BOUNDING TECHNIQUES IN SHAKEDOWN AND RATCHETTING

BY

JOSE RICARDO QUEIROZ FRANCO, M.Sc.,B.Eng.

A thesis submitted for the degree of
Doctor of Philosophy
of the University of Leicester.

January 1987

Bounding Techniques in Shakedown and Ratchetting

Jose Ricardo Queiroz Franco

JANUARY 1987

ACKNOWLEDGEMENTS

I would like to express gratitude to my supervisor Professor Alan R. S. Ponter. He has been a profound source of encouragement and inspiration in the making of this thesis. Mention has to be made of his open mind and vision in matters of research.

I also would like to extend my sincere thanks to the following persons, who somehow helped to see me through the work:

Mr Phillip Brown, Senior Computer Officer, for his constant availability and assistance.

Dr. Keith Carter, for constructive discussions during the course of the research.

Dr. Robert Colls, who so freely volunteered to revise the language of the thesis.

Dr Richard Mobbs, who has also given so freely of his time to improve the presentation of the text.

Mr. Colin Morrison, whose experimental skills made it possible to run the tests so smoothly.

Dr. Dimitrios Papadakos, for his help with part of the graphical routines.

Mrs Helen Townsend, for her skilful typing of the equations.

The Drawing Office Staff, for producing half of the diagrams in this thesis.

My friends in the Computer Office and in the Enginneering Department, whose support and friendship made my work much more pleasant and easy.

My friends from FEMVIEW LTD., who have always been free to advise me regarding the acquisition of computer hardware and software.

Finally I would like to gratefully acknowledge the financial support provided by the Conselho Nacional de Desenvolvimento Cientifico e Tecnologico(CNPq).

To Cecilia, Pedro and Paulo for their love,

patience and encouragement.

BOUNDING TECHNIQUES IN SHAKEDOWN AND RATCHETTING

by

JOSE RICARDO QUEIROZ FRANCO

ABSTRACT

A review of Shakedown and Ratchetting concepts and their extensions is presented in an attempt to recount all the aspects of the problems considered in this research programme. The concept of Stress Concentration Factor was the first to be further investigated, by analysing two representative types of structures operating under severe stress concentration, namely; two-bar structures and cylindrical vessels with variable thickness subjected to cyclic mechanical loads. The material behaviour considered are: elastic-perfectly plastic and isotropic hardening. Such an analytical investigation allowed the assessment of the influence of the Stress Concentration Factor below and above the limit of reversed plasticity.

The primary aim of this research was to develop simplified techniques capable of solving thermal loading problems in the presence of steady mechanical loads. A simplified technique was then developed to analyse a tube subjectd to a complex thermal loading simulating the fluctuation of level of sodium in Liquid Metal Fast Breeder Reactors(LMFBR). The technique was also able to include a second important aspect of shakedown problems which is cases of multiple mechanical loads. The construction of bi-dimensional Bree type diagrams, from tri-dimensional ones obtained for such cases, allowed an easy assessment of the modes of deformation of the structure. The effects of the temperature on the yield stress were explored.

A third aspect of thermal cyclic problems investigated was the experimental verification of the reliablity of the extended Upper Bound Theorem proposed in Chapter 2. This was achieved by experimental tests on portal frames at 400° C. Contours representing states of constant of deformation were obtained from the experimental measurements. A fourth aspect of the problem was the development of theoretical technique to estimate the transient plastic deformation in excess of the shakedown limit which allowed the construction of theoretical contours directly comparable with the experimental ones.

The fifth and major contribution of this thesis was the development of a general technique for the analysis of axi-symmetric shells based in a displacement formulation for the Finite Element Method. Limit analysis and shakedown problems were reduced to minimization problems by developing a technique to obtain consistent relationship between the displacement field and the plastic strain field. Such a technique, based upon a Galerkin type of approach, consist of minimizing the difference between the two representations of the strain within the element; in terms of nodal displacement and in terms of plastic multipliers. The problem was then solved by Linear Programming. Finally, the conclusions and proposal for future work are presented.

CHAPTER 1

INTRODUCTION

1.1 General Considerations 1
1.2 On Some Factors Governing the Shakedown Behaviour of the Structure 3
1.3 Summary of the Objectives of the Present Research 4
1.4 Summary of the Contents of this Thesis 5

CHAPTER 2

A REVIEW OF SHAKEDOWN THEOREMS AND ITS EXTENSIONS

2.1 Introduction 10
2.2 Stress-Strain Relationships and Basic Assumptions 12

2.2.1 State of Stress 13
2.2.2 State of Strain 14
2.2.3 Equilibrium Conditions 14
2.2.4 General Stress-Strain Relations 15

2.3 The Dependence of Shell Performance on the Stress Concentration Factor 19
2.4 Shakedown Theorems 21

2.4.1 Melan's Statical Shakedown Theorem 21
2.4.2 Koiter's Kinematical Shakedown Theorem 22
2.4.3 Extensions of Koiter's Theorems to Include Cyclic Thermal Loading 25
2.4.4 Extension of the Upper Bound Shakedown Theorem (Koiter's) for Cyclically Hardening Materials 27

2.4.4.1 Description of the Problem 27
2.4.4.2 Material and Structural Shakedown for Cyclically Hardening Materials 29
2.4.4.3 The Extended Koiter's Theorem 31

2.4.5 Formulation of the Upper Bound Theorem for Beams and Frames 37

CHAPTER 3

SHAKEDOWN AND RATCHETTING ABOVE THE LIMIT OF REVERSED PLASTICITY; NUMERICAL APPLICATION FOR THE CASE OF CYCLIC MECHANICAL LOADS

3.1 The Two-Bars Structure 44

3.1.1 Notation 44
3.1.2 Introduction 45
3.1.3 Behaviour of two-bars structure 46
3.1.4 Conclusions 48

3.2 Cylindrical Pressure Vessel with Varible Thickness 48

3.2.1 Notation 48
3.2.2 Introduction 49
3.2.3 Elastic Solutions 50

3.2.3.1 Edges Forces Calculations (H,M) 50
3.2.3.2 Global Collapse 51

3.2.4 The Upper Bound Theorem 51

3.2.4.1 The Mechanism of Deformation 51

3.2.5 Limit Design Boundary 52

3.2.5.1 Ratchetting Bound 52
3.2.5.2 Reverse Plasticity Bound 53

3.2.6 Work Hardening Material 54

3.2.6.1 Ratchetting Bound Above Reverse Plasticity 54

3.2.7 Elastic/Perfectly Plastic Material 55

3.2.7.1 Ratchetting Bound Above Reverse Plasticity 56

3.2.8 Numerical Examples 57
3.2.9 Conclusions 58

CHAPTER 4

SIMPLIFIED ANALYSIS OF TUBES SUBJECTED TO MECHANICAL LOADS AND MOVING TEMPERATURE FRONT

4.1 Introduction 78
4.2 The Simplified Analysis 82

4.2.1 Geometry and Loading 82
4.2.2 Thermal Stress Distribution Assumed 82
4.2.3 The Effects of the Simplifications Adopted on the Shakedown Boundary and Modes of Deformation 84

4.3 Simplified Analysis of a Tube Subjected to Constant Axial Load and Moving Temperature Fronts 85

4.3.1 Temperature Independent Calculations 86

4.3.1.1 Applying the Upper Bound Theorem to the Mode of Deformation II 86
4.3.1.2 Applying the Upper Bound Theorem to the Modified Mode of Deformation III 88

4.3.2 Temperature Dependent Calculations 92

4.3.2.1 Mode of Deformation II 92
4.3.2.2 Mode of Deformation III 93

4.4 Simplified Analysis of a Tube Subjected to Internal Pressure and Moving Temperature Fronts . 94

4.4.1 Temperature Independent Calculations 95

4.4.1.1 Mode II of Deformation 95
4.4.1.2 Mode III of Deformation (outward mechanism) 96

4.4.2 Temperature Dependent Calculations 96

4.4.2.1 Mode II of Deformation 96
4.4.2.2 Mode III of Deformation 97

4.5 Simplified Analysis of a Tube Subjected to Axial Load, Internal Pressure and Moving Temperature Fronts 97

4.5.1 Temperature Independent Calculations 100

4.5.1.1 Inward Mechanism for a Predominant Axial Load 100
4.5.1.2 Outward Mechanism for a Predominant Internal Pressure 101
4.5.1.3 Reversed Plasticity Mechanism 102

4.5.2 A Bi-Dimensional Representation of the Tri-Dimensional Bree Type Diagram 103
4.5.3 Temperature Dependent Calculations 106

4.5.3.1 Inward Mechanism for a Predominant Axial Load 106
4.5.3.2 Outward Mechanism for a Predominant Internal Pressure 107
4.5.3.3 Reversed Plasticity Mechanism 107

4.5.4 A Bi-Dimensional Bree Type Diagram for the Temperature Dependent Yield Stress 108

4.6 Conclusions 111

CHAPTER 5

EXPERIMENTAL TESTS ON PORTAL FRAMES OPERATING AT 400°C SUBJECTED TO CYCLIC THERMAL LOADING IN THE PRESENCE OF STEADY MECHANICAL LOAD

5.1 Introduction 129
5.2 Material Behaviour 131

5.2.1 Bending Moment-Curvature Relationship 131
5.2.2 Cyclic Stress-Strain Curve 133

5.3 Theoretical Analysis of a Portal Frame For An Isotropic Material Model 135

5.3.1 Description of Possible Modes of Behaviour .. 135

5.4 Description of the Test Specimens, Apparatus and Equipment 138
5.5 Description of the Experimental Procedure 140

5.5.1 On the Collapse Mechanical Load 140
5.5.2 The Cyclic Loading Test 141

5.6 Analysis of the Experimental Results 142
5.7 A Theoretical Estimate of the Accumulation of Transient Plastic Strain Beyond Shakedown for the Portal Frame 144

5.7.1 The Isotropic Hardening Model 144
5.7.2 On the Calculation of the Transient Plastic Strain 149
5.7.3 Theoretical Contours of Constant Ratchet Strain 153

5.7.3.1 A General Approach 153
5.7.3.2 Uniaxial Behaviour 156

5.7.4 On the Determination of Contours for the Portal Frame 156

CHAPTER 6

A DISPLACEMENT FORMULATION FOR THE FINITE ELEMENT SHAKEDOWN ANALYSIS OF PRESSURE VESSELS

6.1 Introduction 185
6.2 An Approximate Yield Surface for Symmetrically Loaded Thin Shells of Revolution 190
6.3 Discretization of the Axi-Symmetric Shells via Finite Elements 196
6.4 On a Consistent Relationship Between Nodal Displacement Variables and Nodal Plastic Multipliers 201

6.4.1 Stress and Strain Fields as Functions of Generalized Quantities 201

6.5 A General Solution for the Biorthogonality Condition 205
6.6 Approximate Displacement and Strain Fields for Axi-symmetric Shells 209
6.7 The Upper Bound Theorem Applied to Axi-Symmetric Shells Via Finite Element Technique and Linear Programming 211
6.8 The Constraint Equations for the Linear Programming 217
6.9 End Conditions for Axi-Symmetrical Shells 220
6.10 Numerical Solutions 222

6.10.1 Limit Load Problems 224

6.10.1.1 Cylindrical Shells 224
6.10.1.2 Conical Shells 230
6.10.1.3 Spherical Caps 231
6.10.1.4 Toroidal Shells 234
6.10.1.5 Torispherical Vessels 235

6.10.2 Cyclic Thermal Stress Problems (Shakedown Analysis) 238

6.10.2.1 Cylindrical Vessels 238
6.10.2.2 Torispherical Vessels 239

CHAPTER 7

CONCLUSIONS AND PROPOSALS FOR FUTURE WORK

7.1 Conclusions 283
7.2 Proposals for Future Work 288

APPENDIX A 290
APPENDIX B 308
APPENDIX C 311
APPENDIX D 315
APPENDIX E 322

REFERENCES 334

CHAPTER 1

INTRODUCTION

1.1 General Considerations

This chapter aims first to provide a brief description of the several aspects of shakedown problems studied in this thesis, and second to summarize the objectives and achievements of the present research.

Shakedown and Ratchetting concepts have been widely used as an aid to structural design over the last twenty years. During the last 6 years, general finite element codes have appeared(such as ABAQUS) which are capable of analysing structures subjected to complex histories of load and deformation. It has been realized, however, that it is very difficult to extract a general understanding of structural behaviour through a step by step solution of individual cases. It is also impossible to assess the sensitivity of behaviour to variations in geometry, material assumptions and histories of loading. This problem is particularly accute for structures subjected to severe thermal loading. The need to understand ratchetting phenomena has encouraged a reappraisal of the usefulness of shakedown theory as the basis of computer analysis techniques, as the theory is capable of producing, directly, quantities of direct use in design; viz. the limit load, shakedown limit, and the ratchet limit.

However, before the results of computer methods can be accepted as reliable, it is necessary to understand the relationship between classical plasticity theory and ratchetting phenomena. Although the analysis of pressure vessels under cyclic internal pressure based on shakedown theory and the subsequent translation of the results into design methods has greatly contributed to establish shakedown as the basis for design criteria, certain aspects have still to be studied. For example, the effects of stress concentration, the capability of the material to work harden and the type of structure need to be studied. Several papers have been published [10,11,12,13,14] concerning the interpretation of the difference between theoretical and experimental results for mechanical loading problems. The conclusions vary from the strict application of the shakedown concept, as required by the present Codes of Practice, yielding loads which are too high due to an underestimate of the stress concentration factor[9], or to being sometimes unnecessarily conservative. The latter argument is based on the fact that, although metals can withstand several thousands cycles of reversed plasticity, the shakedown limit eliminates both possibilities of ratchetting and reversed plasticity [13,14] without distinguishing between the two phenomena.

More recently, the application of shakedown theory to thermal loading problems has become a major task in the design of components operating at high temperatures and subjected to cyclic thermal loading in the presence of static mechanical loads. These problems have gained

considerable significance with the advent of the Liquid Metal Fast Breeder Reactor(LMFBR) and advanced aeronautical structures such as the solid propellant rocket booster of the Space Shuttles in the USA and the rocket booster of the satellite launcher Ariane in France. The thermal loading problems are now significantly more complicated with much higher temperatures and much more severe thermal conditions. The mechanical loads for such problems may consist of internal pressure, axial load, own weight of the component or the weight of coolant it carries. Although in the literature there exist very few attempts to consider more than one mechanical load, in practice such loads are more likely to occur simultaneously or at least in pairs. The primary aim of the present research is the development of a general technique capable of analysing a wide range of axi-symmetric vessel components under a variety of axisymmetric thermal loading conditions (as described above) and the work contained in this thesis contributes towards such an objective.

1.2 On Some Factors Governing the Shakedown Behaviour of the Structure

The several aspects of shakedown problems considered here can be described as follows:

a) The influence of the Stress Concentration Factor on the shakedown limits.

b) Structural and Material behaviour above the limit of

reversed plasticity; an extended upper bound formulation to define the ratchetting bound above reversed plasticity for cyclic mechanical load problems.

c) Cyclic Hardening above the limit of reversed plasticity.

d) Thermal Loading Problems involving more than one mechanical load; including the effects of the dependence of the material yield stress on the temperature.

e) Experimental Analysis of a Portal Frame operating at high temperatures and subjected to simulated thermal cyclic loading in the presence of mechanical loads; a direct correlation with the extended upper bound formulation and a theoretical estimate of the accumulation of transient plastic deformation beyond shakedown limits.

f) A Displacement Formulation for the Finite Element Shakedown Analysis of a Wide Range of Axi- Symmetric Pressure Vessels.

1.3 Summary of the Objectives of the Present Research

The overall objective of this thesis is to develop a simplified technique, based on a Finite Element Approach and Linear Programming, capable of performing a complete shakedown analysis of axisymmetric thermal loading problems applied to a wide range of axi-symmetric pressure vessels. This technique aims also to encompass, in the future, most of the material and structural features listed above so that a better and more economical design can be achieved by:

a) The use of a simplified but reliable numerical technique for the analysis of complex thermal loading problems.

b) Preventing incremental deformation(ratchetting) in the structure without eliminating the possibility of reversed plasticity.

c) Applying the technique to as many representative vessels components and loading conditions as possible in order to obtain a better picture of the factors which control the behaviour of such structures.

d) Considering different material properties and material models to evaluate the best assumption, when compared with experimental results.

e) Providing the designer with a selection of solutions which could help in the assessment of the circumstances when a more detailed analysis is required or more experimental data is needed.

1.4 Summary of the Contents of this Thesis

The present chapter together with Chapter 2 will provide a clear picture of the several aspects of the problems studied in this research programme. In Chapter 2 there will be a review of Shakedown and Ratchetting concepts and their application to pressure vessels. Sections 2.1 and 2.2 present some aspects of the stress-strain relationships, and the basic assumptions behind them. In Section 2.3 the dependence of the shakedown behaviour of pressure vessels on the stress concentration factor is discussed. The two fundamental shakedown theorems (Melan's and Koiter's) are

presented and discussed in Section 2.4, which in their classical form imply materials obeying elastic/perfectly plastic material properties. The extension of the Upper Bound Theorem for Cyclic Hardening Materials proposed by Ponter and Karadeniz [36,37] is also reviewed in Section 2.4. Such an extension may be used to define bounds separating the region of plastic shakedown from the ratchetting region in a Bree type diagram, which would allow the designer to assess the region where ratchetting can be prevented without eliminating the possibility of reversed plasticity. The extension of Koiter's theorem to include cyclic thermal loading is also considered in Section 2.4.3.

In Chapter 3 two types of structure subjected to cyclic mechanical loads are analysed using the upper bound and the extended upper bound theorems, and their behaviour above the limit of reversed plasticity is also discussed. The structures are analysed considering two different types of materials; elastic-perfectly plastic and isotropic hardening materials. The two types of structures are:

- two-bar structures

- cylindrical vessels with a discontinuity in the thickness

In Chapter 4, a much more complex, thermal loading problem is considered where a simplified analysis is performed of a tube subjected to mechanical loads and moving temperature fronts. Such a problem represents the simulation of the

fluctuation of the level of sodium in a LMFB reactor. The mechanical loads may consist of internal pressure, axial load, self weight of the component or the weight of the coolant it carries. The three combinations of mechanical and thermal loads considered in the calculations can be summarized as follows:

- moving temperature front in the presence of steady axial load

- moving temperature front in the presence of steady internal pressure

- moving temperature fronts in the presence of steady axial load and internal pressure

Two sets of calculations using the upper bound theorem were performed for each case; in the first set the material properties were assumed to be independent of the temperature and in the second set the dependence of the yield stress of the material was considered. The results are presented in the form of Bree type diagrams and for the third loading case such a diagram is a tri-dimensional one. However, a much simpler bi-dimensional diagram may be obtained, where the designer can easily assess the regions of different modes of deformation for the overall design concept.

In Chapter 5 the results of tests performed on portal frames uniformly heated to 400°C and subjected to simulated thermal cyclic loading in the presence of steady mechanical load is

analysed. The material ratchetting and cyclic hardening are assessed and the regions of reversed plasticity and shakedown are defined. Contours representing the bounds of steady state of ratchetting rates are estimated by simple mathematical representations of uniaxial incremental growth of the material (material ratchetting), and compared with the contours obtained experimentally. The sensitivity of the structural behaviour to large variations of temperature is also assessed.

In Chapter 6 a displacement formulation for the Finite Element analysis of pressure vessels is developed in the form of a general technique. The primary aim of this technique is the solution of thermal cyclic loading problems by means of the upper bound theorem. By imposing certain restrictions on the class of mechanisms of deformation assumed, the shakedown or limit analysis problem can be reduced to a minimization problem and solved by Linear Programming. Nevertheless, such problems can only be solved by a minimization process if a consistent relationship between the displacement fields which describe such mechanisms of deformation and the kinematically admissible strain fields can be found. In Section 6.5 a general method of obtaining such a consistent relationship is developed, based upon a Galerkin type technique which minimize the difference between the two representations of strain within each element. This general technique is based upon four basic types of shell elements; cylindrical, conical, spherical and toroidal. The class of displacement fields and the yield condition (Tresca) chosen are such that the

solutions generated can be directly compared with available analytic solutions. However the technique is capable of extension to a wide class of displacement fields and piecewise linear yield conditions. For the purposes of this thesis all the elements were tested individually in limit analysis problems and also torispherical vessels were analysed consisting of the combination of three basic elements.

Finally the conclusions and proposals for future developments are presented in Chapter 7.

CHAPTER 2

A REVIEW OF SHAKEDOWN THEOREMS AND EXTENSIONS

2.1 Introduction

The work presented in this thesis is largely related to shakedown theory and in order to avoid repeating the basic concepts for each particular problem considered, this chapter stands as an attempt to encompass all the necessary features of the shakedown theorems which could be referred to in following chapters.

In the design of components subjected to variable loads and particularly for those operating under cyclic thermal loading, shakedown theory can prove to be a much more powerful tool than the direct application of classical plasticity as a step-by-step incremental problem. This is because the theory is concerned with the evaluation of quantities of direct relevance to design, and because global solutions for a whole class of structures can be constructed. The primary application to pressure vessels has been in the support of design codes and design charts, ie, information and technique which can be used in the early stages of design.

The two existing shakedown theorems present very important complementary features, i.e. to the statical shakedown theorem, which is formulated in terms of stress variables and gives rise to a lower bound on a load parameter,

corresponds a similar theorem of a kinematical type which allows the determination of a upper bound in terms of a compatible strain field. Although shakedown theory was developed for particular classes of problems as long ago as 1926 [1], and has been fairly well understood from the theoretical point of view for many years, only relatively recently has it been used as an aid to design. The delay in the application of these theorems to practical problems is perhaps explained by the complexity of the theory when expressed in its original form (e.g. Koiter's description of the upper bound theorem [28,29]). The definition of either equilibrium stress fields for the lower bound or, consistent strain fields for upper bound, has proved to be rather complicated especially for thermal loading problems where such stress and strain fields depend on the position of the point considered and also on the current time.

The lower bound theorem has been successfully applied in the design of pressure vessels under variable mechanical load [4,5], but the fact that the strict application of the shakedown concept produces bounds on load which eliminate both ratchetting and reversed plasticity altogether, has been cause for serious criticism. The reason for this is that reverse plasticity may be tolerated in design, and that a more general method, which distinguishes between non-ratchetting reverse plasticity and ratchetting reverse plasticity, is required. One of the aims of the present chapter is to present such an extension of shakedown proposed by Ponter and Karadeniz [36,37] based on the classical upper bound shakedown theorem, which extends the

classical shakedown boundary to include the reversed plasticity region. Extensions of the shakedown theorems to include non-uniformly heated bodies and the formulation for beams and frames where the deformation is assumed to be caused only by bending moments are also included in this chapter, with emphasis on the upper bound shakedown theorem.

2.2 Stress-Strain Relationships and Basic Assumptions

Consider an elastic-plastic body of volume V and surface S (Fig.2.1). Assume that at any instant t this body is subjected to body forces per unit of volume bi, surface forces pi prescribed on surface Sp (part of S where the forces are prescribed) where λ is a load parameter and applied surface displacement u_i on Su, the remainder of the total surface where the displacements are prescribed. For the sake of simplicity the discussion of the shakedown theorems will be restricted to cases where the prescribed displacements vanish on surface Su. In addition, it is assumed that a history of temperature $\Theta(x,t)$ may occur for t > 0.

All deformations are assumed to be sufficiently small so that changes in geometry can be disregarded.

2.2.1 State of Stress

The state of stress at an internal point of the body is defined by σij which represents components of a stress tensor in a nine dimensional stress space. Assuming negligible geometric changes during the deformed state it becomes sufficient to refer to the stress tensor in the undeformed state.

A statically admissible stress field must satisfy the following conditions:

a) Equilibrium Equations

$$\sigma_{ij,j} + b_i = 0 \qquad 2.1$$

where the comma denotes partial differentiation with respect to the space variables and bi are the body forces per unit volume.

b) Stress Boundary Conditions

$$\sigma_{ij} n_j = \lambda p_i \qquad 2.2$$

where n_j are the direction cosines of the outward normals to the surfaces.

2.2.2 State of Strain

The state of strain at a point is defined by the symmetric strain tensor ε_{ij} representing an elastic, a plastic and a possible thermal expansion component $\varepsilon^{\theta}_{ij}$.

$$\varepsilon_{ij} = \varepsilon^{e}_{ij} + \varepsilon^{p}_{ij} + \varepsilon^{\theta}_{ij} \qquad 2.3$$

where the elastic part of the constitutive relation is given by Hooke's law

$$\sigma_{ij} = D_{ijhk}\varepsilon^{e}_{ij} \qquad 2.4$$

and D_{ijhk} denotes the tensor of elastic coefficients which is symmetric, positive definite and independent of temperature. The strain-displacement relations for the linear theory is given by

$$\varepsilon_{ij} = \frac{1}{2}\left[\frac{\partial U_i}{\partial x_j} + \frac{\partial U_j}{\partial x_i}\right] \qquad 2.5$$

and likewise the strain rate tensor $\dot{\varepsilon}_{ij}$ is expressed in terms of the velocities $\dot{U}_i$ by an identical expression.

2.2.3 Equilibrium Conditions

The Principle of Virtual Displacement can be used to express the conditions of equilibrium as

$$\int_V \sigma_{ij}\varepsilon^{c}_{ij}dV = \int_V b_i U^{c}_i dV + \lambda \int_{S_p} P_i U^{c}_i dS \qquad 2.6$$

an equation valid for any stress distribution σ_{ij}, in equilibrium in the interior and surface of the body, ie, with b_i and λpi and for any displacement field U_i^c compatible with the corresponding strain distribution ε_{ij}^c. Equation (2.6) also holds if the displacement field and corresponding stress distribution are replaced by a velocity field $\dot{U}_i$ and corresponding strain rate distribution $\dot{\varepsilon}_{ij}$.

2.2.4 General Stress-Strain Relations

The stress state corresponding to stress points within the elastic domain has been referred to as a safe stress state and denominated by $\sigma_{ij}^{(s)}$ whereas admissible stress state $\sigma_{ij}^{(a)}$ is a term given to all the stress points within and at the boundary of the elastic domain. The boundary of the elastic domain is called in geometric terms the yield surface on which any stress point can give rise to increments of plastic strain, ie plastic deformation can develop if the stress distribution in the element satisfy $\phi(\sigma_{ij}) = \sigma_y$ where $\phi(\sigma_{ij})$ defines the yield surface.

Plastic stress-strain relations have been derived using various approaches always involving propositions based on essentially correct but restricted assumptions. The first approach to such relations was proposed by Saint-Venant in 1870 [15] who suggested that the principal stress axes should coincide with the principal axes of strain increment. Levy and von Mises [16,17] later developed, independently,

general three dimensional equations relating the increments of total strain to the stress deviator. In this approach the total strain increments are assumed to be equal to the plastic strain increment, the elastic strain being ignored. Thus it cannot be applied in the elastoplastic range but only to large plastic flow. The generalization of the approach to include both elastic and plastic strain components was proposed by Prandtl [19] and Reuss[20]. These relations all originated from the assumption above proposed by Saint-Venant and have been shown to imply the von Mises yield criterion [23]. A general plastic stress-strain relation for any yield criterion was derived by Drucker [20,21,22] through stability postulates termed the fundamental quasi-thermodynamic postulates. Drucker's first postulate termed stability "in the small" starts with a more precise definition of work hardening which may be formulated as follow:

Consider an element of the continuum in some initial state of stress and then some external agency applies an additional set of stresses with the subsequent slow removal of them. Work hardening implies that the element will remain in equilibrium and

(a) positive work is done by the external agency during the application of the added set of stresses and

(b) the net work performed by the external agency during its application and removal is zero or positive.

It should be emphasized that the work referred to is only the work done by the added set of forces on the resulting displacements. In other words, work hardening implies that useful net energy cannot be extracted from the element and the system of forces acting on it.

Mathematically it can be put as follows: Suppose that an external agency is applied to an element of the continuum initially under a state of stress σ_{ij} and strain ε_{ij} so that the strain and stress at each point is changed by amounts $d\varepsilon_{ij}$ and $d\sigma_{ij}$ respectively where one component of the total strain increment is elastic and the other may be plastic; ie, $d\varepsilon_{ij} = d\varepsilon^e_{ij} + d\varepsilon^p_{ij}$. If the added forces are removed the plastic increments remain in the element.

For work hardening implication (a) gives

$$d\sigma_{ij}d\varepsilon_{ij} > 0 \qquad 2.7$$

and from (b)

$$d\sigma_{ij}(d\varepsilon_{ij} - d\varepsilon^e_{ij}) \geq 0 \qquad 2.8$$

ie

$$d\sigma(d\varepsilon^e_{ij} + d\varepsilon^p_{ij}) > 0$$

thus

$$d\sigma_{ij}d\varepsilon^p_{ij} \geq 0 \qquad 2.9$$

Inequalities (2.8,2.9) represent the mathematical definition of stable work hardening. Drucker's second postulate, stability "in the large", involves the assumption (a) and

(b) applied to a finite change in the external agency. This results in the following inequalities, which had previously been suggested by Hill [29] as the maximum work principle.

$$[\sigma_{ij} - \sigma_{ij}(s)]\dot{\varepsilon}^{p}_{ij} > 0 \qquad 2.10$$

$$[\sigma_{ij} - \sigma_{ij}(a)]\dot{\varepsilon}^{p}_{ij} \geq 0 \qquad 2.11$$

where σij is a state of stress on the yield surface at which plastic strain rates $\dot{\varepsilon}^{c}_{ij}$ occur. It has been shown that in virtue of Equation (2.11) the yield surface is convex and the equality sign is only possible in the absence of plastic deformation. Another form of the postulate (2.7) is expressed by

$$\dot{\sigma}_{ij}\dot{\varepsilon}_{ij} \geq 0 \qquad 2.12$$

where $\dot{\sigma}_{ij}$ is the stress rate corresponding to the plastic strain rate $\dot{\varepsilon}^{p}_{ij}$ and will always be equal to zero for perfectly plastic material. A full derivation of the general plastic stress-strain relations can be found in [23] and [28] and will not be presented here. From the previous definition of work hardening the general form of the stress-strain relations for work hardening and perfectly plastic materials are expressed by the respective associated flow rules:

Work Hardening Material

$$d\varepsilon^{c}_{ij} = G \frac{\partial\phi(\sigma_{ij})}{\partial\sigma_{ij}} d\phi \qquad 2.13$$

where G is a scalar which may depend on stress,strain and history and $\phi(\sigma_{ij})$ is the yielding criterion assumed.

Perfectly Plastic Material

$$d\varepsilon_{ij} = d\mu \frac{\partial\phi}{\partial\sigma_{ij}} \qquad 2.14$$

where $d\mu$ is a scalar. It should be noted here that these postulate can only provide statements about the plastic strain rates. For the total plastic strains the entire history of the element has to be given.

2.3 The Dependence of Shell Performance on the Stress Concentration Factor

Lower bounds of shakedown loads have been obtained by Leckie [4] and Leckie and Penny [5] for radial nozzles in spheres composed of elastic/perfectly plastic materials, based on Melan's theorem which states that; the structure will shake down if any distribution of self-equilibrating residual stresses can be found which, when superimposed on to the elastic stresses due to cyclic load, do not violate the yield condition. The actual self-stress distribution will always be greater than the assumed values since the structure tends to find the best residual distribution.

These lower bound solutions for cyclic pressure have been proved by Rose [2] to depend upon the elastic stress concentration factor (SCF) defined by

$$SCF = \frac{\text{maximum elastic stress}}{\text{membrane stress in the sphere}} \qquad 2.16$$

It has been shown that for small values of SCF, while the permanent residual strain is small, the pressure for initial yielding(p_i) is higher than for large values of SCF where the permanent set is increased. It can also be concluded from Rose (Figs. 2a,b) that for small values of SCF the shakedown pressure (p_s) can be greater than the test pressure and according to Ponter [14] the plastic collapse pressure p_l and the shakedown pressure p_s are equal when the SCF is less than about 2.

If a SCF>2 is considered, shakedown pressure is then the limiting condition, eliminating both possibilities of reversed plasticity and ratcheting. This situation can be better explained by Fig.(2.3) for plane stress. It has been shown by Rose [2] and Leckie and Payne [6] that the maximum achieved shakedown pressure is $p_s=2p_i$ where p_i is the pressure for first yield.

Defining a shakedown factor as $K_s=p_s/p_i$ the maximum value of $K_s=2$ can be found by using Melan's theorem where the residual stresses field is represented by d' and the elastic stresses correspond to line dd' (Fig. 2.3). It can be seen that

$$\rho_{ij} = -\frac{1}{2}\sigma^{e}_{ij} \qquad 2.17$$

2.4 Shakedown Theorems

Before the theorems are stated, it is useful to have some definitions of the terms involved.

SHAKEDOWN: A structure subjected to cyclic load is considered to be in a state of shakedown, if the response of the structure becomes elastic after the appearance of plastic deformation during the first cycle.

REVERSED PLASTICITY: When a small volume of the structure is subjected to an elastic stress range larger than $2\sigma_y$, developing plastic strain, alternatively in tension and compression for each part of the cycle, that part of the structure is said to be operating in a reversed plasticity condition.

RATCHETTING: A structure, when its deformation increases over each loading cycle, is said to be ratchetting.

2.4.1 Melan's Statical Shakedown Theorem

The first general shakedown theorem for elastic-perfectly plastic material, based on a statical approach to the problem of structures operating under several loads varying independently within prescribed limits, was proposed by Melan [24,25,26]. This theorem may be formulated as follows:

Shakedown will occur if a state of residual stress $\rho_{ij}(x)$, independent of time, can be found, such that superposition of this residual stress on the elastic stresses due to prescribed mechanical and thermal cyclic loads $\hat{\sigma}_{ij}(x,t)$ nowhere violate the yield criterion, ie

$$\phi(\sigma^*_{ij}) < \sigma_y \qquad 2.18$$

where

$$\sigma^*_{ij}(x,t) = \hat{\sigma}_{ij}(x,t) + \bar{\rho}_{ij}(x) \qquad 2.19$$

In general, structures do not shake down to a unique shakedown state independent of the loading programme. However, a residual stress field is normally search so that a maximum admissible load variation is obtained. In this sense the application of Melan's theorem leads to lower bounds of the limits of load variation.

The proof of this theorem was given by several authors [27,28,29,30].

2.4.2 Koiter's Kinematical Shakedown Theorem

The second general theorem generally referred to in the literature as Koiter's theorem, is based on kinematical principles and was proposed by Koiter [28]. Here, its form for cyclic loading, with cycle time Δt is discussed.

First, it is convenient to give some definitions as follows: the concept of an arbitrary field of admissible plastic strain rate cycle $\dot{\varepsilon}_{ij}$ is defined by its property that the plastic strain increments during a cycle t = 0 to t = Δt.

$$\Delta\varepsilon^c_{ij} = \int_0^{\Delta t} \dot{\varepsilon}^c_{ij}(t)dt \qquad 2.20$$

constitute a kinematically admissible strain distribution, ie, $\Delta\varepsilon^c_{ij}$ satisfies the compatibility conditions (2.5) and the corresponding displacement field are zero on Su. Corresponding to the plastic strain rate field $\dot{\varepsilon}_{ij}(t)$ there is a unique residual stress rate distribution $\dot{\rho}_{ij}(t)$ and corresponding elastic strain rates. The kinematically admissible total strain rate field

$$\dot{\varepsilon}_{ij} = \dot{\varepsilon}^e_{ij} + \dot{\varepsilon}^c_{ij} \qquad 2.21$$

is obtained from a velocity field $\dot{U}_i$ from (2.5). In addition the total stress rate history is given by

$$\dot{\varepsilon}^e_{ij} = D_{ijk\ell}\dot{\sigma}_{k\ell} \qquad 2.22$$

and $\dot{\rho}_{ij}$ is now defined by $\dot{\rho}_{ij} = \dot{\sigma}_{ij} - \dot{\hat{\sigma}}_{ij}$, where $\dot{\hat{\sigma}}ij$ is the rate of change of elastic stresses for the same loading history. The residual stresses at the end of a cycle t = Δt return to their initial values at time t = 0 as the increments of plastic strains are kinematically admissible; hence

$$\int \dot{\varepsilon}^{e}_{ij}(t)dt = 0 \qquad 2.23$$

while the displacement increments over a cycle time Δt are

$$\Delta U^{c}_{i} = \int \dot{U}_{i}(t)dt \qquad 2.24$$

Koiter's theorem may now be formulated by the following statements: the structure will not reach a state of shake-down, in other words it will either suffer ratchetting or reversed plasticity, if any system of external cyclic loads and any admissible plastic strain rate cycle $\dot{\varepsilon}^{c}_{ij}(t)$ within prescribed limits satify

$$\int_{o}^{T} dt\{\int_{V} b_i(t)\dot{U}^{c}_{i}dV + \lambda \int_{S_p} p_i(t)\dot{U}^{c}_{i}(t)dS\} > \int_{o}^{T} dt \int_{V} D(\dot{\varepsilon}^{c}_{ij})dV \qquad 2.25$$

where $D(\dot{\varepsilon}_{ij})$ is the plastic energy dissipation $D(\dot{\varepsilon}^{c}_{ij}) = \sigma_{ij}\dot{\varepsilon}^{c}_{ij}$ for the admissible strain rate cycle $\dot{\varepsilon}^{c}_{ij}$. However, the structure will shake down if a number $k > 1$ exists so that for the prescribed loading system

$$K\left[\int_{o}^{T} dt\{ \int_{V} b_i(t)\dot{U}^{c}_{i}(t)dV + \lambda \int_{S_p} p_i(t)\dot{U}^{c}_{i}(t)dS\}\right] \leq \int_{o}^{T} dt \int_{V} D(\dot{\varepsilon}_{ij})dV \qquad 2.26$$

is valid for all admissible plastic strain rate cycles $\dot{\varepsilon}^{c}_{ij}$.

Koiter [28,29] and Martin [30] have presented proof for this general theorem.

2.4.3 Extensions of Koiter's Theorems to Include Cyclic Thermal Loading

The shakedown problem when a temperature field is included in the loading programme was first studied by Prager [31] and Rosemblum [32] who presented the proof for the extended version of Melan's theorem.

Koiter's theorem was also extended to non-uniformly heated bodies [33,34,35] in a slightly different formulation. An additional term of the form

$$\int_0^T dt \int_V \dot{\rho}_{ij}\delta_{ij}\alpha\theta(x,t)dV \qquad 2.27$$

has to be added to the left-hand side of (2.25) and (2.26) where α is the coefficient of linear thermal expansion, δ_{ij} is the Kronecker delta ($\delta_{ij}=1$ for $i=j$ and $\delta_{ij}=0$ for $i\neq j$) and $\dot{\rho}_{ij}$ is the residual stress rate produced by the plastic strain rate $\dot{\varepsilon}_{ij}$ where the thermal expansion strains are included in the definition of $\hat{\sigma}_{ij}$. The uniqueness of the residual stress rate $\dot{\rho}ij$ and the corresponding given plastic strain rate $\dot{\varepsilon}_{ij}$ followed by the unique thermal stress distribution $\hat{\sigma}^{\Theta}_{ij}(x,t)$ related to the thermal strain field $\delta_{ij}\alpha\Theta(x,t)$ give rise to the following equation

$$\int_0^T dt \int_V \dot{\rho}_{ij}\delta_{ij}\alpha\theta(x,t)dV = \int_0^T \int_V \hat{\sigma}^{\theta}_{ij}(x,t)\dot{\varepsilon}^c_{ij}dV \qquad 2.28$$

which is a consequence of the virtual work and the reciprocity theorem. Assuming that the body forces b_i and the surface forces λp_i are time independent, Koiter's non-shakedown theorem can now be expressed as

$$\int_V b_i dU^c_i dV + \lambda \int_S p_i dU^c_i dS + \int_0^T dt \int_V \hat{\sigma}_{ij}(x,t)\dot{\varepsilon}^c_{ij}(t)dV > \int_0^T dt \int \sigma^c_{ij}\dot{\varepsilon}^c_{ij}(t)dV$$

2.29

where $\hat{\sigma}_{ij}(x,t)$ denotes the elastic stresses due to the time dependent loads, which could include some variable mechanical load. It may be noted that no additional term was included in Equation (2.29). This inequality depends only on the plastic strain rate $\dot{\varepsilon}^c_{ij}$ and the corresponding displacement increment dU^c_i with no involvement of the residual stress field ρ_{ij} induced by ε_{ij} during the transient part of the cycle. Once a consistent relationship between ε_{ij} and dU_i is defined corresponding to each instant during the elastic stress history $\sigma_{ij}(x,t)$, Equation (2.29) may be used to calculate upper bounds on the load parameter. A systematic technique has been developed and will be presented in a later chapter where a Displacement Formulation for the Finite Element Shakedown Analysis of Pressure Vessels is used to define compatible strain fields for certain classes of linear yield surfaces. The optmization of Equation (2.29) to give minimum upper bounds is achieved by reducing the problem to a Linear Programming Problem.

2.4.4 Extension of the Upper Bound Shakedown Theorem (Koiter's) for Cyclically Hardening Materials

As it has already been stated, the classical shakedown theory eliminates both the possibility of ratchetting and of reversed plasticity. This constitutes a real deficiency of the shakedown concept in structural design. The capability of many metals of work hardening and therefore being able to withstand several thousand cycles of reversed plasticity presents a real need to develop simple techniques to assess the range of the reversed plasticity region F in a Bree type diagram (Fig.2.4). This region would certainly not only provide useful information to the designer but also lead to more economical design, as the possibility of ratchetting and fatigue can be separately assessed.

2.4.4.1 Description of the Problem

Consider the body shown in Fig. 2.1 and the assumptions described in Section 2 with constant body and surface forces and a cyclic history of temperature occuring at point x, for a cyclic time t. The temperature history is given by

$$\theta(x,t) = \theta_o + \bar{\theta}(x,t) \qquad 2.30$$

where Θ_o denote some reference temperature and $\bar{\Theta}(x,t)$ is a quasistatic cycling temperature which has the form

$$\theta(x,t) = \Omega(x)\mu(t)\Delta\theta \qquad 2.31$$

$$0 < \mu < 1 \; ; \; 0 < \Omega < 1$$

where $\Delta\Theta$ denotes the maximum temperature difference and $\Omega(x)$ is a nondimensioanal shape function. This implies that the thermo elastic stress history follows a straight line path in stress space.

Assuming a perfectly plastic material element with a yield stress σ_y, a Bree type diagram (Fig. 2.4) can be obtained with axes proportional to the steady mechanical load P/P_L and to the maximum effective thermal-elastic stress σ_t/σ_y due to the cyclic thermal loading where P_L is defined as the limit load. The classical shakedown region S where an elastic mode of behaviour is achieved after some cycles of transient plastic strain is defined by the boundary ABD. The region of interest of this section is the reversed plasticity region F where plastic strains may occur in alternating directions in some part of the element. This region can be isolated from the ratchetting region R, where incremental plastic strains occur at each cycle, by an extended boundary BC which can be determined by the extended upper bound theorem proposed by Ponter and Karadeniz [36,37].

2.4.4.2 Material and Structural Shakedown for Cyclically Hardening Materials

The conditions for material shakedown of a perfectly plastic material is defined by cyclic stress histories that will not cause incremental growth. Although material data for cyclic loading conditions and especially for cyclic thermal loading is complex and limited at the present time, simple conservative assumptions can still be adopted to develop a reliable theory of analysis such as that proposed by Ponter and Karadeniz [36,37]. This theory can be described as follows: The yield criterion is defined in the stress space by (2.18) and the associated flow rule given by (2.14).

A particular class of stress histories which cannot be contained within the yield surface but cause no strain growth will be defined as the reversed plasticity condition. Despite the shortage of material data for the behaviour of specific materials such as the SS316 under plastic cyclic loading, some general discussion on the subject is presented in Chapter 5. The conditions of material shakedown can, however, be formulated by the use of some simplifying assumptions.

It is assumed that material shakedown will occur for a cyclic history of stress $\sigma^*_{ij}(t)$ and temperature $\Theta(t)$ if either of the following conditions are satisfied :

(a) the stress history is contained within the yield surface, ie, $\phi[\sigma^*_{ij}(t)] < \sigma_y[\Theta(t)]$

(b) for those stress histories which exceed the limits of the yield surface, and for which condition (a) cannot be satisfied, the extremes of the stress history are assumed to be related by $\sigma_{ij}^{*max} = - \sigma_{ij}^{*min}$ during the cycle.

Fig.2.5 shows schematically these conditions. Because of the lack of experimental data to assess it, no effect of the variation of temperature on the cycle has been considered in condition (b). The insensitiveness of the relationship between the stress and strain amplitudes to the mean stress when the cyclic state is reached, has been shown by, for example, Pellisier-Tanon et al. [38] which implies that the stress histories, which occur in practice, belong to class of histories of the form

$$\sigma_{ij}^{*}(x,t) = \lambda\hat{\sigma}_{ij}^{p} + \sigma_{ij}^{\theta}(t) + \bar{\rho}_{ij} \qquad 2.32$$

where $\hat{\sigma}_{ij}^{\Theta}(t)$ denotes a thermo-elastic/plastic stress history for zero applied load, $\hat{\sigma}_{ij}^{p}$ is the elastic solution due to constant applied loads $p_i(x)$ and $\bar{\rho}_{ij}$ is an arbitrary residual stress field in equilibrium with zero applied load on Sp. The construction of σ_{ij}^{Θ} requires that cyclic material behaviour be fully described, what is not normally available. For stress histories within the yield surface the response to the cyclic component will be close to the linear elastic solution, whilst for large amplitudes which imply condition (b) the actual response lies between the predictions of perfect plasticity and linear elasticity.

2.4.4.3 The Extended Koiter's Theorem

The extended upper bound theorem presented in this section defines those states of loading for which no incremental plastic strain occurs after a significant number of cycles, although the state of stresses resulted from it cannot be contained within the yield surface, ie the maximum effective thermoelastic stress $\sigma_t < 2\ \sigma_y$. The extended theorem is identical to the classical theorem when the stress history lies within the yield surface, which implies that it contains the classical upper bound as a special case and provides an upper bound for the definition of a boundary between region R of ratchetting and region F of reversed plasticity.

The conclusion reached by Ponter and Karadeniz [36,37] after considering special cases that the assumption of complete cyclic hardening within the reverse plasticity region of the body would provide the smallest F region, leads to a simplifying assumption on the cyclic stress history which can be stated as follows:

The steady cyclic stress history in (2.32) will assume the form of the linear elastic stress history, ie $\sigma^{\Theta}_{ij} = \hat{\sigma}^{\Theta}_{ij}$ where $\hat{\sigma}^{\Theta}_{ij}$ is the linear elastic stress history. The effect of temperature on the elastic moduli will be neglected in all these arguments as is the case for the classical shakedown theorem. The implication of this assumption is

that no knowledge of the cyclic material behaviour is required.

The total volume V of the body described in Section 2 may be divided into two subvolumes; V_s where the thermal stress history $\hat{\sigma}^{\Theta}_{ij}(x,t)$ can be contained within the limits of the yield surface by a rigid body translation in stress space and V_F where $\hat{\sigma}^{\Theta}_{ij}(x,t)$ exceeds those limits and hence causes reverse plasticity.

In order to formulate the new theorem, a particular form of The residual stress field will now be chosen, so that

$$\bar{\rho}_{ij} = \rho^1_{ij} + \rho^2_{ij} + \rho^3_{ij} \qquad 2.33$$

where ρ^1_{ij} denotes part of the residual stress which cancels $\hat{\sigma}^p_{ij}$ in V_F, ρ^2_{ij} is a residual stress field which enforces condition (b) of the material shakedown in V_F and ρ^3_{ij} is an arbitrary stress field in V_s that ensures that the equilibrium equations are satisfied if V_F were removed.

The total stress history (2.32) now becomes

$$\sigma^*_{ij}(t) = (\lambda\hat{\sigma}^p_{ij} + \rho^1_{ij}) + (\hat{\sigma}^{\theta}_{ij}(t) + \rho^2_{ij}) + \rho^3_{ij} \qquad 2.34$$

To satisfy assumption (b) of the material shakedown in V_F two conditions have to be imposed

- the stress distribution

$$\sigma_{ij}^{p} = \hat{\sigma}_{ij}^{p} + \rho_{ij}^{1} \qquad 2.35$$

must be either zero or a purely hydrostatic state of stress within V_F with the former requirement being sufficient for plane stress states. This condition then implies $\sigma_{ij}^{*} = \hat{\sigma}_{ij}^{\Theta} + \rho_{ij}^{2}$ in V_F, since ρ_{ij}^{3} is defined only in V_s.

- considering that the stress histories generally vary between a maximum extreme $\hat{\sigma}_{ij}^{\Theta max}(t_1)$ and minimum $\hat{\sigma}_{ij}^{\Theta min}(t_2)$ along a linear path in stress space, the residual stress ρ_{ij}^{2} may be identified in V_F as

$$\rho_{ij}^{2} = \frac{1}{2}\left[\hat{\sigma}_{ij}^{\theta max}(t_1) + \hat{\sigma}_{ij}^{\theta min}(t_2) \right] \qquad 2.36$$

so that

$$\sigma_{ij}^{*max} = \frac{1}{2}\left[\hat{\sigma}_{ij}^{\theta max}(t_1) - \sigma_{ij}^{\theta min}(t_2) \right] = - \sigma_{ij}^{*min} \quad \text{in } V_F \qquad 2.37$$

It is important to note that ρ_{ij}^{2} given by assumption (b) in V_F must also be defined in V_s.

The analysis now reduces to a shakedown problem within V_s which can be formulated by the following theorem:

The structure will shake down if an arbitrary stress field such as (2.35) exists so that

(1) Within V_F $\sigma^p_{ij} = 0$ which implies that condition (b) of the material assumption can be satified by a residual stress field of the type shown in (2.36)

(2) $\phi(\sigma^*_{ij}) < \sigma_y$ within V_s for a σ^*_{ij} is given by

$$\sigma^*_{ij}(t) = \lambda\sigma^p_{ij} + \bar{\sigma}^\theta_{ij} + \rho^3_{ij} \qquad 2.38$$

where $\lambda\sigma^p_{ij}$ is in equilibrium with the applied load in V_s, $\bar{\sigma}^\theta_{ij} = \hat{\sigma}^\theta_{ij} + \rho^2_{ij}$ and ρ^3_{ij} is an arbitrary residual stress in Vs. The following inequality now holds:

2.39

$$\lambda \int p_i dU^c_i dS < \int_0^T dt \int_{V_S} \left[\sigma^c_{ij} - \hat{\sigma}^\theta_{ij}(t)\right]\dot{\varepsilon}^c_{ij} dV - \int_0^T dt \int_{V_F} \frac{1}{2}\left[\hat{\sigma}^{\theta max}_{ij}(t_1) + \hat{\sigma}^{\theta min}_{ij}(t_2)\right]\dot{\varepsilon}_{ij} dV$$

This theorem may be proved by applying the upper bound to V_s to give

$$\lambda \int_S p_i dU^c_i dS \leq \int dt \int_{V_S} (\sigma^c_{ij} - \bar{\sigma}^\theta_{ij})\dot{\varepsilon}_{ij} dV + \int_V \rho^3_{ij} d\varepsilon^c_{ij} dV \qquad 2.40$$

where $d\varepsilon^c_{ij} = \int \dot{\varepsilon}_{ij}\, dt$. The integral involving ρ^3_{ij} sums to zero since the residual stress field is in equilibrium with zero applied loads in V_s. Considering that the thermal stress field on the right hand side of Equation (2.40) is $\bar{\sigma}_{ij} = \hat{\sigma}^\theta_{ij} + \rho^2_{ij}$ then

$$\int_o^T dt \int_{V_S} \overline{\sigma}^{\theta}_{ij} \varepsilon^c_{ij} dV = \int_o^T dt \int_{V_S} \hat{\sigma}^{\theta}_{ij} \dot{\varepsilon}^c_{ij} dV + \int_o^T dt \int_{V_S} \rho^2_{ij} \dot{\varepsilon}^c_{ij} dV \qquad 2.41$$

where the second term on the right hand side is given by

$$\int_o^T dt \int_{V_S} \rho^2_{ij} \dot{\varepsilon}^c_{ij} dV = \int_o^T dt \int_V \rho_{ij} \dot{\varepsilon}^c_{ij} dV - \int_o^T dt \int_{V_F} \rho^2_{ij} \dot{\varepsilon}^c_{ij} dV \qquad 2.42$$

As the residual stress ρ^2_{ij} is in equilibrium with zero load in the total volume V, the first integral on the right hand side of (2.42) is also zero. Hence the upper bound, Equation (2.40) becomes (2.39), which is determinate for prescribed $\dot{\varepsilon}^c_{ij}(t)$. It can be noted that the term involving the elastic thermal cyclic stress history $\hat{\sigma}^{\Theta}_{ij}$ in V_s is the only term which depends upon an arbitrary time during the cycle. Once the strain rate $\dot{\varepsilon}^c_{ij}$ is prescribed, Equation (2.39) may be used to search for the minimum value of corresponding to a particular time "to" during the cycle. This condition can be better described in geometric terms, which is shown schematically in Figs. 2.6,2.7. The instant "to" corresponds to the stress point on the yield surface, where the cyclic stress history $\hat{\sigma}^{\Theta}_{ij}(t)$ touches when translated in the stress space as a rigid body by the action of the constant mechanical stresses σ^p_{ij}, if such a translation is admissible.

This translation can also result in the cyclic stress history touching the yield surface at two points during the cycle as shown in Fig. 2.7. In that case two plastic flows $d\varepsilon^1_{ij}$ and $d\varepsilon^2_{ij}$ are activated at different times, corresponding to the two extremes of the cycle t_1 and t_2. Thus, the total plastic strain during the cycle can be written as

$$d\varepsilon^c_{ij} = d\varepsilon^1_{ij} + d\varepsilon^2_{ij} \qquad 2.43$$

Hence, the first term on the right hand side of Equation (2.39) becomes

$$\int_0^T dt \int_V \left[\sigma^c_{ij} - \hat{\sigma}^\theta_{ij}(t)\right]\dot{\varepsilon}_{ij} dV =$$

$$\int_{V_S} \left[\sigma^c_{ij} - \hat{\sigma}^\theta_{ij}(t_1)\right] d\varepsilon^1_{ij} dV + \int_{V_S} \left[\sigma^c_{ij} - \hat{\sigma}^\theta_{ij}(t_2)\right] d\varepsilon^2_{ij} dV \qquad 2.44$$

The applicability of the extended upper bound theorem (Equation (2.39)) to thermal cyclic problems is limited to some class of structures for which design in the reversed plasticity regions is possible. They can be identified as those structures capable of bearing certain loading conditions, within some restricted volume V_F, in excess of the classical shakedown limits without excessively or/and incrementally deforming. In such a category of structures, the thermal loading may suffer large variations and there would still exist some region in the structure capable of transmitting the mechanical load through the structure. The first step to assess the applicablity of (2.39) is to identify volumes V_F and V_s. The condition whether the region V_s is capable of transmitting the loads λpi has then

to be examined. In other words, Equation (2.39) can only be applied if a volume Vs exists, which does not contain a mechanism of deformation, in which case a boundary separating the regions of reversed plasticity F and ratchetting R may be determined.

2.4.5 Formulation of the Upper Bound Theorem for Beams and Frames

This formulation is based on the assumption that bending moments are the only agencies producing deformation. Because of its easy availability in the literature [99, 101, 101], only a brief summary will be presented here, with emphasis on the problem experimentally analysed in Chapter 5. Some information on material behaviour is also given in Chapter 5.

Let the loads consist of cyclic thermal loading in the presence of a steady mechanical load which will both generate bending moments. The bending moment in a generic section i, due to the cyclic thermal load alone, will vary between a maximum value $\hat{M}_i^{\Theta max}(t_1)$ and a minimum value $\hat{M}_i^{\Theta min}(t_2)$. During the early cycles of loading, plastic transient deformation introduces residual bending moments m_i to the structure. Shakedown will occur when the following inequalities are satisfied for any generic section i:

$$\lambda_s(\hat{M}_i^P + \hat{M}_i^{\theta max}(t_1)) + m_i \leq M_p^i \qquad 2.45$$

$$\lambda_s(\hat{M}_i^P + \hat{M}_i^{\theta_{min}}(t_2)) + m_i \geq -M_p^i \qquad 2.46$$

where λ_s is the shakedown load factor, $\hat{M}_i^P$ is the bending moment (assumed positive) due to the mechanical load and M_p^i is the plastic moment defined in Chapter 5. For an upper bound formulation a mechanism of incremental collapse is assumed with hinge rotations Θ_i's occuring in positions where the bending moment equals the plastic moment. Whatever the sign convention, any plastic moment M_i^P and the corresponding hinge rotation Θ_i will have an identical sign, ie, corresponding to a positive M_p^i there is a positive Θi and vice-versa. For any section where a hinge is formed, inequalities (2.45, 2.46) are replaced by equalities:

$$\lambda_s(\hat{M}_i^P + \hat{M}_i^{\theta_{max}}) + m_i = M_p^i$$

$$\lambda_s(\hat{M}_i^P + \hat{M}_i^{\theta_{min}}) + m_i = -M_p^i \qquad 2.47$$

If the hinge rotation Θ_i of the assumed mechanism is introduced to Equations (2.47) gives

$$\lambda_s \begin{Bmatrix} \hat{M}_i^P + \hat{M}_i^{\theta_{max}} \\ \hat{M}_i^P + \hat{M}_i^{\theta_{min}} \end{Bmatrix} \theta_i + m_i\theta_i = |M_p^i\theta_i| \qquad 2.48$$

where the right hand side of Equation (2.48) is always positive. When all the hinges of the assumed mechanism is considered and the Equations summed gives

$$\lambda_s \sum \begin{Bmatrix} \hat{M}_i^P + \hat{M}_i^{\theta_{max}} \\ \hat{M}_i^P + \hat{M}_i^{\theta_{min}} \end{Bmatrix} \theta_i = \sum |M_p^i \theta_i| \qquad 2.49$$

since the residual moments are in equilibrium with zero load and

$$\sum m_i \theta_i = 0 \qquad 2.50$$

Equation (2.49) can either yield upper bounds of the shakedown load or its actual value if the true mechanism of incremental collapse is known.

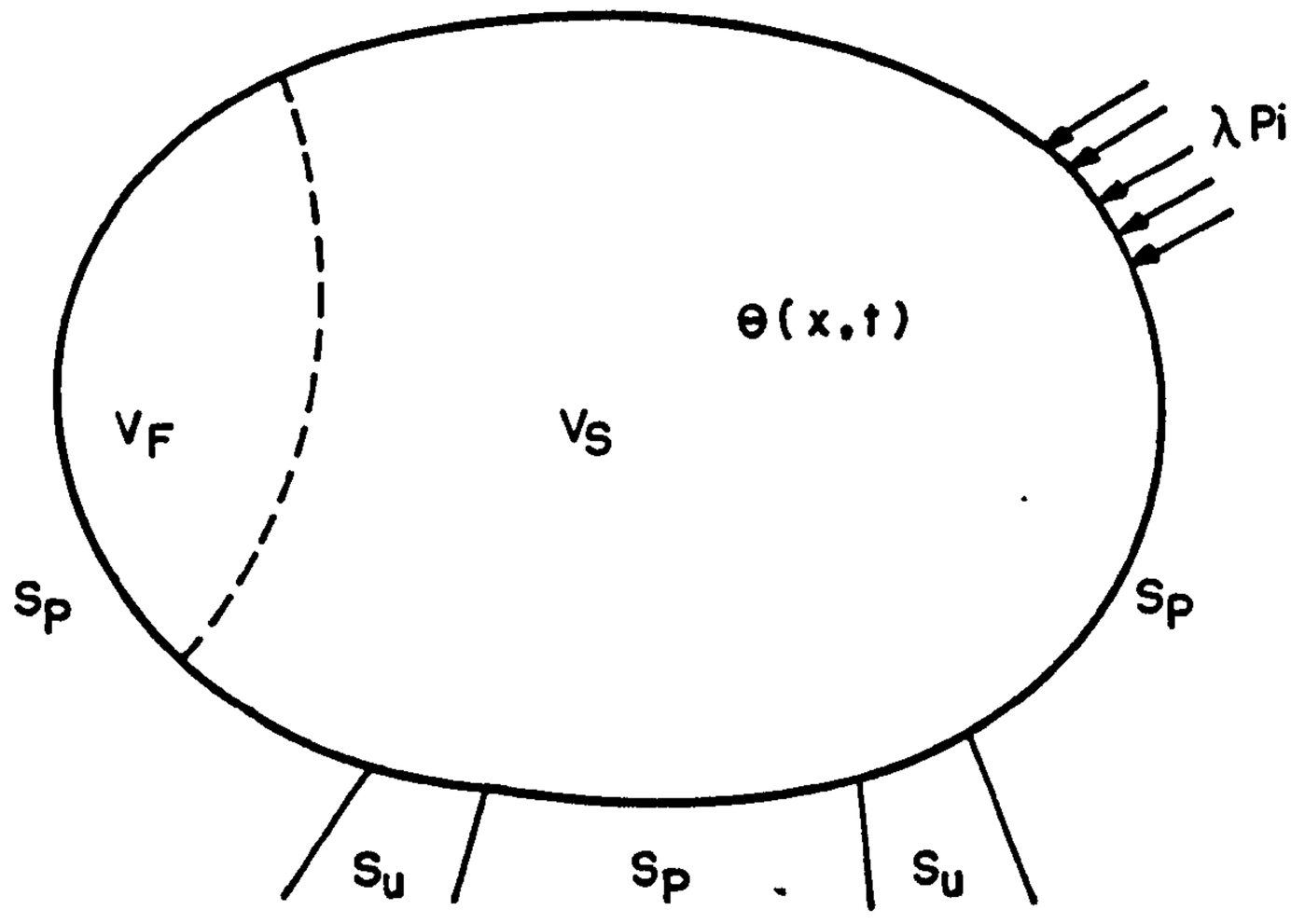

Fig. 2.1- TWO-DIMENSIONAL BODY

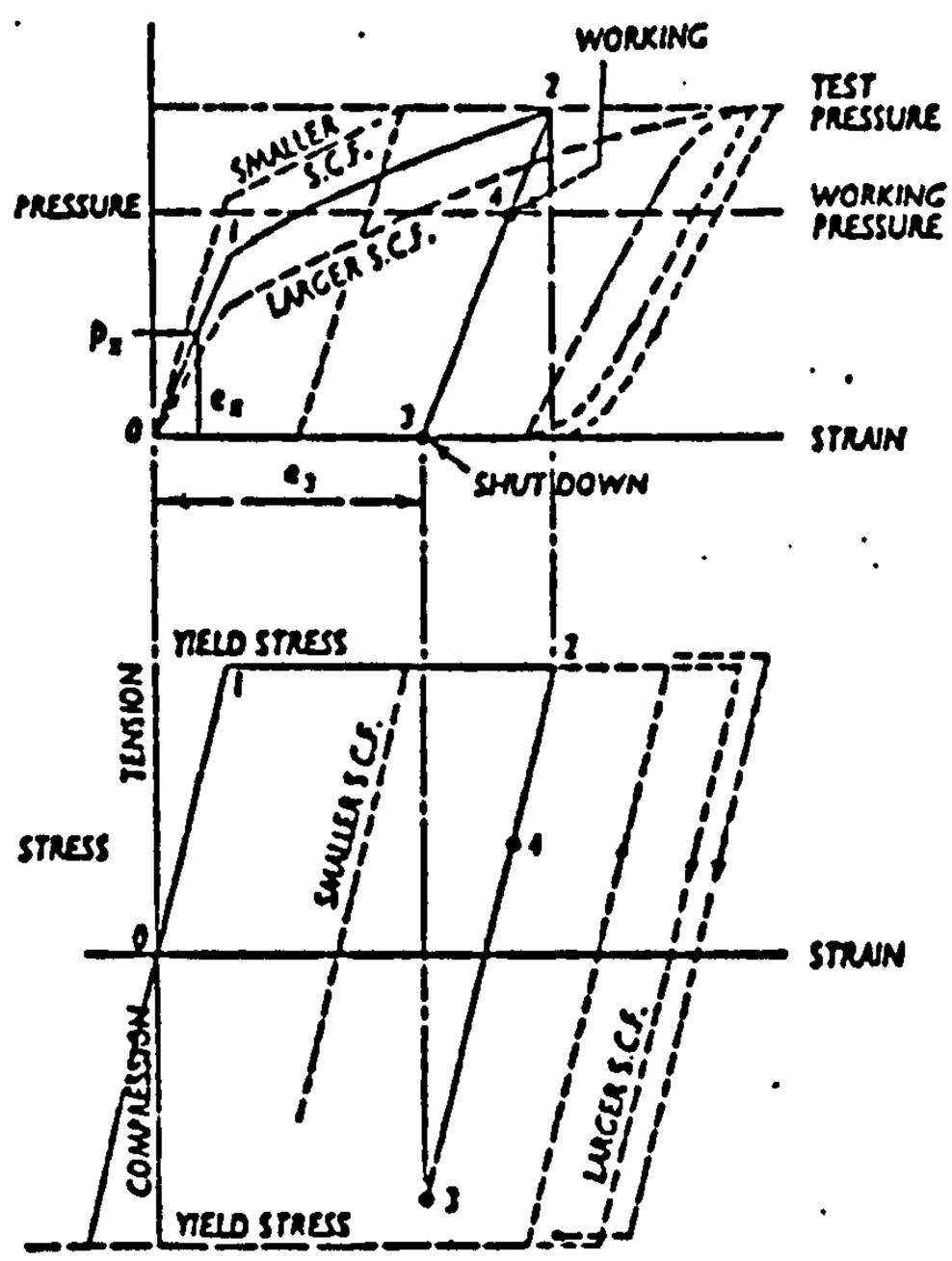

Fig. 2.2a,b -Pressure-strain and stress-strain curves

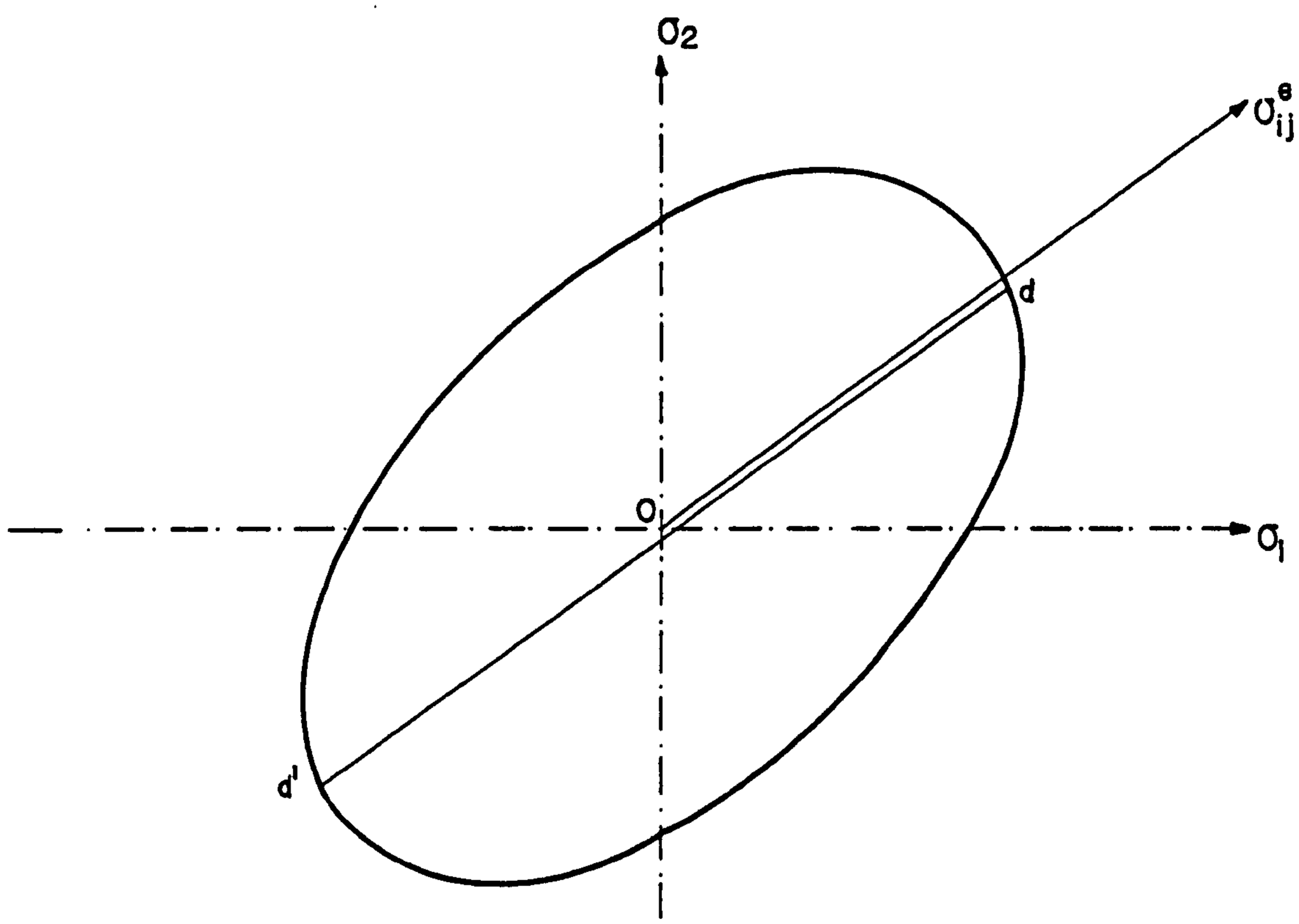

Fig. 2.3 - SHAKEDOWN OF PRESSURE VESSELS (PERFECT PLASTICITY) [14]

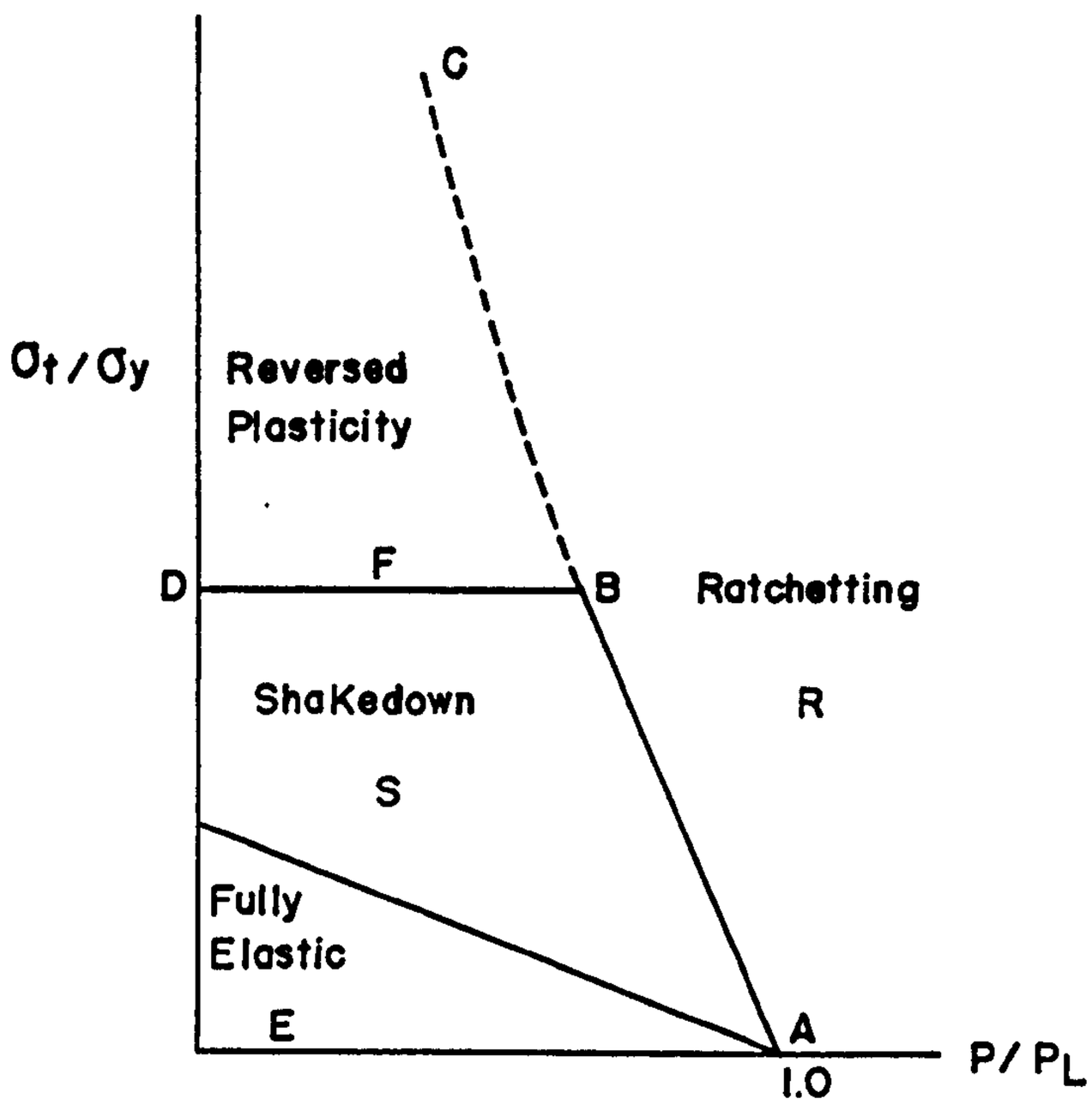

σt: MAXIMUM THERMO-ELASTIC EFFECTIVE STRESS

P_L: PLASTIC LIMIT LOAD PARAMETER

Fig. 2.4 - BREE TYPE DIAGRAM

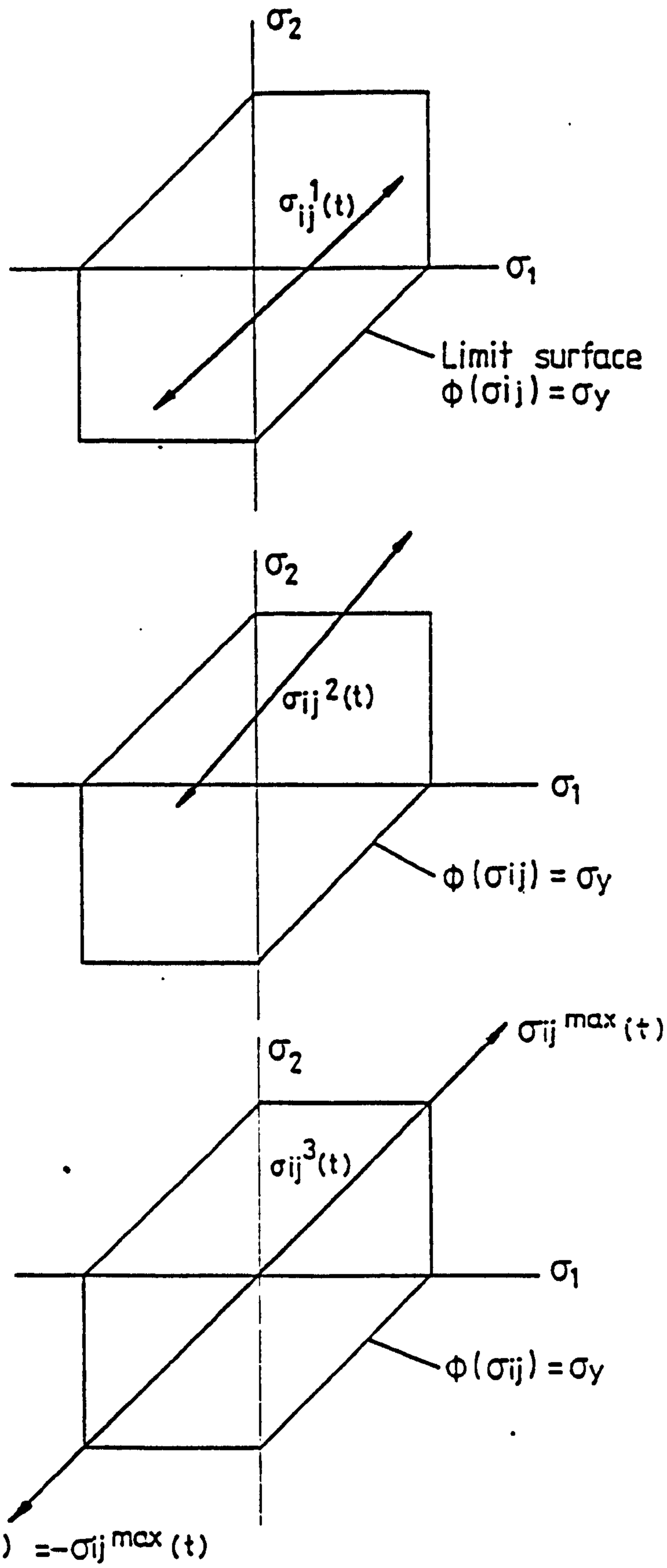

σ_{ij}^{1} No incremental growth
σ_{ij}^{2} Possible incremental growth
σ_{ij}^{3} No incremental growth (Reversed plasticity condition)

Fig. 2.5 Schematic representation of material shakedown conditions [60]

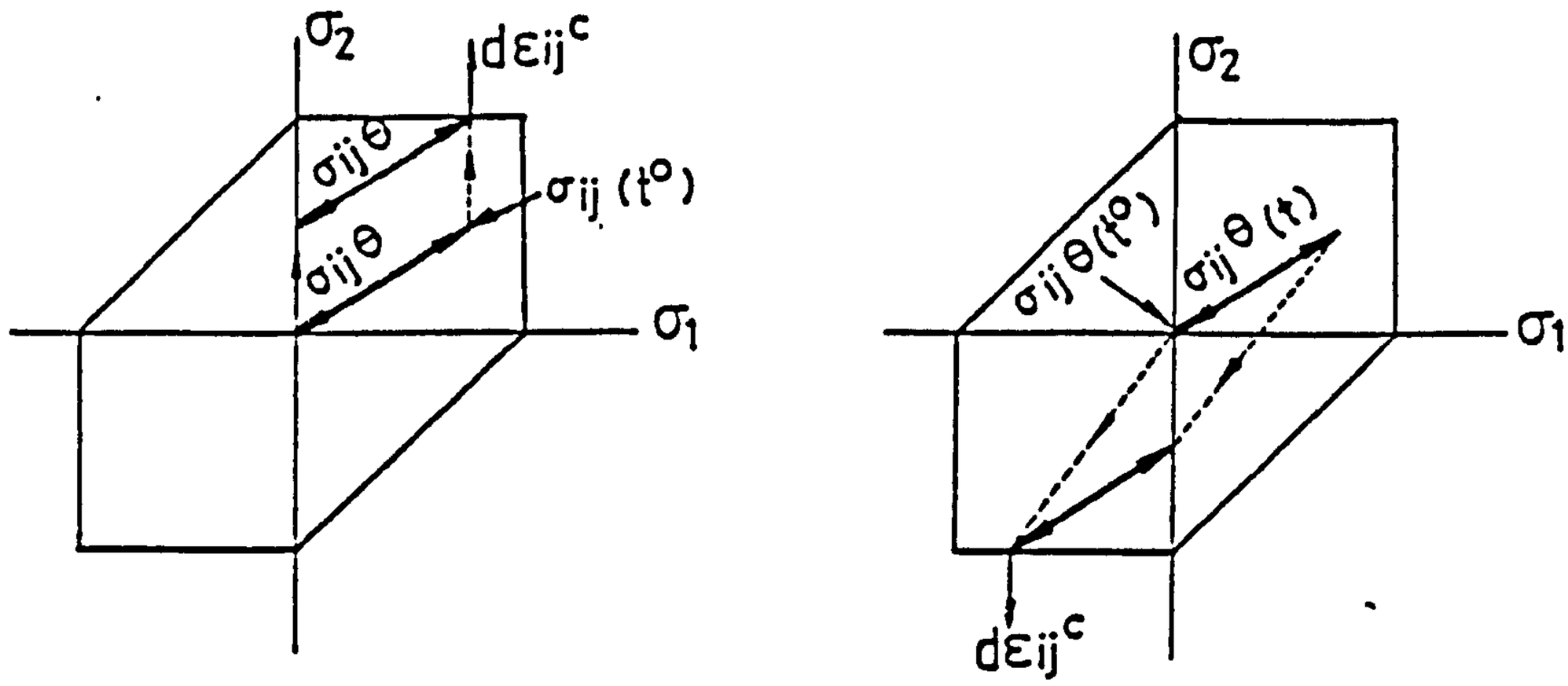

Fig. 2·6 The definition of t^o : for a prescribed $d\varepsilon_{ij}^c$, σ_{ij}^θ (t^o) contacts the limit surface at the stress point associated with $d\varepsilon_{ij}^c$ when the stress trajectory $\sigma_{ij}^\theta(t)$ is given a rigid body translation in stress space [60]

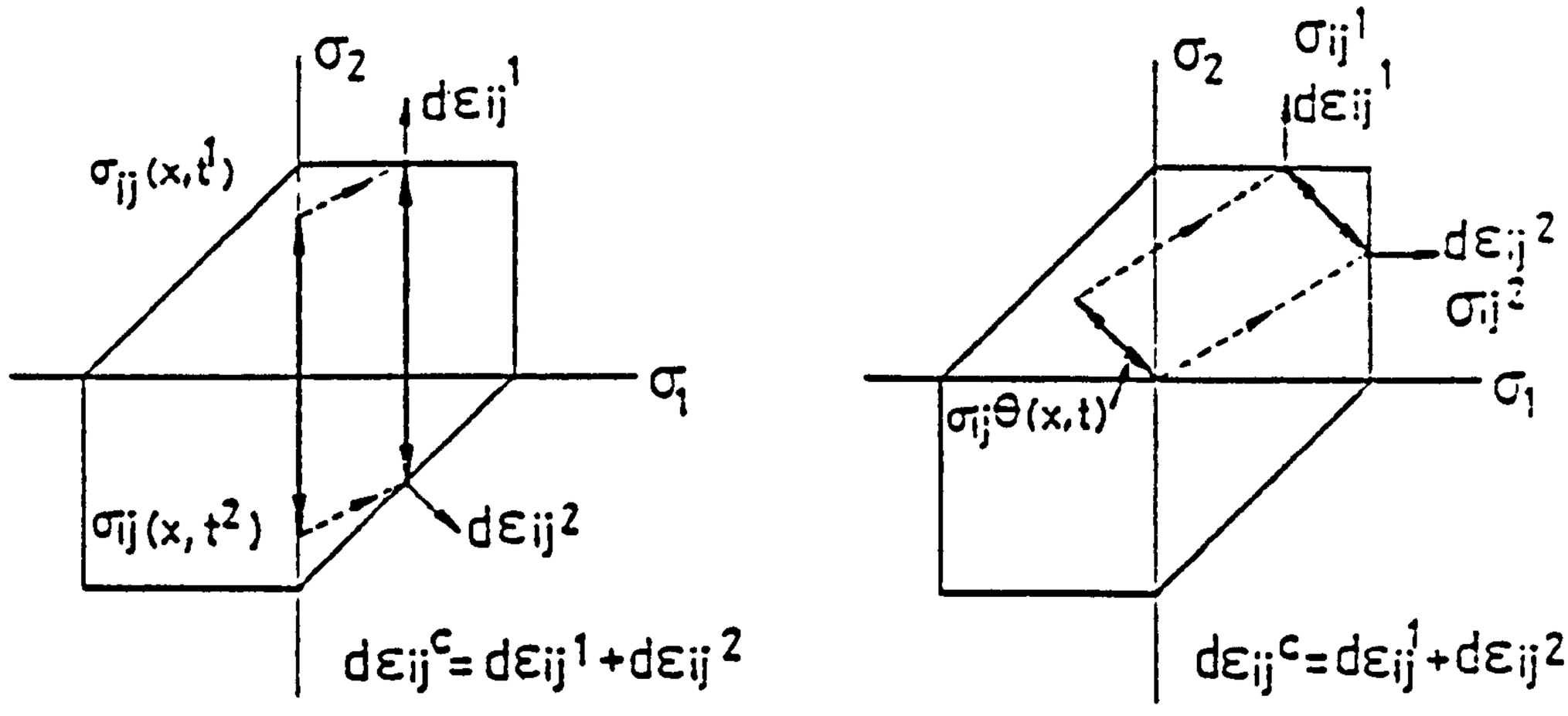

Fig. 2.7 The particular class of stress histories the times t_1 and t_2 can be defined so that plastic strainsoccur at the two extremes $t = t_1$ and $t = t_2$ [60]

CHAPTER 3

SHAKEDOWN AND RATCHETTING ABOVE THE LIMIT OF REVERSED PLASTICITY; NUMERICAL APPLICATION FOR THE CASE OF CYCLIC MECHANICAL LOADS

The purpose of the present numerical analysis is to study the dependence of the shakedown behaviour on the stress concentration factor and on the type of structure for mechanical loading problems.

Two types of structures are considered in the calculations, and the behaviour of such structures above the limit of reversed plasticity for two different types of material is explored. The two types of structures and material considered are: two-bar structures subjected to variable axial loads, and cylindrical vessels with variable thickness and under cyclic internal pressure. The materials considered are the elastic/perfectly plastic and the isotropic hardening materials.

3.1 The Two-Bars Structure

3.1.1 Notation

l	length of bar 1
n	ratio of the lengths of the bars

k ratio of the cross areas of the bars

P_L limit load P_s shakedown load

σ_y yield stress of material

σ_1^* stress in bar 1 after first cycle

σ_2 stress in bar 2

ρ_1, ρ_2 residual stresses

$\sigma_2^* = \sigma_2 + \rho_2$

$\bar{p}$ additional load after cyclic hardening

3.1.2 Introduction

The lower bound theorem was used to study the two-bar structure (Fig. 3.1) assuming first the bars made of elastic/perfectly plastic material.

The load history is shown in Fig.(3.2) and the elastic stresses can be calculated by equations

$$\sigma_1^* = \frac{\eta P}{(\eta + k)A} \qquad 3.1$$

$$\sigma_2 = \frac{P}{(\eta + k)A} \qquad 3.2$$

The load that will make the structure collapse is given by:

$$P_L = (1 + k)A\sigma_y \qquad 3.3$$

3.1.3 Behaviour of two-bars structure

The stress-strain diagrams for a load which makes bar 1 yield, but not bar 2, can be seen in Fig.(3.3a,b). In the first cycle the stress difference $\Delta\sigma_1$ (Fig.(3.3a) which should be supported by bar 1, is transferred to bar 2. At the end of the first cycle $\Delta\sigma_1$ and $\Delta\sigma_1/k$ will appear as residual stresses and will keep the relation $\rho_1=-k\rho_2$. If the same load is maintained, the structure will behave elastically.

Increasing the load may cause one of two conditions: the first condition is when the limit load is reached first. This is always the case for the ratio of the lengths of the bars within the range $\eta\leq 2k/(k-1)$. The stress-strain diagrams are represented by Fig.(3.4 a,b) and it can be said that the shakedown load is equal to the limit load.

The second condition (Fig.3.5 a,b), for $\eta>2k/(k-1)$, implies a reduction of the shakedown load with the increase of η. This reduction is due to the dependence of the shakedown load on the stress concentration in bar 1, which increases with η. The shakedown load for such cases is given by

$$P_s = \frac{2(\eta+k)P_L}{\eta(1+k)} < P_L \qquad 3.4$$

If an η equal to infinity is considered, the shakedown load becomes

$$P_s = \frac{2P_L}{(1+k)} \qquad 3.5$$

which tends to zero as k tends to infinity. The elastic stresses in the two bars for $\eta=\infty$ and $k\neq\infty$ are

$$\sigma_1^* = \frac{P_s}{A} \quad , \quad \sigma_2 = 0 \qquad 3.6$$

Bar 2 will, therefore, only receive the load transferred from bar 1 to maintain the equilibrium of the residual stresses. From the relationships $\rho_2=-\rho_1/k$ and $\rho_1=-\sigma_y$ we can see that the stress in bar 2 can be very low, depending upon the value of k. This conclusion encourages the increasing of the load over the limit of reversed plasticity, since the possibility of ratcheting is eliminated by the elastic behaviour of bar 2. The possibility of failure by fatigue must then be investigated. The stress-strain diagrams for loads greater than P_s is shown in Fig. 3.6. Fig. 3.7 represents the limit condition when $P_s=P_L$.

If the possibility of cyclic hardening is considered, for $P_s=P_L$ and $\eta>2k/(k-1)$, bar 1 will increase its capacity of receiving load and will transfer less load to bar 2 each cycle. Fig. 3.8 represents the process, which stabilizes after a few cycles with no transference of load in the end.

Then, as the stress in bar 2 is less than σ_y, the structure can now support an additional load P before failure. The non-dimensinal additional load can be calculated by

$$\frac{\bar{P}}{P_L} = \frac{[\eta(k-1) - 2k]}{2k\ (1+k)} \qquad 3.7$$

Plotting the non-dimensional load P/P_L against η, for particular values of k, Fig. 3.9 is obtained. Region E represents completely elastic behaviour of the structure. Elastic shakedown will happen in S region while plastic shakedown will occur within the PS region in the absence of ratchetting. The region of plastic shakedown with hardening is also represented and shows loads greater than P_L.

3.1.4 Conclusions

From this theoretical analysis it can be concluded that depending on the capacity of the material to withstand cyclic load without failing by fatigue, the structure can work subject to operating conditions above the shakedown limit. The elimination of ratchetting will be assured by the elastic behaviour of bar 2 which prevents great displacements up to the structure rupture.

3.2 Cylindrical Pressure Vessel with Varible Thickness

3.2.1 Notation

R	radius of cylinder
T_1	thickness of thicker cylinder
T	thickness of thinner cylinder
t	thickness of the elastic part
k	t/T
α	T_1/T

β	R/T
Δ_p	variable pressure
p	primary constant load
p_L	limit pressure
H,M	edge force and bending moment per unit of circumference
$N_x, N\phi$	axial and hoop forces
σ_x, σ_ϕ	axial and hoop stresses
σ_1, σ_2	extreme axial stresses

3.2.2 Introduction

Present day design rules for pressure vessels under cyclic load have as a limiting condition the lower bound shakedown estimates which are quite safe but do not give much information about the general behaviour of the structure. For this reason, in the study of cylindrical pressure vessels with variable thicknesses, which follows, the upper bound theorem was used instead. The other important point that justifies the determination of the upper bound is the great possibility of guessing the actual mechanism of deformation in pressure vessels, which gives the exact bound.

When a cylindrical pressure vessel has a variation in its thickness (Fig. 3.10a) the junction constitutes a point of weakness because of the local stress concentration that takes place. Depending upon the geometry of the vessel, it can fail either as a membrane or due to the stress

concentration at the junction. If the vessel is considered to be composed of two cylinders with different thicknesses it can be assumed that the maximum stresses occur in the thinner one. The load history is shown in Fig. 3.10b and in order to obtain general results, the elastic stresses will be calculated as a function of the two nondimensinal geometric parameters:

$$\alpha = \frac{T_1}{T}$$

$$\beta = \frac{R}{T}$$

where T_1, T, and R are defined (Fig. 3.10a).

3.2.3 Elastic Solutions

3.2.3.1 Edges Forces Calculations (H,M)

Elastic Solutions were obtained by ensuring compatibility of displacements between the two cylinders. This analysis was made using the theory of thin shells, superimposing on to the membrane solution the effect of edge forces H and M(Fig. 3.11). Equations 3.8 and 3.9 give the values of H and M in terms of the nondimensional parameters:

ν = Poisson's ratio

$$f_1 = \frac{(\alpha^3+\sqrt{\alpha})(\alpha-1)}{[2\alpha\sqrt{\alpha}(\alpha+1) + (\alpha^4+1) + 2\alpha^2]}$$

$$f_2 = \frac{(\alpha^3-\alpha)(\alpha-1)}{[2\alpha\sqrt{\alpha}(\alpha+1) + (\alpha^4+1) + 2\alpha^2]}$$

$$H = \sqrt{\beta} \quad \sqrt{3(1-\nu^2)}\, T\, f_1(\alpha) p \qquad 3.8$$

$$M = \beta\, T^2\, f_2(\alpha) p/2 \qquad 3.9$$

3.2.3.2 Global Collapse

Considering the Tresca yield condition, the collapse will occur if the geometry of the vessel is such that the hoop stress reaches yield before the axial stress, as indicated in Fig. 3.12. Details of the calculations for this mode of deformation are given in Appendix A and the equation which defines the bound for such a collapse to occur is given by

$$\frac{\Delta p}{P_L} + 2\,\frac{\bar{p}}{P_L} = 1 \qquad 3.10$$

3.2.4 The Upper Bound Theorem

3.2.4.1 The Mechanism of Deformation

The assumed axial mechanism of deformation is shown in Fig.(3.13). Equation (3.11) represents the upper bound theorem. The left hand side term(I) expresses the internal dissipation of energy at plastic rupture. The first term on the right side(II) expresses the work done by the primary constant load p and the last term(III) of Equation (3.11) represents the work corresponding to the maximum positive stresses due to varying loads.

$$\underset{\substack{\uparrow \\ \text{stress at yield} \\ \text{I}}}{\int_V \sigma_{ij}^c \, d\varepsilon_{ij}^c dV} \geq \underset{\substack{\uparrow \\ \text{constant load} \\ \text{II}}}{\int_S \bar{p} \, d u_i^c dS} + \underset{\substack{\uparrow \\ \text{variable load} \\ \text{III}}}{\int_V \sigma_{ij}^{\Delta p}(z,t_o) \, d\varepsilon_{ij}^c dV} \qquad 3.11$$

The limit load is assumed to be the load which makes the axial membrane stress reach yield and can be calculated by

$$P_L = \frac{2T\sigma_y}{R} = \frac{2\sigma_y}{\beta} \qquad 3.12$$

The calculations of the upper bound using Equation (3.11) and the collapse mechanism shown in Fig. 3.13 are given in Appendix A.

3.2.5 Limit Design Boundary

3.2.5.1 Ratchetting Bound

Equation 3.13 is obtained in Appendix A in terms of non-dimensional groups

$$1 = \frac{\bar{p}}{P_L} + \frac{(36f_2^2(\alpha) + 1)}{24f_2(\alpha)} \times \frac{\Delta p}{P_L} \qquad 3.13$$

where p and Δ_p are, respectively, the primary constant pressure and variable pressure, p_L is the limit load, and f_2 is a function of the geometric parameter $\alpha(=T_1/T)$ previously defined. Equation (3.13) defines a line which is the ratchetting bound for variable loads smaller than the shakedown limit. This line corresponds to the beginning of

axial incremental growth.

3.2.5.2 Reverse Plasticity Bound

If a Tresca yield condition is considered (Fig. 3.14) the axial shakedown limit is calculated by superimposing on to the membrane stress the stress due to the edge moment M (Equation 3.14).

$$\sigma_x(\Delta p/2) = \frac{\Delta p}{4T} + \frac{6M(\Delta p/2)}{T^2} = \sigma_y \qquad 3.14$$

which gives

$$\frac{\Delta p}{P_L} = \frac{2}{[1 + 6 f_2(\alpha)]} \qquad 3.15$$

The boundary constituted by the two bounds AB and BC in Fig. 3.15 is the one used in the design of pressure vessels. To complete the ratchetting bound above the reverse plasticity limit ($\Delta\sigma > 2\sigma_y$) it is necessary to assume two different regions in the vessel thickness as proposed by Ponter and Karadeniz [36,37]: V_{F1} and V_S (Fig. 3.16). V_{F1} is the region where reversed plasticity occurs and can take no primary load (p). Therefore the upper bound is applied to V_S only, where the stresses remain within the yield surface.

3.2.6 Work Hardening Material

The first material to be analysed was the isotropic hardening material, which theoretically maintains the linearity of the stress distribution,reaching stresses greater than the yield stress in the plastic region V_{F1} (Fig.3.16).

3.2.6.1 Ratchetting Bound Above Reverse Plasticity

Again all the calculations are presented in Appendix A which give rise to Equation 3.16 when the extended upper bound theorem is applied to the volume V_s alone.

$$\frac{\bar{p}}{p_L} = \frac{1}{12f_2(\alpha)}\left[\frac{1}{\Delta p/p_L} - \left(\frac{1}{4} - 3f_2(\alpha) + 9f_2^2(\alpha)\right)\frac{\Delta p}{p_L} - (1 - 6f_2(\alpha))\right] \quad 3.16$$

Equation 3.16 is used in range $\sigma_2<\sigma_y$. When $\sigma_2>\sigma_y$ another region (V_{F2}) of plastic stresses appears as indicated in Fig. 3.17.

The same procedure is used to obtain the final part of the limit curve for ratchetting in a work hardening material (Equation 3.17).

$$\frac{\bar{p}}{p_L} = \frac{1}{6f_2(\alpha)}\cdot\frac{1}{\Delta p/p_L} \quad 3.17$$

Depending on the geometry of the vessel, the membrane stress A ($=\Delta pR/4T$) can be greater than the stress due to edge moment $BT/2(=6M/T^2)$. In other words A > BT/2. The stress

distribution for this case is shown in Fig. 3.18. It can be seen that only the positive part of the load cycle is considered ($\Delta_p>0$).

The extended upper bound theorem is again applied to obtain Equation 3.18.

$$\frac{\bar{p}}{p_L} = \frac{1}{12f_2(\alpha)}\left[\frac{1}{\Delta p/p_L} - \left(3f_2(\alpha) - 9f_2^2(\alpha) - \frac{1}{4}\right)\frac{\Delta p}{p_L} - (1-6f_2(\alpha))\right] \qquad 3.18$$

3.2.7 Elastic/Perfectly Plastic Material

When the same vessel which has previously been considered is composed of elastic/perfectly plastic material, a different equilibrium must be satisfied. The stress diagram through the thickness for this particular material can be divided in two different parts (Figs. A 6a,b) as shown in Appendix A. For the region where the stresses remain within the yield surface, the stress diagram is linear and a function of z (Equation 3.19). For the plastic region the stress is constant and equal to σ_y (Equation 3.20).

$$\sigma_x^1 = A + Bz \qquad 3.19$$

$$\sigma_x^2 = \sigma_y \qquad 3.20$$

3.2.7.1 Ratchetting Bound Above Reverse Plasticity

The application of the upper bound theorem to V_S in Figs (3.19a,b,c) is given with some detail in Appendix A.

The Equation representing the first part of the bound separating the region of reversed plasticity from the ratchetting region, obtained in Appendix A is

$$\frac{\bar{p}}{p_L} = \frac{k^3}{12\left[f_2 \frac{\Delta p}{p_L} - (1-k)\right]}\left[3 - \frac{1}{k^2}\left[\frac{9}{k^2} f_2^2 - \frac{3}{k} f_2 + \frac{1}{4}\right]\left(\frac{\Delta p}{p_L}\right)^2 + \right.$$

$$+ \frac{1}{k}\left[\frac{18(1-k)}{k^3} f_2 - \frac{3(1-k)}{k^2}(1 + 2f_2) + \frac{(1-k)}{k} - 2\right]\frac{\Delta p}{p_L} - \quad 3.21$$

$$\left. - \frac{(1-k)}{k}\left[\frac{9(1-k)}{k^3} - \frac{6(1-k)}{k^2} + \frac{(1-k)}{k} - 4\right]\right] .$$

Figs. 3.20a,b represent the new stress distribution within the thickness where a new plastic zone (V_{F2}) is forming. The calculations of the new stress distribution is given in Appendix A and the equation for the second part of the ratchetting/reversed plasticity bound is found to be

$$\frac{\bar{p}}{p_L} = \frac{k^3}{\left(6f_2(\alpha) - \frac{3}{4}\frac{\Delta p}{p_L}\right)\frac{\Delta p}{p_L} - 3(1-k^2)} \qquad 3.22$$

for $f_2(\alpha) > 0.5$. The problems when $f_2(\alpha) < 0.5$ are also discussed in Appendix A.

3.2.8 Numerical Examples

For a vessel of small α (=2), it can be seen from Fig. 3.21 that the global collapse will be the most important factor. Before reaching ratchetting or reverse plasticity, the vessel will collapse as a membrane.

If α=8 is adopted, analysis of the results can be done for two different materials: the work hardening and the elastic/ perfectly plastic materials.

The results in the case of a work hardening material are presented by different regions of the diagram shown in Fig. 3.22. The vessel behaviour will be purely elastic for loads within region E. The response of the structure will still be elastic for working conditions in region ES after initial yield during the first cycle. In region PS some parts of the vessel suffer reverse plasticity. Finally the structure will fail as a membrane if the loads go to the area GC. It is interesting to notice that for an isotropic hardening material these theoretical results indicate that global collapse occurs always before ratchetting.

If the material of the vessel is assumed to be elastic/perfectly plastic however, the theoretical results change considerably as shown in Fig. 3.23. Perhaps the actual curve representing the ratchetting limit condition, for loads above the alternating plasticity is neither one of these but any other that lies between.

The limit case, for equal to infinity, is shown in Fig. 3.24. The important conclusion in this case, and in those cases where the stress concentration is high, is the fact that depending on the load the global collapse will not be reached first. These results can, perhaps, provide encouragement to experimental work, mainly with the zone of plastic shakedown (PS) in mind. It can be seen in Fig. 3.24 that theoretically, for elastic/perfectly plastic material, ratchetting can occur before the vessel collapses as a membrane.

3.2.9 Conclusions

The theoretical analysis presented has shown that for cylindrical vessels with variable thicknesses the upper bound theorem gives a general picture of the vessel behaviour. From the results obtained it is possible to conclude that it would be an interesting experimental test if these vessels were submitted to working conditions in the region of plastic shakedown. The possibility of ratchetting, but not of reversed plasticity, would then be eliminated and the problem is likely to be one of low cycle fatigue analysis instead.

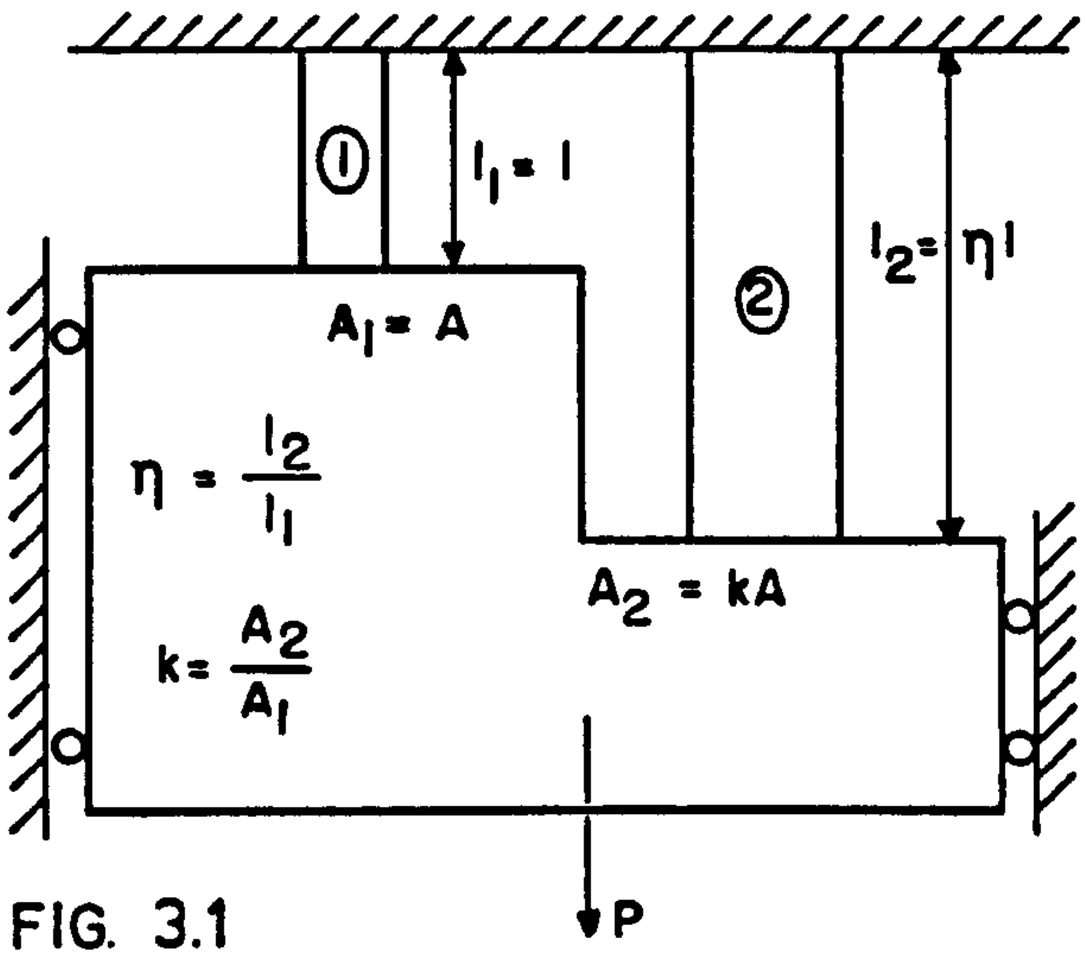

FIG. 3.1

THE GEOMETRY OF TWO-BARS STRUCTURE

ELASTIC SOLUTION

$$\sigma_1^* = \frac{\eta P}{(\eta + k)A}$$

$$\sigma_2 = \frac{P}{(\eta + k)A}$$

$P_L = (1 + k)A\sigma_y$ (LIMIT LOAD)

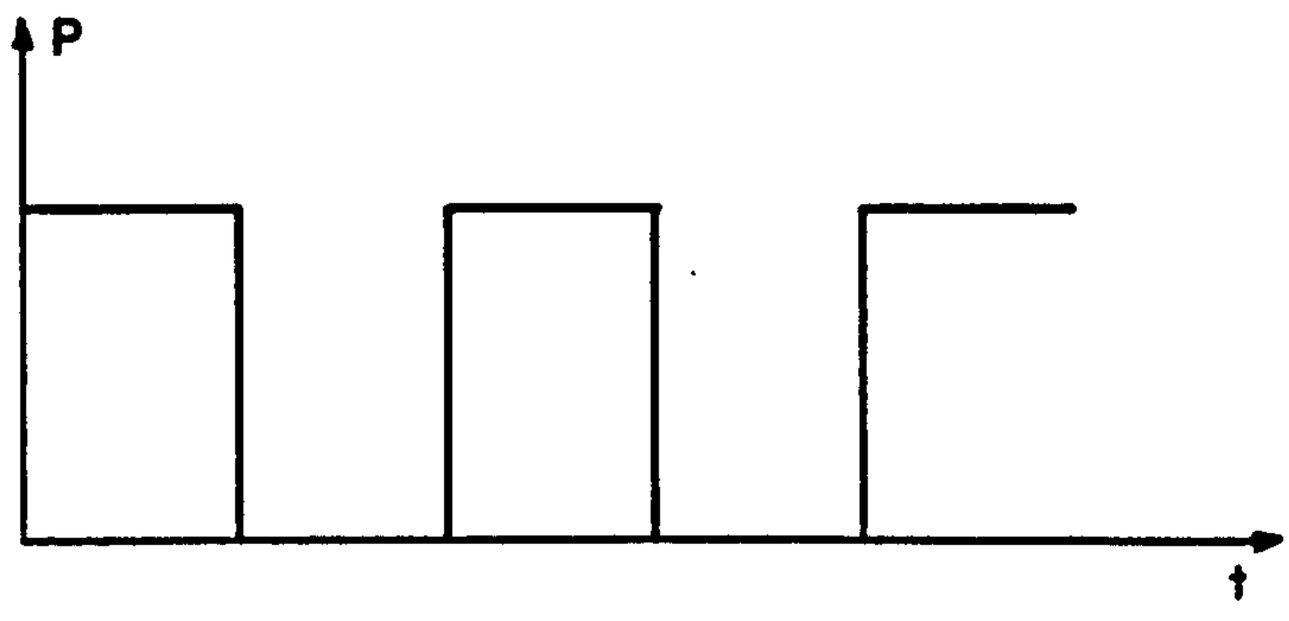

FIG. 3.2

LOAD HISTORY

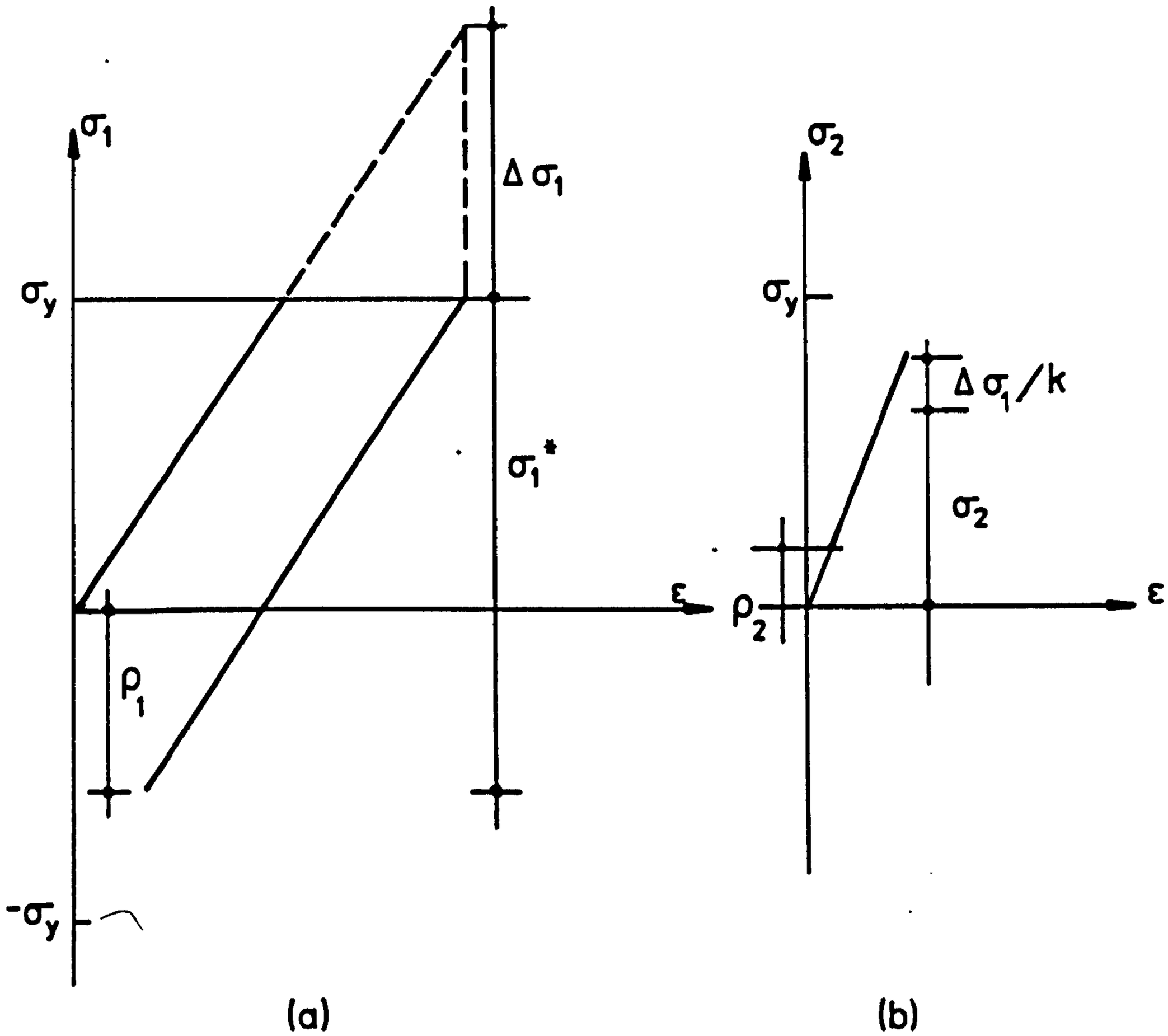

FIG: 3.3 STRESS-STRAIN DIAGRAMS

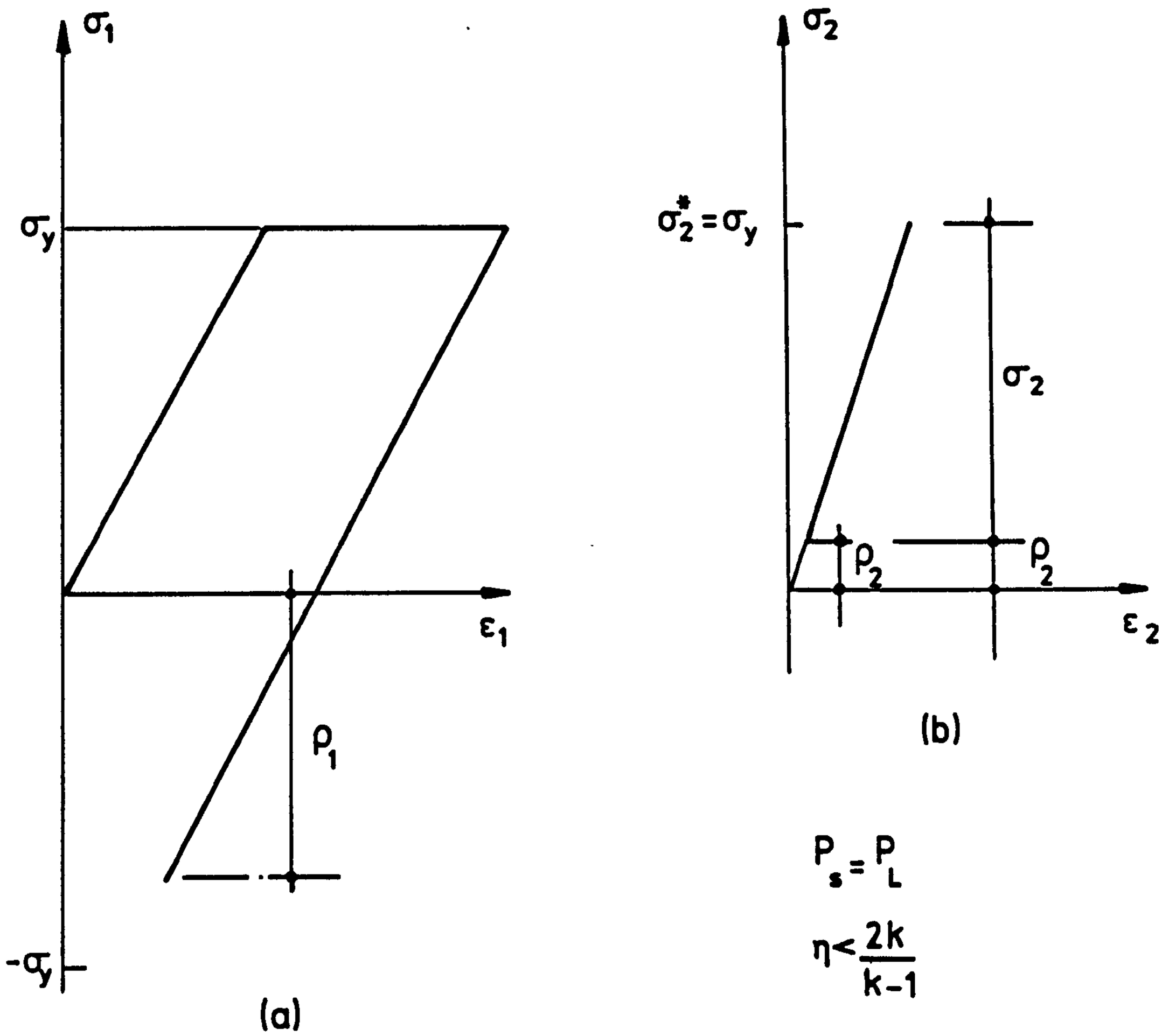

FIG. 3.4 STRESS-STRAIN DIAGRAM FOR LIMIT LOAD

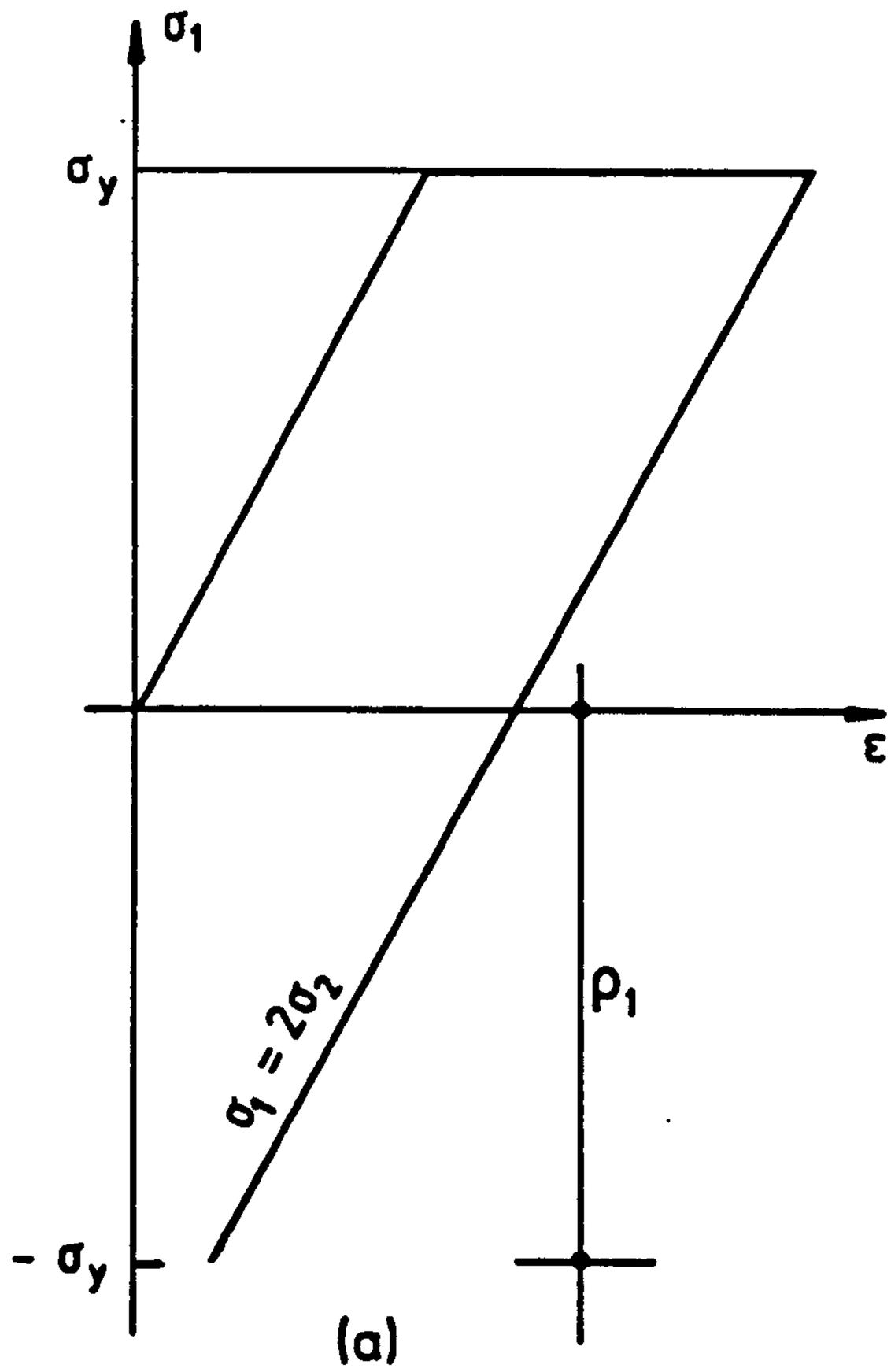

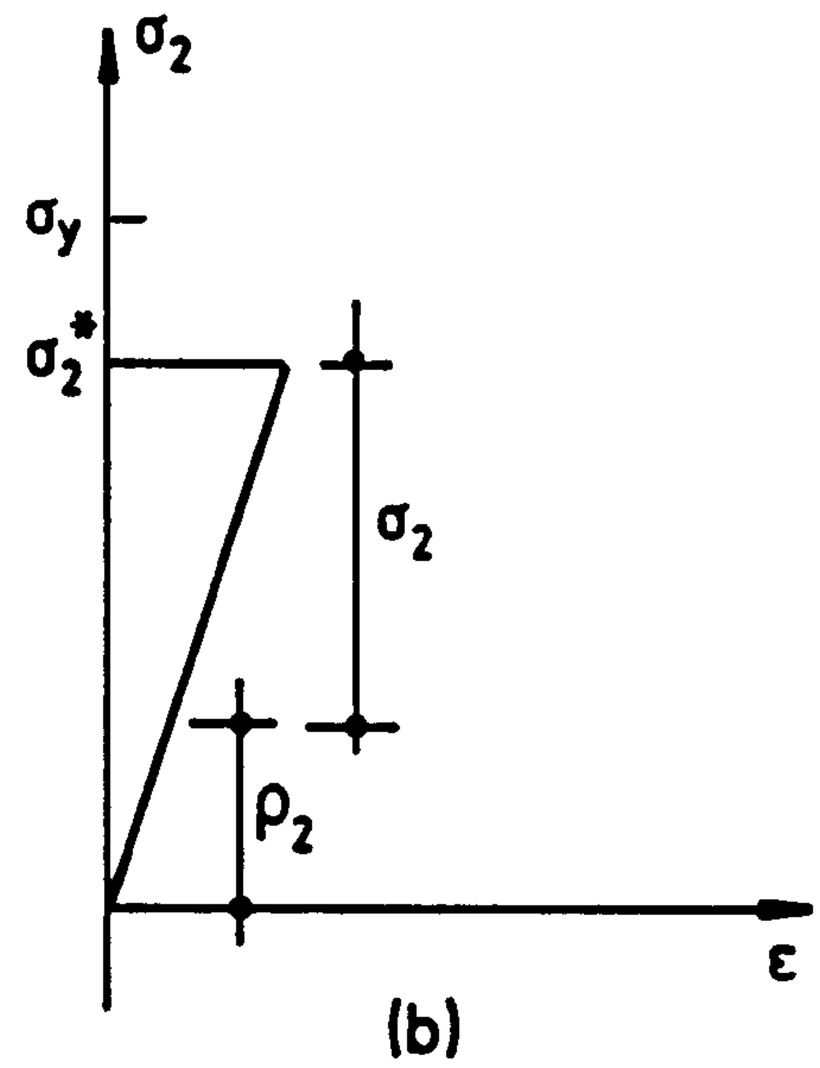

$$P_S = \frac{2(\eta + k)P_L}{\eta(1+k)} < P_L$$

$$\eta > \frac{k2}{k-1}$$

FIG. 3.5 STRESS-STRAIN DIAGRAM FOR SHAKEDOWN LOAD

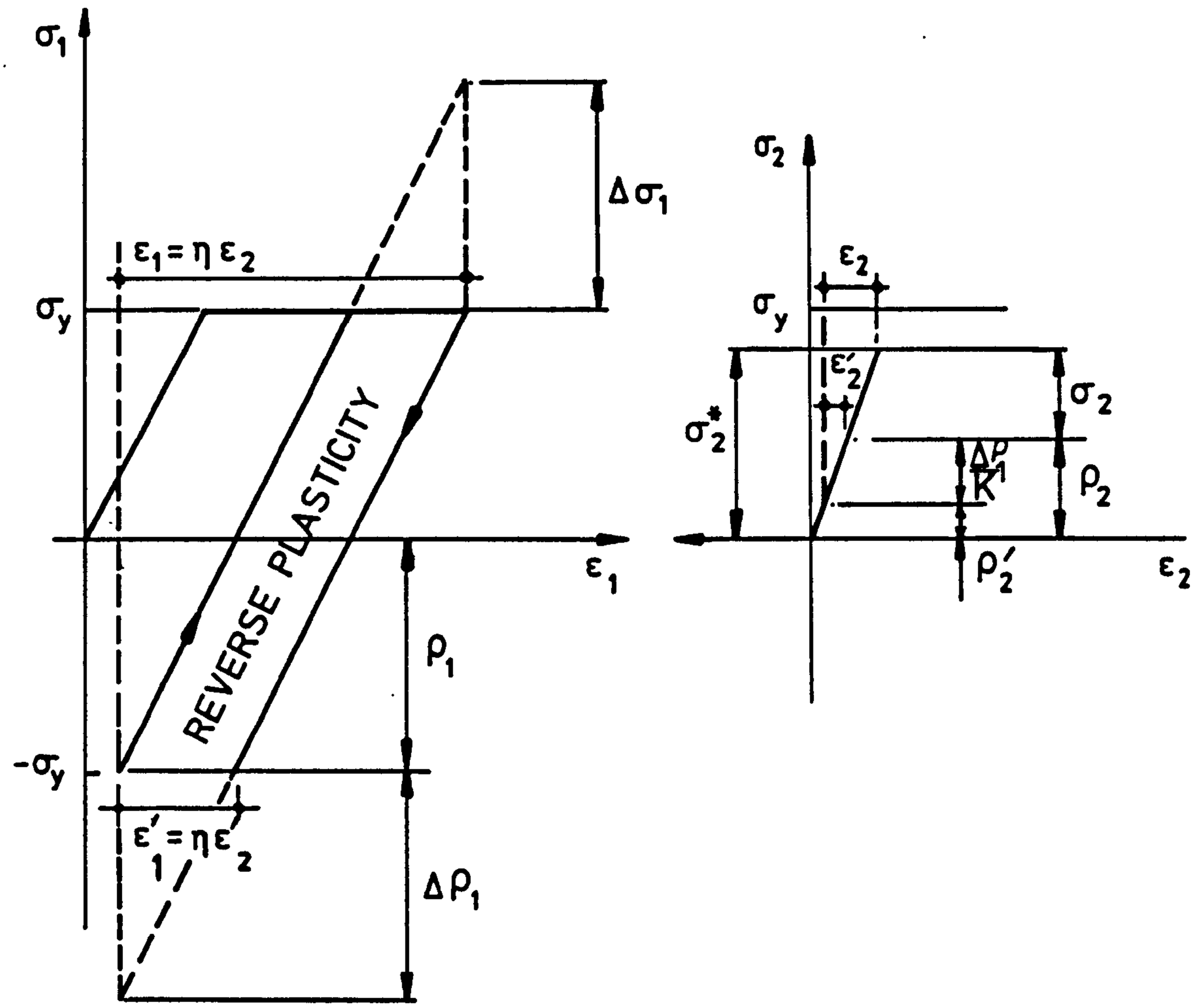

FIG. 3.6 PLASTIC SHAKEDOWN

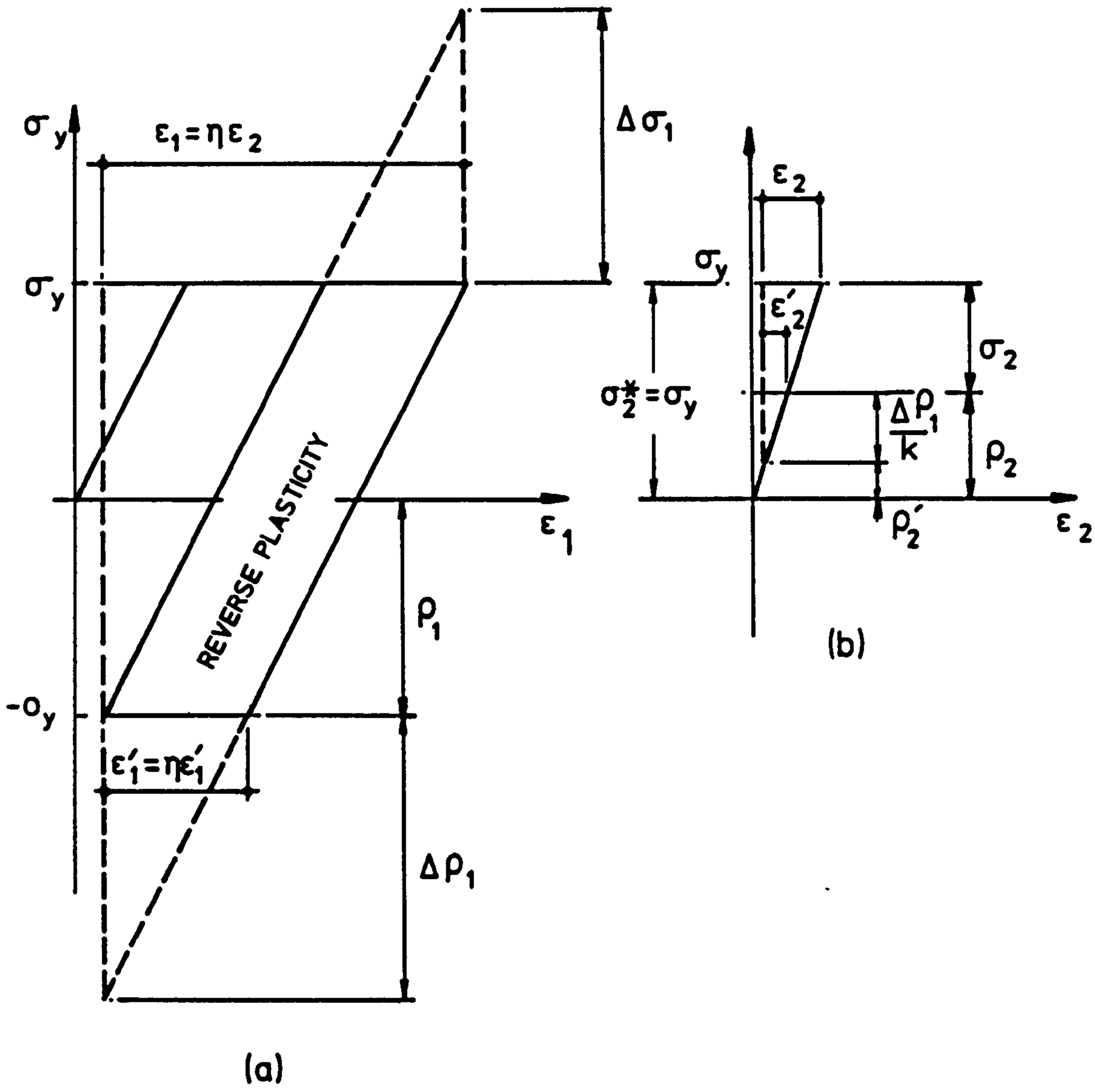

FIG. 3.7 LIMIT CONDITION FOR REVERSED PLASTICITY

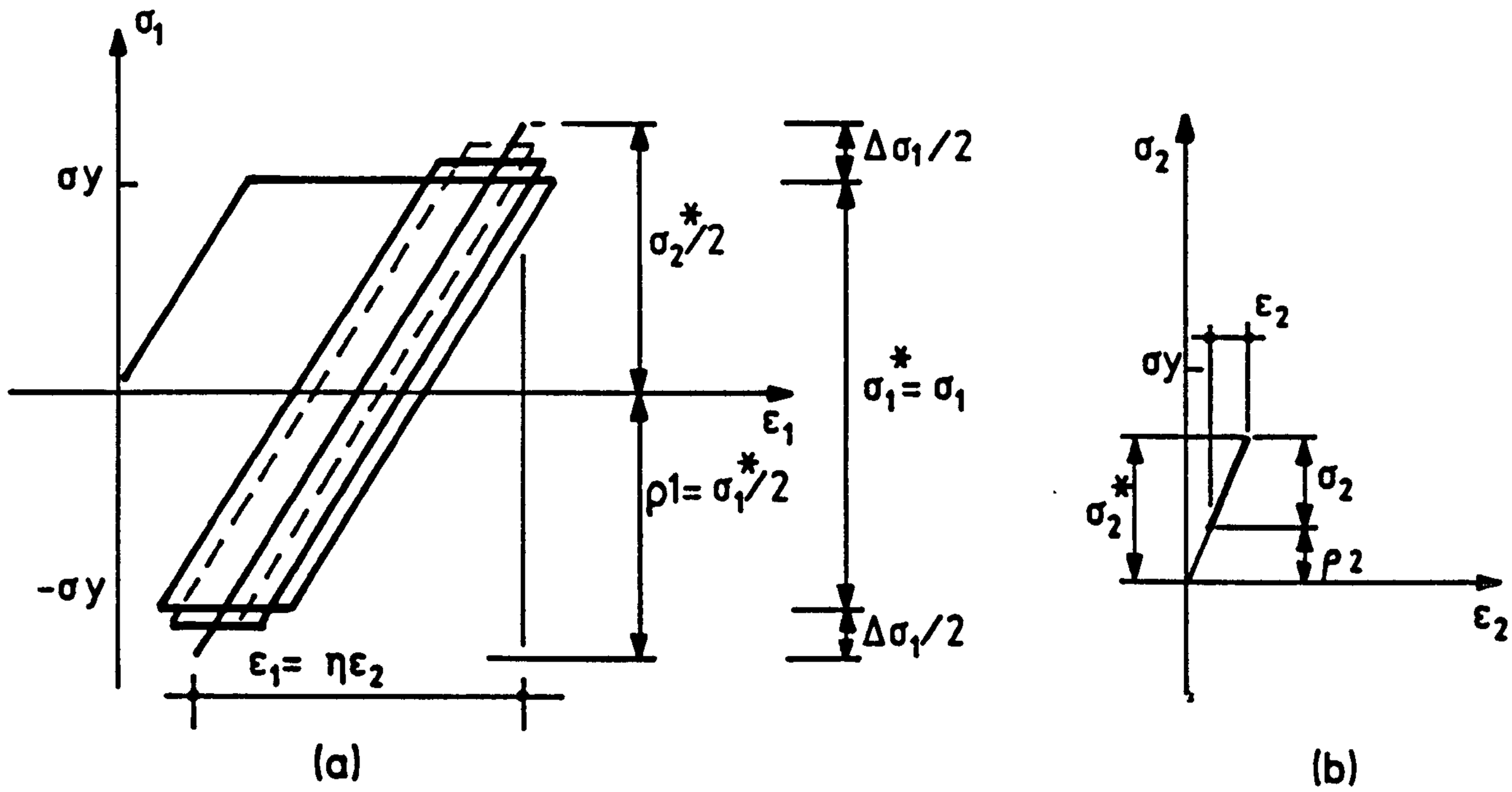

FIG. 3.8 CYCLIC HARDENING ($\Delta\rho_1 = 0$ - NO REVERSED PLASTICITY)

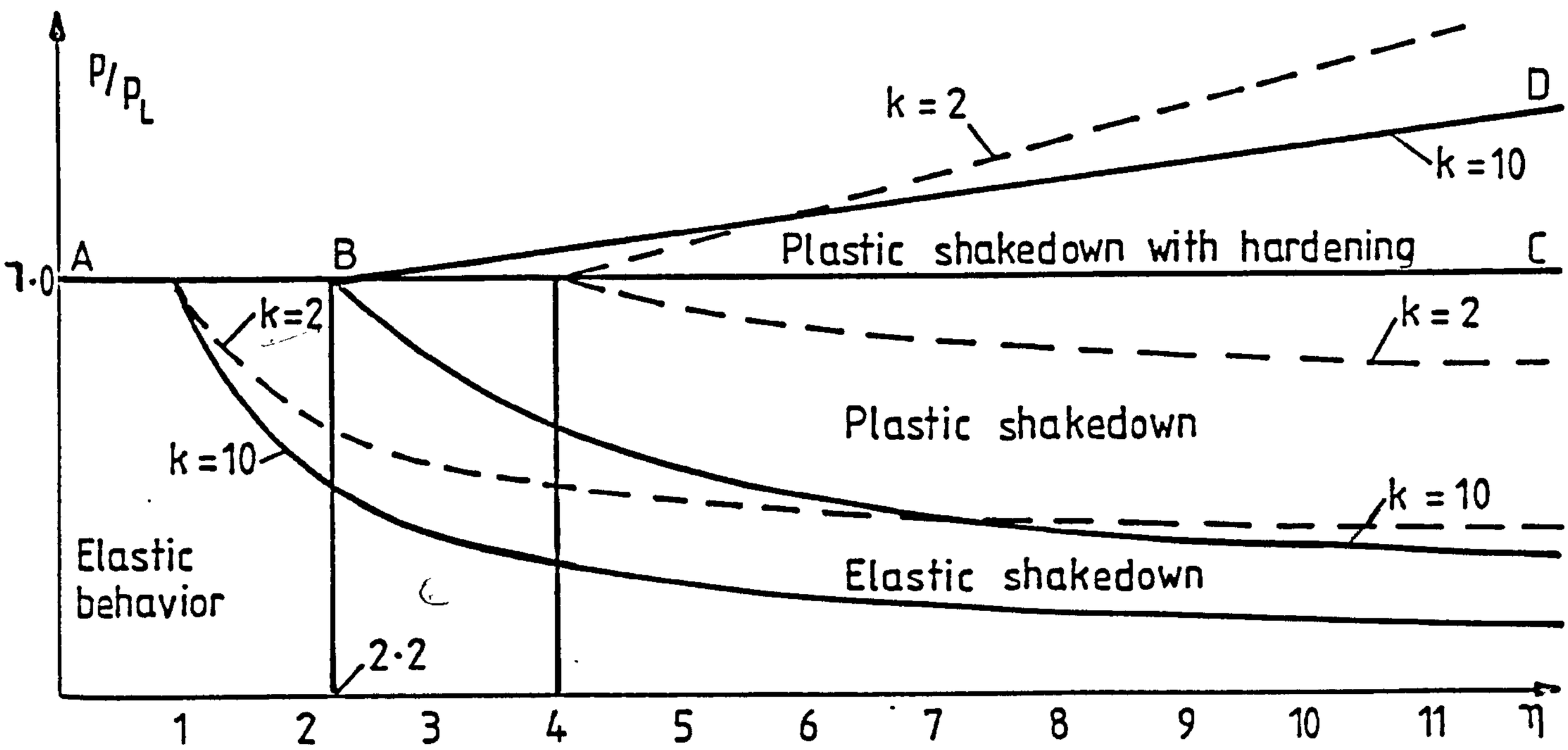

FIG. 3.9 BOUNDARIES FOR THE STRUCTURE MODES OF BEHAVIOUR

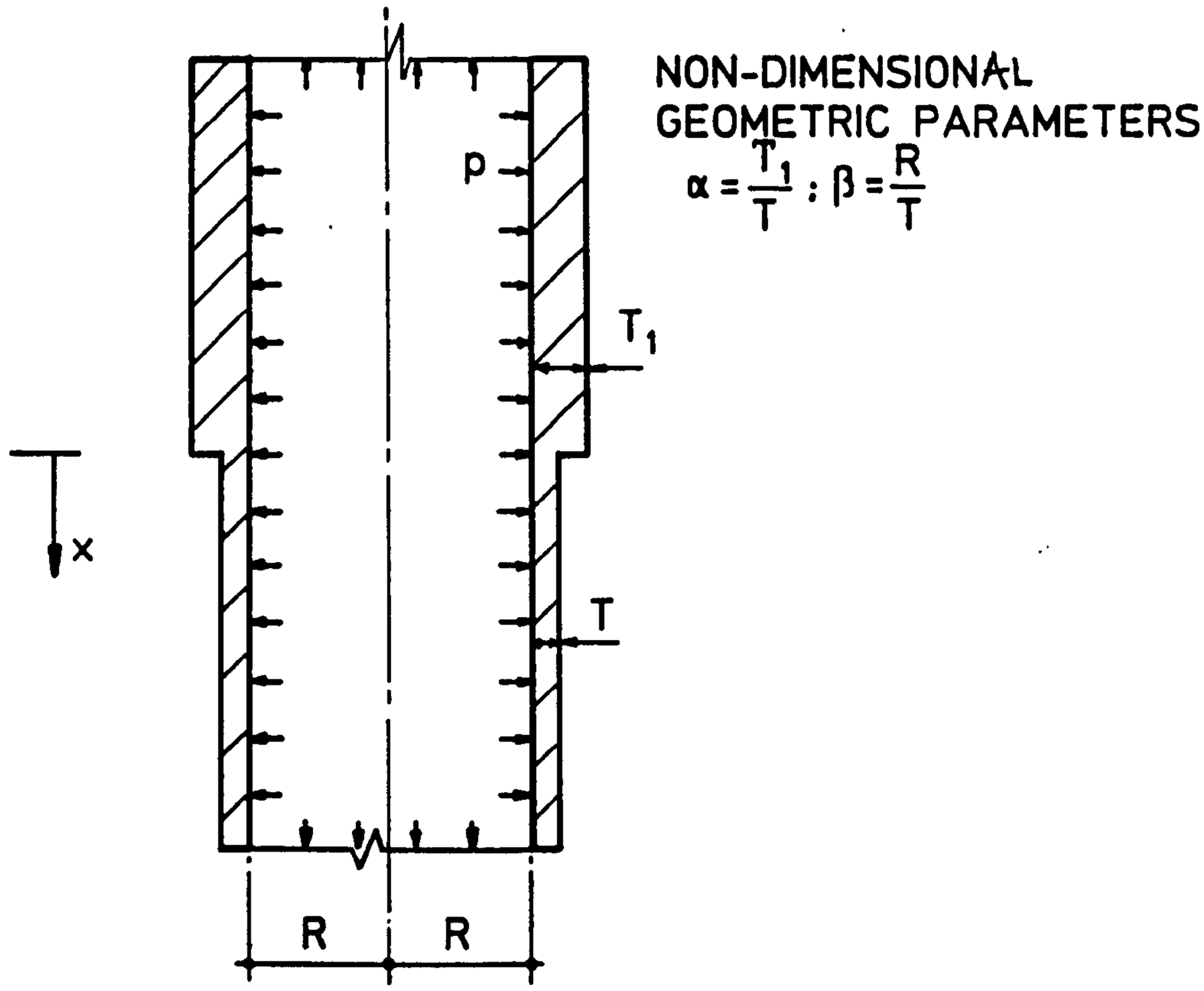

(a) THE VESSEL GEOMETRY

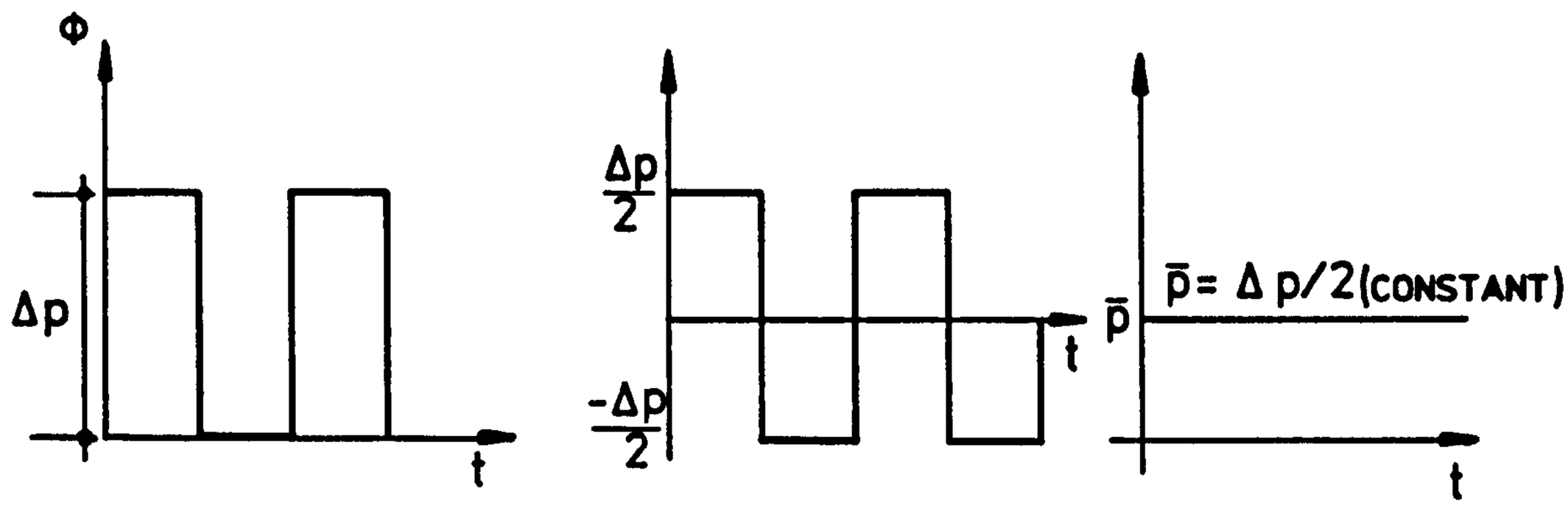

(b) THE LOAD

FIG. 3.10

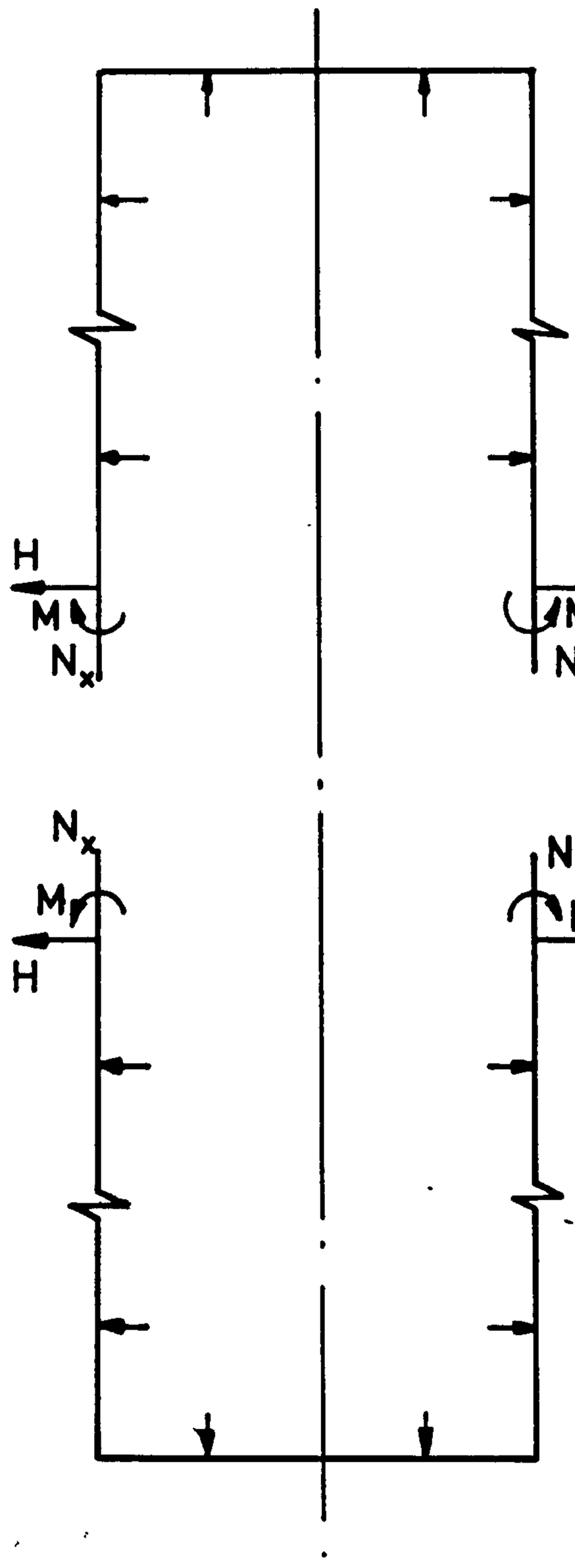

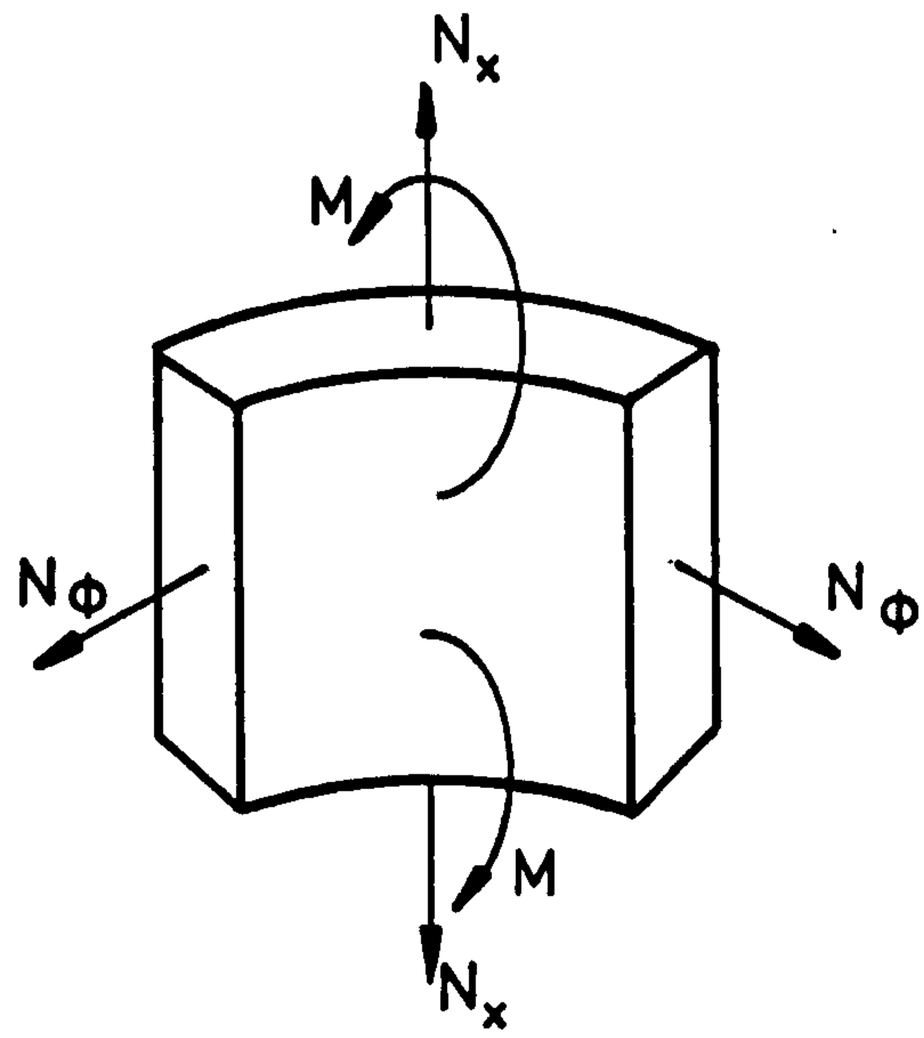

STRESS ELEMENT FOR THE CYLINDER

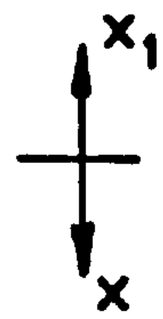

$$H = \sqrt{\beta}\sqrt{3(1-\nu^2)}\, T\, f_1(\alpha)\, \Delta p/2$$

$$M = \beta\, T^2 f_2(\alpha)\, \Delta p/4$$

FIG 3.11 THE ELASTIC STRESSES CALCULATIONS

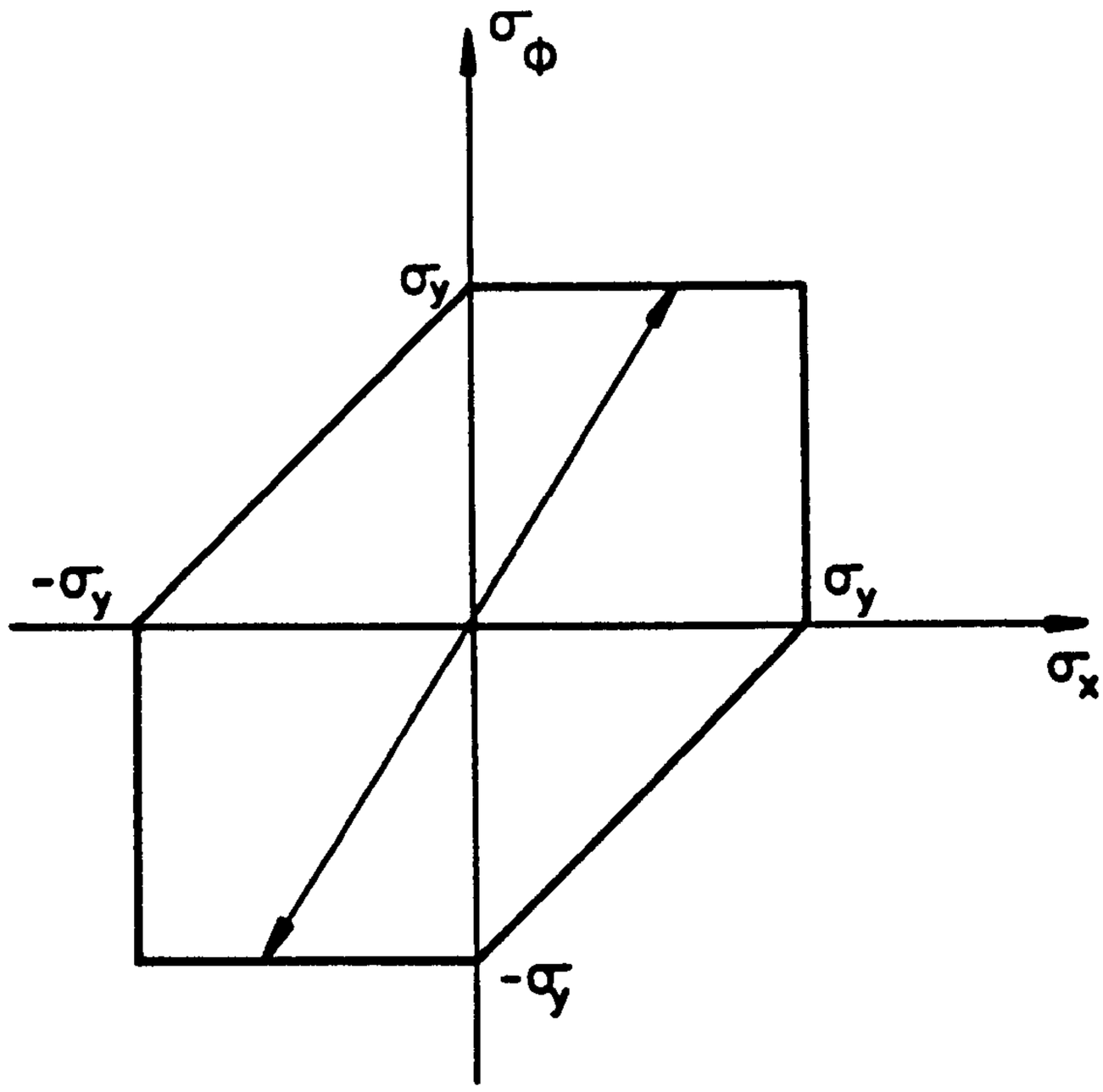

FIG 3.12 GLOBAL COLLAPSE

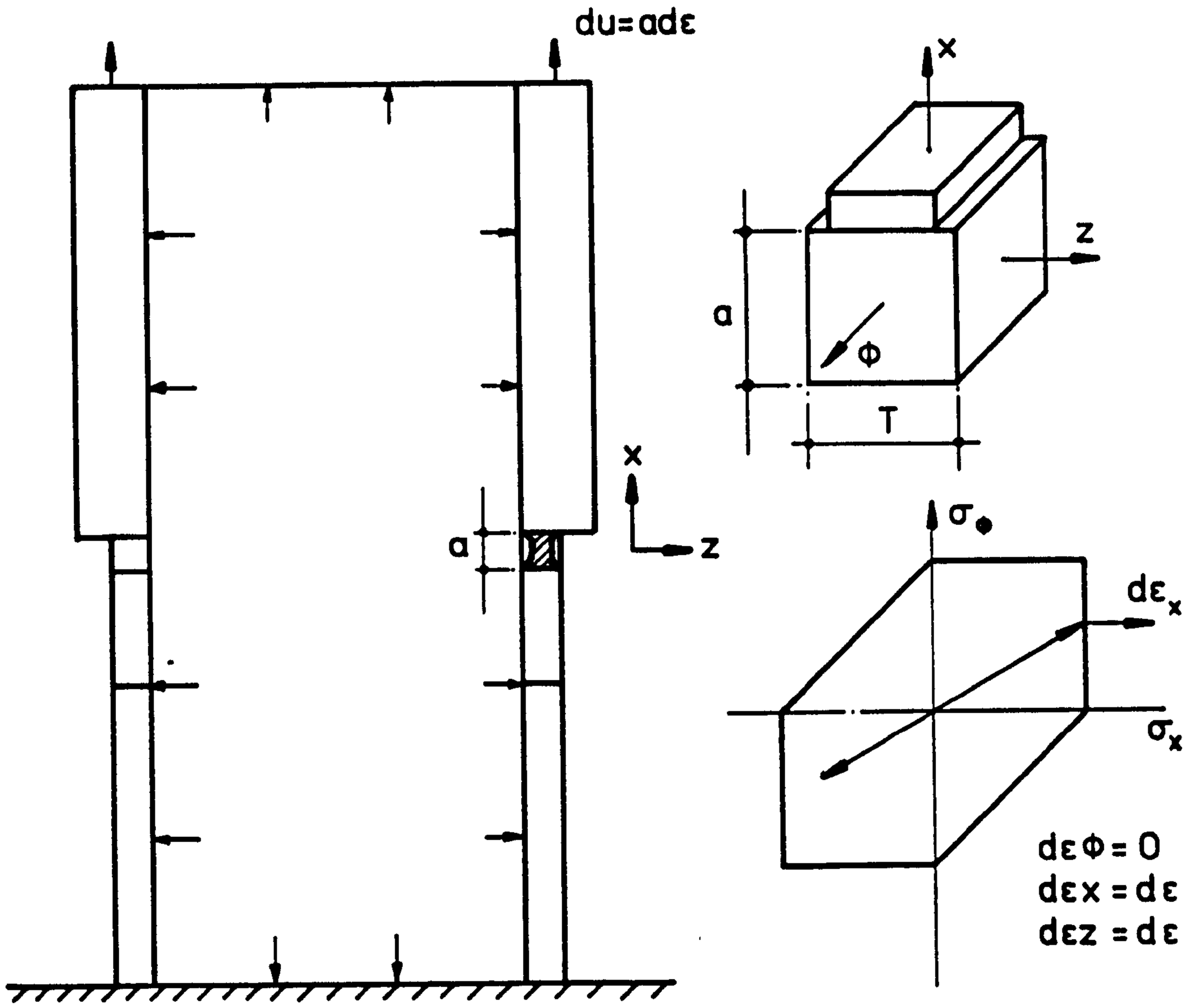

FIG 3.13 MECHANISM OF DEFORMATION

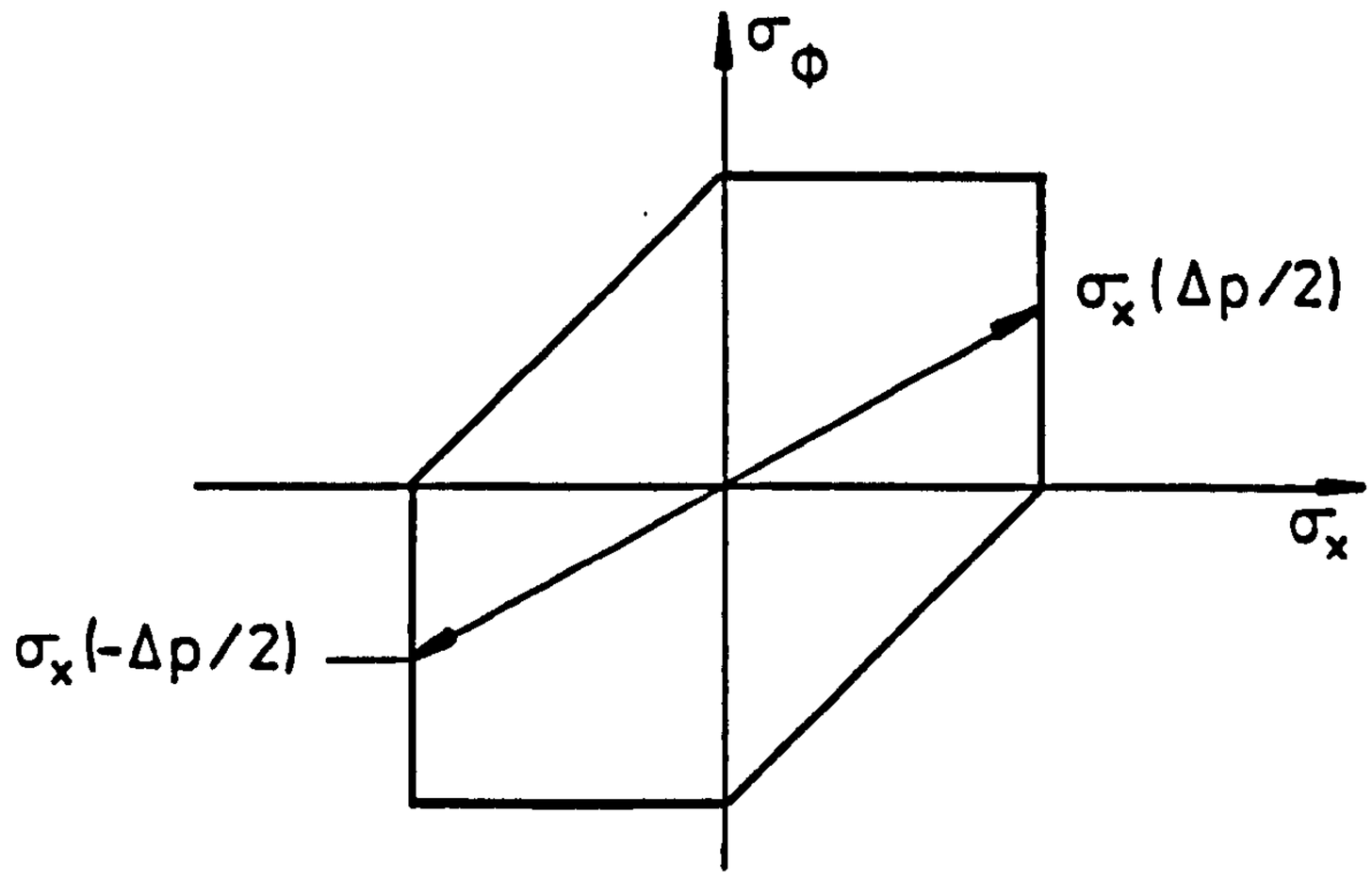

FIG. 3.14 SHAKEDOWN LIMIT

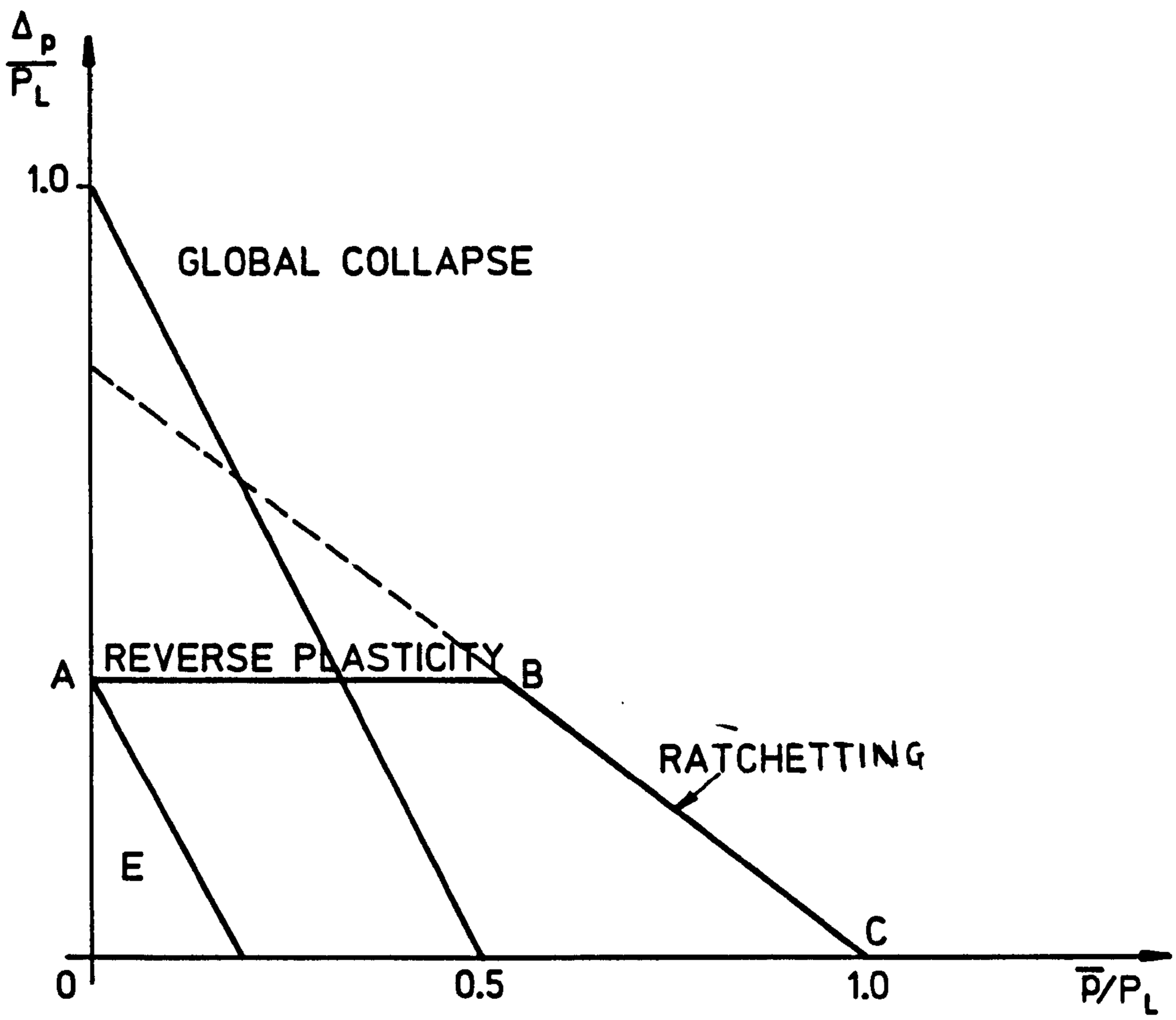

FIG. 3.15 DESIGN BOUNDARY FOR PRESSURE VESSELS

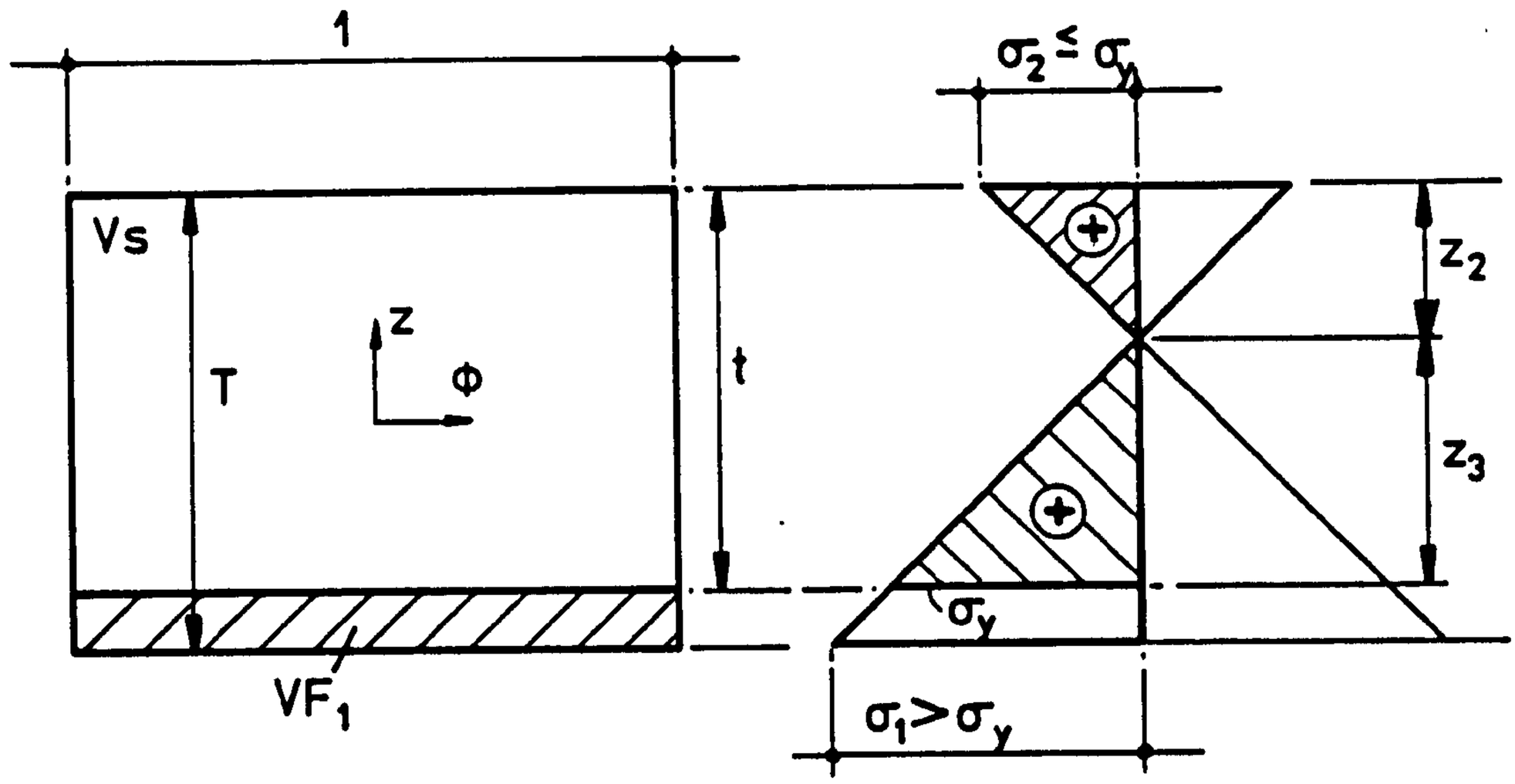

FIG. 3.16 STRESS DISTRIBUTION FOR WORK HARDENING MATERIAL

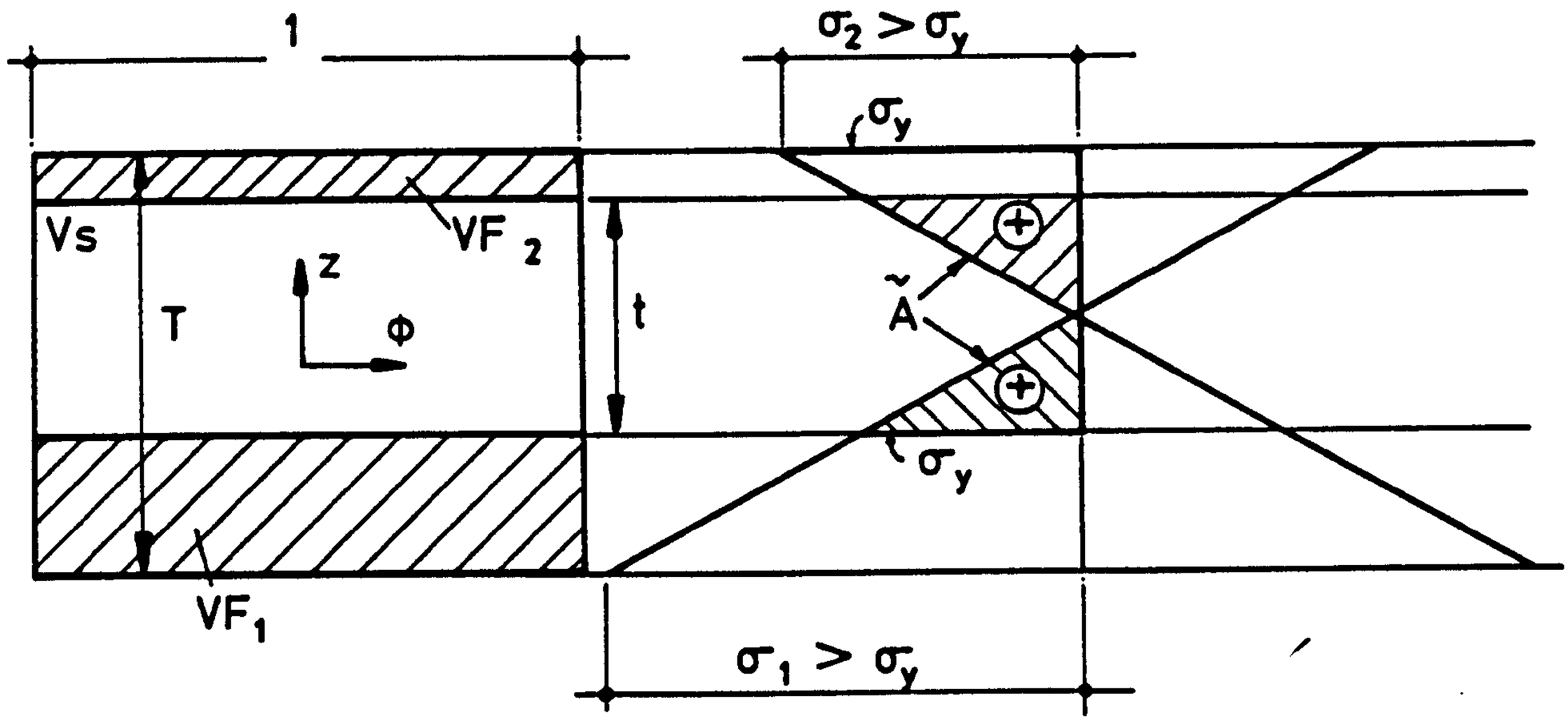

FIG 3.17 NEW REGION OF PLASTIC SHAKEDOWN

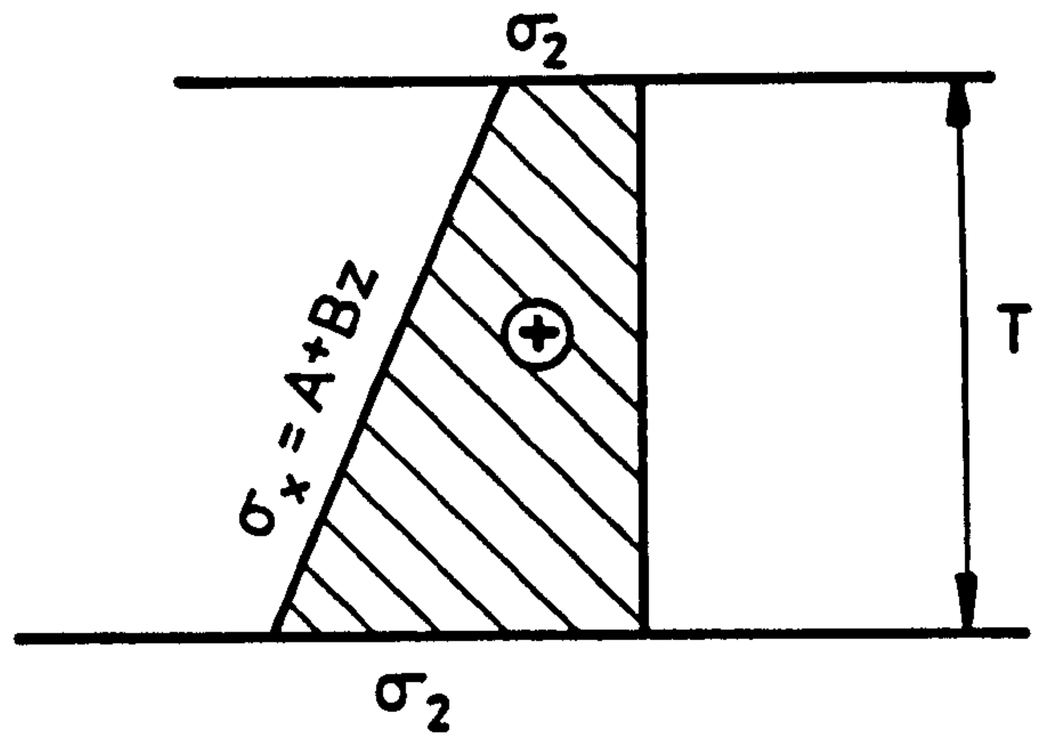

FIG. 3.18 STRESS DISTRIBUTION FOR A>BT/2

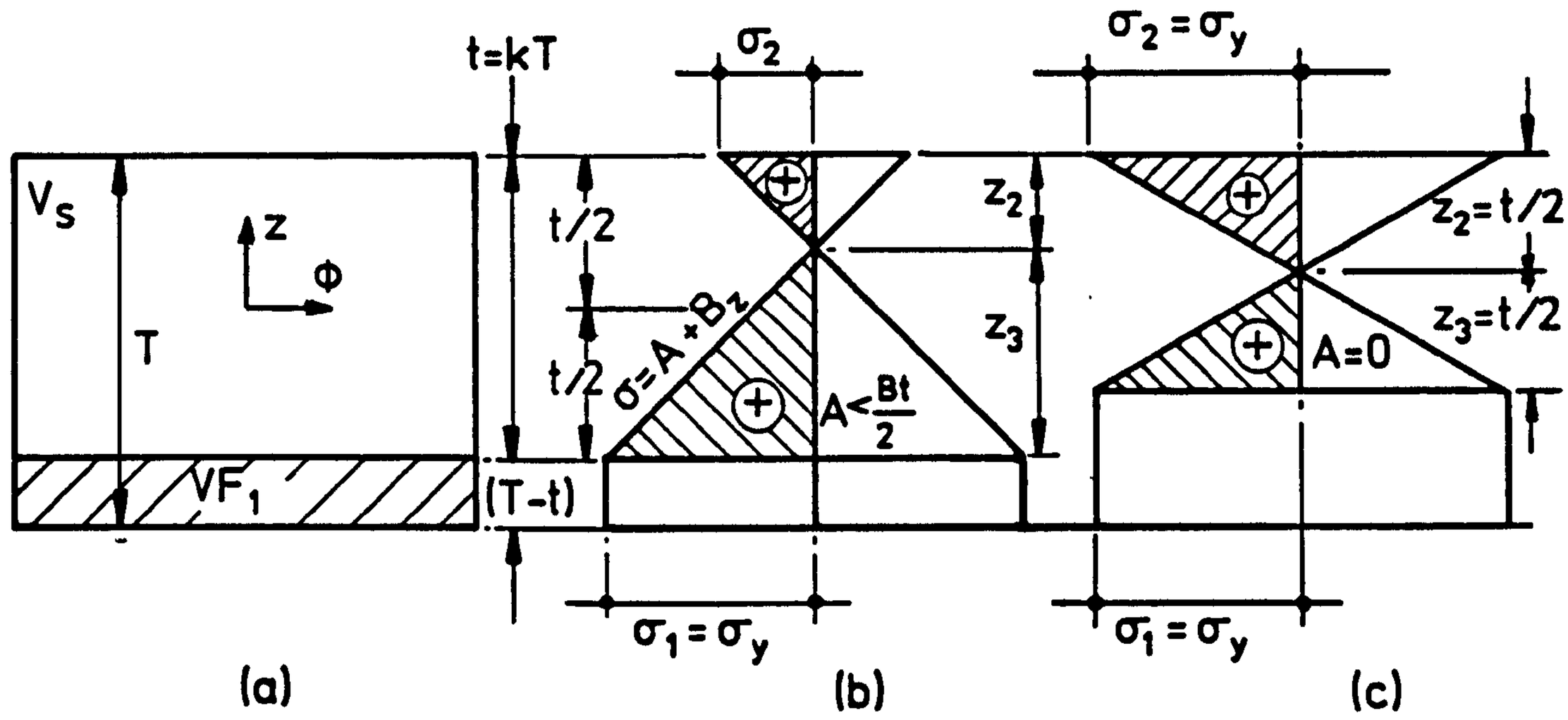

FIG.3.19 STRESS DISTRIBUTION FOR ELASTIC/PERFECTLY PLASTIC MATERIAL

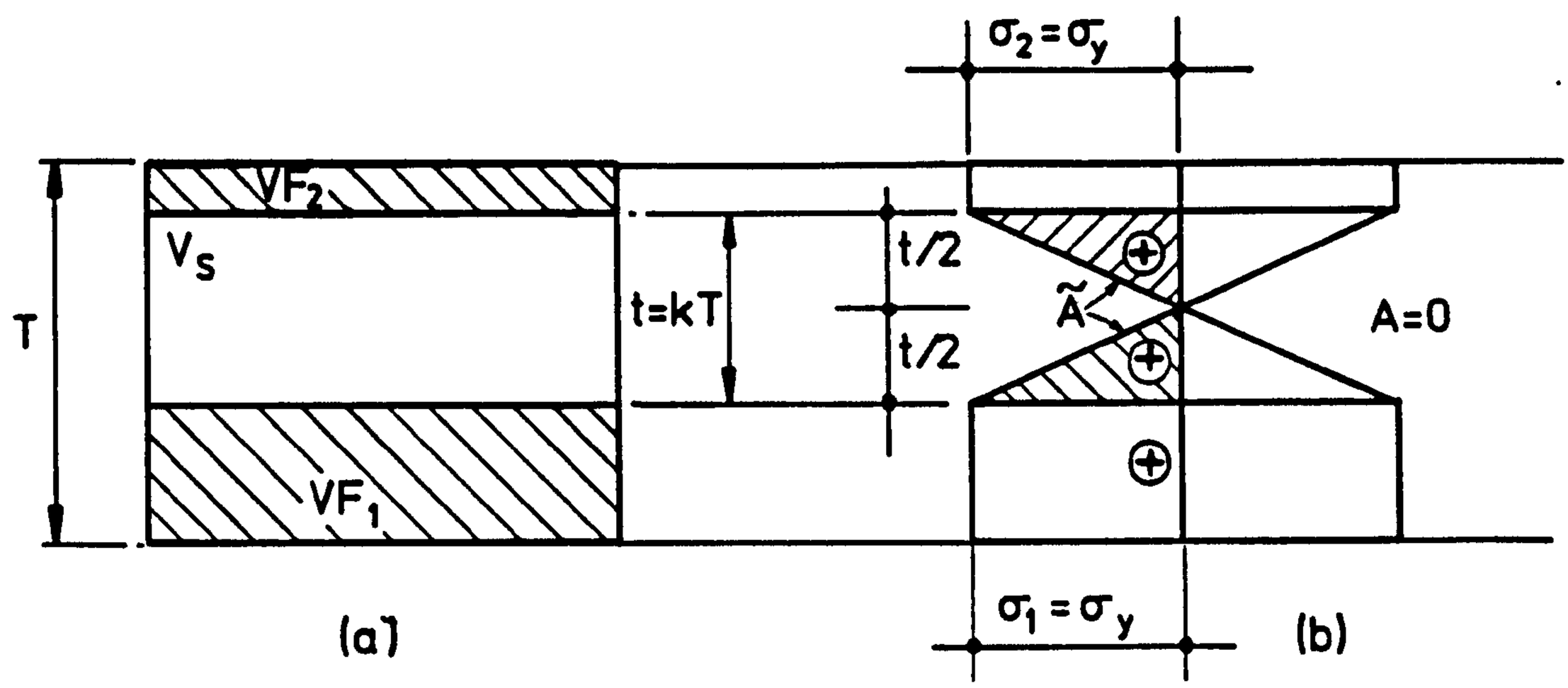

FIG.3.20 NEW REGION OF PLASTIC SHAKEDOWN

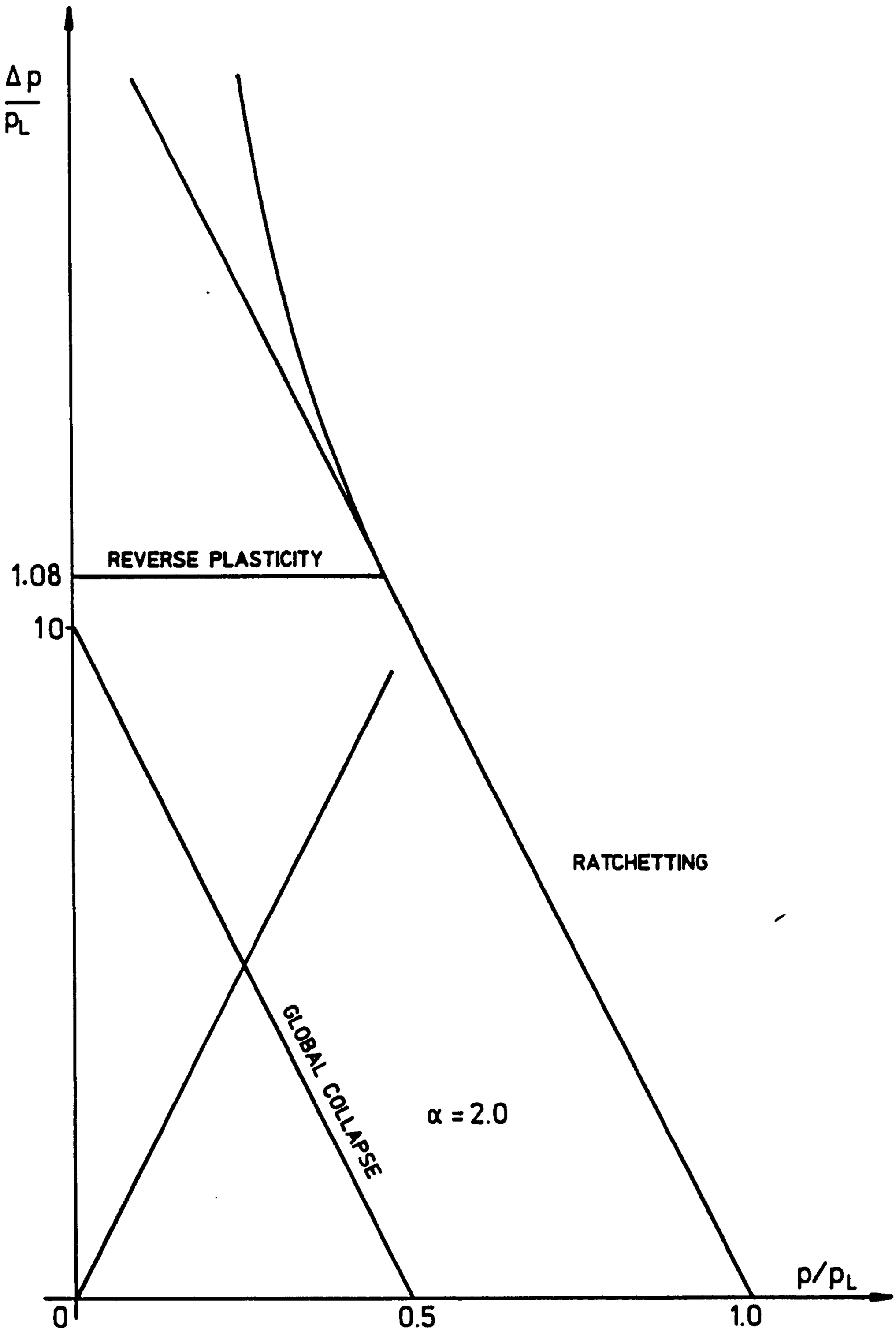

FIG.3.21 LOAD REGIMES FOR CYLINDER WITH VARIABLE THICKNESS

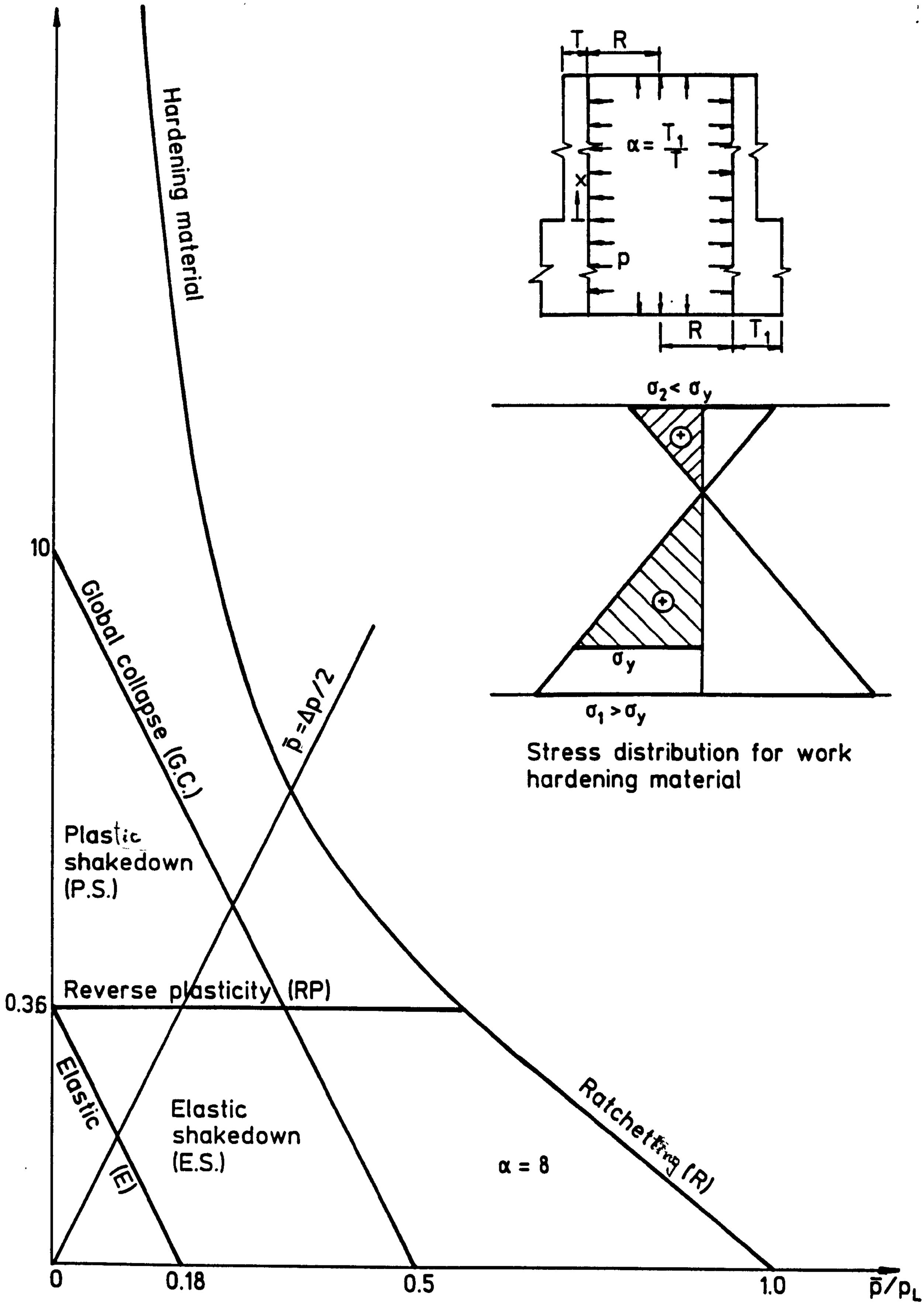

Stress distribution for work hardening material

FIG 3·22 LOAD REGIMES FOR CYLINDER WITH VARIABLE THICKNESS

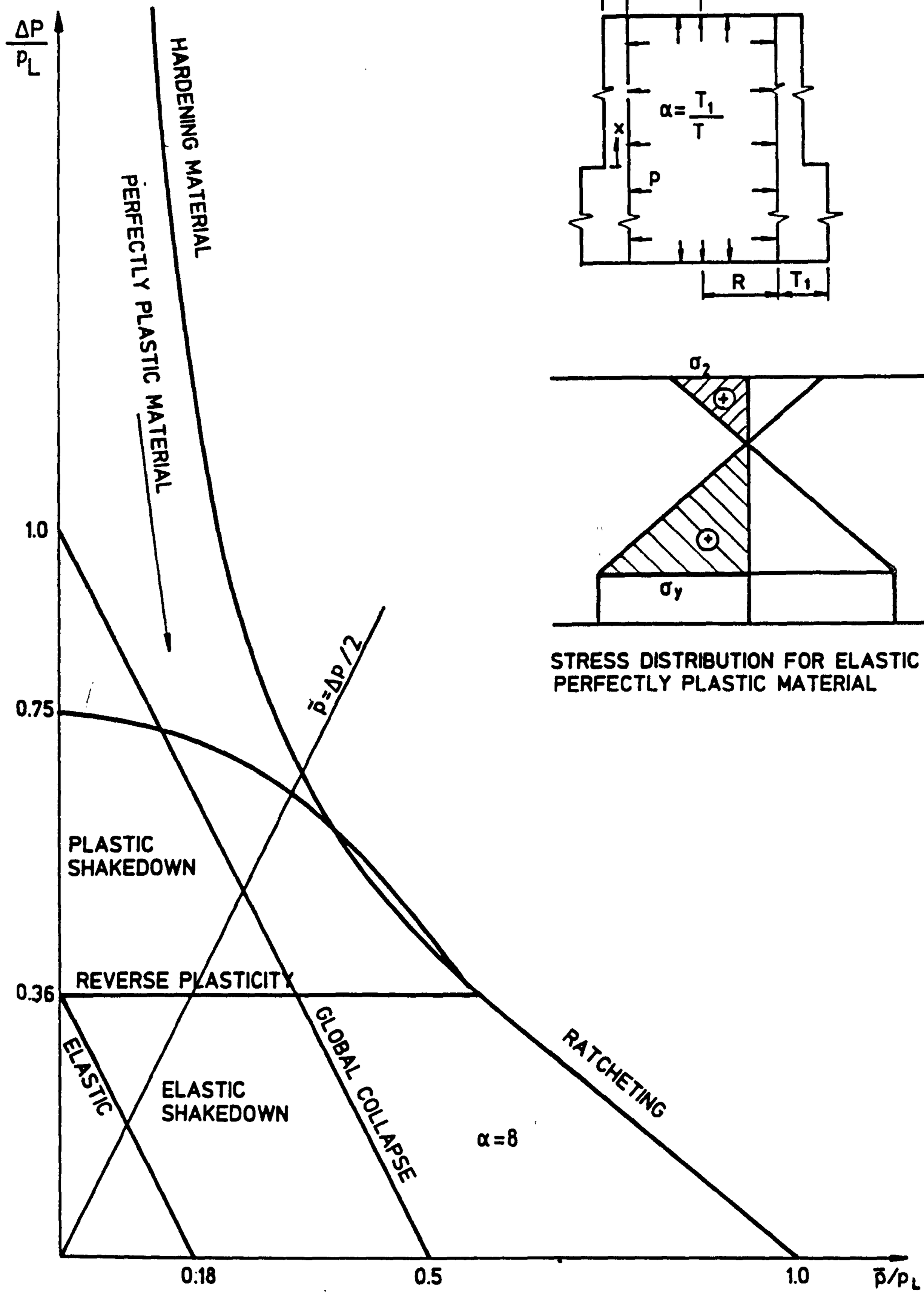

FIG 3·23 LOAD REGIMES FOR CYLINDER WITH VARIABLE THICKNESS

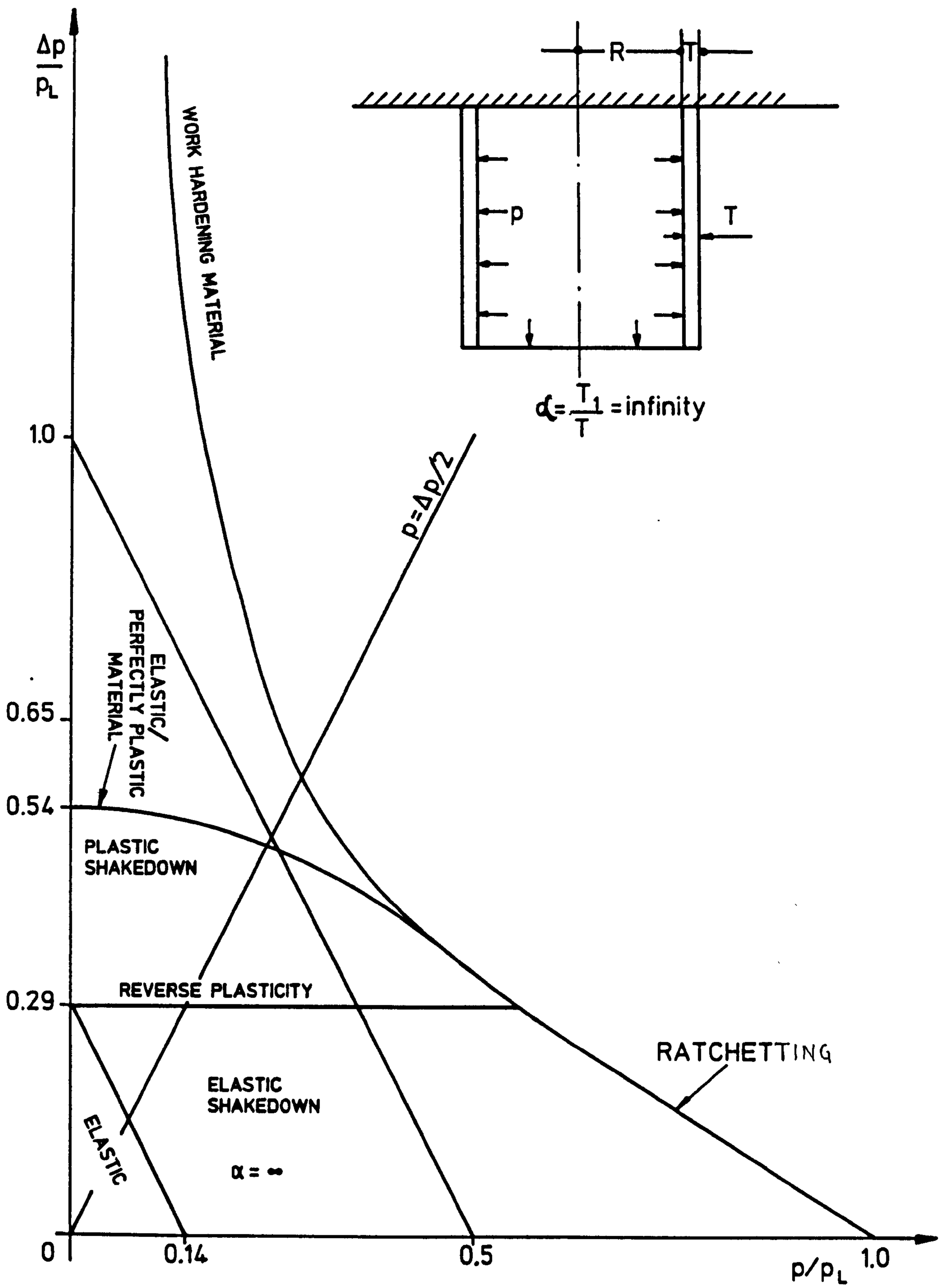

FIG.3.24 LOAD REGIMES FOR THE LIMIT CASE WHEN $\alpha = \infty$

CHAPTER 4

SIMPLIFIED ANALYSIS OF TUBES SUBJECTED TO MECHANICAL LOADS AND MOVING TEMPERATURE FRONT

4.1 Introduction

The problem of shakedown and ratchetting at elevated temperature in components of Nuclear Reactors has been the subject of extensive study since 1959 when Miller [39] first derived criteria to determine limits on the stresses to prevent incremental growth or to estimate the expansion per cycle when that was due to occur. In particular, Miller studied the problem of the behaviour of nuclear reactor fuel cans under the effects of cyclic thermal loading and constant internal pressure. Bree [40] extended his work to include a more complete material model capable of introducing to the calculations effects of work-hardening, dependence of the yield stress on the temperature and also the effects of creep. A more detailed study of the effect of creep was subsequently published by Bree [41]. Other authors [42-46] following similar procedures ie, using uniaxial models to predict thermal ratchet mechanisms, succeeded in obtaining exact solutions for simplified versions of practical engineering problems. Nevertheless, the ever-increasing demand for nuclear energy in recent years has brought the construction of more advanced reactors such as the Liquid Metal Fast Breeder Reactors (LMFBR) which operate in conditions of much higher and complex loading

systems. The consequence of this rapid development in nuclear technology is that engineering problems related to thermal cyclic loading have become more complicated and considerable effort has been devoted in recent years to better understand the new aspects of the problem.

New materials selected for the new reactors (LMFBR) had exhibited a Bauschinger effect, as pointed out by Mulcahy [47,48]. In consequence, the thermal ratchetting response of a kinematic hardening material model representing an idealised Bauschinger effect, had to be studied.

Although the current design codes still require conservative shakedown boundaries which impose design and operating conditions completely free of ratchetting, more precise methods of analysis had to be developed by means of simplified numerical techniques to avoid the cost and time required to perform a complete inelastic F.E. analysis for such problems. The development of these numerical techniques of detailed analysis for the design of structures at elevated temperatures has received great support in the last decade.

One contribution to this development has been made by Arnaudeau et al. [49] analysing the upper part of the French LMFBR main vessel with consists of a thin cylinder subjected to axisymmetrical thermal load and axial mechanical load representing the weight of the vessel. A bi-dimensional model was used in their approach in an attempt to apply more precise rules to the analysis instead of the classical

uniaxial model mentioned previously and a comparison was made for a perfectly plastic material.

The new problems of designing fast breeder reactors has been the subject of thorough study at the University of Leicester in the last 10 years. Several papers have been published encompassing different aspects of structural and material behaviour. At first, simple structural models like the two-bars structure were analysed by Megahed [50] to simulate the fuel can of a sodium cooled reactor where a theoretical analysis was performed to study the modes of behaviour of such a simple structure under rapid cooling cyclic or down shock loading. The need to understand the effect of thermal loading in the design of LMFBR's beyond the restrictions of the present codes which will prevent not only ratchetting but also reversed plasticity was pointed out later by Ponter [14] who proposed an alternative approach to simplified analysis which would allow a much more detailed method. Ponter's technique consists of defining conservative bounds separating the region F of reversed plasticity and the region R of ratchetting for Bree-like structures. The technique has been developed recently [36,37] and applied to a number of thermal transient problems. The solutions shown in [37] demonstrate that ratchetting can occur in the presence of very moderate mechanical load when the thermal cyclic load is high, as in the case of the liquid-metal fast breeder reactors. Also the realization that the ratchetting mode of behaviour depends considerably on the variation of the yield stress with the temperature and that it becomes possible even in the absence of mechanical load, has been a

great contribution to the understanding of the effects of thermal cyclic transients.

Subsequently a more systematic method of analysis was developed by Karadeniz and Ponter [51] for thin cylindrical shells subjected to cyclic thermal loading based upon the upper bound kinematic shakedown theorem (Koiter's Theorem) and a Finite Element Approach. The solution of the problem was achieved by choosing a suitable displacement field and reducing the upper bound theorem to a problem in linear programming. The generalization of this technique for several different types of shells was further developed and will be presented in a later chapter of this thesis.

In this chapter a simplified analysis of a similar problem of a tube subjected to mechanical loads and moving temperature fronts as presented in [51] will show how simple calculation can predict the behaviour of a tube under rather complicated combinations of load. The analysis is extended to combine more than one mechanical load (internal pressure/axial load) with the moving temperature front. Such analyses are only possible without becoming excessively complex, by assuming some simplifications. Apart from these simplifications all the assumptions in [51] will also hold here and an analogous procedure will be used by analysing individually the combination of the mechanical loads, axial load and internal pressure with the moving temperature front. A third loading system is then considered consisting of the combination of the two mechanical loads applied simultaneously with the thermal cyclic loading. In fact,

the last case is the one more likely to occur in practice where the internal pressure can be due to the release of gaseous fission materials from the fuel and the axial load represents any dead weight or the own weight of the vessel.

4.2 The Simplified Analysis

4.2.1 Geometry and Loading

The problem of the fluctuation of the level of sodium in LMFB reactors which is here simulated by the moving temperature front has been the subject of an international benchmark project on simplified methods for elevated temperature design and analysis [52]. The temperature distribution through the thickness of the tube is assumed to be constant and the thermal stresses arise from a step of temperature $\Delta\Theta$ moving along a prescribed length of the tube in alternating directions. The geometry of the tube and the mechanical loads considered are illustrated in Fig. 4.1a whilst the thermal loading is shown in Fig. 4.1b.

4.2.2 Thermal Stress Distribution Assumed

The thermal stress distribution used in [51] was given by Arnaudeau et al. [49] for the steady step variation $\Delta\Theta$ as shown schematically in Fig. 4.2a.

$$\hat{\sigma}_\theta^\theta = -\sigma_t e^{-\beta x}\cos\beta x + 2\eta\nu\xi\sigma_t e^{-\beta x}\sin\beta x \quad \text{for} \quad x > 0$$

$$\hat{\sigma}_\theta^\theta = -\sigma_t e^{\beta x}\cos\beta x + 2\eta\nu\xi\sigma_t e^{\beta x}\sin\beta x \quad \text{for} \quad x < 0$$

$$\hat{\sigma}_x^\theta = 2\eta\nu\xi\sigma_t\, e^{-\beta x}\sin\beta x \quad \text{for} \quad x > 0$$

$$\hat{\sigma}_x^\theta = 2\eta\nu\xi\sigma_t\, e^{\beta x}\sin\beta x \quad \text{for} \quad x < 0$$

where

$$\xi = \{3/(1-\nu^2\}^{1/2} \; ; \; \beta = \left\{\frac{3(1-\nu^2)}{R^2h^2}\right\}^{0.25}$$

$$\sigma_t = \frac{E\alpha\Delta\theta}{2}$$

ν is Poisson's ratio, η is the distance across the thickness and the origin is at the temperature discontinuity ($x = 0$). The same assumptions made by Karadeniz [60], Karadeniz and Ponter [51] that the maximum thermal stress amplitude is $2\sigma_t$ and that it occurs at $x = 0$ will hold here. Its worth mentioning that the thermal stress distributions are of a localized nature and as such will give rise to localized hinge-conical mechanisms or to localized thinning due to net deformation in the axial direction. For the present simplified analysis, only the maximum thermal hoop stress will be considered to contribute to the deformation pattern between hinges, as shown in Fig. (4.2b).

4.2.3 The Effects of the Simplifications Adopted on the Shakedown Boundary and Modes of Deformation

In order to clarify the implications of the simplified assumptions adopted for the present analysis, some discussion is required about their effects on the results when compared with those obtained in [51].

The sequence of contours defining the shakedown limit in a Bree type diagram presented in [51] (Fig. 4.3) was divided in regions corresponding to different modes of deformation of the tube. The stress histories and the corresponding modes of mechanism are illustrated in Fig. 4.4.

For these calculations the following simplified assumptions will be introduced:

- the incremental collapse deformation between hinges will be caused mainly the maximum thermal hoop stress

- the axial stress will contribute to the energy dissipation in the formation of hinges and with the axial strain for the case of axial load

- mode I in Fig. 4.4 will no longer be possible since only the maximum thermal hoop stresses will be taken into consideration

- the three hinge global mechanism(mode III, Fig. 4.4) will be assumed as symmetric despite the axial strain in the case of the axial mechanical load. Such symmetry does not affect the shakedown limit but only the positions of the hinges, which in this case are imposed to be symmetric.

Mode II representing an incremental deformation in the axial direction will still be valid here, hence for the present calculations the possible mechanisms of deformation are the one represented by mode II (Fig. 4.4) and a slightly modified(symmetric) three hinges mechanism shown in Fig. (4.5) with the respective stress history. Defining these two modes of response "a priori" allows a direct application of the Upper Bound Theorem to determine the bounds which will define the shakedown boundary for the problem.

4.3 Simplified Analysis of a Tube Subjected to Constant Axial Load and Moving Temperature Fronts

In this section two sets of calculations will be carried out for the problem of a tube subjected to a step of temperature moving in alternating directions along a certain length of the tube in the presence of sustained axial load. First the material properties are assumed to be independent of the temperature and in the second set of calculations the effect of the temperature on the yield stress is considered.

The upper bound theorem is given by Equation (2.39)

$$\int_S P \, dU^c dS \leq \int_o^{\Delta t} \int_V [\sigma_{ij}^c(t) - \hat{\sigma}_{ij}^{\theta}(x,y,t)\dot{\varepsilon}_{ij} dt dV \qquad 4.1$$

where $\sigma_{ij}^c(t)$ is generally the yield stresses dependent on temperature and $\sigma_{ij}^{\theta}(x,t)$ is the maximum thermal stresses in the hoop direction, both corresponding to the plastic strain $\dot{\varepsilon}_{ij}^c$ at time "t" .

4.3.1 Temperature Independent Calculations

4.3.1.1 Applying the Upper Bound Theorem to the Mode of Deformation II

The mechanism of deformation and the stress history for this mode is shown in Fig. (4.6) in some more detail. The bound obtained by applying Equation (4.1) to this mechanism defines the loading points where axial increments of strain accumulate whilst the hoop strain is cancelled by yielding in tension and compression during the cycle. This bound coincides with the straight line BC (Fig. 4.3) given in [51].

The line equation is obtained as follows:

(a) The energy dissipation W_I is given by

$$\sigma_{ij}^c d\varepsilon_{ij}^c = \sigma_{ij}^{c_1} d\varepsilon_{ij}^{c_1} + \sigma_{ij}^{c_2} d\varepsilon_{ij}^{c_2} \qquad 4.2$$

where

$$\sigma_{ij}^{c_1} d\varepsilon_{ij}^{c_1} = \sigma_{ij}^{c_2} d\varepsilon_{ij}^{c_2} = \sigma_y \cdot \lambda \qquad 4.3$$

Thus

$$W_I = \int_V \sigma_{ij}^c d\varepsilon_{ij}^c dV = \int_o^{\Delta X} 2\,\sigma_y\,\lambda 2\pi R h dx = 4\pi R h \lambda \sigma_y \Delta X \qquad 4.4$$

b) The external work W_E due to $\hat{\sigma}_{ij}^{\theta}(x,t)$ is

$$\hat{\sigma}_{ij}^{\theta}(x,t)\ \dot{\varepsilon}_{ij}^c(t) = \hat{\sigma}_{ij}^{\theta}(x,t_1) d\varepsilon_{ij}^c(t_1) + \hat{\sigma}_{ij}^{\theta}(x,t_2) d\varepsilon_{ij}^c(t_2) \qquad 4.5$$

or

$$\hat{\sigma}_{ij}^{\theta}(x,t)\ \dot{\varepsilon}_{ij}^c(t) = \sigma_t \lambda + (-\sigma_t)\ (-\lambda) = 2\lambda\sigma_t \qquad 4.6$$

Thus

$$W_E = \int_o^{\Delta t} \int_V \hat{\sigma}_{ij}^{\theta}(x,t)\ \dot{\varepsilon}_{ij}(t) dt dV = \int_o^{\Delta X} 2\lambda\sigma_t 2\pi R h dx = 4\pi R h \lambda \sigma_t \Delta X \qquad 4.7$$

c) The external work due to the mechanical load

$$\int_S P\ dU^c dS = \pi R^2 P \lambda \Delta X \qquad 4.8$$

The equation for such a line can then be written

$$\frac{P}{P_L} = 2\left(1 - \frac{\sigma_t}{\sigma_y(\theta_R)}\right) \qquad 4.9$$

where P_L is defined as $P_L = 2\sigma_y h/R$.

4.3.1.2 Applying the Upper Bound Theorem to the Modified Mode of Deformation III

Consider a tube subjected to a stress history as indicated in Fig. (4.5) arising from the thermal axial load and cyclic loading shown in Figs. (4.1a,b) respectively. The upper bound theorem can then be applied to the inward three hinge mechanism (Fig. 4.5) which is a consequence of yielding occuring at the maximum temperature. Making use of the mechanism symmetry, the radial displacement can be described as

$$w = w_o\left(1 - \frac{x}{a}\right) \qquad 4.10$$

where w_o and a are defined in Fig. 4.5. The strains in the axial and circumferential directions can be defined by

$$d\varepsilon_\phi = \frac{w}{R} \quad ; \quad d\varepsilon_x = \frac{dU^c}{dx} \qquad 4.11$$

The axial and hoop strains can be determined from Equations (4.10), (4.11) and Fig. (4.5) to give

$$d\varepsilon_\phi = \frac{-w_o}{R}\left(1 - \frac{x}{a}\right) \qquad 4.12$$

and in addition

$$d\varepsilon_x = - d\varepsilon_\phi \qquad 4.13$$

The axial displacement needed for the left hand side of

Equation (4.1) can be calculated from the axial strain relation $d\varepsilon_x = du^c/dx$ so that

$$dU^c = \frac{w_o}{R}\left(1 - \frac{x}{a}\right) dx \qquad 4.14$$

Hence

$$\Delta u = \int_o^a dU^c = \int_o^a \frac{w_o}{R}\left(1 - \frac{x}{a}\right) dx = \frac{w_o}{R}\frac{a}{2} \qquad 4.15$$

All the terms in Equation (4.1) are now in a position to be calculated. The term on the left hand side is thus

$$\int_S P\, dU^c dS = F\, \Delta U^c = \pi R^2 P \frac{w_o}{R}\frac{a}{2} \qquad 4.16$$

The term involving σ_{ij}^c in (4.1) represents the energy dissipation and needs to be integrated within two different volumes; the hinges volumes and the volumes of the elements between hinges, so that

$$\int_V \sigma_{ij}^c d\varepsilon_{ij}^c dV = \int_{V_{Element}} \sigma_{ij}^c d\varepsilon_{ij}^c dV + \int_{V_{Hinge}} \sigma_{ij}^c d\varepsilon_{ij}^c dV \qquad 4.17$$

If the symmetry is to be taken into consideration, only half of the mechanism is needed for the calculations. Thus, the energy dissipation within the element becomes

$$\sigma_{ij}^c d\varepsilon_{ij}^c = \sigma_\phi\, \varepsilon_\phi^c + \sigma_x d\varepsilon_x^c \qquad 4.18$$

Substituting Equation (4.13) into (4.17) gives

$$\sigma_{ij}^c d\varepsilon_{ij}^c = (\sigma_x - \sigma_\phi) d\varepsilon_x^c \qquad 4.19$$

The first term on the right hand side of (4.17) then gives

$$\int_{V_{Element}} \sigma_{ij}^{c} d\varepsilon_{ij}^{c} dV = \int_{o_{Element}}^{a} \sigma_y \frac{w_o}{R} \left(1 - \frac{x}{a}\right) 2\pi R h dx = \pi h a w_o \sigma_y \qquad 4.20$$

The detailed calculation for the energy dissipation during the formation of a hinge, will be given in Appendix D. In this section only the final equation for such energy dissipation will be given which is

$$W_H = \frac{\sigma_y h^2}{4} 2\pi R\theta \qquad 4.21$$

where Θ is the curvature or rotation at the hinge, compatible with the mechanism. For the present symmetrical conical mechanism (Fig. 4.5), half of the total energy dissipation during the formation of the hinges is given by

$$\int_V \sigma_{ij}^{c} d\varepsilon_{ij}^{c} dV = \frac{\sigma_y}{4} 2\pi R \left(\frac{w_o}{a} + \frac{w_o}{a}\right) = \sigma_y h \pi R \frac{w_o}{a} \qquad 4.22$$

Similarly the integral involving the thermal cyclic load can be written as

$$\int_V \hat{\sigma}_{ij}^{\theta} d\varepsilon_{ij}^{c} dV = \int_o^{\Delta X/2} (-\sigma_t) \left[\frac{-w_o}{R} \left(1 - \frac{x}{a}\right)\right] 2\pi R h dx \qquad 4.23$$

since only the maximum cyclic hoop stress will be considered. Thus (4.23) becomes

$$\int_V \hat{\sigma}_{ij}^{\theta} d\varepsilon_{ij}^{c} dV = \sigma_t w_o 2\pi h \left(\frac{4a\Delta X - \Delta X^2}{8a}\right) \qquad 4.24$$

Substituting Equations (4.16),(4.20),(4.21) into (4.1) gives

$$\frac{PRa}{2} = \sigma_y h \frac{(a^2+Rh)}{a} - \sigma_t h \frac{(4a\Delta X - \Delta X^2)}{4a} \qquad 4.25$$

which in terms of non-dimensional parameters becomes

$$\frac{P}{P_L} = \frac{(a^2+Rh)}{a^2} - \frac{\sigma_t}{\sigma_y} \frac{(4a\Delta X - \Delta X^2)}{4a^2} \qquad 4.26$$

Taking the derivative of Equation (4.26) w.r.t. "a" and making it equal to zero, gives the size of the mechanism as a function of the travel length of the moving temperature front corresponding to a minimum P/P_L.

$$\frac{a}{x} = \frac{1}{2} + \frac{2Rh}{\Delta X} \frac{1}{\sigma_t/\sigma_y(\theta_R)} \qquad 4.27$$

Substituting Equation (4.27) into (4.26) gives Equation (4.28), which represents shakedown bounds as shown in Fig. (4.7), defining operating points where the inward mechanism would occur when the yield stress is assumed to be independent of the temperature.

$$\frac{P}{P_L} = 1 - \frac{\left[\left(\frac{\sqrt{Rh}}{\Delta X}\right)^2 + \frac{1}{4} \frac{\sigma_t}{\sigma_y(\theta_R)} \right]}{\left[\frac{1}{2} + 2 \left(\frac{\sqrt{Rh}}{\Delta X}\right)^2 \frac{1}{\sigma_t/\sigma_y(\theta_R)} \right]^2} \qquad 4.28$$

The contours obtained using Equation (4.27) are shown in

Fig. (4.7). Comparison with the contours presented by Karadeniz and Ponter [51] for the same problem, shows that despite the simplifications adopted for these calculations they are very close as shown in Fig. (4.8). The greatest difference seems to be in the region where Mode I of deformation was defined in [51] (Fig. 4.4), which was not considered in the present analysis.

4.3.2 Temperature Dependent Calculations

4.3.2.1 Mode of Deformation II

In order to include the effects of temperature on the yield stress of the material, the calculations were repeated using the yield stress values dependent upon the temperature given in Table 1-14.5 of Code N47 for the 316SS [53]. The calculations were then normalized in terms of the yield stress at a fixed temperature Θ_R = 150°C. The stress history for Mode II of deformation (Fig. 4.6) indicates that yielding occurs during the cycle, in tension and compression in the hoop direction and therefore cancelling each other. On the other hand a localized thinning due to the axial strain develops incrementally in each cycle. Taking into account the dependence of yield stress on the temperature for this stress history, the maximum stress which produces tensile yielding corresponds to the basic yield stress at 150°C whilst the minimum stress arises out of compressive yielding at a temperature of 150°C + $\Delta\Theta$ and the corresponding yield stress has to be considered. Applying

Equation (4.1) to the mechanism shown in Fig. 4.6 but taking into account different yield stresses for the two extremes of the cycle, gives

$$\frac{P}{P_L(\theta_R)} = 1 + \frac{\sigma_y(\theta_R+\Delta\theta)}{\sigma_y(\theta_R)} - 2\,\frac{\sigma_t}{\sigma_y(\theta_R)} \qquad 4.29$$

which again coincides with the bound found in [51]. The diagram with a complete classic shakedown boundary for temperature dependent yield stress is shown in Fig. (4.9).

4.3.2.2 Mode of Deformation III

Equation (4.28) was then adapted to include the variation of the yield stress with the temperature by normalizing it in terms of $\sigma_y(\theta_R)$ as follows: The left hand side in Equation (4.27) became

$$\frac{P}{P_L(\theta_R+\Delta\theta)} = \frac{\sigma_y(\theta_R)}{\sigma_y(\theta_R+\Delta\theta)}\;\frac{P}{P_L(\theta_R)} \qquad 4.30$$

and

$$\frac{\sigma_y}{\sigma_y(\theta_R+\Delta\theta)} = \frac{\sigma_t}{\sigma_y(\theta_R)}\;\frac{\sigma_t(\theta_R)}{\sigma_y(\theta_R+\Delta\theta)} \qquad 4.31$$

which gives

$$\frac{P}{P_L(\theta_R)} = \frac{\sigma_y(\theta_R+\Delta\theta)}{\sigma_y(\theta_R)}\left\{1 - \frac{\left(\frac{\sqrt{Rh}}{\Delta X}\right)^2 + \frac{1}{4}\,\frac{\sigma_t}{\sigma_y(\theta_R)}\,\frac{1}{\sigma_y(\theta_R+\Delta\theta)/\sigma_y(\theta_R)}}{\left[\frac{1}{2} + 2\left(\frac{\sqrt{Rh}}{\Delta X}\right)^2\,\frac{\sigma_y(\theta_R+\Delta\theta)/\sigma_y(\theta_R)}{\sigma_t/\sigma_y(\theta_R)}\right]^2}\right\} \qquad 4.32$$

and

$$\frac{a}{\Delta X} = \frac{1}{2} + 2\left(\frac{\sqrt{Rh}}{\Delta X}\right)^2 \frac{\sigma_y(\theta_R \mp \Delta\theta)/\sigma_y(\theta_R)}{\sigma_t/\sigma_y(\theta_R)} \qquad 4.33$$

Again, this more simplified technique was able to predict contours (Fig. 4.9) which were nearly coincident with those produced by a rigorous F.E. analysis in [51]. Such comparison is shown in Fig. (4.10).

4.4 Simplified Analysis of a Tube Subjected to Internal Pressure and Moving Temperature Fronts

In this section a thin cylindrical shell with closed ends will be analysed under the effect of constant internal pressure p and an axially moving temperature front identical to that in the previous cases. Again, in the first set of calculations the effects of temperature on material properties will be ignored. Despite the similarity with the axial loading case the present solution exhibits significant independent characteristics listed as follows:

- although region LO (Fig. 4.3) had been neglected in the axial load case due to the simplification of the axial stress history, in the present calculations mode I of deformation actually does not occur and therefore the possible modes of deformation are still the ones used in the previous cases.

- for the present case mode III(global mechanism) involves radial displacement and three hinges with no axial elongation and the symmetry is an actual fact not a simplification as in the case of the axial loading.

- in contrast to the yielding condition at the hot side of the cycle for the case of the axial load which gave rise to an inward mechanism, the internal pressure will produce yielding at maximum positive hoop stress and minimum temperature resulting in a outward mechanism.

Mode II of deformation is still valid here as a local yielding mechanism with axial strain increment taking place at the lower half cycle whilst the hoop strains sum to zero.

4.4.1 Temperature Independent Calculations

4.4.1.1 Mode II of Deformation

A similar procedure to the axial load case is used to determine the reversed plasticity bound(line BC in Fig. 4.12). For this case, however, reversed plasticity ie, yielding occuring at both extremes of the cycle, arises at a much higher thermal load. This difference in mode of response can perhaps be explained by the amount of energy dissipation required to reach such a state of deformation for each loading case. Equation (4.34) defines the reversed plasticity bound.

$$\frac{p}{p_L} = 4\left(1 - \frac{\sigma_t}{\sigma_y(\theta_R)}\right) \qquad 4.34$$

4.4.1.2 Mode III of Deformation(outward mechanism)

The mechanism of deformation and the stress history for the present case is shown in Fig. (4.11). Applying Equation (4.1) to this mechanism gives rise to the same Equation (4.28) with the difference that the limit mechanical load is now $pL = \sigma_y(\theta_R)h/R$. Hence the equation defining the shakedown bounds for the internal pressure is

$$\frac{p}{p_L} = 1 - \frac{\left[\left(\frac{\sqrt{Rh}}{\Delta X}\right)^2 + \frac{1}{4}\frac{\sigma_t}{\sigma_y(\theta_R)}\right]}{\left[\frac{1}{2} + 2\left(\frac{\sqrt{Rh}}{\Delta X}\right)^2 \cdot \frac{1}{\sigma_t/\sigma_y(\theta_R)}\right]^2} \qquad 4.35$$

The resulting diagram with shakedown bounds for a range of values of travel length is shown in Fig. (4.12).

4.4.2 Temperature Dependent Calculations

4.4.2.1 Mode II of Deformation

The same procedure as in Section 4.3.2.2 can be applied here to find the reversed plasticity bound equation (line BC in Fig. 4.13) which gives

$$\frac{p}{p_L} = 2\left[1 + \frac{\sigma_y(\sigma_R+\Delta\theta)}{\sigma_y(\theta_R)} - 2\frac{\sigma_t}{\sigma_y(\theta_R)}\right] \qquad 4.36$$

In contrast to the hinge-conical mechanism (mode III) the localized thinning type of mechanism is very much dependent upon the effects of temperature on the yield stress as shown in Fig. (4.13).

4.4.2.2 Mode III of Deformation

As previously stated the internal pressure will give rise to yielding at the basic temperature θ_R due to maximum hoop stresses which makes this mode of deformation independent of the variation of the temperature. Consequently, Equation (4.35) is still valid to define the shakedown limits shown in Fig. 4.13.

4.5 Simplified Analysis of a Tube Subjected to Axial Load, Internal Pressure and Moving Temperature Fronts

To the author's knowledge there has been no attempt to analyse thermal loading problems in the presence of more than one mechanical load, although the papers by Leckie and Penny [5,8] present a simple graphical technique, using the lower bound theorem to solve the problem of multiple mechanical loading applied to pressure vessels. As emphasized by Leckie [13] the application of the lower bound theorem when two or more variable loads are acting on the shell is excessively complicated even when the problem involves only mechanical loads. Simple techniques like that suggested in [13] have great appeal for the design of

pressure vessels since they avoid complex calculations and the cost associated with them and also allow more complex problems to be tackled while still providing a high level of confidence in the integrity of the structure.

For the particular case of fast nuclear reactor components, the primary or mechanical loads are normally internal pressure and dead weight which, so far, have been considered individually in the solution of particular thermal cyclic problems for such components. Several papers have been published [39,40,41,51,55] where the internal pressure is taken as the primary load which could be in practice due to the release of gaseous fission products as pointed out by Bree [40]. On the other hand, the problem of dead weight acting as primary load has also been the subject of study by several authors [49,51,54,55] in search of better design techniques for fast-reactor components. Arnaudeau [49], for example, assumes the self-weight of the vessel, which is always present, as an axial load, whilst Goodman [54] considers the weight of the fluids sustained by the vessel which could be assumed to produce internal pressure as well. Independent of the agent responsible for causing the primary loads, it is very likely in practice that during the life-time of the vessel more than one mechanical load will be present most of the time.

The simplicity of the technique applied in the previous sections and the fact that the results obtained from it compare closely with those presented by Karadeniz and Ponter [51], as shown in Figs. 4.8 and 4.10, provided the necessary

encouragement to carry on with the study of the moving temperature fronts in a tube in the presence of both internal pressure and axial load.

The problem now involves a system of three loads and if a Bree type diagram is to be plotted it will be a three dimensional one as shown in Fig. 4.14 for a temperature independent yield stress. Obviously many more bounds have to be determined to define the limits for the different modes of behaviour which can be described as follows from Fig. 4.14:

- elastic limit; defined by planes AGFH and AEH

- plastic collapse due to axial load alone; defined as point E

- plastic collapse due to the internal pressure; defined as line GF

- plastic collapse due to the combination of the two mechanical loads in the absence of thermal load; defined as line FE

- plastic collapse due to the combination of the two mechanical loads in the presence of thermal load below the ratchetting limit; defined as plane FEMJ

- incremental collapse (shakedown limit) for a particular travel length($\overline{\Delta X} = 2.1$) of the temperature

front; defined as surface KGFJ; the incremental collapse mechanism for an operating point at surface KGFJ is the outward conical-hinge mechanism

- incremental collapse (shakedown limit) for the same travel length($\overline{\Delta X}$ = 2.1) of the temperature front referred above; defined as surface LEM; the incremental collapse mechanism for an operating point at surface LEM is the inward conical-hinge mechanism

- reversed plasticity limit; defined as plane ABCD; for the same particular travel length ($\overline{\Delta X}$ = 2.1) of the temperature front related to the shakedown limit above, the reversed plasticity limit is confined to the area AKJML of the plane ABCD

When the effects of the temperature on the yield stress is taken into account, a similar diagram may be plotted by normalizing the three coordinates in terms of the yield stress $\sigma_y(\Theta_R)$ corresponding to a fixed temperature Θ_R= 150°C as in the previous cases. Fig. 4.15 shows the Bree type diagram produced when the temperature dependent yield stress is included in the calculations. Details of this diagram will be discussed in Section 4.5.3.

4.5.1 Temperature Independent Calculations

4.5.1.1 Inward Mechanism for a Predominant Axial Load

The inward mechanism formed due to the current mechanical loads and the respective stress history are shown in Fig. 4.5. Applying Equation (4.1) to such mechanism considering the internal pressure and the axial load acting simultaneously with the thermal cyclic load gives

$$\frac{P}{P_L(\theta_R)} = \left\{ 1 - \frac{\left[\left(\frac{\sqrt{Rh}}{\Delta X}\right)^2 + \frac{1}{4}\frac{\sigma_t}{\sigma_y(\theta_R)} \right]}{\left[\frac{1}{2} + 2\left(\frac{\sqrt{Rh}}{\Delta X}\right)^2 \frac{1}{\sigma_t/\sigma_y(\theta_R)} \right]^2} \right\} + \frac{1}{2}\frac{p}{p_L} \qquad 4.37$$

Equation (4.37) represents the equation of a surface which depends on the travel length of the temperature front. One of such surfaces for a particular travel length ($\overline{\Delta X}$ = 2.1) is illustrated as LEM in Fig. 4.14. The intersection of this surface with the plane ABCD defines one of the bounds of the confined reversed plasticity region shown as curve LM for this particular travel length.

4.5.1.2 Outward Mechanism for a Predominant Internal Pressure

Similarly, Equation (4.1) can be applied again assuming the ratchetting mechanism and the stress history shown in Fig. 4.11. As can be seen from Fig. 4.11, the axial load makes no contribution to the formation of the outward mechanism. As a result the upper bound theorem (Equation (4.1)) gives rise to the same Equation (4.35) as that obtained in Section 4.4.1.1 which is independent of the axial load.

Equation (4.35) represents in this case a surface perpendicular to the plane ABGO in Fig. (4.14) which depends upon the travel length and defines the boundary of the shakedown region for an outward mechanism. The curve KJ shown in Fig. (4.14) defines the intersection between this surface and the plane ABCD which is the other bound of the reversed plasticity boundary for the travel length value $\overline{\Delta X}$ = 2.1. Similar curves to KJ and LM can be obtained for different values of the travel length.

4.5.1.3 Reversed Plasticity Mechanism

When two mechanical loads are considered in the application of the upper bound theorem (Equation (4.1)) to the localized thinning mechanisms such as those described in previous sections, the resulting bound is a plane which for the particular case of internal pressure and axial load is given by

$$\frac{1}{2}\frac{P}{P_L} + \frac{1}{4}\frac{p}{p_L} + \frac{\sigma_t}{\sigma_y} = 1 \qquad 4.38$$

Such a plane defined in Fig. 4.14 as ABCD is limited by the planes BCFG, CDFE and ADEO representing the different combinations of the mechanical loads capable of causing plastic collapse alone, ie, independent of the thermal stress. However, when a moving temperature front along any travel length is considered, the reversed plasticity region is reduced to a sector of the plane ABCD similar to that defined as AKJML in Fig. 4.14 for the particular value of ΔX

= 2.1. Sector AKJML is limited by the intersection of the plane ABCD with the two surfaces representing the shakedown bounds corresponding to any travel length for the two possible incremental collapse mechanisms.

4.5.2 A Bi-Dimensional Representation of the Tri-Dimensional Bree Type Diagram

The tri-dimensional diagram provides a global picture of the several bounds separating the regions of modes of deformation and allows the plotting of results for various travel lengths if necessary. However, the actual plotting of the results can be tedious, even though it can be programmed to be plotted by computer. For design purposes a bi-dimensional diagram representing the projection of the bounds for various modes of behaviour on the plane positive quadrant defined by the mechanical loads axes P/P_L and p/pL is much more convenient. As it will be shown later in this section, for simplicity, it is better to plot one of such diagrams for each different travel length making possible an easy comparison between two or more diagrams.

A better understanding of the bi-dimensional diagram can be provided by a detailed analysis of such a diagram for the particular value of travel length $\overline{\Delta X}$ = 2.1 as shown in Fig. (4.16).

The possible modes of deformation can be described as follows from Fig. (4.16):

- the region marked as LEM defines where the axial load predominates and the inward mechanism is due to occur depending on the level of thermal load. Line NP, and the lines parallel to it, are the projections on the plane of the diagram of points on the shakedown boundary corresponding to constant normalized thermal stresses. Any point on line NP, for example, corresponds to a point on the shakedown boundary at a normalized stress $\sigma_t/\sigma_y = 0.70$. Any increase in the thermal stress for that particular combination of mechanical loads defined by line NP will give rise to an incremental collapse with the formation of a inward cone-hinge mechanism.

- the region marked as ALMJK is the reversed plasticity region. Line PQ across this region represents the projection of the points on the reversed plasticity boundary at the same level of normalized thermal stress $\sigma_t/\sigma_y = 0.70$. A net of axial deformation will result if the thermal stress is increased for the points on line PQ. The lines parallel to PQ correspond also to projections of points on the reversed plasticity boundary but at different levels of thermal stress.

- for mechanical loading points described by line AI, ie, $P/P_L = 1.5\ p/p_L$ the only possible mode of deformation is the localized axial thinning at the reversed plasticity limit. In this case the tube will respond elastically for any thermal stress below that

limit and no shakedown region exists. Line AI also defines the regions where one of the mechanical loads becomes predominant, ie, region AIE for the axial load and AIFG for the internal pressure

- the region marked as KJCB is where internal pressure predominates and the inward mechanism occurs. Line QR at the normalized thermal stress $\sigma_t/\sigma_y = 0.70$ and the other lines parallel to it represent the projection of the shakedown boundary for the outward incremental mechanism at different levels of thermal stress. As has already been pointed out, this mode of behaviour is independent of the axial load which can be seen by the lines projections of the boundary parallel to the axis P/P_L.

- the lines DC and CB are the bounds for the plastic collapse caused by the combination of the mehanical loads alone, ie, without any thermal load.

A sequence of Bree type diagrams are shown in Fig. (4.17) for several values of $\overline{\Delta X}$ which illustrate the way the bounds change with the length of travel. By comparing the various diagrams it can be seen that the bounds are much more sensitive to the length of short travels resulting in great reduction of the reversed plasticity region for a small increase in the travel length. In other words, a small increase in the length of a short travel causes a considerable reduction of the mechanical loads at the shakedown limit. For large movements of the temperature

front the two regions where hinge-conical mechanisms can occur tend to close-in towards line AI eliminating the reversed plasticity region. This can be better visualized from Fig. 4.14 where the shakedown limit surfaces tend to flatten towards the elastic limit planes for large movements of the temperature front, eliminating in this way not only the reversed plasticity region but, most importantly, the shakedown region as well.

4.5.3 Temperature Dependent Calculations

4.5.3.1 Inward Mechanism for a Predominant Axial Load

A similar procedure as used in earlier sections will give rise to the equation of a new shakedown limit surface which includes the effects of the temperature on the yield stress. The basic temperature was again taken as 150°C and the resulting equation for such a surface is given by

$$\frac{P}{P_L(\theta_R)} = \frac{\sigma_y(\theta_R+\Delta\theta)}{\sigma_y(\theta_R)} \left\{ 1 - \frac{\left(\frac{\sqrt{Rh}}{\Delta X}\right)^2 + \frac{1}{4}\,\frac{\sigma_y}{\sigma_y(\theta_R)}\,\frac{1}{\sigma_y(\theta_R+\Delta\theta)/\sigma_y(\theta_R)}}{\left[\frac{1}{2} + 2\left(\frac{\sqrt{Rh}}{\Delta X}\right)^2 \frac{\sigma_y(\theta_R+\Delta\theta)/\sigma_y(\theta_R)}{\sigma_t/\sigma_y(\theta_R)}\right]^2} \right\} + \frac{1}{2}\,\frac{p}{p_L(\theta_R)} \qquad 4.39$$

For the travel length $\overline{\Delta X} = 2.1$, Equation (4.39) gives rise to the surface L'E'M' shown in Fig. 4.15 which intersects the plane A'B'C'D' through the curve L'M'. The planes

C'D'E'F' and B'C'F'G', which define the bounds for plastic collapse due to the mechanical loads alone, are no longer independent of the thermal stress, ie, parallel to thermal load axis. Instead of being perpendicular to the positive quadrant limited by the mechanical loads axes, they now form an angle with it due to the effects of the temperature on the yield stress (Fig. 4.15).

4.5.3.2 Outward Mechanism for a Predominant Internal Pressure

As has been already stated the outward mechanism occurs for the maximum positive circumferential stress at the cold side of the temperature front which is at the basic temperature Θ_R = 150°C. As a result Equation (4.35), independent of the effects of the temperature on the yield stress and of the axial load, defining the shakedown limit surface perpendicular to the plane A'B'G'O', is still valid here.

The intersection of this surface with the plane A'B'C'D' for the travel length $\overline{\Delta X}$ = 2.1 is shown as curve K'J' in Fig. (4.15).

4.5.3.3 Reversed Plasticity Mechanism

The resulting bound from the application of the upper bound theorem to such a mode of deformation when the temperature dependent yield stress is taken into account is the plane

shown as A'B'C'D' in Fig. (4.15) given by the following equation

$$\frac{P}{P_L(\theta_R)} = 1 + \frac{\bar{\sigma}_y(\theta_R+\Delta\theta)}{\sigma_y(\theta_R)} - 2\,\frac{\sigma_t}{\sigma_y(\theta_R)} - \frac{1}{2}\,\frac{p}{p_L(\theta_R)} \qquad 4.40$$

As in the previous case, this plane is intersected by the shakedown limit surfaces corresponding to any travel length of the temperature front through curves like those shown in Fig. (4.15) as K'J' and L'M' for the particular travel length $\overline{\Delta X} = 2.1$. These intersections will occur at a much lower level of thermal stress since the reversed plasticity plane in Fig. (4.15) has substantially moved downwards due to the effects of the temperature on the yield stress. The consequences of this change in the reversed plasticity bound will be discussed in the next section.

4.5.4 A Bi-Dimensional Bree Type Diagram for the Temperature Dependent Yield Stress

Following similar procedures as those presented in Section 4.5.2, a detailed description of the bi-dimensional Bree type diagram will again provide a better understanding of several important features of the results. Fig. (4.18) shows such a diagram for a temperature dependent yield stress corresponding to the travel length $\overline{\Delta X} = 2.1$.

The diagram shown in Fig. (4.18) exhibits many similar features to those presented in the temperature independent case. Therefore, only the significant differences will be described here as follows:

- the shakedown limit region for the inward mechanism has substantially increased at the cost of a reduction of the reversed plasticity region.

- the projections of the points defined by the intersection of the shakedown limit surfaces with the plane C'D'E'F' (Fig. 4.15), bound of the plastic collapse due to the mechanical loads alone, at different levels of thermal loads, will no longer coincide with line E'F' at zero thermal stress. This is due to the dependence of the mode of deformation represented by the plane C'D'E'F' on the thermal stress. The projections of those points on the present diagram (Fig. 4.18) are now shown as curves E'M' and F'J'.

- in contrast with the inward mechanism, the outward mechanism will have its shakedown region reduced in favour of a much larger reversed plasticity area. The curved bound K'J' which separates the regions of these two modes of deformation has moved inside the outward mechanism region due to the effects of the temperature on the yield stress whilst the shakedown surface bound has remained unchanged.

From Fig. 4.18 it can be concluded that the dependence of the yield stress on the temperature gives rise to a reduction of the reversed plasticity region where the axial load is predominant, whilst the opposite takes place in the region where the internal pressure imposes the formation of an outward hinge-cone mechanism. When a sequence of diagrams for a number of travel length values (Fig. 4.19) is plotted in order to show how sensitive to the length of the travel the various bounds are, a very similar pattern of behaviour to those for the temperature independent yield stress is obtained. This set of solutions, however, shows that for a prevailing axial load and large values of $\overline{\Delta X}$ the reversed plasticity region is reduced to such extent that incremental deformation in the form of inward mechanism starts taking place even for zero applied loads. At the limit, the sector of the reversed plasticity region corresponding to the inward mechanism (A'L'M'H'in Figs. 4.15 and 4.18) disappears completely as shown in Fig. (4.19).

The inclusion of temperature dependence of yield stress in the analysis leads to incremental deformation at much lower combinations of mechanical and thermal loads. Furthermore ratchetting in the form of inward conical mechanism of deformation prevails upon the localized thinning mechanism for it requires less energy dissipation to occur.

A considerably different situation from one where the axial load is predominant can be seen for the outward mechanism region which is reduced due to the increase of the reversed plasticity region under the influence of the yield stress

temperature dependence. In addition, ratchetting occurs at the same combinations of mechanical and thermal loads.

4.6 Conclusions

The assumption of simple mechanisms and a simplified analysis has been able to predict the same behaviour of a tube under rather complex loading conditions, as the solution produced by a rigorous Finite Element analysis. Further, the solution could be extended to include more than one mechanical load in the analysis which in practice is more likely to occur. Such simplified techniques provides also a better picture of the structural and material behaviours when compared with those solutions obtained by a step by step analysis.

FIG.4.1 (a) THE TUBE GEOMETRY

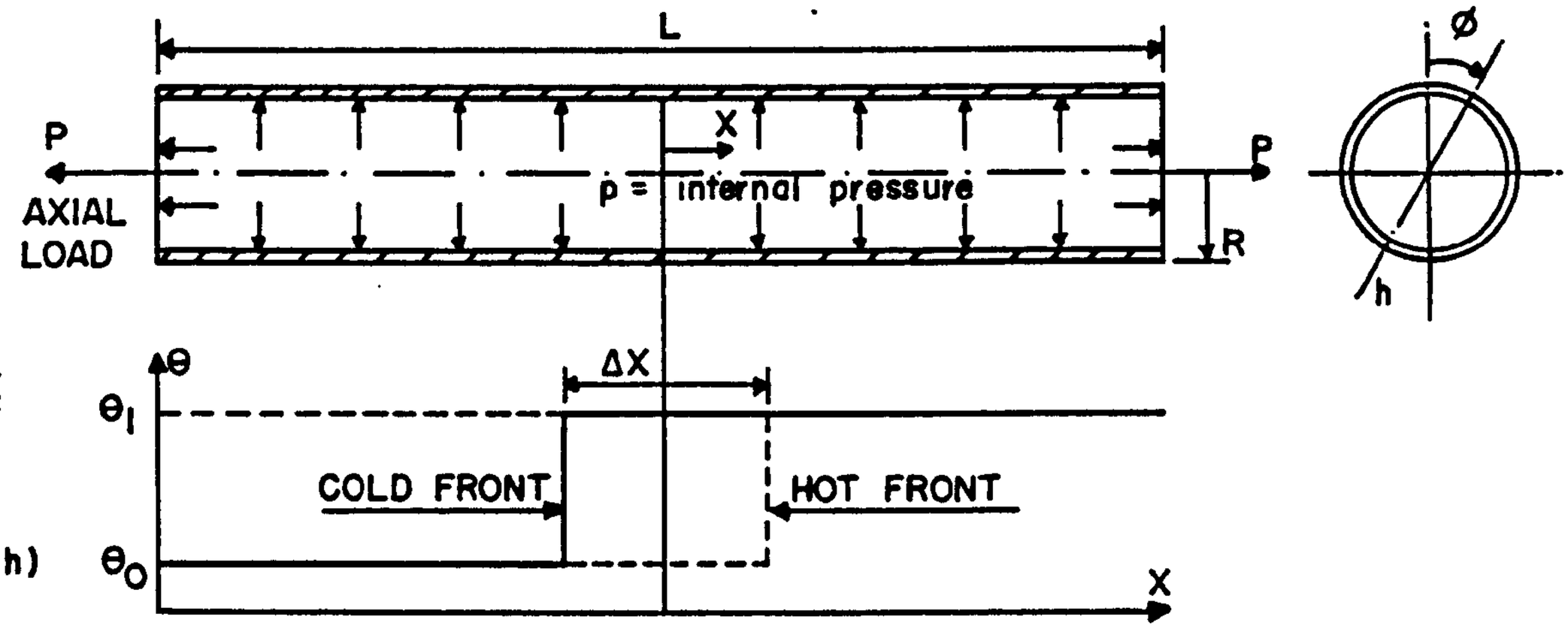

FIG.4.1 (b) THE THERMAL LOAD

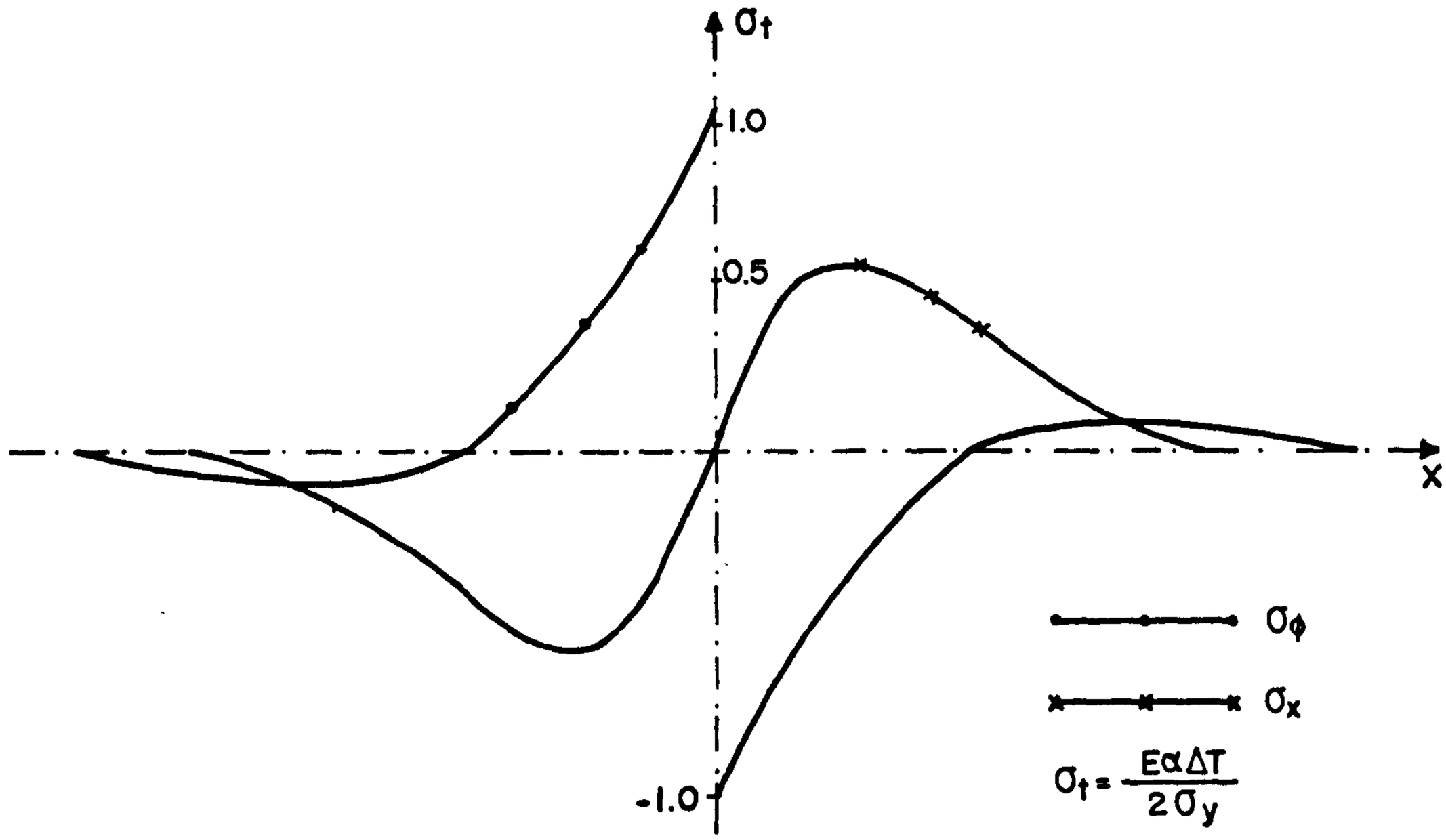

Fig. 4.2a- ELASTIC THERMAL STRESS DISTRIBUTION FOR A TUBE SUBJECTED TO A STEP CHANGE IN TEMPERATURE $\Delta\theta$ [51]

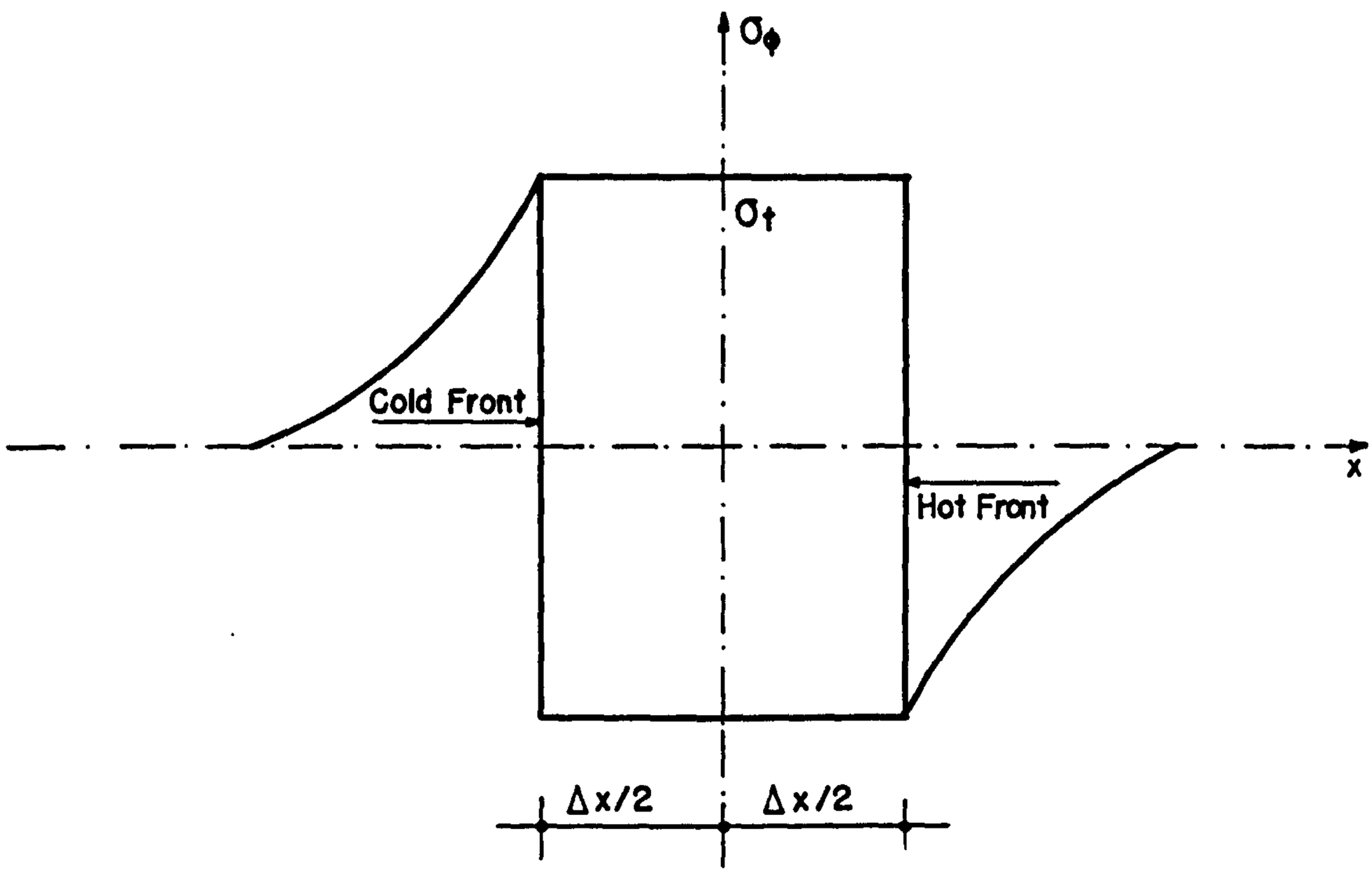

Fig. 4.2(b) SIMPLIFIED HOOP STRESS ASSUMED

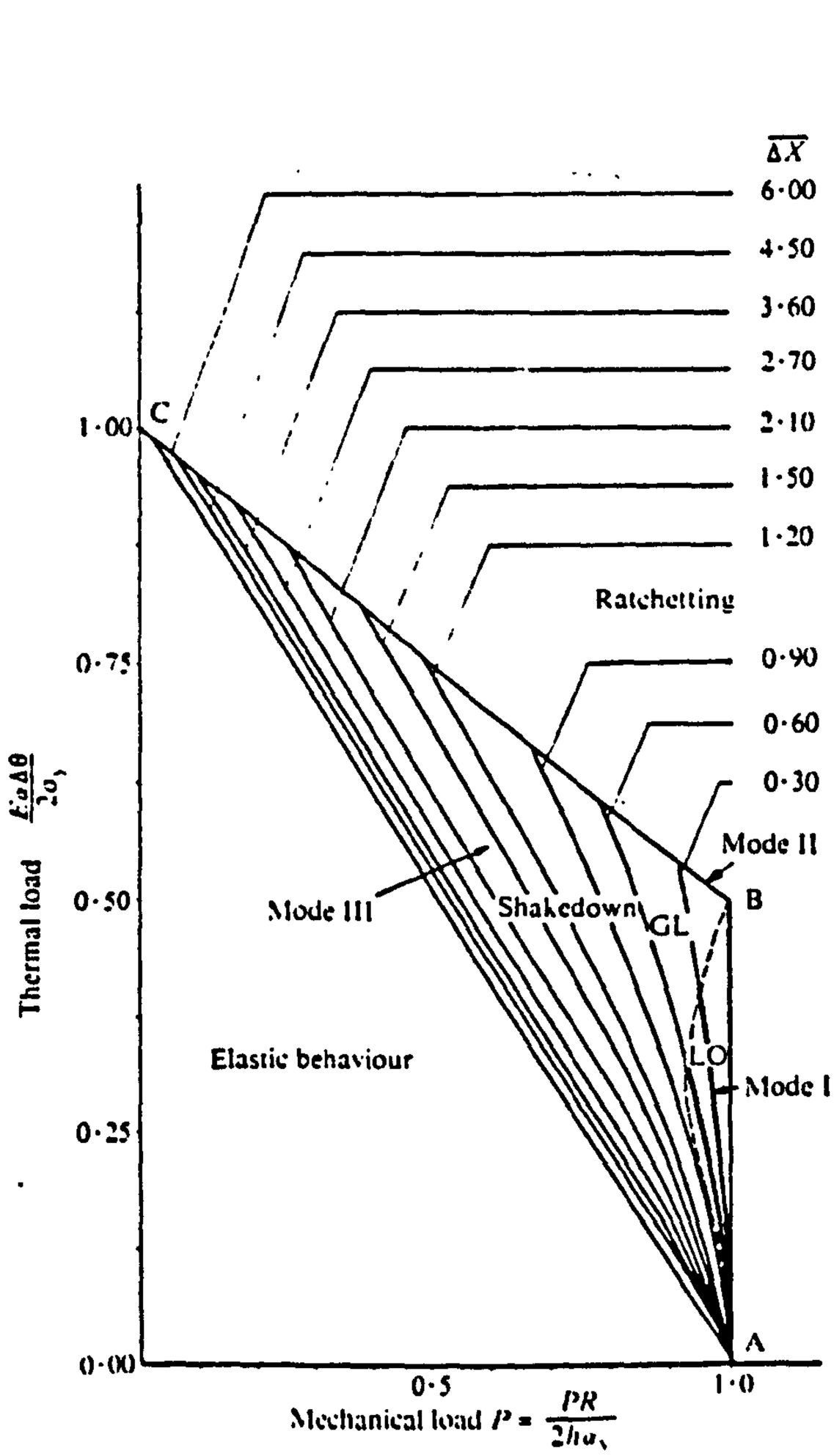

Fig 4·3 Bree type diagram for a tube subjected to a steady axial mechanical load and moving temperature fronts [51]

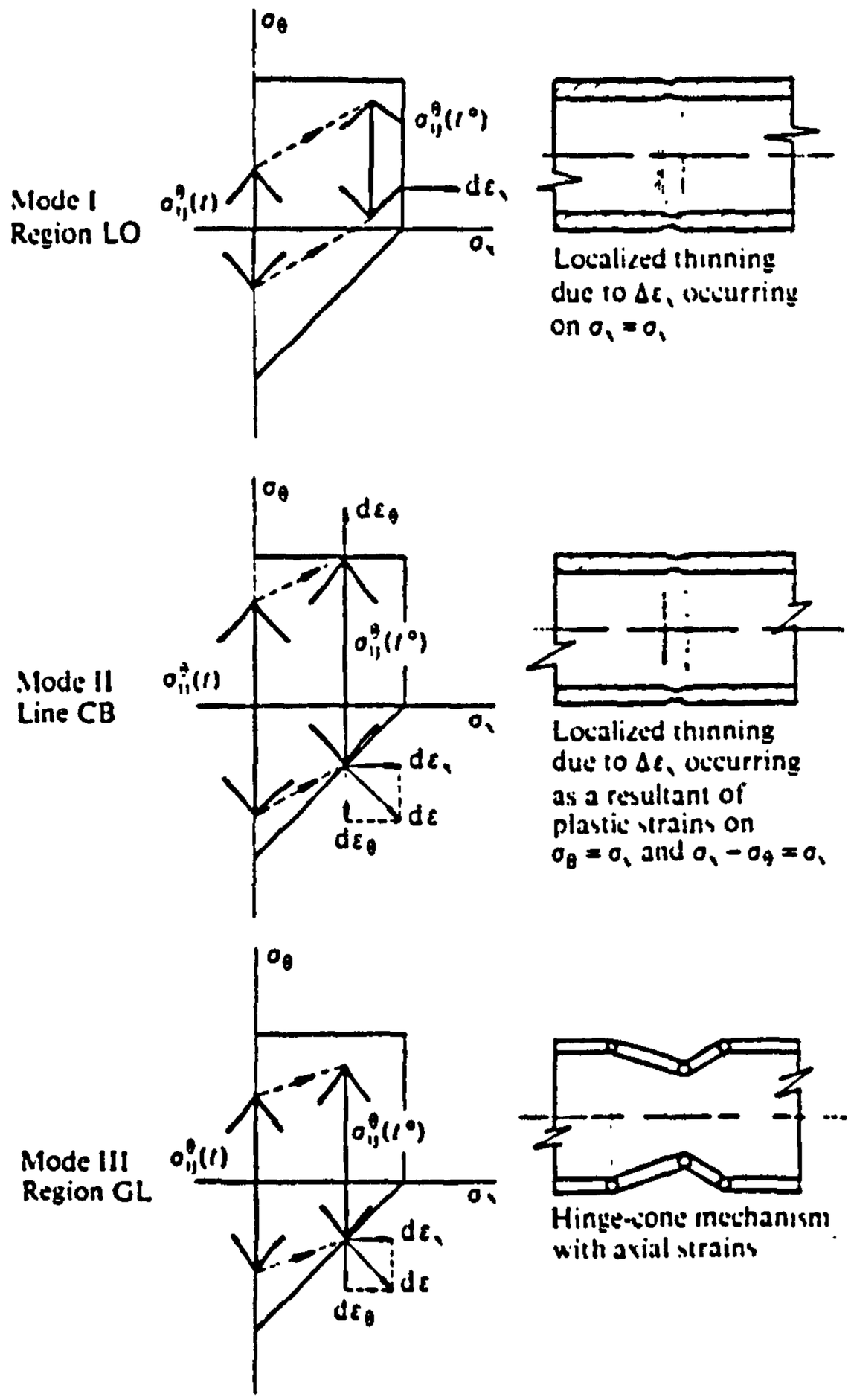

Fig 4·4 Schematic representation of shakedown states and corresponding mechanisms of deformation for a tube subjected to a steady axial mechanical load and axially moving temperature fronts for regions of Fig. 4·3 [51]

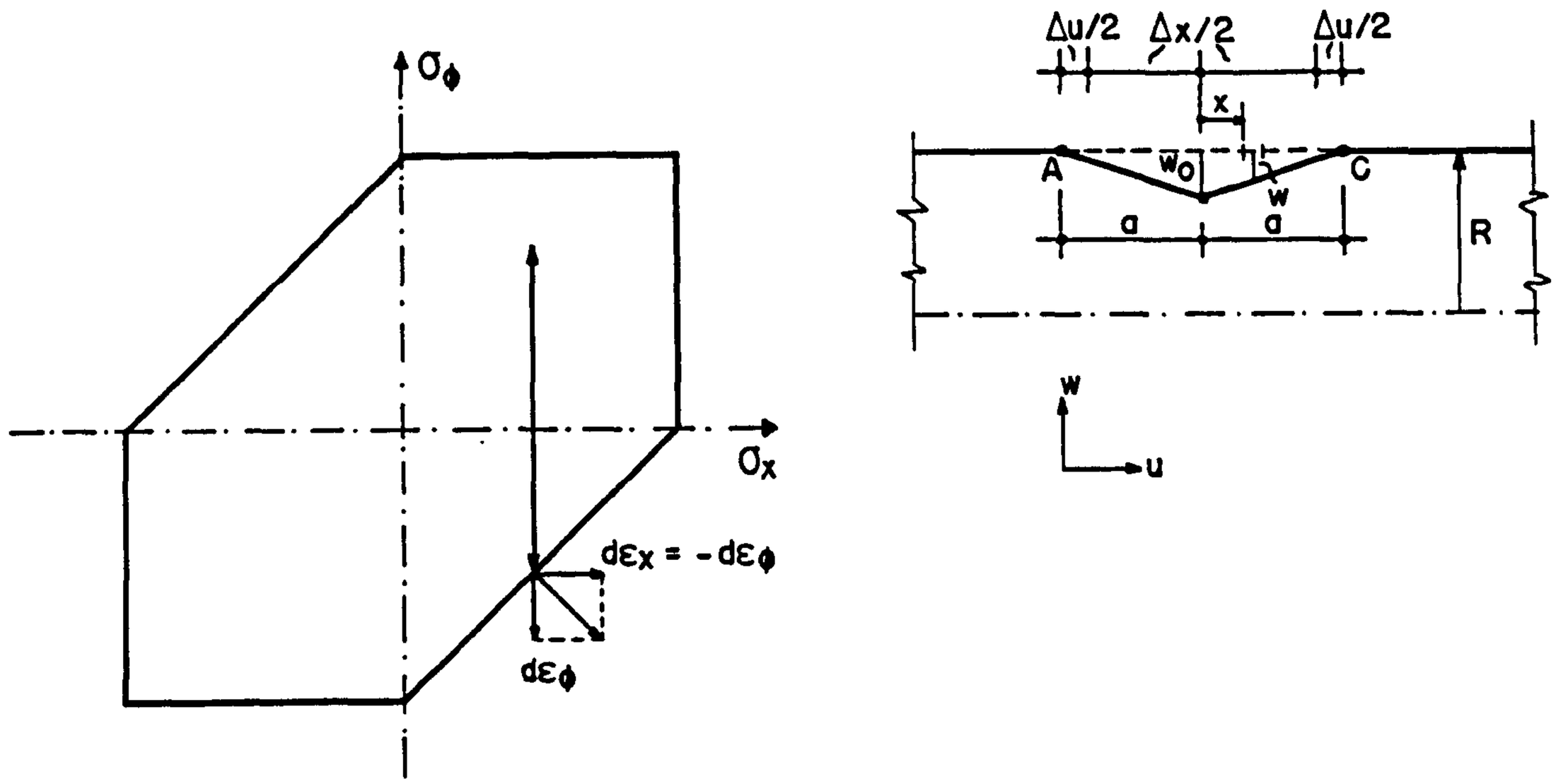

Fig. 4.5- SHAKEDOWN STATE OF STRESS AND CORRESPONDING MECHANISM OF DEFORMATION FOR MOVING TEMPERATURE FRONTS IN THE PRESENCE OF AXIAL LOAD

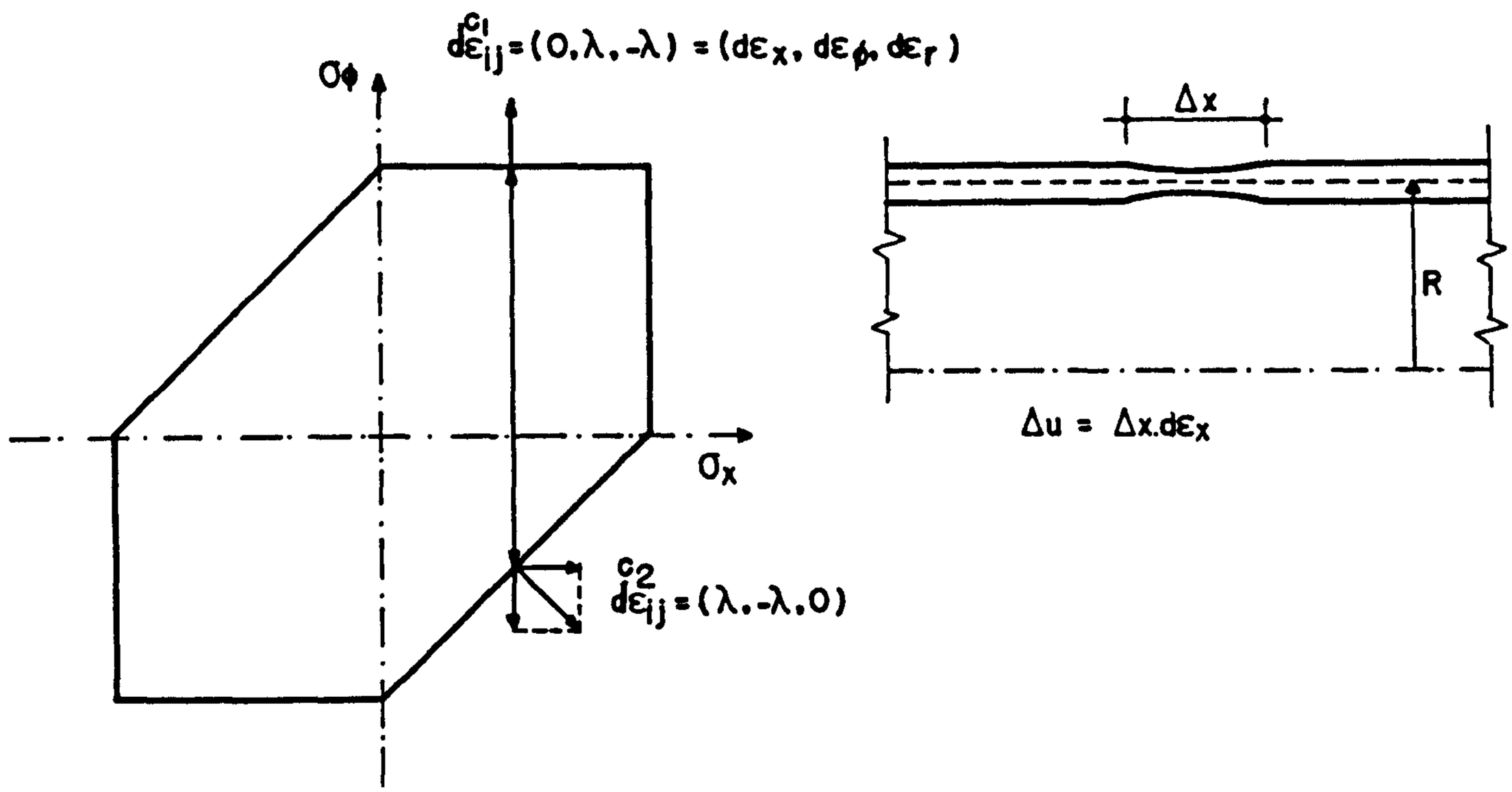

Fig. 4.6- REVERSED PLASTICITY STATE OF STRESS AND CORRESPONDING MECHANISM OF DEFORMATION FOR MOVING TEMPERATURE FRONT IN THE PRESENCE OF MECHANICAL LOAD

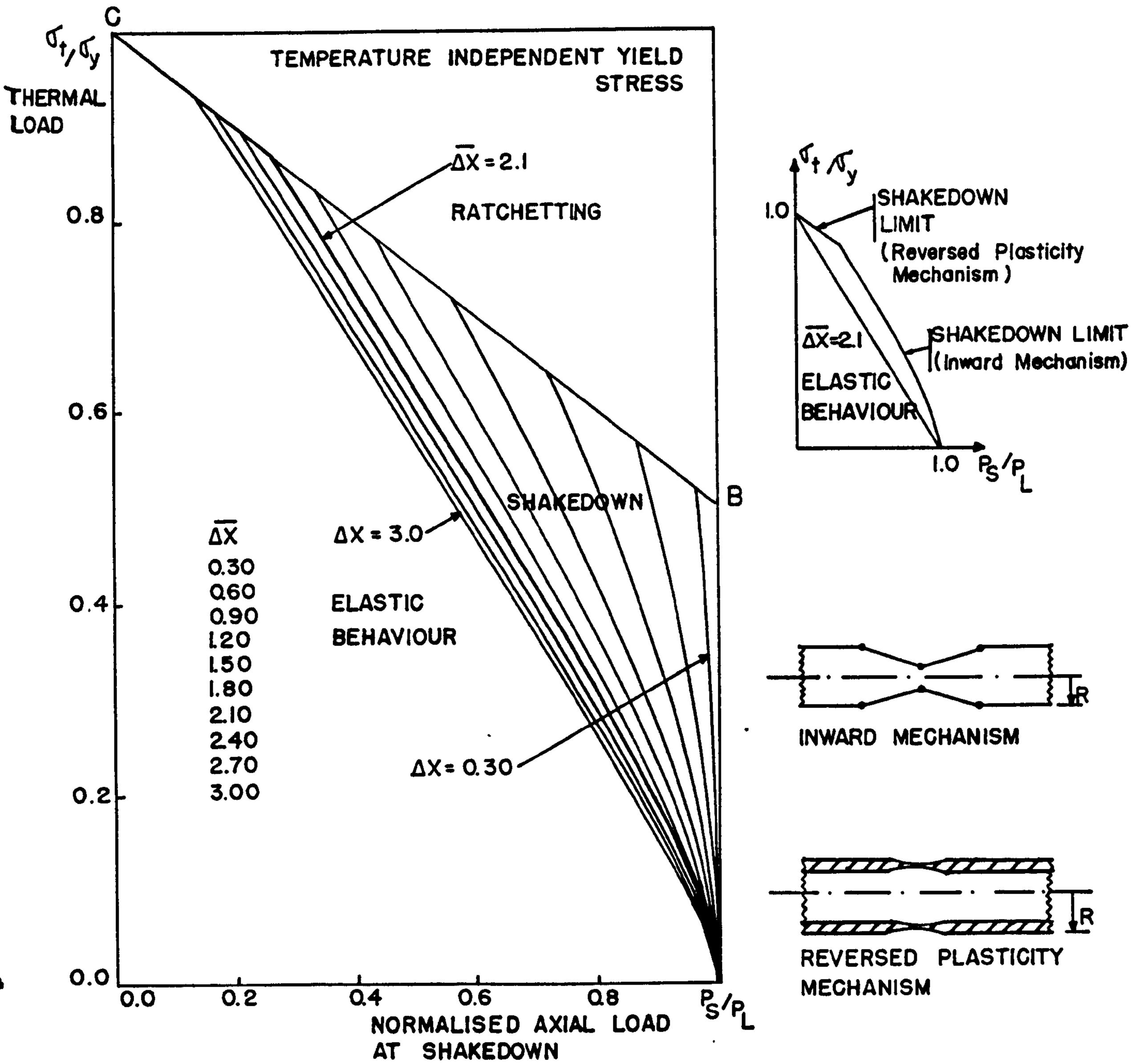

FIG.4.7 - BREE TYPE DIAGRAM FOR A TUBE SUBJECTED TO A STEADY AXIAL LOAD AND MOVING TEMPERATURE FRONT

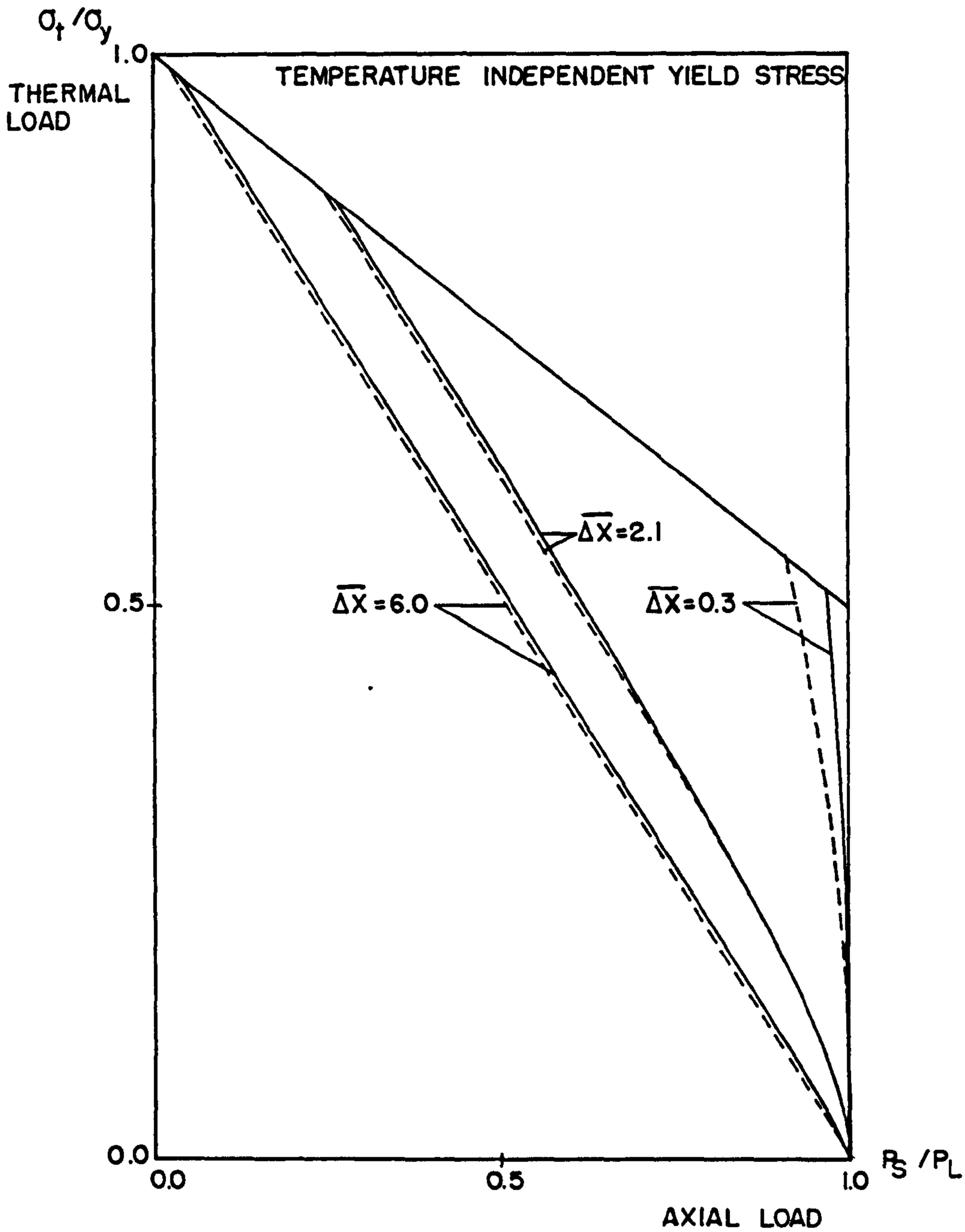

Fig. 4.8- DIRECT COMPARISON WITH THE RESULTS OBTAINED IN [51] FOR PARTICULAR TRAVEL LENGTHS OF THE TEMPERATURE FRONT

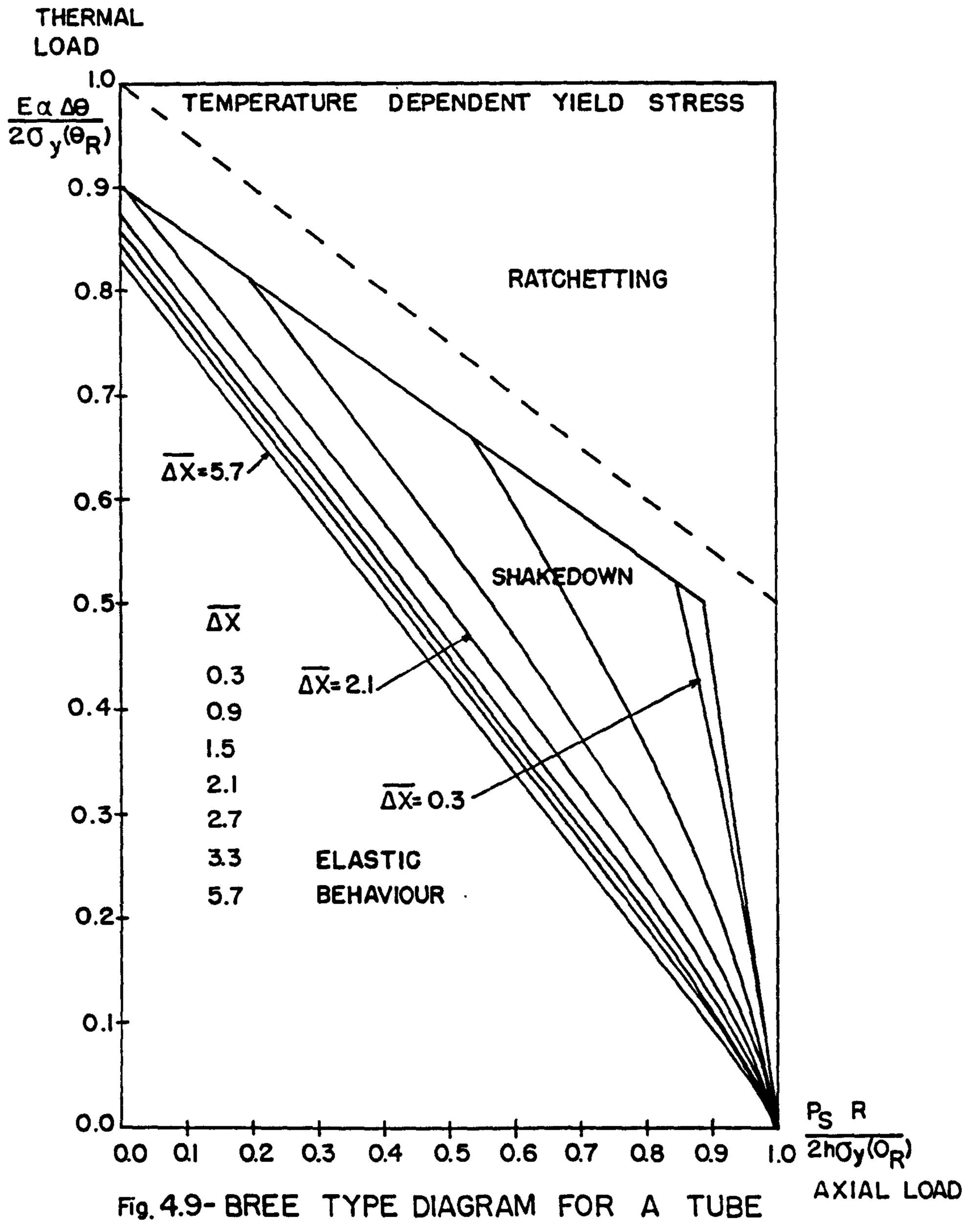

Fig. 4.9- BREE TYPE DIAGRAM FOR A TUBE SUBJECTED TO A STEADY AXIAL LOAD AND MOVING TEMPERATURE FRONT

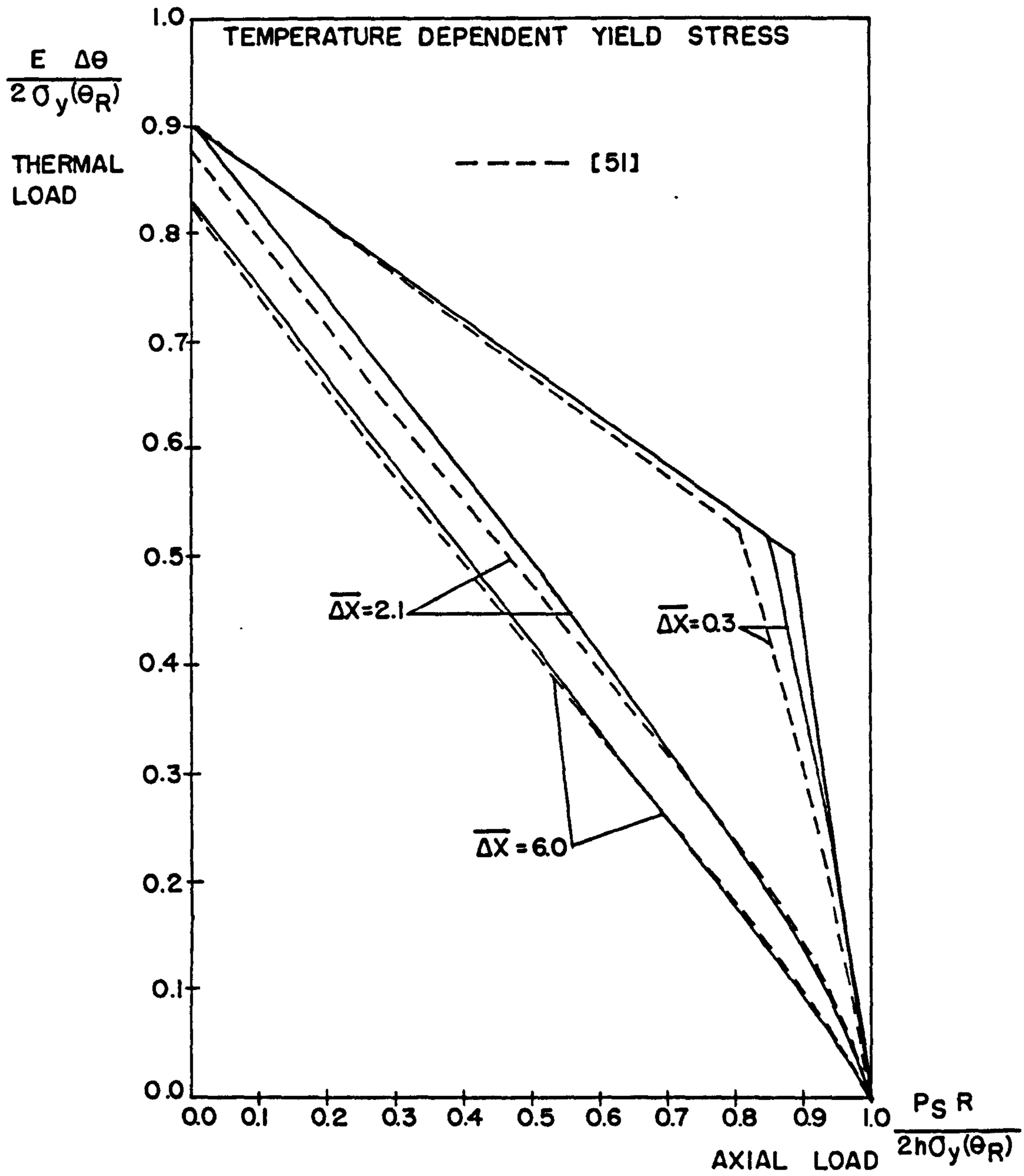

Fig. 4.10- DIRECT COMPARISON WITH THE RESULTS OBTAINED IN [51] FOR PARTICULAR TRAVEL LENGTHS OF THE TEMPERATURE FRONT

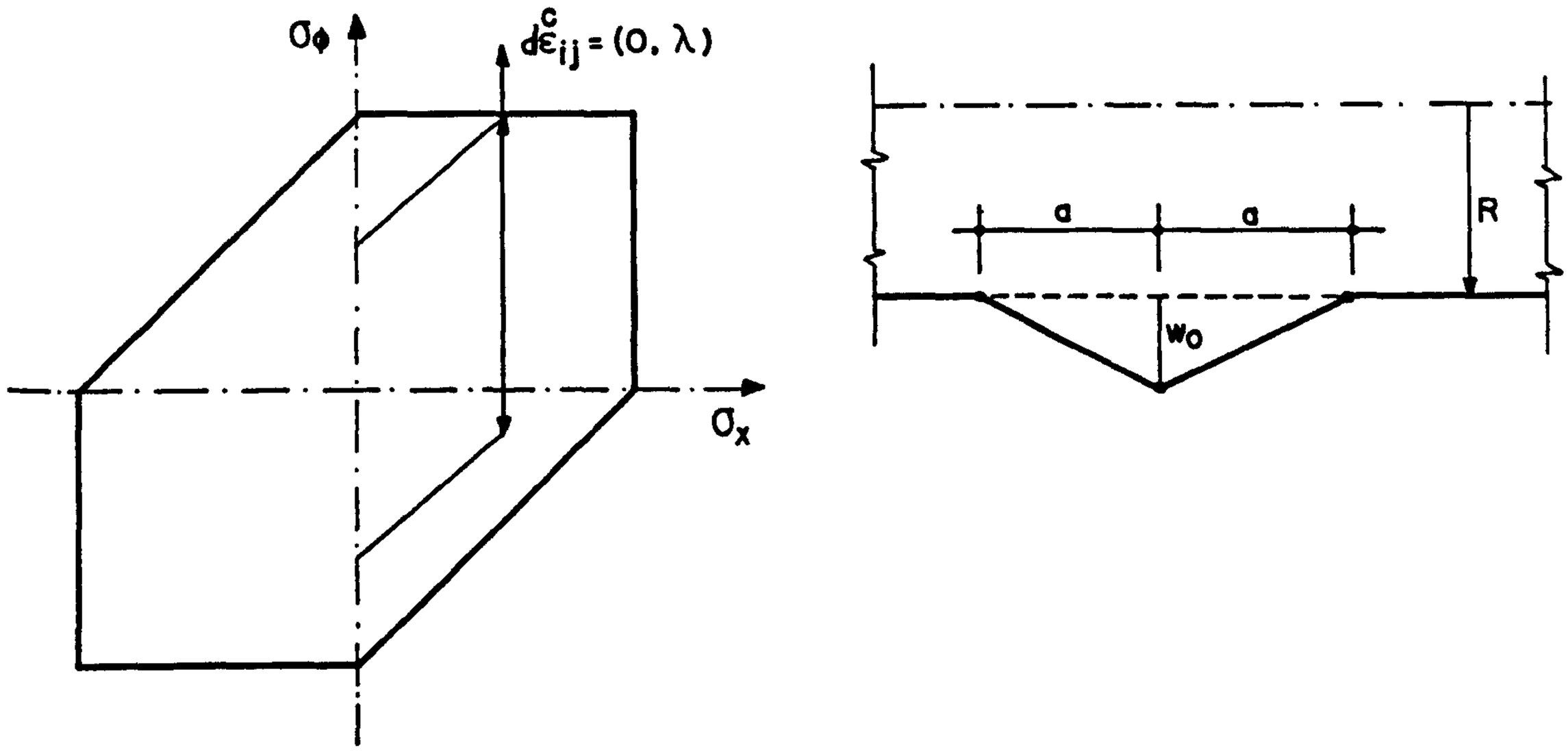

Fig. 4.11- SHAKEDOWN STATE AND CORRESPONDING MECHANISM OF DEFORMATION FOR THE MOVING TEMPERATURE FRONT IN THE PRESENCE OF INTERNAL PRESSURE

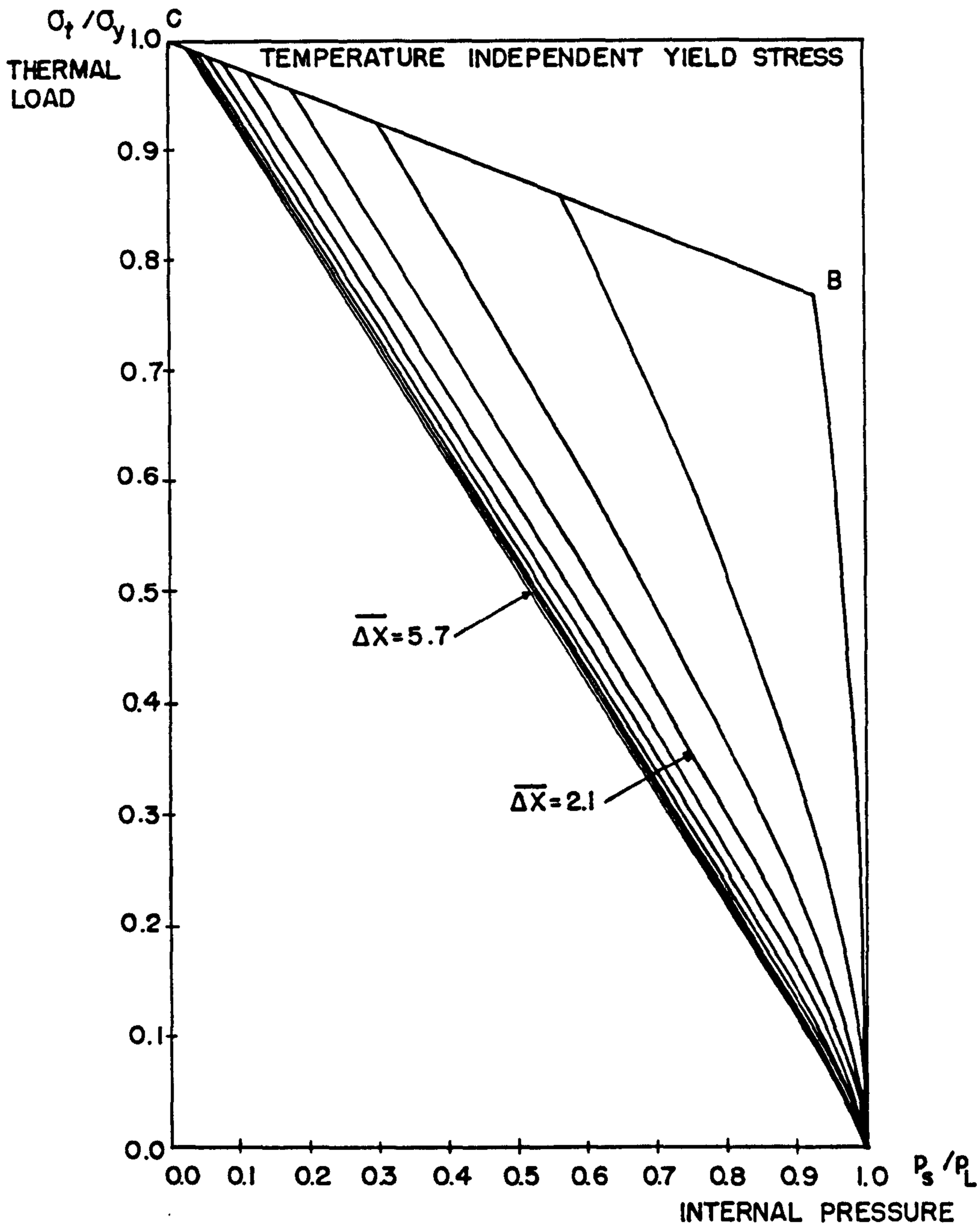

Fig. 4.12- BREE TYPE DIAGRAM FOR A TUBE SUBJECTED TO INTERNAL PRESSURE AND MOVING TEMPERATURE FRONT

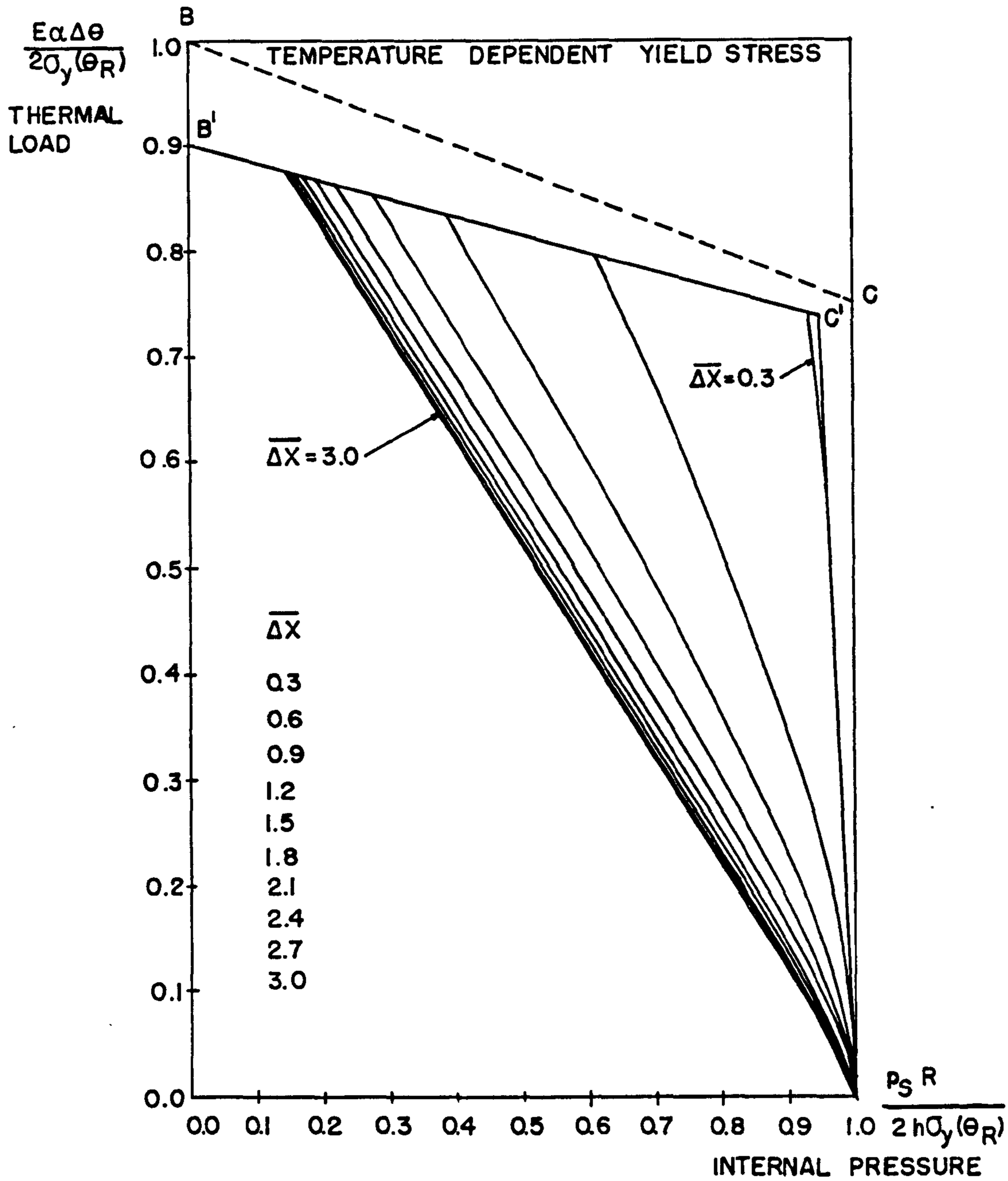

Fig. 4.13- BREE TYPE DIAGRAM FOR A TUBE SUBJECTED TO A STEADY INTERNAL PRESSURE AND MOVING TEMPERATURE FRONT

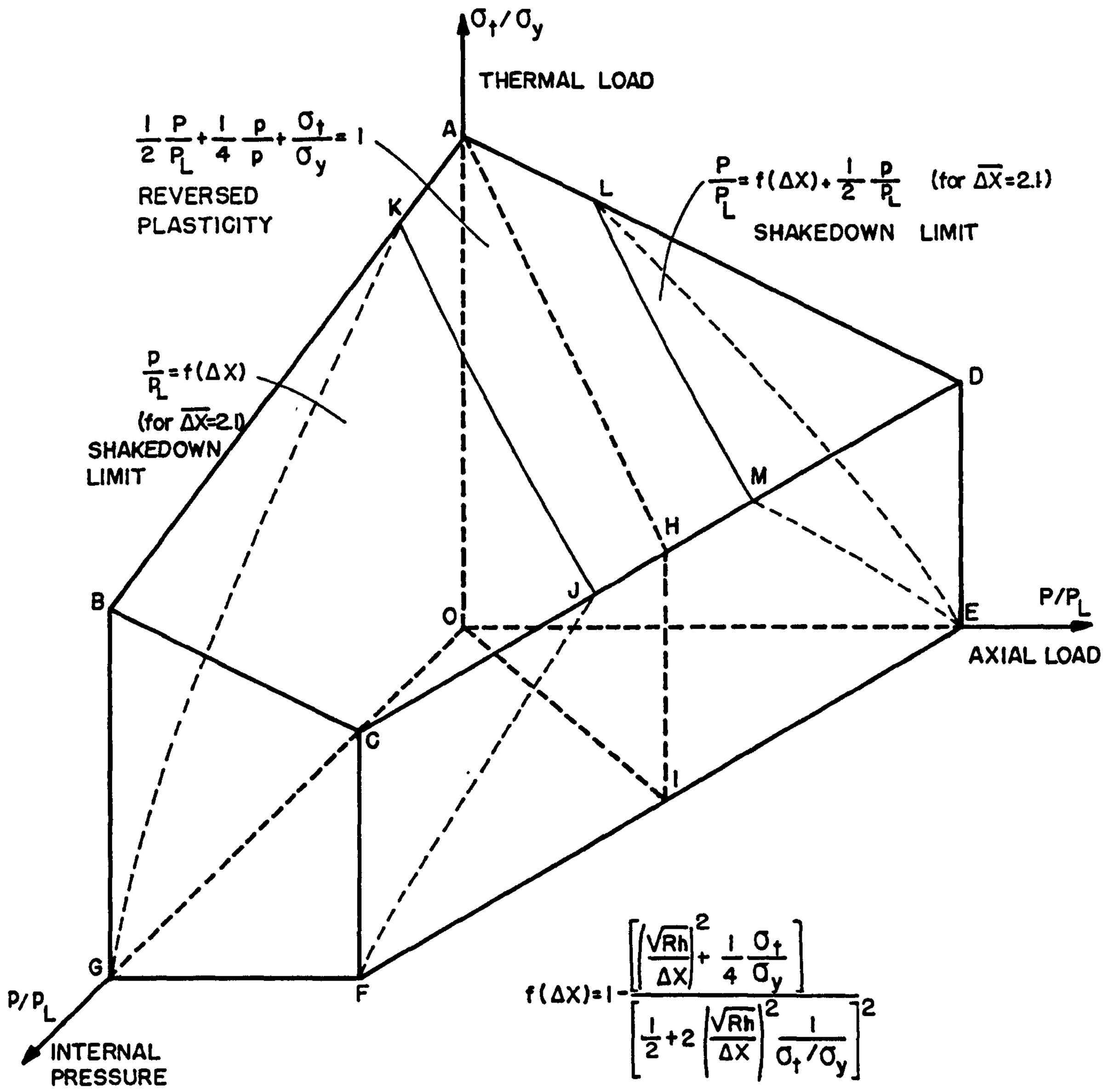

Fig. 4.14- TRI-DIMENSIONAL BREE TYPE DIAGRAM
TEMPERATURE INDEPENDENT

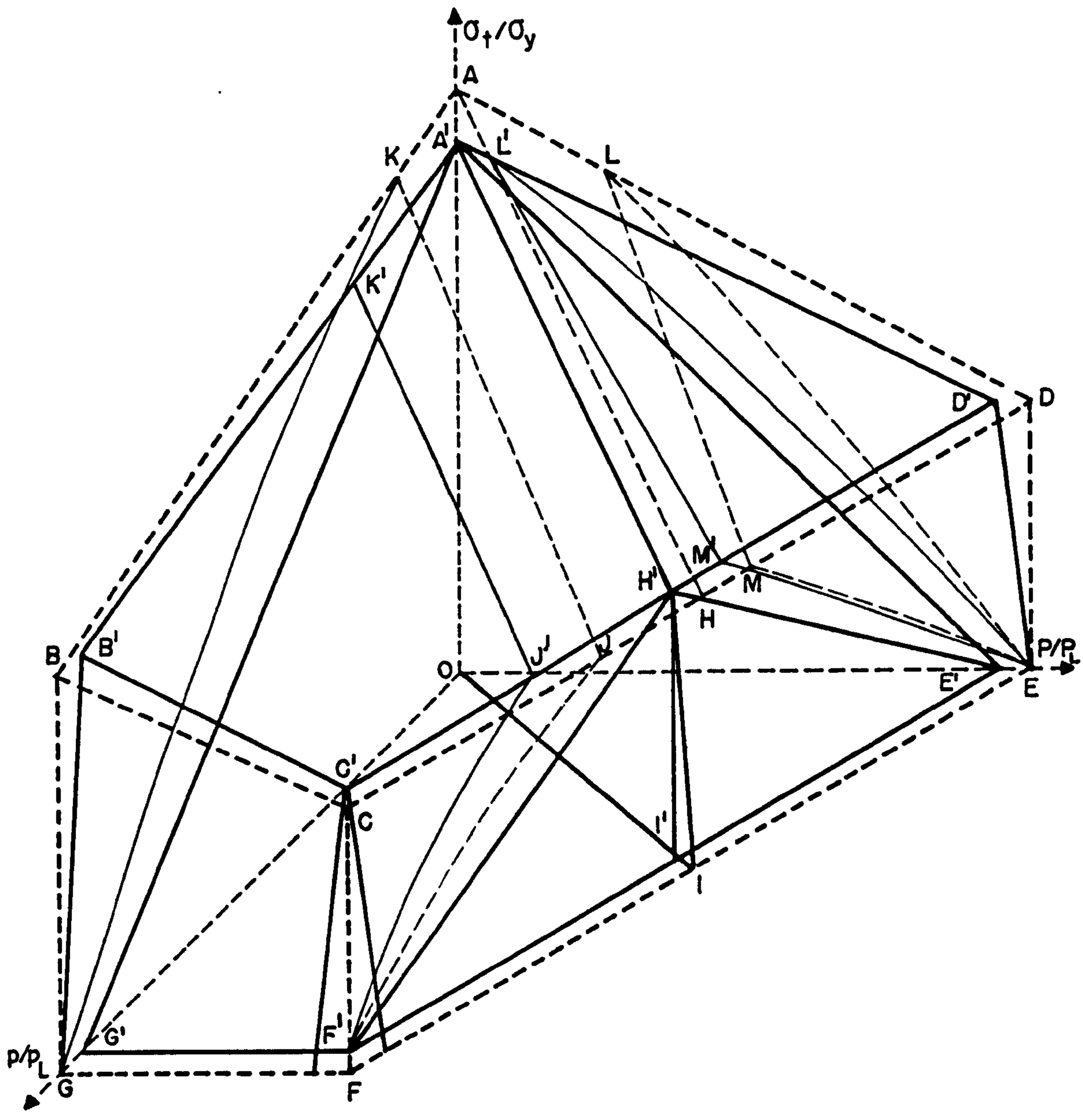

Fig. 4.15 - TRI-DIMENSIONAL BREE TYPE DIAGRAM TEMPERATURE DEPENDENT

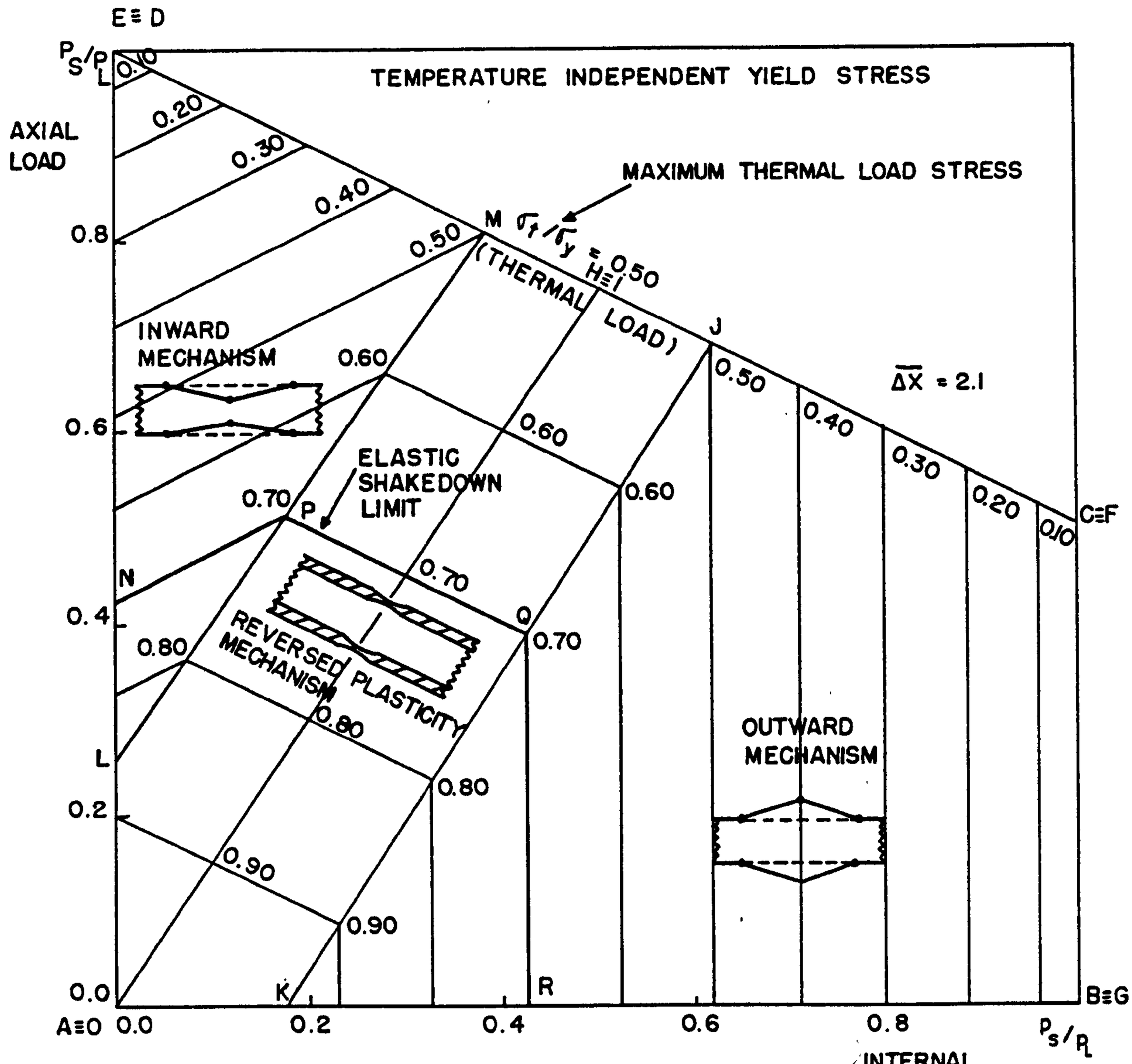

FIG. 4.16 - BI - DIMENSIONAL BREE TYPE DIAGRAM

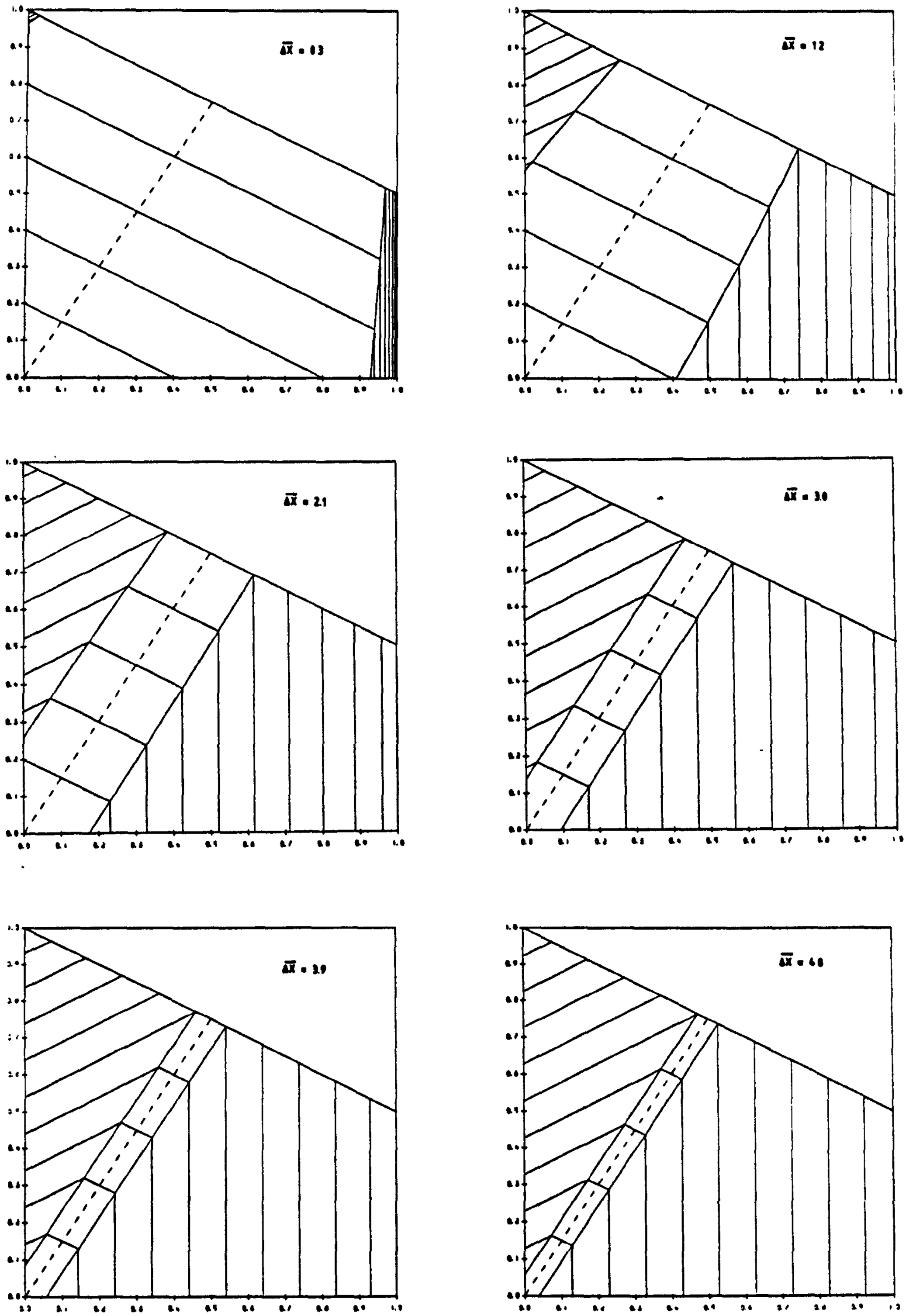

Fig. 4.17 A SEQUENCE OF BI-DIMENSIONAL DIAGRAMS SHOWING THE EFFECTS OF LENGTH OF TRAVELS ON THE REGIONS OF DIFFERENT MECHANISMS OF DEFORMATION.

TEMPERATURE INDEPENDENT

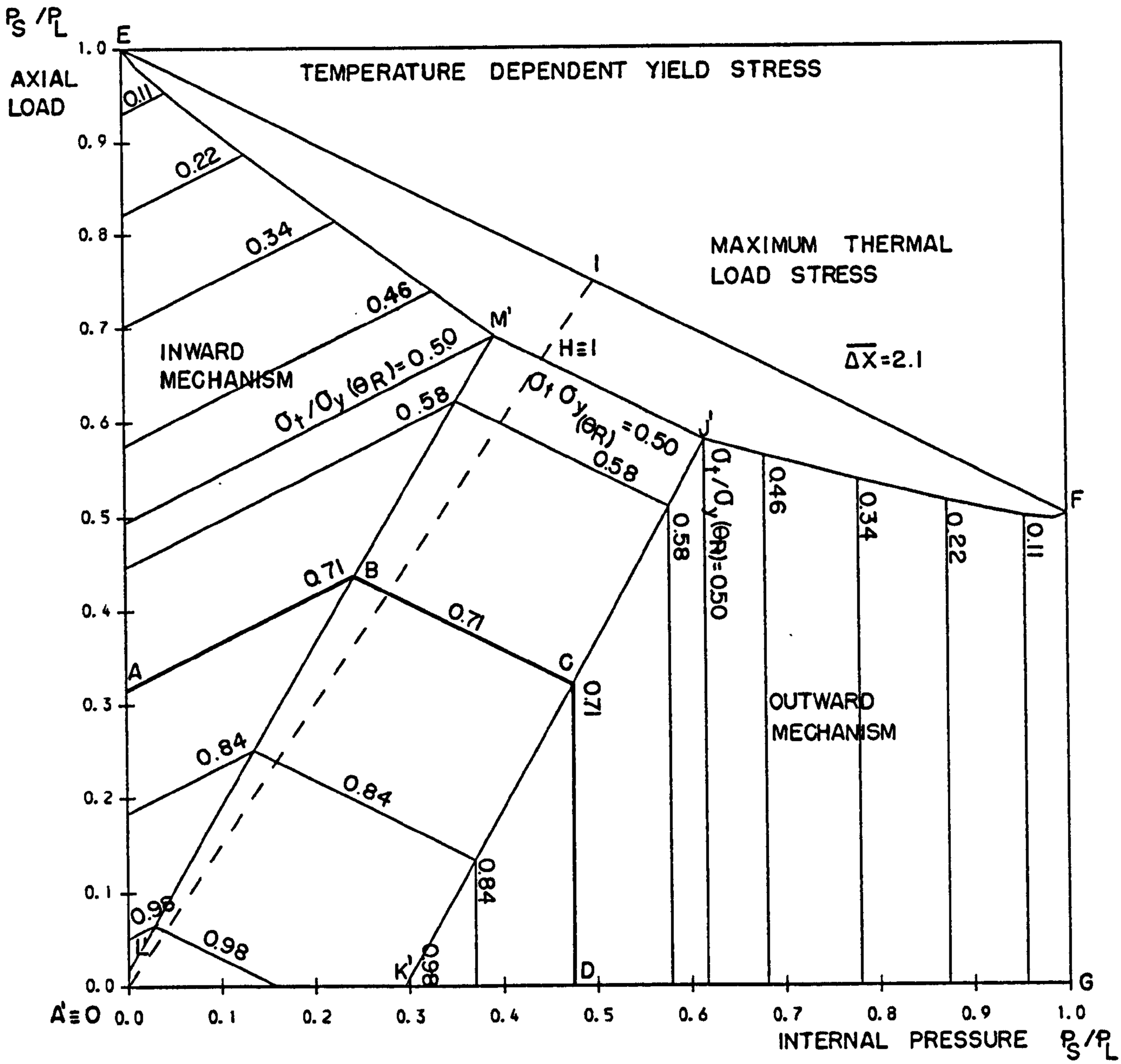

Fig. 4.18 - BI-DIMENSIONAL BREE TYPE DIAGRAM

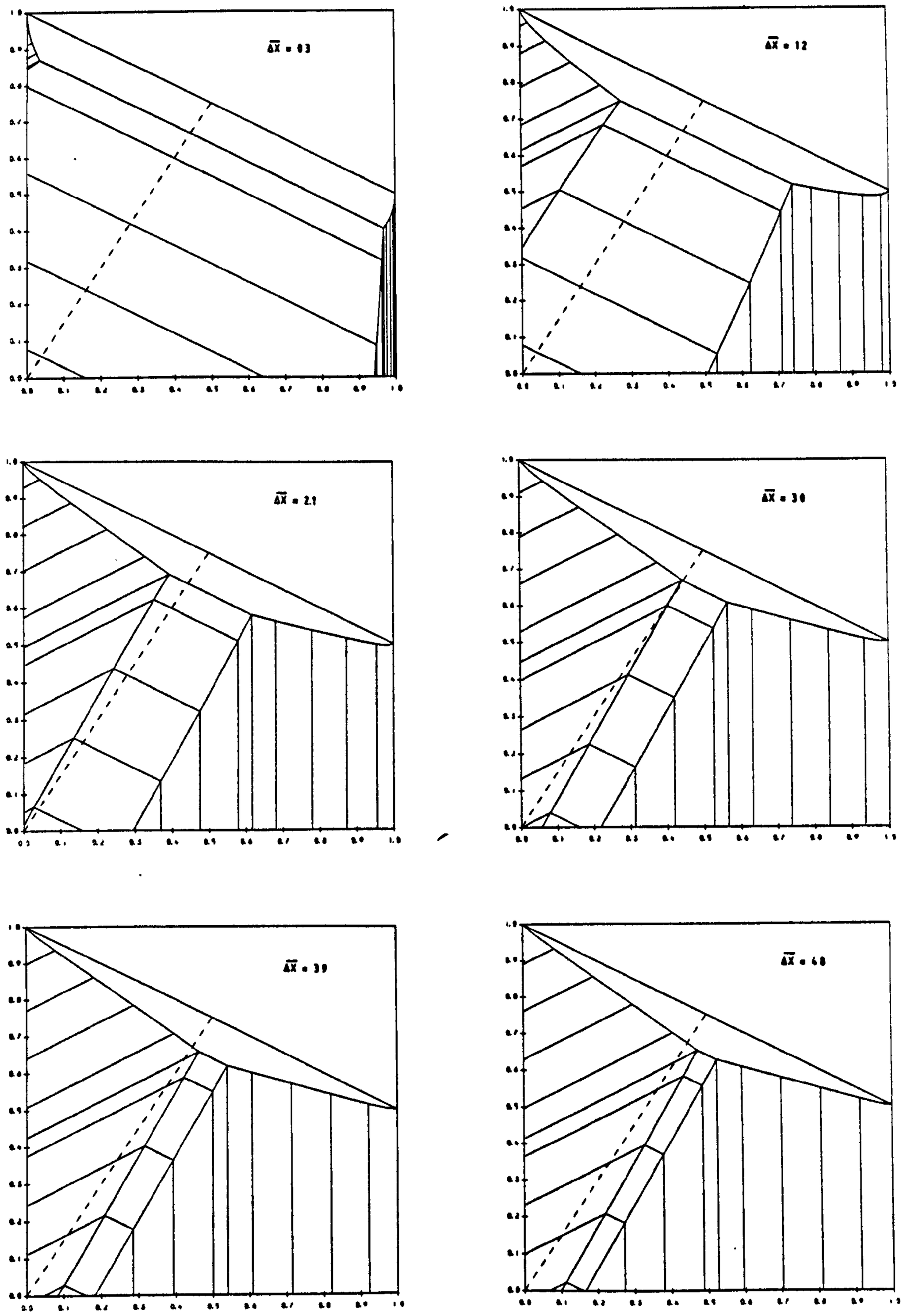

Fig. 4.19 A SEQUENCE OF BI-DIMENSIONAL DIAGRAMS SHOWING THE EFFECTS OF LENGTH OF TRAVELS ON THE REGIONS OF DIFFERENT MECHANISMS OF DEFORMATION.

TEMPERATURE DEPENDENT

CHAPTER 5

EXPERIMENTAL TESTS ON PORTAL FRAMES OPERATING AT 400°C SUBJECTED TO CYCLIC THERMAL LOADING IN THE PRESENCE OF STEADY MECHANICAL LOAD

5.1 Introduction

Detailed analysis in support of the design of structure which operates under cyclic thermal loading and at high temperatures has required a considerable amount of research in recent years. As a result there has been considerable progress in the development of new analytical methods, in the understanding of material behaviour and even in the improvement of design criteria. Nevertheless, there is still insufficient experimental data which can be used to verify the correlation between the various theoretical assumptions proposed and the actual behaviours of materials and structures.

The present experimental investigation has been undertaken because of the lack of experiments capable of substantiating or not the increasing theoretical data available. It has also been motivated by the need to demonstrate that the extended shakedown theory, described in Chapter 2, is capable of describing real behaviour.

The theory used to analyse this particular class of problems, which involves cyclic thermal loading in the

presence of high temperatures and mechanical loads, has been developed from classical models based upon the theory of plasticity, and then extended to more complete constitutive equations which include new important features of metal behaviour under cyclic loading. Two of these material cyclic phenomena have already been identified as playing a major role in the description of the properties of metals used in nuclear reactor structures,viz.: material ratchetting and cyclic hardening [102]. Material ratchetting, a phenomenon which is not completely understood, is a form of softening of the material due to incremental growth of the material under cyclic loading conditions in the plastic range. It has become clear that much more experimental data has to be produced for a better comprehension of the effects of this particular material behaviour on the performance of the structure. The other important characteristic of some materials selected for nuclear structures is cyclic hardening when operating in the regime of reverse plasticity. Many components in fast breeder reactors operate subject to small constant primary load and large thermal cyclic loading which makes this regime particularly important for the design of such components. It has been found that for the SS316 at 400°C cyclic hardening is significant but material ratchetting is absent.

The purpose of the present set of experiments is to define the extent of the reverse plasticity and shakedown regions with the inclusion of cyclic hardening in simple constitutive relations for the structural analysis. This was achieved by analysing the structural behaviour of portal

frames made of SS316 operating under simulated cyclic thermal gradients and a horizontal mechanical load at 400°C.

Simple mathematical representation of the uniaxial incremental growth of the material was used to predict a state of constant plastic deformation.

5.2 Material Behaviour

A knowledge of the most important features of material cyclic behaviour can provide a better understanding of structural behaviour and therefore the class of constitutive equations has to be chosen or even developed so that these main features are included in the analysis. Unfortunately, the main cause of the lack of development in mathematical material models which contain most of the already experimentally observed cyclic behaviour is the limited applicability they may have due to the complex form they are likely to take. Nevertheless, some of the most relevant features of the SS316 will be presented in this section for later use together with the two most commonly used hardening rules; isotropic and kinematic hardening.

5.2.1 Bending Moment-Curvature Relationship

It will be assumed throughout this chapter that the deformation occurs only as a result of bending of the members of the frame and the bending moment- curvature will

provide useful information about some characteristics of a hardening material such as the stainless steel 316 proved to be.

Plotting values of curvature against the corresponding bending moment gives rise to a curve similar to that shown in Fig. 5.1. The modes of behaviour along the diagram can be described as follows:

- elastic behaviour from O to A, ie, the curvature varies linearly with the bending moment and unloading leads to the return to the initial state.

- above point A the behaviour is no longer elastic or linear; a complete unloading will result in some permanent curvature as illustrated by the dashed line BE in Fig. 5.1.

- for a strain-hardening material a slow increase of the bending moment above point C in Fig. 5.1 will still be followed by an increase of the curvature. Depending upon the capacity of the material to strain-harden the increase of the curvature can be quite considerable. For some materials the bending moment can reach the collapse value soon above point C as shown by the dashed curve CD'in Fig. 5.1. Such behaviour is not relevant for the material used in the experiment (SS316) and will not be considered here.

5.2.2 Cyclic Stress-Strain Curve

For most engineering metals the hysteresis loops formed during each cycle (Fig. 5.2) will have their proportions changed as cycling progresses. It is said that the material is capable of cyclically hardening when the stress amplitude increases for a constant strain cycling, whereas cyclic softening takes place if the material presents the opposite behaviour. For both strain-hardening and softening materials the phenomenon observed when plastic cycling takes place between prescribed strain [103,104,105] or stress [106] limits is of a very rapid rate of hardening or softening during the first cycles which decreases continously towards a steady cyclic state. A significant result of experimental investigations is the discovery of the uniqueness of the steady cyclic state irrespective of the initial condition of the material for many metals and alloys. As an example of this, the experimental hysteresis loops for cold-worked and annealed copper at a plastic strain amplitude of 1% obtained by Oldroyd [107,108] are shown in Figs. 5.3a,b. Nearly the same stress range was reached at the cyclic state despite the considerable contrast in the initial condition of the two materials.

A set of steady cyclic hystereses loops for different strain amplitudes is shown schematically in Fig. 5.4. The curve passing through the tips of these loops is known in the literature as the cyclic stress-strain curve, skeleton curve or backbone curve. The backbone curve can show features which differ significantly from the monotonic stress-strain

curve and has considerable importance for both shakedown analysis and low cycle fatigue problems. As a measure of the hardening or softening of the material it can be said that the metal cyclically hardens if the backbone curve is above the monotonic stress-strain curve or the metal cyclically softens if it falls below it [105].

Experimental observation has shown that the SS316 exhibits a considerable amount of transient strain-hardening when subjected to cyclic loading in the plastic range. Fenn [109] has obtained experimentally a set of hysteresis loops for the 316 stainlees steel at a total prescribed strain amplitude of 2% which showed similar cyclic transient behaviour to that of the TPHC copper. Later Ponter and Karadeniz [36,37] constructed the cyclic stress-strain curve for the SS316 at 400°C using mainly material data supplied by the UKAEA laboratories at Risley. This curve and the monotonic stress-strain curve are presented in Fig. 5.5 together with other curves representing the classical material models; ie, perfect plasticity, isotropic and kinematic hardening. From Fig. 5.5 it is evident that although the monotonic curve shows some strain hardening the cyclic curve shows a much greater cyclic hardening. The cyclic stress-strain curve will, therefore, be much more realistic for the determination of the bound separating the regions of reversed plasticity and ratchetting for the present problem of portal frames subjected to steady mechanical load and thermal cyclic loading. Modelling the monotonic curve using either isotropic or kinematic hardening gives rise to substantially different responses

under reverse loading. The isotropic hardening is expected to overestimate the amount of cyclic hardening whilst the kinematic hardening, coinciding with the monotonic curve, underestimate the capacity of the material to cyclically harden as shown in Fig. 5.5. From the two models the isotropic hardening may lead to solutions more consistent with the actual response of the portal frame in question.

5.3 Theoretical Analysis of a Portal Frame For An Isotropic Material Model

The portal frame considered in this analysis is shown in Fig. 5.6 where the loading history is composed of a sustained horizontal load at node C and a cyclic horizontal movement of node A, simulating a cyclic thermal load, as shown in Fig. 5.7. The material used was 316 stainless steel which will be modelled as a linear isotropic hardening material. The uniaxial stress/strain curve is shown in Fig. 5.8.

5.3.1 Description of Possible Modes of Behaviour

Relevant values of the elastic solution are shown in Table (5.1). The response of the frame when operating under the combination of the two loads depends upon the values of P and δ. The alternatives for the structural behaviour within the classical shakedown boundary and during the first half cycle are:

- elastic behaviour
- plastic deformation starting at either nodes B,C or D and the rest of the structure deforming elastically

Boundaries defining the above modes of behaviour of the structure can be analytically determined as functions of the loads and can be usefully plotted as a Bree type diagram. The classical shakedown boundary is composed of two bounds. The first bound is defined by the cyclic load necessary to form a reversing plastic hinge at node B (reversed plasticity) and the second occurs when a mechanism of incremental collapse consisting of plastic hinges at nodes B,C and D (Fig. E3)is assumed to operate. For loads in excess of these boundaries the following modes of behaviour are expected to occur:

- alternating plasticity at the hinge at node B with zero strain growth
- ratchetting or incremental growth

A safe estimate of the boundary separating the reverse plasticity region and the ratchetting region can be achieved by using the extended shakedown theorem [36,37] which assumes that the material cyclically hardens towards a state of fully elastic behaviour in the same manner as isotropic hardening. In the case of this particular problem, the volume of the frame is divided into two subvolumes:

- V_F where the stress history due to the cyclic thermal loading cannot be contained within the yield surface and will, therefore, cause alternating plasticity. The volume V_F of the portal frame can be identified as a region developing from node B where the moment due to the cyclic loading first exceeds the assumed moment necessary to form a hinge.

- V_S where the stress history is contained within the yield surface. This volume is represented by the remainder of the structure.

According to the extended upper bound theorem the classical upper bound theorem can then be applied to the remainder volume V_S by removing V_F from the calculations which, for the particular case of the portal frame corresponds to treating node B as a hinge, ie, to analyse a frame like that shown in Fig. 5.9. The volume V_S is further reduced when the limit moment is next exceeded at node D and a second hinge starts to develop from there. The upper bound theorem can again be applied to the reduced structure shown in Fig. 5.10 where the new volume V_S has nodes B and D operating as hinges. The bounding conditions representing the different modes of behaviour described above are calculated in Appendix E

5.4 Description of the Test Specimens, Apparatus and Equipment

The portal frames used for the experiments were manufactured out of 5/8" 316 austenitic stainless steel sheets by a spark erosion technique as shown in Fig. 5.11 and Fig. 5.12. Two frames were produced from each sheet. The frames were then painted with a protective coating to prevent excessive oxidation during the heat-treatment which consisted of an annealing process at 1050°C for approximately one hour and a subsequent rapid air cooling. The dimensions of the frame are given in Section 5.6.

The apparatus and data-recording equipment used during the experiments are shown in Fig. 5.13 and Fig. 5.14. A brief description can be summarized as follows:

- A mains transformer (on the right of Fig. 5.13) induced high secondary current into the frame so that it could be uniformily heated to the desired temperature (400°C). The temperature was controlled by a P.I.D. temperature controller, with a thermocouple (Nickel Chrome/Nickel Aluminium) welded to the frame as control feedback, shown on the left of Fig. 5.13.

- The mechanical loading system can be seen in Fig. 5.13 and consists of dead weights hanging from a wire coupled to the bottom left hand node or for multi-step loads by use of a motorized ball-screw jactuator driven by a servo-amplifier with the load as a feedback.

- The portal frame support at the botton right is clamped and the pinned support at the top right is constrained to allow vertical movements above and below the unloaded position (Fig. 5.13). Such cyclic displacements, $+\delta_A$, simulating thermal cyclic loading, were applied to the frame by a servo-hydraulic jack, controlled by a DC Servo Amplifier, shown at the top of Fig. 5.13.

- Linear Variable Differential Transformers (LVDT) were used to measure the control displacements $+\delta_A$ and the displacements at the top of the frame as shown in Fig. 5.13. The control LVDT mounted in the jack would also feedback the displacement to the amplifier control system.

- The loads required to produce the displacements $\pm\delta_A$ were measured by means of a Load-cell situated between the jack and the pinned support.

- The values of force and displacement together with the feedback to the servo control system were all plotted continuously by a chart recorder during the whole experiment. The plotter is shown in Fig. 5.14.

- The experiments were controlled by an RML micro computer (Fig. 5.14) and a program in Basic language had to be written to enable the generation of the command codes to the D/A (Digital to Analog) convertor and the digital relay board. The data was collected by an Apple based

scanning/recording system (Fig. 5.14) which was initiated by the digital relay board. This method enabled dual tasking to be effected without hold periods. The data was transfered from the Apple disk to the mainframe at the end of each test. Fig 5.14 shows a overall view of the control system.

- Figs. 5.15a,b show the experiment running at the two extremes of the cycle, ie at $\pm\delta_A$.

5.5 Description of the Experimental Procedure

5.5.1 On the Collapse Mechanical Load

A step by step collapse test of the frame at 400°C was carried out by increasing load in increments of 1Kg. The load was left still for a few minutes to assess the effects of creep, and increments were added until the frame was considerably deformed. The horizontal displacements were measured, and the results are displayed in Fig. 5.16. Assuming that P_L is given by linear extrapolation for elastic behaviour and collapse behaviour, a value of P_L = 45Kg was obtained. A theoretical Bree diagram, schematically illustrated in Fig. 5.17, based upon an isotropic hardening model was then plotted using the following quantities.

- the limit load obtained from the collapse test
- the frame dimensions defined previously

- the value of EI obtained from the tests within the elastic range

This Bree diagram was used as a reference for the analysis of results of the tests which are presented in the form of contours of states of constant plastic displacements, ie $u_p = u - u_e$ where u is the measured displacement and u_e the elastic displacement calculated assuming an elastic behaviour of the structure.

5.5.2 The Cyclic Loading Test

A sequence of 20 tests on portal frames at 400°C was carried out during which the mechanical load remained constant. For each level of constant mechanical load P the node A was cycled through controlled horizontal displacements $\pm\delta_A$ for 100 cycles at a sequence of increasing values. The number of times the cyclic loading had to be incremented varied from 6 to 13 depending upon the value of the mechanical load applied to the test. During the tests the following data was recorded for the subsequent analysis.

- the control displacement varying from $-\delta_A$ to $+\delta_A$
- the horizontal force necessary to impose such displacement, ie the horizontal reaction at node A.
- the horizontal displacement at B

Data values were read every 5 cycles intercalated by maximum and minimum values. At the end of each block of 100 cycles,

values corresponding to neutral cyclic loading, ie, δ_A = 0.0, were read before the load was increased. The data was transferred to the University main frame computer which produced plots showing variations with the number of cycles carried out during the test. A set of data for particular combinations of loading are shown in Figs. 5.18a,b,c

5.6 Analysis of the Experimental Results

The theoretical equation for the elastic horizontal displacement of a portal frame with dimensions shown in Fig. 5.19 is:

$$U_e = \frac{13}{132}\frac{P\ell^3}{EI} \pm \frac{5}{22}\delta_A \qquad 5.1$$

or in a more general way

$$U_e = A*P + B*\delta_A \qquad 5.2$$

where A and B are constants dependent upon the geometry and on the material. When the mechanical load is the only load applied to the frame and is in the elastic range the horizontal displacement measured in the experiment can be used to calculate EI as follow:

$$EI = \frac{13}{132}\frac{P\ell^3}{U_e^P} \qquad 5.3$$

where U_e is the displacement due to P alone in the elastic range read during the test and "L" is the length of each of the three bars composing the frame. Similar procedures can be used to calculate constant B in Equation (5.2). Instead of adopting the theoretical value 5/22 shown in Equation (5.1), B can be determined by simple subtraction once A has been found, as proposed above, provided the combination of the two loads still remains in the elastic range. The total displacement of the portal frame when operating subjected to a loading system outside the elastic range is:

$$U_T = U_e + U_p \qquad 5.4$$

where Up is the plastic component. While U_e can be calculated from (5.2), U_T is obtained from the experiment as a direct reading and the plastic component is calculated by simple subtraction.

For each test corresponding to a constant mechanical load, these plastic displacements were then plotted against the various incremented cyclic thermal load δ_A to produce a set of curves as shown in Fig. 5.20. From these curves a set of contours were plotted superimposing the Bree diagram allowing a direct comparison between the theoretical extended shakedown boundary and the actual behaviour of the structure under cyclic loading. These contours represent a state of constant plastic deformation after transient plastic deformations accumulate over a few initial cycles. This observation is consistent with several other works [13,14,60,110,111] which have already concluded that

components subjected to small primary loads and high thermal gradients may be operating under regimes of reversed plasticity without ratchetting. The Bree diagram and the approximate contours are shown in Fig. 5.21a. Fig. 5.21b shows the plastic displacement plotted against the increment of mechanical load corresponding to contours of constant plastic deformation. It corresponds to assume that only increments of mechanical load occur beyond the limit of shakedown, ie δ_A remain constant. Although the curves obtained seem to follow no regular pattern, it can be seen in Fig. 5.21b that the curve corresponding to $\delta_A = 0$ constitutes a upper bound as expected.

5.7 A Theoretical Estimate of the Accumulation of Transient Plastic Strain Beyond Shakedown for the Portal Frame

The contours obtained from the tests on the portal frames can be directly compared with theoretical contours calculated from estimates of cyclic states of constant plastic deformation after initial transient strain for the isotropic hardening material model.

5.7.1 The Isotropic Hardening Model

A slightly modified isotropic rule will be used for the purpose of the present calculations. The uniaxial stress-strain curve for the kinematic hardening model for the 316SS used in the experiments and for the assumed isotropic

hardening model, is shown in Fig. 5.22. The isotropic hardening will prevail until a plastic hinge is formed corresponding to the plastic moment when the cross section will not be able to take any more increment of moment.

The stress $\sigma = 3\sigma_y/2$ corresponds to the plastic moment M_L. The equations for the elastic moments at nodes B,C and D from Table (1) can be used.

For Line BC in the Bree diagram

$$M_B = \frac{5}{22} P L \pm \frac{12}{11}\frac{EI}{\ell^2} \delta_A$$

$$M_C = \frac{-7}{22} P_L \pm \frac{3}{11} \frac{EI}{\ell^2} \delta_A \qquad 5.5$$

$$M_D = \frac{10}{22} P_L \mp \frac{9}{11} \frac{EI}{\ell^2} \delta_A$$

The accumulation of strain over a number of initial cycles depends very much upon the combination of the loads which determines how the hinges extend from the nodes along the bars of the frame. This can be better understood by rearranging the elastic moment Equations (5.5) in terms of non-dimensional parameters and as functions of the plastic moment as follows:

The collapse mechanical load has already been defined in Appendix E as $P_L = 3\ M_L/L$ and the cyclic load to form a hinge at node B was also defined as

$$\delta_L = \frac{11}{36}\frac{\ell^2}{EI}\,3M_L \qquad 5.6$$

The maximum elastic moments can then be written as:

$$M_B = \left(\frac{15}{22}\frac{P}{P_L} + \frac{\delta}{\delta_L}\right) M_L$$

$$M_C = -\left(\frac{21}{22}\frac{P}{P_L} + \frac{\delta}{\delta_L}\right) M_L \qquad 5.7$$

$$M_D = \left(\frac{30}{22}\frac{P}{P_L} + \frac{3}{4}\frac{\delta}{\delta_L}\right) M_L$$

In order to estimate the amount of transient strain accumulated during initial cycles it is necessary to have an estimate of how far the hinges will spread along the bars of the frame for the particular hardening model. As has been said previously, it depends on the combination of the loads. The estimation will be exemplified here through numerical calculation using the data from the experiments carried out on the portal frames. Table (5.2) shows the values of moments at nodes B,C and D for different operating points at the boundary.

The examples chosen correspond to the same values of the mechanical loads applied in the experiments so that a direct comparison can be made. Although approximate, the calculations give reasonable estimates of the actual extension of the hinges. The set of operating points are taken from the bound BC on the Bree Diagram.

Table (5.2) shows that loading points at the bound BC will produce moments which are redistributed through the structure in two different ways:

Consider, for example, the moment distribution for P = 35Kg which is illustrated in Fig. 5.23. The classical isotropic hardening model would allow the moment at node D to be greater than the plastic moment, but for the model assumed here any cross section subjected to M_L will operate as a plastic hinge and therefore will be unable to take any more increment of moment. For this particular loading point only M_D is in excess of M_p by an amount of $\Delta M_D = 0.311$ which has to be redistributed to the rest of the structure (Fig. 5.23). Assuming that the redistribution will take place proportionally to the current moment at the cross section, give:

$$\Delta M_D = \Delta M_B + \Delta M_C \qquad 5.8$$

and

$$\frac{\Delta M_B}{\Delta M_C} = k \qquad 5.9$$

hence

$$\Delta M_C = \frac{\Delta M_D}{1+k} \qquad 5.10$$

and

$$\Delta M_B = \frac{k}{1+k} \Delta M_D \qquad 5.11$$

For the particular case of P = 35Kg and ΔM_D = 0.311 give ΔM_C = 0.152 and ΔM_B = 0.159. Hence, M_B = 1.023 and M_C = 0.978 which needs to be once more redistributed but now in the same way as the other cases shown in Table (5.2) for the bound BC. The other mode of redistribution of moments occurs when the loading points produce elastic moments at B and C greater than M_p. Table (5.2) shows that this is the case for all the other mechanical loads considered. In these cases two hinges will start to extend; one from node B and the other from D. Fig. 5.24 illustrates the way it occurs:

An estimate of the extent of the hinges is given by

$$d^B s = \frac{\Delta M_B}{M_C + M_D} L \qquad 5.12$$

$$d^D s = \frac{\Delta M_D}{M_D + M_C} L \qquad 5.13$$

The values that will be used on the estimates of the accumulation of the transient strain is the total extension consisting of the sum of the values for each node. Table (5.3) shows the total extension of the hinges for the various mechanical loads.

5.7.2 On the Calculation of the Transient Plastic Strain

According to the Prandtl-Reuss equations [23], the plastic stress increment is proportional to the instantaneous stress deviation at any point of the loading, ie, $d\varepsilon^p_{ij} = S_{ij}d\lambda$ which corresponds to state that the increments of plastic strain depends on the current state of deviatoric stress and not on the increment of stress required to achieve this condition . Mendelson [23] has demonstrated that $d\lambda$ can be determined by using the yield criterion to give

$$d\varepsilon^p_{ij} = \frac{3}{2}\frac{d\varepsilon_p}{\sigma_e} \qquad 5.14$$

where σ_e and $d\varepsilon_p$ are called equivalent or effective stress and plastic strain increment, respectively defined as:

$$\sigma_e = \frac{1}{\sqrt{2}}\left[(\sigma_x-\sigma_y)^2 + (\sigma_y-\sigma_z)^2 + (\sigma_z-\sigma_x)^2 + 6(\tau^2_{xy}+\tau^2_{yz}+\tau^2_{zx})\right]^{1/2} \qquad 5.15$$

$$d\varepsilon_p = \frac{\sqrt{2}}{3}\left[(d\varepsilon_x^p - d\varepsilon_y^p)^2 + (d\varepsilon_y^p - d\varepsilon_z^p)^2 + (d\varepsilon_z^p - d\varepsilon_x^p)^2 + 6(d\varepsilon_{xy}^p)^2 + 6(d\varepsilon_{yz}^p)^2 + 6(d\varepsilon_{zx}^p)^2\right]^{1/2} \qquad 5.16$$

For an uniaxial tensile test in the x direction the effective stress and effective plastic strain increment become $\sigma_e = \sigma_x$ and $d\varepsilon_p = d\varepsilon_x$. Comparing the equivalent stress with the von Mises yield criterion it is seen that they are identical and since the Prandtl-Reuss relations make use of it the von Mises yield criterion is implied.

The concept of strain energy density or plastic work per unit volume is frequently used in theory of plasticity and is given by

$$dW_p = S_{ij}\, d\varepsilon_{ij}^p \qquad 5.17$$

It can be demonstrated that this plastic work can be written in terms of the equivalent stress and the equivalent strain increment as

$$dW_p = \sigma_e\, d\varepsilon_p \qquad 5.18$$

The Prandtl-Reuss relations, Equation (5.14) can also be written in terms of the plastic work to give:

$$d\varepsilon_{ij}^p = \frac{3}{2}\frac{dW_p}{\sigma_e^2} S_{ij} \qquad 5.19$$

The equivalent plastic strain was used by Mendelson [23] as a measure of work hardening where the yield function was assumed to be a function of the equivalent plastic strain. As the equivalent stress has been assumed to be the same as the von Mises yield function for the Prandtl-Reuss equations gives:

$$\sigma_e = F(\varepsilon_p) \qquad 5.20$$

where

$$\varepsilon_p = \int d\varepsilon_p \qquad 5.21$$

The functional relationship between the equivalent plastic strain ε_p and the yield function can be obtained experimentally and then substituted into Equation (5.20) to calculate the plastic strain increments. This experimental relationship given by Equation (5.20) can be taken from the uniaxial tensile test diagram shown in Fig. 5.25 where the abscissa and ordinate are replaced by ε_p ($= \int d\varepsilon_p$) and σ_e respectively. The slope of this curve in the plastic range is given by:

$$E' = \frac{d\sigma_e}{d\varepsilon_p} \qquad 5.22$$

Substituting Equations (5.18) and (5.22) into (5.19) give

$$d\varepsilon_{ij}^{p} = \frac{3}{2}\frac{d\sigma_e}{E'}\frac{S_{ij}}{\sigma_e} \qquad 5.23$$

which in terms of actual stresses become

$$d\varepsilon_x^p = \frac{d\sigma_e}{E'\sigma_e}\left[\sigma_x - \frac{1}{2}(\sigma_y+\sigma_z)\right]$$

$$d\varepsilon_y^p = \frac{d\varepsilon_p}{E'\sigma_e}\left[\sigma_y - \frac{1}{2}(\sigma_z+\sigma_x)\right]$$

$$d\varepsilon_z^p = \frac{d\varepsilon_p}{E'\sigma_e}\left[\sigma_z - \frac{1}{2}(\sigma_x+\sigma_y)\right] = -(d\varepsilon_x^p+d\varepsilon_y^p) \qquad 5.24$$

$$d\varepsilon_{xy}^p = \frac{3}{2}\frac{d\varepsilon_p}{E'\sigma_e}\tau_{xy}$$

$$d\varepsilon_{yz}^p = \frac{3}{2}\frac{d\varepsilon_p}{E'\sigma_e}\tau_{yz}$$

$$d\varepsilon_{zx}^p = \frac{3}{2}\frac{d\varepsilon_p}{E'\sigma_e}\tau_{zx}$$

In the case of uniaxial problems, say in the x direction, Equations 5.24 simplify to

$$d\varepsilon_x^p = d\varepsilon_p \qquad 5.25$$

$$\sigma_e = \sigma_x \qquad 5.26$$

and the actual uniaxial stress-strain curve (Fig. 5.26) can be used to find the experimental relationship given by Equation (5.20).

5.7.3 Theoretical Contours of Constant Ratchet Strain

5.7.3.1 A General Approach

Any loading point on the shakedown boundary will be associated with a certain mechanism of ratchet which after a number of cycles will either reach a state of steady incremental growth or a cyclic state of constant plastic deformation. The latter is more likely to occur if the material is able to work harden under cyclic loading. The material considered here is a work hardening material and it will be assumed that for an operating point beyond the shakedown limit the ratchet mechanism will remain the same.

At some time of the cycle "to" the stress point in a material element will be on the yield surface, and associated with it there is a transient plastic strain vector which is compatible with a plastic ratchet mechanism. This stress is given by

$$\sigma_{ij} = \sigma^{p}_{ij} + \sigma^{\theta}_{ij}(t_o) + \rho_{ij} \qquad 5.27$$

Assuming that only the primary load will be incremented by an amount ΔP in excess of shakedown, transient plastic

strain will dominate during the first few cycles followed by a state of constant plastic deformation. According to the hardening rule suggested by Prager [112] the yield surface moves in translation during the transient plastic deformation. Despite the special cases pointed out in [113] no deformation of the yield surface will be considered and therefore the original form of Prager's rule applies here only to von Mises' yield condition (Fig. 5.27) which is consistent with the calculations of the previous section. The increment of stress on the element due to the increment of primary load ΔP is given by

$$\Delta\sigma^{*}_{ij} = \Delta\hat{\sigma}^{p}_{ij} + \Delta\rho_{ij} \qquad 5.28$$

The convexity of the yield surface and the fact that the stress point must lie inside it after translation can be demonstrated from the mathematical definition of strain-hardening (Equation 5.29 obtained from [23]).

$$\Delta\sigma_{ij}\, d\varepsilon^{p}_{ij} > 0 \qquad 5.29$$

These two facts allow the following inequality to hold

$$(\Delta\sigma_{ij} - \Delta\sigma^{*}_{ij})\, d\varepsilon^{p}_{ij} > 0 \qquad 5.30$$

where $\Delta\sigma^{*}_{ij}$ is given by Equation (5.28) and $\Delta\sigma_{ij}$ represents the new position of the translated yield surface as shown in Fig. 5.27. The transient strain rate vector $d\varepsilon^{p}_{ij}$ is assumed to be compatible with the incremental mechanism and is given by Equation (5.23) which is a generalized equation including

both elastic and plastic components of strain.

Substituting Equations (5.23) and (5.28) into (5.30) and integrating over the volume give:

$$\frac{2}{3}\frac{E'\sigma_e}{S_{ij}}\int_V d\varepsilon^p_{ij}\ d\varepsilon^p_{ij}\ dV > \int_V \Delta\sigma^p_{ij}\ d\varepsilon^p_{ij}\ dV + \int_V \Delta\rho_{ij}\ d\varepsilon^p_{ij}\ dV \qquad 5.31$$

The fact that the residual stress $\Delta\rho_{ij}$ is in equilibrium with zero applied load makes the second integral on the right hand side equal to zero and Equation (5.31) becomes

$$\frac{2}{3}\frac{E'\sigma_e}{S_{ij}}\int d\varepsilon^p_{ij}\ d\varepsilon^p_{ij}\ dV > \Delta P\Delta u \qquad 5.32$$

The compatibility between the strain increment and the assumed incremental mechanism is given by

$$d\varepsilon^p_{ij} = \Delta u P_{ij}(x) \qquad 5.33$$

where $P_{ij}(x)$ is a function of geometric parameters and position. From Equation (5.32) the displacement Δu is given by

$$\Delta u > \frac{3}{2}\frac{S_{ij}\Delta P}{E'\sigma_e} / \int_V P_{ij}(x)\ P_{ij}(x)\ dV. \qquad 5.34$$

5.7.3.2 Uniaxial Behaviour

The uniaxial behaviour of the material element transforms the inequality of Equation (5.34) into an equality. When the following expression for the stress deviation (for the uniaxial case)

$$S_{ij} = \frac{2}{3}\sigma_x \qquad 5.35$$

is substituted into Equation (5.34), along with $\sigma_e = \sigma_x$, it becomes

$$\Delta u = \frac{\Delta P}{E'} \Big/ \int_V P_{ij}(x)\, P_{ij}(x)\, dV \qquad 5.36$$

Equation (5.36) will be used in the next section to determine theoretical contours of constant plastic strain for the portal frame which will allow a direct comparison with the experimental results.

5.7.4 On the Determination of Contours for the Portal Frame

Equation (5.36) shows that function $P_{ij}(x)$ is the only parameter in the equation which has to be calculated for each type of structure. For the portal frame it will be determined as follows:

Consider that hinges have extended from the nodes along the bars of the frame for a total distance ds producing plastic deformation compatible with the plastic horizontal displacement as shown in Fig. 5.28. The relationship between the plastic strain and plastic displacement of the material element is given by

$$d\varepsilon = \frac{y\Delta u}{dsL} \qquad 5.37$$

where Δu and L are defined in Fig. 5.28 whilst y and ds are defined in Fig. 5.29 which represents the material element as the sum of the hinges extended along the bars joined together.

Substituting Equation (5.37) into the integral of (5.36) and integrating over the volume give

$$\frac{E'\Delta u\ b\ h^3}{ds\ \ell^2\ 12} = \Delta P \qquad 5.38$$

or

$$\Delta P = \frac{EI}{k}\frac{\Delta u}{\ell^2 ds} \qquad 5.39$$

where k was defined in Fig. 5.26 as the strain hardening parameter $E' = E/k$. For the particular 316SS used in the experiments k has been defined from the monotonic stress-strain curve obtained experimentally (Fig. 5.30) as 22.5. For the cyclic stres-strain constructed by Ponter and

Karadeniz [36,37] k = 7. The values presented in Table (5.3) for total ds were used to define theoretical contours corresponding to both values of k and compared with the contour obtained experimentally for the case of u = 4mm. (Fig. 5.31).

EQUATIONS FOR THE PRIMARY LOAD	
HORIZONTAL REACTION AT NODE A	$H_A = \frac{5}{22} P$
VERTICAL REACTION AT NODE A	$V_A = \frac{6}{11} P$
MOMENT AT B	$M_B = \frac{5}{22} Pl$ (MIN)
MOMENT AT C	$M_C = \frac{-7}{22} Pl$
MOMENT AT D	$M_D = \frac{10}{22} Pl$ (MAX)
ELASTIC DISPLACEMENT AT B	$U_B = \frac{13}{132} Pl^3$
ELASTIC LOAD LIMIT	$P_E = 0.49\, P_L$
LOAD TO FORM A HINGE AT D	$P_M = 0.73\, P_L$
EQUATIONS FOR THE CYCLIC THERMAL LOAD	
HORIZONTAL REACTION AT NODE A	$H_A = \frac{12}{11} \frac{EI}{l^3} \delta_A$
VERTICAL REACTION AT NODE A	$V_A = \frac{3}{4} H_A = \frac{9}{11} \frac{EI}{l^3} \delta_A$
MOMENT AT B	$M_B = \frac{12}{11} \frac{EI}{l^2} (\pm \delta_A)$ (MAX)
MOMENT AT C	$M_C = \frac{3}{11} \frac{EI}{l^2} (\pm \delta_A)$ (MIN)
MOMENT AT D	$M_D = -\frac{9}{11} \frac{EI}{l^2} (\pm \delta_A)$
ELASTIC DISPLACEMENT AT B	$U_B = \frac{5}{22} (\pm \delta_A)$
ELASTIC LIMIT	$\delta_E = \frac{11}{54} \frac{l^3}{EI} P_L$
LOAD TO FORM A HINGE AT B	$\delta_L = \frac{11}{36} \frac{l^3}{EI} P_L$

TABLE 5.1

	P	P/P	δ /δ	M_B/M_L	M_C/M_L	M_D/M_L
P	35	0.778	0.333	0.864	-0.826	1.311
BC	23	0.511	-0.733	1.082	-0.671	1.247
	18	0.4	0.9	1.173	0.607	1.22
	15	0.333	1.0	1.227	-0.568	1.205

TABLE 5.2

P	ΔMB	ΔMD	d_S^B (mm)	d_S^D (mm)	d_S^T
35	0.023	0.311	1.72	20	21.7
23	0.082	0.247	7	19	26
18	0.173	0.22	14.6	18	32.6
15	0.227	0.205	19	17	34

TABLE 5.3

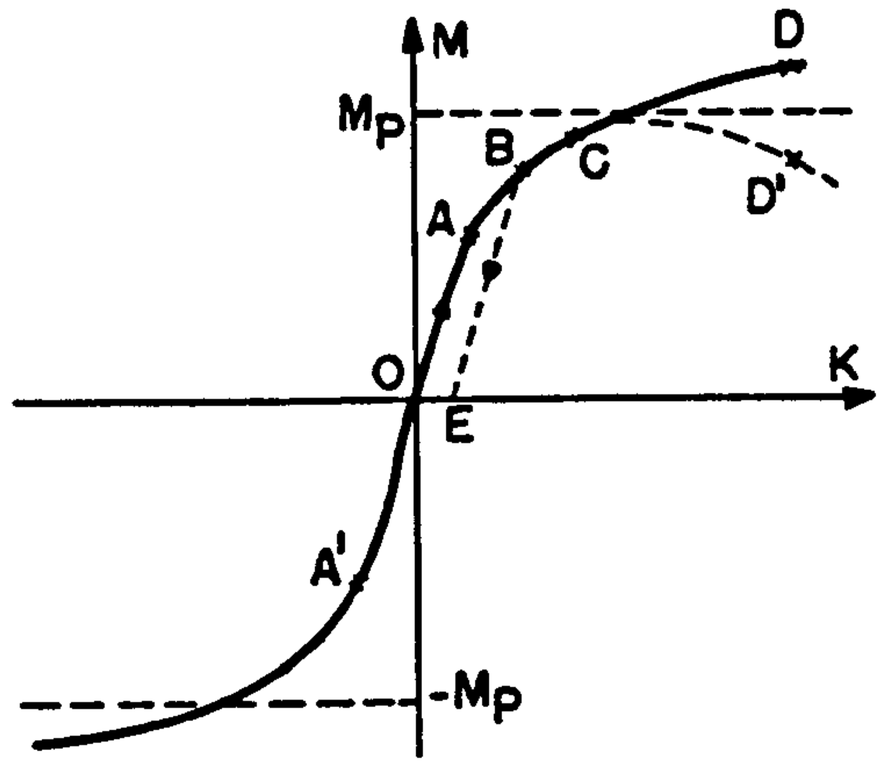

Fig. 5.1 -

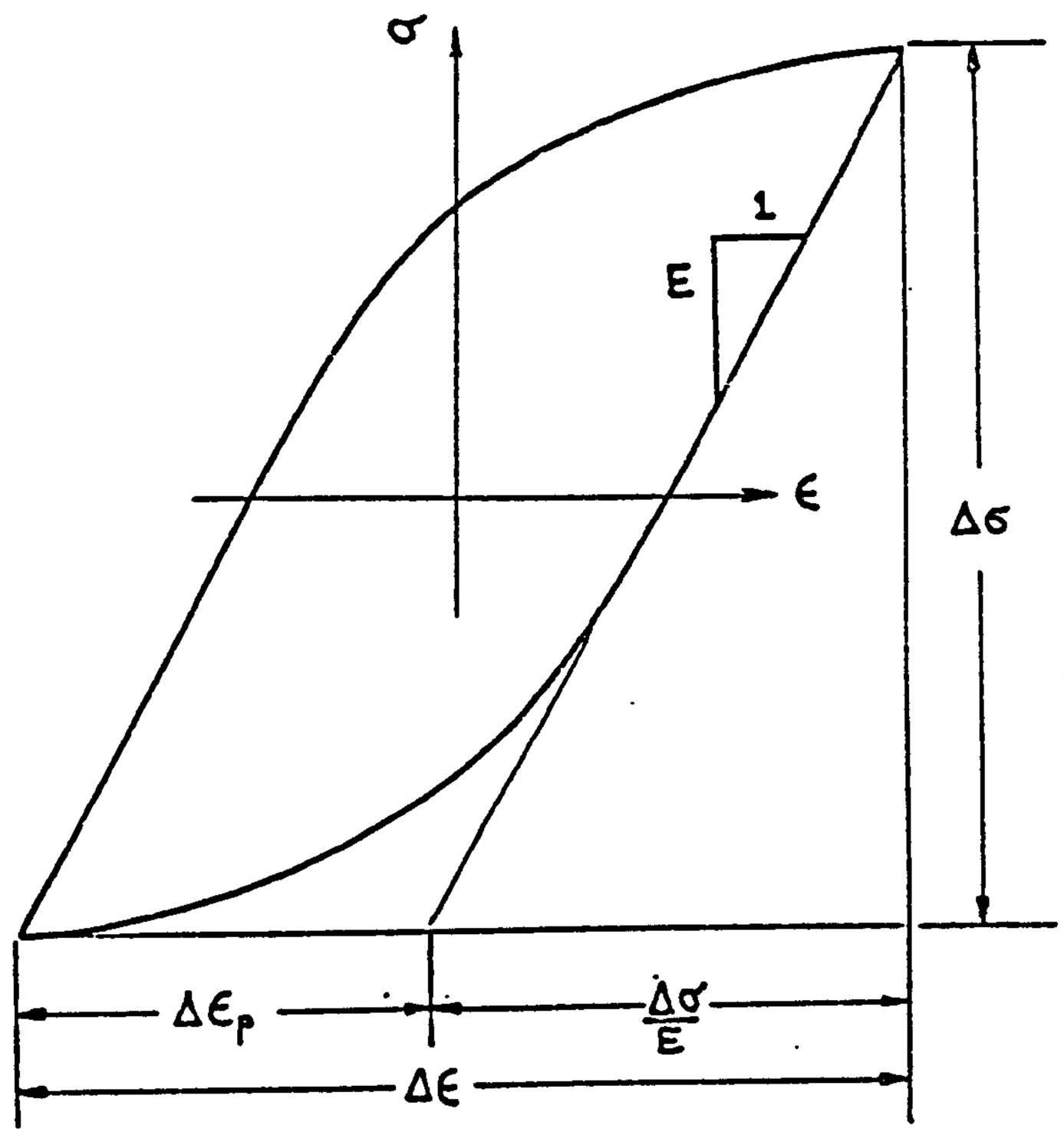

FIG.5.2 — Stress-strain hysteresis loop.

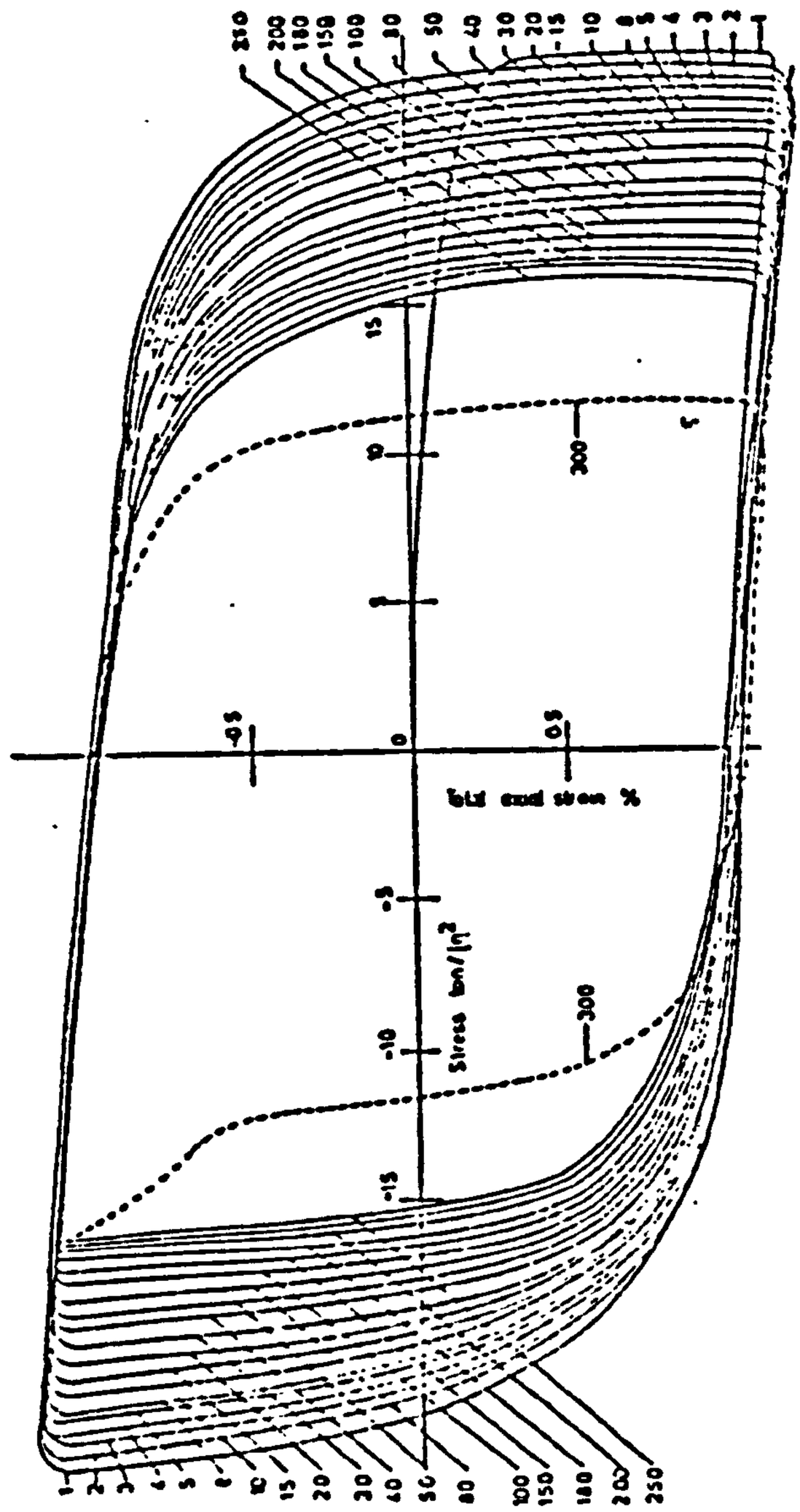

FIG.5.3a- Cyclic softening of initially work-hardened OFHC copper at a plastic strain amplitude of ±1% 106

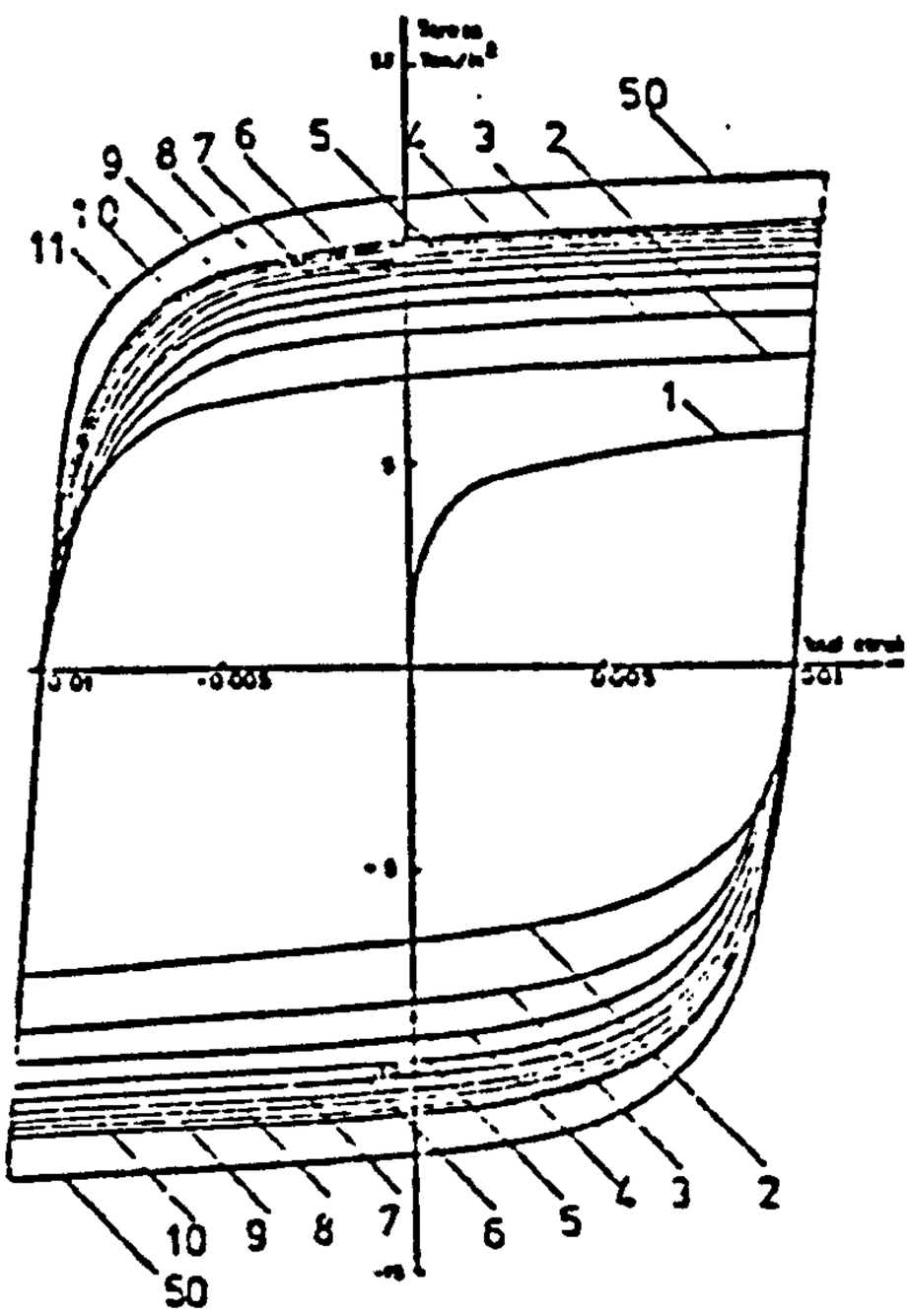

FIG.5.3b Cyclic hardening of initially annealed OFHC copper at a plastic strain amplitude of ±1% 107

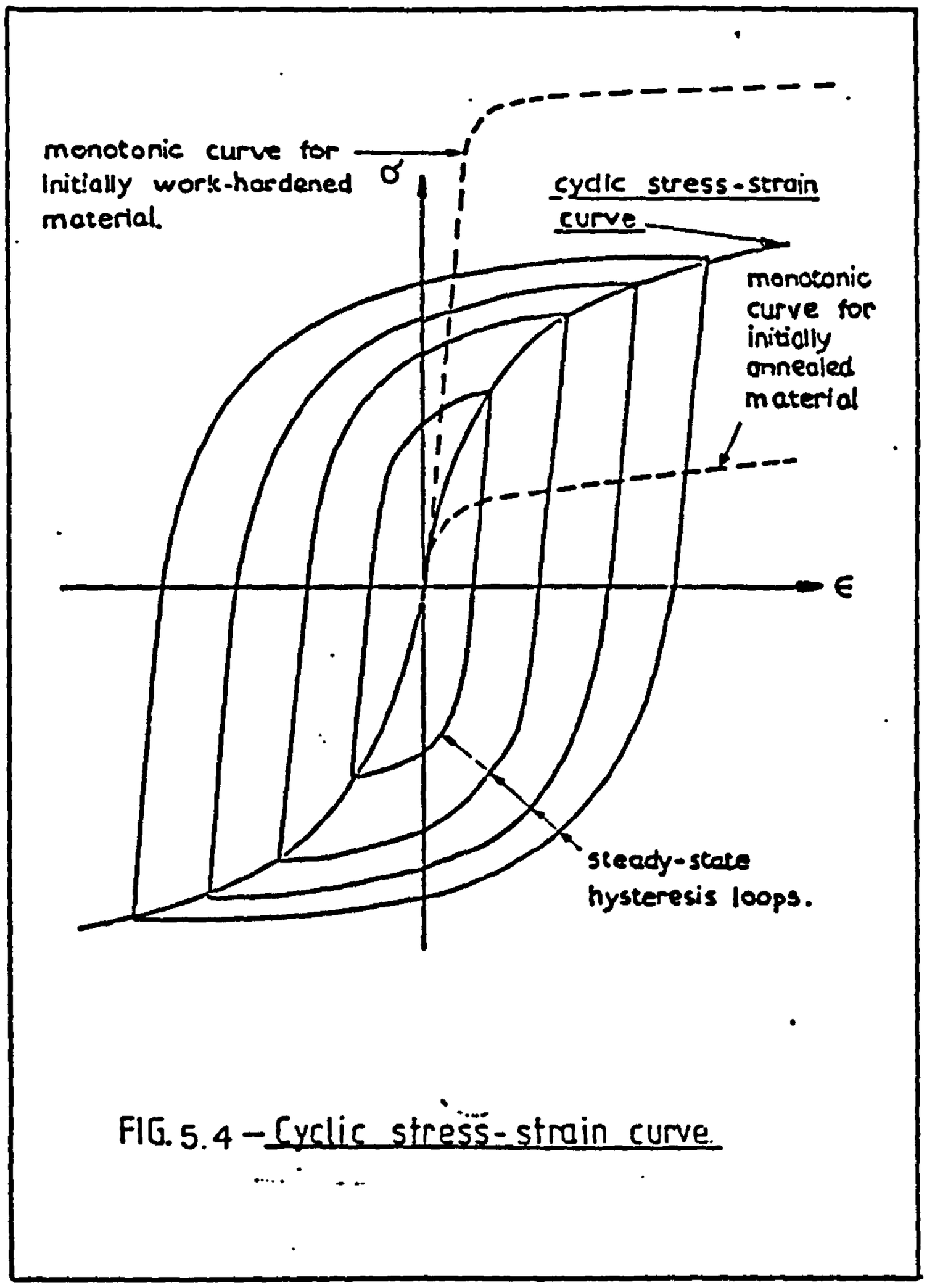

FIG. 5.4 – Cyclic stress-strain curve.

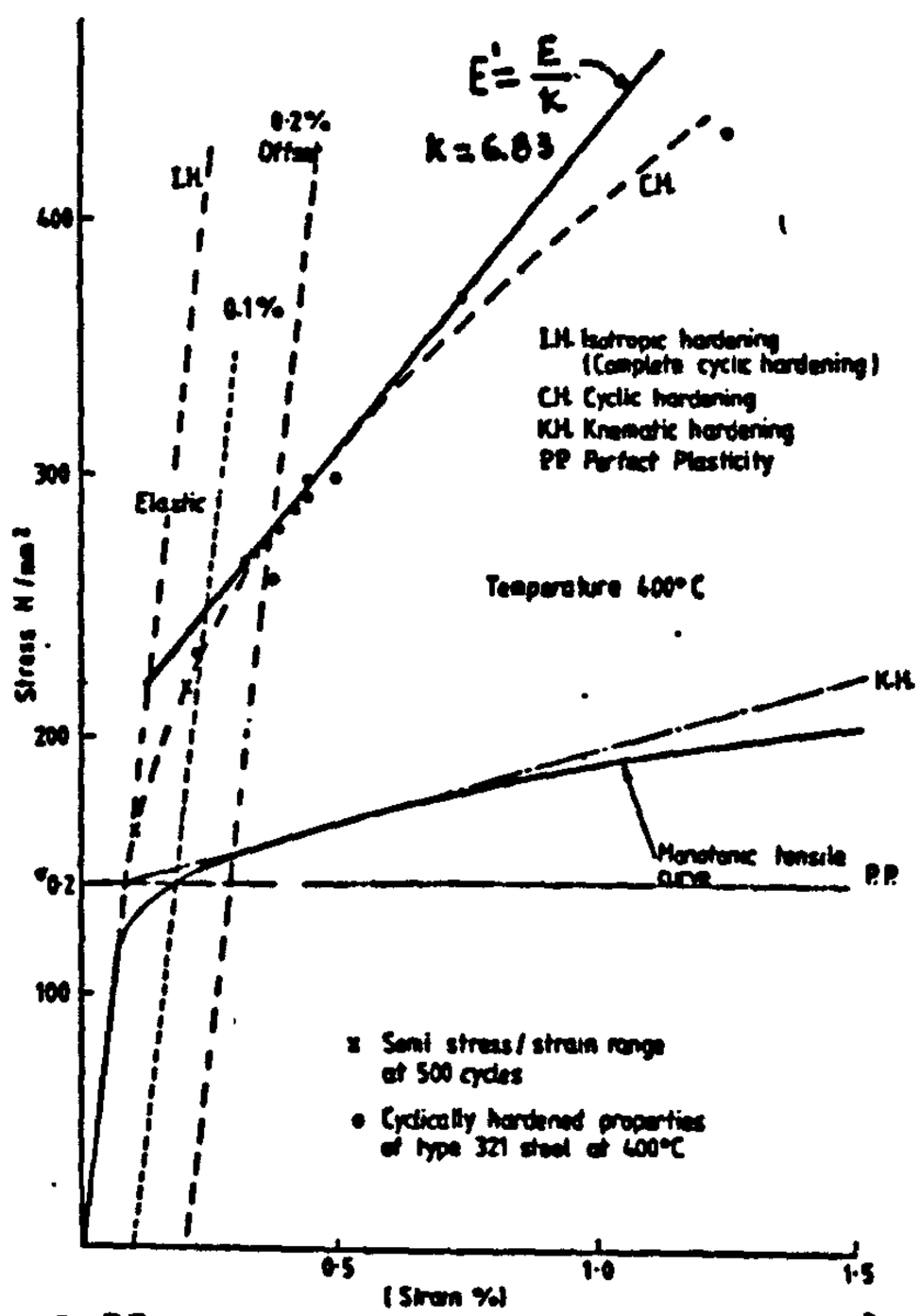

Fig.5.5 Cyclic and monotonic stress-strain curve for type 316SS [36]

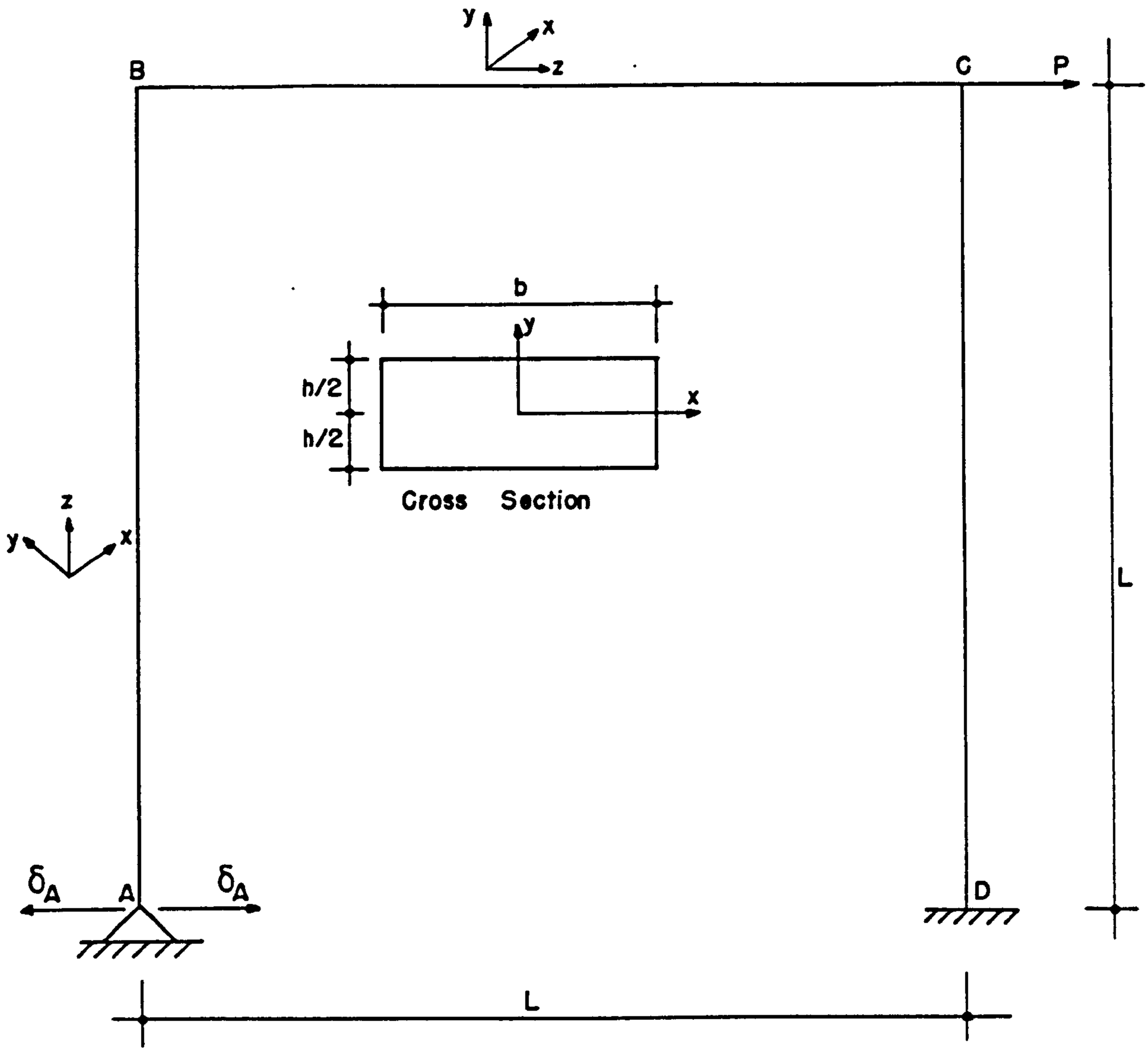

Fig. 5.6 - SIMPLIFIED REPRESENTATION OF THE PORTAL FRAME GEOMETRY

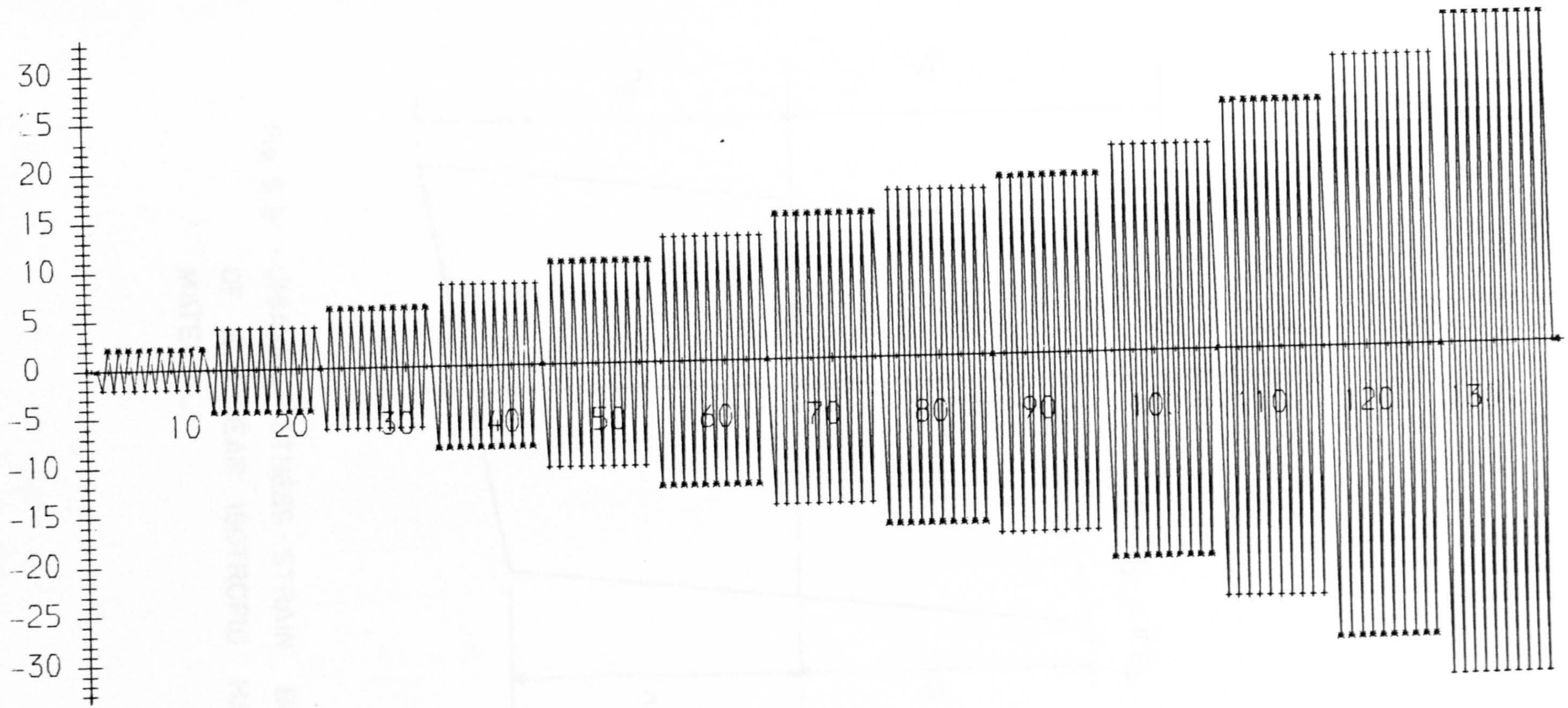

FIG. 5.7 CONTROL DISPLACEMENT $\pm \delta_A$ SIMULATING A CYCLIC THERMAL LOADING

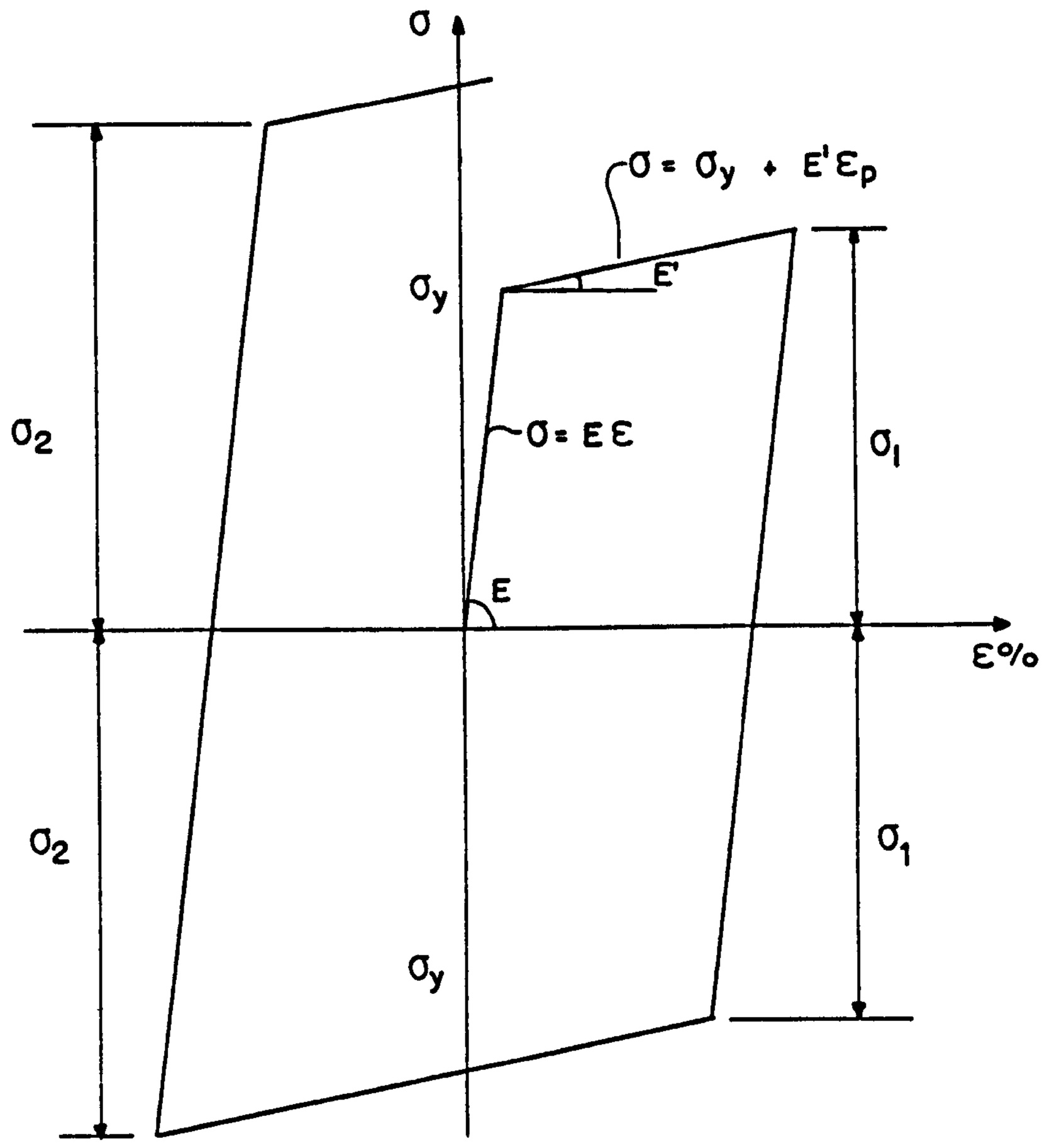

Fig. 5.8 - UNIAXIAL STRESS - STRAIN BEHAVIOUR OF A LINEAR ISOTROPIC HARDENING MATERIAL

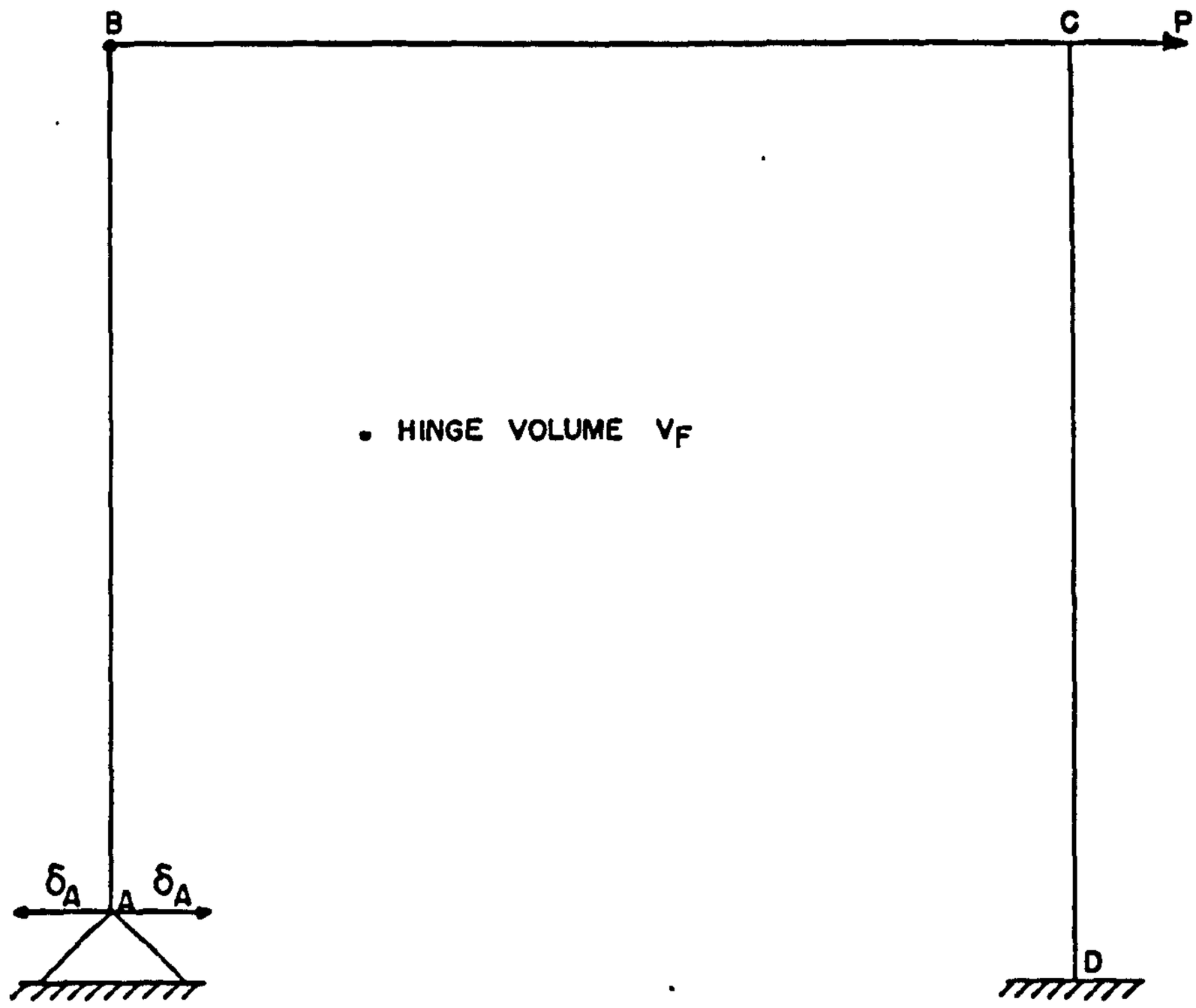

Fig. 5.9 - REMAINDER PORTAL FRAME CORRESPONDING TO BOUND BD IN THE BREE DIAGRAM AFTER A PLASTIC HINGE IS FORMED AT NODE B

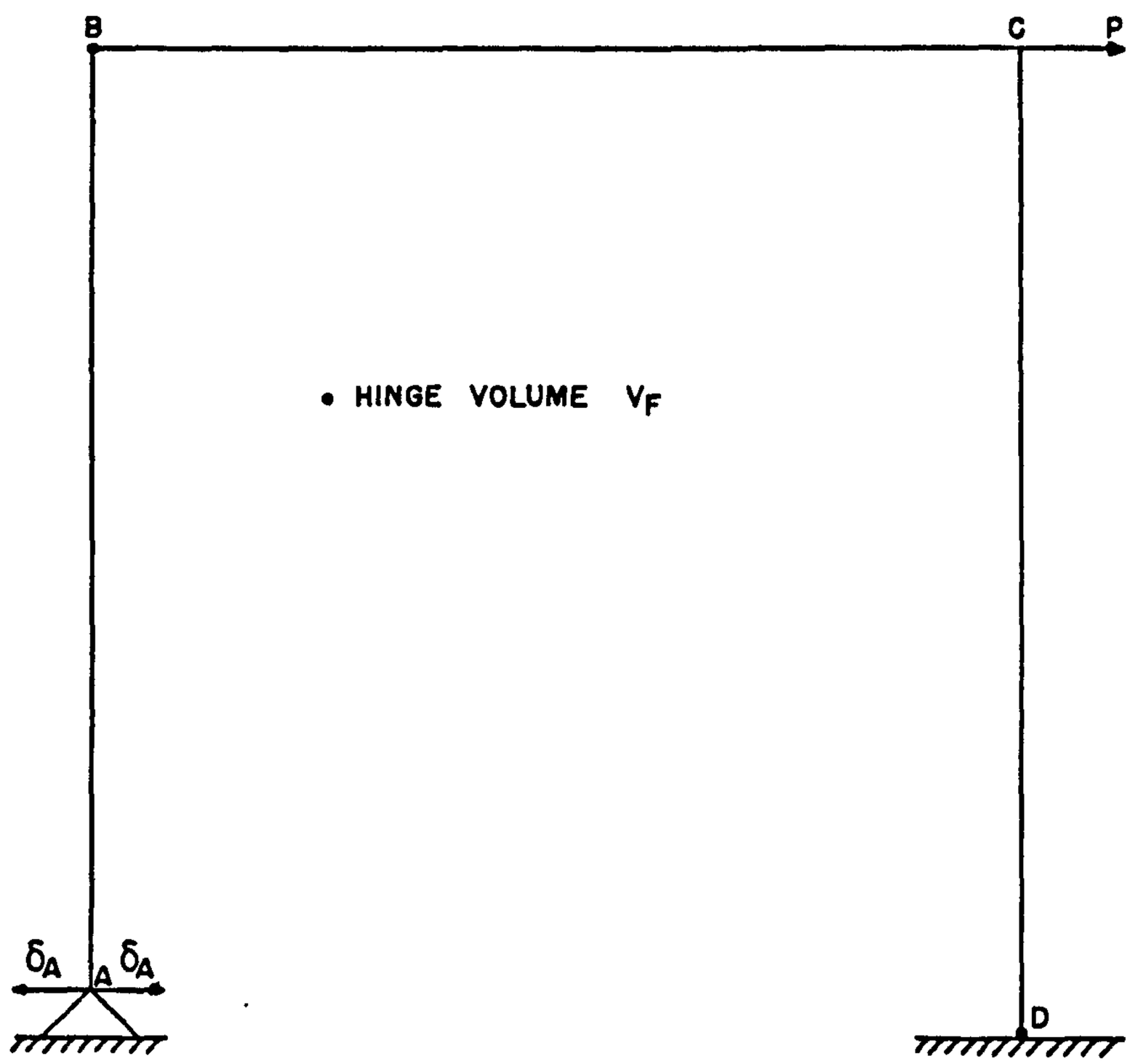

Fig. 5.10 - REMAINDER OF THE PORTAL FRAME CORRRESPONDING TO BOUND DE IN THE BREE DIAGRAM AFTER PLASTIC HINGES ARE FORMED AT NODES B AND D

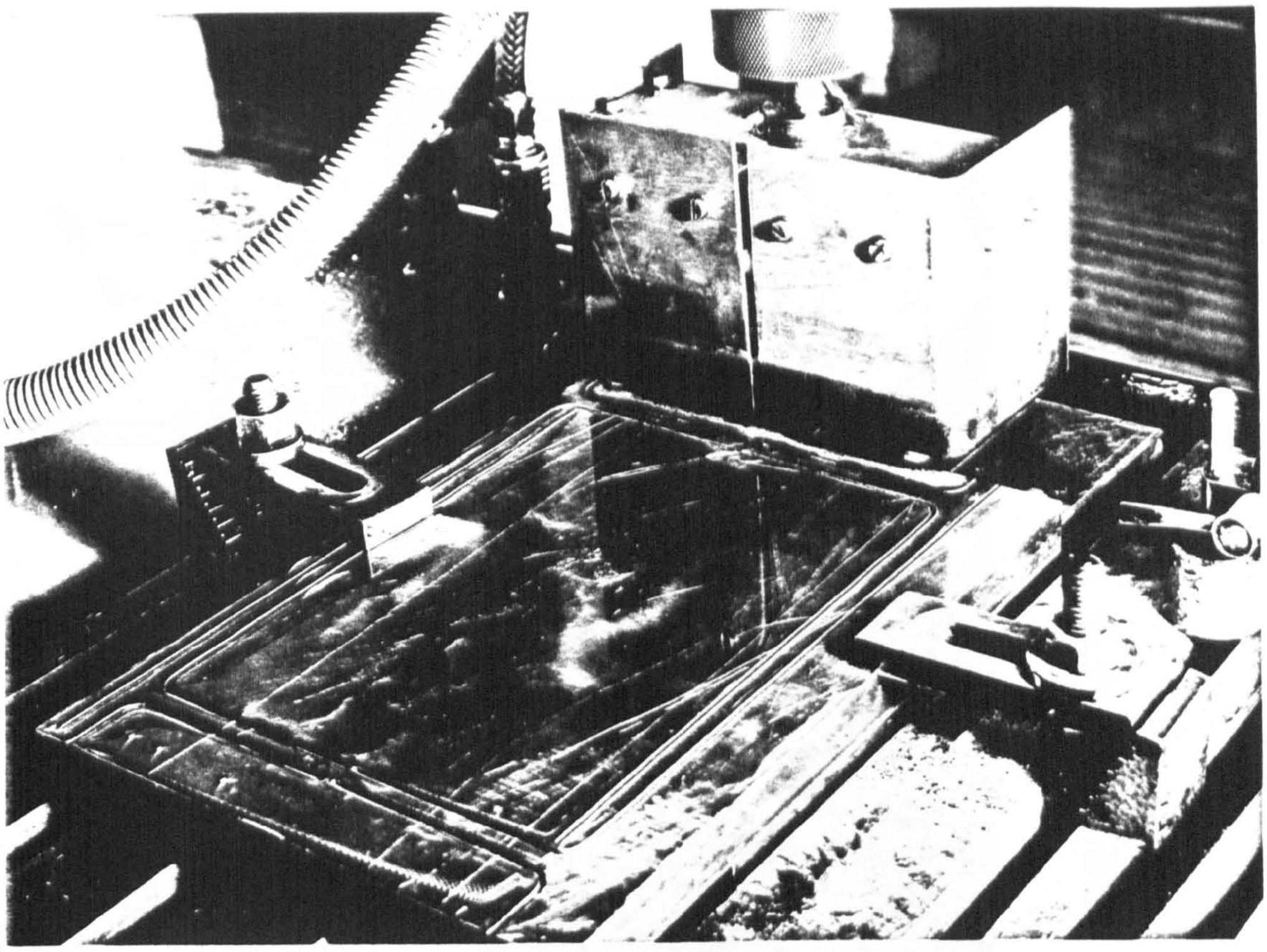

FIG. 5.11 SPARK EROSION TECHNIQUE

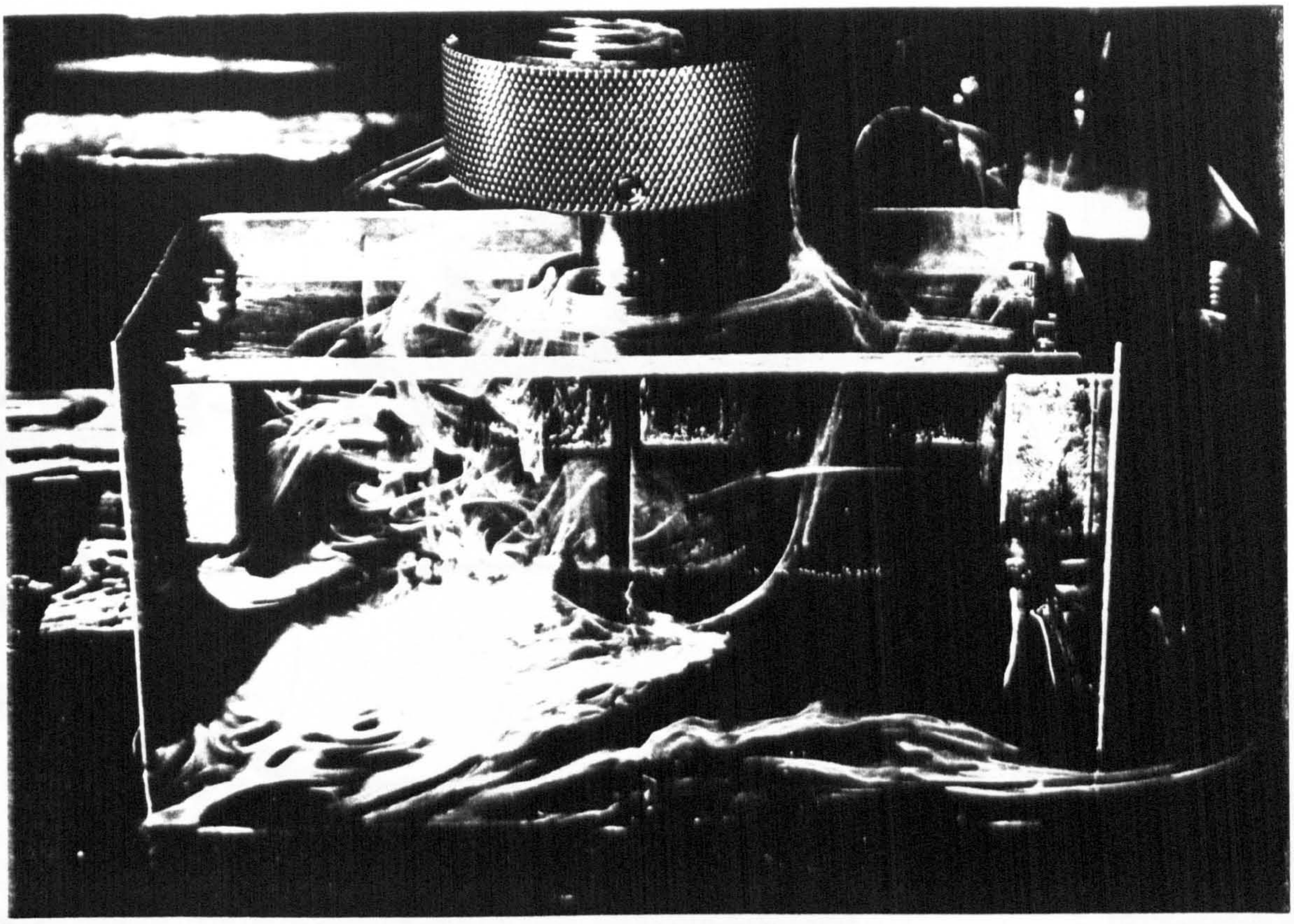

FIG. 5.12

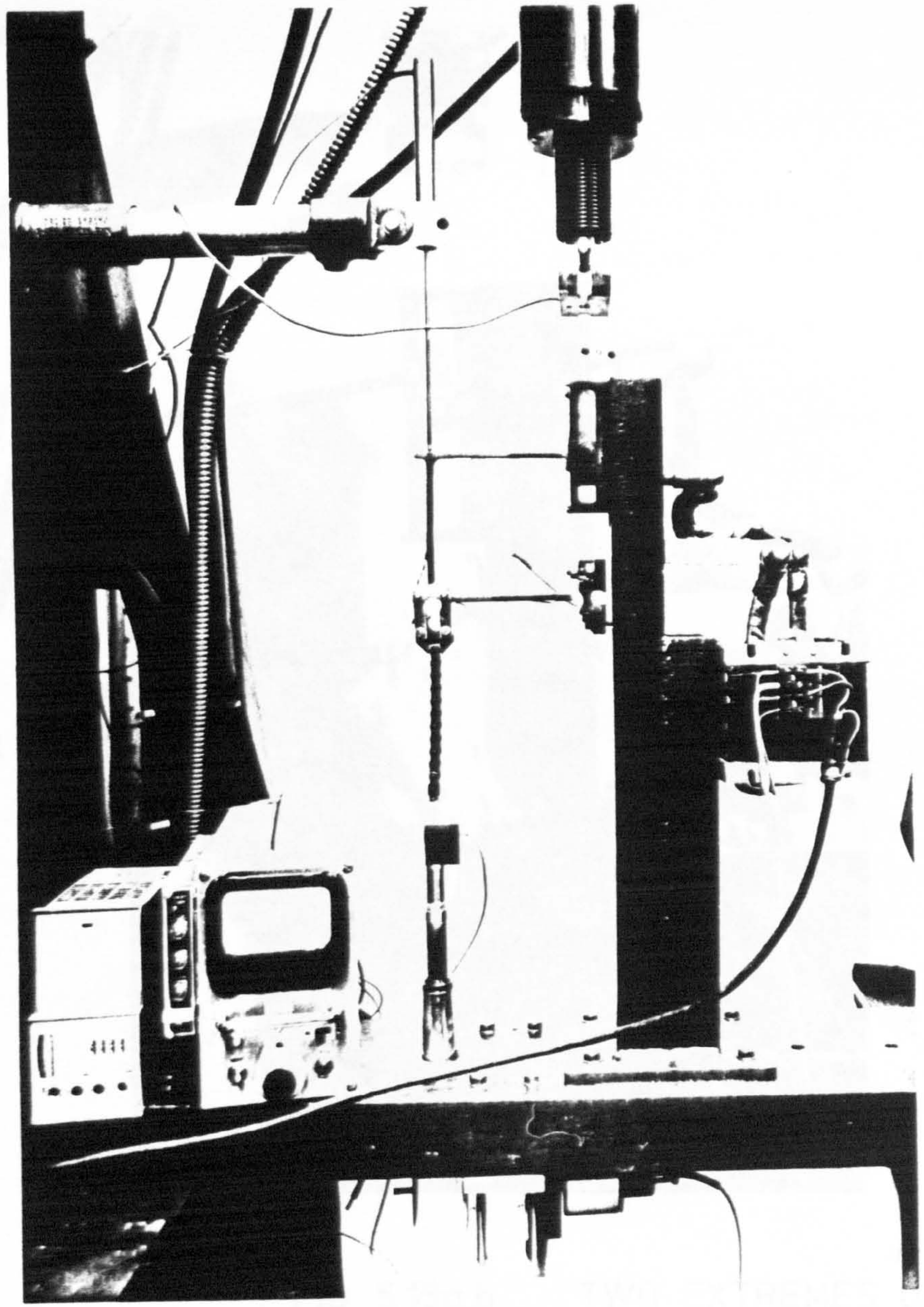

FIG. 5.13 THE APPARATUS

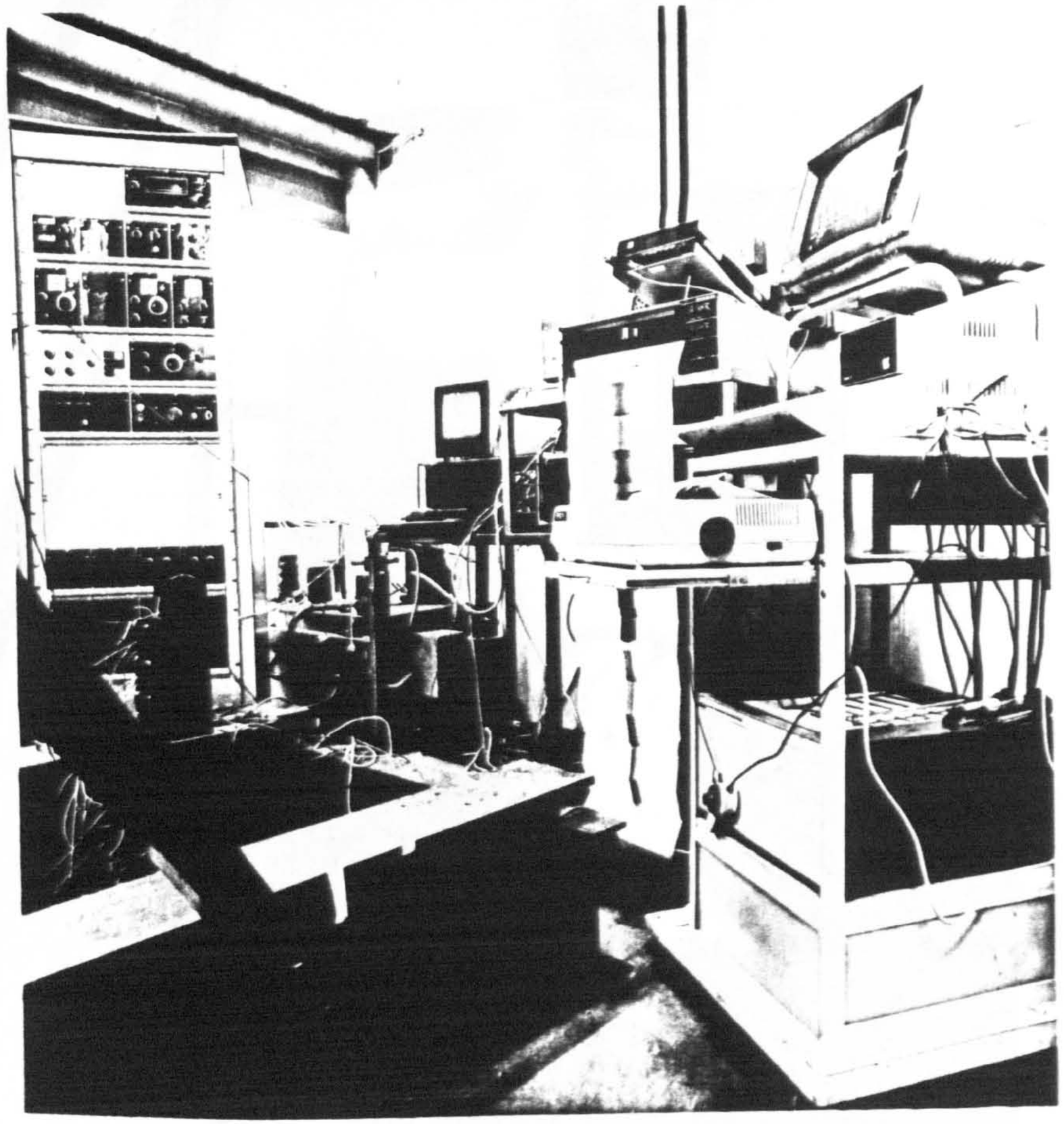

FIG. 5.14 DATA RECORDING EQUIPMENT

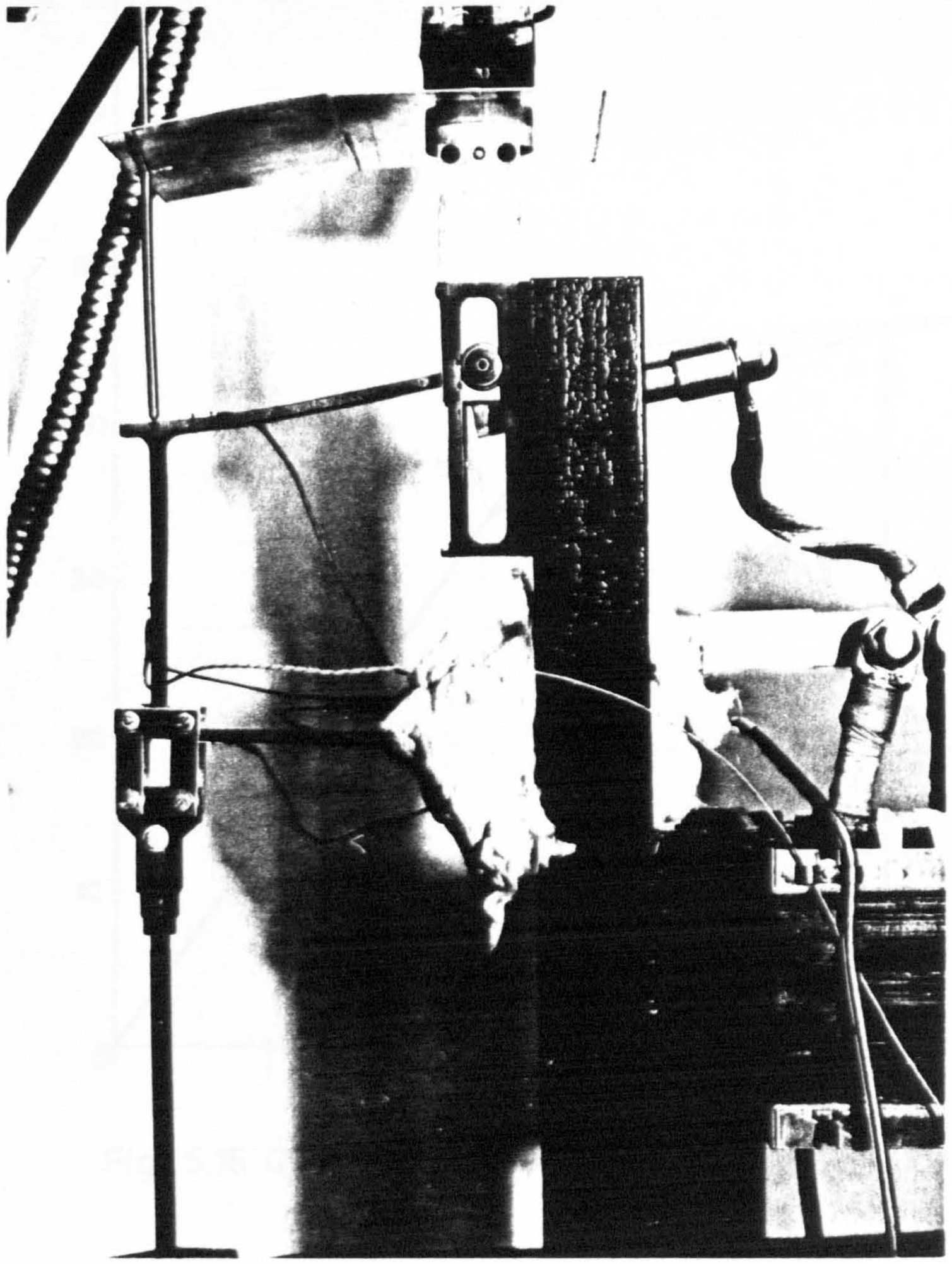

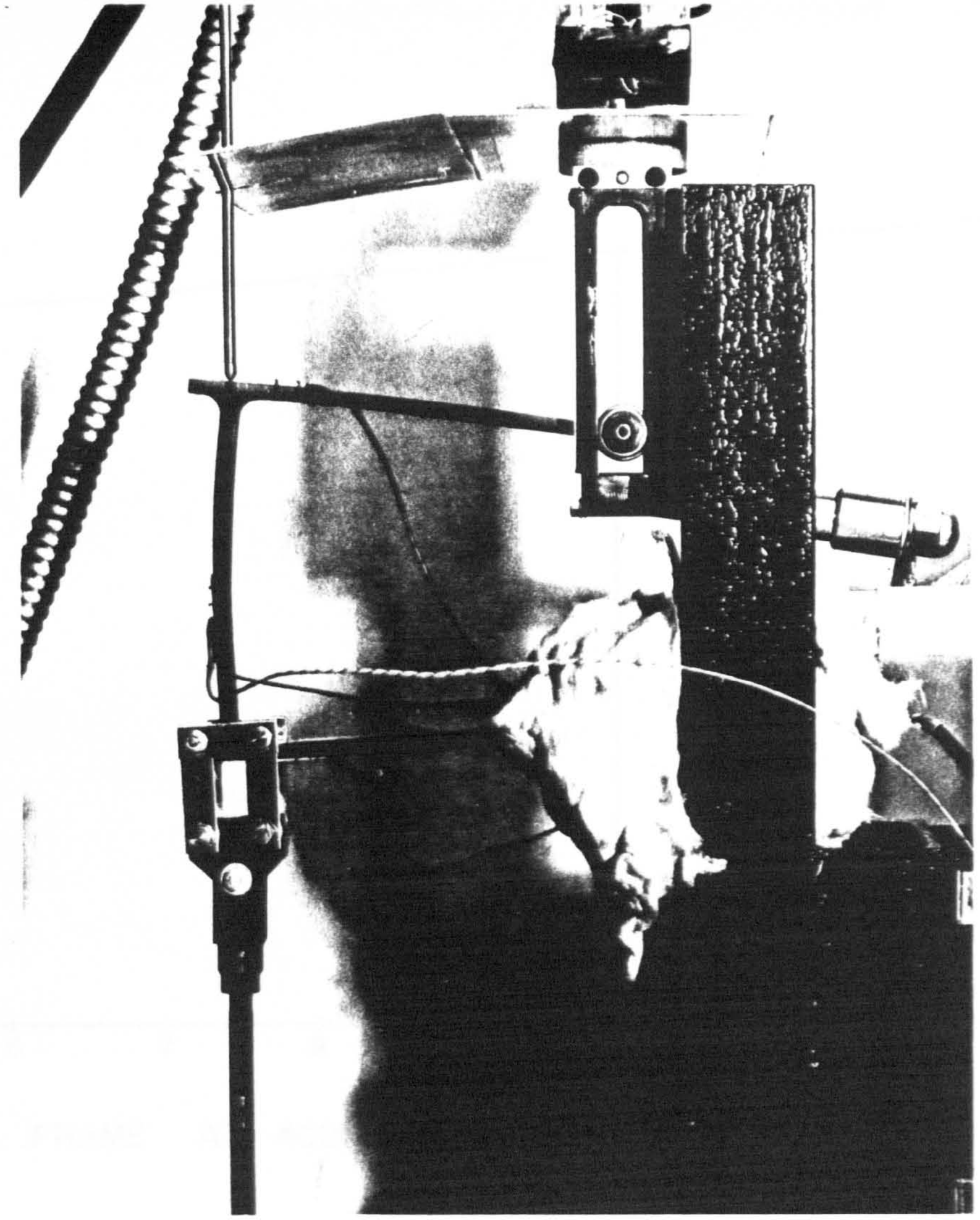

FIG. 5.15a,b. TWO EXTREMES OF THE CYCLE $\pm \delta_A$

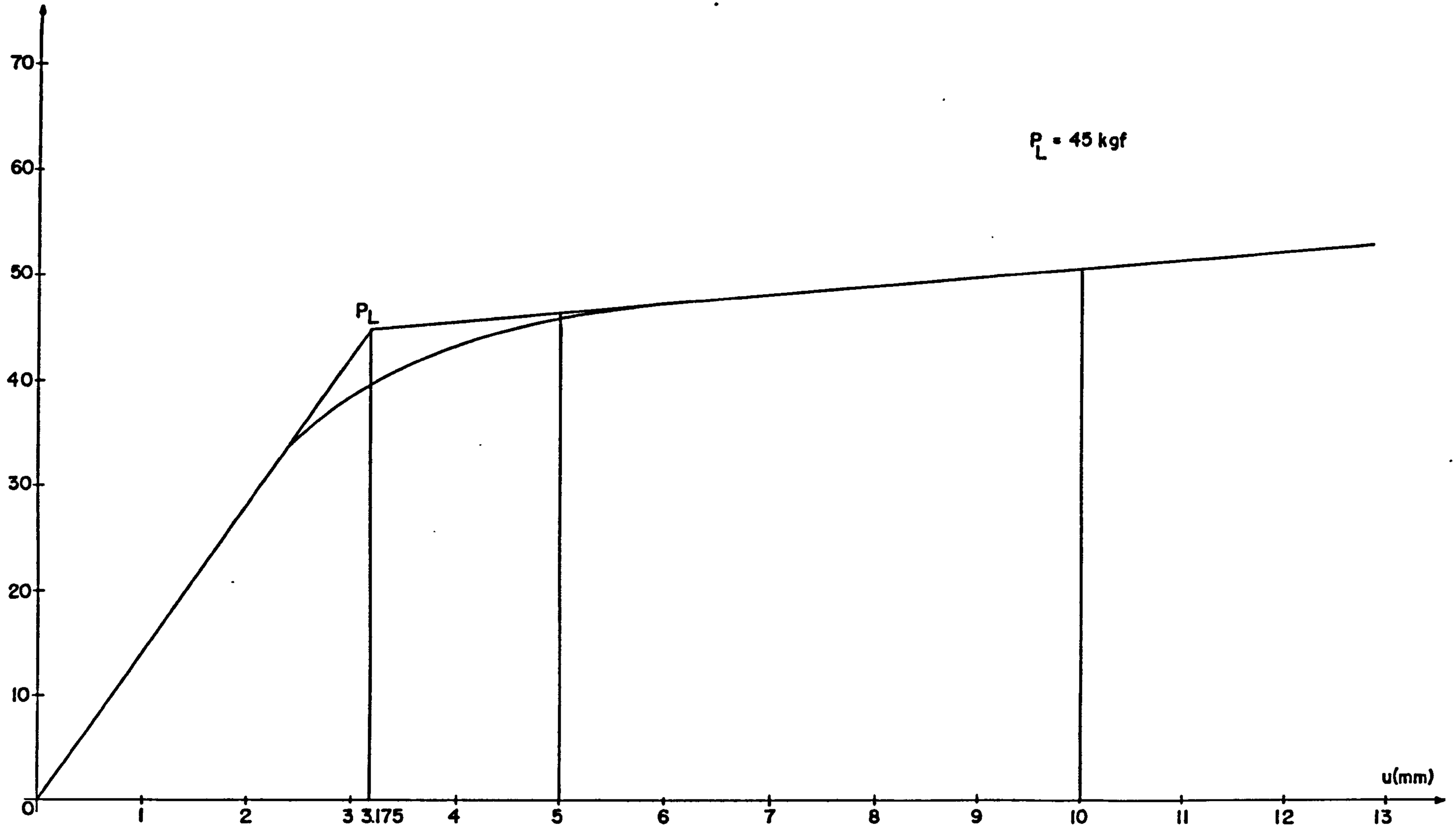

Fig. 5.16 COLLAPSE LOAD TEST ON SS316 PORTAL FRAME AT 400°C

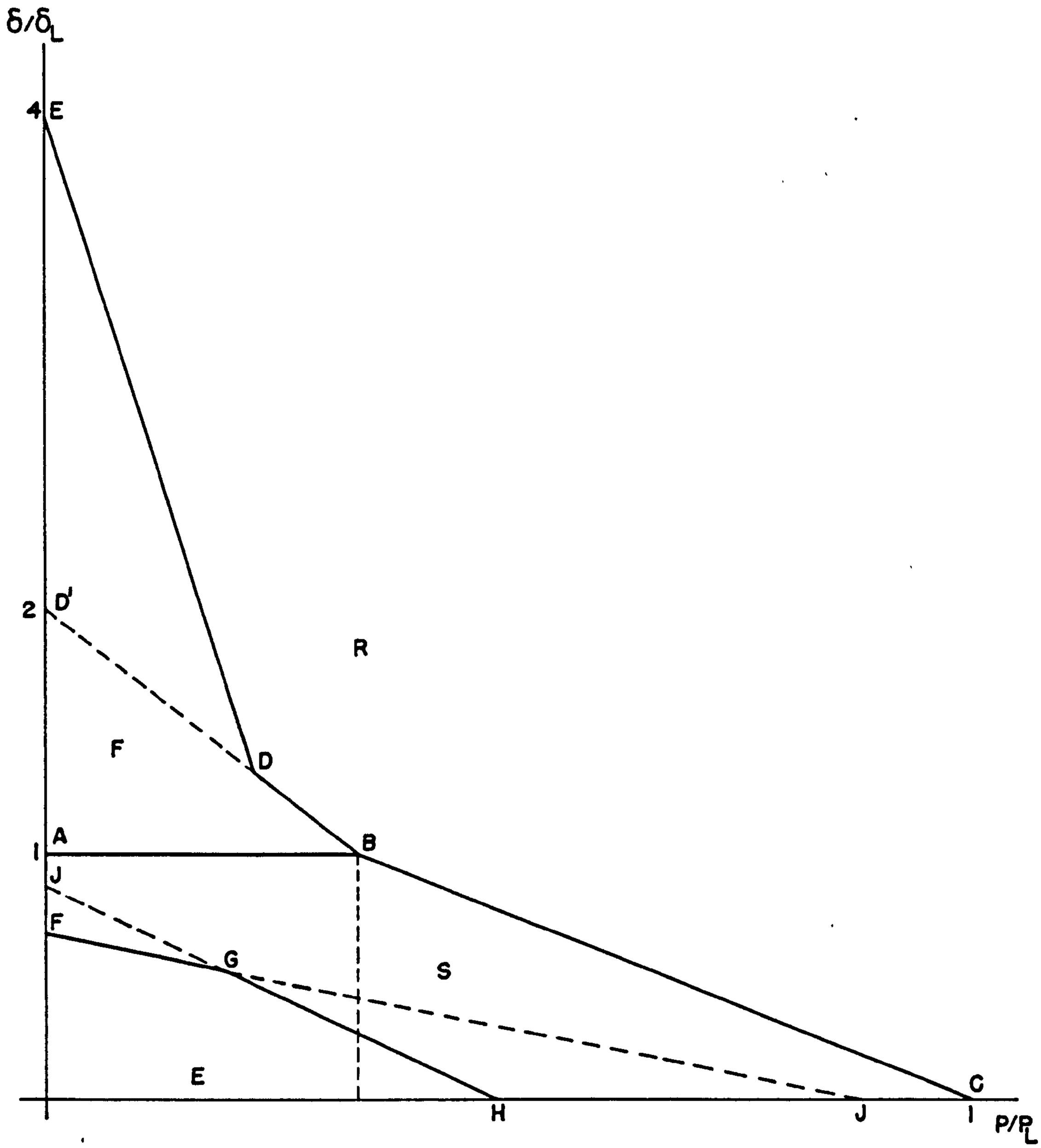

Fig. 5.17 - SKETCH OF THE BREE DIAGRAM SHOWING THE REGIONS OF DIFFERENT MODES OF BEHAVIOUR

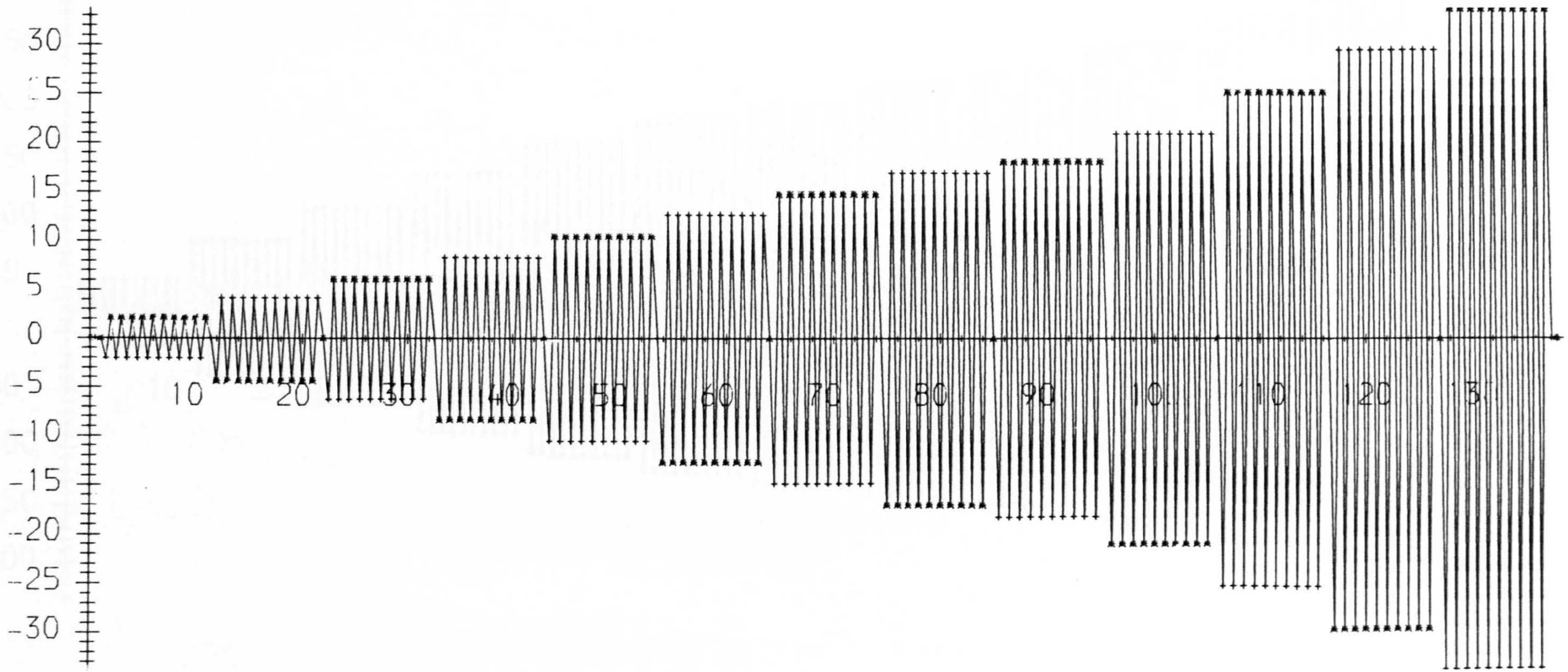

FIG. 5.18a. CONTROL DISPLACEMENT

CYCLES

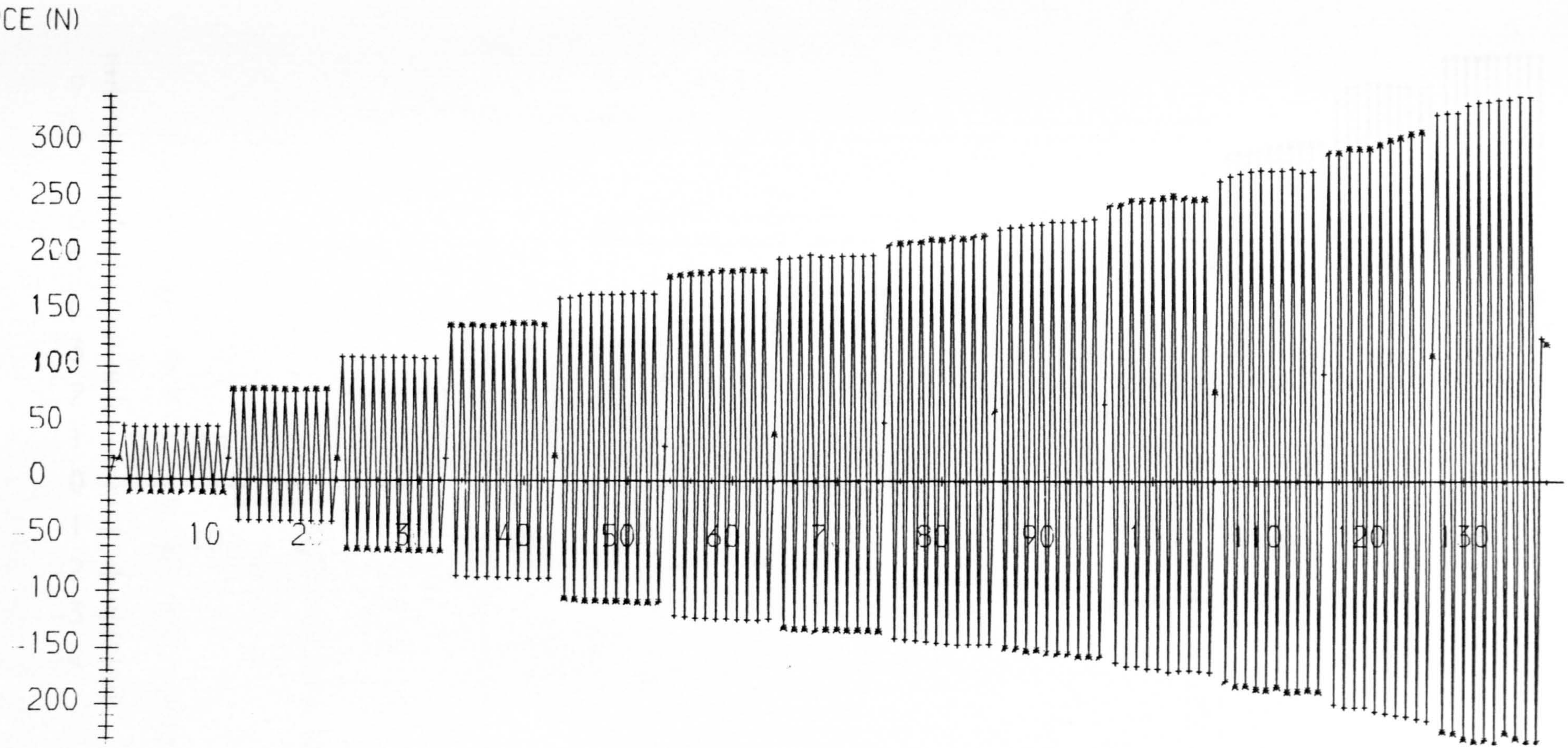

FIG. 18b FORCE REQUIRED TO PRODUCE THE DISPLACEMENTS $\pm \delta_A$

CYCLES

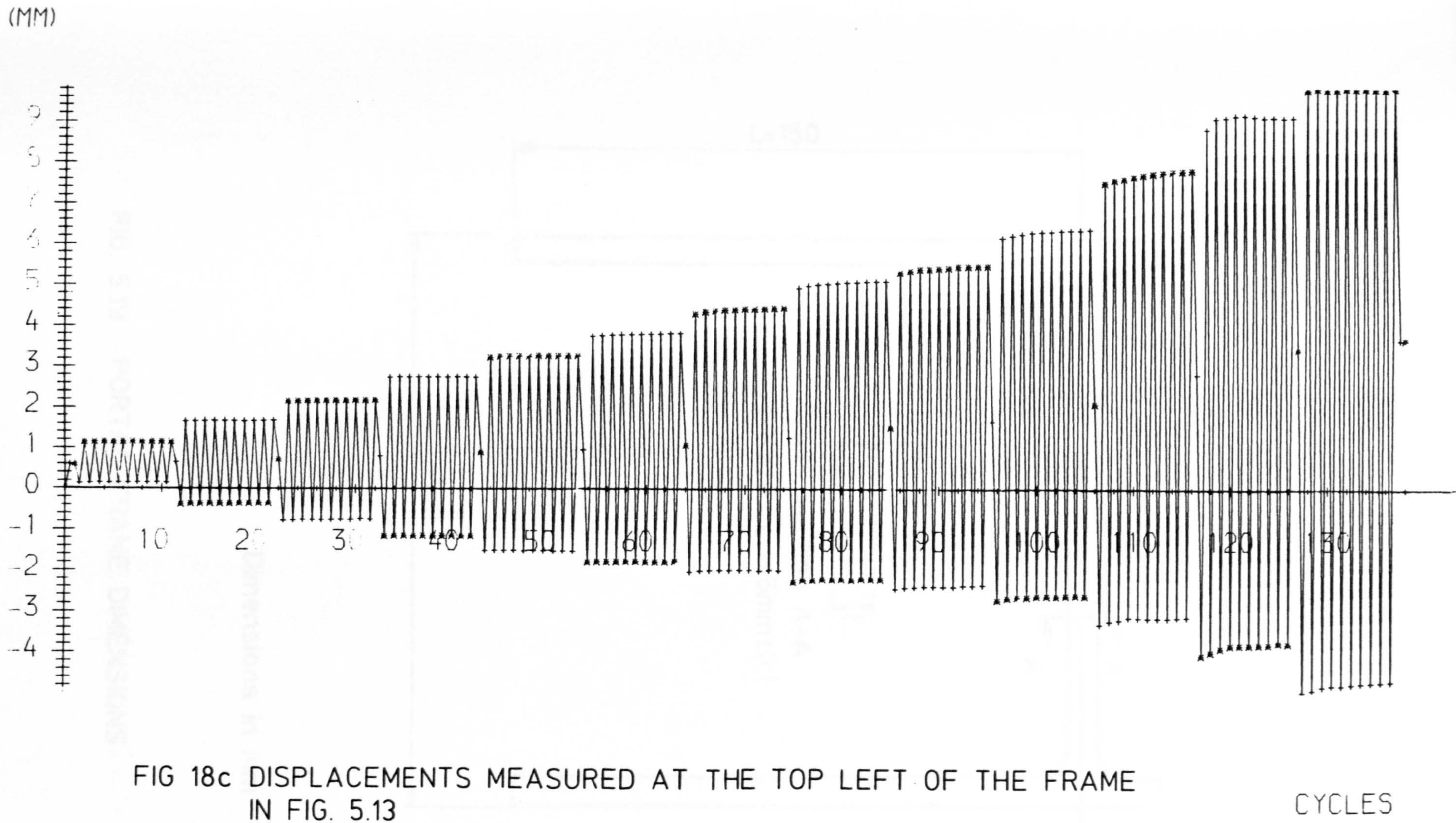

FIG 18c DISPLACEMENTS MEASURED AT THE TOP LEFT OF THE FRAME IN FIG. 5.13

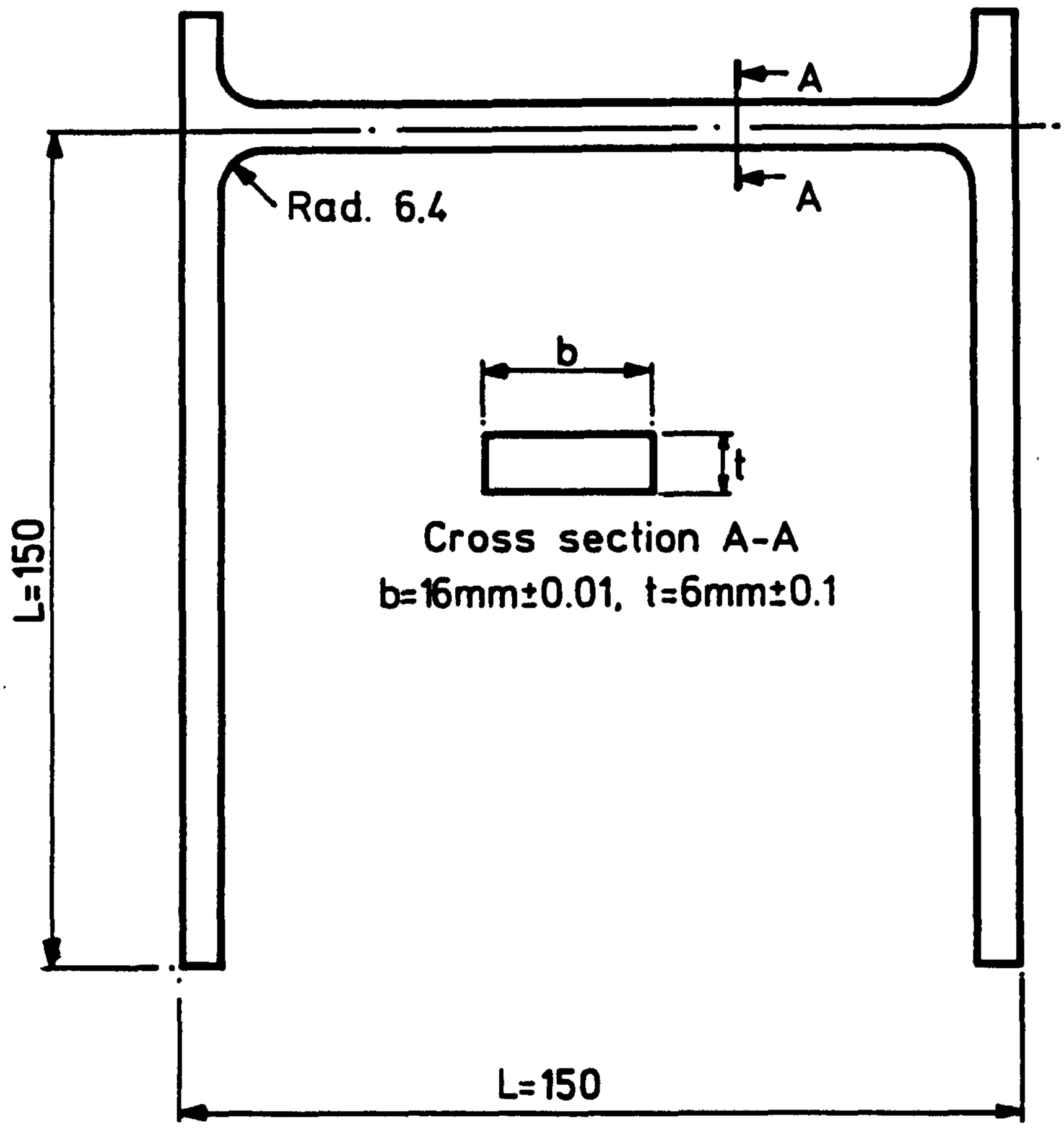

Dimensions in mm

FIG. 5.19 PORTAL FRAME DIMENSIONS

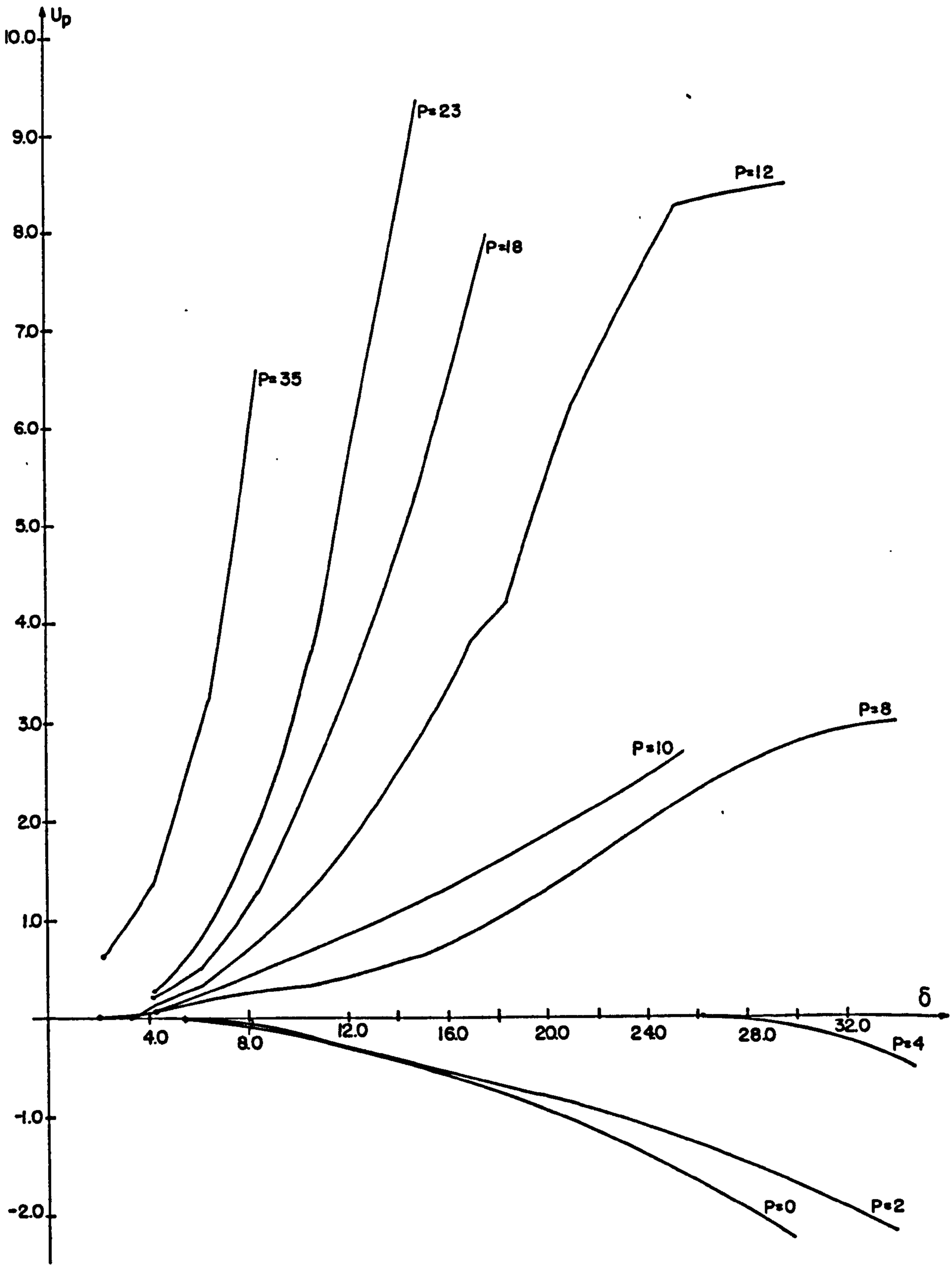

Fig. 5.20 PLASTIC DISPLACEMENT/CONTROL DISPLACEMENT DIAGRAM

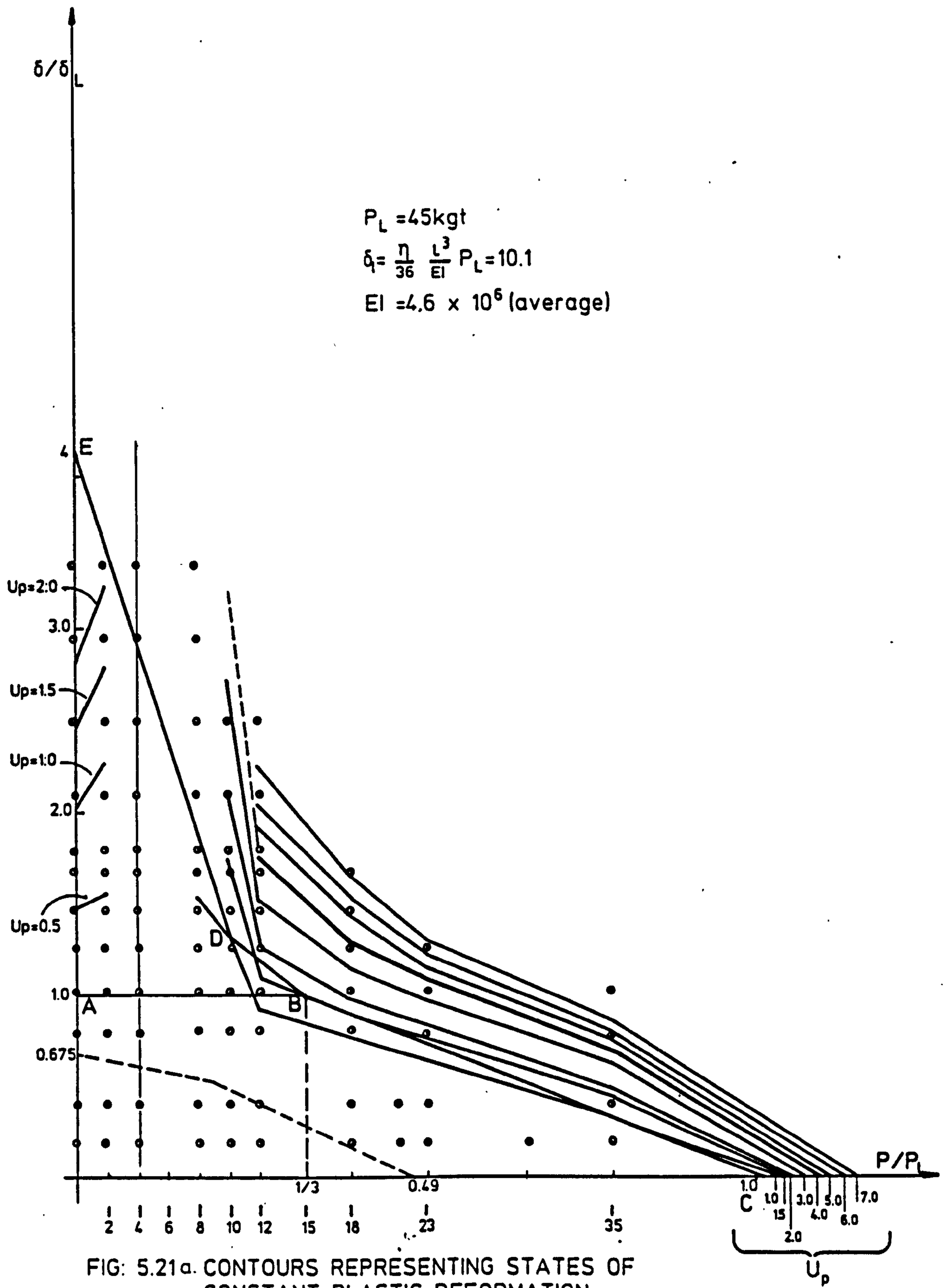

FIG: 5.21a. CONTOURS REPRESENTING STATES OF CONSTANT PLASTIC DEFORMATION

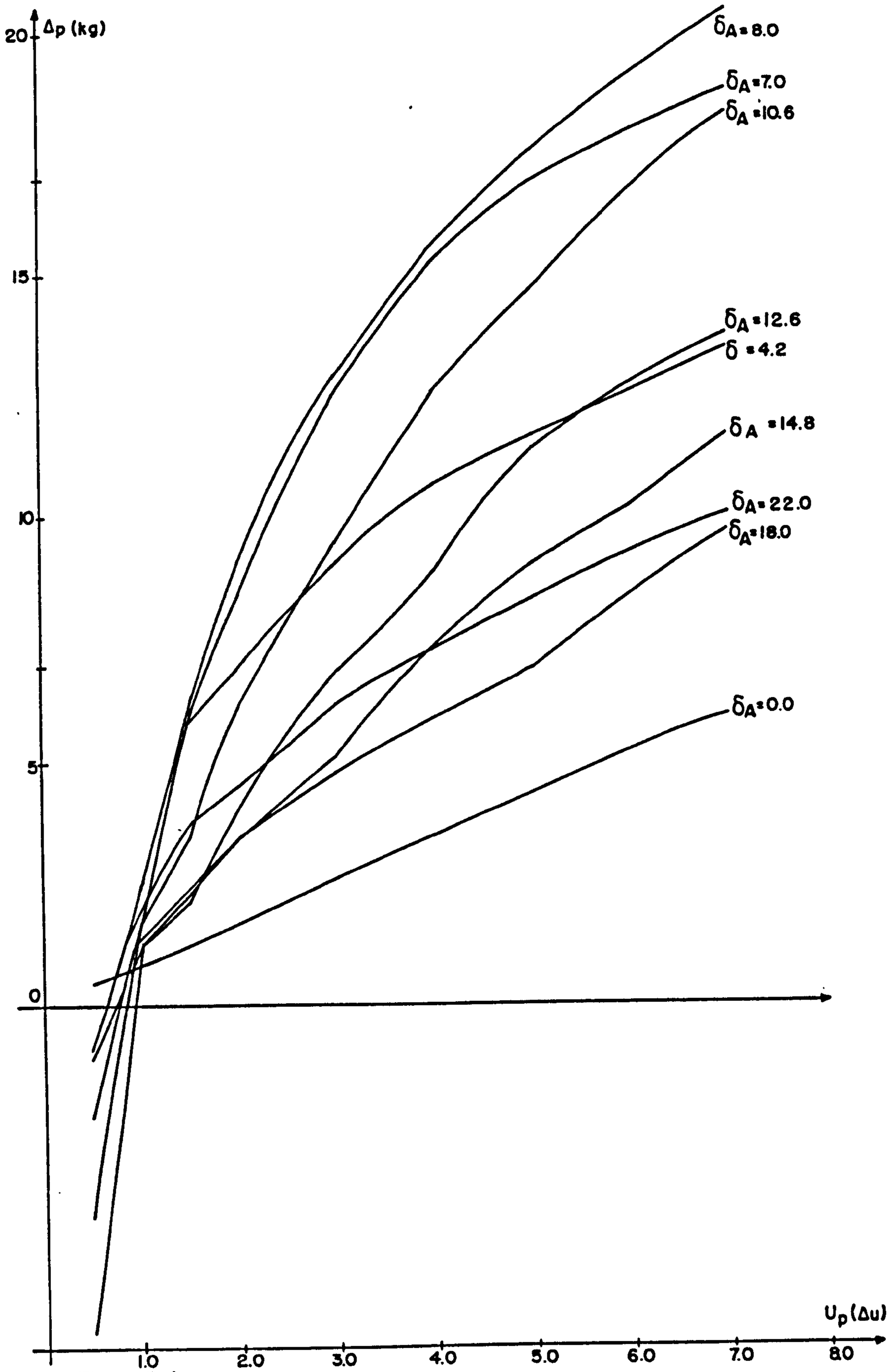
Δp (kg)
20
15
10
5
0
δA = 8.0
δA = 7.0
δA = 10.6
δA = 12.6
δ = 4.2
δA = 14.8
δA = 22.0
δA = 18.0
δA = 0.0
Up (Δu)
1.0
2.0
3.0
4.0
5.0
6.0
7.0
8.0
Fig. 5.21b

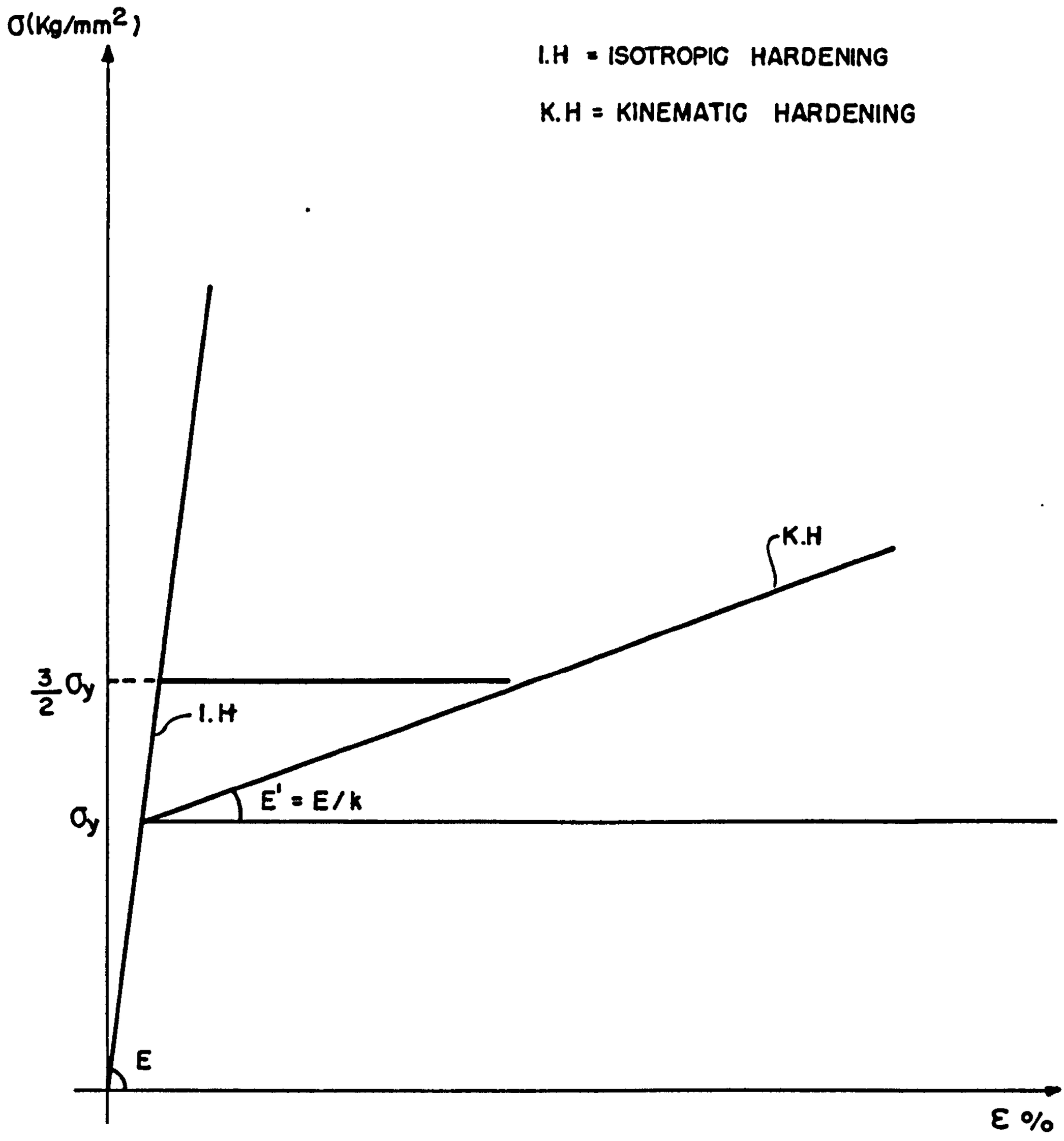

Fig. 5.22 - UNIAXIAL STRESS-STRAIN DIAGRAM FOR THE ISOTROPIC AND KINEMATIC HARDENING MODELS

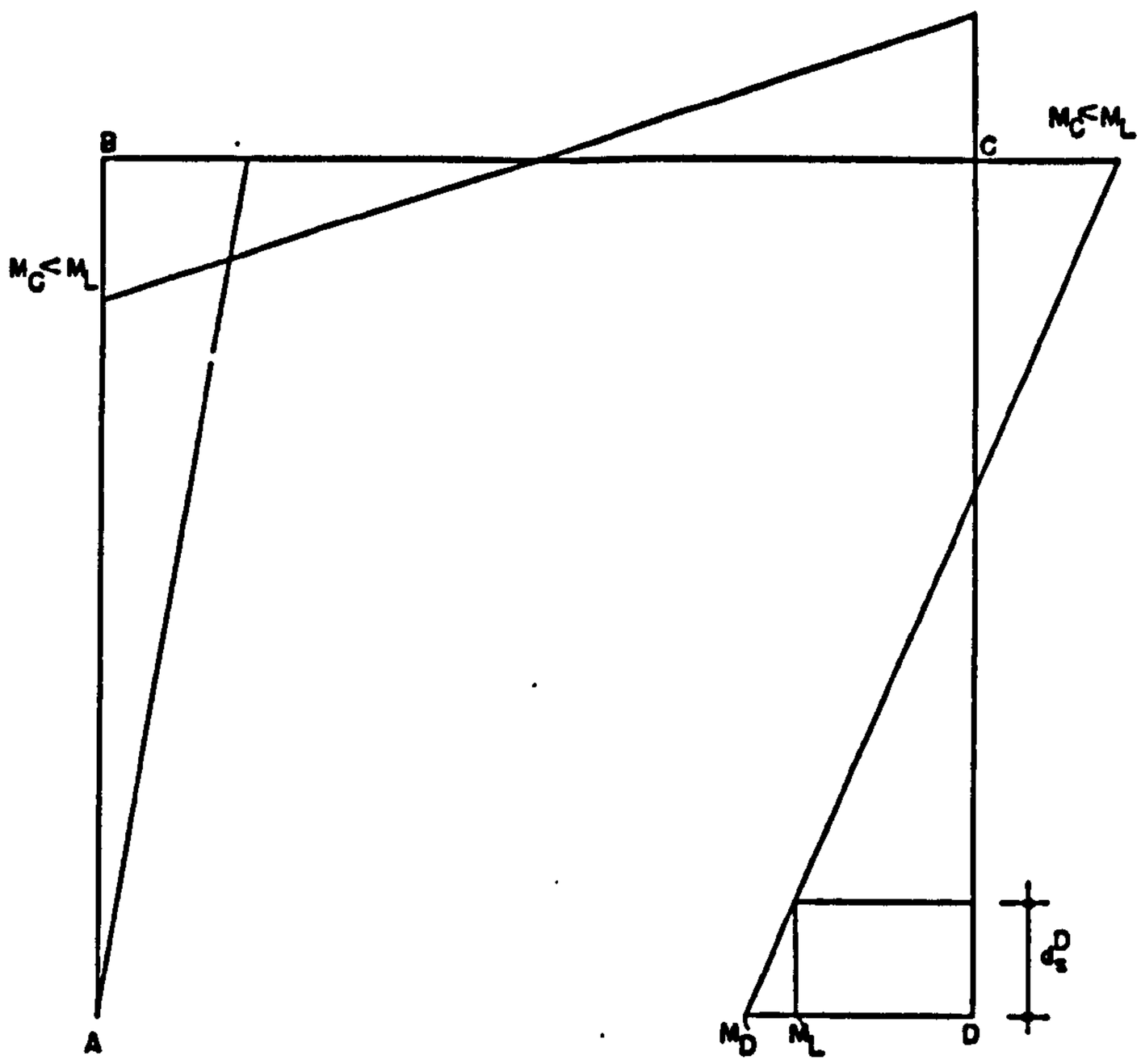

Fig. 5.23 - MOMENT DISTRIBUTION FOR AN OPERATING POINT AT THE SHAKEDOWN BOUNDARY CORRESPONDING TO P = 35 Kg

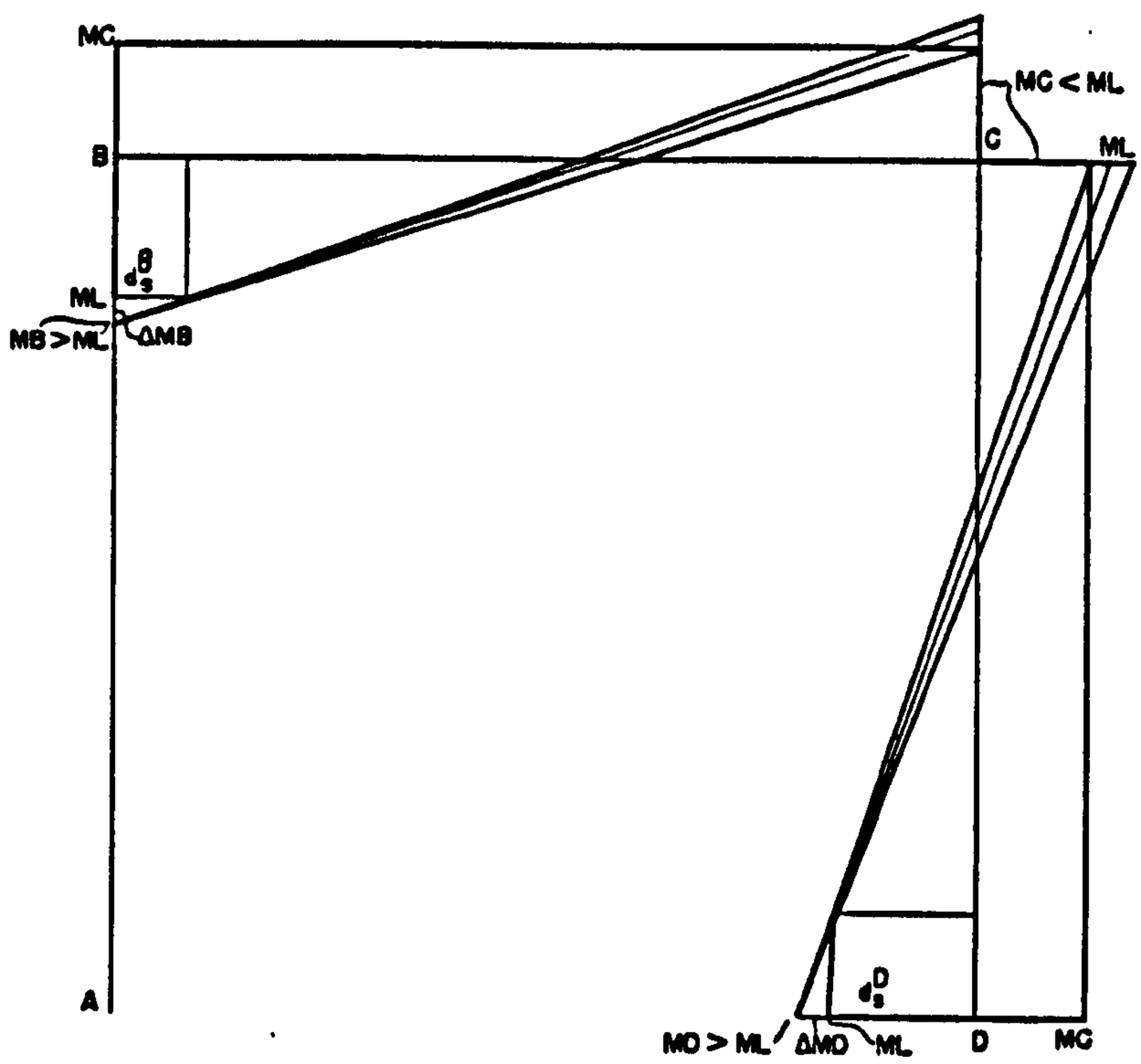

Fig. 5.24 - MOMENT DISTRIBUTION FOR SOME OPERATING POINTS AT BOUND BC OF THE BREE DIAGRAM

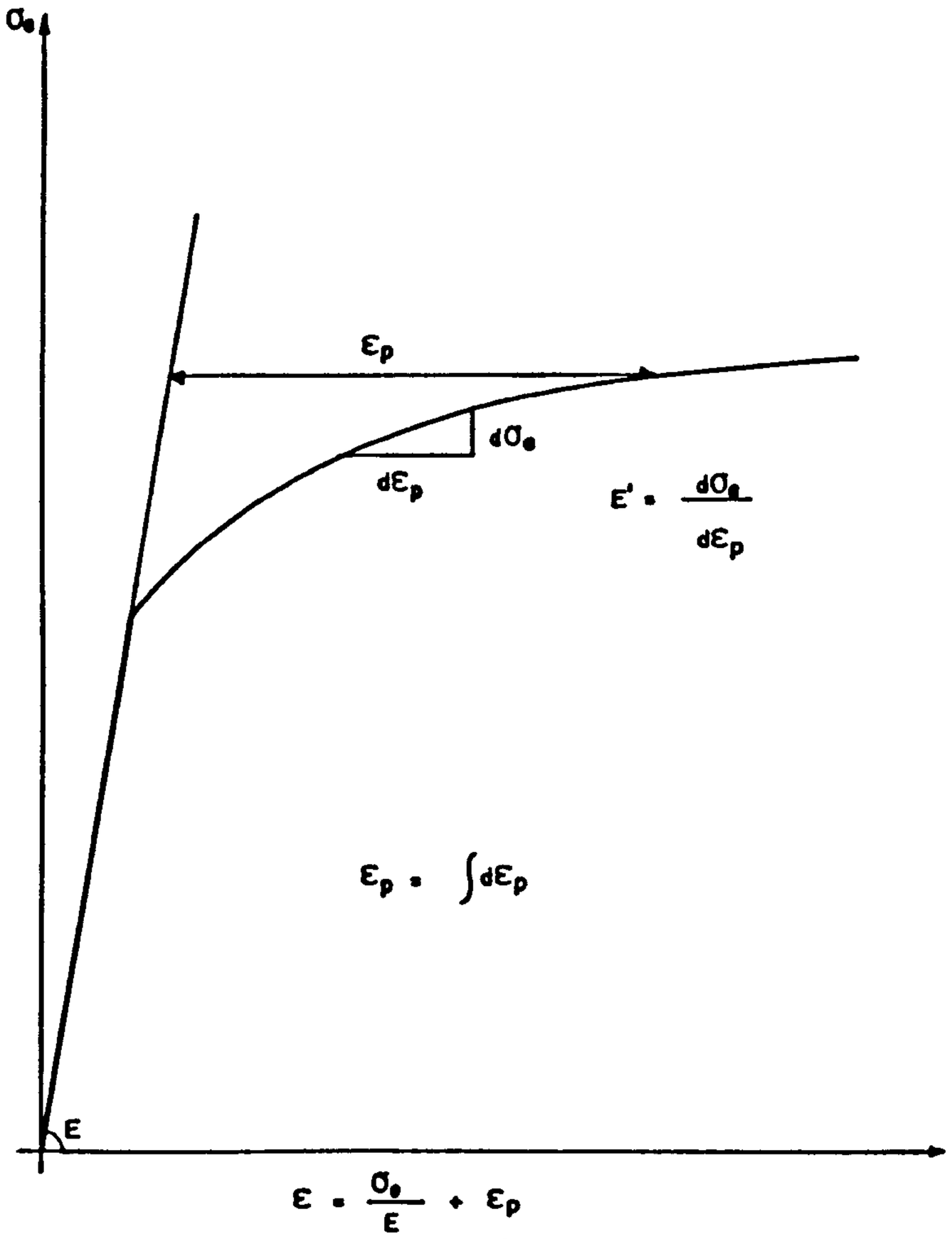

Fig. 5.25 EQUIVALENT STRESS/ EQUIVALENT PLASTIC STRAIN DIAGRAM

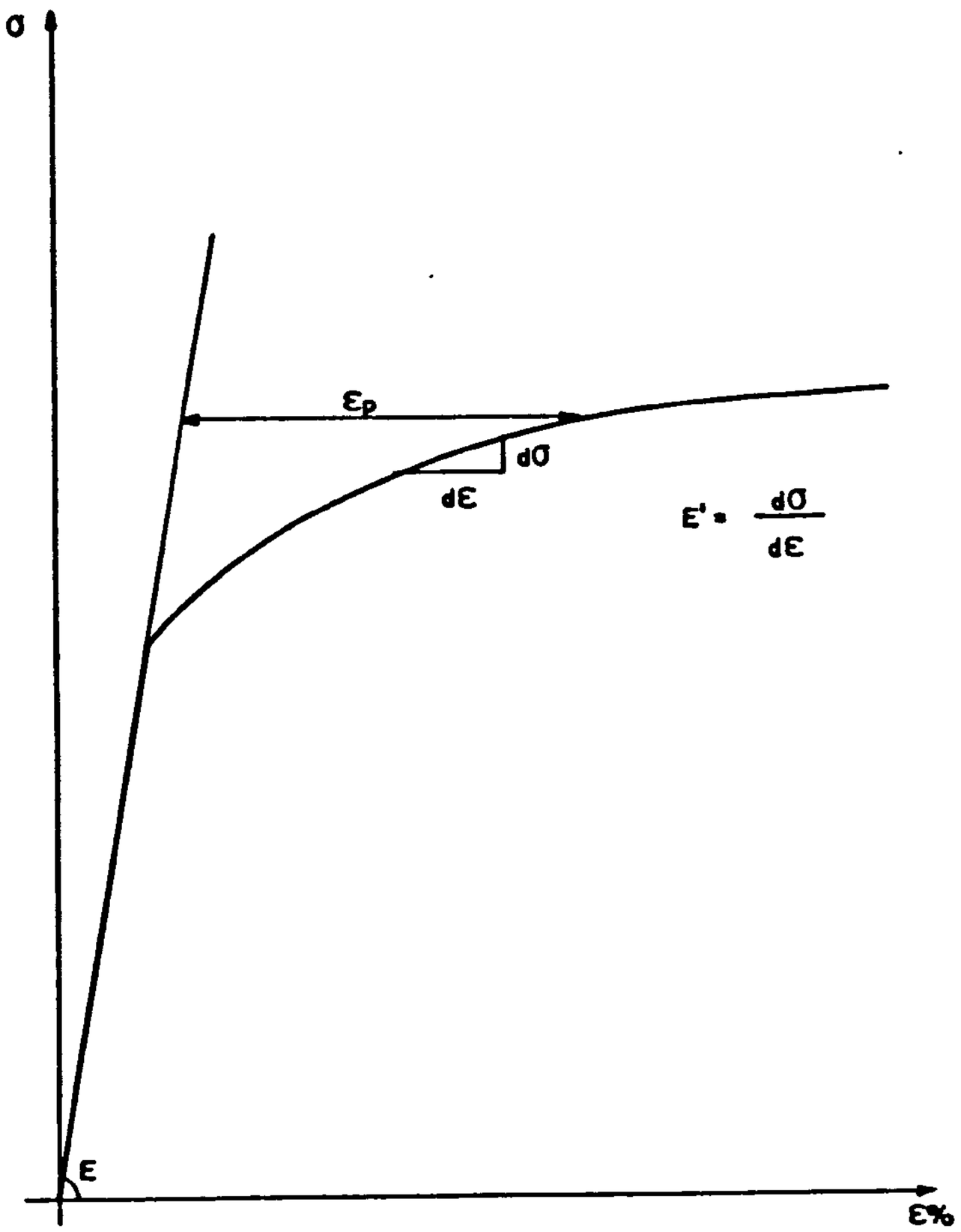

Fig. 5.26 STRESS-STRAIN DIAGRAM FOR A MONOTONIC UNIAXIAL TENSILE TEST

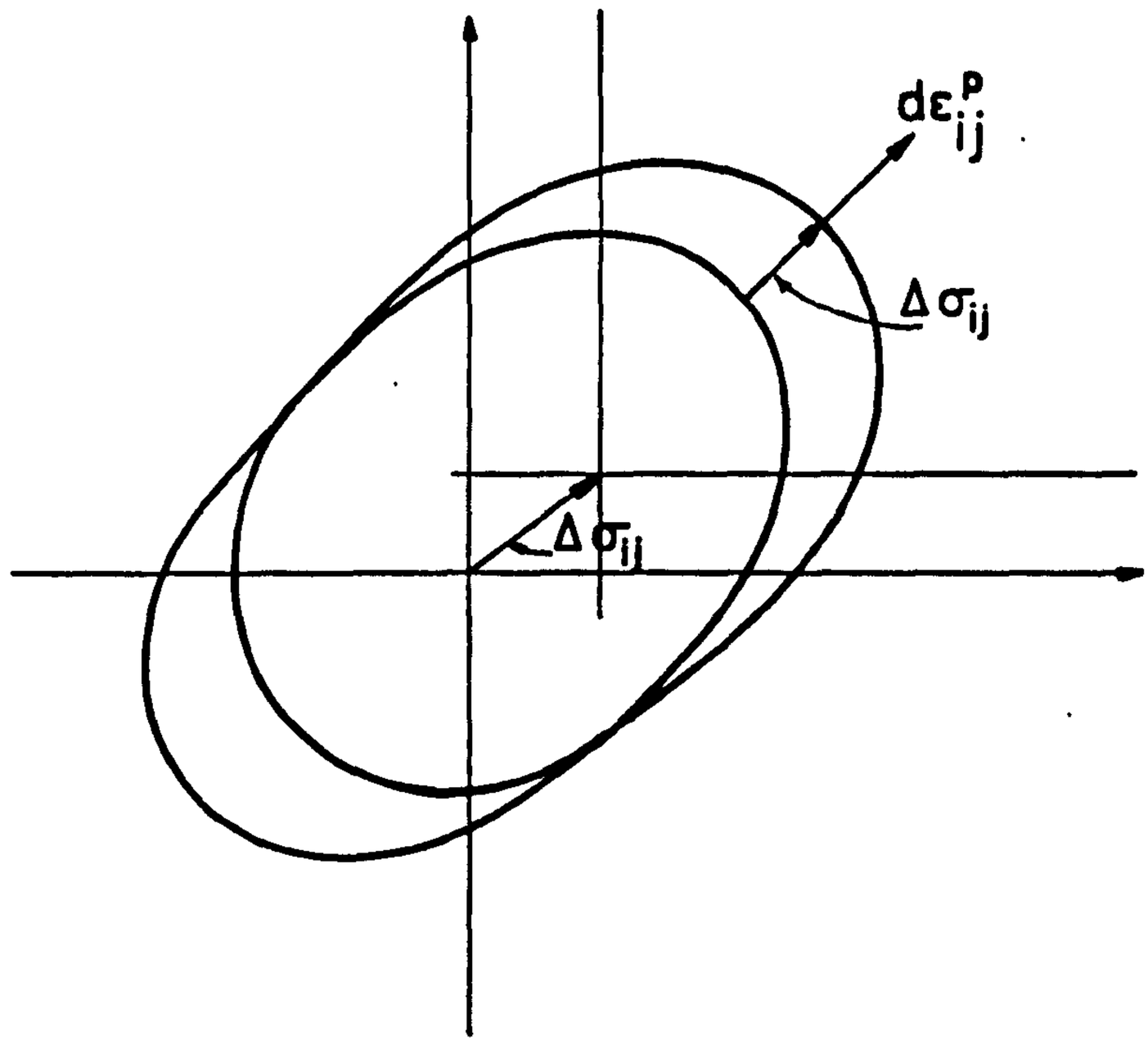

Fig. 5.27 PRAGERS RULE

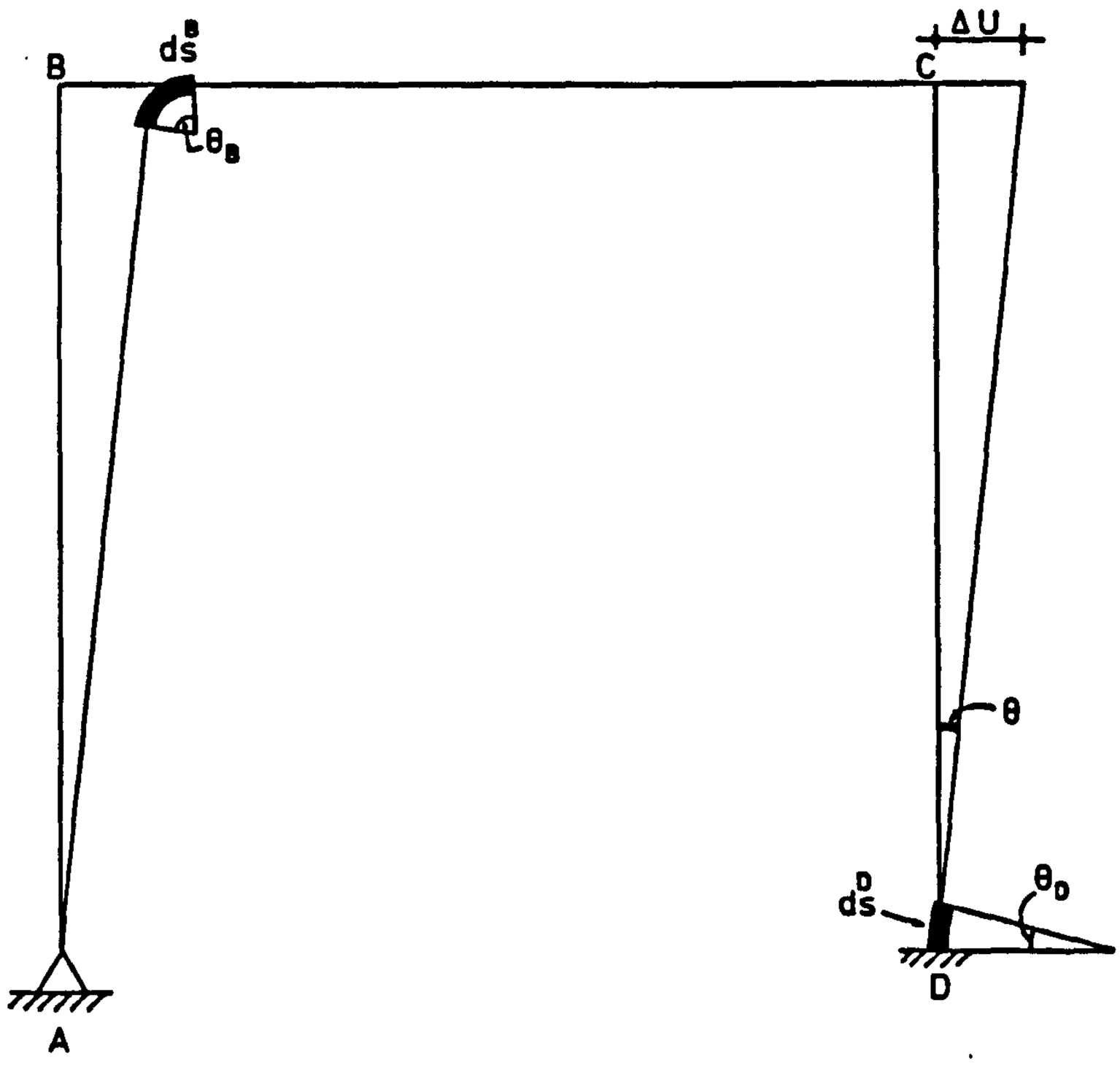

Fig. 5.28 SCHEMATIC REPRESENTATION OF THE HINGES EXTENT

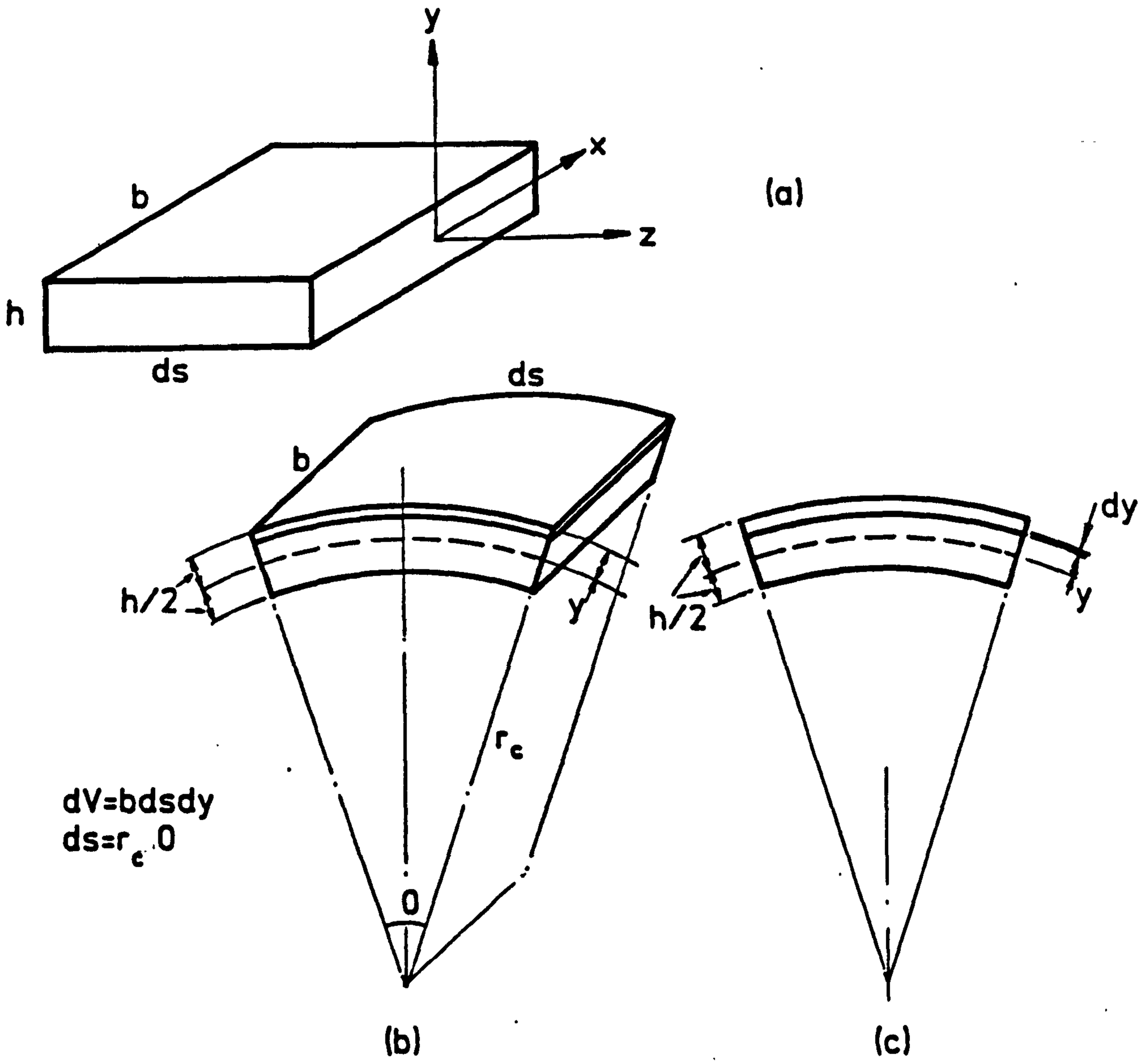

FIG. 5.29 THE TOTAL EXTENT OF THE HINGES

a) The geometry of the material element
b) The element deformed as a hinge
c) A frontal view

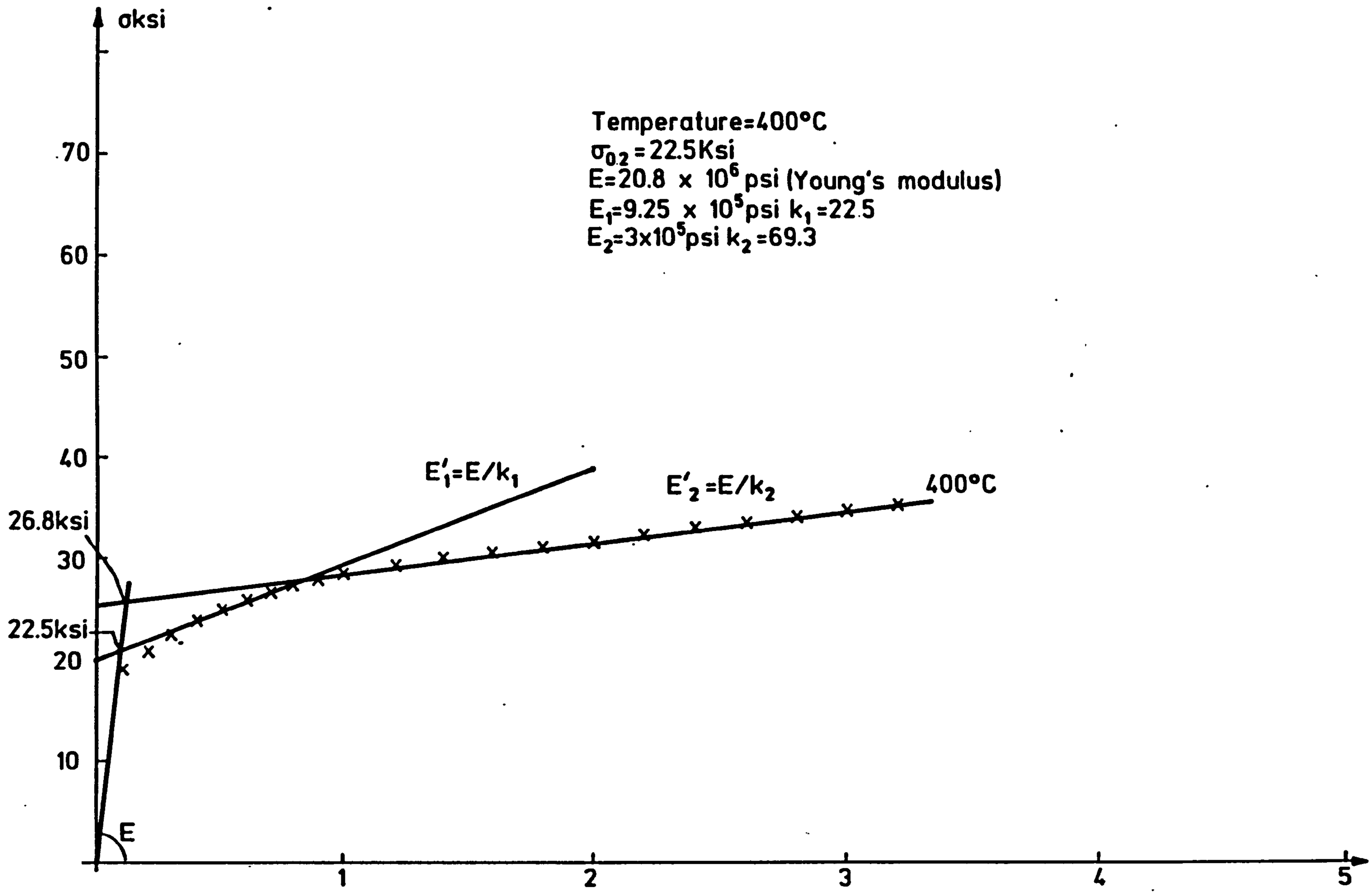

FIG: 5.30 MONOTONIC CURVES AT 400°C

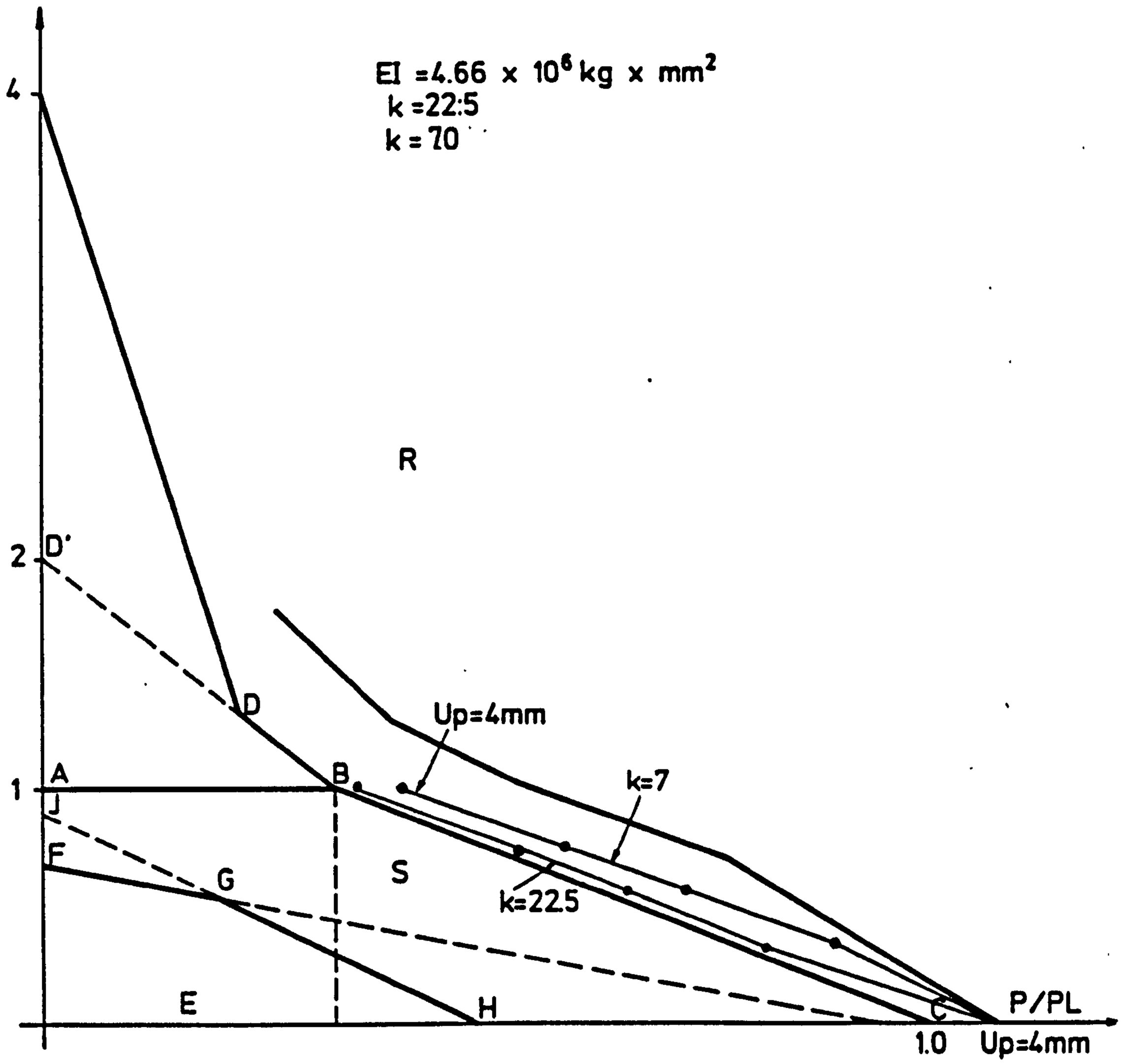

FIG. 5.31 COMPARISON BETWEEN THE EXPERIMENTAL AND THEORETICAL CONTOURS FOR U_p=4mm

CHAPTER 6

A DISPLACEMENT FORMULATION FOR THE FINITE ELEMENT SHAKEDOWN ANALYSIS OF PRESSURE VESSELS

6.1 Introduction

In recent years the application of mathematical programming methods to the solution of shakedown and limit analysis problems has received a great deal of attention in civil engineering structural problems [59]. The selection of numerical methods, such as the Finite Element Method(FEM), as a means of discretizing continuous structural problems for the application of these methods to shell problems [51,60,61,62,63,64], is beginning to contribute to the development of simplified techniques capable of reliably solving such problems. The approaches used in these techniques are generally based upon a statement on the equilibrium of forces, ie, a lower bound(STATICS) or upon a statement on the compatibility of deformations, ie, an upper bound (KINEMATICS). The simplified procedures adopted to make the development of these techniques viable rely upon the use of perfect plasticity, but it is hoped that it may be possible to use more complete constitutive relations to describe the structural behaviour of the material. For example, Zarka [64] has described a technique for linear kinematic hardening material. The STATIC, the KINEMATIC and the CONSTITUTIVE relations constitute the fundamentals of a structural mechanics problem, although they are established

independently of each other with no implied relationship between statics and kinematics. One practical solution is to obtain a lower bound based on the equilibrium of the loading system which agrees as close by as possible with an upper bound based on structural geometry. An accepted important feature of Structural Mechanics is a duality which, when satisfied at every stage of the calculations, consists of a reliable criterion for the FEM formulation. In addition, the use of Linear Programming in shakedown analysis on the basis of the classical shakedown theorems constitutes a dual pair which allows one to switch from one formulation to the other by means of certain mathematical rules.

There has been some progress in the development of techniques involving FEM [61,62,66,67] and mathematical programming to solve shakedown problems but only very recently have attempts been made to include thermally loaded structures in such numerical approaches [51,60,63,64]. Another feature of most of the existing techniques is the emphasis of their applicability to beams and framed types of structure more common to civil engineers as became evident in the EUROMECH 185 conference [59]. The lower bound theorem (Melan's Theorem) seems also to have some preference among the techniques available and the shakedown concept applied via such theory is well established as the basis for design criteria for pressure vessels, although its application has been primarily limited to mechanical loads [4,5,6,7,8]. The application of the lower bound theorem to pressure vessel design by means of an analytical approach was

first proposed by Leckie [4]. Subsequently, the technique was developed by Leckie and Penny [5] by using linear programming to obtain lower bound shakedown estimates of the applied loads. Several papers have latterly contributed to the understanding of this particular problem and the technique proposed to solve it [6,8,9], and for its simplicity it is worthwhile mentioning the description and discussion of the shakedown concept applied to pressure vessels presented by Findlay and Spence [7].

The kinematic shakedown formulation has recently been applied by Karadeniz and Ponter [51] and Karadeniz [60] to the problem of cylindrical pressure vessels subjected to a programme of cyclic thermal and steady mechanical loading whose solution was obtained by adapting the problem to a linear programming standard form where the actual continuous structure is replaced by a compatible system of finite elements. Such a method of analysis allows the construction of an interactive diagram for the shakedown limit for classes of thermal loading history in the form of a Bree diagram, as well as also providing a picture of the deformation patterns liable to occur. Although the technique used to obtain the solutions presented in [51,60] has some degree of generality, its application is limited to the peculiarities of cylindrical vessels' geometry. A Tresca yield condition was used together with a restricted class of displacement fields.

In the present chapter a general technique will be developed based upon a upper bound displacement formulation for the Finite Element Method applied to shakedown analysis of axi-

symmetric pressure vessels by using linear programming, for Tresca type yield surfaces. The kinematic shakedown theorem (Koiter's) will be used according to its reformulated form presented in Chapter 2 and the results will yield upper bounds.

This general technique for pressure vessels will be associated with four basic types of axi-symmetrical elements, namely

- cylindrical
- conical
- spherical
- toroidal

Theoretically the method would allow any combination of such elements, although for the present work the technique has been applied only to vessels composed of the basic elements individually and for torispherical vessels composed of the combination of cylindrical, toroidal and spherical elements. The results obtained are compared with other solutions obtained either from analytical methods or from numerical techniques already available and will be discussed in a later section. The computer code written to obtain the solutions was quite flexible, in the sense that the inclusion of a new type of shell resulting from a different combination of the basic elements proved possible with relative ease.

The emphasis upon the upper bound theorem arises from two considerations. Although the main emphasis in Section 6.10 is on the solution of limit load problems, in the longer term the solution of thermal loading problems is of much greater importance. The application of the lower bound theorem has not produced particularly good results, as pointed out by Ponter [14]. The reason for this is that the residual stress fields required to produce a good lower bound are often quite complex. For example, in the classic Bree problem [40] the residual stress field at the shakedown limit is not linear through the plate thickness, but involves two regions of linear variation with a discontinuity on the centre surface. Using finite elements it is very difficult to define classes of approximating residual stresses which can provide this type of variation, and the use of linearly varying fields, or even continuous fields, yields poor lower bounds. On the other hand, the classes of displacement field associated with the shakedown limit are of a simple form and can be easily represented by suitable classes of finite element displacement distributions. Although the results are upper bounds, the choice of a sufficiently wide class of displacement fields will ensure acceptably accurate solutions.

The method described in Section 6.5 is expressed in a general form for a Tresca yield condition. For applications the same class of simple displacements is chosen as that used by Karadeniz and Ponter [51] as a means of demonstrating the technique and to allow comparison with known solutions. The displacement field assumes that all

the meridional curvature occurs at nodal points, ie, plastic hinge lines, and the meridional and circumferential strains occur within the element with no curvature. This displacement field, together with the Tresca yield condition, give rise to identical results for limit load calculations as those obtained by using the limited interaction yield surface of Drucker and Shield [75] expressed in terms of membrane forces and bending moments. It is worth noting that for thermal loading problems, the use of the upper bound in terms of generalized forces implies the assumption of residual stress fields varying linearly through the thickness of the shell. However, as commented previously, it is known that this is generally not the case and if the upper bound is used in terms of stresses and strains, no such assumption is made and the resulting upper bound is greatly improved.

In the next section, the argument used by Drucker and Shield and others for the simplification of yield surfaces are recounted, although subsequently, for the reasons given above, the general technique is described in terms of stress and strain tensors.

6.2 An Approximate Yield Surface for Symmetrically Loaded Thin Shells of Revolution

The derivation of appropriate yield surfaces for axially-symmetric loaded shells of revolution in terms of force and moments resultants is rather more complex than it is in the

case of a biaxial state of plane stress. The problem of a symmetrically loaded cylindrical shell was extensively studied by several authors with the inclusion of axial and circumferential forces acting individually or simultaneously with bending moment [69,70,71,72,73]. Onat and Prager [74] extended the investigation to general shells of revolution (Fig. 6.1). Drucker and Shield [75] have shown that the yield surface for a thin cylindrical shell can be used for any axi-symmetric thin shell of revolution as a very good approximation. They also propose the use of an hexagonal prism approximation obtained from the actual yield surface. The method proposed in [75,76] for obtaining these yield surfaces can be summarized as follows:

In the case of general shells of revolution, both meridional and circumferential bending moments $M\phi$ and $M\Theta$ appear in the equilibrium equations, which are, for example according to reference 57 and Fig. 6.1

$$r\frac{dN_\phi}{d\phi} + (N_\phi - N_\theta)R_1\cos\phi - rQ + rR_1T = 0 \qquad 6.1$$

$$r\ N_\phi + R_1N_\theta\sin\phi + \frac{d}{d\phi}(rQ) + rR_1p = 0 \qquad 6.2$$

$$r\frac{dM_\phi}{d\phi} + R_1(M_\phi - M_\theta)\cos\phi - rR_1Q = 0 \qquad 6.3$$

The significance of the circumferential moment $M\Theta$ for the yield criterion will be discussed later.

The yield surface for such a case is in a four-dimensional stress space by the two moment limited interaction surface

proposed by Hodge [78] in the form

$$f(N_\phi, N_\theta, M_\phi, M_\theta) = k^2 \qquad 6.4$$

In general, due to its complexity, the applicability of such a yield criterion is restricted to simple problems [74]. For this reason it was essential to develop simplified versions of this yield surface which would allow its direct application to practical problems without compromising the reliability of the results. The search for more practical yield surface started from the observation that for the cylindrical case, within the framework of small displacement theory, the circumferential bending moment $M\Theta$ plays no role in the load bearing capacity of the shell. It has been described as an induced or passive moment although equal to $M\phi/2$ if a Poisson's ratio of 0.5 (ie, incompressibility) is always assumed for the plastic range. The yield surface may then be described in three dimensions

$$f(N_\phi, N_\theta, M_\phi) = k^2 \qquad 6.5$$

and $M\Theta$ does not appear in the equations of equilibrium. On the other hand, for the general axisymmetric case the moment $M\Theta$ does enter into the equilibrium equations and also does work during deformation due to changes in the circumferential curvature. However, for thin shells, ie, $h/R_o \ll 1$, the contribution of $M\Theta$ to the yield criterion becomes negligible and the term containing $(M\phi - M\Theta)$ in the equilibrium Equation (6.3) can be ignored. Two interpretations of that assumption were given in [75] and it

enables the use of the yield condition (6.5) in the analysis of general shells of revolution.

The way $M\Theta$ should be treated in the equation of equilibrium (6.3) proposed in [75] is as follows: In the equilibrium equation (6.3) the order of magnitude of the term involving $(M\phi - M\Theta)$ can be neglected when compared with the other two terms, except for portions of the shell near the axis of revolution where h/R_o may not be small. This interpretation was used by Gill [79] to calculated lower and upper bounds to the limit pressure for flush cylindrical nozzle in spherical pressure vessels. The second interpretation, which was later reinforced by Dinno and Gill [80], corresponds to putting $M\Theta = M\phi$ in Equation (6.3). The theorems of limit or shakedown analysis given in [81] and [28] respectively, could then be applied using the resulting equations of equilibrium in conjunction with any particular four-dimensional interaction yield surface to calculate a true lower bound. In addition, as pointed out in [80], since $M\Theta = M\phi$ the one-moment limited interaction surface will be contained within, or on, such a yield surface and therefore may be used. Dinno and Gill [80] have also proposed another way of dealing with $M\Theta$ in Equation (6.3), which is to assume $M\Theta = 0$. That again would lead to the use of the one-moment limited surface but they concluded that the additional work involved for most practical problems makes the use of it less encouraging.

Despite all the simplification the use of the one moment limited interaction yield surface may bring to the analysis

of general shells of revolution, its original form presents a high level of complexity which is still incompatible with the necessary practicability of analysis as an aid to design. Therefore, for the sake of simplicity and convenience of practical design inscribed and circumscribed linearized surfaces (Hexagonal Prism, Fig. 6.2), which give rise to lower and upper bounds respectively have been proposed. Since the lower and upper bounds computed from inscribed and circumscribed hexagonal prisms respectively would be too far apart for engineering purposes, the use of an intermediate sized inscribed prism has been proposed which would allow the application of the static theorem to provide reliable lower bound answers. In addition, Drucker and Shield [75] proposed that the upper bound theorem based upon the circumscribed hexagonal prism could then be reduced by multiplying by a factor 7/8. This proposition has been used by Gill [79] who obtained a limit pressure factor smaller than the shakedown factor calculated by Leckie [4] for the same type of vessel. This contradiction raised the question whether the shakedown factor obtained by Leckie was too high? The answer, which seems to be reasonable, was given in two ways; first, experimental investigation indicated that the result obtained by Leckie was a lower bound of the true value and it was also consistent with Gill's unmodified values, ie, his results obtained before multiplying by 7/8. In fact, as suggested by Leckie this factor should not be included in the analysis except for some physical reason. A second reason why the reducing factor 7/8 should not necessarily be used was subsequently given by Dinno and Gill [80] where the lower bound results obtained by assuming $M\Theta =$

0 in the equilibrium equations coincided with the upper bound results [79], both based on a circumscribing yield surface.

Thus, it seems proper to adopt the circumscribed surface (Fig. 6.2), for comparison, because the conclusions discussed above appear to be reasonable.

An important feature of thin shells is their high bending flexibility which leads to a primary membrane behaviour, except for some localized curvature. This characteristic has been widely used [79,80,82,83,75,51,76,84] to separate the distinct volumes of the shell where either bending or membrane behaviour are independently relevant. These volumes are the plastic hinges where curvatures ($k\Theta$,$k\phi$) are unrestricted and the regions between two adjacent hinges where only circumferential (ε_Θ) and meridional (ε_ϕ) strains occur. This important conclusion was drawn from the normality condition and from the convexity of the hexagonal prism yield surface [75]. The several analytical solutions for plastic collapse problems referenced above had a deformation pattern consisting of localized three hinges mechanism where the positions of the hinges are obtained generally from the lower bound approach by finding the positions where the bending moment is maximum, ie, where $dM_\phi/d\phi = 0$. For the application of the upper bound for constant load using a displacement field, which consists of discrete hinges at the nodes of a finite element subdivision and zero curvature within the element(hinge-cone displacement field), results in identical upper bounds to those obtained

using the non-interactive yield surface (Fig.6.2). Such a displacement field separates membrane action from bending action as in the case of the approach using Fig. 6.2 in terms of $(M_\phi, N_\phi, N_\Theta)$ and corresponding deformations $(k_\phi, \varepsilon_\phi, \varepsilon_\Theta)$. However, for thermal loading problems, quite complex variations of thermal stress have to be included, both through the thickness of the shell and along the centre line. The use of generalized stresses implies that the residual stress in the exact solution can be satisfactorily described in terms of linear variations through the shell thickness and it is known for the Bree problem that the actual residual stresses are not of that form. For this reason, the upper bound theorem will be applied directly for the Tresca yield condition, but with the knowledge that the choice of the hinge-cone type mechanism will yield limit load solutions directly comparable with the analytical solutions, generated from the non-interactive yield surface of Fig. 6.2. When the same technique is applied to thermal loading problems, however, there exists no restriction on the variation of the residual stress through the thickness of the shell. In addition, the method may also be applied to a wide class of displacement and this is discussed later in this chapter.

6.3 Discretization of the Axi-Symmetric Shells via Finite Elements

The elastic-plastic deformation pattern for thin shells may be defined in terms of the displacement field of its middle

surface $U_e(s)$ and the plastic strains in terms of plastic multipliers $\lambda_k(s)$ which characterize the plastic behaviour of the material. It is convenient to describe the displacement field using global displacement components in the outward horizontal direction W(s) and in the downward vertical direction U(s), respectively perpendicular and parallel to the axis of symmetry, as shown in Fig. 6.3. The local displacement components normal w(s) and tangential u(s) to the meridional direction can be obtained by a simple transformation. The finite element formulation for the elastic-plastic problem of thin shells may be derived from suitable interpolation of the displacement field and of the plastic multipliers as a function of nodal values. For this purpose, let the shell be discretized into NE finite elements. The displacement field within each element i (i = 1,...,NE) may be expressed in terms of nodal displacements $\{UN\}^i$ as

$$\{U_e^i(s)\} = \{U_o^i\} + [\Omega^i(s)]\,\{U_n^i\} \qquad 6.6$$

where $\Omega^i(s)$ is a matrix of suitably chosen interpolation functions which ensures the continuity between adjacent elements when the assemblage is performed. The element nodal displacements $\{UN\}^i$ can be divided into two independent parts; constant rigid body motions $\{U_o^i\}$ which give no contribution to the strain field and the so called natural displacements which generate the straining modes $\{U_n^i\}$.

Multiplying the global displacement by an appropriate transformation matrix [T] gives rise to the local displacement field with components normal and tangential to the meridional surface of the shell (Fig. 6.3).

$$\{u_e^i(s,\phi)\} = [T]^i \{U_e^i(s)\} \qquad 6.7$$

where

$$[T]^i = \begin{bmatrix} \sin\phi & \cos\phi \\ -\cos\phi & \sin\phi \end{bmatrix} \qquad 6.8$$

Substituting (6.6) into (6.7) gives

$$\{u_e^i(s,\phi)\} = [T]\{U_o^i\} + [T]\,[\Omega^i(s)]\,\{U_n^i\} \qquad 6.9$$

Compatible strain fields within the element i as functions of nodal displacements can be obtained by applying equation (2.5) to (6.9) to produce the classical relation independent of the rigid body motions

$$\{\varepsilon^i\} = [B]^i \{U_n^i\} \qquad 6.10$$

where

$$\{\varepsilon^i\} = \begin{Bmatrix} \varepsilon_\phi^i \\ \varepsilon_\theta^i \end{Bmatrix} \qquad 6.11$$

Details of such displacement and strain fields assumed for the case of axi-symmetric shells, are given in Appendix B.

The plastic strains can also be related to the plastic multiplier fields via a suitable matrix for any linearized yield surface. For the Tresca yield condition, assuming no variation of strain through the shell thickness, the relation between plastic strains and plastic multipliers can be defined from Fig. 6.4 as follows:

$$\{\varepsilon_2^i\} = [N]\ \{\lambda_k^i(s)\} \quad \text{for} \quad k = 1,6 \qquad 6.12$$

where

$$\{\varepsilon_2^i\} = \begin{Bmatrix} \varepsilon_\phi^2 \\ \varepsilon_\theta^2 \end{Bmatrix} \qquad 6.13$$

$$[N] = \begin{bmatrix} 1 & 0 & -1 & -1 & 0 & 1 \\ 0 & 1 & 1 & 0 & -1 & -1 \end{bmatrix} \qquad 6.14$$

Similarly to the displacement field, the plastic multipliers field for the element can be interpolated in terms of nodal parameters λ_k^n in a finite element approximation

$$\{\lambda^i(s)\} = [\Lambda^i(s)]\ \{\lambda_k^n\} \qquad 6.15$$

where the only restriction on $\{\Lambda^i(s)\}$ is

$$[\Lambda^i(s)] \geq 0 \qquad 6.16$$

within the element for any $\{\lambda_k^n\} > 0$.

The reduction of the upper bound theorem (Equation 2.39) to a linear programming problem requires that the two separate descriptions of the plastic strain increments ε_{ij}, given by Equation (6.10) and (6.12), must be consistent with each other at both nodes and within the element. Karadeniz and Ponter [51] show that, for cylindrical shells, suitable shape functions Ω_i and Λ_i could be found so that forcing equality of strains for (6.10) and (6.12) at the nodes would imply that equality was also satisfied within the element. Generally, however, this cannot be achieved and there do not exist shape functions which give such consistency for other shapes of shell element. Therefore, a means by which (6.10) and (6.12) may be made consistent with each other, in a average sense, has to be found. This problem is similar to the problem discussed by Corradi [66] for incremental finite element solutions, where evaluation of the stress within an element is given by the relationship

$$\{\sigma_{ij}^e\} \quad [D] \left\{ \{\varepsilon_{ij}^i\} - [N] \{\lambda_k^i\} \right\} \qquad 6.17$$

where [D] is the elastic stiffness coefficient matrix. This equation can give poor results, if separate descriptions of the total strain and of the plastic multipliers are adopted. Corradi used a procedure suggested by Oden [85,86] to obtain improved results. Oden [85] describes a procedure, which

produces a continuous stress field $\{\sigma_{ij}\}$ that is consistent with the discontinuous stress field $\{\sigma^e_{ij}\}$ obtained, using the traditional Finite Element procedure, from the elastic strains, by imposing the condition

$$\int_V \{\sigma_{ij}\}^T\{\varepsilon_{ij}\}dV = \int_V \{\sigma^e_{ij}\}^T\{\varepsilon_{ij}\}dV \qquad 6.18$$

Such a condition has to be satisfied for all possible strain fields $\{\varepsilon_{ij}\}$ belonging to the class assumed in the finite element method. The solution to this problem is claimed by Oden [85,86] to be unique, and the procedure is discussed in the following section.

6.4 On a Consistent Relationship Between Nodal Displacement Variables and Nodal Plastic Multipliers

6.4.1 Stress and Strain Fields as Functions of Generalized Quantities

Assuming that the behaviour of individual elements may be described in terms of generalized variables, the stress and strain fields within the element can be expressed as follows:

Let [b(s)] be a suitable interpolation matrix which gives rise to an internal distribution of strain in terms of generalized strain quantities {E}.

$$\{\epsilon^i_{ij}\} = [b^i]\ \{E_i\} \qquad 6.19$$

Similarly, let the stress field be written in terms of generalized stress quantities $\{\Sigma\}$ by means of matrix $[\psi(s)]$

$$\{\sigma^i_{ij}\} = [\psi^i_{ij}]\ \{\Sigma_i\} \qquad 6.20$$

Note that the stress distribution defined by Equation (19), although apparently independent of the constitutive law, when applied to an elastic material the constitutive equation imposes constraints on the form of [b] and $[\psi]$, which then define the stiffness matrix of the element. By the following argument, Oden suggests a relationship between [b] and $[\psi]$ independent of the constitutive law:

The generalized stresses and strains within the element must satisfy the principle of virtual displacements [87] which states that

$$\{\Sigma_i\}^T\{E_i\} = \int_V \{\sigma^i_{ij}\}^T\{\epsilon^i_{ij}\}\ dV \qquad 6.21$$

Equations (6.19) and (6.21) imply the biorthogonality condition

$$\int_V [\psi^i_{ij}]\ [b^i]\ dV = [I] \qquad 6.22$$

A solution of Equation (6.22) can be obtained by imposing

$$[\psi_{ij}] = [b^i]\ [C]^i \qquad 6.23$$

as proposed in [85,86], where $[C]^i$ is a symmetric and non-singular matrix defined as

$$[C]^i = \left\{ \int_V [b^i]^T [b^i] dV \right\}^{-1} \qquad 6.24$$

Note that this result is independent of the constitutive relationship. Corradi [66] uses the functions $[\psi]$ of (6.23) to calculate internal stresses from nodal values $\{\Sigma\}^i$ which have been generated by the solution of the finite element formulation. He obtains improved results compared to the conventional approach.

In the present formulation, the generalized strains are replaced by the displacement $\{U_n^i\}$ with the rigid body translation removed and the generalized stresses are replaced by forces $\{F\}^i$, so that

$$\{F\}^T \{U_n\} = \{\Sigma\}^T \{E\} = \int_V \{\sigma_{ij}\}^T \{\varepsilon_{ij}\} dV \qquad 6.25$$

where the strain distribution field within the element $\{\varepsilon_{ij}\}$ is defined by Equation (6.10), and the stress distribution field is assumed to be described in terms of the generalized forces by means of a matrix $[\psi]$ of suitable interpolation functions

$$\{\sigma_{ij}\} = [\psi_{ij}] \{F\} \qquad 6.26$$

Equality (6.25) will now always be satisfied for any $\{U_n\}$ and $\{F\}$ if

$$[\psi_{ij}] = [B]\ [\bar{C}] \qquad 6.27$$

where $[\bar{C}]$ is given by

$$[\bar{C}] = \left\{ \int_V [B]^T [B] dV \right\}^{-1} \qquad 6.28$$

A consistent relationship between the two strain fields $\{\varepsilon^1_{ij}\}$ and $\{\varepsilon^2_{ij}\}$ can now be defined by requiring that

$$\{F\}^T \{U_n\} = \int_V \{\sigma_{ij}\}^T \{\varepsilon^1_{ij}\} dV = \int_V \{\sigma_{ij}\}^T \{\varepsilon^2_{ij}\} dV \qquad 6.29$$

where $\{\sigma_{ij}\}$ was defined in (6.26) for arbitrary values of $\{F\}$. Substituting (6.10), (6.26), (6.27) and (6.28) into (6.29) gives the result

$$\{U_n\} = [L]\ \{\lambda^n_k\} \qquad 6.30$$

where

$$[L] = [\bar{C}] \int_V [B]\ [K(s)] dV \qquad 6.31$$

and

$$[K(s)] = [N]\ [\Lambda(s)] \qquad 6.32$$

This gives the required relationship between the nodal values λ^n_k of the plastic multipliers and the nodal displacements $\{U_n\}$ so that the consistent relationship (6.29) is always satisfied.

6.5 A General Solution for the Biorthogonality Condition

In the case of axi-symmetrical shells, the elements which show constant and conical deformation patterns are those whose meridian angles are constant and in this case it might be expected that Equations (6.26), (6.27) and (6.28) satisfy the required condition (6.25). For curved elements however, the deformation pattern $\{\varepsilon^1_{ij}\}$ varies as a function of the meridional angles along the element and it is no longer linear. Although the approximate solution given by (6.27) will also satisfy the required condition (6.25) for a non-linear deformation pattern, it will be shown in Section 6.10 that, using (6.27) the difference between the two strain fields $\{\varepsilon^1_{ij}\}$ and $\{\varepsilon^2_{ij}\}$ is not neglegible. However, a general solution for (6.25) different from (6.30) can be obtained as follows: let [R] be a matrix of the same size as [B] so that

$$[H] = \left\{ \int_V [B]^T [R] dV \right\}^{-1} \qquad 6.33$$

is a non-singular matrix. Hence, the following statement can be proved: Equation (6.25) can be satisfied if a matrix [R] can be found such that

$$[\psi] = [R][H] \qquad 6.34$$

Then

$$\int_V [\psi]^T [B] dV = \int_V [H]^T [R]^T [B] dV \qquad 6.35$$

where

$$[H]^T = \left\{ \int_V [R]^T [B] dV \right\}^{-1} \qquad 6.36$$

which leads to

$$\int [\psi] [B] dV = [I] \qquad 6.37$$

Thus, the solution given by (6.27) is a special case for [R] = [B].

Let the consistent relationship between the two strain fields, Equation (6.29), be written in the form of the orthogonality condition

$$\int_V \{\sigma\}^T (\{\varepsilon_1\} - \{\varepsilon_2\}) dV = 0 \qquad 6.38$$

where $\{\sigma\}$ is defined by (6.26) and (6.27) so that (6.38) holds for all $\{U_n\}$, $\{\lambda_k^n\}$ and $\{F\}$. It seems that this condition will only provide reliable displacement-plastic multipliers relation for [R] = [B] if $\{\varepsilon^1\}$ is linear, as $\{\varepsilon^2\}$ assumed for the present case. Hence, Equations (6.30) to (6.32) provide a consistent relation between displacement field and the plastic multipliers field only if the entries of matrix [B] are at most linear.

However, when the entries of [B] are polynomials of higher order or not polynomials, a more general solution for the biorthogonality condition (6.37), such as that given by (6.34), is required, so that

$$\{U_n\} = [H] \left\{ \int_V [R]^T [K] dV \right\} \{\lambda_k^n\} \qquad 6.39$$

when (6.26) and (6.34) are substituted into (6.29). Let matrix [L] now be

$$[L] = [H] \left\{ \int_V [R]^T [K] dV \right\} \qquad 6.40$$

Hence,

$$\{U_n\} = [L]\{\lambda_k^n\} \qquad 6.41$$

Equation (6.41) enforces a general consistency relation between displacement field and plastic multipliers field for each individual element and therefore gives rise to two such relations for each nodal displacement. Once assemblage is performed, interelement continuity may be ensured by taking the average of the nodal values, relative to the sharing node of adjacent elements. Details of this averaging process is given in Appendix C.

The difficulty of this approach is that the matrix [R] is arbitrary and there is no obvious criteria for its choice. In order to discuss a procedure to choose a consistent matrix [R], let the relationship (6.39) be rearranged in a

simpler form by multiplying both of its sides by $\{\int_V [R]^T [B]\, dV\}$, which gives the condition

$$\int [R]^T([B]\{U_n\} - [K]\{\lambda_k^n\})\, dV = 0 \qquad 6.42$$

ie,

$$\int_V [R]^T(\{\varepsilon_1\} - \{\varepsilon_2\})\, dV = 0 \qquad 6.43$$

Such a condition requires that the difference between $\{\varepsilon^1\}$ and $\{\varepsilon^2\}$ shall be orthogonal to the arbitrary matrix [R]. The elements of [R] need, therefore, to be chosen so that the strain difference is as small as possible. Expanding (6.43) into its individual components given by (6.11) and (6.13), results in

$$\int_V R_{11}(\varepsilon_\theta^1-\varepsilon_\theta^2)dV + \int_V R_{21}(\varepsilon_\phi^1-\varepsilon_\phi^2)dV = 0 \qquad 6.44$$

$$\int_V R_{12}(\varepsilon_\theta^1-\varepsilon_\theta^2)dV + \int_V R_{22}(\varepsilon_\phi^1-\varepsilon_\phi^2)dV = 0 \qquad 6.45$$

$$\int_V R_{13}(\varepsilon_\theta^1-\varepsilon_\theta^2)dV + \int_V R_{23}(\varepsilon_\phi^1-\varepsilon_\phi^2)dV = 0 \qquad 6.46$$

where $dV = 2\pi R(s)h(s)ds$. The components of [R] can now be seen to be a set of functions in a Galerkin type procedure for the minimization of the strain differences. The final choice was as follows

$$[R] = \begin{bmatrix} 1 & 0 & 0 \\ 0 & (1-s/\ell_i)/R & (s/\ell_i)/R \end{bmatrix} \qquad 6.47$$

This choice implies that Equation (6.44) becomes

$$\int_V (\varepsilon_\phi^1-\varepsilon_\phi^2)dV = 0 \qquad 6.48$$

ie, $(\varepsilon_\phi^1-\varepsilon_\phi^2)$ is zero in the mean within each element and the combination of Equations (6.45) and (6.46) is equivalent to

$$\int_V [A(1-s/\ell_i) + B\ s/\ell_i]\ (\varepsilon_\theta^1-\varepsilon_\theta^2)/R_2 dV = 0 \qquad 6.49$$

which represents the ortogonality of $(\varepsilon_\Theta^1-\varepsilon_\Theta^2)$ to an arbitrary linear function. It has been found that this gives the identical result to [R] = [B] for cylindrical and conical elements, but a markedly different result for any curved element. The numerical results are discussed in the Section (6.10).

6.6 Approximate Displacement and Strain Fields for Axi-symmetric Shells

For the current stage of the present technique, the displacement field within the element will be assumed to be interpolated by linear functions. The equations defining the displacements and strain fields will be given here directly in a matrix form and all the algebraic development is given in Apendix B. Equation (6.50) represents the global displacement field (defined in Section 6.3) which for an axi-symmetric shell element (Fig. 6.3) becomes

$$\{U_e(s)\} = \begin{Bmatrix} U(s) \\ \\ W(s) \end{Bmatrix} = \begin{Bmatrix} U_i \\ \\ 0 \end{Bmatrix} + \begin{bmatrix} s/\ell_i & 0 & 0 \\ \\ 0 & (1-s/\ell_i) & s/\ell_i \end{bmatrix} \begin{Bmatrix} U_{i+1}-U_i \\ W_i \\ W_{i+1} \end{Bmatrix} \qquad 6.50$$

where l_i is the length of a generic element i, and the rigid body translation and the nodal displacements are defined by the vectors

$$\{U_o\} = \begin{Bmatrix} U_i \\ \\ 0 \end{Bmatrix} ; \ \{U_n\} = \begin{Bmatrix} U_{i+1}-U_i \\ W_i \\ W_{i+1} \end{Bmatrix} \qquad 6.51$$

The local displacement field is given by

$$\begin{Bmatrix} u(s,\phi) \\ \\ W(s,\phi) \end{Bmatrix} = \begin{Bmatrix} U_i \sin\phi \\ \\ -U_i \cos\phi \end{Bmatrix} + \begin{bmatrix} \frac{s}{\ell_i}\sin\phi & (1-\frac{s}{\ell_i})\cos\phi & \frac{s}{\ell_i}\cos\phi \\ \\ -\frac{s}{\ell_i}\cos\phi & (1-\frac{s}{\ell_i})\sin\phi & \frac{s}{\ell_i}\sin\phi \end{bmatrix} \begin{Bmatrix} U_{i+1}-U_i \\ W_i \\ W_{i+1} \end{Bmatrix} \qquad 6.52$$

where $\phi = \phi(s) = \phi_i + s/R_1$ (Fig. 6.3)

The strain field (see Appendix B) may now be written as

$$\begin{Bmatrix} \varepsilon_\phi(s,\phi) \\ \\ \varepsilon_\theta(s,\phi) \end{Bmatrix} = \begin{bmatrix} \frac{\sin\phi}{\ell_i} & -\frac{\cos\phi}{\ell_i} & \frac{\cos\phi}{\ell_i} \\ \\ 0 & (1-\frac{s}{\ell_i})/(R_2\sin\phi) & (\frac{s}{\ell_i})/(R_2\sin\phi) \end{bmatrix} \begin{Bmatrix} U_{i+1}-U_i \\ W_i \\ W_{i+1} \end{Bmatrix} \qquad 6.53$$

or

$$\{\varepsilon(s,\phi)\} = [B]\ \{U_n\} \qquad 6.10$$

6.7 The Upper Bound Theorem Applied to Axi-Symmetric Shells Via Finite Element Technique and Linear Programming

For the current stage of development of the present technique the extended upper bound theorem (Equation (2.39)) will become identical to the classical form, ie, it will be applied only for stress histories contained within the yield surface. Equation (2.39) can thus be written as

$$\lambda \int_S p_i dU_i dS \leq \int_o^{\Delta t} dt \int_V [\sigma^c_{ij}(t) - \hat{\sigma}^\theta_{ij}(x,y,t)]\dot{\varepsilon}_{ij}(t)dV \qquad 6.54$$

when the effects of temperature on the yield stress is considered. Equation (6.54) implies a search for a minimum value of the right hand side for a prescribed value of

$$W_E = \int_S p_i dU^c_i dS = 1 \qquad 6.55$$

This can be achieved by defining the instants during the the cycle, when the term [$\sigma^c_{ij}(t)-\hat{\sigma}^\theta_{ij}(x,t)$] corresponding to $\dot{\varepsilon}^c_{ij}(t)$ is a minimum. In the case of limit analysis problems, ie, for $\hat{\sigma}^\theta_{ij}(x,t) = 0$ in (6.54), the calculations are independent of time. For problems involving cyclic thermal loading, however, an additional requirement, relating the plastic strain field rate $\dot{\varepsilon}_{ij}(t)$ and the

corresponding time in the cyclic thermal stress history $\sigma_{ij}^{\Theta}(x,t)$ is necessary to ensure an absolute minimum value for the mechanical load within $0 < t < T$. As stated previously this kinematic theorem requires the prescription "a priori" of the deformation mode defined by the strain and displacement fields. The class of mechanism of deformation, following definition in Section 6.2, will be precribed as that in which plastic hinges may occur at nodal points whilst a uniform membrane strain is assumed to distribute linearly along the element.

In this way, the shakedown problem is reduced to a minimization problem and the present technique will use Linear Programming to search for the absolute minimum value for the the mechanical load multiplier λ, by assuming that the integral on the left hand side of (6.54) is constant. Such an assumption will only define the size of the prescribed mechanism and will appear in the calculations as an additional constraint for the Linear Programming problem to be solved. The cost function for a standard Linear Programming problem can now be

$$\lambda^{s} \leq \int_{o}^{\Delta t} dt \int_{V_{element + hinge}} [\sigma_{ij}^{c}(t) - \hat{\sigma}_{ij}^{\theta}(x,y,t)]\dot{\varepsilon}_{ij}(t)dV \qquad 6.56$$

if the general constraint condition (6.55) is introduced to the problem. Inequality (6.56) may be split, for integration purposes, into two different volumes:

$$\lambda^s \leq I_1 + I_2 = \int_0^{\Delta t} dt \int_{V_{element}} [\sigma_{ij}^c(t) - \hat{\sigma}_{ij}^\theta(x,y,t)\ \dot{\varepsilon}_{ij}(t)dV +$$

$$\int_0^{\Delta t} dt \int_{V_{hinge}} [\sigma_{ij}^c(t) - \hat{\sigma}_{ij}(x,y,t)]\dot{\varepsilon}_{ij}(t)dV \qquad 6.57$$

The general consistent relation between displacement field and plastic strain field described by plastic multipliers λ_k's, discussed in Sections 6.4 and 6.5 (Equation (6.41)), will be used as a basic concept for the present technique. All the variables involved in the solution of the Linear Programming problem need to appear in the equations as functions of the plastic multipliers. Most of the detailed calculations involving matrix manipulations, following the substitution of Equation (6.41) into the appropriate equations governing the behaviour of the assembled system of elements, will be given in the Appendices. In this section, only some details of the basic principles involved are discussed.

On the Minimization of the Cost Function (6.57): Let the first integral on the right of Equation (6.57) be written in terms of plastic multipliers by means of (6.41) for a generalized element "i" of a axi-symmetric shell to give

$$I_1 = \int_0^{\Delta t} dt \int_V [\sigma_{ij}^c(t) - \hat{\sigma}_{ij}^\theta(t)]\,[N]\{\lambda_k(t)\}\,dV \qquad 6.58$$

where [N] was defined in Section 6.3 and will be rearranged as follows

$$I_1 = \sum_{k=1}^{6} \int_{V_{element}} [\sigma_{ij}^{c} - \hat{\sigma}_{ij}^{\theta}(t_k)]\{N_{ij}\}_k\{\lambda_k(t_k)\}\, dV \qquad 6.59$$

with $\{N_{ij}\}_1 = [1\ 0]$, $\{N_{ij}\}_2 = [0\ 1]$ and so on. The absolute minimum of (6.57) has to be found in two levels. For a yield stress independent of the temperature the construction shown in Fig. 6.5 can be used to define the instants t_k's during the cycle, corresponding to each plastic multiplier, when the term $[\sigma_{ij}^{c} - \hat{\sigma}_{ij}^{\theta}(s,t_k)]\ \{N_{ij}\}_k$ is a local minimum. Inequality (6.57) becomes thus

$$\lambda^{s} < \sum_{k=1}^{6} \int_{V_{element}} [\sigma_{ij}^{c} - \hat{\sigma}_{ij}^{\theta}(t_k)]\{N_{ij}\}_k\{\lambda_k(t_k)\}dV + \int_{V_{hinge}} [\sigma_{ij}^{c} - \hat{\sigma}^{\theta}(t_k)]d\varepsilon_{ij}(t_k)dV = I_1 + I_2 \qquad 6.60$$

for a particular element "i". The second integral, I2, on the right side of (6.57), over the volume of the hinge, is discussed in detail in Appendix D. The minimization of λ given by inequality (6.58), for all λ_k^n's defining the compatible strain field and the nodal variables defining the hinge rotations in I2 (see next section), is achieved by Linear Programming, when the assemblage of elements is performed. The solution of the problem consists of the minimum value of λ and the mechanism of collapse requiring the least amount of energy dissipation defined by the values of the plastic multipliers λ_k^n's, which contributed to the mode of deformation and the nodal positions where plastic hinges have formed.

On the General Constraint Equation (6.55): Equation (6.55) represents the external work produced by the mechanical loads, which for the current stage of the present technique will be limited to two cases:

(a) Internal Pressure

Consider the generic element "i" of an axi-symmetric shell shown in Fig. 6.6. The elemental contribution to the external work due to the internal pressure is given by (6.55) as

$$W_E = \int_S p_i d\, U_i^c dS = \int p_i w(s) dS + F \int \frac{dU^c}{ds} ds \qquad 6.61$$

where the first integral on the right represents the work done in the radial direction and the second integral represents the work due to axial displacements when the shell has its end(s) closed by a rigid plate(s).

The radial displacement w(s) is given by (6.52) and the work in that direction becomes

$$\begin{aligned} \int_S p\, w(s) dS = 2\pi p_i \Bigg\{ & \left[- \int_o^{\ell_i} \cos\phi\, r(s) ds \right] U_i \; + \\ & \left[- \frac{1}{\ell_i} \int^{\ell_i} s \cos\phi\, r(s) ds \right] (U_{i+1} - U_i) \; + \\ & \left[\int_o^{\ell_i} (1 - \frac{s}{\ell_i}) r(s) ds \right] W_i \; + \\ & \left[\frac{1}{\ell_i} \int_o^{\ell_i} s \cos\phi\, r(s) ds \right] W_{i+1} \end{aligned} \qquad 6.62$$

where $dS = 2\pi r(s)ds$. The geometric parameters R_1, r_o, ϕi etc., describing the shell, are defined in Fig. 6.6 with

$$r(s) = R_1 \sin\phi - r_o \qquad 6.63$$

where ϕ was defined in (6.54). The sign convention for r_o is positive from the left to the right as indicated in Fig. 6.6. Thus, Equation (6.64) represents the work due to the internal pressure on the radial direction for the element i. The total work resulting from the sum of the contribution of all NE elements can be written as

$$W_E = 2\pi p_i \sum_{i=1}^{NE} [IFWUI(i)U_i + IFWU(i)(U_{i+1}-U_i) + IFWI(i)\, W_i + IFWIP1(i)\, W_{i+1}] \qquad 6.64$$

where the following definitions hold

$$IFWU(i) = \frac{1}{\ell_i}\int_o^{\ell_i} s \cos\phi\, r(s)ds$$

$$IFWUI(i) = -\int_o^{\ell_i} \cos\phi\, r(s)ds \qquad 6.65$$

$$IFWI(i) = \int_o^{\ell_i}\left(1 - \frac{s}{\ell_i}\right) \sin\phi\, r(s)ds$$

$$IFWIP1(i) = \frac{1}{\ell_i}\int_o^{\ell} s \sin\phi\, r(s)ds$$

Equation (6.64) defines a general additional constraint to be satisfied.

The Linear Programming problem will be solved in terms of nodal plastic multipliers λ_k^n's and the global nodal

displacements in (6.64) have to be substituted as functions of λ_k^n's by means of (6.41). Some details of such a substitution, which involves fairly complex matrix manipulations, is given in Appendix D.

b) Ring Load Applied to Node "i"

Fig. 6.7 shows schematically the ring load case applied to a generic node "i" connecting two adjacent elements. The equation defining the external work produced by such a load in the radial direction is

$$W_E = 2\pi r_i P_i w_i \qquad 6.66$$

where $w_i = -U_i \cos\phi_i + \sin\phi_i W_i$. Equation (6.66) is valid for any node not coincident with the axis of revolution, where $r_i = 0$. Again the global displacements have to enter Equation (6.66) as functions of the plastic multipliers.

6.8 The Constraint Equations for the Linear Programming

In addition to the general constraint (6.64), there are a set of nodal constraints, related to the formation of plastic hinges, which must be satisfied, defining the unrestricted curvatures (rotations) at the nodes in terms of displacement variables. These nodal plastic rotations contribute to the internal energy dissipation and also to the work done by thermal cyclic loading, when meridional bending moments are induced by it. Fig. 6.8 illustrates such

a rotation in a generic node "i" with an appropriate sign convention, and the constraint equation may be defined at each node as

$$\theta_i = \frac{dw}{ds}(\ell_i - 1) + \frac{dw}{ds}(0) \qquad 6.67$$

In order to ensure that the Linear Programming will be dealing with non-negative variables as required, the following auxiliary non-negative variables will be introduced

$$\theta_i = \theta_i^{(+)} - \theta_i^{(-)} \qquad 6.68$$

for $\theta_i^{(+)} > 0$ and $\theta_i^{(-)} < 0$ so that

$$\theta_i^{(+)} = \theta_i \qquad 6.69$$

$$\text{if } \theta_i > 0$$

$$\theta_i^{(-)} = 0$$

and

$$\theta_i^{(+)} = 0$$

$$\text{if } \theta_i < 0 \qquad 6.70$$

$$\theta_i^{(-)} = -\theta_i$$

The derivative of the radial displacement (6.52) for the element "i" is

$$\frac{dw}{ds}(s) = \frac{U_i}{R_1}\sin\phi + \left(\frac{s}{R_1}\sin\phi - \cos\phi\right)\frac{(U_{i+1}-U_i)}{\ell_i} +$$

$$\left[\left(1 - \frac{s}{\ell_i}\right)\frac{\cos\phi}{R_1} - \frac{1}{\ell_i}\sin\phi\right]W_i + \qquad 6.71$$

$$\left[\frac{s}{R_1}\cos\phi + \sin\phi\right]\frac{W_{i+1}}{\ell_1}$$

Substituting (6.71) into (6.67) for the respective values of "s" corresponding to node "i" on two generic parental elements gives

$$\theta_i = \theta_i^{(+)} - \underline{\theta_i^{(-)}} = CU_1(i)(U_i-U_{i-1}) + C_1(i)\,\underline{W_{i-1}} + \qquad 6.72$$

$$C_2(i)\,W_i + C_3(i)\,W_{i+1} + CU_2(i)\,(U_{i+1}-U_i)$$

where

$$CU_1(i) = \cos\phi_i/\ell_i \;;\quad CU_2(i) = -\cos\phi_i/\ell_i$$

$$C_1(i) = \sin\phi_i/\ell_{i-1};\quad C_2(i) = -\sin\phi_i\left(\frac{\ell_i+\ell_{i-1}}{\ell_i\,\ell_{i-1}}\right) \qquad 6.73$$

$$C_3(i) = \sin\phi_i/\ell_i$$

The constraint equations relative to each node can then be written in terms of nodal plastic multipliers by means of (6.41) for the Linear Programming procedures. From equation (6.72) it can be seen that the constraint equations involve displacements from three nodes. When such displacements are substituted into (6.72) in terms of plastic multipliers, using the relationships given in Appendix C, each constraint equation will be dealing with λ's from five nodes. Thus,

the set of variables for each constraint equation, corresponding to a particular node, consists of 30 plastic multipliers and the two nodal variables $\Theta_i^{(+)}$ and $\Theta_i^{(-)}$ representing the hinge rotation. If Equation (6.72) is rearranged in terms of plastic multipliers for all the nodes, the set of constraint equations for the Linear Programming may be schematically represented as shown in Fig. 6.9.

6.9 End Conditions for Axi-Symmetrical Shells

Assuming that both ends of the shell are fully constrained the following conditions must be satisfied at the extreme nodes

At Node 1

$$u(1) = U_1 \sin\phi_1 + W_1 \cos\phi_1 = u_1 \text{ (prescribed)} \qquad 6.74$$

$$w(1) = -U_1 \cos\phi_1 + W_1 \sin\phi_1 = w_1 \text{ (prescribed)} \qquad 6.75$$

Node NN(last node)

$$u_{(NN)} = U_N \sin\phi_N + W_N \cos\phi_N = u_N \text{ (prescribed)} \qquad 6.76$$

$$w_{(NN)} = -U_N \cos\phi_N + W_N \sin\phi_N = w_N \text{ (prescribed)} \qquad 6.77$$

For the case of axi-symmetric loading, one single external displacement constraint in the direction of the axis of

revolution is sufficient to avoid the shell translating as a rigid body. This condition is generally imposed at one or at both ends of the shell as follows

$$U_1 = 0 \quad \text{which implies} \quad U_N = \sum_{i=1}^{NE} (U_{i+1} - U_i) \qquad 6.78$$

or

$$U_N = 0 \quad \text{for} \quad U_1 = - \sum_{i=1}^{NE} (U_{i+1} - U_i) \qquad 6.79$$

Conditions (a) and (b) may be introduced to the Linear Programming as constraint equations by substituting $(U_{i+1} - U_i)$ as functions of λ_k^n's as shown in Appendix C.

The internal constraints, which actually enforce the end conditions of the shell, are defined by the local displacements at the extreme nodes (u(1),w(1)) and (u(NN),w(NN)). Assuming the global condition (b)(Equation (6.79)), for example, the end conditions for both ends fully constrained become

At Node 1

$$u(1) = - \sum_{i=1}^{NE} (U_{i+1} - U_i) \sin\phi_1 + W_1 \cos\phi_1 = u_1 \text{ (prescribed)} \qquad 6.80$$

$$w(1) = \sum_{i=1}^{NE} (U_{i+1} - U_i) \cos\phi_1 + W_1 \cos\phi_1 = w_1 \text{ (prescribed)} \qquad 6.81$$

For $u_1 = w_1 = 0$ the end conditions at node 1 will be satisfied by simply imposing

$$\sum_{i=1}^{NE} (U_{i+1} - U_i) = 0 \qquad 6.82$$

$$W_1 = 0 \qquad 6.83$$

At Node NN

The assumption of condition (b) implies $U_N = 0$ and therefore the local meridional and radial displacements can be determined from (6.76) and (6.77) as

$$w_{(NN)} = W_N \sin\phi_N = w_N \text{ (prescribed)} \qquad 6.84$$

$$u_{(NN)} = W_N \cos\phi_N = u_N \text{ (prescribed)} \qquad 6.85$$

These two equations become redundant if the prescribed displacements are zero, ie, $u_N = w_N = 0$, and it is sufficient to have the condition

$$W_N = 0 \qquad 6.86$$

Again these end conditions must be introduced to the LP as consistent functions of the plastic multipliers by substituting the global displacements as functions of λ_k^n's.

6.10 Numerical Solutions

As already stated in Section (6.1) the numerical solutions for the present stage of development of the technique

proposed, will only consider problems involving the basic shell elements individually, described previously, and problems involving torispherical vessels. The first set of calculations are concerned with the solution of limit analysis problems and the results are compared either with exact solutions obtained analytically, or with other numerical solutions. A versatile code (CONRE) has been written in a way that allows the easy inclusion of further developments of the technique. CONRE current structure is likely to suffer only minor changes as a result of improvements and future developments.

The integrations involved in the calculations are perfomed using Gaussian quadrature, where a suitable number G of Gaussian points (usually 5) within the element are chosen. Thus, an integral over the element volume can be reasonably estimated by means of the following expression

$$\int_V f(x)dV = \sum_{k=1}^{G} y_k W_k \qquad 6.87$$

where $y_k = f(x_k)$ and the weighting factors W_k are given by Zienkiewicz [88].

Some observations on the element discretization of the shell may be useful to clarify some points about the end conditions which the Code (CONRE) allows to be considered in the calculations. First, let the axis of revolution be considered in the vertical position so that the shell can be described from top to bottom as illustrated in Fig. 6.10. The numbering system adopted for the nodes and elements is

also shown in Fig. 6.10, starting with node 1 at the top and ending with node NN at the botton. For curved elements, the meridional angle will be measured clockwise, with the origin coincident with the axis of revolution.

6.10.1 Limit Load Problems

6.10.1.1 Cylindrical Shells

Case 1: Cylindrical Vessels Subjected to a Ring of Pressure

Such a simple example has already been solved analytically by several authors [69,73,89,90,91] where the influence of the end conditions and of the length of the vessel on the limit load is analysed. Drucker [69] was the first to approach such a problem for an infinitely long cylindrical shell, where he uses different limit yield conditions, including the exact one, from which he defines approximations of rectangular and hexagonal shape. Drucker's solutions are based on the yield surfaces shown in Fig. 6.11 and his normalized lower bounds for each yield condition are given by

$$\frac{p}{p_L} = \beta\sqrt{Rh} \qquad 6.88$$

where β is a constant dependent on the yield criterion and p_L is defined as

$$p_L = \frac{\sigma_y h}{R} \qquad 6.89$$

which represents the pressure at which the shell would fail as a membrane. The values of β for the various yield surfaces (Fig. 6.11) are presented in Table 6.1.

Table 6.1

Yield Condition	β
Inscribed Rectangle	1.5
Hexagon	1.73
Exact	1.82
Circumscribed	2.00

As pointed out by Drucker [69], if the upper bound theorem is applied to a hinge-cone deformation pattern (Fig. 6.12) for the hexagonal or exact yield criterion the same upper bound $\beta = 2.00$ is found. He concludes that the conical shape of the mechanism chosen agrees with the requirement of zero rate of curvature between hinges implied be the normality condition. Nevertheless, the hexagonal and exact yield criteria require a non-zero curvature for their sloping and curved sides, respectively, which explains the divergence of the upper and lower bounds for such yield surfaces and the agreement for the rectangular. The optimum size of the mechanism, ie, the mechanism which would lead to a minimum value of P/σ_y may be easily found as

$$a = \sqrt{Rh} \qquad 6.90$$

and may be considered as the length of the shell OVER WHICH P is effectively carried.

The "a priori" knowledge that the optimum size of the mechanism is given by (6.90) allows the choice of an element discretization, which would lead to a solution coincident with Drucker's. That in a sense, demonstrates the reliability of the present technique despite the simplicity of the problem. If no knowledge of this kind were available, a fine mesh of elements would be required to ensure an accurate result.

Some examples will be given to illustrate the application of this technique to such problems:

Numerical Examples: Consider the cylindrical vessel discretized into finite elements as shown in Fig. 6.13 where the geometric parameters are defined. From (6.90) the optimum size of the mechanism would be $a = 0.045$. The element structure chosen, however, enforces a mechanism, at the best, of $a = 0.05$, which is the size of the elements and consequently the limit load obtained (Fig. 6.13) is sightly greater than the value given by (6.88) which implies the optimum mechanism. If a more precise limit load is required, the problem may be solved by refining the mesh, for example, by assuming smaller elements, say $l_i = 0.045$ (Fig. 6.14) and the optimum solution is obtained.

The strain distribution along the elements involved in the formation of the collapse mechanism, is shown in Fig. 6.15. The discussion about the strain distribution on cylindrical vesels will be given at the end of this section.

Case 2: Cylindrical Vessels under Internal Pressure

The analysis of cylindrical shells under uniform pressure has been thoroughly studied by Hodge [78], where various support conditions were considered. Although Hodge provides solutions for both sandwich and uniform shells, for the purposes of the present work only uniform shells will be considered. The shells are assumed to be open at the ends and the various end support conditions for the present numerical analysis are as follows:

End Condition 1: Unconstrained Ends

Such condition may be thought of as the shell being supported by elastic rings, which would allow the vessel to expand freely in the radial direction. The limit load for such a case is simply the membrane limit pressure given by (6.89) and the normalized solution become $p/p_L = 1$. The deformation pattern consists of a uniform expansion with respect to the axis of revolution as shown in Fig. 6.16 for a particular shell geometry.

The strain distribution within a particular element of the shell is shown in Fig. 6.17.

End Condition 2: Bottom Fully Constrained and Top Free

Such problem (Fig. 6.18) has been analysed by Onat [70], by means of the exact yield surface for cylindrical shells (see Section 6.2), defined in terms membrane forces and bending moments. Onat also considers a compressive load applied, simultaneously with an internal pressure, at the top of the vessel, which for simplicity will be ignored here.

The expression for the limit load given in [70] for the internal pressure alone is

$$\frac{p}{\sigma_y} = \frac{h}{R} + \frac{1}{2}\frac{h^2}{L^2} \qquad 6.91$$

Equation (6.91) applied to this problem gives p/σ_y = 0.050078 which compares very well with the result given in Fig. 6.19 of 0.050156.

Fig. 6.20 show the strain distribution for a particular elements of the discretized shell.

End Condition 3: Clamped Ends

A complete analytical solution for the problem of cylindrical shells under internal or external pressure with both ends fully constrained (Fig. 6.21) has been given by Hodge [78].

The solution given in [78] for the approximate rectangular yield surface (Fig. 6.11) is

$$\frac{p}{\sigma_y} = \frac{h}{R} + \frac{h^2}{L^2} \qquad 6.92$$

Hodge's lower bound solution implies a symmetric three-hinges mechanism and seems to be independent of the length of the cylindrical shell. Such a solution coincides with that obtained by applying the upper bound theorem to a similar mechanism and therefore may be thought of as an exact solution for short cylinders. However, due to the localized nature of the bending moment, for long thin cylindrical shells, failure may occur due to hinges forming near the ends, where the bending moments are concentrated, and not as a membrane as Equation (6.92) seems to indicate. Nevertheless, the solution given by (6.92) seems to be reliable whatever the length of the vessel.

Quite recently some numerical solutions for this problem have been given by Morelle and Hung [61] using Melan's theorem (lower bound) and Tresca's sandwich yield condition [78]. Morelle [62] has also proposed an upper bound formulation for the same yield condition. The former paper claims to obtain the same limit pressure as in [78] with 8 elements, whilst the convergence of the upper bound in [62] seems to require as many elements as 20. In order to compare the solution of the present upper bound technique for such a problem, with those in [61], [78] and [62], the same problem was solved assuming two different element structures shown in Figs. 6.22 & 6.23.

It can be seen that both element structures yield the same solution and the exact limit pressure is obtained with only two elements (Fig. 6.22). The strain distribution is shown in Fig. 6.24 for a particular element.

For all the cases involving cylindrical shells and axi-symmetric loading, the axial strain turned out to be zero as expected for such cases and only the hoop or circumferential strain distribution is plotted for some elements. It can be seen that for all the cases, the ortogonality condition of the difference between $\{\varepsilon^1\}$ and $\{\varepsilon^2\}$ and matrix [R], as discussed in Section 6.5 is exactly satisfied, ie, $\{\varepsilon^1\}$ is coincident with $\{\varepsilon^2\}$. In the case of the shell with free ends, the strain distribution is not only coincident but also constant along the elements, as one would expect for such a uniform expansion.

6.10.1.2 Conical Shells

The analysis for such a shell will be carried out for the loading case of internal pressure and the end conditions considered are for the shell fully constrained or clamped (Fig. 6.25). Lower and upper bounds for this problem have been found by Biron and Chawla [92] using a numerical technique. Hung and Ransart [93] have also analysed the same problem via FEM and found what they called quasi-lower and upper bounds. Both papers have used non-linear programming and von Mises' sandwich yield condition. Quite

recently, Morelle [62] used an upper bound formulation to analyse this problem for sandwich shells and Tresca sandwich yield condition. His results consist of an upper bound value and the corresponding collapse mechanism for an element structure containing 40 elements. Ponter and Carter [94] have also used a numerical upper bound approach for the analysis of a similar problem, based on a strain formulation, where again upper bounds and mechanism of deformation are produced. The lower and upper bounds obtained by the different methods above are compared in Table 6.2 with the upper bound obtained using the present technique. The collapse mechanisms from [62] and [94] are directly compared in Fig. 6.26, with the mechanism yield from the current approach, which used a 10 element structure. Although examples such as this conical shell, seems to be mainly academic, it serves very well to demonstrate the reliability of the technique. In a sense it justifies the aims of such simplified methods, which are to obtain good solutions using as few elements as possible, therefore avoiding the cost and time required to solve problems involving shells with more complex geometries and loading systems.

6.10.1.3 Spherical Caps

The limit analysis of this classical example of a shell structure (Fig. 6.27), subjected to hydrostatic pressure, has been performed by several authors in the past. The solutions vary from the simple determination of upper and

lower bounds on the critical pressure to some more complete solutions where the associated stress and velocity fields are also provided. Onat and Prager's [74] analytical approach, for example, involves a complete four dimensional yield surface for thin uniform shells and the fundamental theorems given in [81], and provides the first crude bounds for such problems.

The problem for sandwich shells was solved by Hodge [89,95] who found much closer bounds. The need to develop simpler yield conditions soon became evident and Hodge [96] considered such an approach, which was followed later by the investigation of the bearing capacity of a spherical shell, assuming a variety of yield conditions carried out by Mroz and Xu [97]. The numerical method proposed by Biron and Chawla [92] was applied to similar problems using the von Mises sandwich shell yield criterion, where upper and lower bounds are obtained as results. As pointed out by Lee and Onat [98], in addition to bounds on the limit pressure, it is very important to have as much information as possible on the respective stress field and deformation patterns. In this sense, as stated previously, the present technique yields solutions which generate the velocity fields together with the critical pressure, since it is based on an upper bound formulation. The problems investigated for the purposes of this thesis are related to clamped uniform shells, whose solutions may be easily compared with those in [78], when the limit pressures are plotted against the cap half angle α, which is defined in Fig. 6.27. Such a diagram is shown in Fig. 6.28. Two sets of spherical caps' geometries were

used for comparison (Fig. 6.28), ie, two typical values of the shell thinckness parameter $H = h/4\ \dot{R}$ as defined in [78], for which the limit pressure curves are drawn in terms of the cap angle α. For large cap angles the solutions tend to the solution of a membrane shell. For some reason which could not be explained the results obtained here are coincident with those given in [78] for simply suported spherical caps as shown in Fig. 6.28.

To complete the set of numerical examples on spherical caps, the solution of a cap with cutout closed by a rigid boss, free to move axially, as shown in Fig. 6.29, is presented.

The limit load and deformation pattern is shown in Fig. 6.30a. Figs. 30b,30c show the strain distribution in the meridional and circumferential directions for a particular element.

At this point, it is possible to make a direct comparison between the solutions for spherical elements obtained by using matrix [B] and matrix [R] as discussed in Sections (6.4 & 6.5). The solutions for a particular spherical cap using both matrices are shown in Figs. 6.31 & 6.32 together with the respective strain distributions for some elements of the discretized shell. It can be seen that for the solution obtained by using matrix [B] (Fig. 6.31), the value of the limit load is poor and the difference $\varepsilon^1 - \varepsilon^2$ is unacceptably large. However, when [R] is used, the limit load value compares well with that given by [78] and the strain difference is acceptable. When [B] is used only a

few elements near the clamped end are activated in the deformation pattern. All the others elements move as rigid bodies. It is worth noting that due to the fact that the general constraint Equation (6.57) was set arbitrarily equal to 1, for simplicity, to enforce the size of the mechanism, it will also control artificially the values of the strains distributed along the element. Therefore, the values appearing on the plots of the strain distributions are not actual values.

6.10.1.4 Toroidal Shells

To the author's knowledge, the only numerical solution for such basic types of shell under internal pressure, considered individually, has been given by Drucker and Shield [75]. The problem analysed in [75] can be described as follows: consider a toroidal knuckle with one end clamped and the other bounded by a rigid plate(boss) as illustrated in Fig. 6.33.

The numerical geometric parameters used in [75] are given in Table 6.3, which will be also used here for comparison. Equations (6.93) and (6.94) represents Drucker and Shield solutions corresponding, respectively, to a lower and upper bound formulation.

$$\frac{p}{\sigma_y} = \frac{h}{L}\left(229\ \frac{h}{L} + 0.335\right) = 0.00159 \quad \text{(lower bound)} \qquad 6.93$$

$$\frac{p}{\sigma_y} = \frac{h}{L}\left(13.9\ \frac{h}{R} + 0.34\right) = 0.00161 \quad \text{(upper bound)} \qquad 6.94$$

which compare closely with each other. The current solution for the same problem is shown in Fig. 6.34, where an upper bound of $p/\sigma_y = 0.00163$ is obtained.

Again the strain distribution for a particular element is shown in Figs. 6.35a & 6.35b. This last example completes the series of problems involving individual basic elements. In the next section, the technique will be applied to a shell composed of three of the basic elements.

6.10.1.5 Torispherical Vessels

Shakedown analyses of this type of pressure vessel, subjected to thermal cyclic loading in the presence of steady mechanical loads, is very likely to become one of the major tasks of the present research. Therefore, the prime objective of the technique in development here is not to solve limit analysis problems as such, although they may be assumed to be the simplest kind of problems this technique can be applied to, whenever the thermal loading is zero. However, solutions for such shakedown problems, described above, seem to be rarely available in the literature. In contrast, limit analysis solutions, which serve very well to test the applicability of this technique to more complex shells, may be readily found for quite a number of types of vessels and loading conditions. In the particular case of torispherical vessels, for example, the limit analysis for the ASME standard torispherical vessel has been performed by

Shield and Drucker [76] and their bounds and collapse mechanism may be directly compared with those produced here. The bounds determined by Biron and Chawla [92] for clamped torispherical heads may also be used for comparison with the values calculated here. Quite recently, Ponter and Carter [94] have presented solutions for the shakedown problem on such vessels using a technique based on a deformation formulation for the Finite Element Approach. They considered two different types of geometric parameters for torispherical vessels, ie, the ASME standard vessels with a small torus and a non-standard vessel with a much larger knuckle. Their solutions, with the upper bounds and kinematic patterns, will also be used for direct comparison.

The ASME Standard Torispherical Vessel

The geometry of such a vessel is illustrated in Fig. 6.37a where the various geometric parameters are defined and the deformation pattern proposed by Shield and Drucker [76] is shown in Fig. 6.37b. For the particular example chosen in [76], it is claimed that the hinge circle labelled as A in Fig. 6.37b moves to the junction of the torus and cylinder when the thickness ratio h/D = 0.00058 with a value of p/σ_y = 0.02378E-02. The solutions obtained here may lead to a slightly different conclusion by analysing the mechanisms shown in Figs. 6.38a & 6.38b. It has been found that the location of the hinge A apparently does not change but the hinge angle at A becomes very small and an extra hinge forms at the junction torus-cylinder. This kinematic pattern seems to occur for small thickness ratio h/D as it can be

seen in Figs. 6.38a & 6.38b. Fig. 6.38 shows a sequence of solutions for various thickness ratios with the respective deformation mechanisms. In order to have a direct comparison with the bounds obtained by Shield and Drucker, upper bounds for various geometric parameters, determined by the present technique, are plotted on Fig. 6.39 where the variation of $pD/2\sigma_y h$ with h/D given in [76] is shown. The solution, for a ASME standard torispherical vessel with a particular thickness, given by Ponter and Carter [94], is shown in Fig. 6.40 where the collapse mechanism is also illustrated. Such a solution can be directly compared with the solution given in Fig. 6.38b.

Non-Standard Torispherical Vessels

Ponter and Carter [94] have also solved the problem of the non-standard torispherical vessel shown in Fig. 6.41a whose bound on the limit pressure and collapse mechanism is given in Fig. 6.41b. Such a case can be directly compared with the solution obtained here, which is shown in Fig. 6.42. It can be seen that the solutions compare closely, although the element structures are not the same.

Finally, the problems of clamped torispherical heads, numerically analysed by Biron and Chawla [92] (Fig. 6.43), may be considered. The bounds in [92] are plotted against the ratio crown-radius/knuckle-radius (Fig. 6.44) covering a wide range of geometries, including the head of a ASME standard vessel for a thickness h = 0.04. The bounds obtained here are also plotted in Fig. 6.44 and the solution

for some particular cases are shown in Fig. 6.45.

6.10.2 Cyclic Thermal Stress Problems (Shakedown Analysis)

The problems considered here involve only two types of vessels subjected to cyclic thermal loading in the presence of steady internal pressure. Such vessels are: cylindrical and torispherical vessels(ASME heads). The thermal cyclic loading is identical to that used by Bree[40,41], ie high temperature gradient varying linearly through the thickness of the vessel. Due to a lack of time it was not possible to include an extra subroutine in the Code CONRE which could generate cost coefficients for thermal loading problems. However, since the problems solved here are identical to those solved by Ponter and Carter [94], their cost coefficients could be directly used, for the cost functions which define the problem to be solved are also identical. The only requirement in this case is to maintain the same geometric parameters, end conditions, and discretized element structure. The flexibility of the computer code CONRE was once again tested and only a simple interface program was necessary to read the cost coefficients provided.

6.10.2.1 Cylindrical Vessels

The cylindrical vessel considered is fully constrainted at one end and closed by a rigid plate at the other. This

problem is identical to that analysed by Bree [40,41] when a bi-dimensional state of stress is considered. The solutions for several levels of cyclic thermal loading are shown in Fig. 6.46 where a direct comparison with the solutions given by Ponter and Carter [94] may also be made. The Bree type diagram obtained in [94] is shown in Fig. 6.47. The same problem was also analysed for temperature dependent yield stresses with the solutions and Bree diagram, for such cases, shown in Fig. 6.48 and Fig. 6.49 respectively.

6.10.2.2 Torispherical Vessels

A torispherical vessel geometrically identical to that shown in Fig. 6.38b, subjected to the same loading conditions of the previous case, was considered for the shakedown analysis. The solutions produced by Ponter and Carter [94] and those obtained here are shown in Fig. 6.50 where a direct comparison can be made. It may be noticed that the value of the limit load obtained for zero thermal load is slightly higher than that given in Fig. 6.38b, which shows just how important the element structure is for obtaining good solutions. The Bree type diagram given in [94] is shown is Fig. 6.51. It is worth mentioning that the bounds separating the regions of ratchetting and reversed plasticity in Fig. 6.47, Fig. 6.49 and Fig. 6.51 were obtained using the extended upper bound theorem presented in Chapter 2.

REFERENCE	TYPE OF FORMULATION	P/σ_y
92	LOWER BOUND	0.050432
92	UPPER BOUND	0.05324
93	LOWER BOUND	0.049624
93	UPPER BOUND	0.054064
62	UPPER BOUND	0.048168
94	UPPER BOUND	0.0518
PRESENT TECHNIQUE	UPPER BOUND	0.052114

TABLE 6.2

GEOMETRIC PARAMETER	VALUE
α	60°
R_1/L	0.06
D/L	1.06
R_1/r_o	6/47
r_o/L	0.47
h/R_1	1/30
h/L	0.002

TABLE 6.3- GEOMETRIC PARAMETER FOR THE TOROIDAL SHELL IN [75]

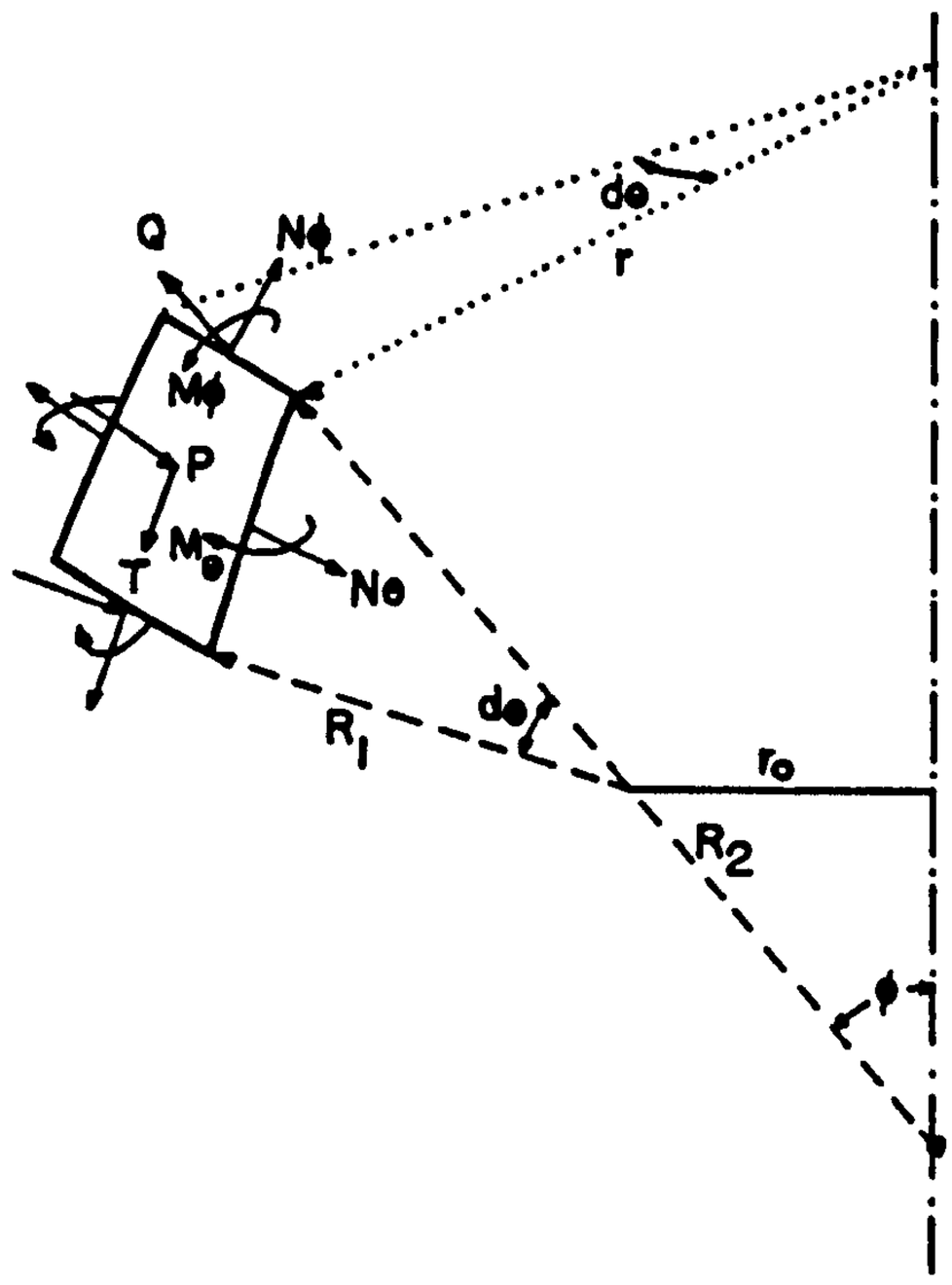

Fig. 6.1 - THIN SHELL OF RESOLUTION

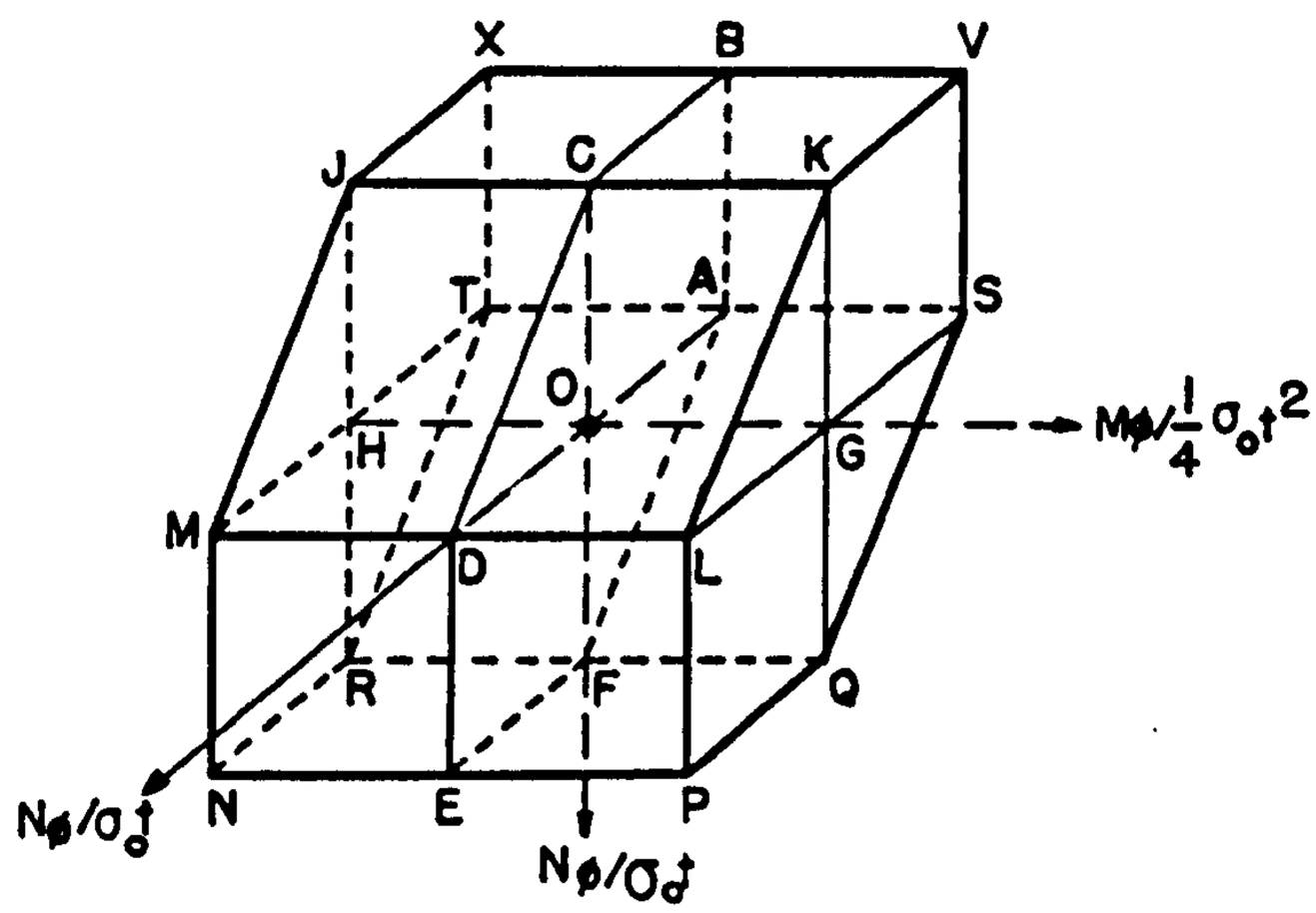

Fig. 6.2-SIMPLER CIRCUMSCRIBED YIELD SURFACE

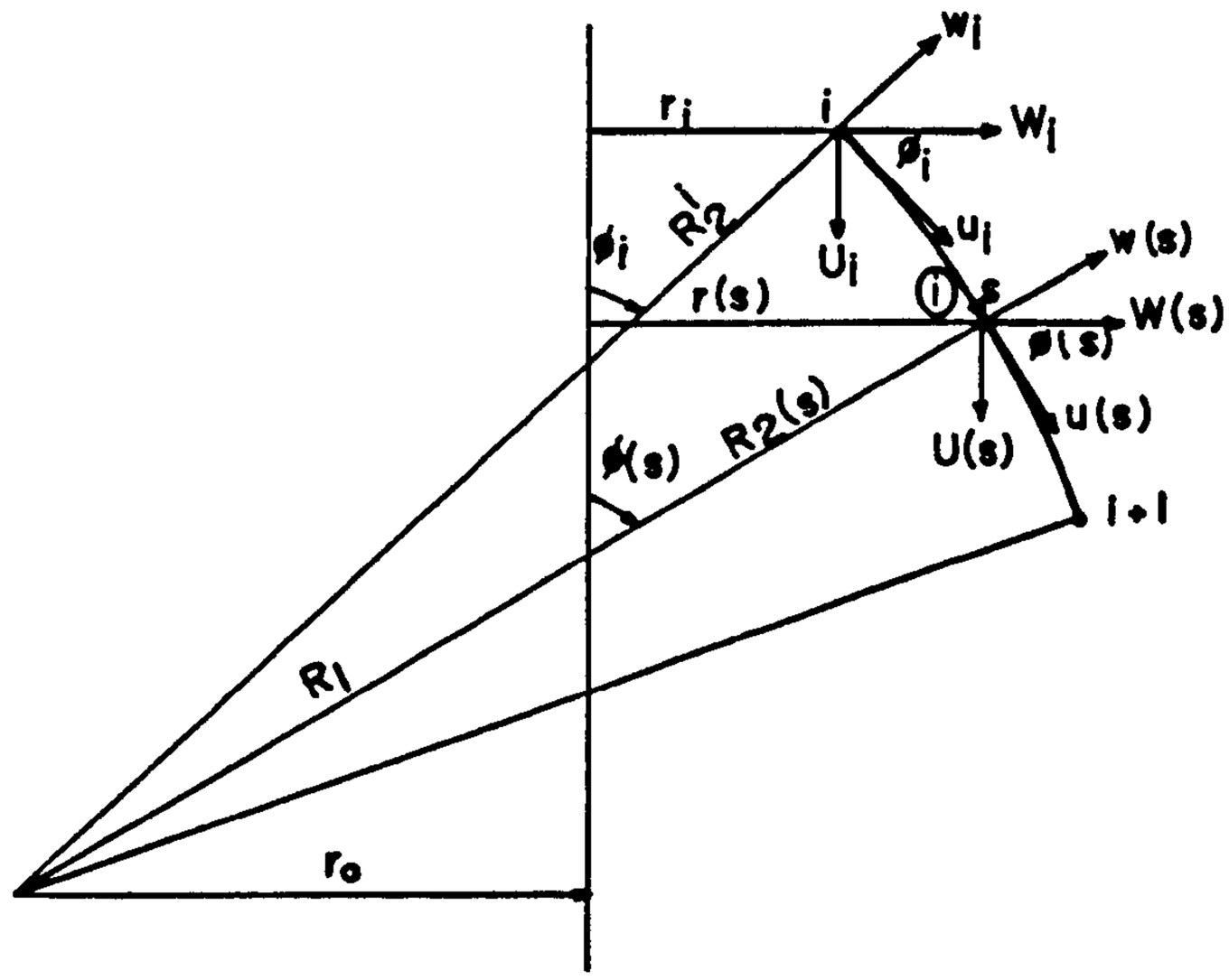

Fig. 6.3- ELEMENT GLOBAL AND LOCAL DISPLACEMENT

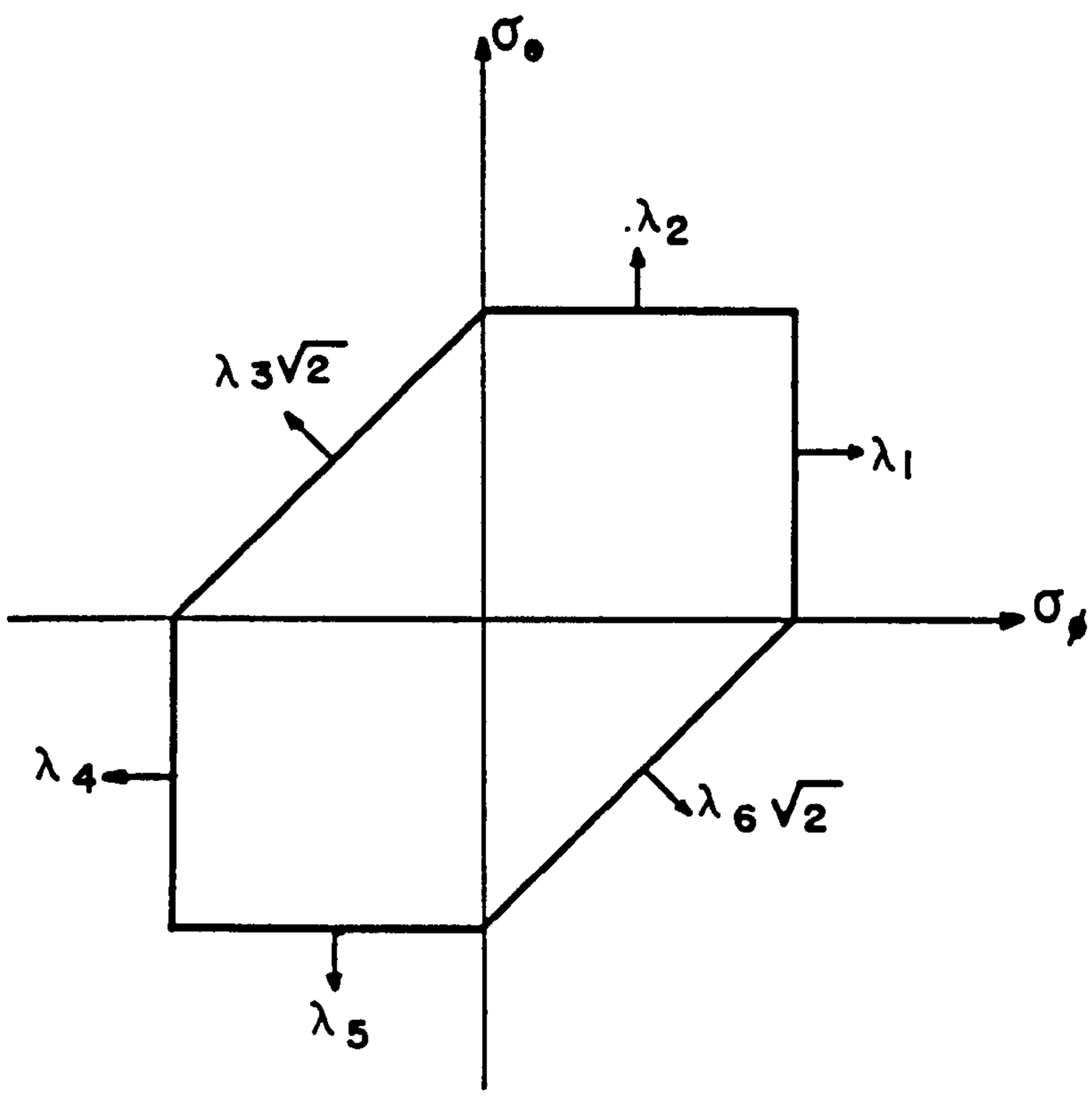

Fig. 6.4- TRESCA YIELD SURFACE AND THE PLASTIC MULTIPLIERS

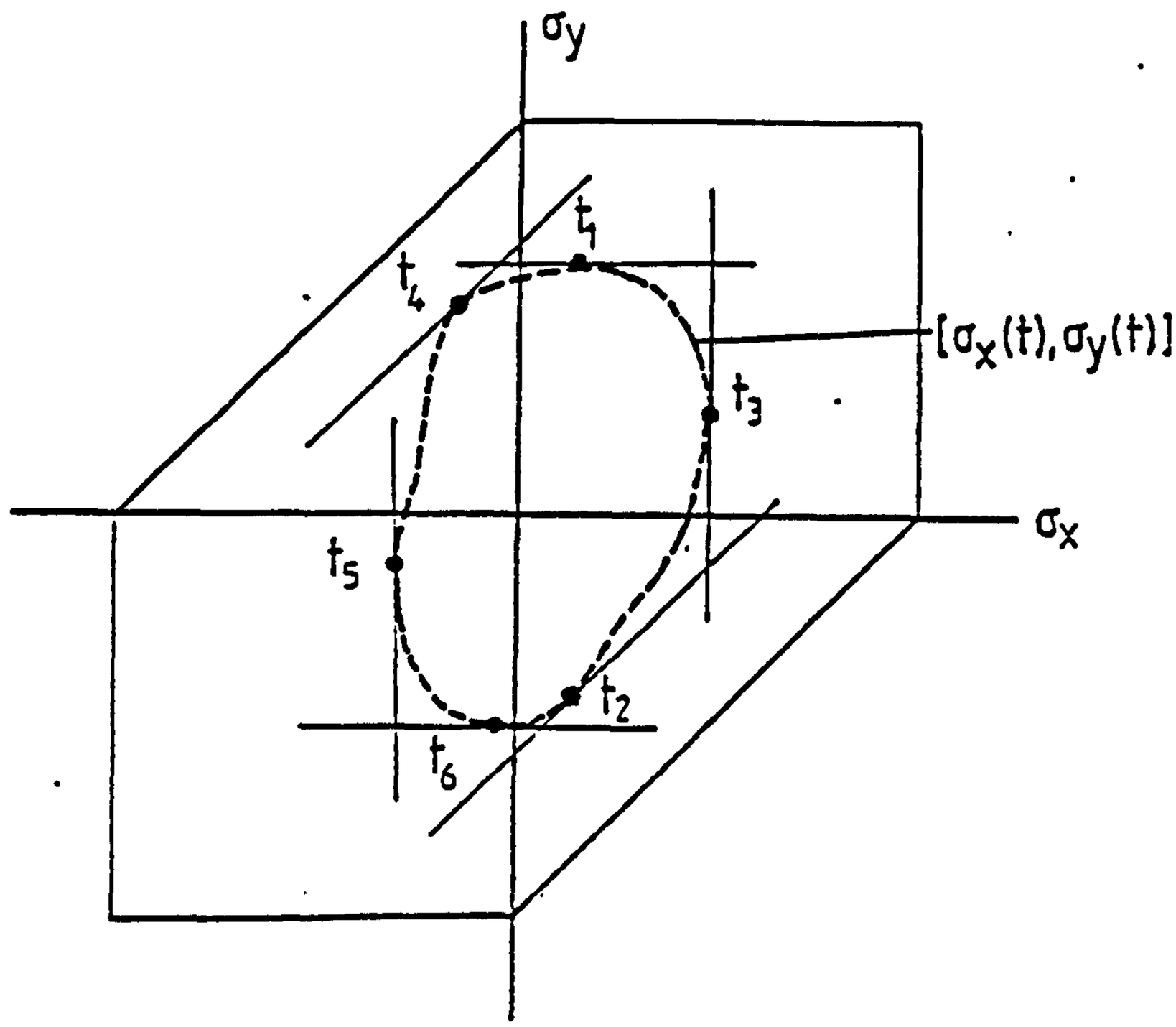

Fig. 6·5 The selection of times t_1 to t_6 of equation (6·60) which maximises the individual terms of this equation [51]

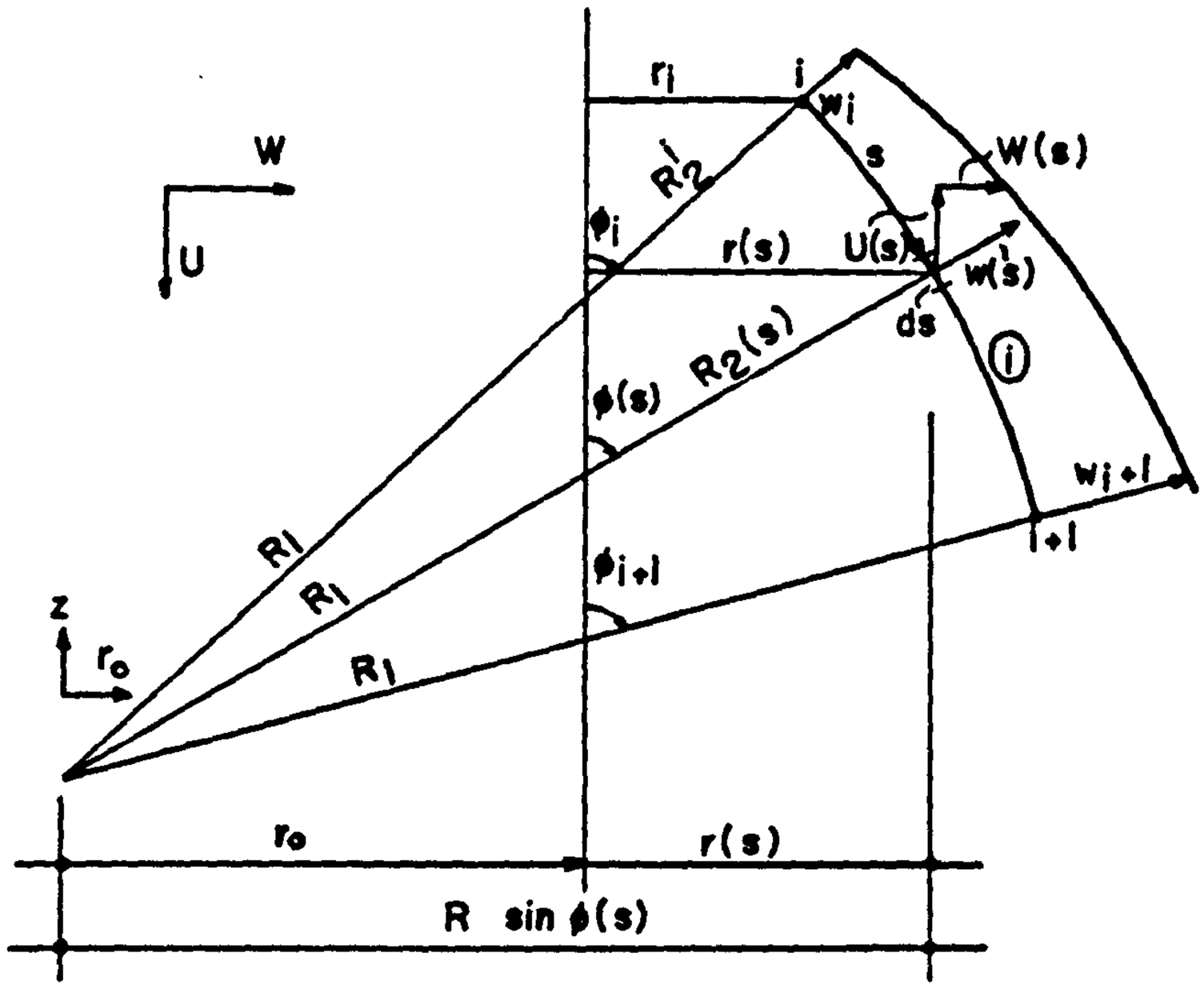

Fig. 6.6 - SCHEMATIC DISPLACEMENT OF A GENERIC ELEMENT UNDER INTERNAL PRESSURE

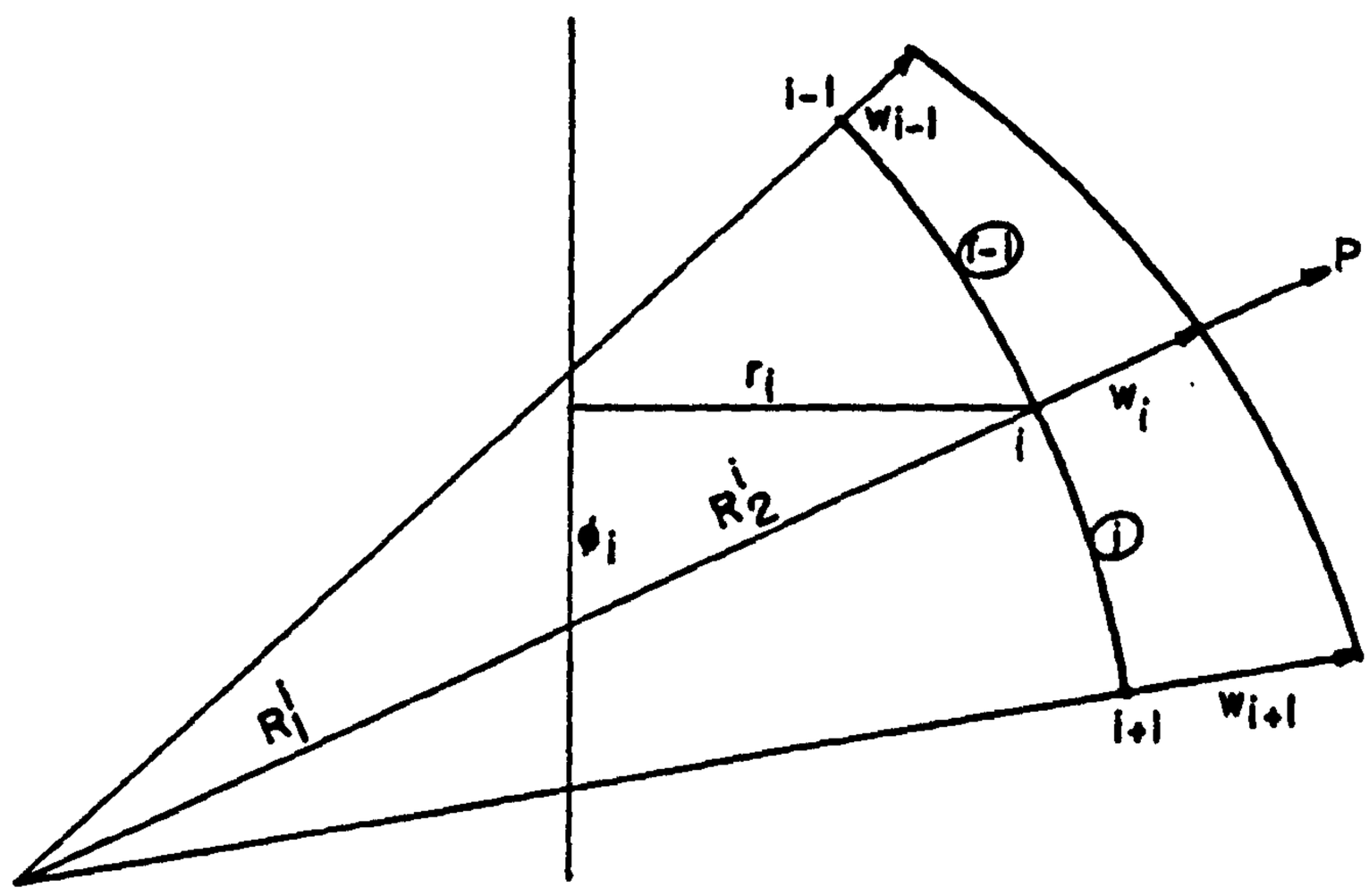

Fig. 6.7- SCHEMATIC DISPLACEMENT OF A GENERIC ELEMENT SUBJECTED TO A RING LOAD

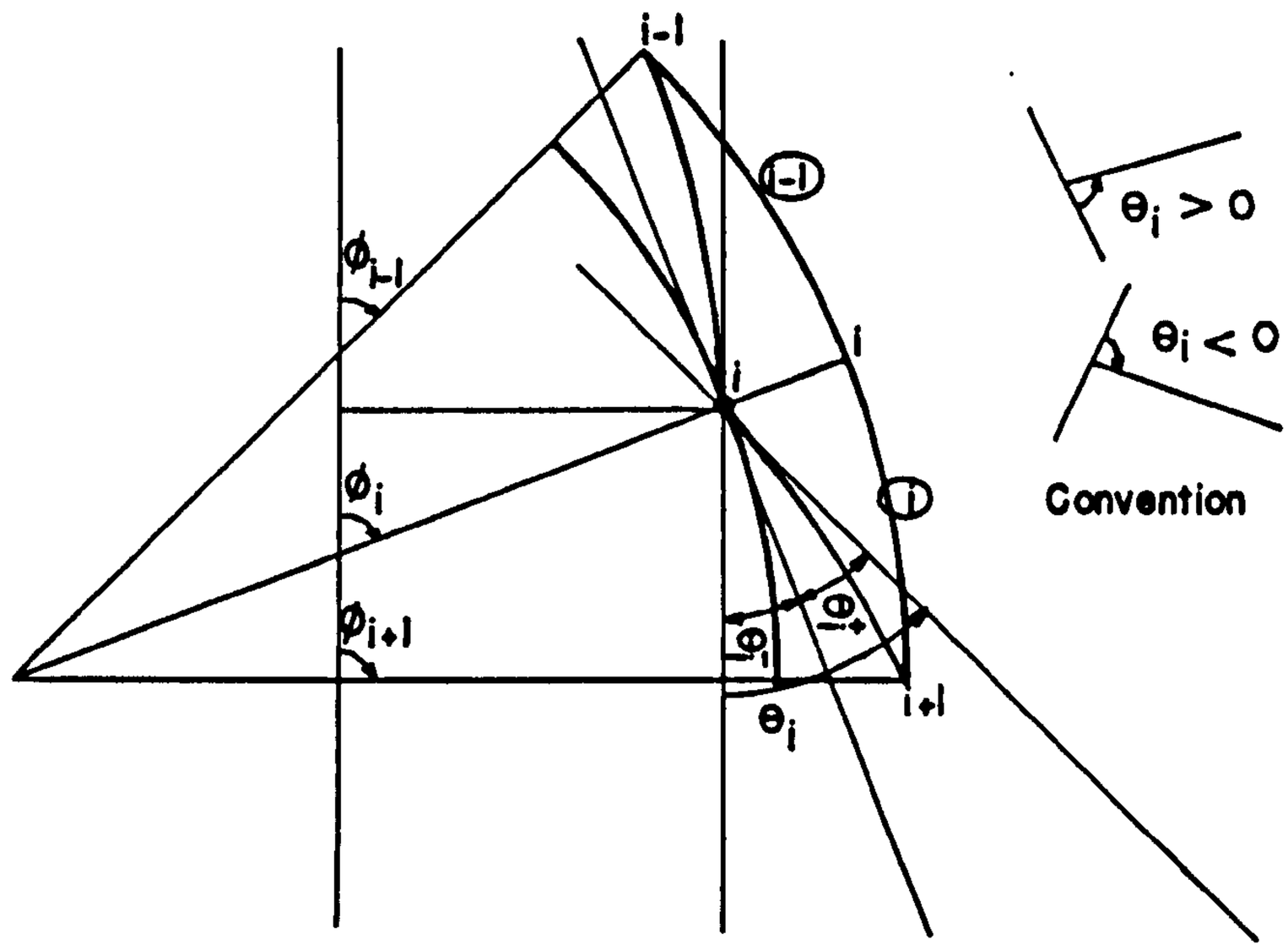

Fig. 6.8 - HINGE ROTATION

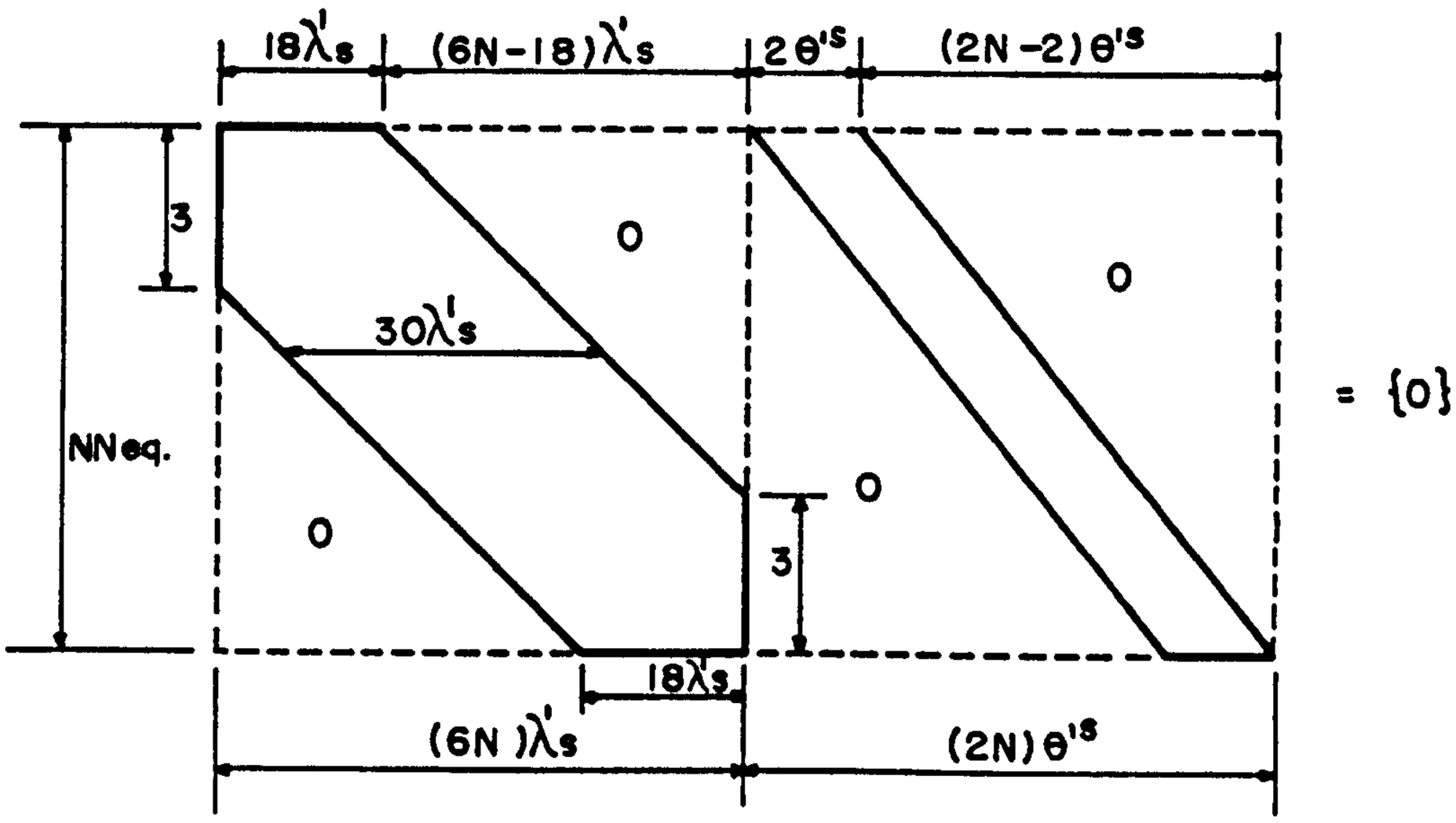

Fig. 6.9 -SCHEMATIC REPRESENTATION OF THE CONSTRAINT EQUATIONS (NNx8NN) COEFICIENTS

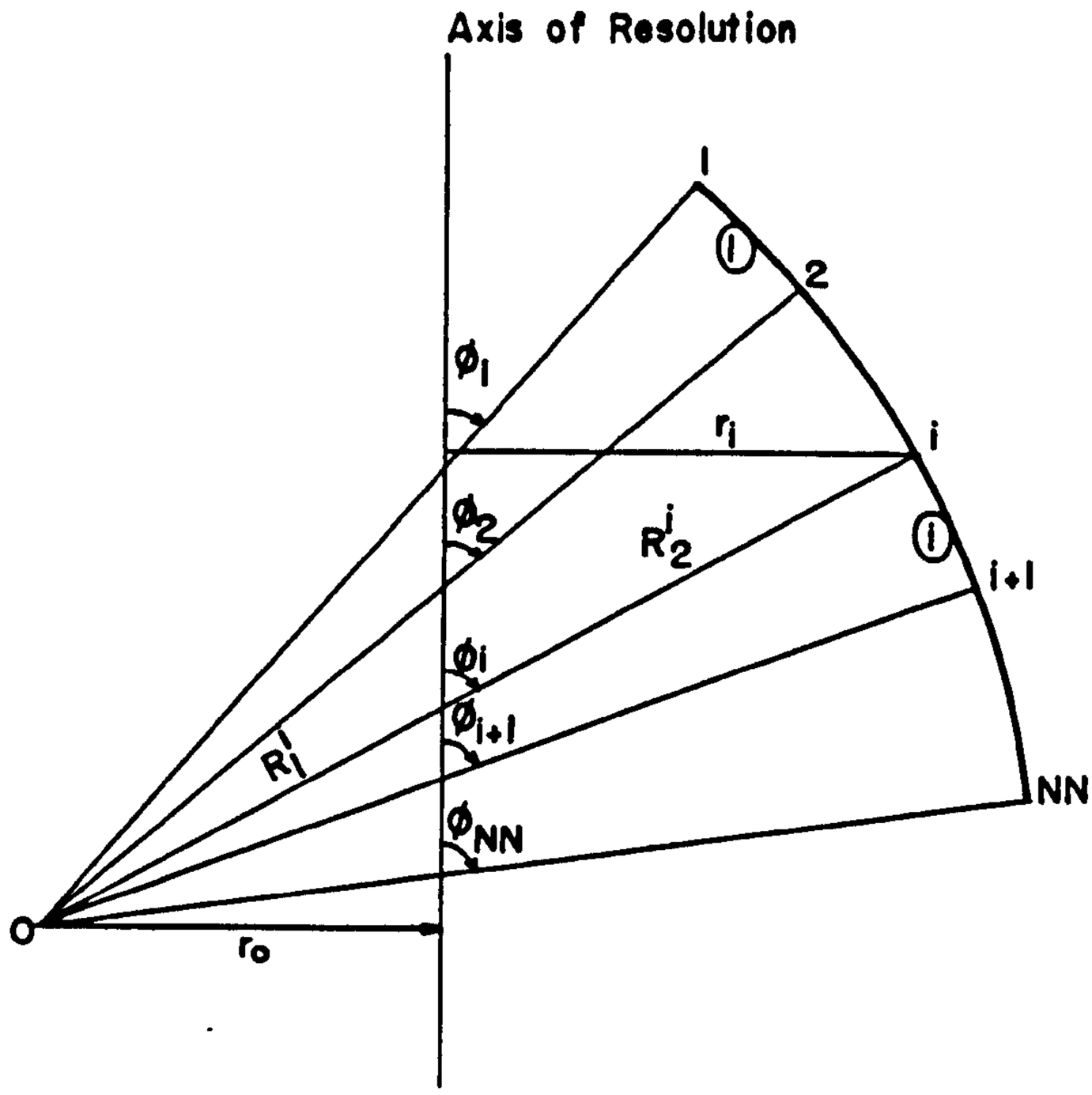

Fig. 6.10 - DISCRETIZED SHELL

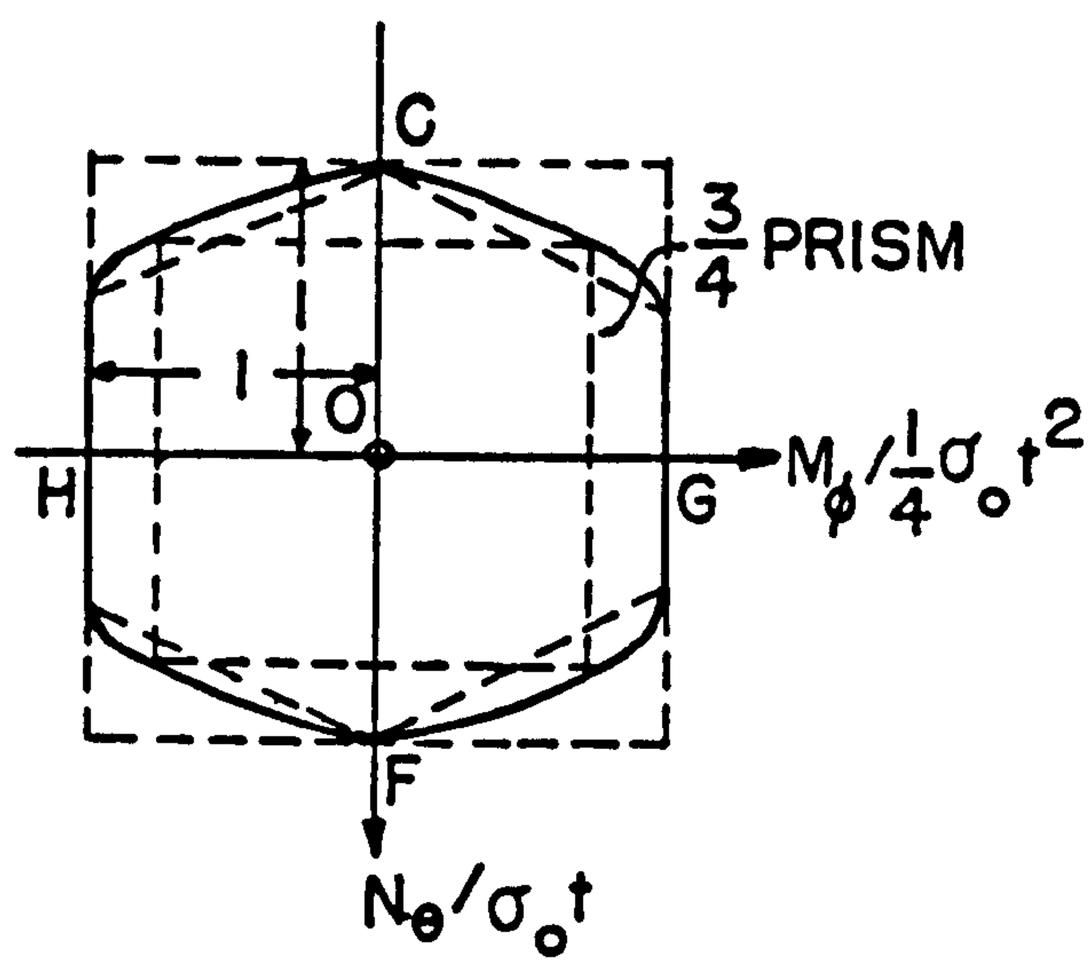

Fig. 6.11 - YIELD CURVE FOR CYLINDER WITH $N_\phi = 0$

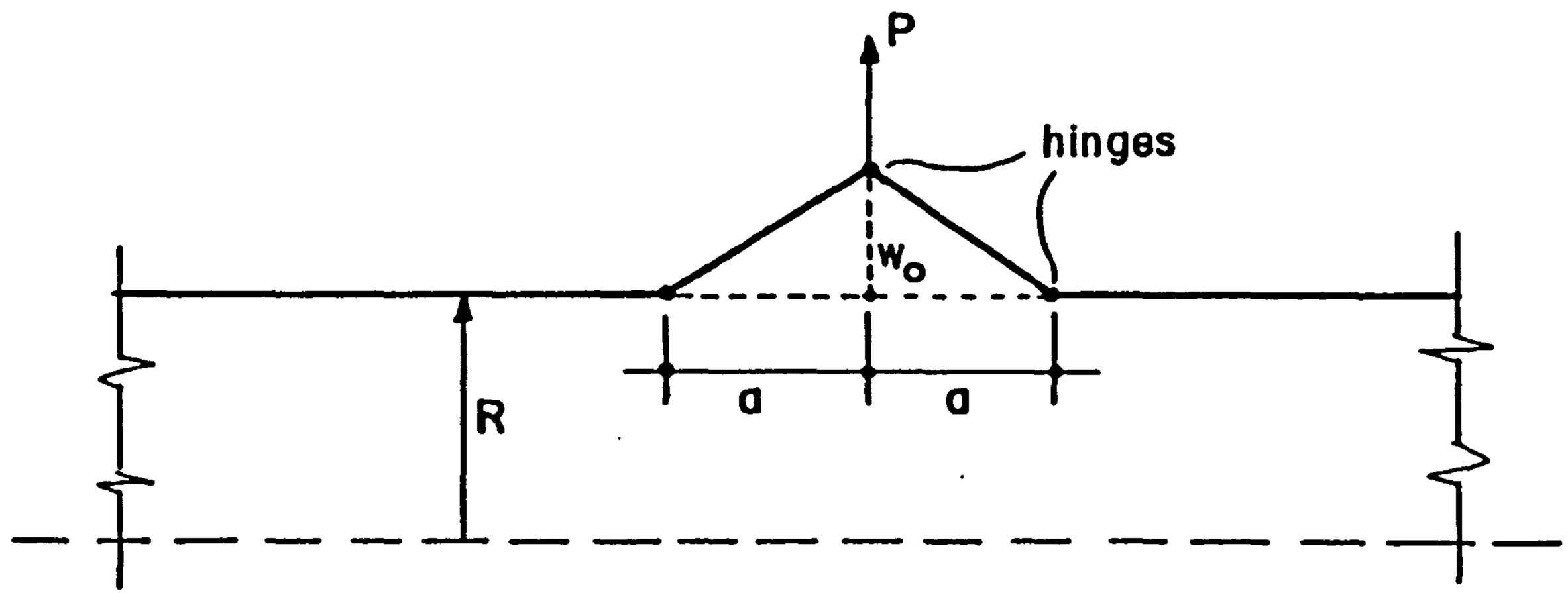

Fig. 6.12- HINGE-CONE DEFORMATION PATTERN

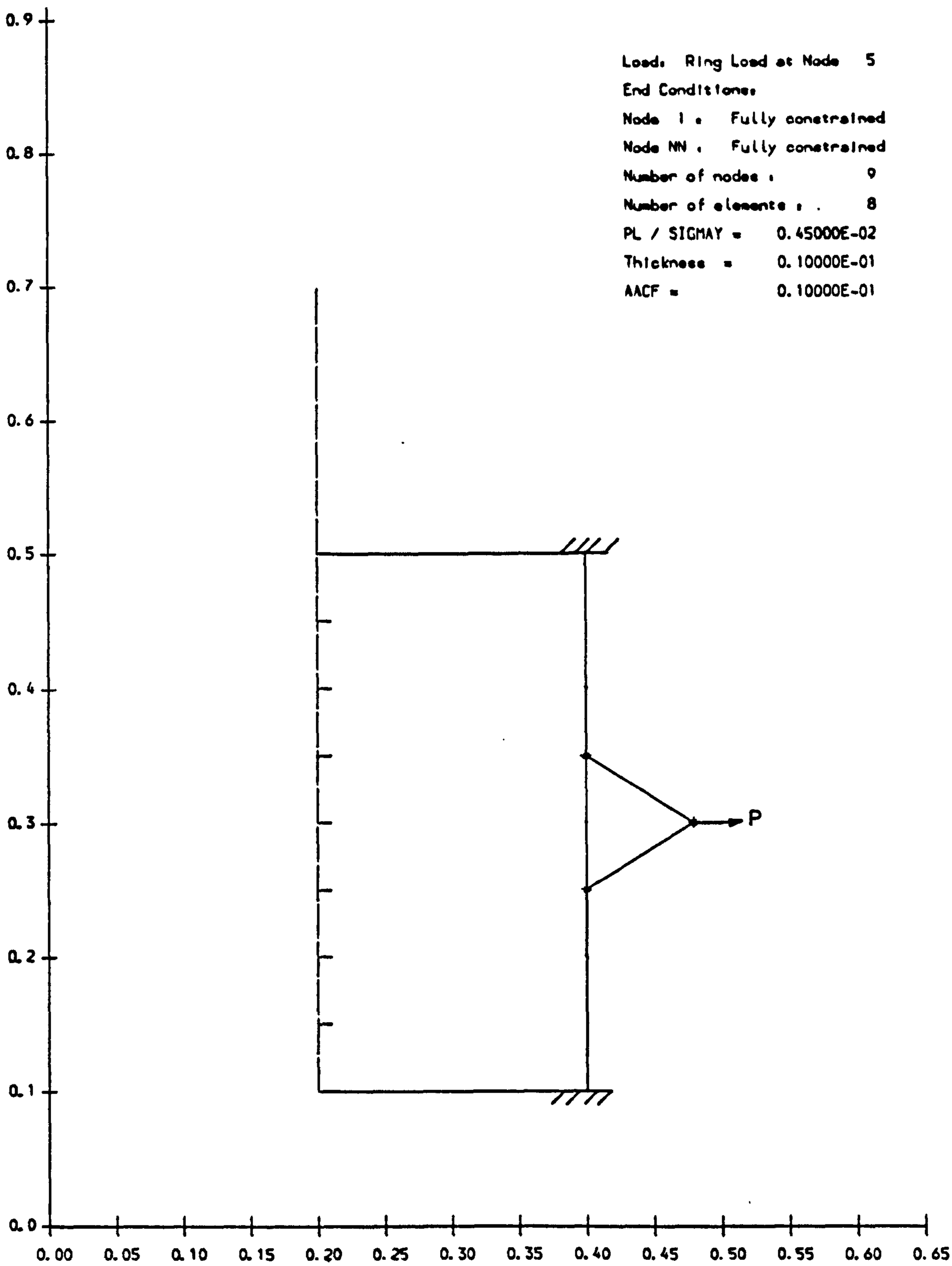
Load: Ring Load at Node 5
End Conditions:
Node 1 : Fully constrained
Node NN : Fully constrained
Number of nodes : 9
Number of elements : 8
PL / SIGMAY = 0.45000E-02
Thickness = 0.10000E-01
AACF = 0.10000E-01
P
0.0
0.1
0.2
0.3
0.4
0.5
0.6
0.7
0.8
0.9
0.00
0.05
0.10
0.15
0.20
0.25
0.30
0.35
0.40
0.45
0.50
0.55
0.60
0.65

Fig. 6.13 -

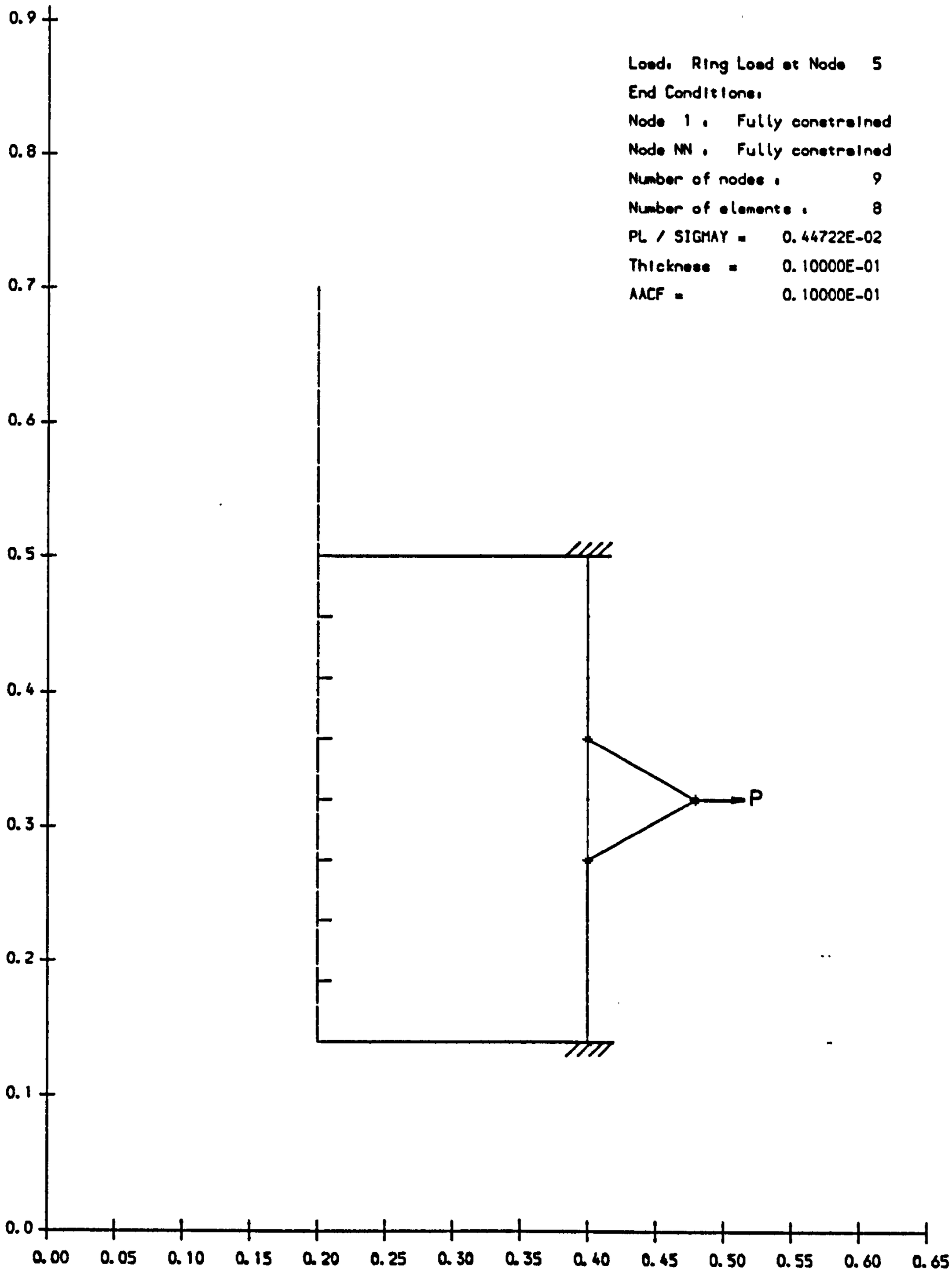
Load: Ring Load at Node 5
End Conditions:
Node 1 : Fully constrained
Node NN : Fully constrained
Number of nodes : 9
Number of elements : 8
PL / SIGMAY = 0.44722E-02
Thickness = 0.10000E-01
AACF = 0.10000E-01
P
0.0
0.1
0.2
0.3
0.4
0.5
0.6
0.7
0.8
0.9
0.00
0.05
0.10
0.15
0.20
0.25
0.30
0.35
0.40
0.45
0.50
0.55
0.60
0.65

Fig. 6.14 -

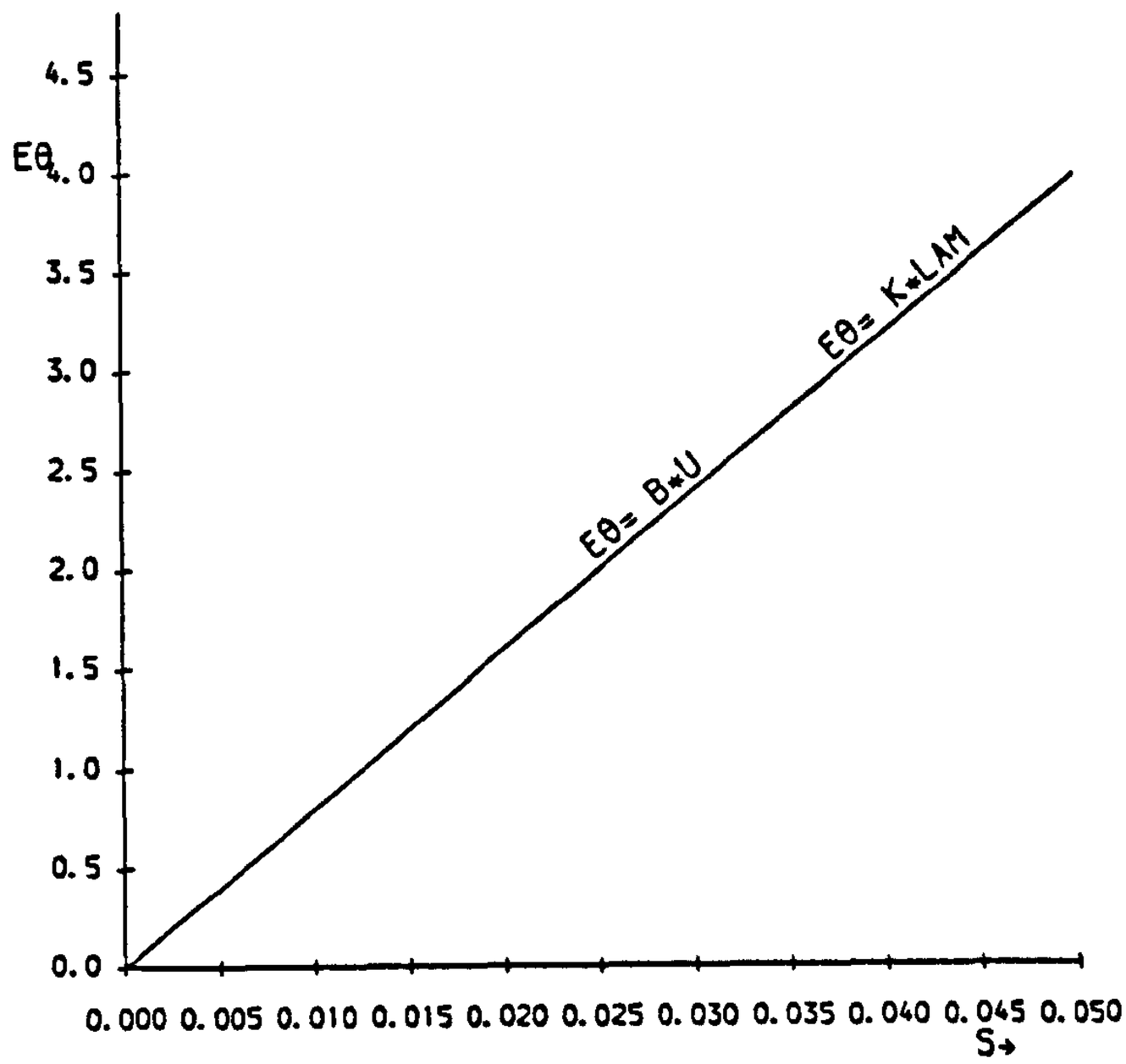

Fig.6.15a- CIRCUMFERENTIAL STRAIN DISTRIBUTION ON ELEMENT 4 OF A CYLINDRICAL SHELL

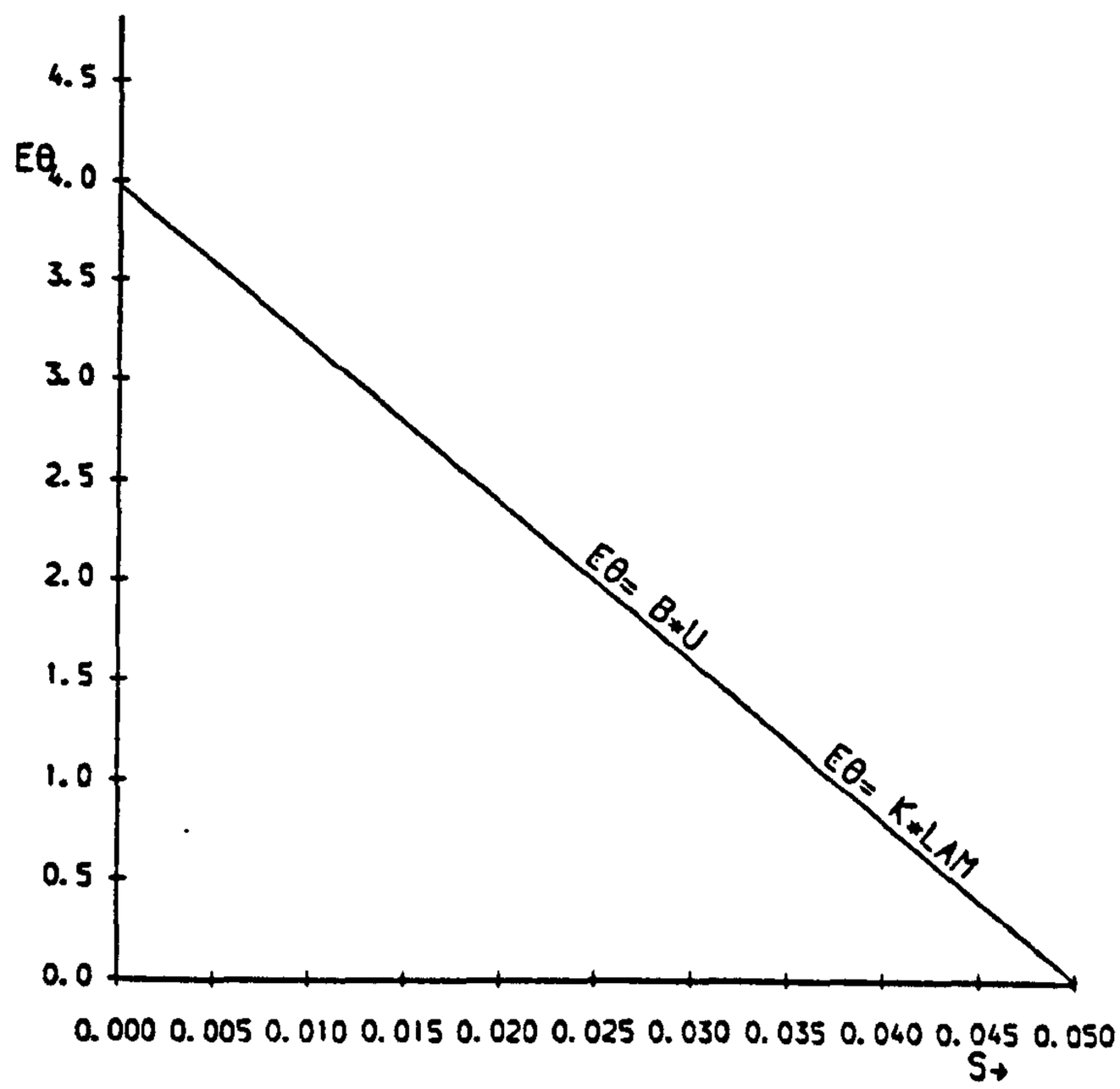

Fig.6.15b- CIRCUMFERENTIAL STRAIN DISTRIBUTION ON ELEMENT 5 OF A CYLINDRICAL SHELL

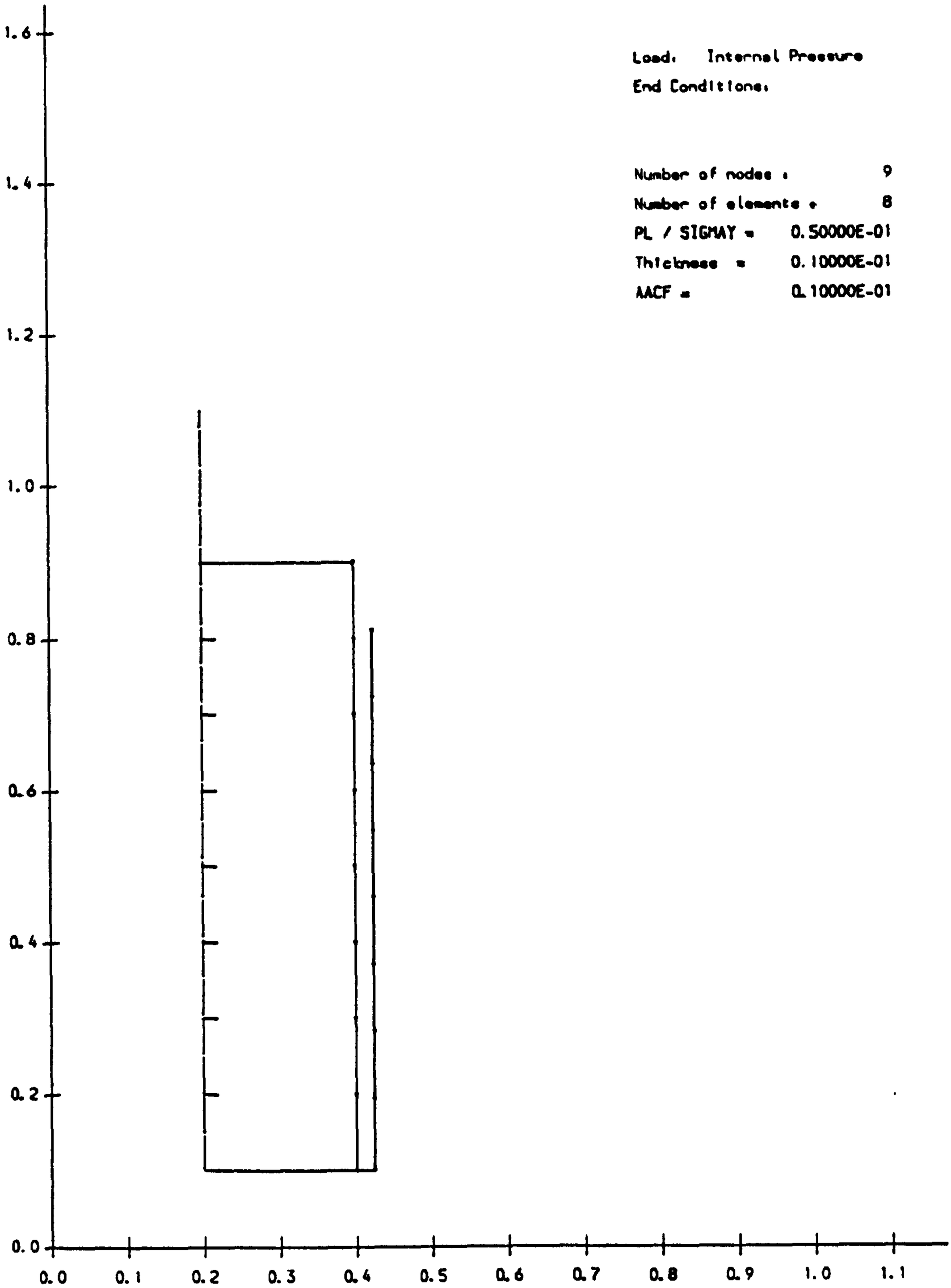
Load: Internal Pressure
End Conditions:
Number of nodes : 9
Number of elements : 8
PL / SIGMAY = 0.50000E-01
Thickness = 0.10000E-01
AACF = 0.10000E-01
1.6
1.4
1.2
1.0
0.8
0.6
0.4
0.2
0.0
0.0
0.1
0.2
0.3
0.4
0.5
0.6
0.7
0.8
0.9
1.0
1.1

Fig. 6.16 -

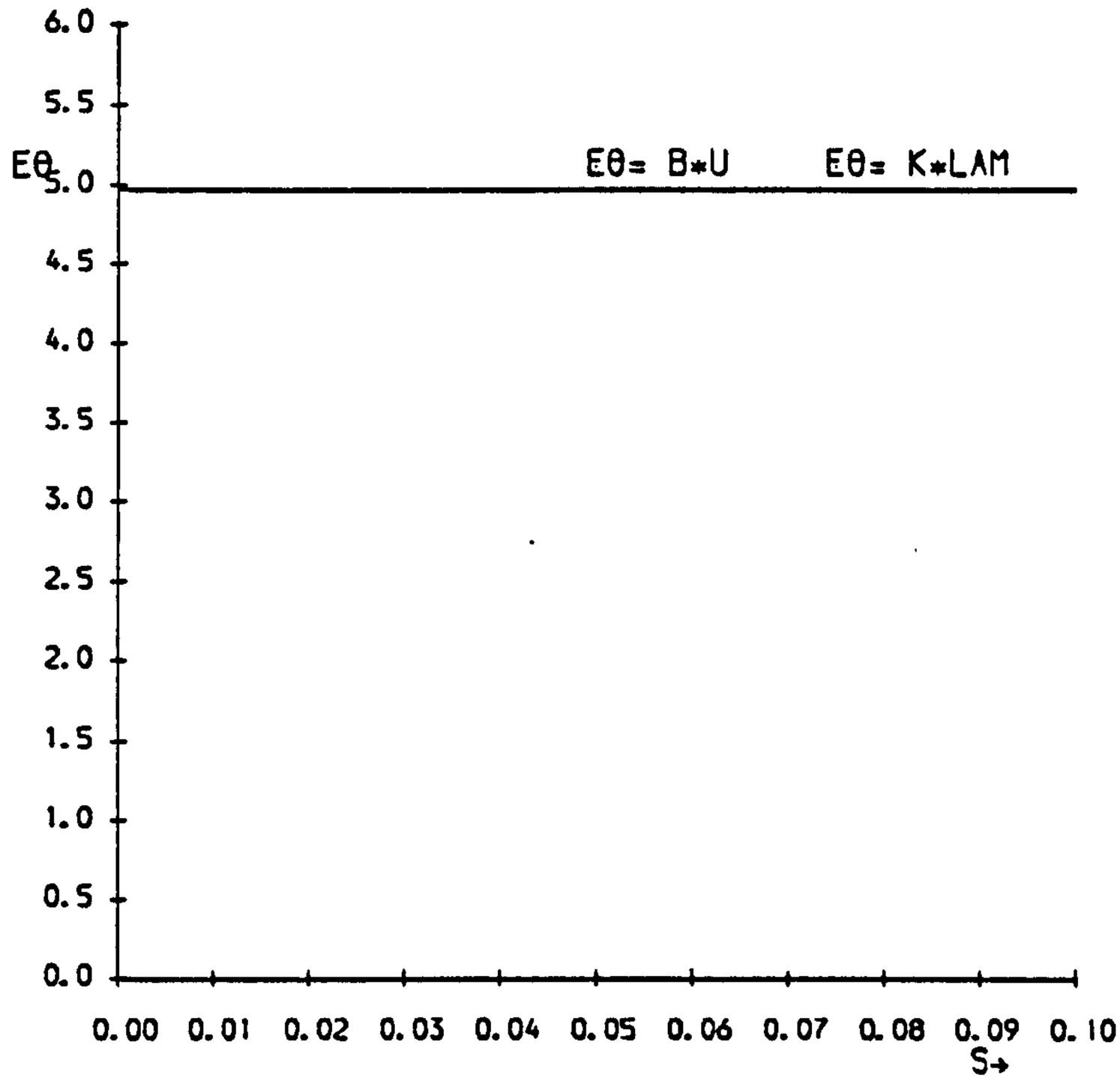

Fig.6.17 - CIRCUMFERENTIAL STRAIN DISTRIBUTION ON ELEMENT 4 OF A CYLINDRICAL SHELL

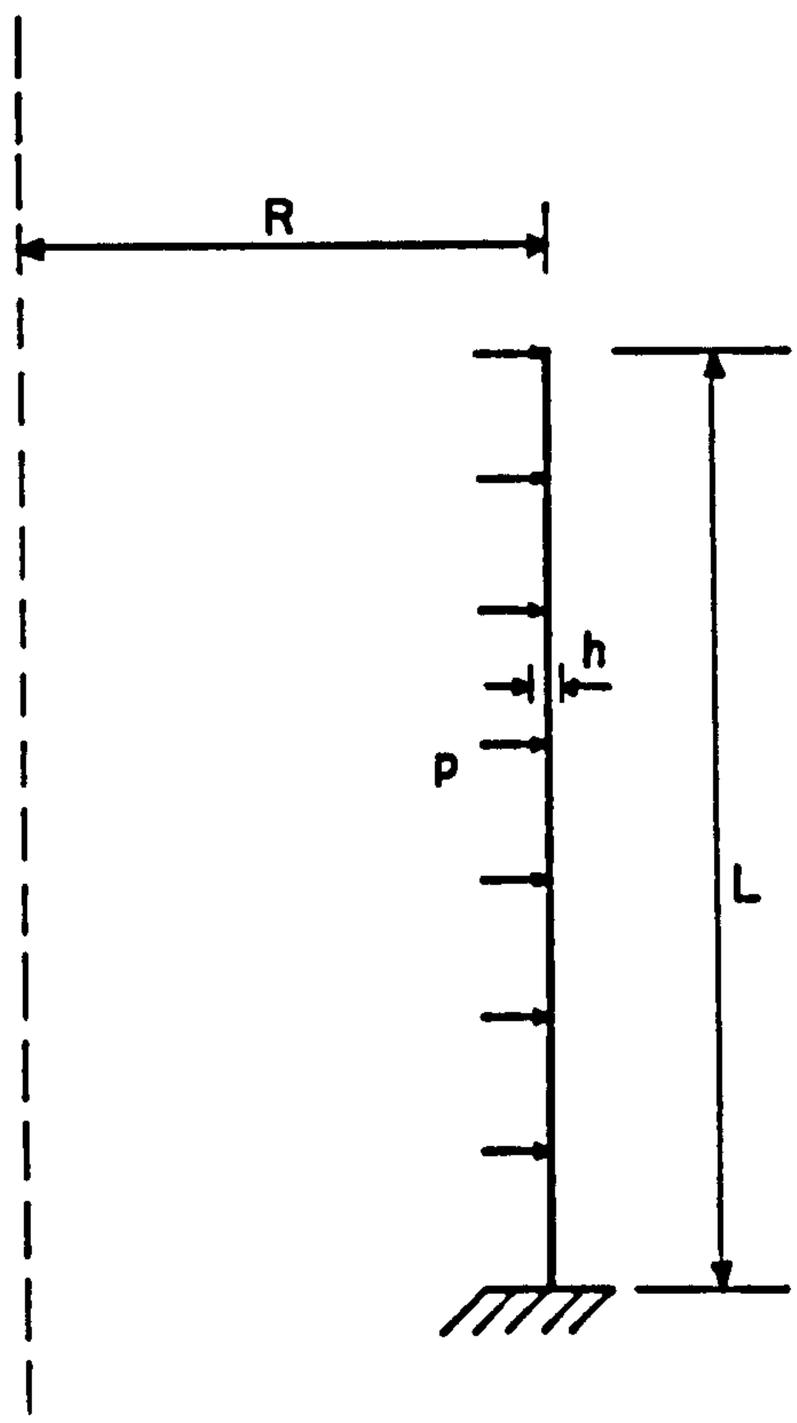

Fig. 6.18

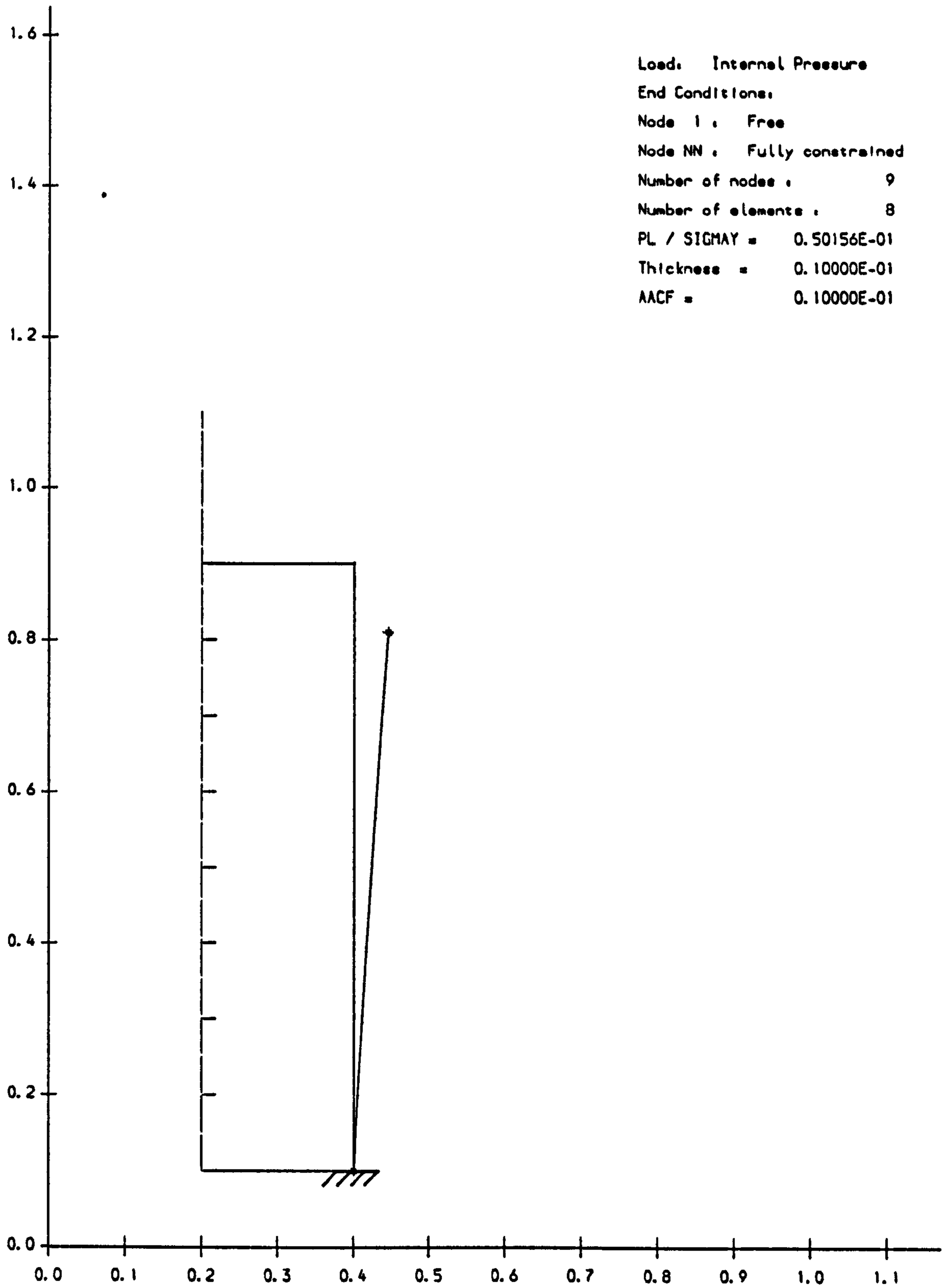
Load: Internal Pressure
End Conditions:
Node 1 : Free
Node NN : Fully constrained
Number of nodes : 9
Number of elements : 8
PL / SIGMAY = 0.50156E-01
Thickness = 0.10000E-01
AACF = 0.10000E-01
1.6
1.4
1.2
1.0
0.8
0.6
0.4
0.2
0.0
0.0
0.1
0.2
0.3
0.4
0.5
0.6
0.7
0.8
0.9
1.0
1.1

Fig. 6.19 -

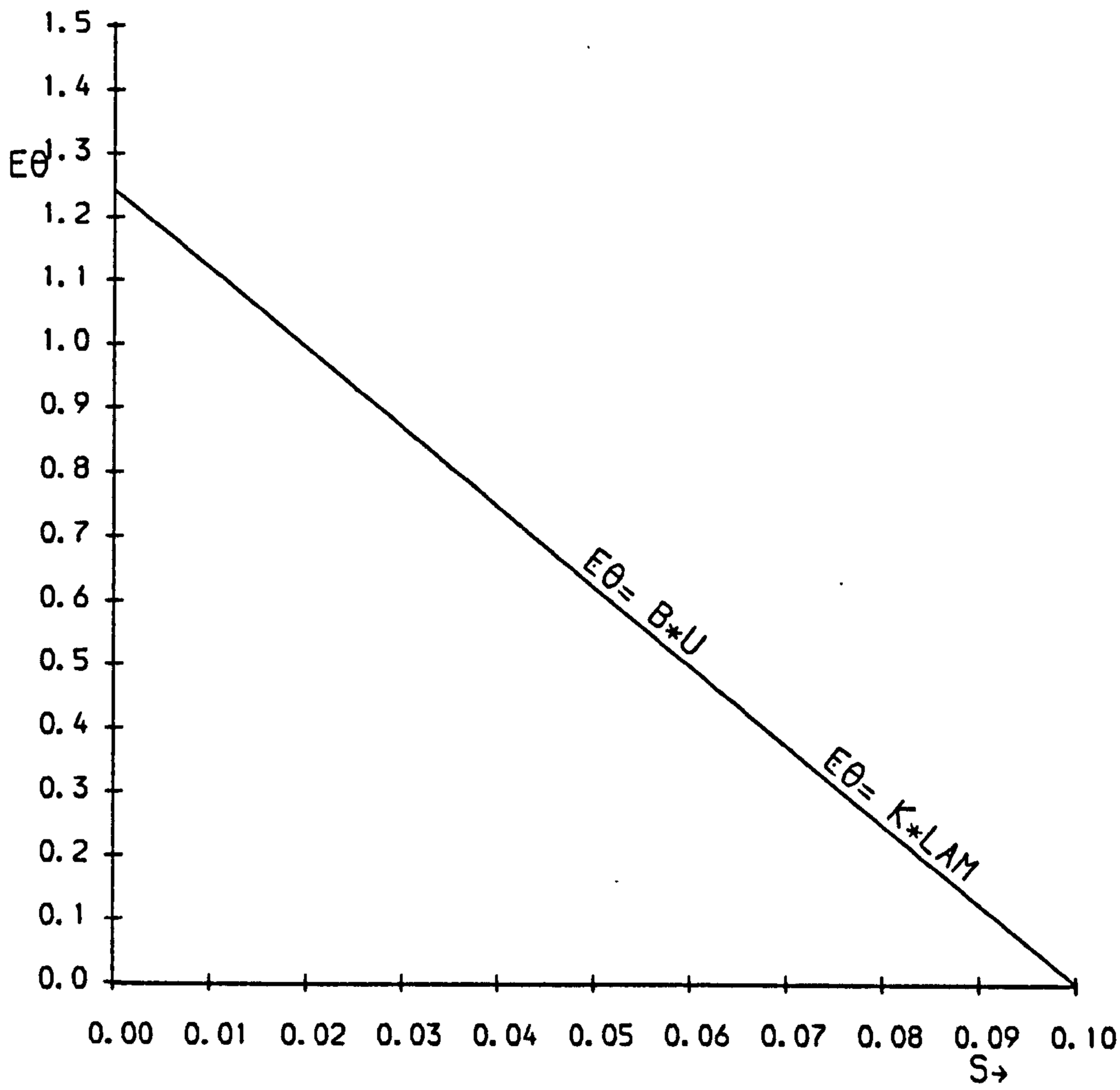

Fig.6.20- CIRCUMFERENTIAL STRAIN DISTRIBUTION ON ELEMENT 8 OF A CYLINDRICAL SHELL

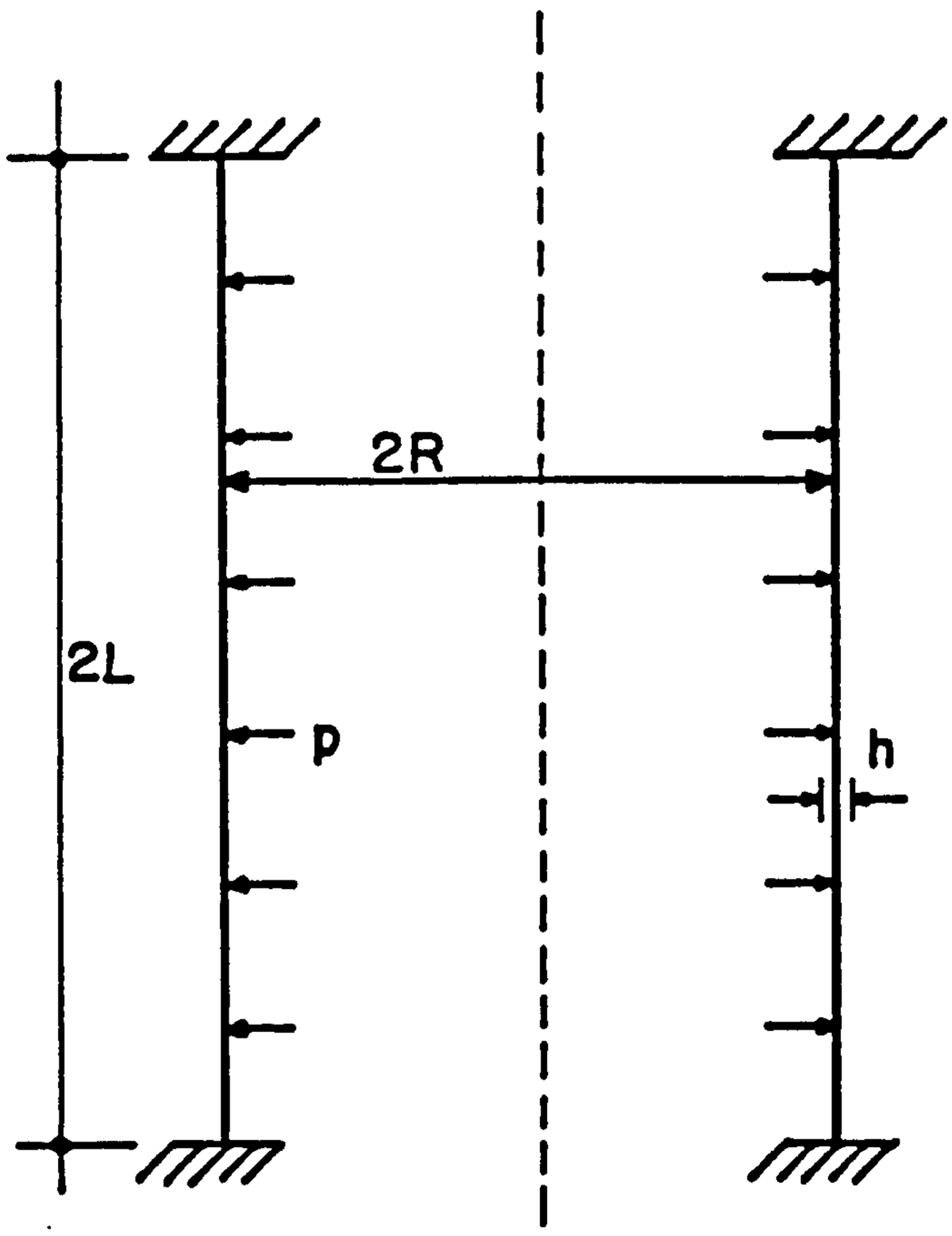

Fig. 6.21 - CLAMPED CYLINDRICAL VESSEL

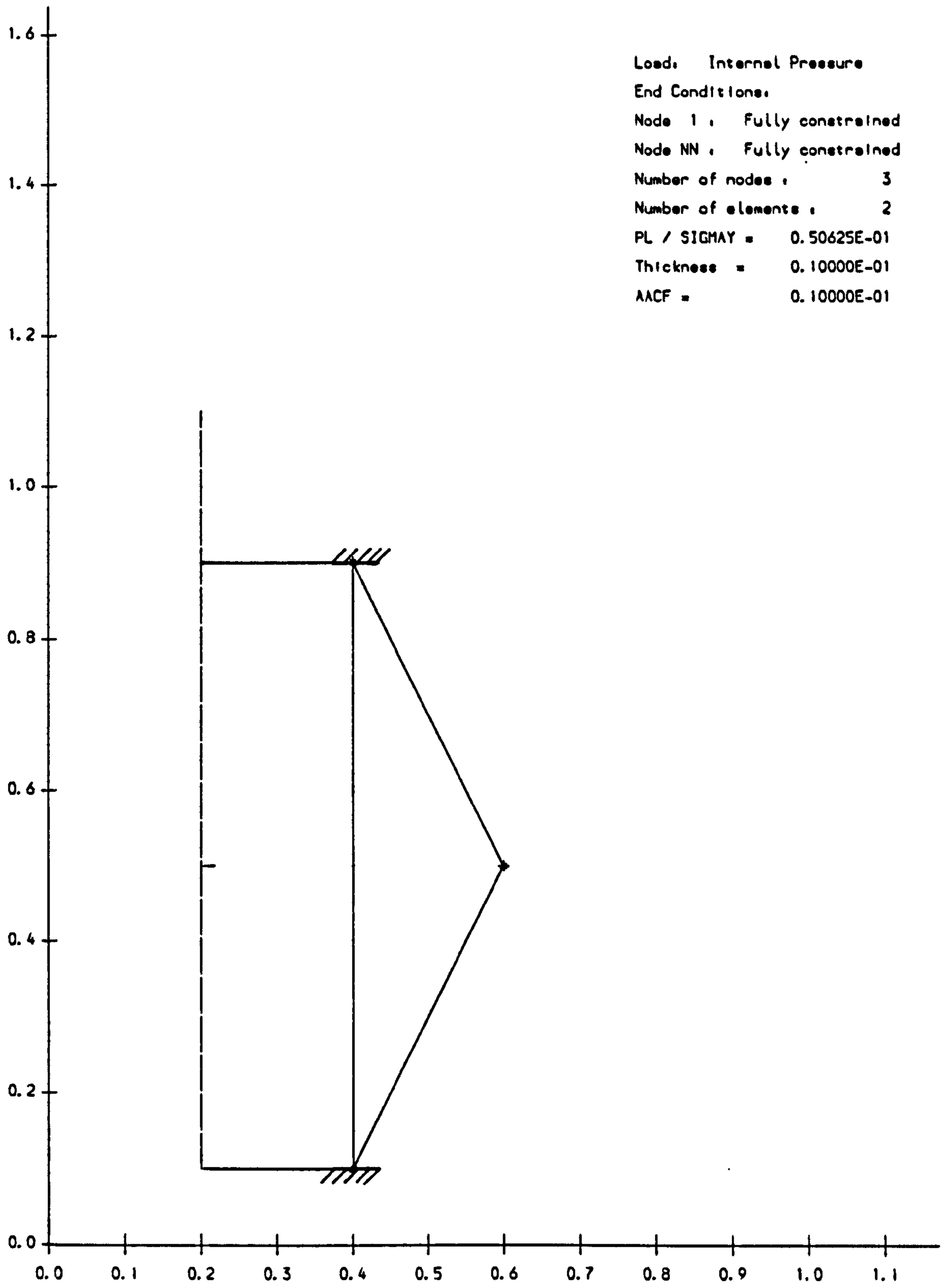
Load: Internal Pressure
End Conditions:
Node 1 : Fully constrained
Node NN : Fully constrained
Number of nodes : 3
Number of elements : 2
PL / SIGMAY = 0.50625E-01
Thickness = 0.10000E-01
AACF = 0.10000E-01
1.6
1.4
1.2
1.0
0.8
0.6
0.4
0.2
0.0
0.0
0.1
0.2
0.3
0.4
0.5
0.6
0.7
0.8
0.9
1.0
1.1

Fig. 6.22 -

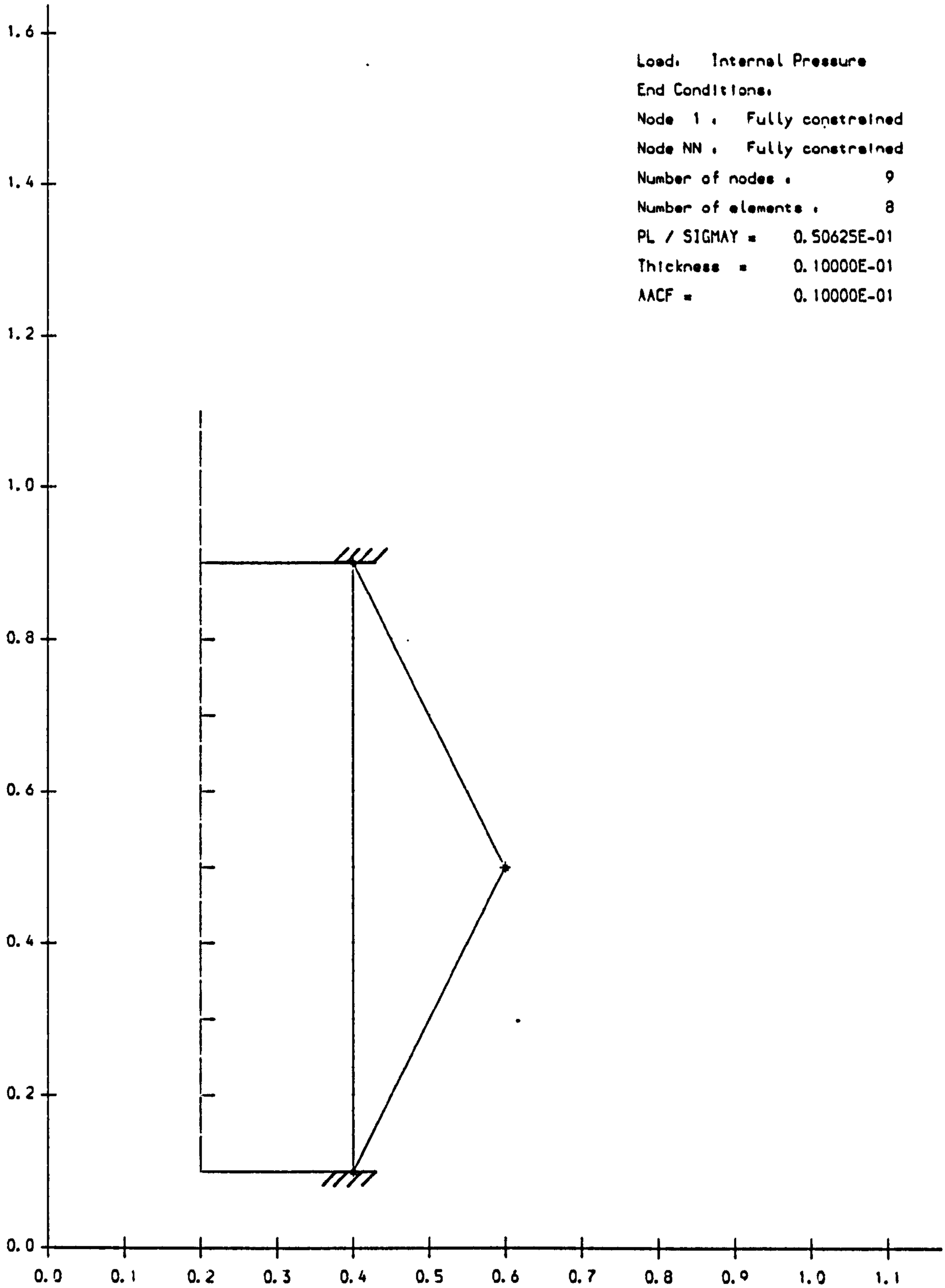
Load: Internal Pressure
End Conditions:
Node 1 : Fully constrained
Node NN : Fully constrained
Number of nodes : 9
Number of elements : 8
PL / SIGMAY = 0.50625E-01
Thickness = 0.10000E-01
AACF = 0.10000E-01
1.6
1.4
1.2
1.0
0.8
0.6
0.4
0.2
0.0
0.0
0.1
0.2
0.3
0.4
0.5
0.6
0.7
0.8
0.9
1.0
1.1

Fig. 6.23 -

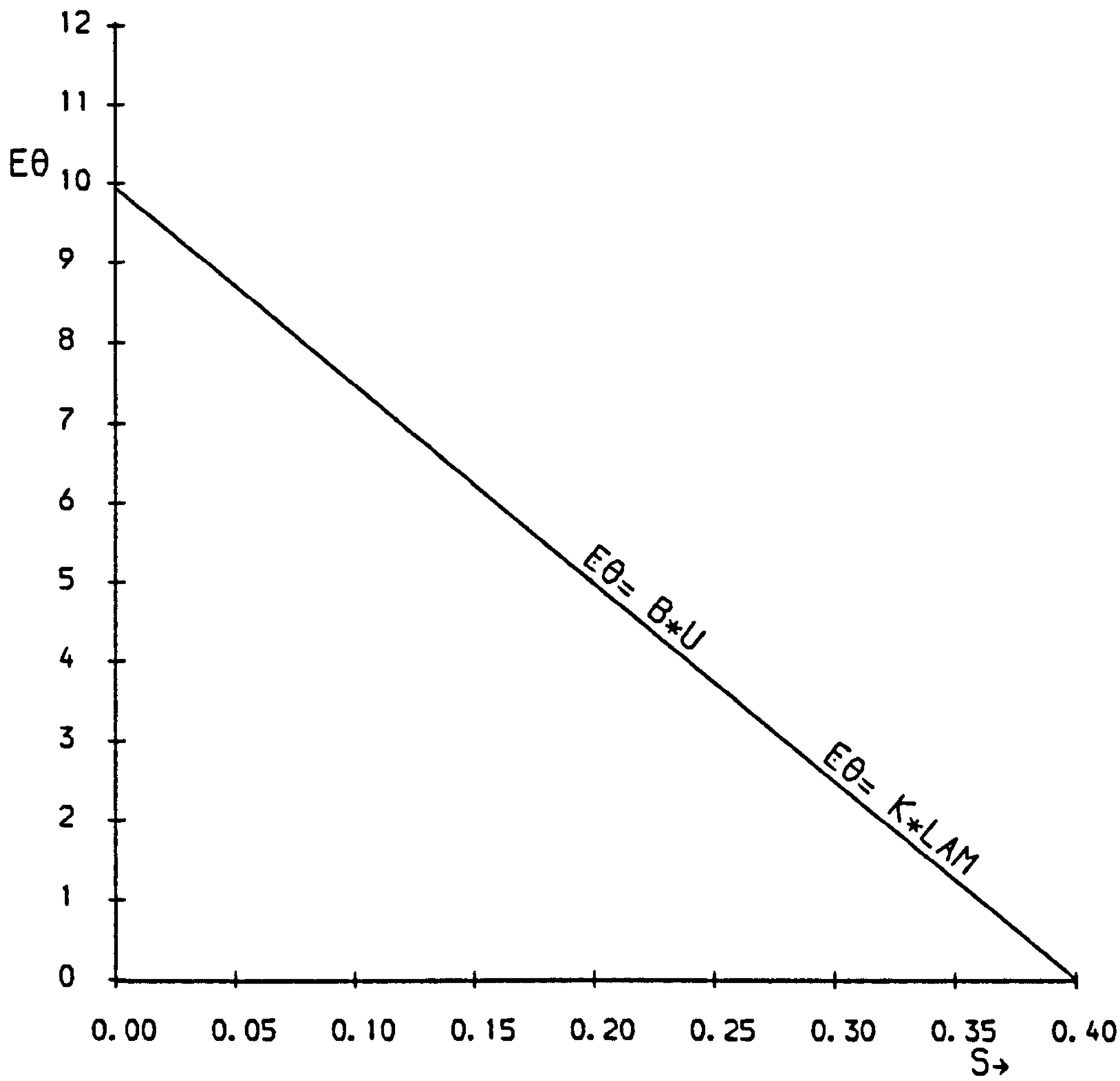

Fig.6.24 - CIRCUMFERENTIAL STRAIN DISTRIBUTION ON ELEMENT 2 OF A CYLINDRICAL SHELL

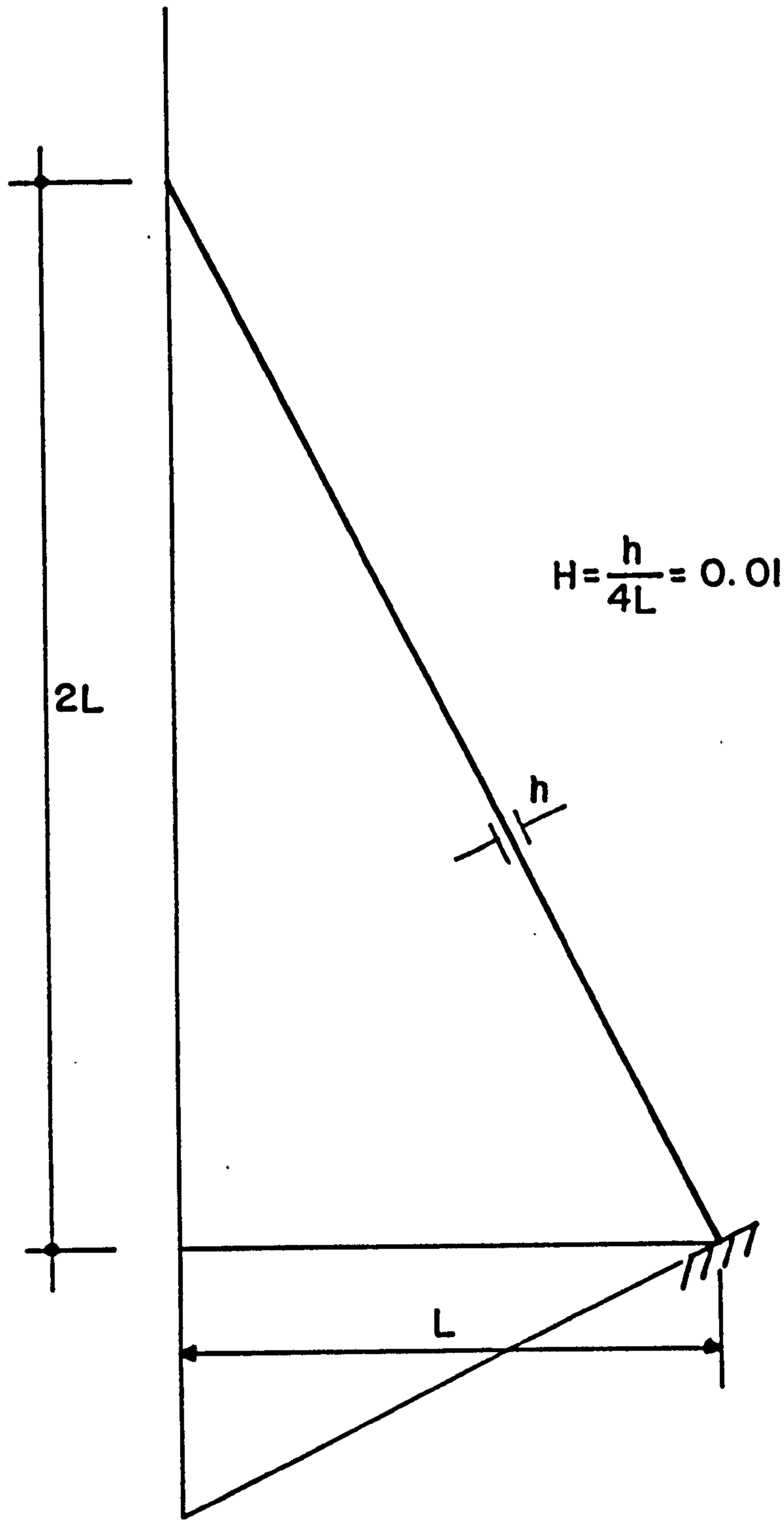

Fig. 6.25 - CONICAL SHELL

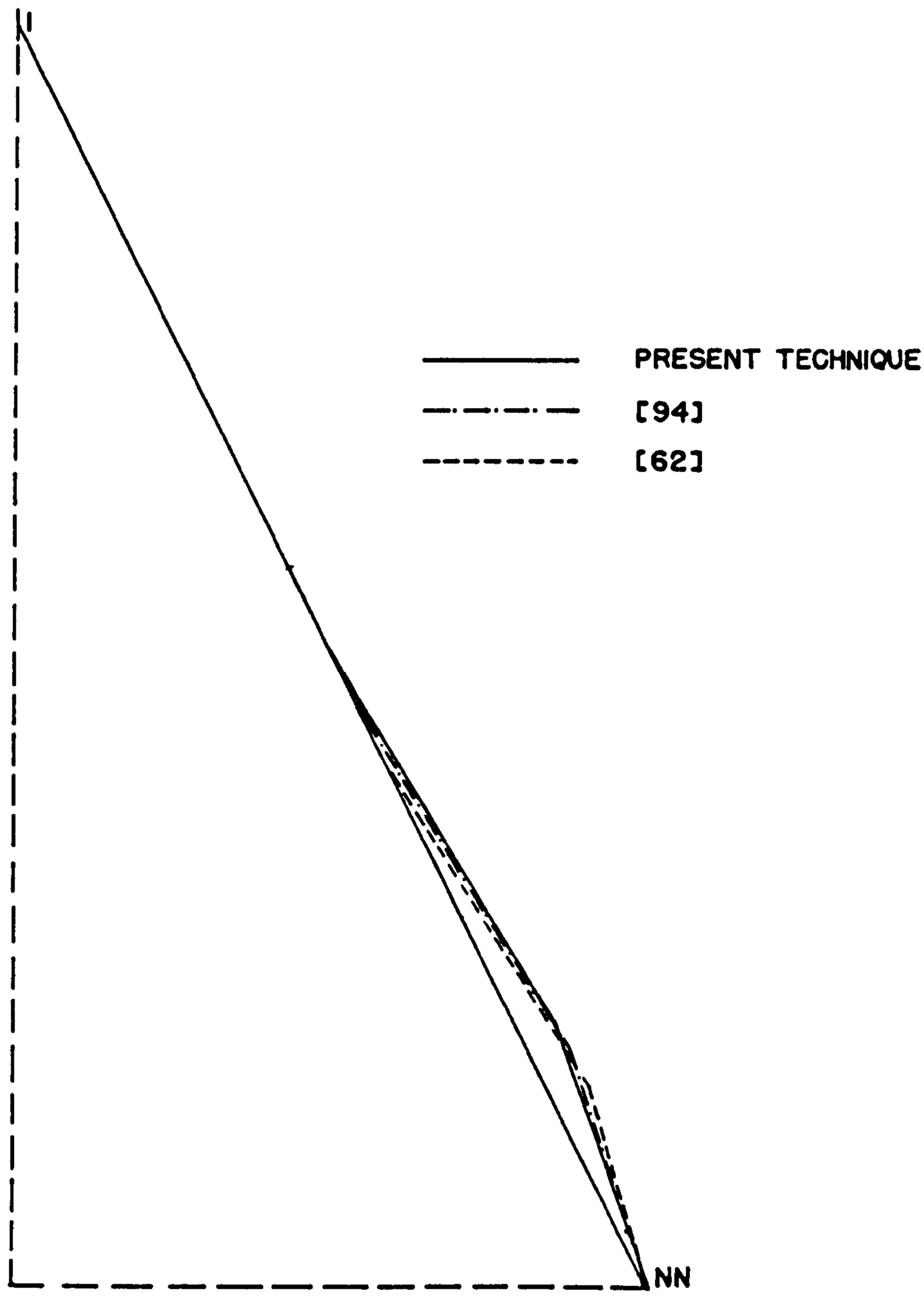

Fig. 6.26- COMPARISON OF THE MECHANISM OF DEFORMATION OF THE PRESENT TECHNIQUE WITH THOSE OBTAINED IN [62] AND [94]

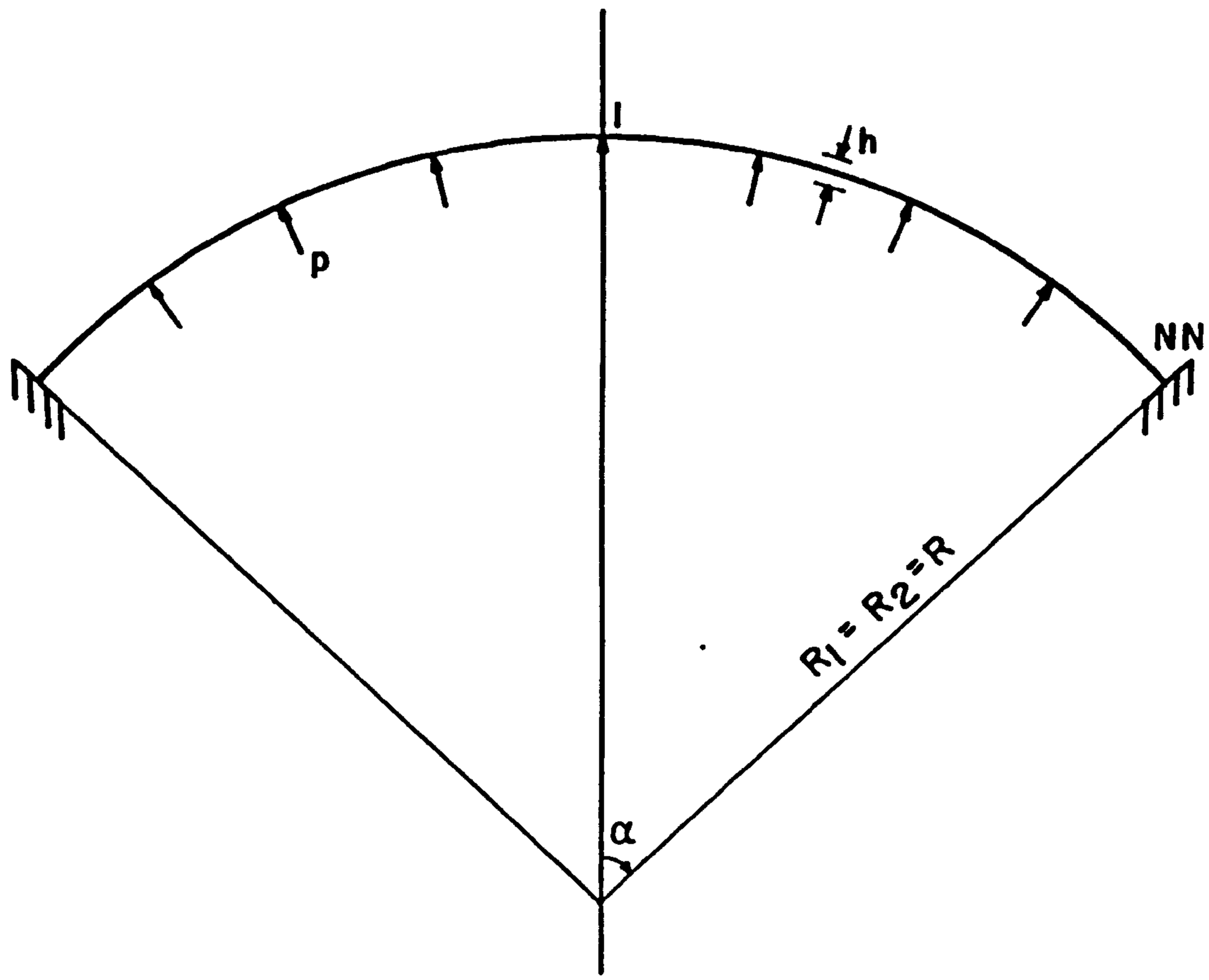

Fig. 6.27- SPHERICAL CAP

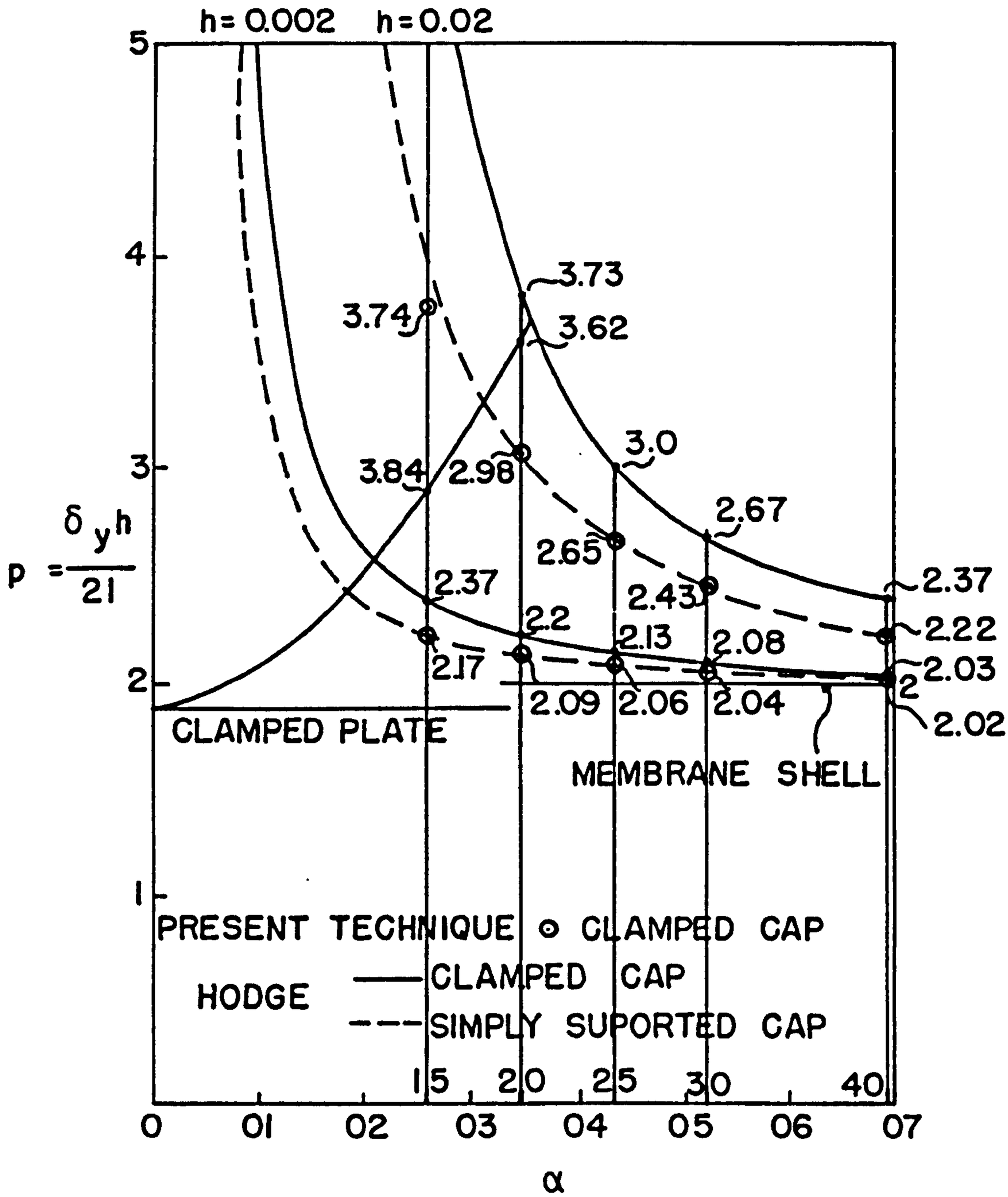

Fig.6.28-LIMIT PRESSURE FOR SPHERICAL CAPS

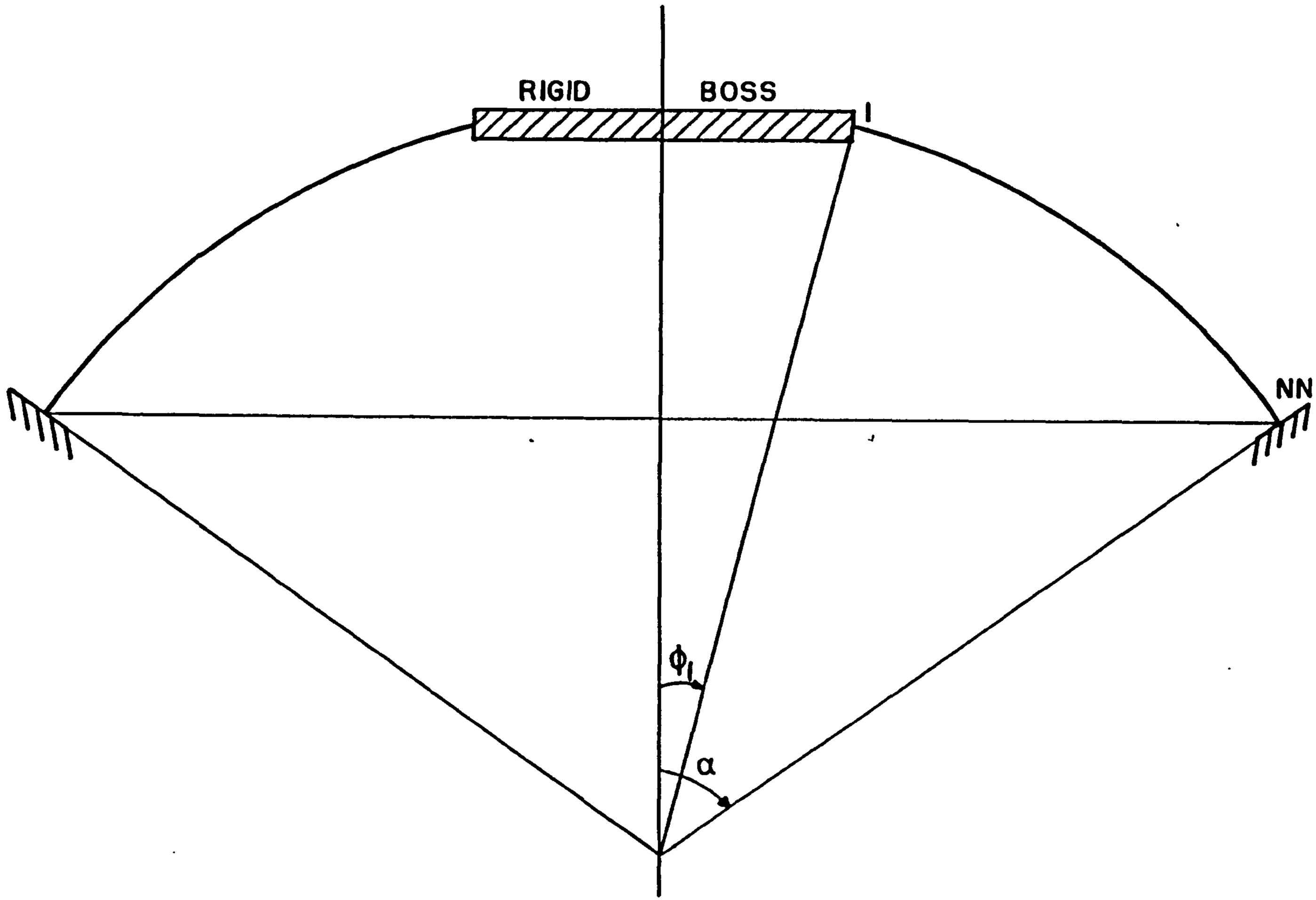

Fig. 6.29- SPHERICAL CAP WITH A RIGID BOSS

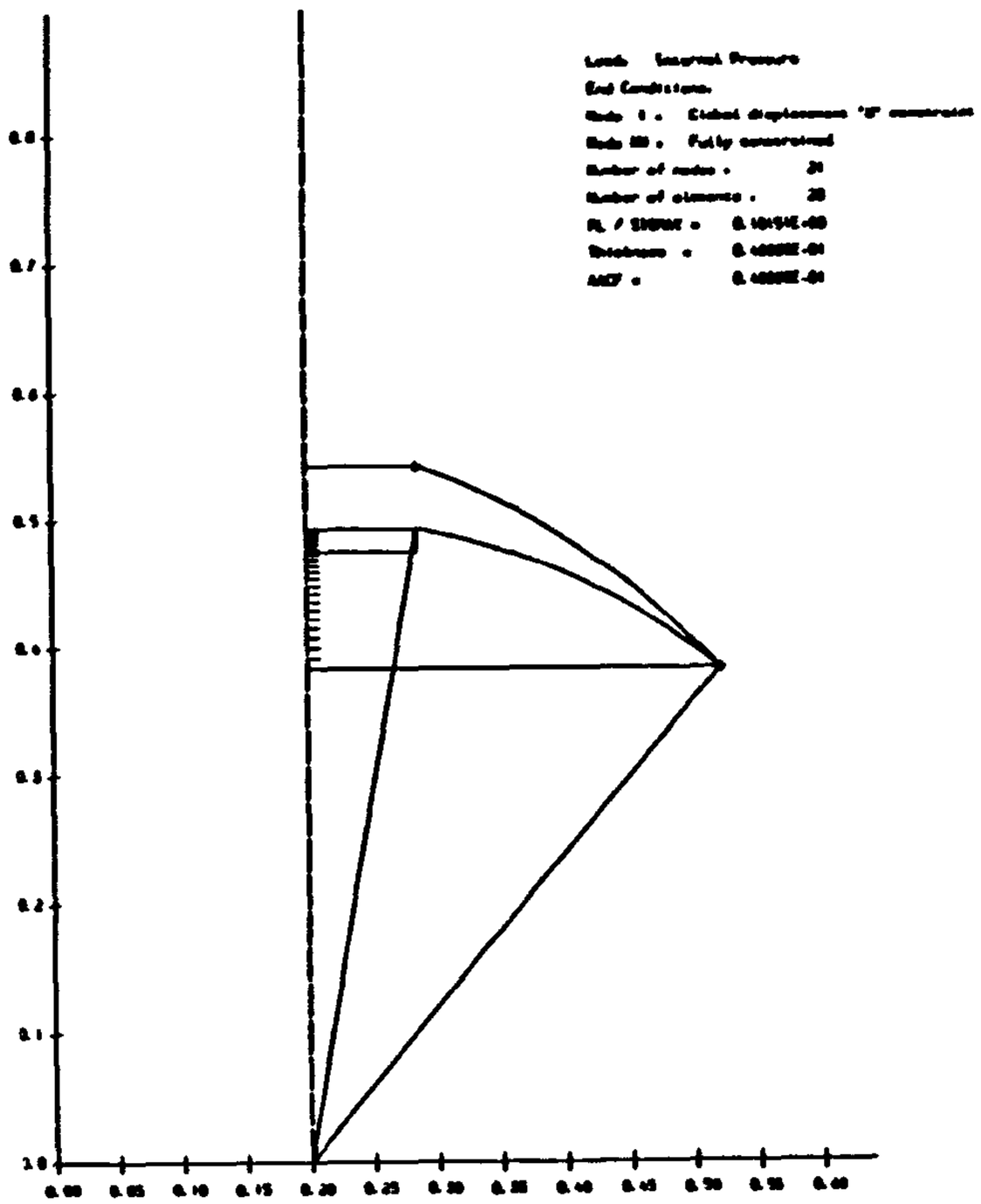

Fig 6 30a

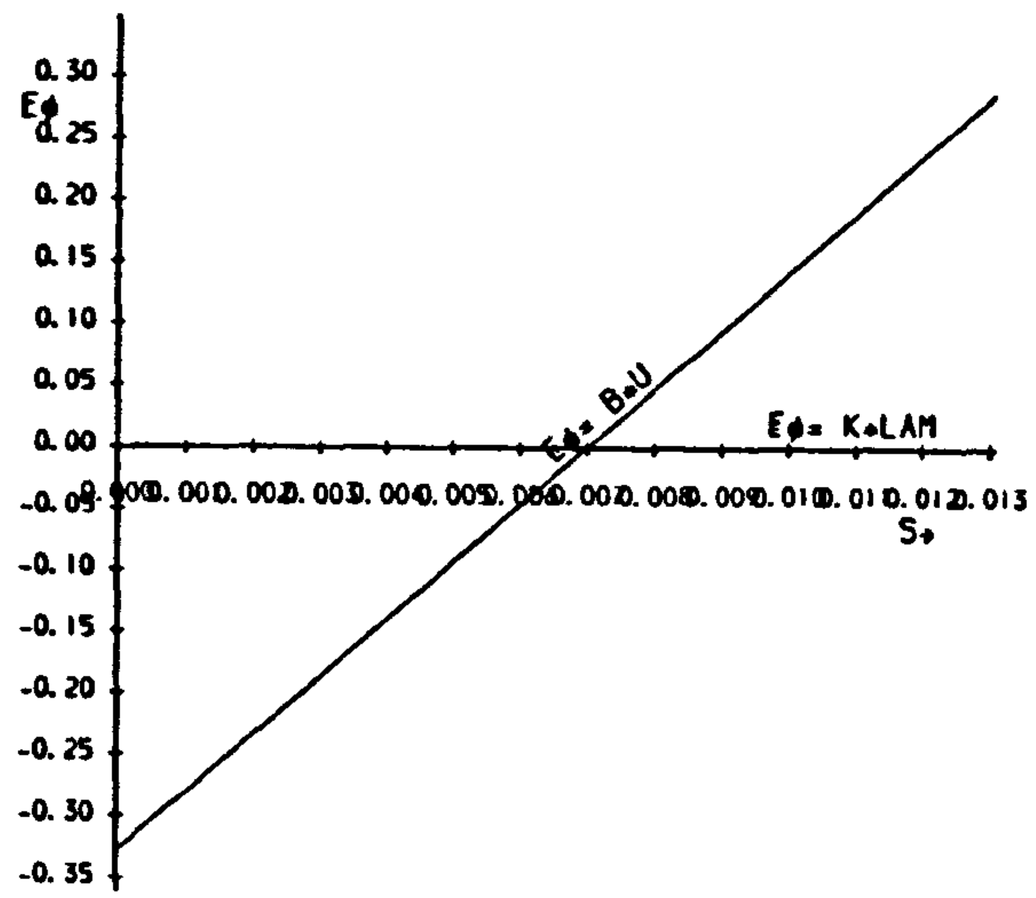

Fig 6 30b MERIDIONAL STRAIN DISTRIBUTION ON ELEMENT 5 OF A SPHERICAL CAP

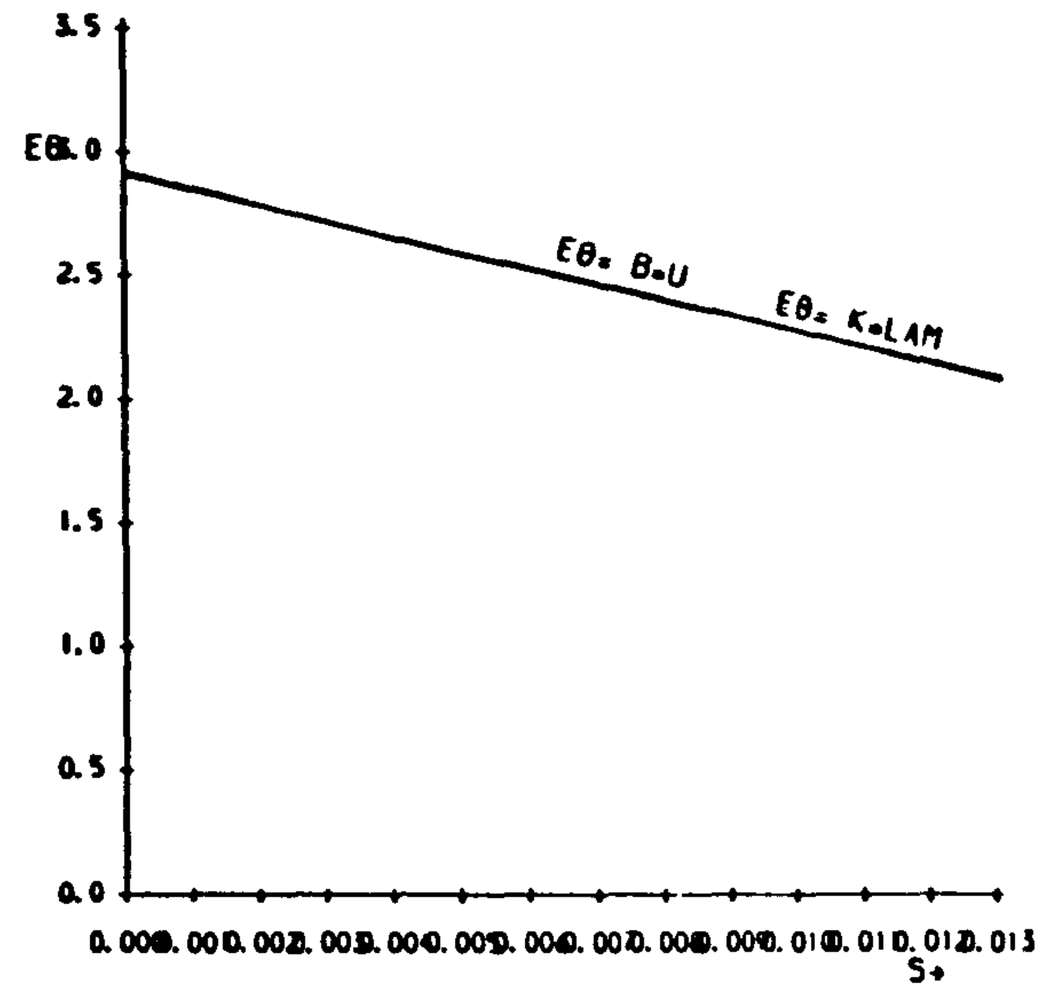

Fig 6 30c - CIRCUMFERENTIAL STRAIN DISTRIBUTION ON ELEMENT 5 OF A SPHERICAL CAP

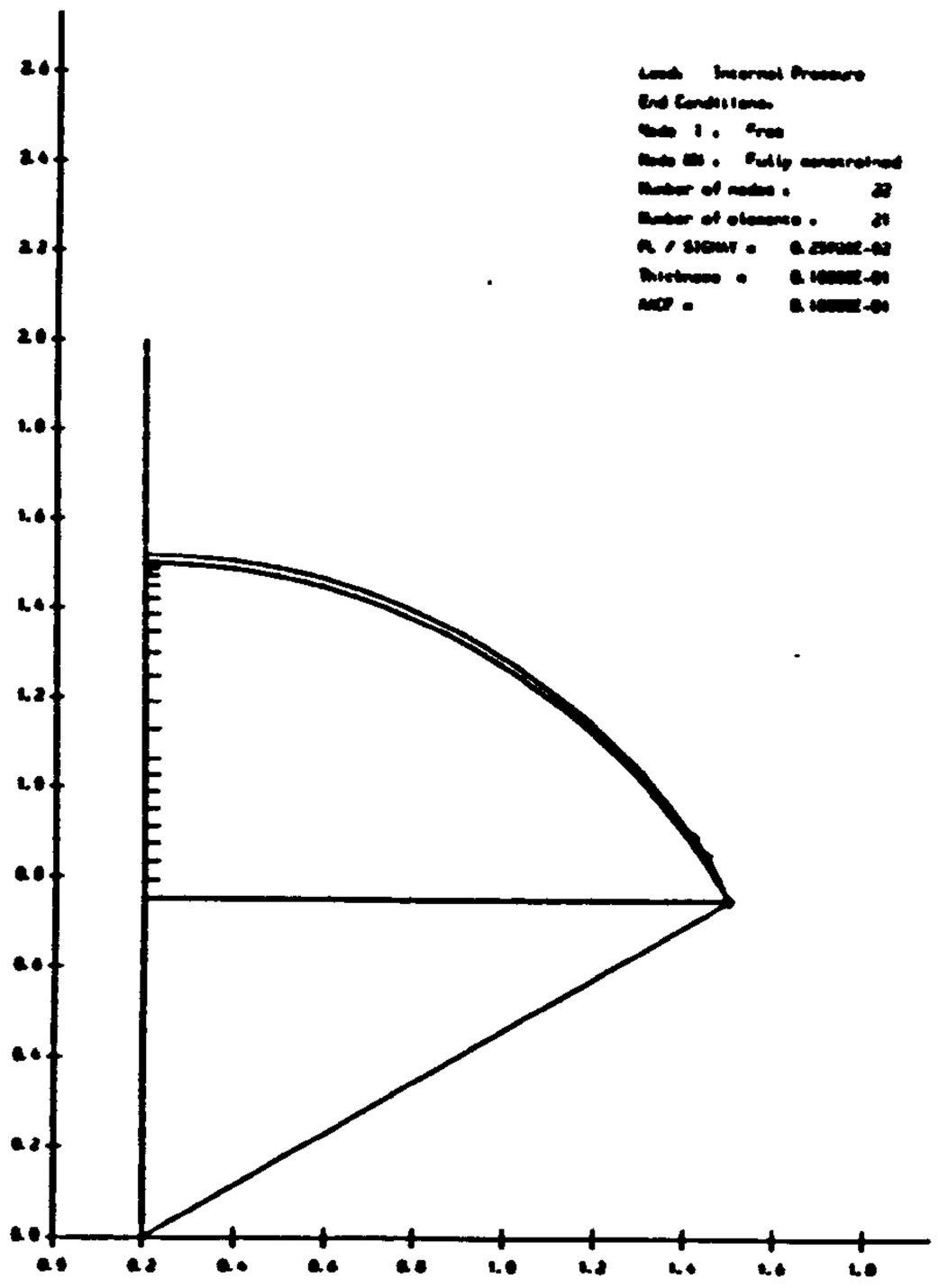

Fig 6.31a

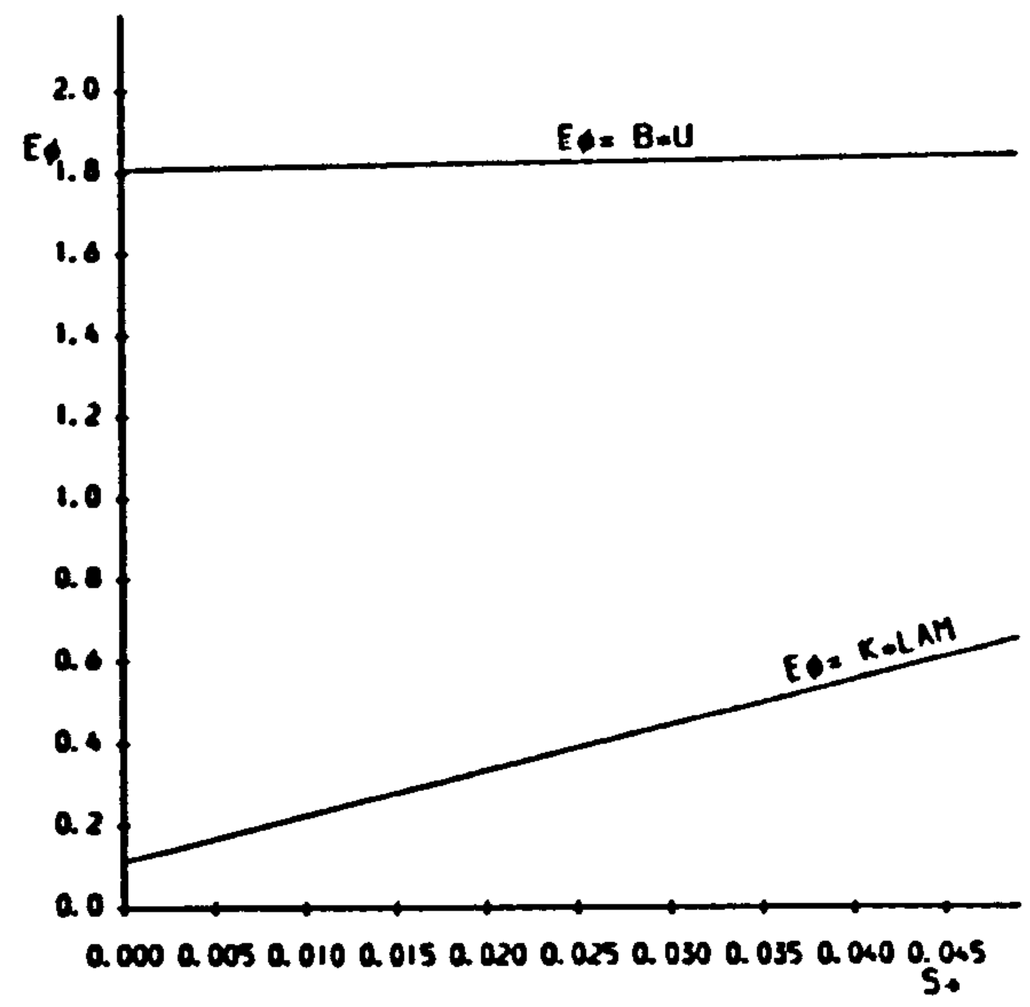

Fig 6.31b - MERIDIONAL STRAIN DISTRIBUTION ON ELEMENT 21 OF A SPHERICAL CAP

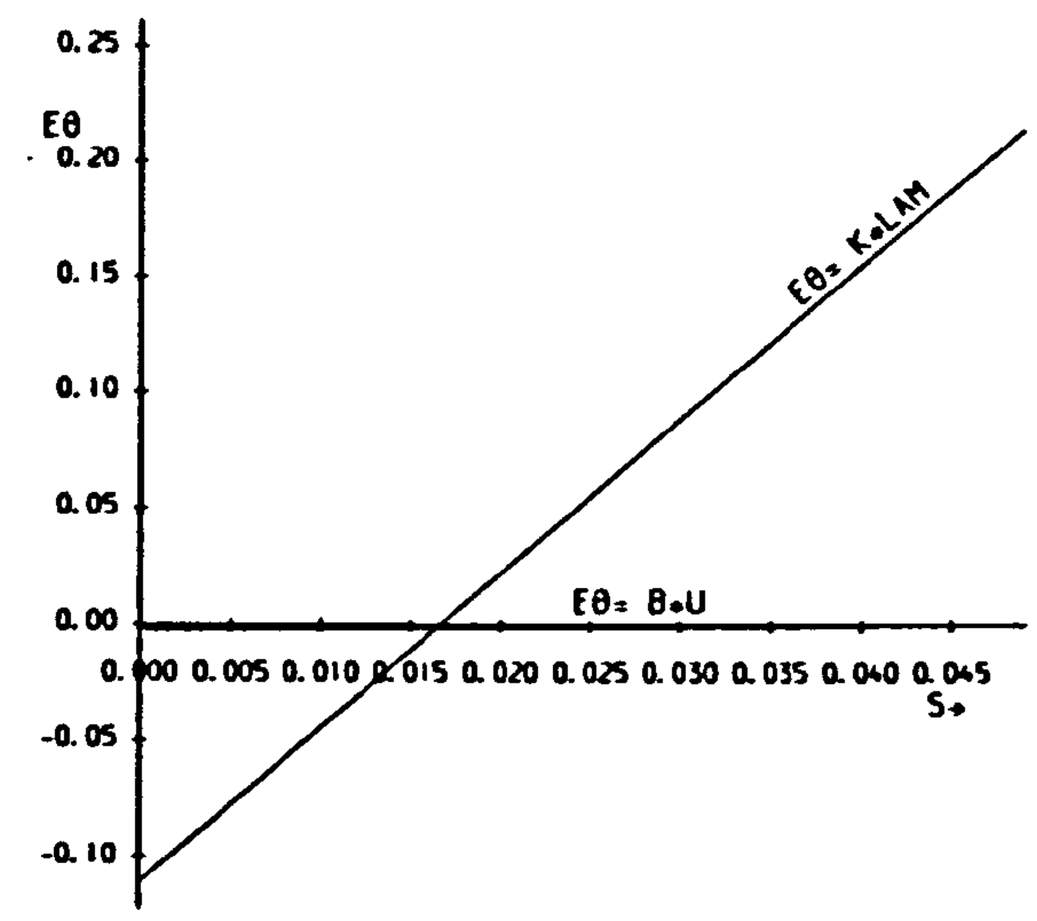

Fig 6.31c - CIRCUMFERENTIAL STRAIN DISTRIBUTION ON ELEMENT 21 OF A SPHERICAL CAP

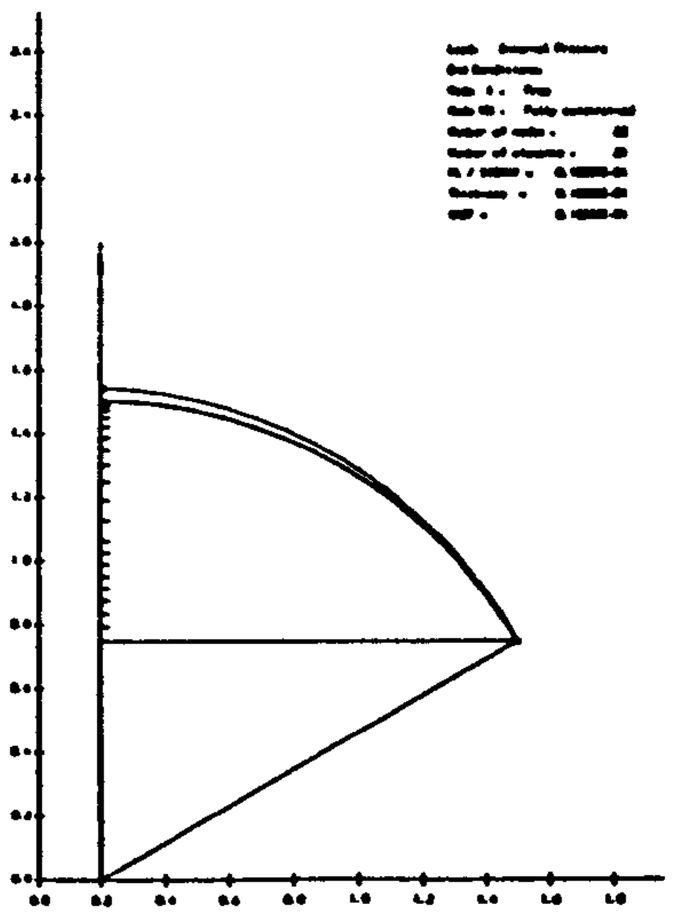

Fig 6 32a

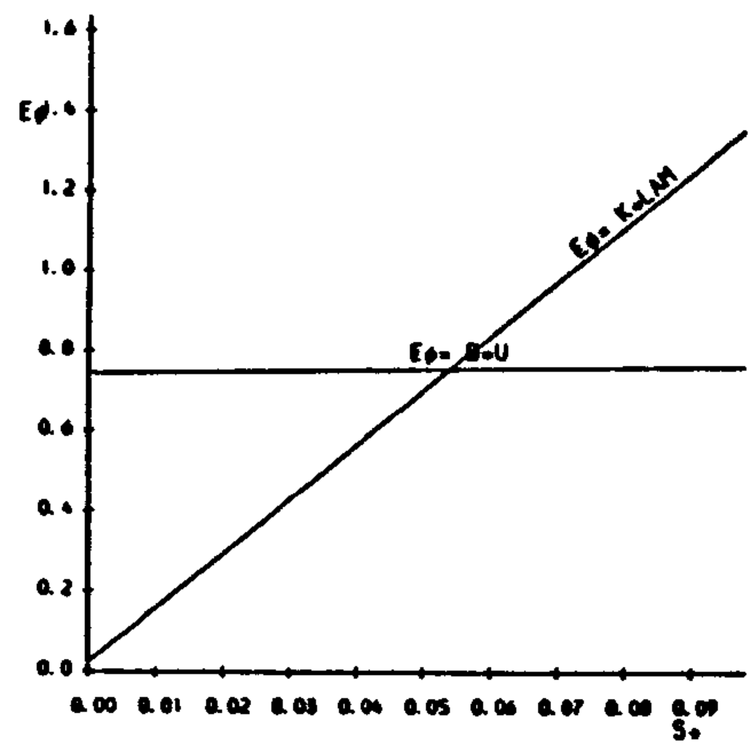

Fig 6 32b - MERIDIONAL STRAIN DISTRIBUTION ON ELEMENT 3 OF A SPHERICAL CAP

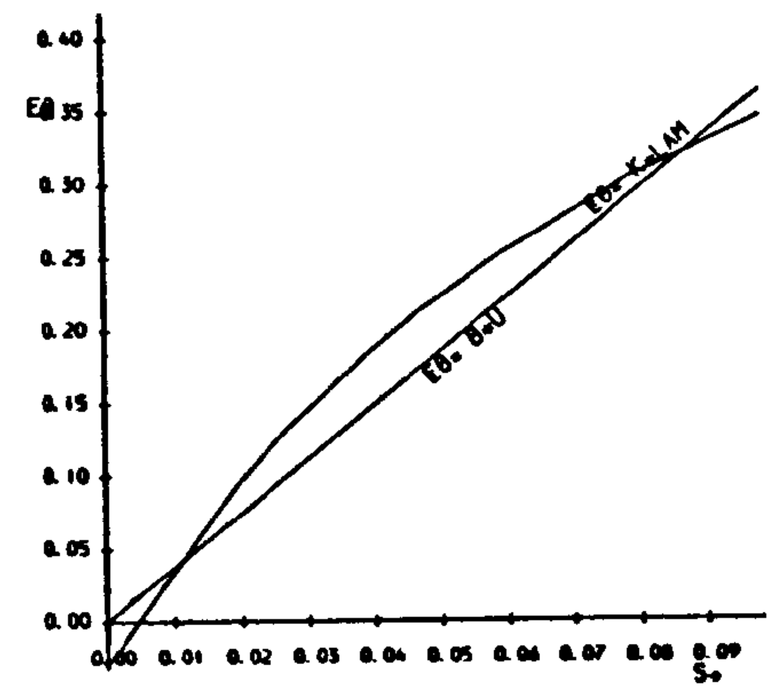

Fig 6 32c - CIRCUMFERENTIAL STRAIN DISTRIBUTION ON ELEMENT 3 OF A SPHERICAL CAP

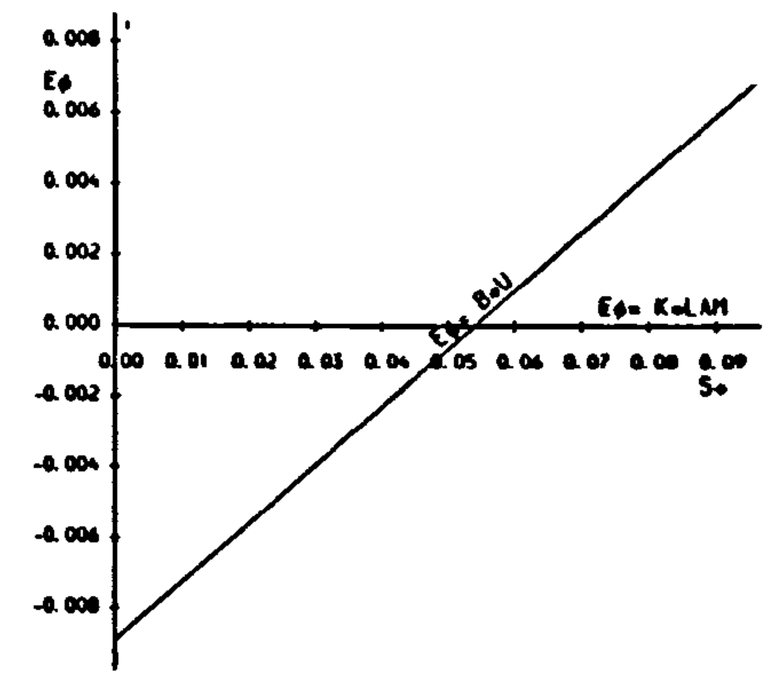

Fig 6 32d - MERIDIONAL STRAIN DISTRIBUTION ON ELEMENT 10 OF A SPHERICAL CAP

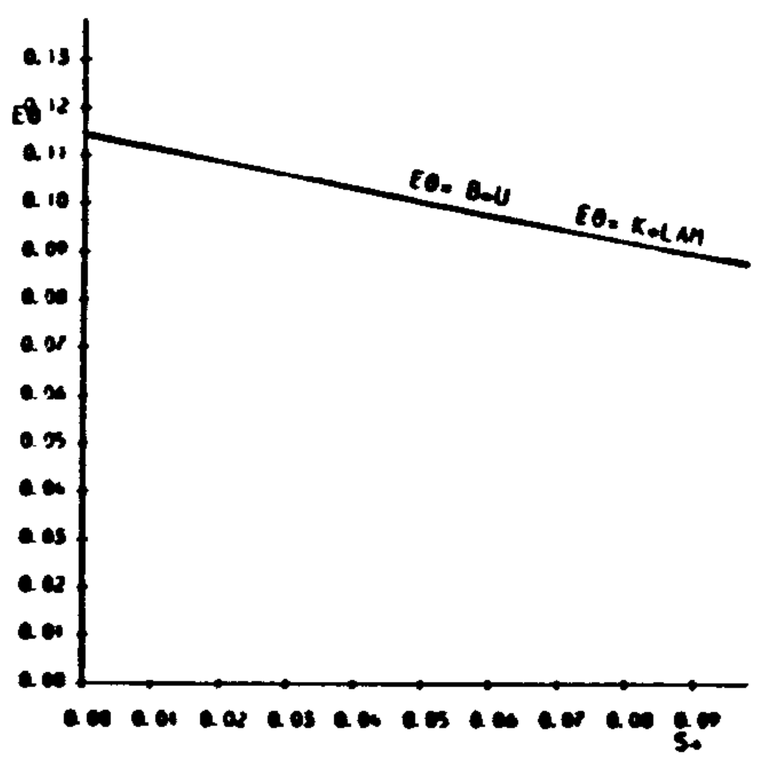

Fig 6 32e - CIRCUMFERENTIAL STRAIN DISTRIBUTION ON ELEMENT 10 OF A SPHERICAL CAP

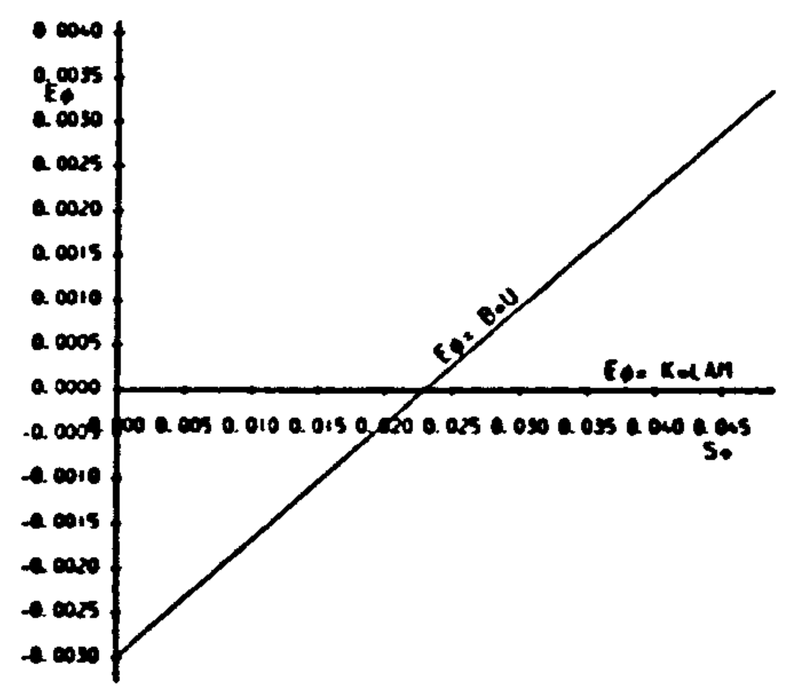

Fig 6.32f - MERIDIONAL STRAIN DISTRIBUTION ON ELEMENT 21 OF A SPHERICAL CAP

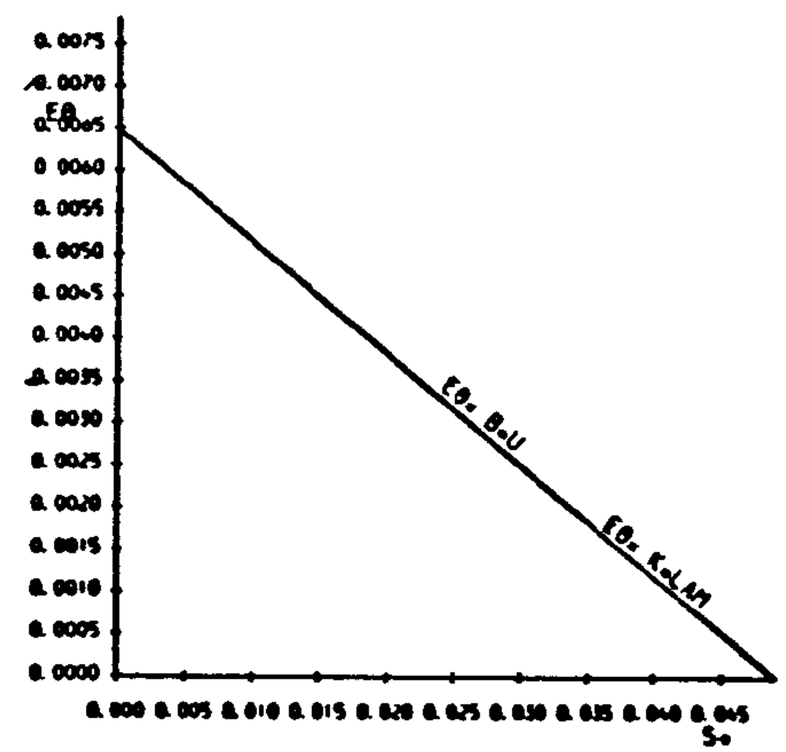

Fig 6 32g - CIRCUMFERENTIAL STRAIN DISTRIBUTION ON ELEMENT 21 OF A SPHERICAL CAP

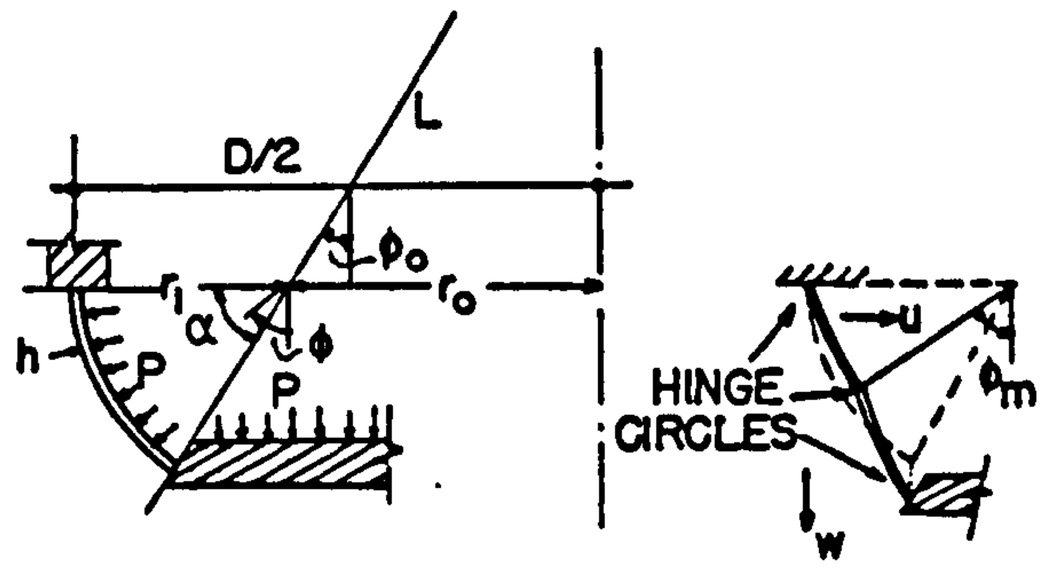

Fig. 6.33- TOROIDAL SHELL AND THE MECHANISM OF DEFORMATION PROPOSED IN [75]

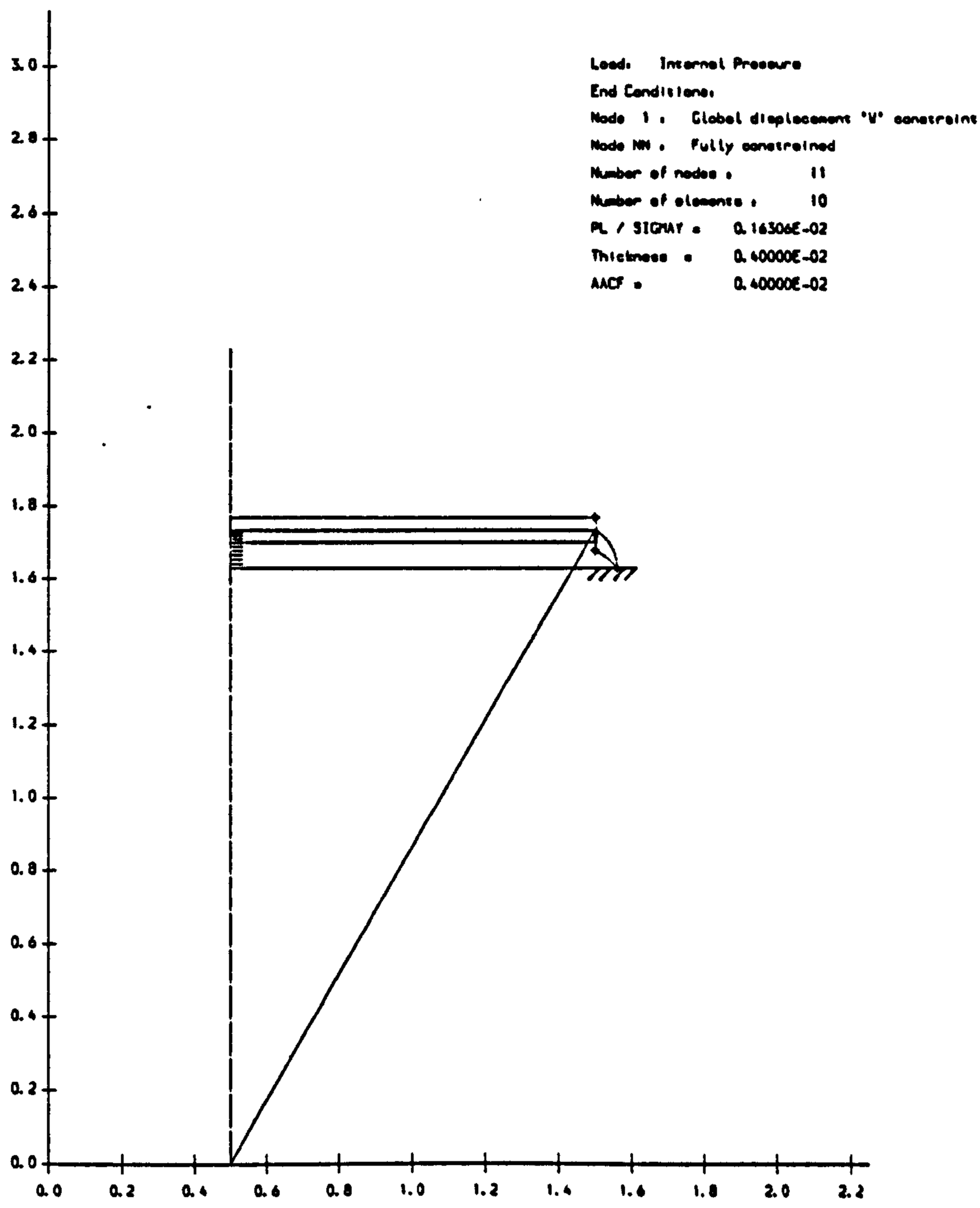

Fig. 6.34 -

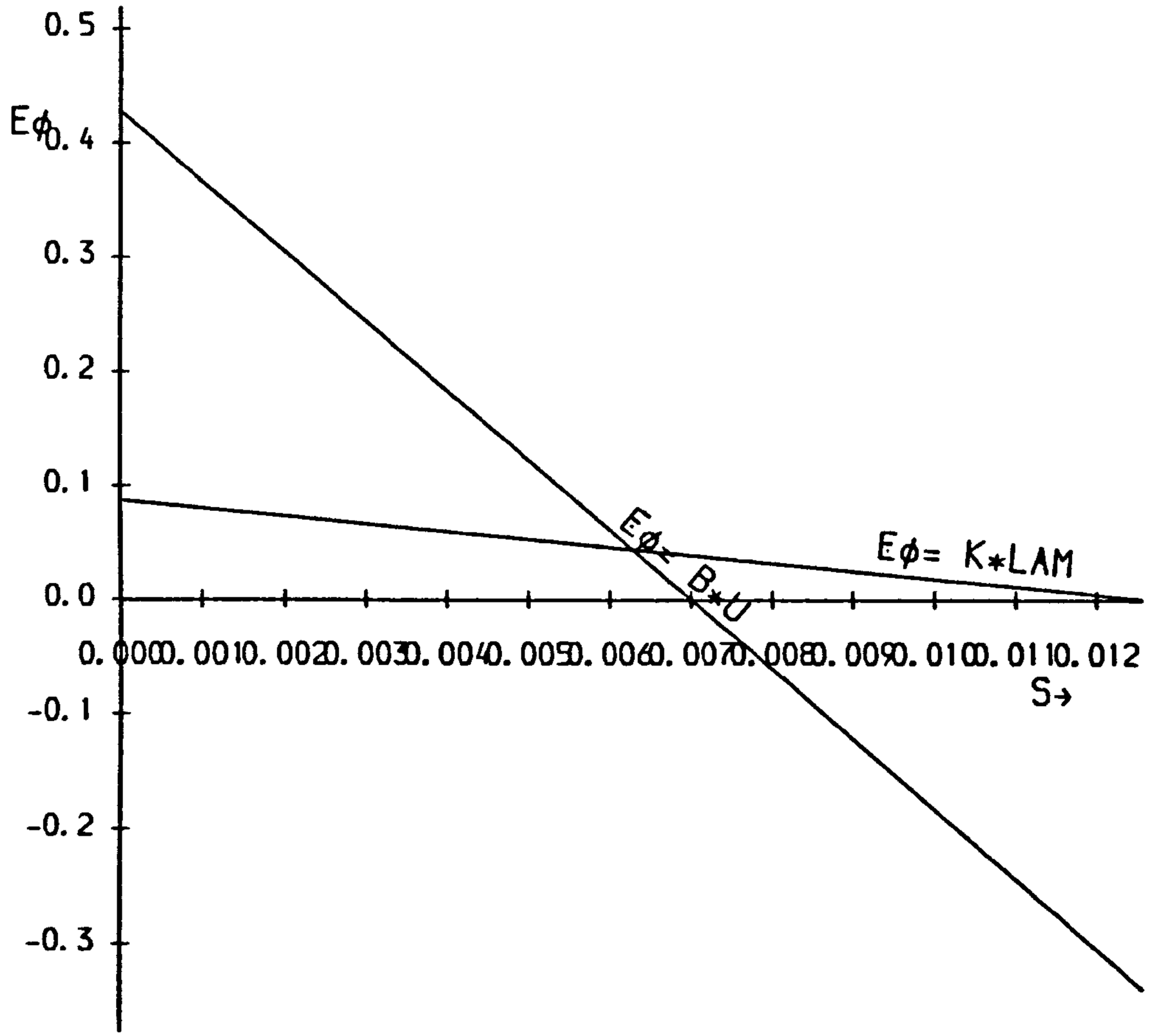

Fig.6.35 - MERIDIONAL STRAIN DISTRIBUTION ON ELEMENT 10 OF A TOROIDAL SHELL

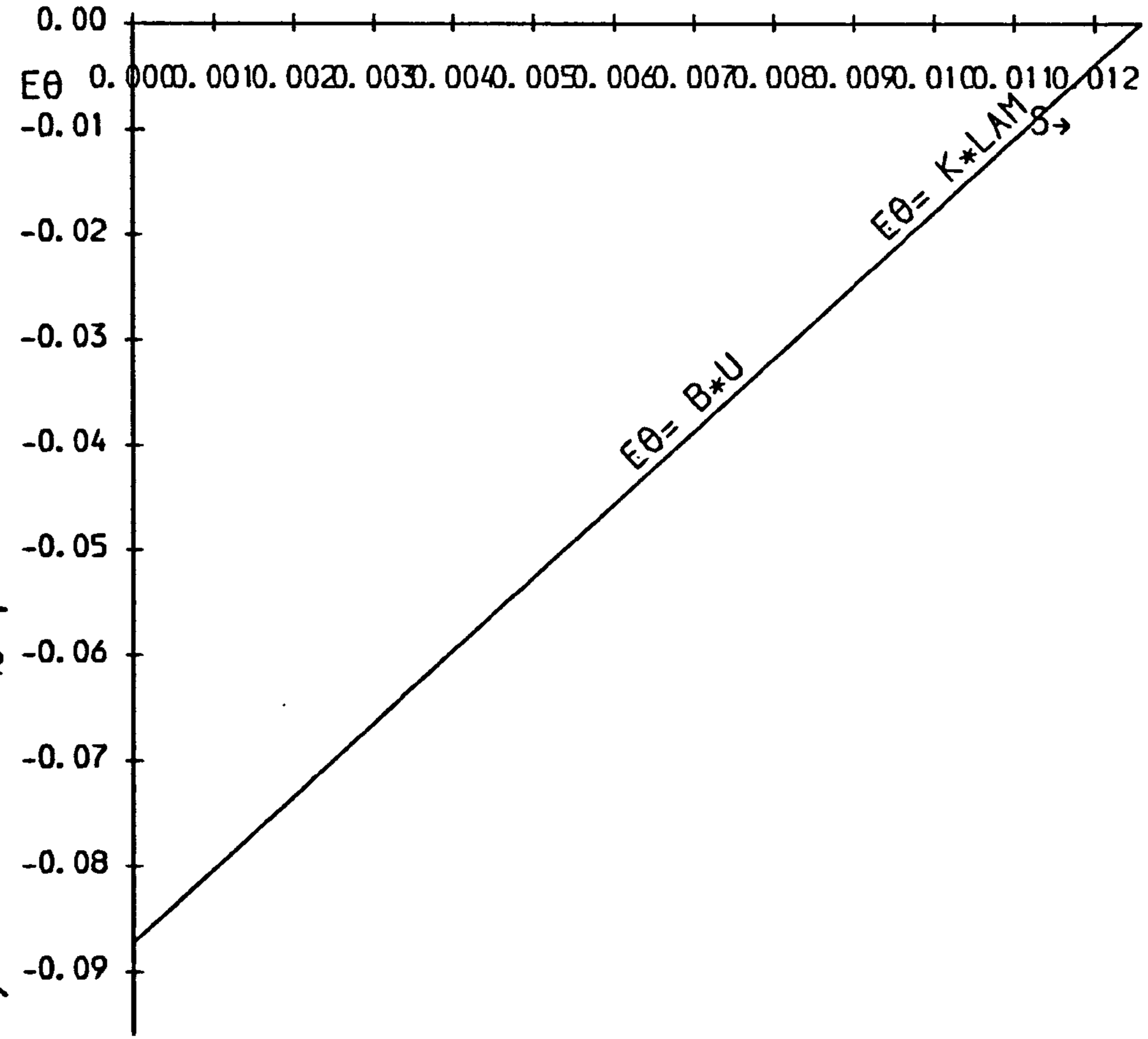

Fig.6.36 - CIRCUMFERENTIAL STRAIN DISTRIBUTION ON ELEMENT 10 OF A TOROIDAL SHELL

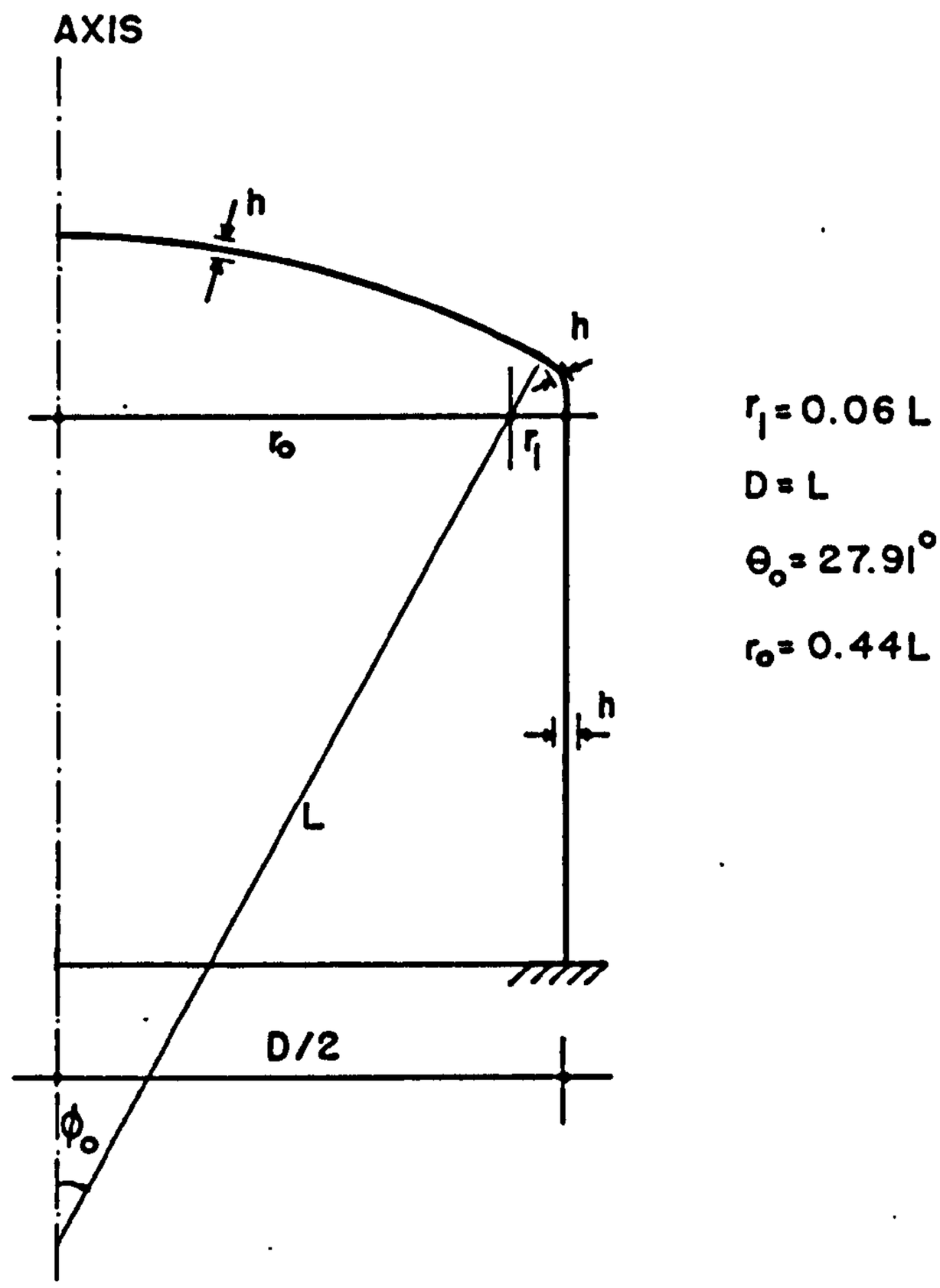

Fig. 6.37a-ASME TORISPHERICAL VESSEL

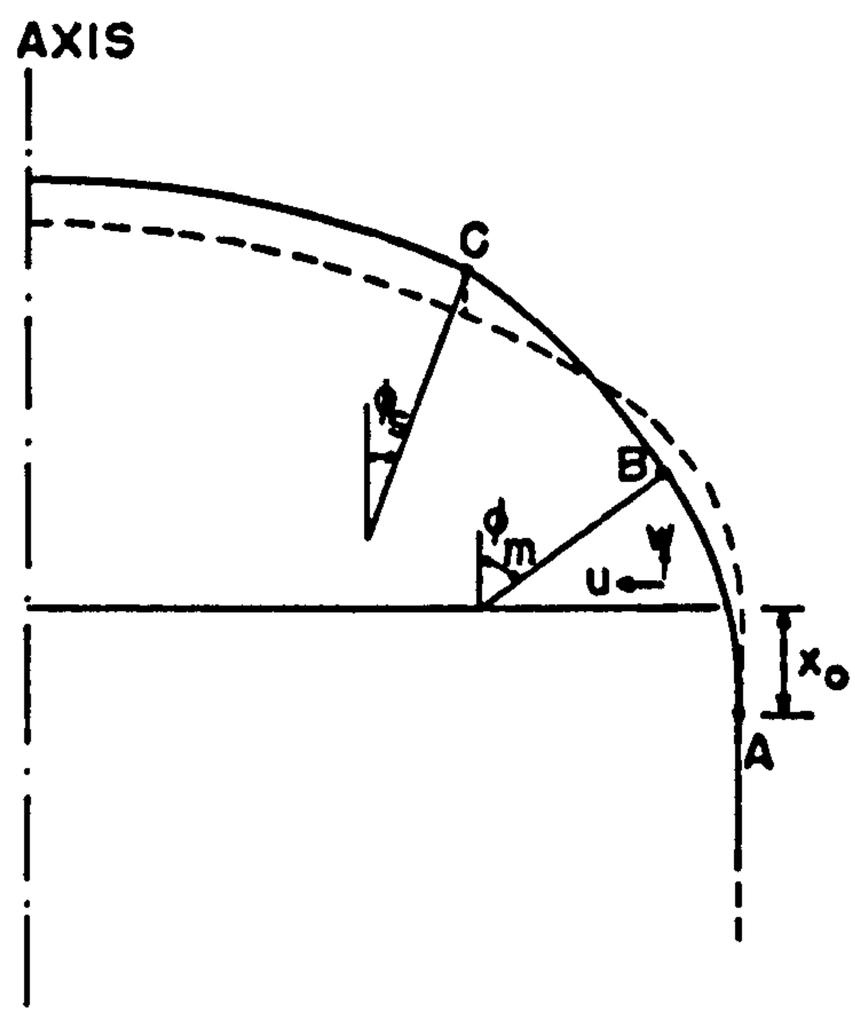

Fig 6.37b-DIAGRAMMATIC REPRESENTATION OF THE DEFORMATION PATTERN; HINGE CIRCLES AT A, B AND C

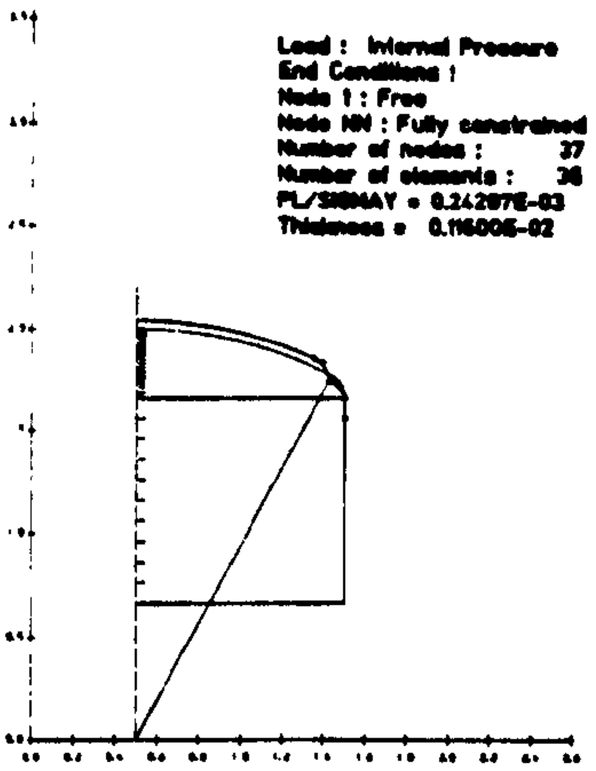

Fig 6.38a

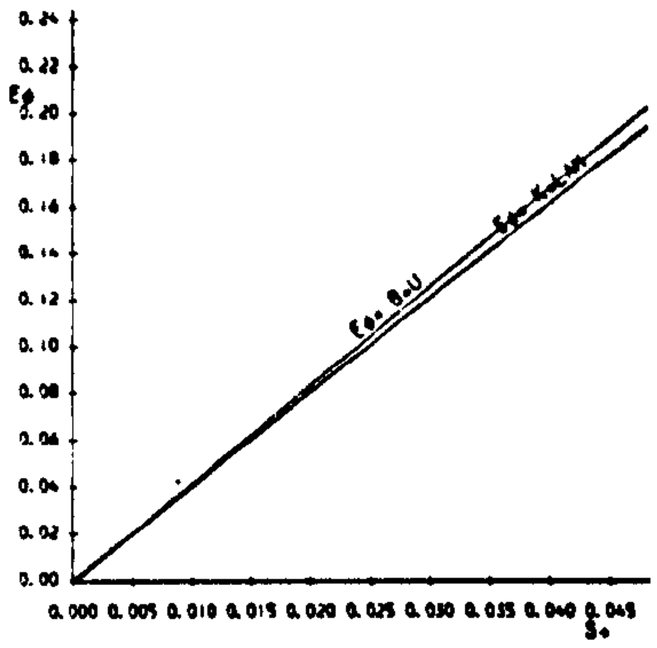

Fig 6.38a$_1$ - MERIDIONAL STRAIN DISTRIBUTION ON ELEMENT 21 OF A TORISPHERICAL SHELL

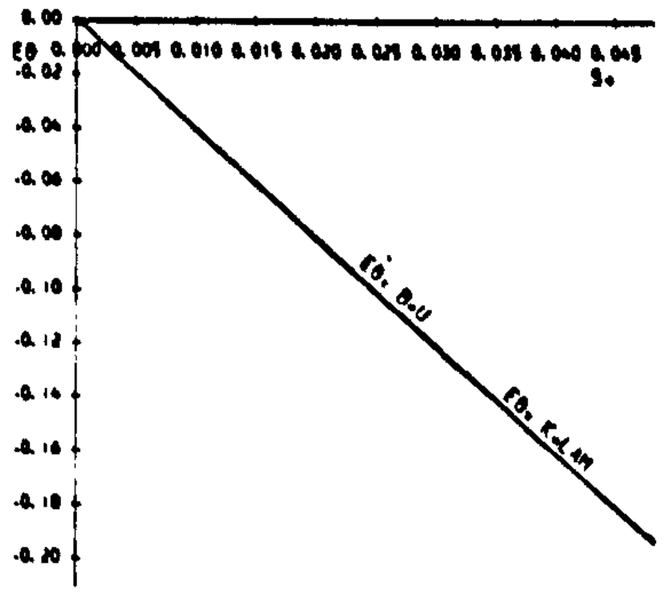

Fig 6.38a$_2$ - CIRCUMFERENTIAL STRAIN DISTRIBUTION ON ELEMENT 21 OF A TORISPHERICAL SHELL

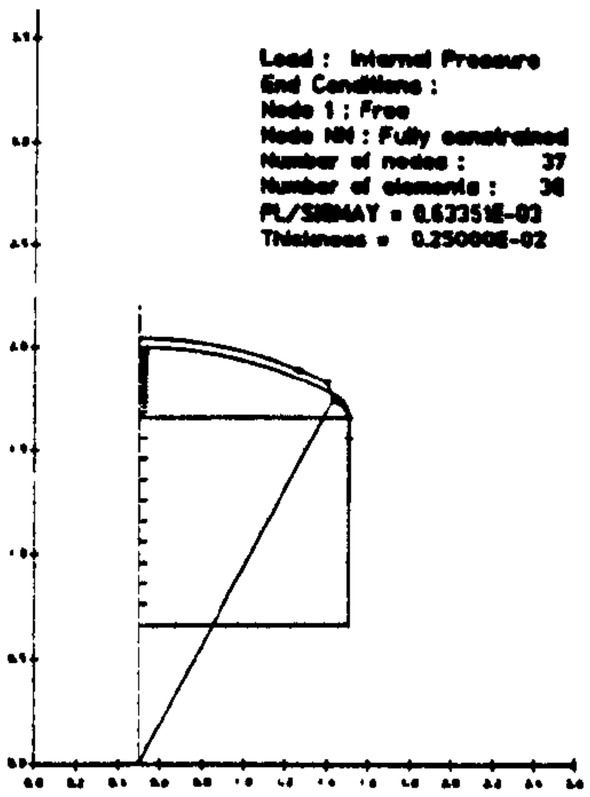

Fig 6.38b

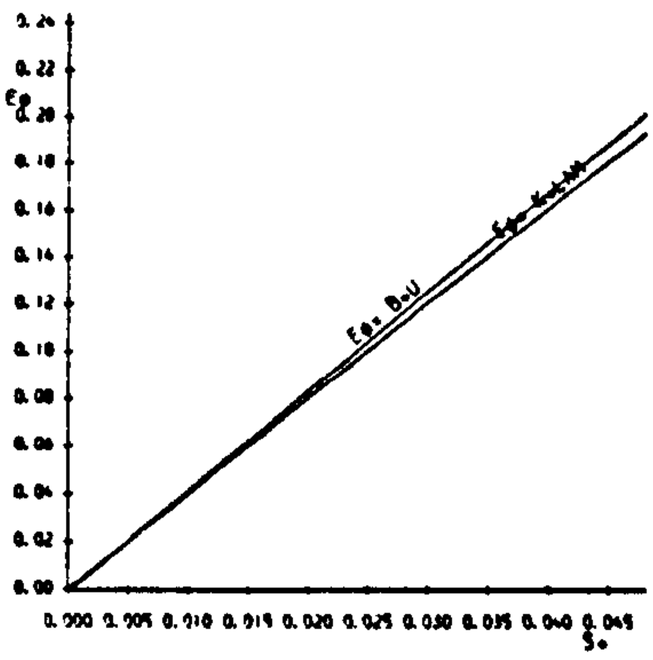

Fig 6.38b$_1$ - MERIDIONAL STRAIN DISTRIBUTION ON ELEMENT 21 OF A TORISPHERICAL SHELL

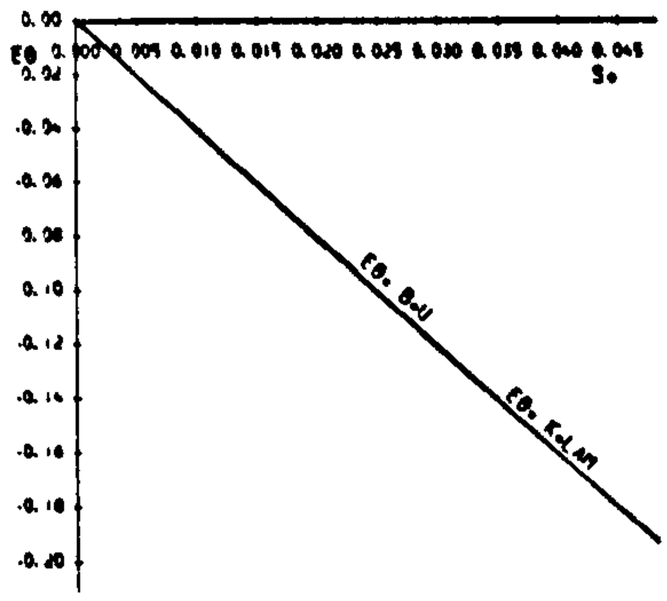

Fig 6.38b$_2$ - CIRCUMFERENTIAL STRAIN DISTRIBUTION ON ELEMENT 21 OF A TORISPHERICAL SHELL

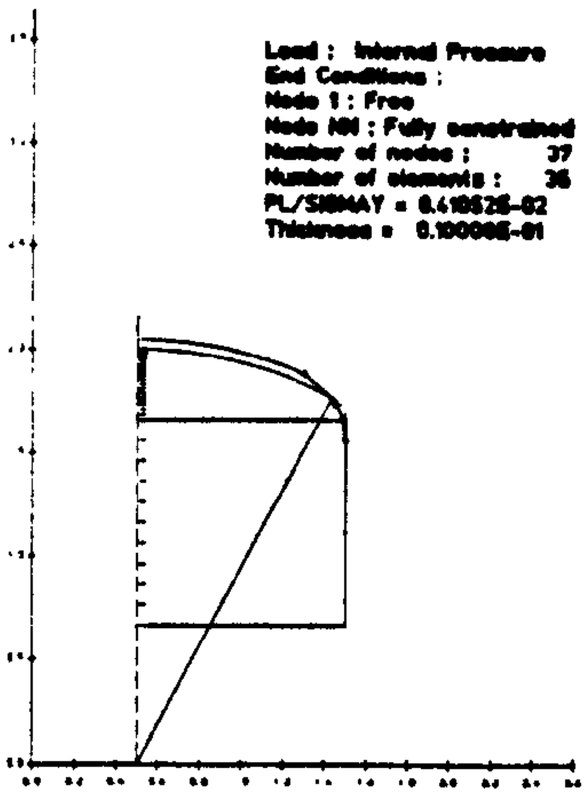

Fig 6.38c

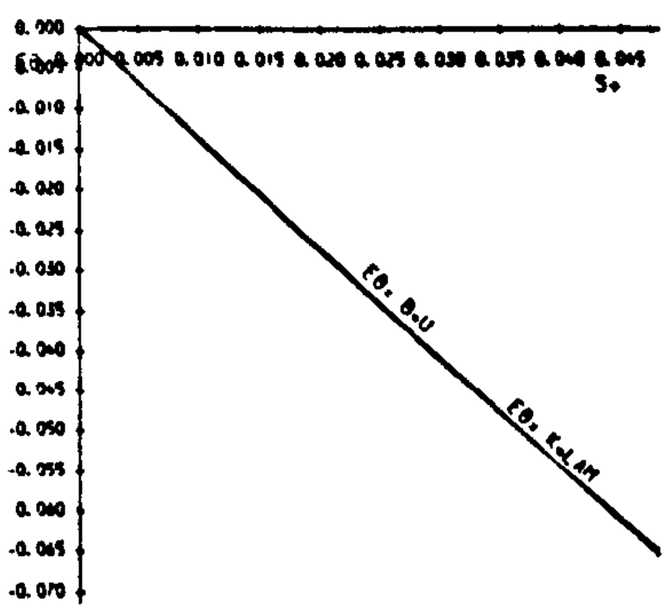

Fig 6.38c$_1$ - CIRCUMFERENTIAL STRAIN DISTRIBUTION ON ELEMENT 19 OF A TORISPHERICAL SHELL

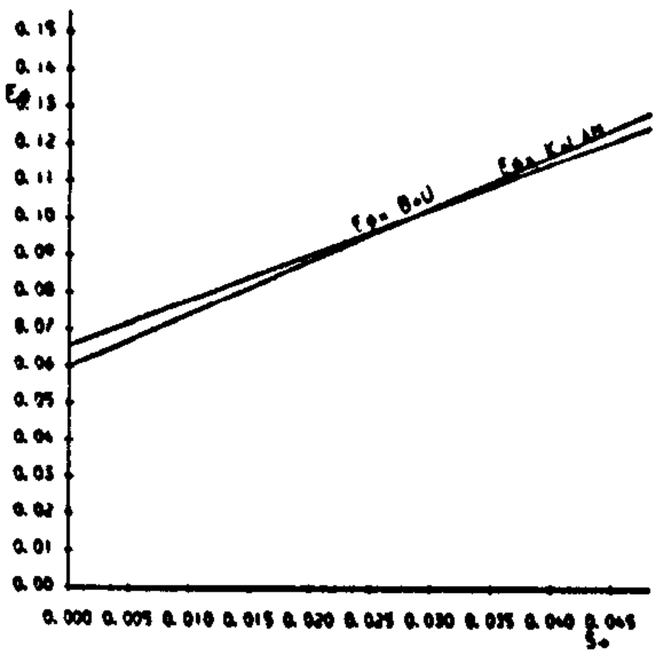

Fig 6.38c$_2$ - MERIDIONAL STRAIN DISTRIBUTION ON ELEMENT 20 OF A TORISPHERICAL SHELL

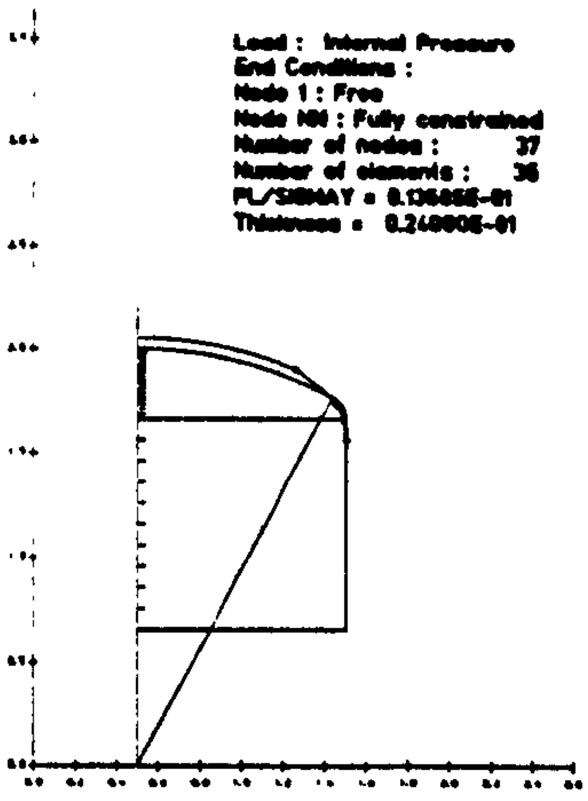

Fig 6.38d

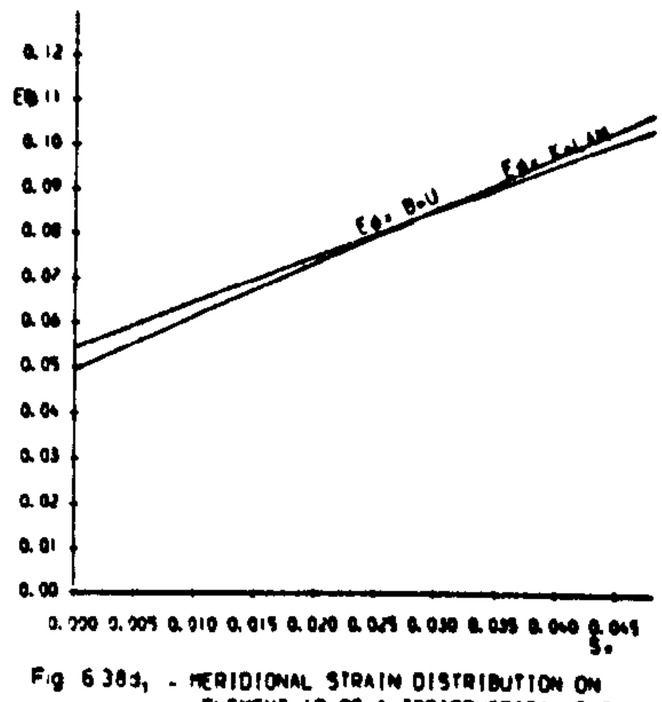

Fig 6.38d$_1$ - MERIDIONAL STRAIN DISTRIBUTION ON ELEMENT 19 OF A TORISPHERICAL SHELL

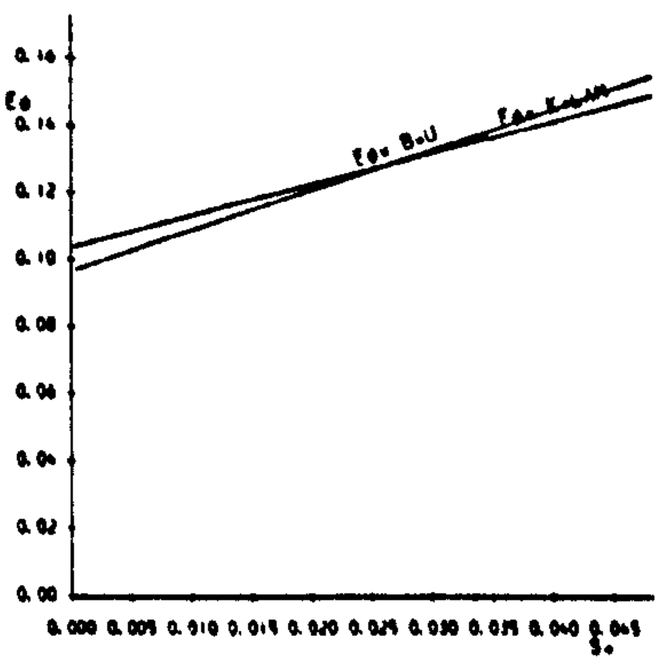

Fig 6.38d$_2$ - MERIDIONAL STRAIN DISTRIBUTION ON ELEMENT 20 OF A TORISPHERICAL SHELL

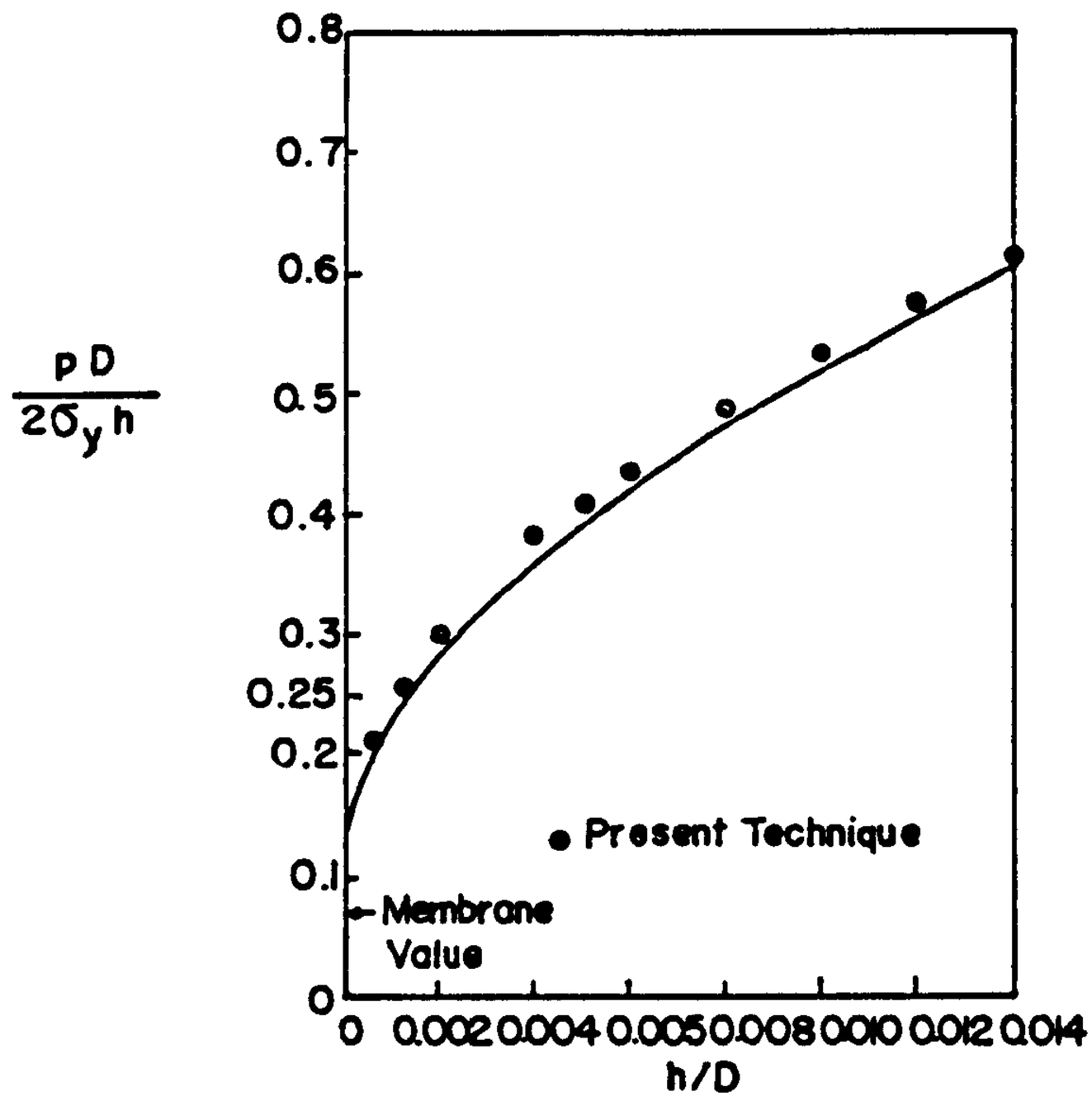

Fig.6.39- LIMIT PRESSURE FOR ASME STANDARD HEAD (HEXAGONAL PRISM YIELD SURFACE) [75]

ASME STANDARD TORISPHERICAL HEAD

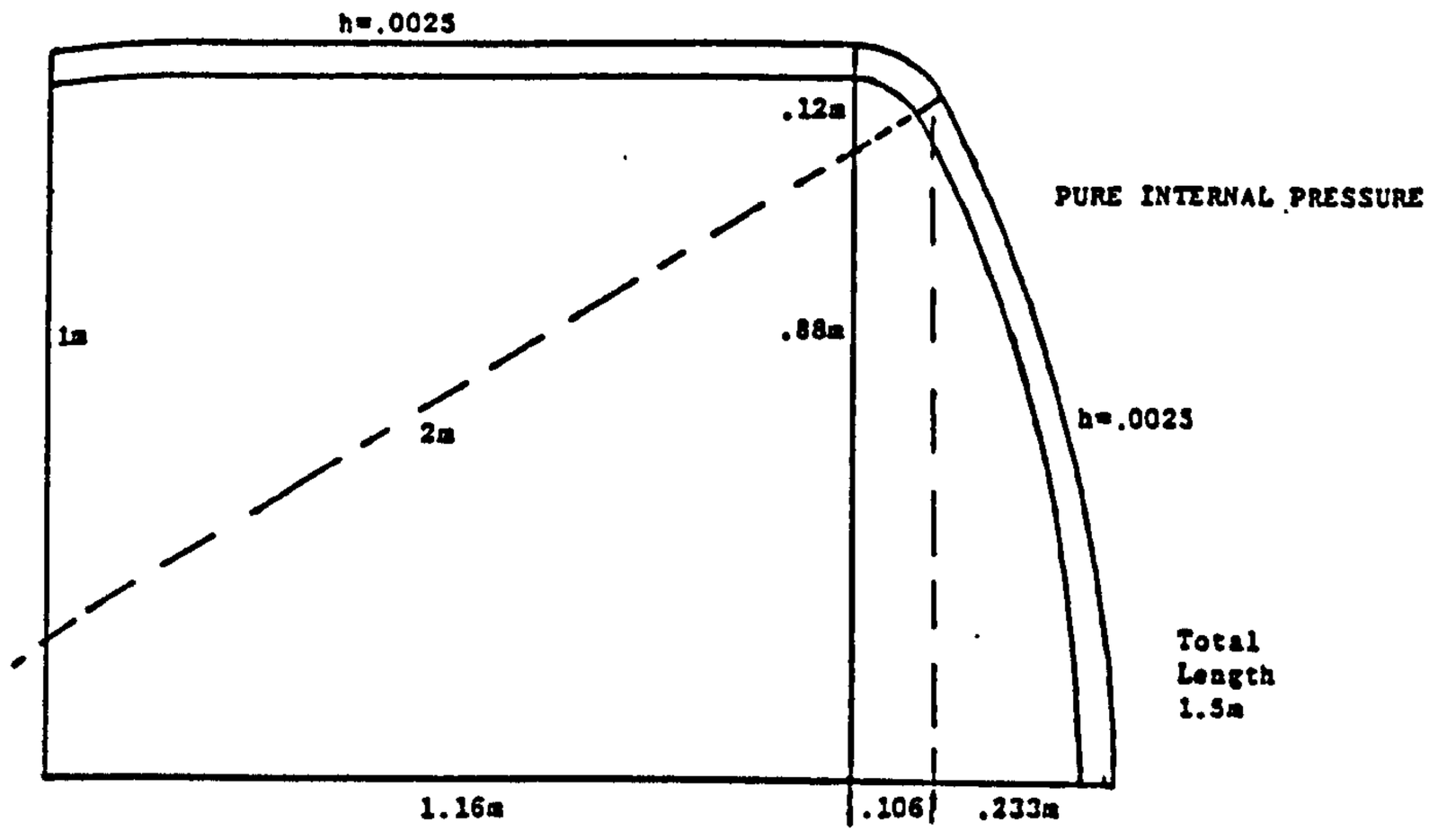

(a)

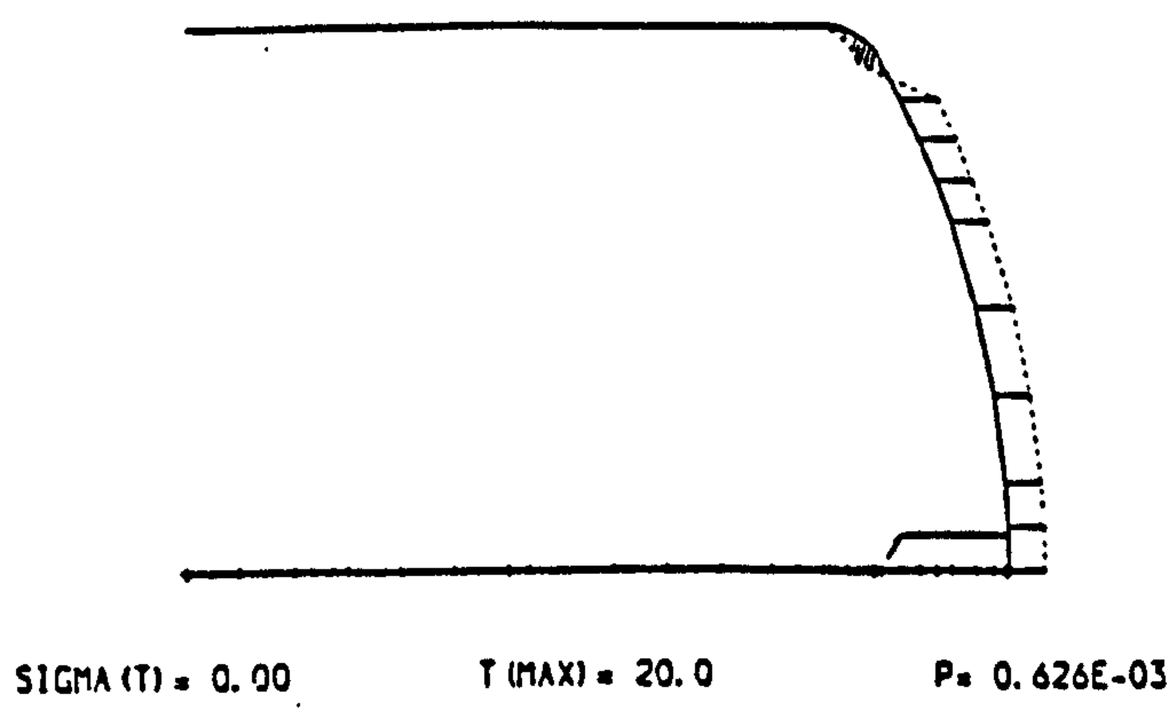

(b)

Fig. 6·40

CASE 8

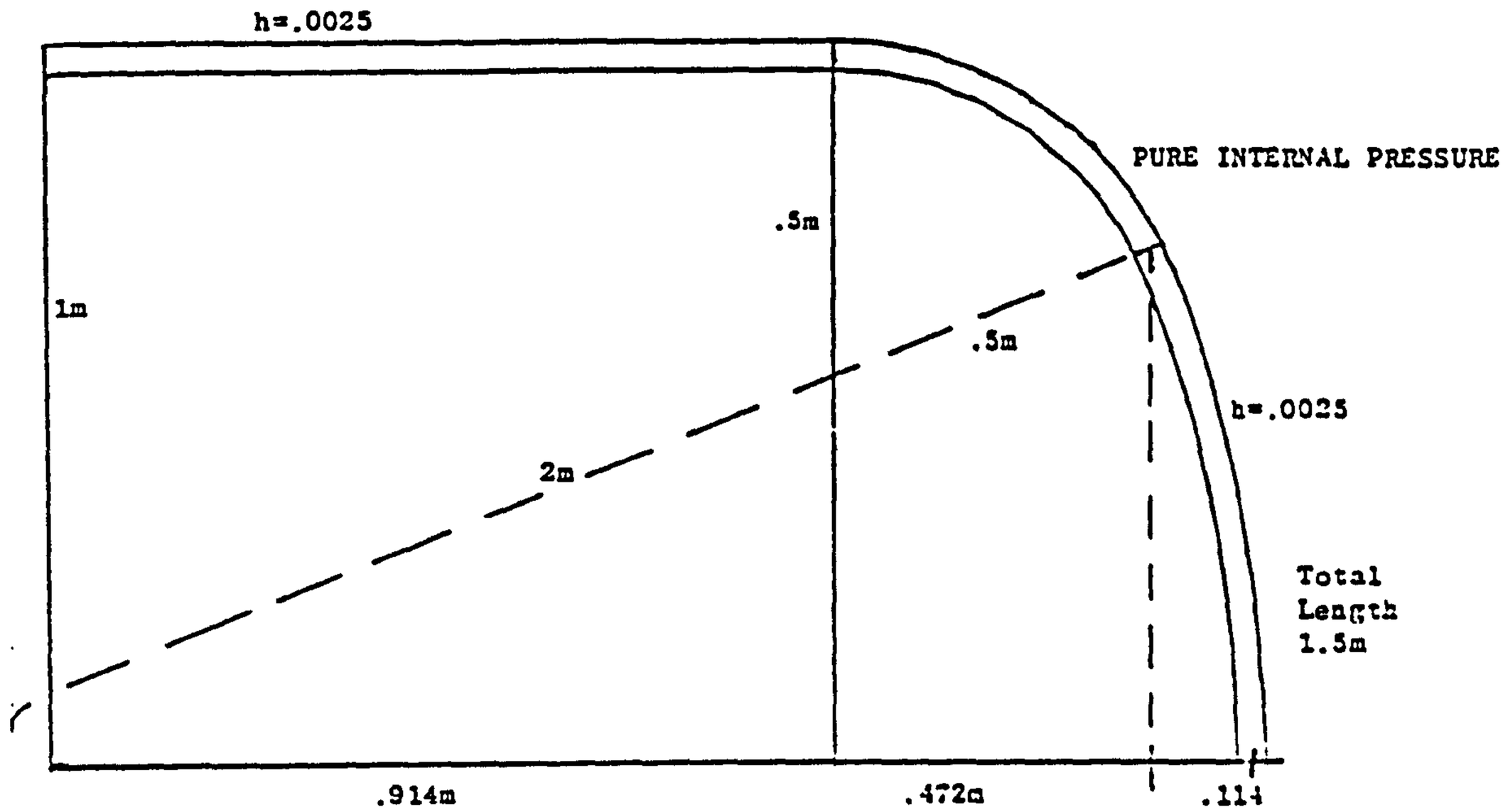

(a)

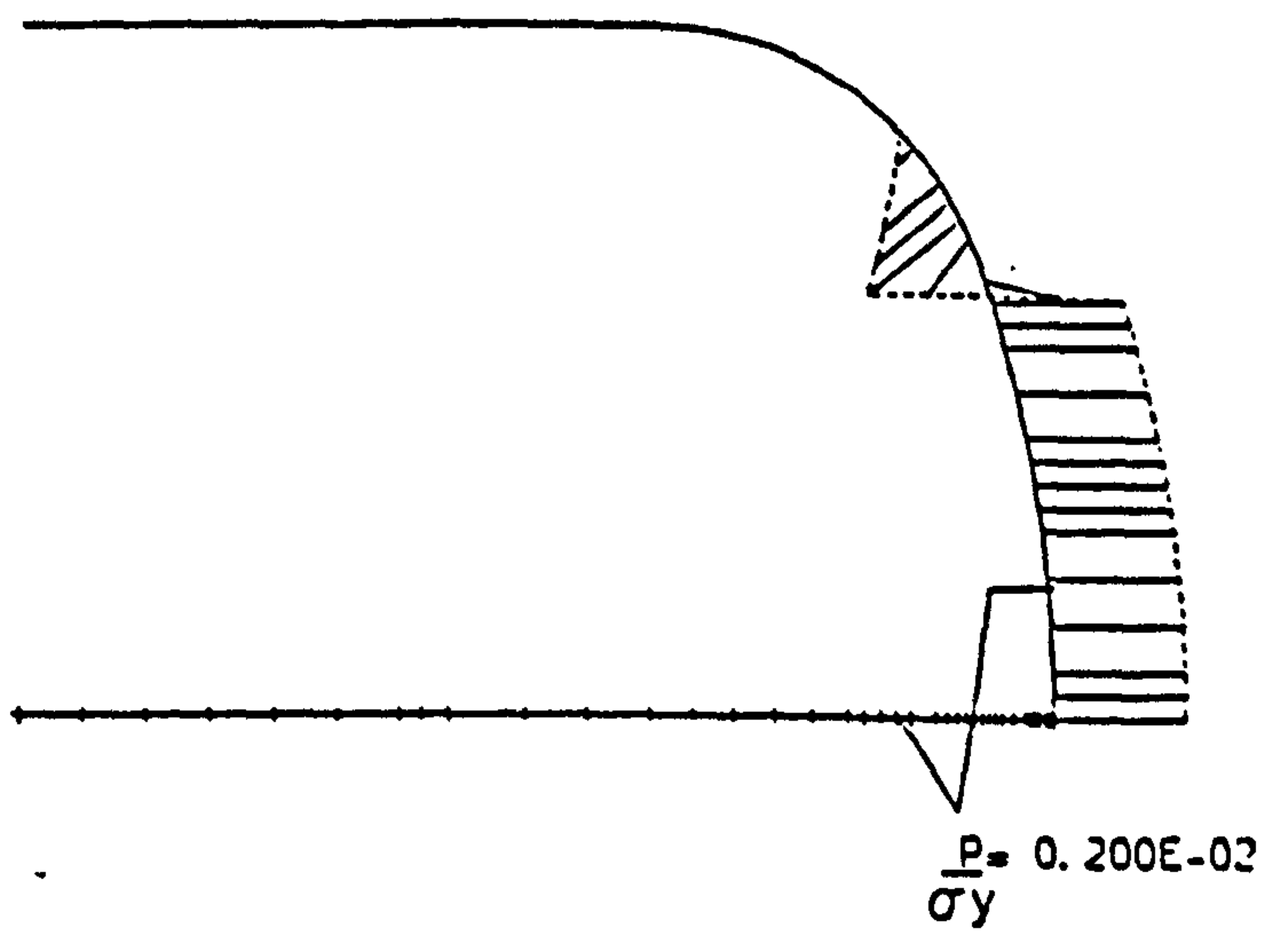

(b)

Fig. 6·41

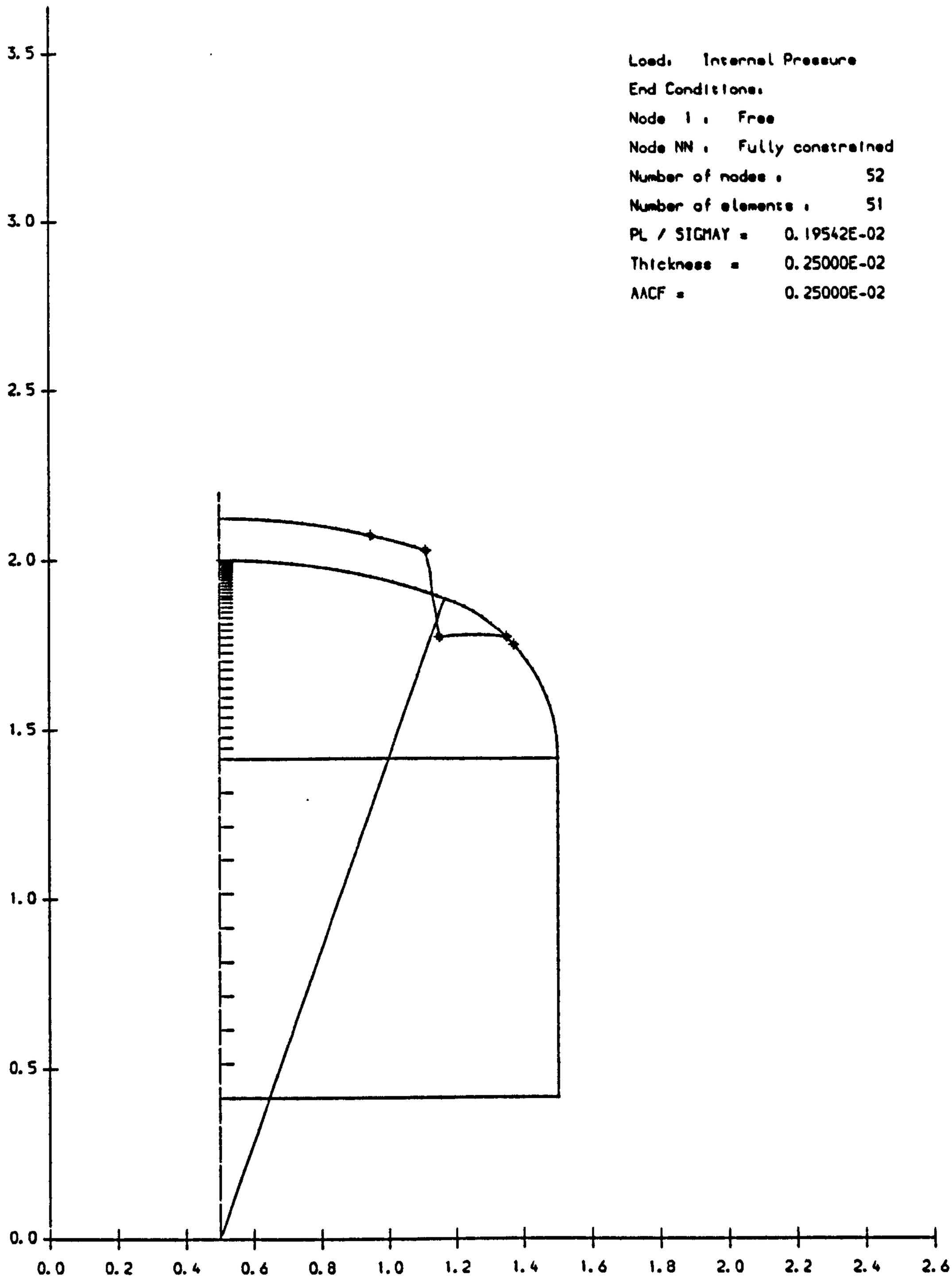
Load: Internal Pressure
End Conditions:
Node 1 : Free
Node NN : Fully constrained
Number of nodes : 52
Number of elements : 51
PL / SIGMAY = 0.19542E-02
Thickness = 0.25000E-02
AACF = 0.25000E-02
3.5
3.0
2.5
2.0
1.5
1.0
0.5
0.0
0.0
0.2
0.4
0.6
0.8
1.0
1.2
1.4
1.6
1.8
2.0
2.2
2.4
2.6

Fig. 6.42-

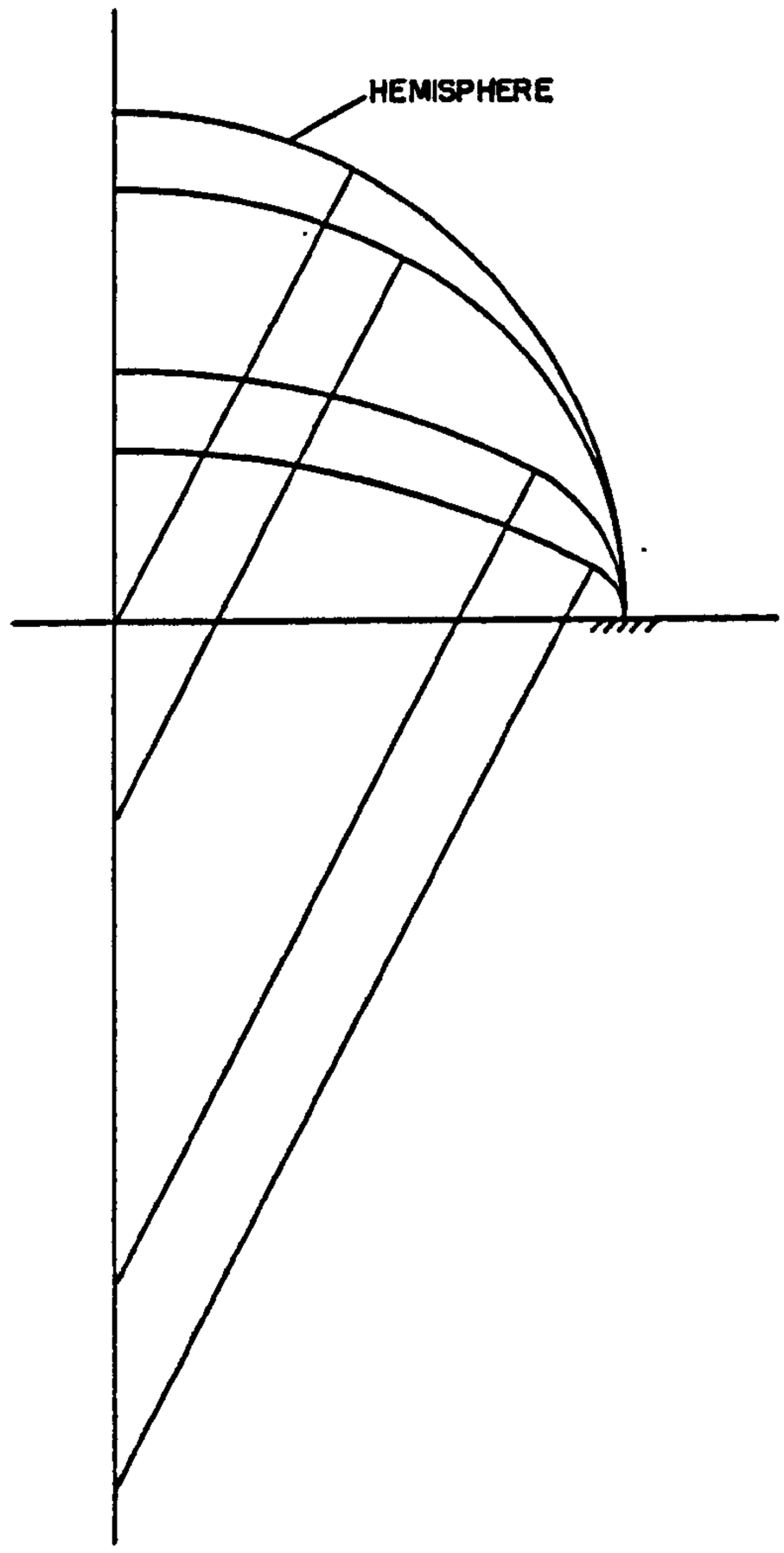

Fig. 6.43- CLAMPED TORISPHERICAL HEADS [92]

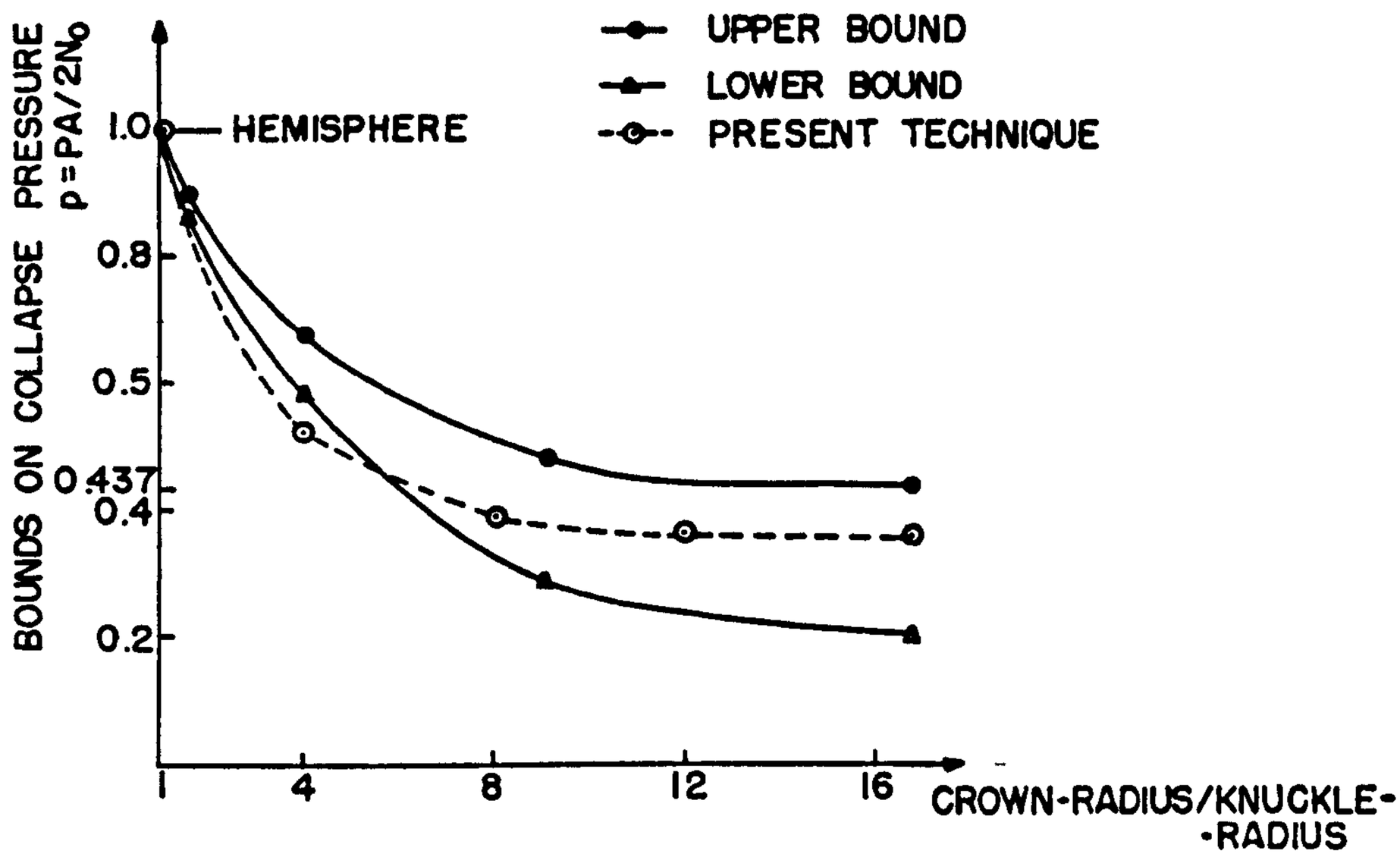

Fig. 6.44- RESULTS FOR TORISPHERICAL HEADS [92]

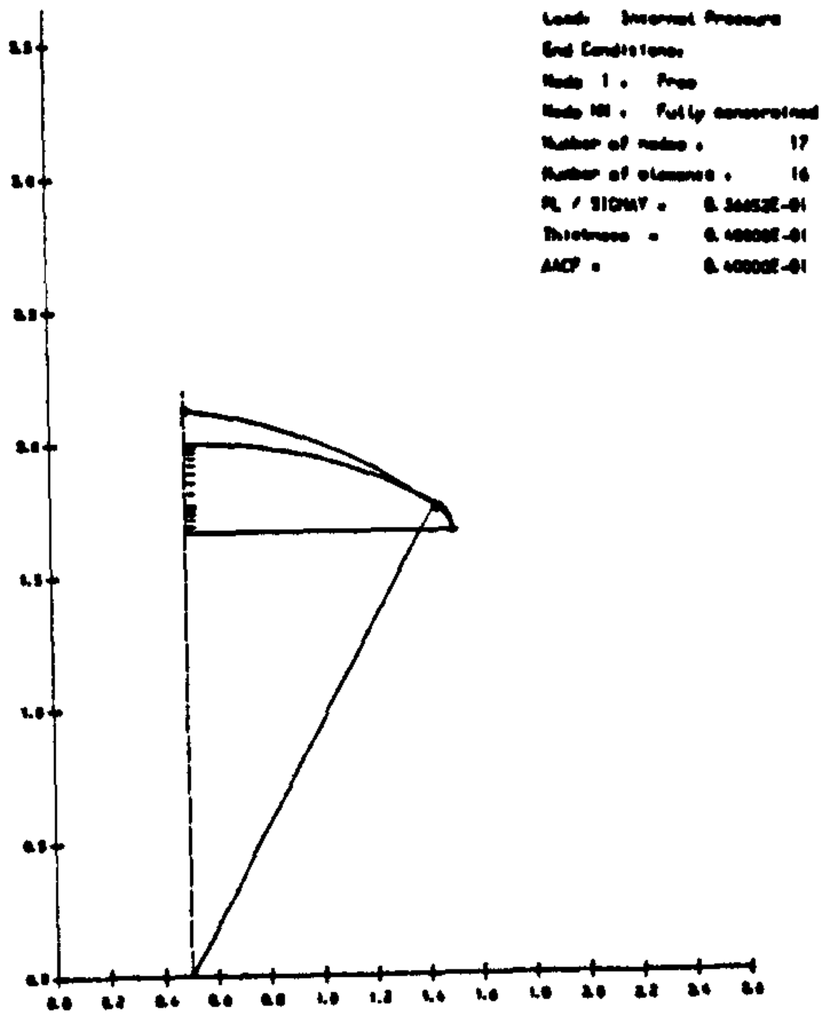

Fig 6.45a

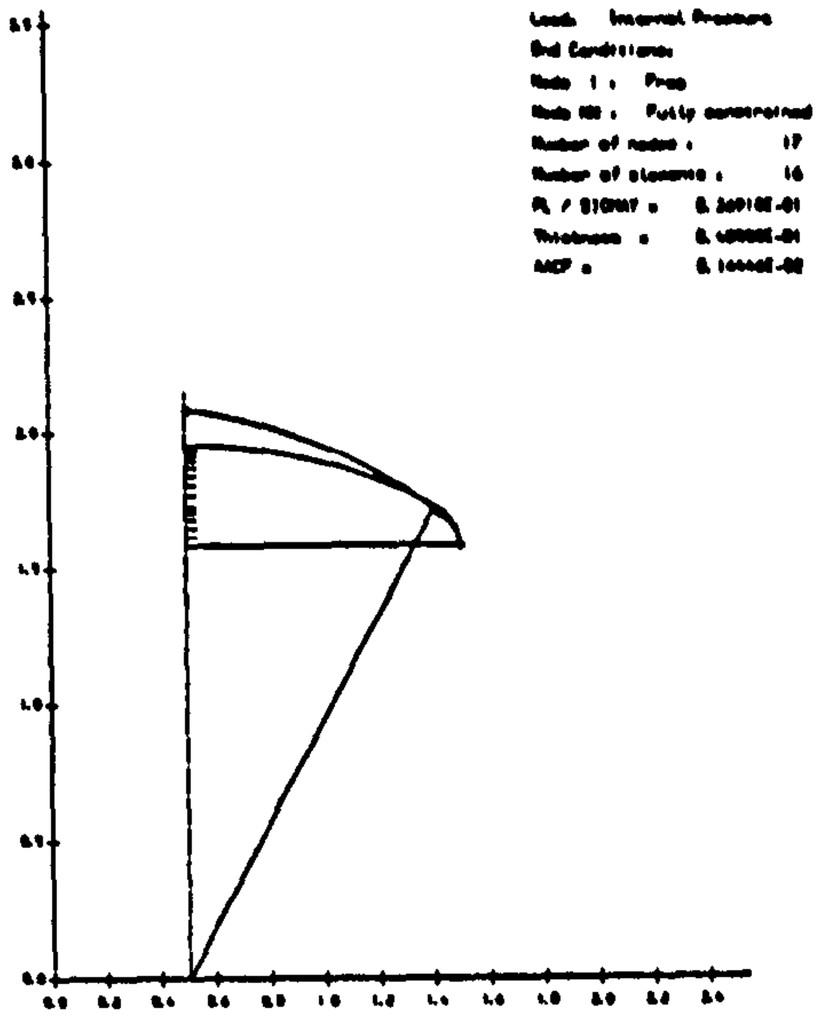

Fig 6.45b

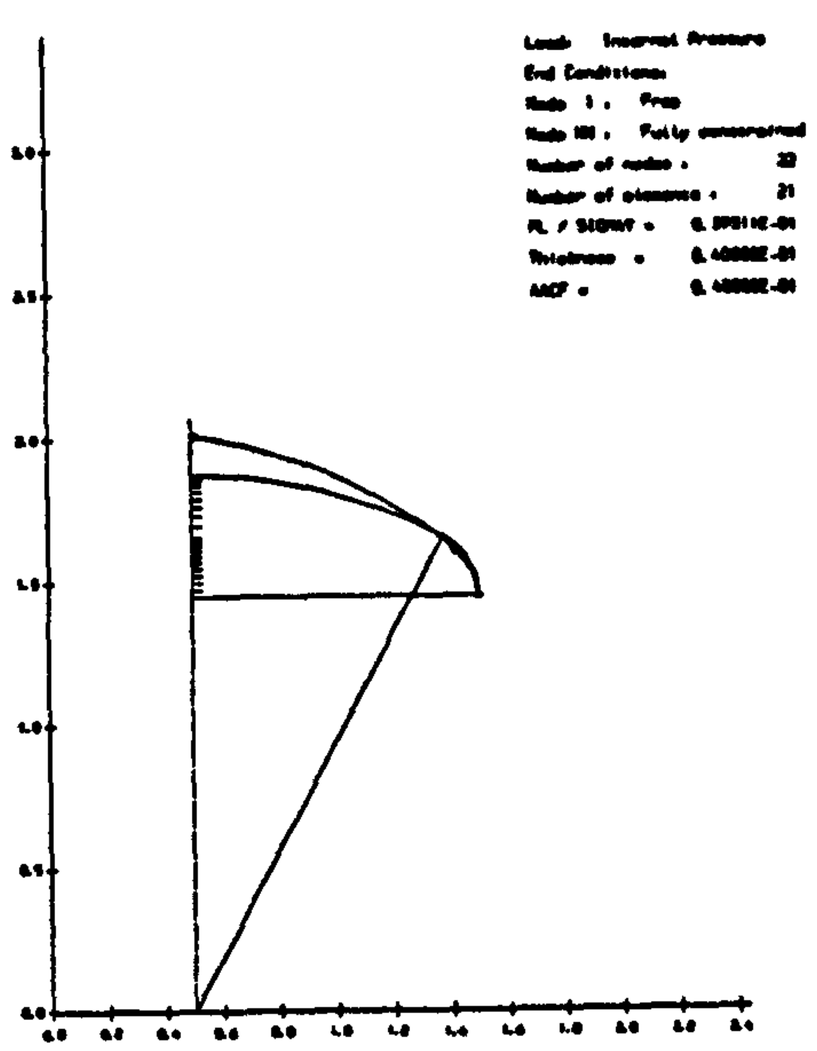

Fig. 6.45c

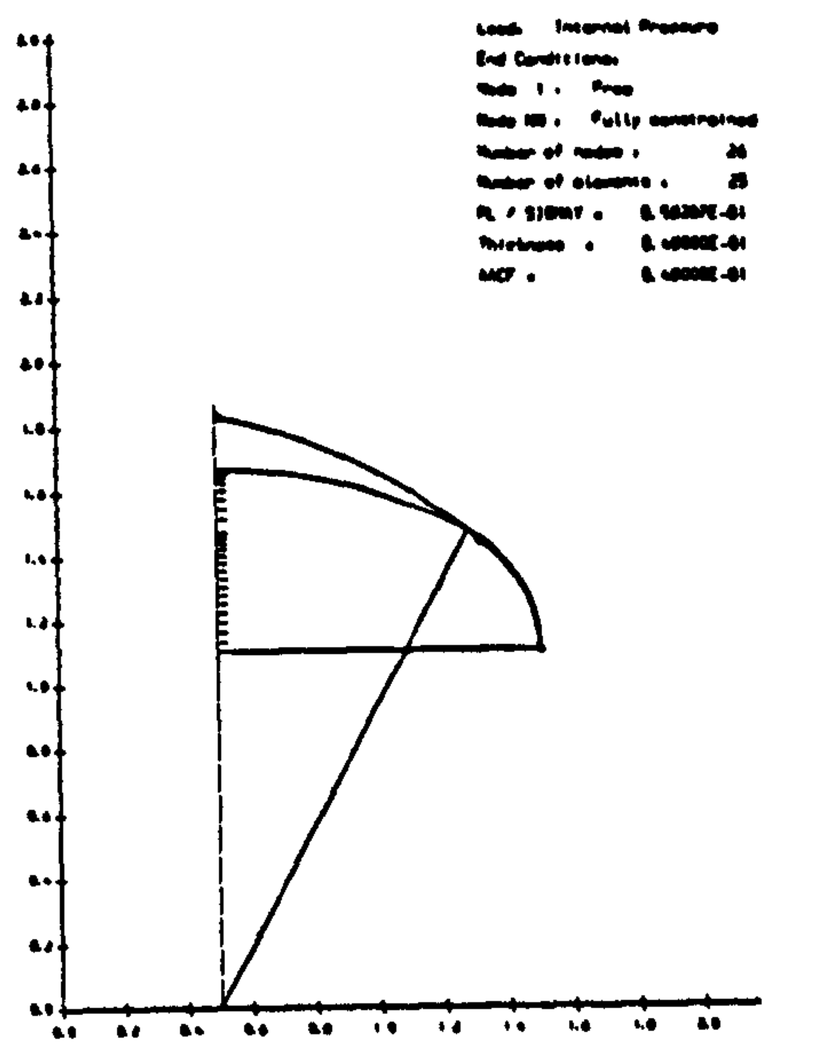

Fig 6.45d

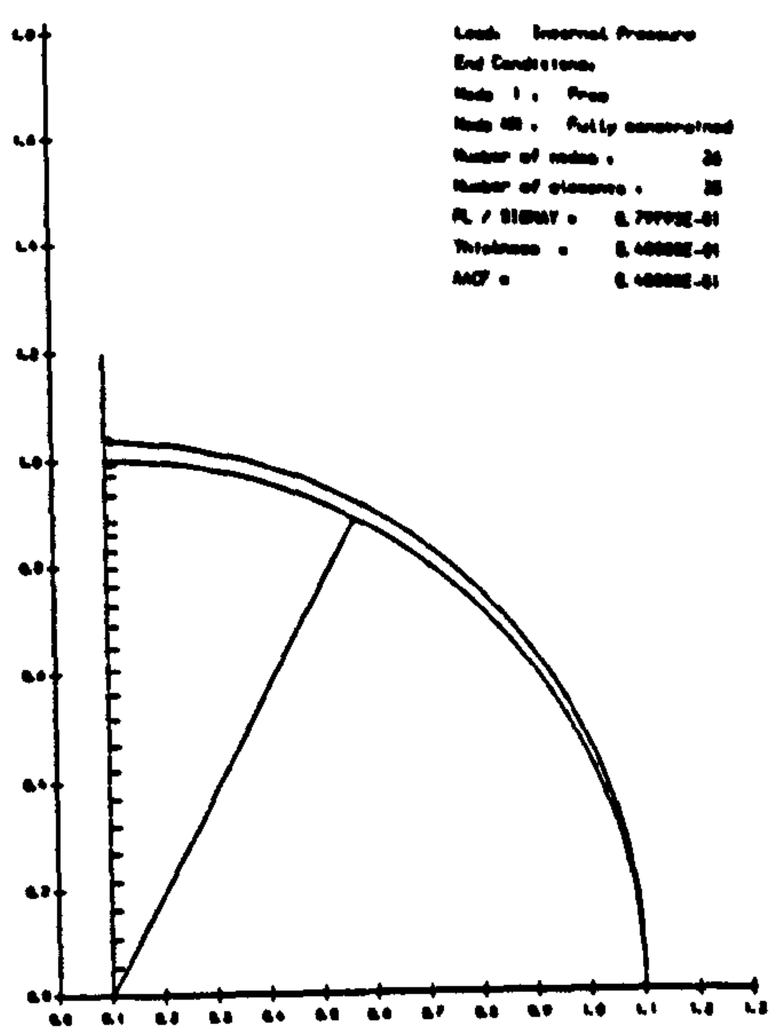

Fig. 6.45e

Fig. 6.46 - BREE PROBLEM — TEMPERATURE INDEPENDENT

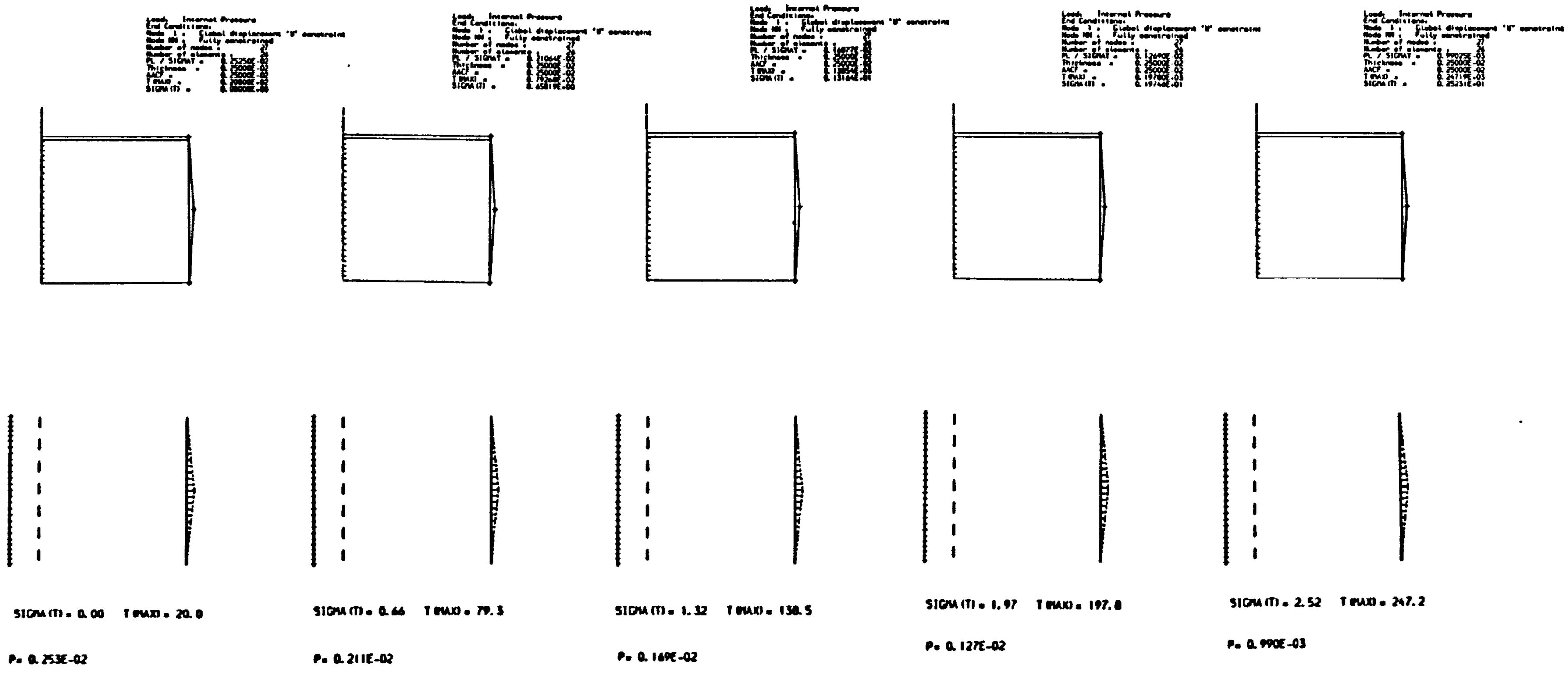

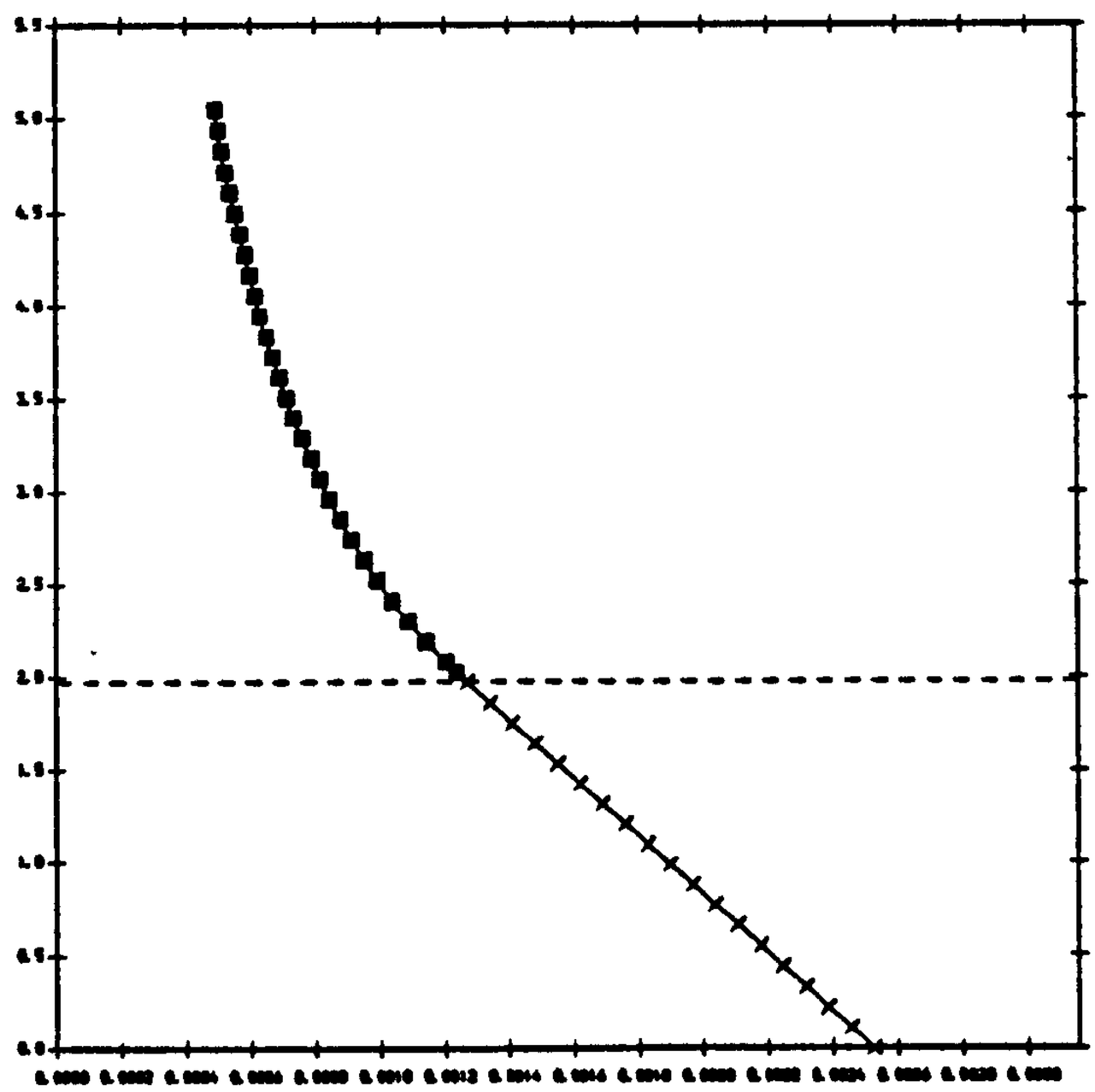

Fig. 6.47 - BREE TYPE DIAGRAM - TEMPERATURE INDEPENDENT [94]

Fig. 6.48 - BREE PROBLEM — TEMPERATURE DEPENDENT

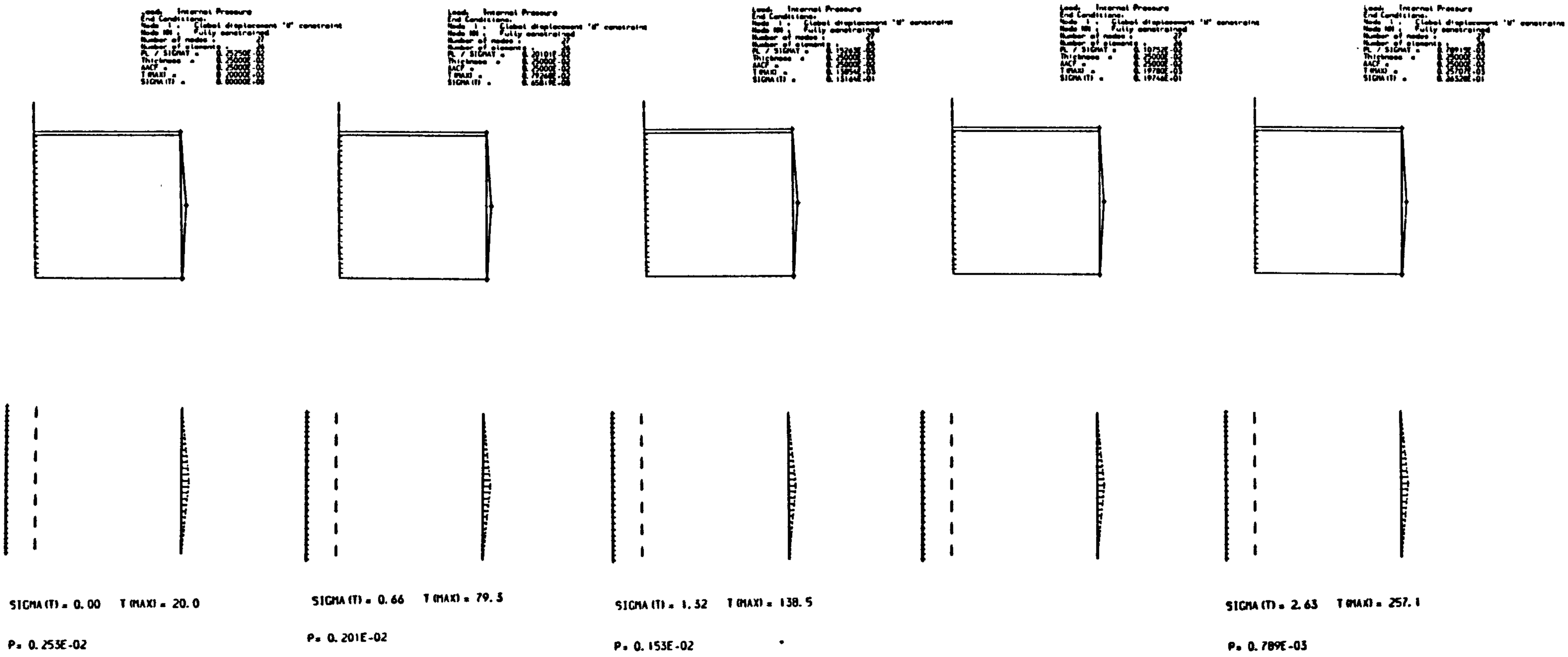

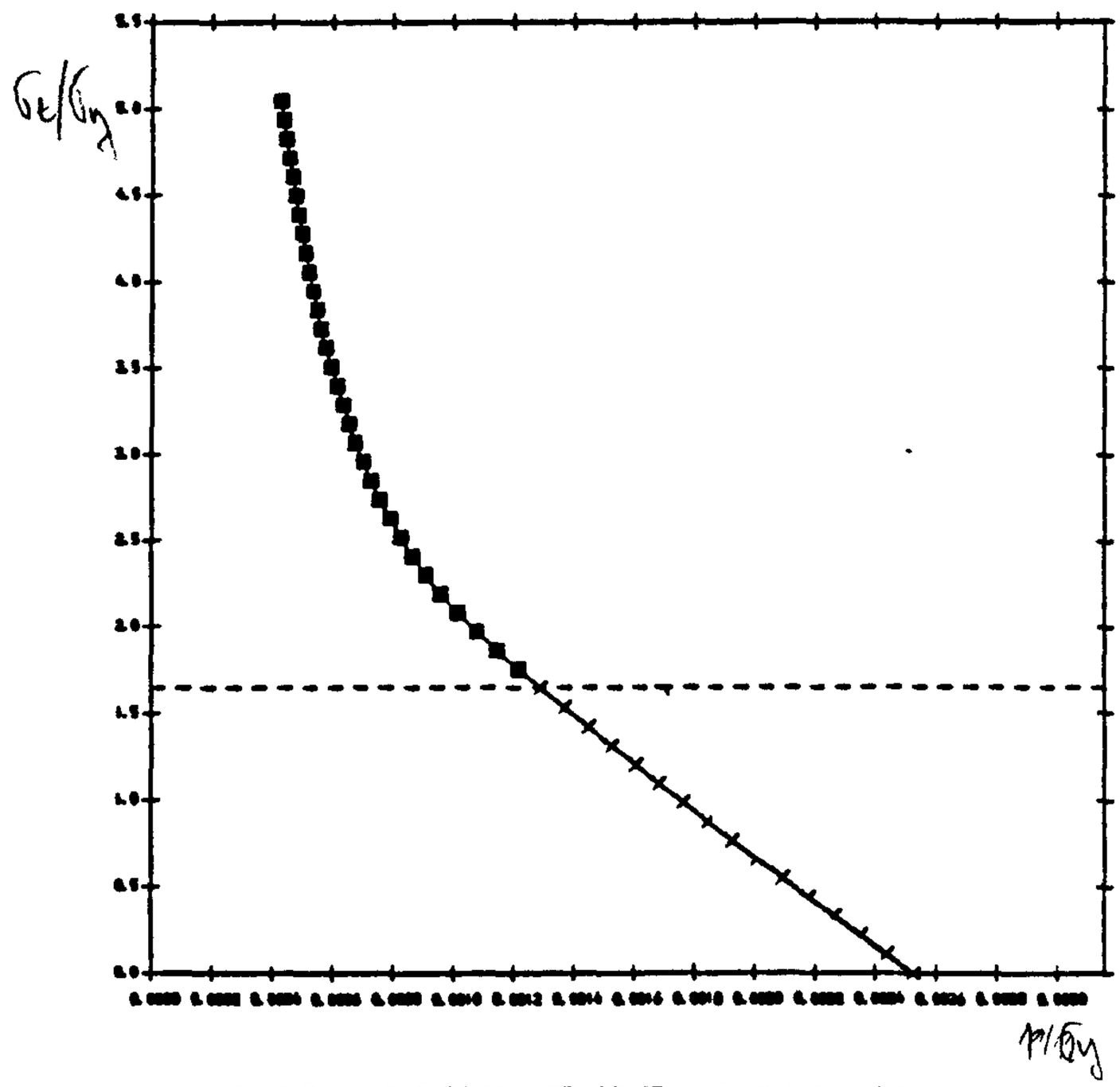

Fig. 6.49 - BREE TYPE DIAGRAM - TEMPERATURE DEPENDENT [94]

SIGMA (T) = 0.00 T MAX = 20.0 P= 0.729E-05

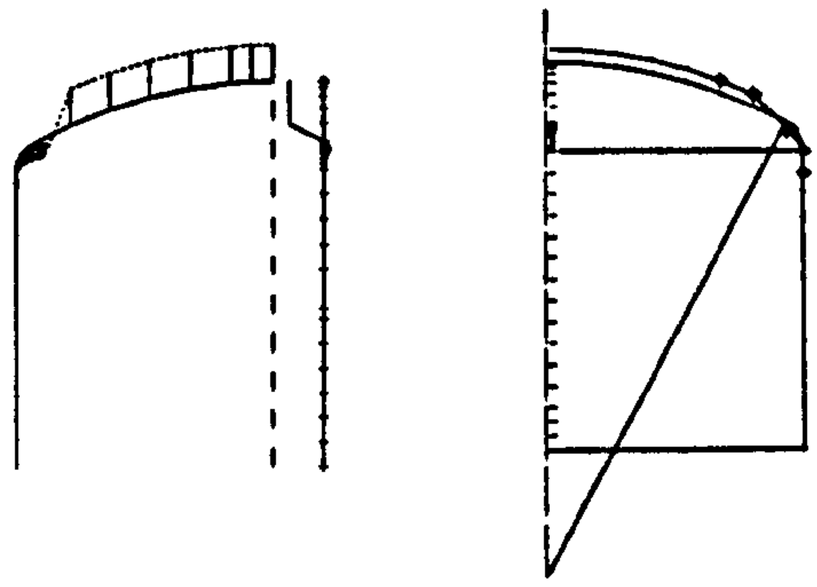

Load: Internal Pressure
End Conditions:
Node 1 : Free
Node NN : Fully constrained
Number of nodes : 31
Number of elements : 30
PL / SIGMAY = 0.70256E-03
Thickness = 0.25000E-02
AACF = 0.43844E-02
T (MAX) = 0.20000E+02
SIGMA (T) = 0.00000E+00

SIGMA (T) = 0.55 T MAX = 69.4 P= 0.646E-03

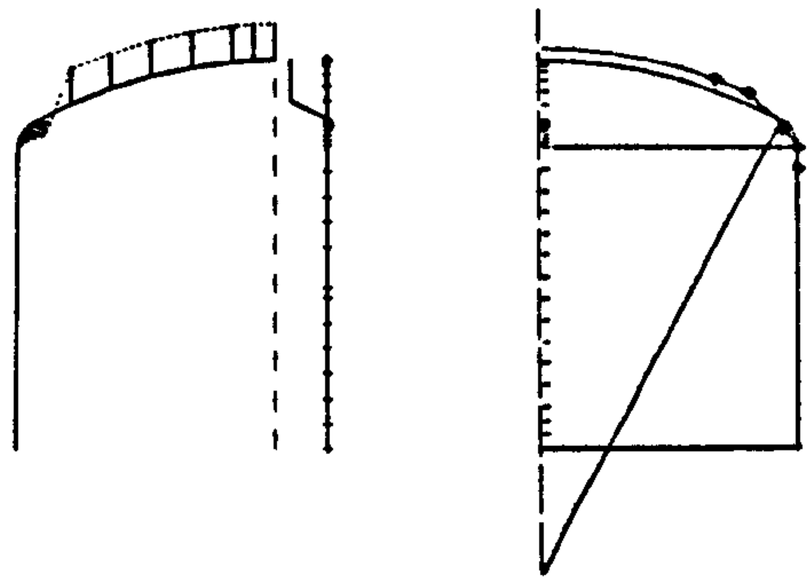

Load: Internal Pressure
End Conditions:
Node 1 : Free
Node NN : Fully constrained
Number of nodes : 31
Number of elements : 30
PL / SIGMAY = 0.61688E-03
Thickness = 0.25000E-02
AACF = 0.43844E-02
T (MAX) = 0.69590E+02
SIGMA (T) = 0.54849E+00

SIGMA (T) = 1.10 T MAX = 118.8 P= 0.553E-03

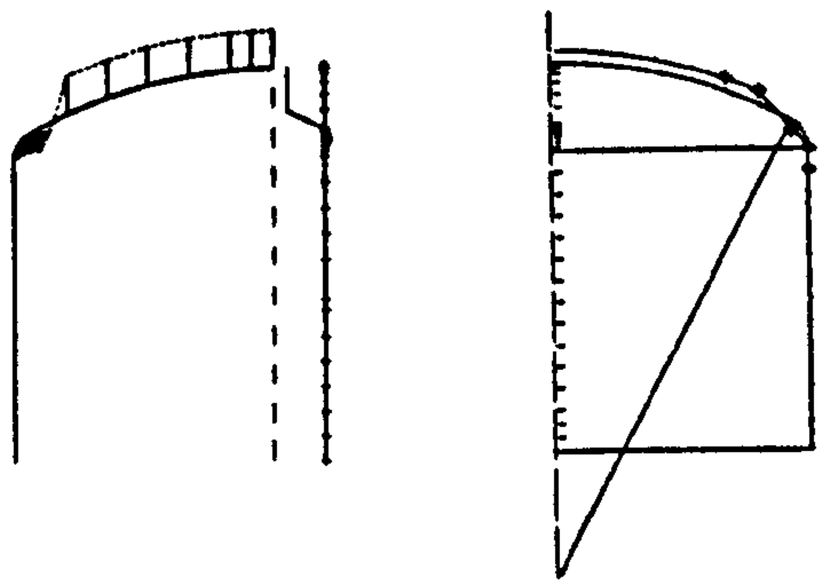

Load: Internal Pressure
End Conditions:
Node 1 : Free
Node NN : Fully constrained
Number of nodes : 31
Number of elements : 30
PL / SIGMAY = 0.50927E-03
Thickness = 0.25000E-02
AACF = 0.43844E-02
T (MAX) = 0.11878E+03
SIGMA (T) = 0.10970E+01

SIGMA (T) = 1.65 T MAX = 168.2 P= 0.397E-03

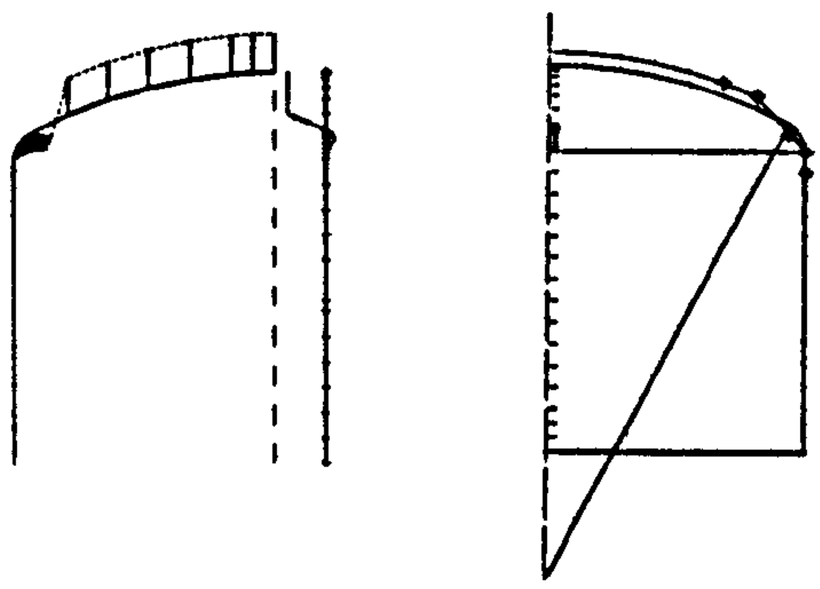

Load: Internal Pressure
End Conditions:
Node 1 : Free
Node NN : Fully constrained
Number of nodes : 31
Number of elements : 30
PL / SIGMAY = 0.36042E-03
Thickness = 0.25000E-02
AACF = 0.43844E-02
T (MAX) = 0.16817E+03
SIGMA (T) = 0.16455E+01

SIGMA (T) = 2.19 T MAX = 217.6 P= 0.270E-03

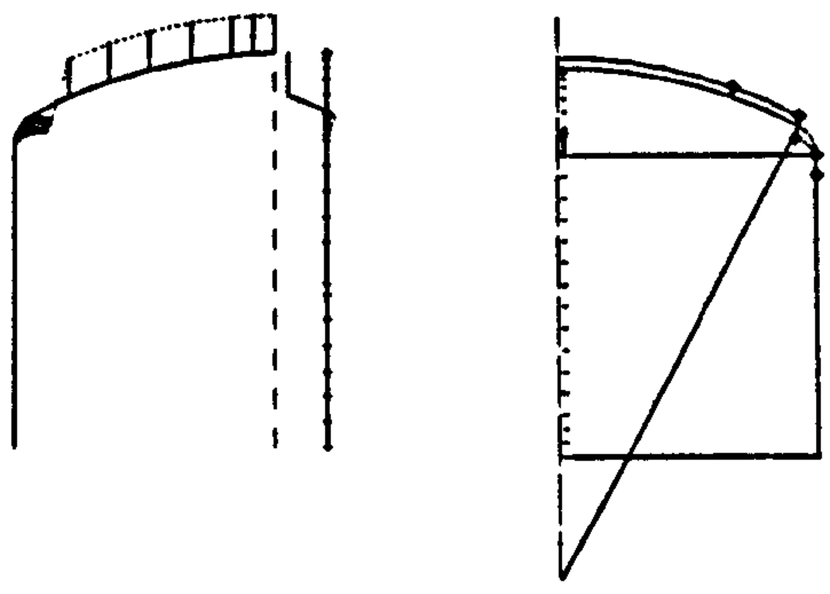

Load: Internal Pressure
End Conditions:
Node 1 : Free
Node NN : Fully constrained
Number of nodes : 31
Number of elements : 30
PL / SIGMAY = 0.22986E-03
Thickness = 0.25000E-02
AACF = 0.43844E-02
T (MAX) = 0.21756E+03
SIGMA (T) = 0.21940E+01

Fig. 6.50 - BREE TYPE PROBLEM - TEMPERATURE DEPENDENT

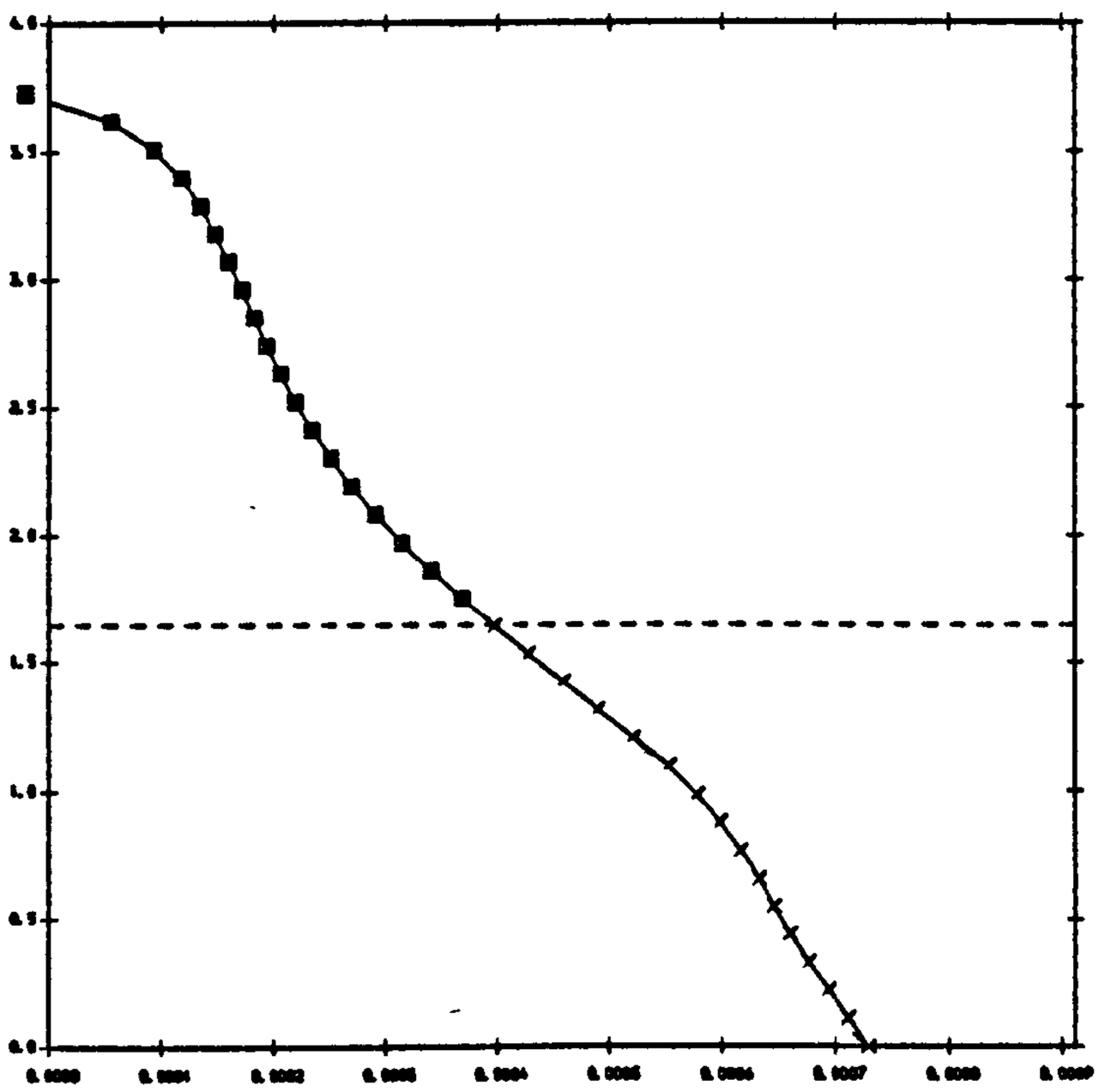

Fig. 6.51 - BREE TYPE DIAGRAM - TEMPERATURE DEPENDENT [94]

CHAPTER 7

CONCLUSIONS AND PROPOSALS FOR FUTURE WORK

7.1 Conclusions

The present research project has contributed to a better understanding of several aspects of the shakedown behaviour of shell structures. The following are the contributions and achievements of the present work:

- The review presented in Chapter 2 contributes by recounting most of the shakedown and ratchetting concepts, extended theorems, and their application with emphasis on the extended upper bound proposed in [36,37].

- By using the extended upper bound theorem the structural and material behaviour of structures operating above the limit of reversed plasticity was analysed. The dependence of shakedown behaviour on the type of structure was demonstrated by the analysis of two cases. The first, a two-bar structure, showed no incremental deformation (ratchetting) up to plastic collapse assuming perfectly plastic behaviour. When cyclic hardening was considered in the calculations, the results obtained showed the ratchet limit to be greater than the limit load.

The second example was the case of the cylindrical vessel with a thickness discontinuity subjected to cyclic internal pressure. A bound defining the ratchet limit was constructed by means of the same extended upper bound. It was shown that, for extreme cases when the Stress Concentration Factor (SCF) is very high, failure may theoretically occur due to incremental deformation for small constant mechanical load in the case of perfectly plastic material. In the case when cyclic hardening was included, the global collapse always prevails and the vessel fails as a membrane when the limit load is reached. In both cases the problem of low cyclic fatigue has to be considered.

- Assessments of structural behaviour at stress concentrations due to mechanical load.

The overall conclusions for these calculations are as follows: The influence of the SCF on the performance of structures subjected to cyclic mechanical load has been investigated with the conclusion that the SCF plays a role in the way structures deform within the shakedown limits, where plastic strains which are small could be ratified. In addition, the dependence of the shakedown limit on the SCF was also confirmed. When the value of the SCF is high, the reversed plasticity shakedown limit is reduced and a higher transient residual strain is obtained at a given load level. However, when the analysis was performed beyond the shakedown limit it was found that the SCF has very little influence on the ratchet limit. In such cases, the analysis

and design may be performed to prevent incremental growth but not reversed plasticity and the structure would be allowed to operate subjected to stress amplitudes $\Delta\sigma > 2\sigma_y$. Thus, the problem to be analysed is likely to be one of low cycle fatigue or alternatively, the parameter which governs structure reliability may be the limit load.

- A simplified technique was used to evaluate the shakedown bounds for thermal loading problems in cylindrical vessels. The technique was able to predict results obtained by Karadeniz and Ponter [51] using a Finite Element analysis technique, and also to extend the analysis to include multiple loadings. A graphical form of presenting the results allows an easy assessment of the regions of differing modes of deformation and this approach has considerable appeal for design purposes. The effects of the temperature on the yield stress of the material were also explored with a considerable change on vessel behaviour.

- The tests performed on portal frames at 400°C confirmed the non-ratchetting material property of the SS316 at this temperature, as well as its capability of cyclic hardening. A theoretical analysis of such a portal frame was made by means of the extended upper bound theorem and as a result a Bree type diagram was constructed. This diagram was used as a reference for the analysis of the experimental results which were

presented as contours of states of constant plastic deformations which were reached after some transient during the first few cycles. An interesting feature of these contours was the way states of constant plastic deformation were reached for small mechanical loads. In contrast with the behaviour of the frames carrying large mechanical loads, the deformation tended to accumulate towards a stable state in the direction opposite to the direction of the mechanical load. It seemed that for the frame loaded with a P = 4 Kg a neutral sort of behaviour was reached without any noticeable plastic deformation. Such behaviour could not be predicted by the theory used but for $\delta/\delta_L < 2.5$ the theory gave a very good estimate of the ratchet limit. An attempt was made to predict theoretically the stable state of constant deformation in excess of the shakedown limit. A simplified calculation was used to estimate the total extent of the hinges along the bars of the frame and the transient plastic deformation was calculated using the method proposed by Mendelson [23]. Theoretical contours were then obtained for a transient deformation of u = 4mm and for two different strain hardening parameters obtained, respectively, from the cyclic stress-strain curve contructed by Ponter and Karadeniz [36,37] with k = 7 (Fig. 5.5), and from the monotonic stress-strain curve in Fig. 5.30 with k = 22.5. Although both curves are conservative when compared with the contour obtained experimentally, the contour corresponding to the cyclic stress-strain curve [36,37] is much closer to the experimental one and therefore less conservative.

- The general technique developed for the shakedown analysis of pressure vessels is probably the major contribution of this research, in the sense that it will possibly be able to accomodate all the aspects of the shakedown problem studied here. The primary aim of the technique which is to solve thermal cyclic loading problems for axisymmetric shells has been achieved and the technique is already able to cope with a wide range of loading problems and differing types of pressure vessels. The basis of the technique was to reduce the shakedown problem to a minimization problem which could be solved as a Linear Programming problem. This could be achieved only by developing a method for obtaining a consistent relationship between the displacement field the kinematically admissible strain field and the plastic strain field assumed. By means of a Galerkin-type technique, the difference between the two representations of the strain, ie the strain in terms of nodal displacements and in terms of plastic multipliers, was minimized and a general and consistent relationship between displacement and strain fields was obtained. Such a relationship has been able to produce good solutions when compared with known solutions for all the cases analysed in this thesis, although, as pointed out in the next Section, it still can be improved by using a better displacement field.

7.2 Proposals for Future Work

The current state of development of the Finite Element technique proposed in this research programme is still incomplete and is capable of considerable development. The technique still needs to go through several important stages of optimization which will increase the reliability of the solutions. In addition, the inclusion of a variety of types of shell elements will greatly increase its potential as a tool for the shakedown analysis of axi-symmetric shells. For the immediate future the technique needs to be implemented with the following developments:

- The inclusion of a variety of additional practical thermal loading cases among the ones already considered in this thesis.

- The inclusion of a wider range of axi-symmetrical shell elements.

- The use of a better displacement field which would allow the inclusion of bending curvature within the element. At the moment the displacement field within the elements is assumed to be interpolated by linear functions with the meridional and circumferencial strains being described in terms of 3 nodal quantities only. By assuming an intermediate node within the element, a compatible displacement field of the second order involving a fourth quantity would, perhaps, be a better approximation for the actual displacement field. Such a

choice of displacement field would lead to a similar orthogonality condition for the meridional strain difference. This would result in a orthogonality condition for both the circumferential and meridional strain to an arbitrary linear function. Such a condition would be much stronger than the condition presently obtained for the strain difference in the meridional direction which is zero in the mean within the element.

- The use of a better yield surface such as the 12λ's obtained from the composition of the Tresca and von Mises yield surface as shown in Fig. 7.1.

- The generalization of the technique to cope with multiple loading.

In a long term the technique could perhaps be extended to analyse asymmetric shells and therefore complete the range of shell structures it is potentially able to analyse.

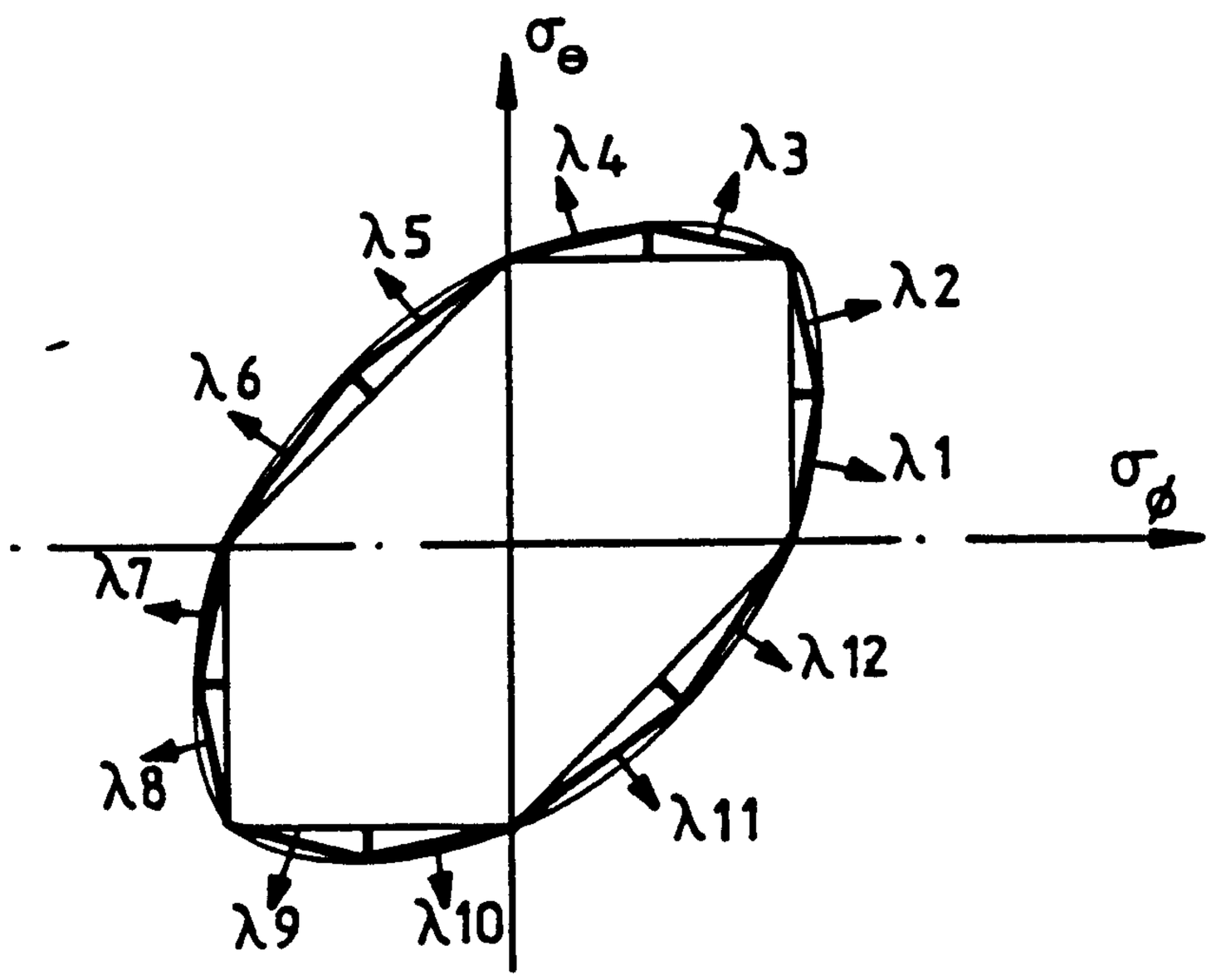

Fig. 7.1 A 12 λ's yield surface

APPENDIX A

A.1 The Calculations for Cylindrical Pressure Vessels with Variable Thickness

The details of the loading and geometry for this problem are given in Chapter 3 and the purpose of this appendix is to provide some details of the calculations involved.

ELASTIC SOLUTIONS

Elastic solutions for thin cylindrical shells are easily available from [57] and [58] and the equations of the edge forces obtained for this particular problem are quoted directly in Chapter 3.

MOMENT AND HOOP FORCE DISTRIBUTIONS

The distributions of bending moments and hoop forces due to the edge forces (H,M) for a particular cylinder (α=4, β=200) are shown in Figs. A1 and A2. Only the distributions in the thinner cylinder are illustrated.

The superposition of the membrane hoop forces and the hoop forces due to H and M is shown in Fig A3. It can be seen that global collapse (or membrane failure) is more likely to happen at the section where the hoop stress due to edge forces is maximum. It is assumed in this analysis, however,

that this maximum hoop force can be neglected in comparison with the membrane hoop force. The global collapse bound is then very easily determinated.

GLOBAL COLLAPSE

The loading condition for a global collapse to occur for a Tresca yield condition is represented in Fig. 3.12. If the effect of the edge forces is neglected, the membrane hoop forces can be calculated by

$$N_\phi = N_\phi^m(\Delta p/2) + N_\phi^m(\bar{p}) \qquad \text{A1}$$

which gives

$$N_\phi = \frac{\Delta pR}{2} + \bar{p}R \qquad \text{A2}$$

The hoop stress is then

$$\sigma_\phi = \frac{\Delta pR}{2T} + \frac{\bar{p}R}{T} \qquad \text{A3}$$

For the global collapse bound the following expression is obtained

$$\frac{\Delta pR}{2T} + \frac{\bar{p}R}{T} = \sigma_y \qquad \text{A4}$$

in terms of Δp and p. The same equation can be written as a function of nondimensional parameters

$$\frac{\Delta p}{P_L} + 2\,\frac{\bar{p}}{P_L} = 1 \qquad \text{A5}$$

THE UPPER BOUND THEOREM

Equation 3.11 represents the upper bound theorem which will be applied to the mechanism shown in Fig. 3.13. Such an equation was divided into three terms which can be calculated as follows:

DETERMINATION OF THE TERMS

Term I ($\int \sigma^c_{ij}\, d\,\varepsilon^c_{ij}\, dV$)

$$\sigma^c_{ij}\, d\,\varepsilon^c_{ij} = \sigma^c_x\, d\,\varepsilon^c_x + \sigma^c_\phi\, d\,\varepsilon^c_\phi = \sigma^c_x\, d\varepsilon + \sigma^c_\phi \times 0 = \sigma_y\, d\varepsilon \text{ (constant)} \qquad \text{A6}$$

The assumed element is shown schematically in Fig. A4.

$$\int \sigma^c_{ij} d\,\varepsilon^c dV = 2\pi R a T \sigma_y d\varepsilon \qquad \text{A7}$$

Term II ($\int p\, d\, u^c dS$)

$$du = a d\varepsilon \qquad \text{A8}$$

$$\int \bar{p}\, d\, u^c dS = \bar{p} a d\varepsilon \int dS = \bar{p} a \pi R^2 d\varepsilon \qquad \text{A9}$$

Term III ($\int \sigma^{\Delta p}_{ij}(z,t) d\, \varepsilon^c_{ij}\, dV$)

$$\sigma^{\Delta p}_{ij}(z,t) d\,\varepsilon^c_{ij} = \sigma^{\Delta p}_x\, d\,\varepsilon^c + \sigma^{\Delta p}_\phi \cancelto{0}{d\,\varepsilon^c_\phi} = \sigma^{\Delta p}_x(z,t) d\varepsilon^c \qquad \text{A10}$$

(maximum when $\sigma^{\Delta}_{xp}(z,t)$ is maximum positive)

$$dV = 2\pi Radz \qquad \text{A11}$$

$$\sigma_{ij}^{\Delta p}(z,t)d\,\varepsilon_{ij}^{c} = 2\pi Rad\varepsilon \int_{o}^{T} \sigma_{x}^{\Delta p}(z,t)dz \qquad \text{A12}$$

Equation 3.11 becomes

$$2\pi RaTd\varepsilon\sigma_{y} = pa\pi R^{2}d\varepsilon + 2\pi Rad\varepsilon \int_{o}^{T} \sigma_{x}^{\Delta p}(z,t)dz \qquad \text{A13}$$

or

$$T\sigma_{y} = \frac{\bar{p}R}{2} + \tilde{A} \qquad \text{A14}$$

where

$$\tilde{A} = \int_{o}^{T} \sigma_{x}^{\Delta p}(z,t)dz \qquad \text{A15}$$

STRESS DISTRIBUTION

Assuming a linear stress distribution through the thickness of the vessel, the stress diagram is shown in Fig. A5. The shaded area corresponds to the value of A.

RATCHETTING BOUND ABOVE REVERSE PLASTICITY

The upper bound theorem can now only be applied to V_s, where the stresses lie below the shakedown limit. The extreme stresses σ_1 and σ_2 are expressed by

$$\sigma_1 = A + BT/2 \qquad \text{A16}$$

$$\sigma_2 = - A + BT/2 \leq \sigma_y \qquad \text{A17}$$

where

$$A = \frac{\Delta pR}{4T} \quad ; \quad B = \frac{12M(\Delta p/2)}{T^3} \quad \text{and} \quad A < BT/2 \qquad \text{A18}$$

Applying the upper bound to V_s gives

$$\sigma_y t = \frac{\bar{p}R}{2} + \tilde{A} \qquad \text{A19}$$

where

$$t = z_2 + z_3 \qquad \text{A20}$$

$$\tilde{A} = \frac{1}{2}\,(z_2\sigma_2 + z_3\sigma_y) \qquad \text{A21}$$

$$z_2 = \frac{\left(- A + \frac{BT}{2}\right)}{B} \quad ; \quad z_3 = \frac{\sigma_y}{B} \qquad \text{A22}$$

Substituting the values of A20, A21 and A22 into A19 gives

$$\sigma_y = \frac{(2\sigma_y + BT - 2A)}{2B} = \frac{pR}{2} + \frac{1}{2}\left(\frac{A^2 - ABT + \frac{BT}{2} + \sigma_y^2}{B}\right) \qquad \text{A23}$$

which in terms of nondimensional groups becomes

$$\frac{\bar{p}}{p_L} = \frac{1}{12f_2(\alpha)}\left[\frac{1}{\Delta p/p_L} - \left(3f_2(\alpha) - 9f_2^2(\alpha) - \frac{1}{4}\right)\frac{\Delta p}{p_L} - (1-6f_2(\alpha))\right] \qquad \text{A24}$$

EQUILIBRIUM EQUATIONS FOR PERFECTLY PLASTIC MATERIALS

Figs. (A6a,b) represent the stresses distribution diagram assuming first $\sigma_2 \leq \sigma_y$. The thickness of the elastic region can be related to the total thickness as

$$t = kT \qquad \text{A25}$$

where k=constant.

Equilibrium of the axial forces is satisfied by equation

$$N_x = \int d\,F_1 + F \qquad \text{A26}$$

From Figs. A6a,b) it can be seen that

$$dF_1 = \sigma_x^1\, dS = (A + Bz)dS \qquad \text{A27}$$

$$F = \sigma_y\,(T - t) = \sigma_y\,(1 - k)T \qquad \text{A28}$$

Introducing this into A26 gives

$$N_x = A\int dS + B\cancelto{0}{\int z\, dS} + F \qquad \text{A29}$$

rewriting

$$A = \frac{N_x - F}{S} \qquad \text{A30}$$

where

$$S = 1 \times t = kT \qquad \text{A31}$$

The equilibrium of the edge moment with the moment due to the internal forces is expressed by

$$M = \int z \, dF_1 + M_p \qquad \text{A32}$$

Here M_p is a plastic moment given by Figs. (A6a,b)

$$M_p = F \times z_p \quad ; \quad z_p = T/2 \qquad \text{A33}$$

Equation A32 becomes

$$M = \int (A + Bz) \, z \, dS + F \frac{T}{2} \qquad \text{A34}$$

or

$$M = A \cancelto{0}{\int z \, dS} + B \int z^2 \, dS + F\frac{T}{2} \qquad \text{A35}$$

then

$$B = \frac{2M - FT}{2I} \quad \text{where} \quad I = \frac{t^3}{12} \qquad \text{A36}$$

As the plastic zone constitutes a small zone of the vessel, it is assumed that the edge moment M and the axial force N_x remain unchanged.

$$M_x = \frac{\beta T^2 f_2(\alpha)\Delta p}{4} \quad ; \quad N_x = \frac{\Delta pR}{4T} \qquad \text{A37}$$

RATCHETTING BOUND ABOVE REVERSE PLASTICITY

Using the procedure previously presented , the upper bound theorem is applied to V_s in Figs. (3.19a,b,c) with the initial assumption that A < BT/2.

Equation A38 is then obtained

$$\sigma_y t = \frac{\bar{p}R}{2} + \frac{A^2 - ABt + \left(\frac{Bt}{2}\right)^2 + \sigma_y^2}{2B} \qquad \text{A38}$$

where

$$A = \frac{\Delta pR - 4F}{4S} \quad ; \quad B = \frac{2M - FT}{2I} \quad ; \quad S = kT \qquad \text{A39}$$

$$F = \sigma_y (1-k)T \quad ; \quad I = \frac{t^3}{12} \quad ; \quad t = kT \qquad \text{A40}$$

Equation A38 can be rewritten in terms of nondimensional paramenters as

$$\frac{\bar{p}}{p_L} = \frac{k^3}{12\left[f_2 \frac{\Delta p}{P_L} - (1-k)\right]}\left[3 - \frac{1}{k^2}\left[\frac{9}{k^2} f_2^2 - \frac{3}{k} f_2 + \frac{1}{4}\right]\left(\frac{\Delta p}{P_L}\right)^2 + \right.$$

$$+ \frac{1}{k}\left[\frac{18(1-k)}{k^3} f_2 - \frac{3(1-k)}{k^2}(1 + 2f_2) + \frac{(1-k)}{k} - 2\right]\frac{\Delta p}{p_L} - \qquad \text{A41}$$

$$\left. - \frac{(1-k)}{k}\left[\frac{9(1-k)}{k^3} - \frac{6(1-k)}{k^2} + \frac{(1-k)}{k} - 4\right]\right]$$

The extreme stresses are now

$$\sigma_1 = \sigma_y = A + Bt/2 \qquad \text{A42}$$

$$\sigma_2 = A - Bt/2 \gtrsim -\sigma_y \qquad \text{A43}$$

From A42 it can be seen that $\sigma_1 = \sigma_y =$ constant. Substituting the values of A and B into this equation gives

$$\frac{\Delta p}{p_L} = \frac{2(3-2k)}{(k + 6f_2(\alpha))} \qquad \text{A44}$$

In the limit for $|\sigma_2| = \sigma_y$, as shown in Fig. (3.18c), a new plastic zone will start developing. From this relationship Equation A45 is obtained

$$\frac{\Delta p}{p_L} = \left[\frac{k^3 + 3(1-k)}{3f_2(\alpha)} \right] \qquad \text{A45}$$

Equations A44 and A45 must be satisfied simultaneously to define the limit point where the new plastic zone starts. Hence

$$\frac{2(3-2k)}{k + 6f_2} = \frac{k^2 + 3(1-k)}{3f_2} \qquad \text{A46}$$

which gives

$$k^2 + (6f_2-3)k - (6f_2-3) = 0 \qquad \text{A47}$$

Solving this equation

$$k_L = \frac{-(6f_2-3) \pm \sqrt{(6f_2-3)^2 + 4(6f_2-3)}}{2} \qquad \text{A48}$$

that is the value of $k(=t/T)$ when $\sigma_2 = \sigma_y$. Equations A41

and A44 define part of the ratcheting curve in the range $k_L \leq k \leq 1$. Prescribing k in this range, the values of $\Delta p/p_L$ are found by using Equation A44. The values of p/p_L are then calculated by introducing k and $\Delta p/p_L$ into A41.

When the new plastic zone (V_{F2}) is formed (Figs. 3.20a,b) a new equilibrium must be established. For the elastic/perfectly plastic material the extreme stresses σ_1 and σ_2 will now remain constant and equal to σ_y (Equations A49, A50).

$$\sigma_1 = A + \frac{Bt}{2} = \sigma_y \qquad \text{A49}$$

$$\sigma_2 = A - \frac{Bt}{2} = -\sigma_y \qquad \text{A50}$$

It can be seen that A=0 and it is only necessary to determinate B. Using the procedure previously presented the expression below is obtained

$$B = \frac{4\sigma_y M(\Delta p/2) - [\sigma_y^2(1-k^2)T^2 + N_x^2]}{4\sigma_y I} \qquad \text{A51}$$

Equation A49 or A50 can be used to calculate $\Delta p/p_L$

$$\sigma_y = \frac{Bt}{2} \qquad \text{A52}$$

which gives

$$\frac{3}{8}\left(\frac{\Delta p}{p_L}\right)^2 - 3f_2\frac{\Delta p}{p} + \frac{3-k^2}{2} = 0 \qquad \text{A53}$$

Solving the equation

$$\frac{\Delta p}{p} = 2\,\frac{(6f_2) \pm \sqrt{(6f_2)^2 - 3(3-k^2)}}{3} \quad \text{for} \quad k_L \geq k \geq 0 \qquad \text{A54}$$

The upper bound theorem can now be applied in the range $k_L \geq k \geq 0$ to complete the ratchetting curve by prescribing the values of k.

$$\sigma_y t = \frac{\bar{p}R}{2} + \tilde{A} \qquad \text{A55}$$

From Fig. 3.20a,b an expression for $\tilde{A}$ is obtained

$$\tilde{A} = \frac{\sigma_y^2}{B} \qquad \text{A56}$$

The upper bound gives

$$\frac{\bar{p}}{p_L} = \frac{k^3}{\left(6f_2(\alpha) - \frac{3}{4}\frac{\Delta p}{p_L}\right)\frac{\Delta p}{p_L} - 3(1-k^2)} \qquad \text{A57}$$

From Equation A48

$$(6f_2-3)^2 + 4(6f_2-3) \geq 0 \qquad \text{A58}$$

or

$$f_2(\alpha) \geq 0.5 \qquad \text{A59}$$

Therefore, for vessels with $f_2 < 0.5$ no k_L can be found. Analysing a vessel with this geometry ($\alpha = 4$) may possibly demonstrate that the extreme stress σ_2 starts decreasing as the plastic zone advances (Fig. A7). Then the limiting condition to define the range of this part of the curve is

now $\sigma_2 = 0$. From this condition

$$\frac{\Delta p}{p_L} = \frac{2(1-k)(k-3)}{(k-6f_2)} \qquad \text{A60}$$

which must be satisfied simultaneously with

$$\frac{\Delta p}{p_L} = \frac{2(3-2k)}{(k+6f_2(\alpha))} \qquad \text{(previously defined)} \quad \text{A44}$$

to give

$$k_z = \frac{-(6f_2-6) \pm \sqrt{(6f_2-6)^2 + 4(12f_2-6)}}{2} \qquad \text{A61}$$

Equations A41 and A44 can still be used since nothing has changed but the range of validity of k that now is $k_z \leq k \leq 1$.

For $k < k_z$, $\sigma_2 > 0$ and the problem lies in the range where $A > Bt/2$ (Fig. A8).

The upper bound theorem gives

$$\frac{\bar{p}}{p_L} = 1 - \frac{1}{2}\frac{\Delta p}{p_L} \qquad \text{A62}$$

This equation can also be used for vessels whose geometry leads to $A > Bt/2$ from the begining of the load history.

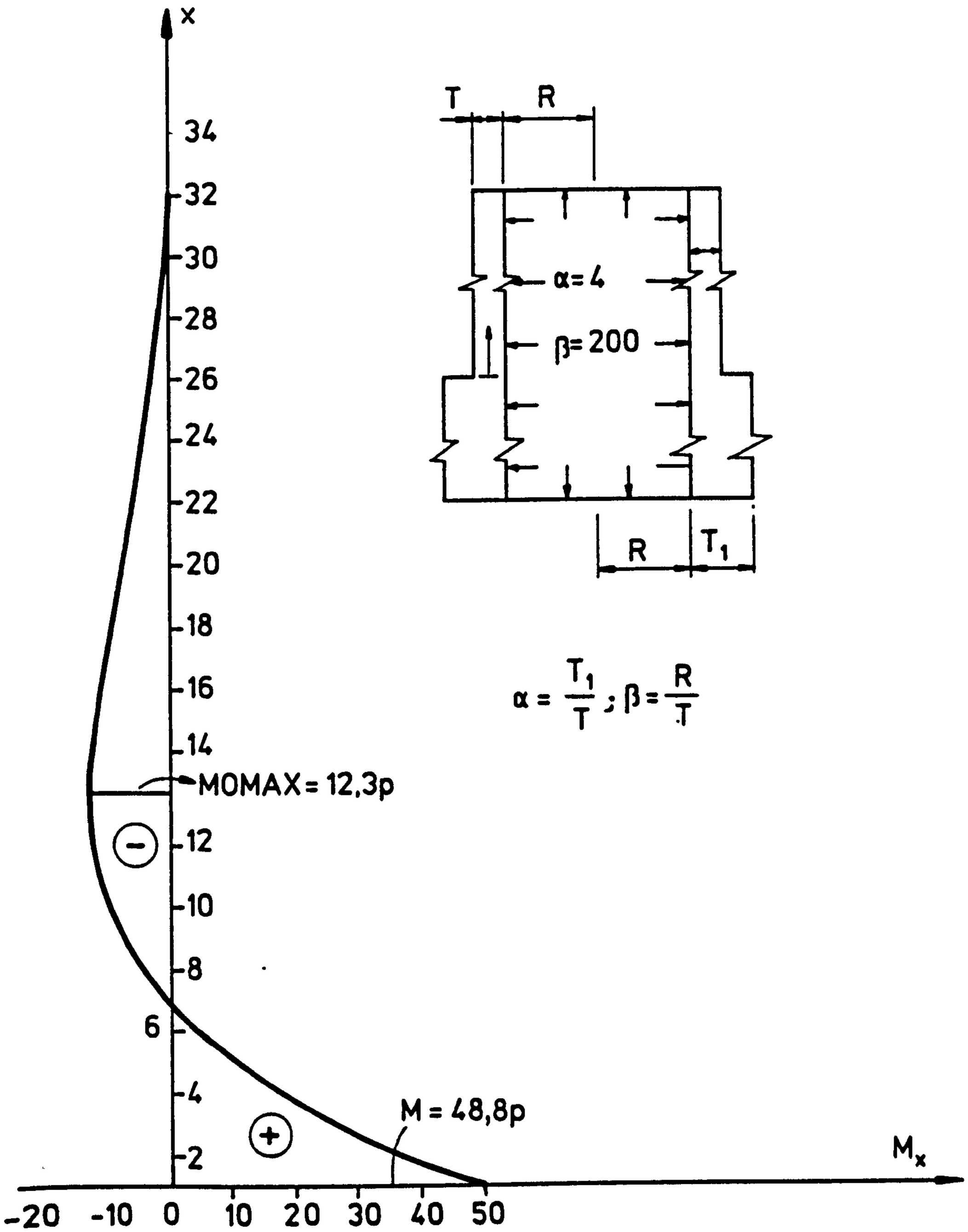

FIG A1 MOMENT DISTRIBUTION DUE TO EDGE FORCES H AND M IN THE THINNER CYLINDER

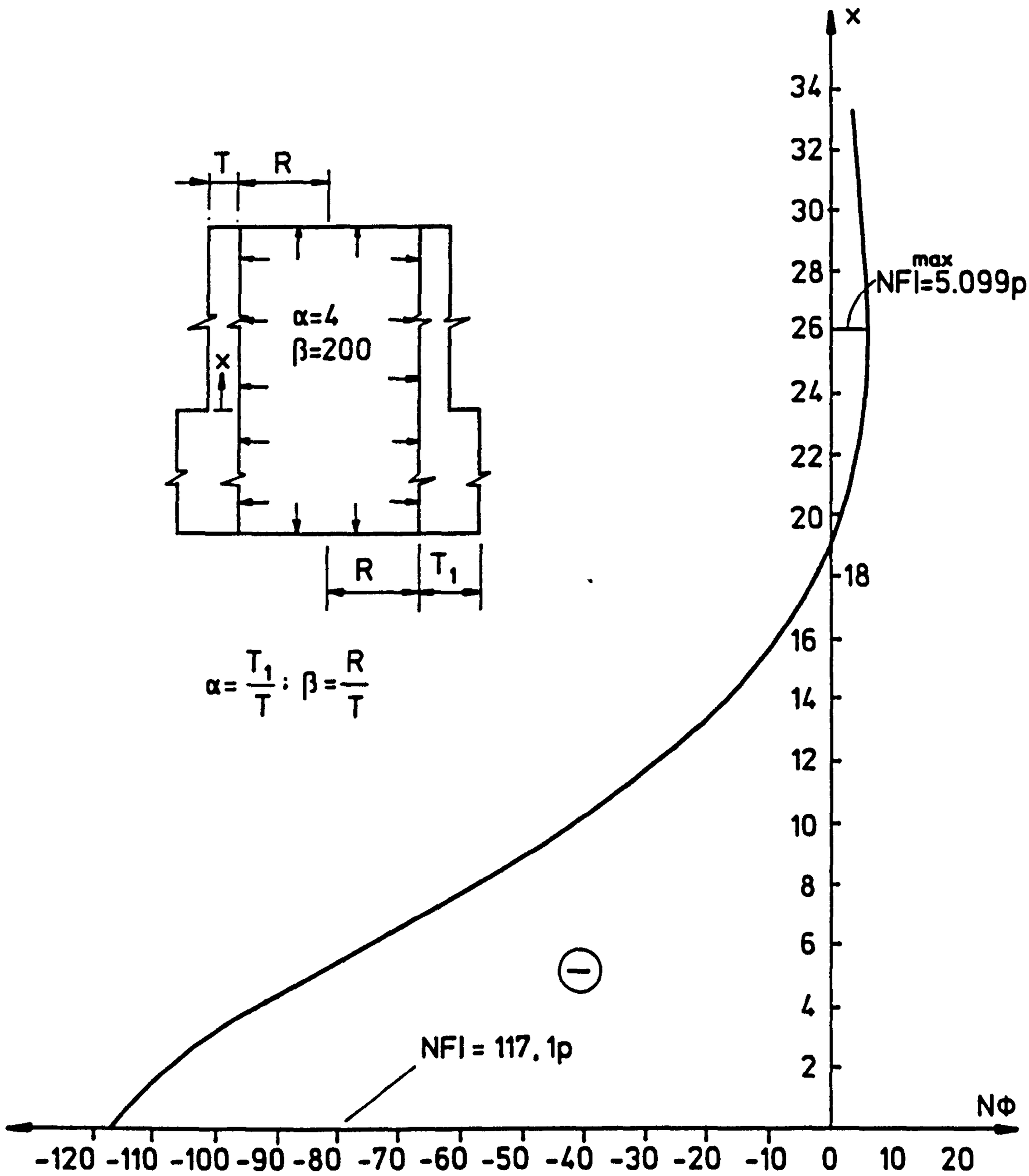

FIG. A2 HOOP FORCE DISTRIBUTION DUE TO EDGE FORCES H & M IN THE THINNER CYLINDER

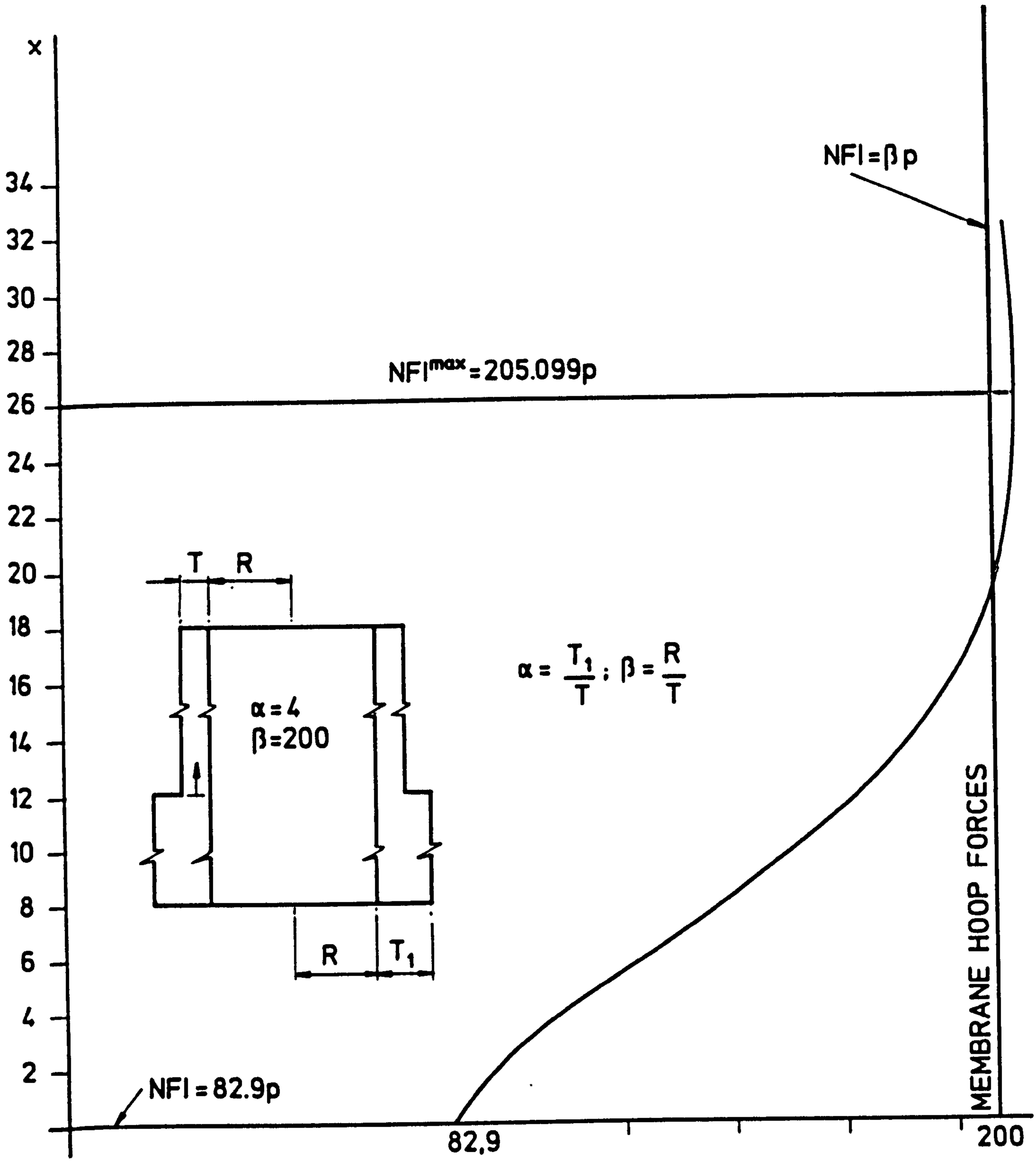

FIG. A3 FINAL HOOP FORCE DISTRIBUTION

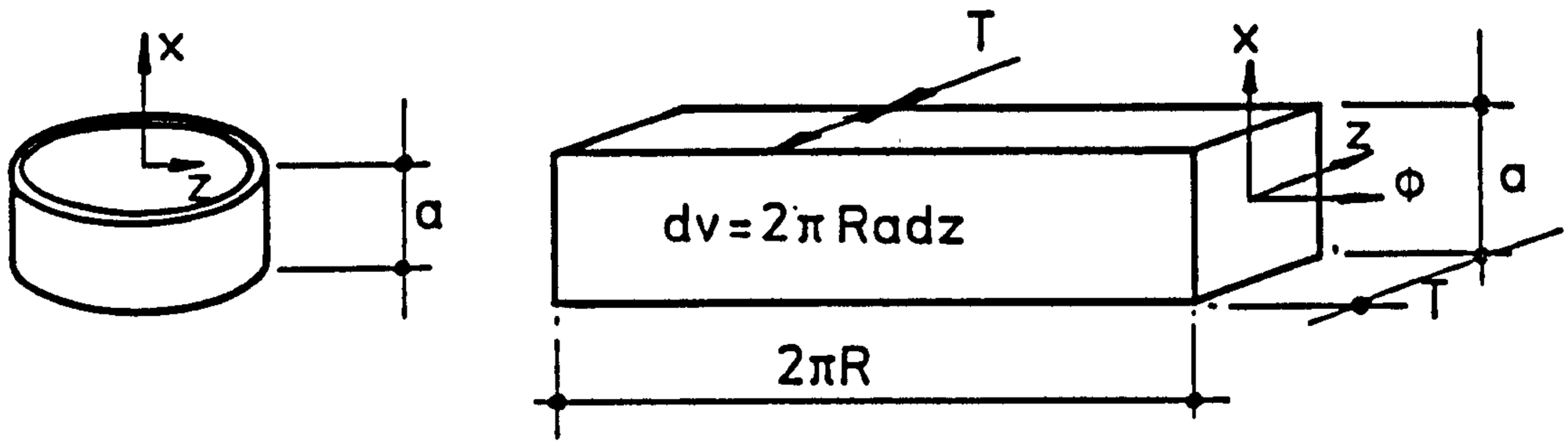

FIG. A4

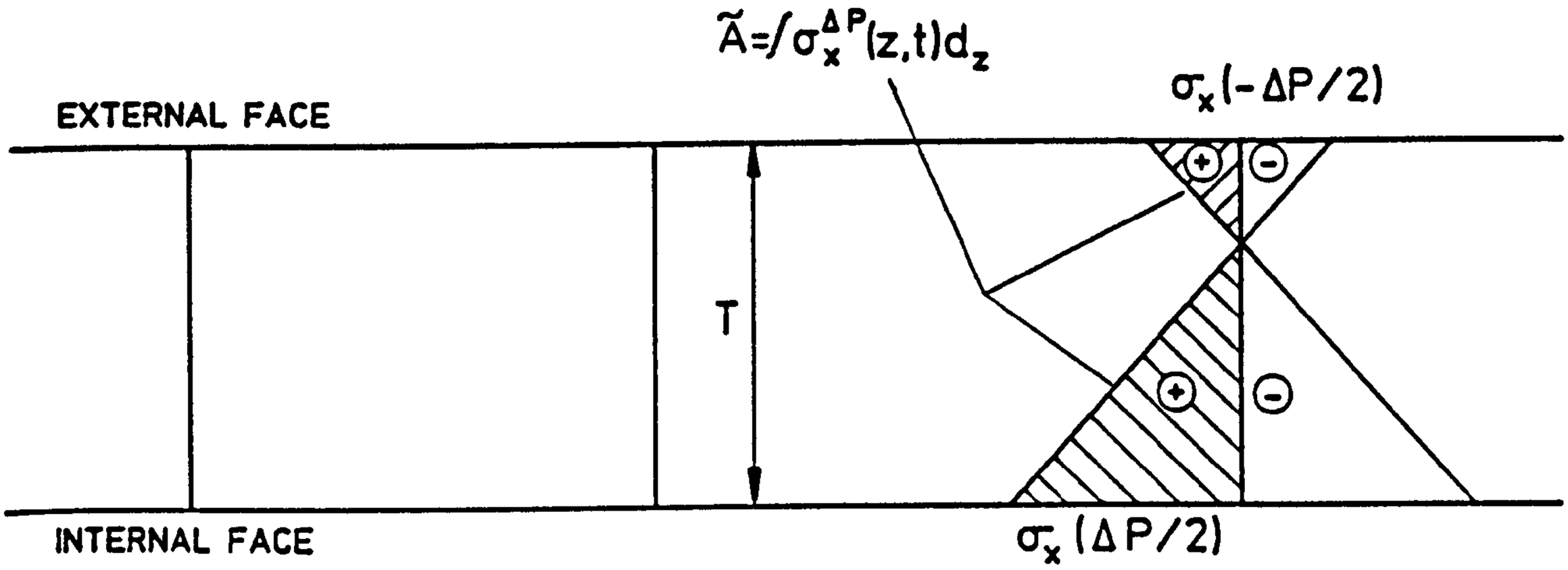

FIG. A5 STRESS DISTRIBUTION

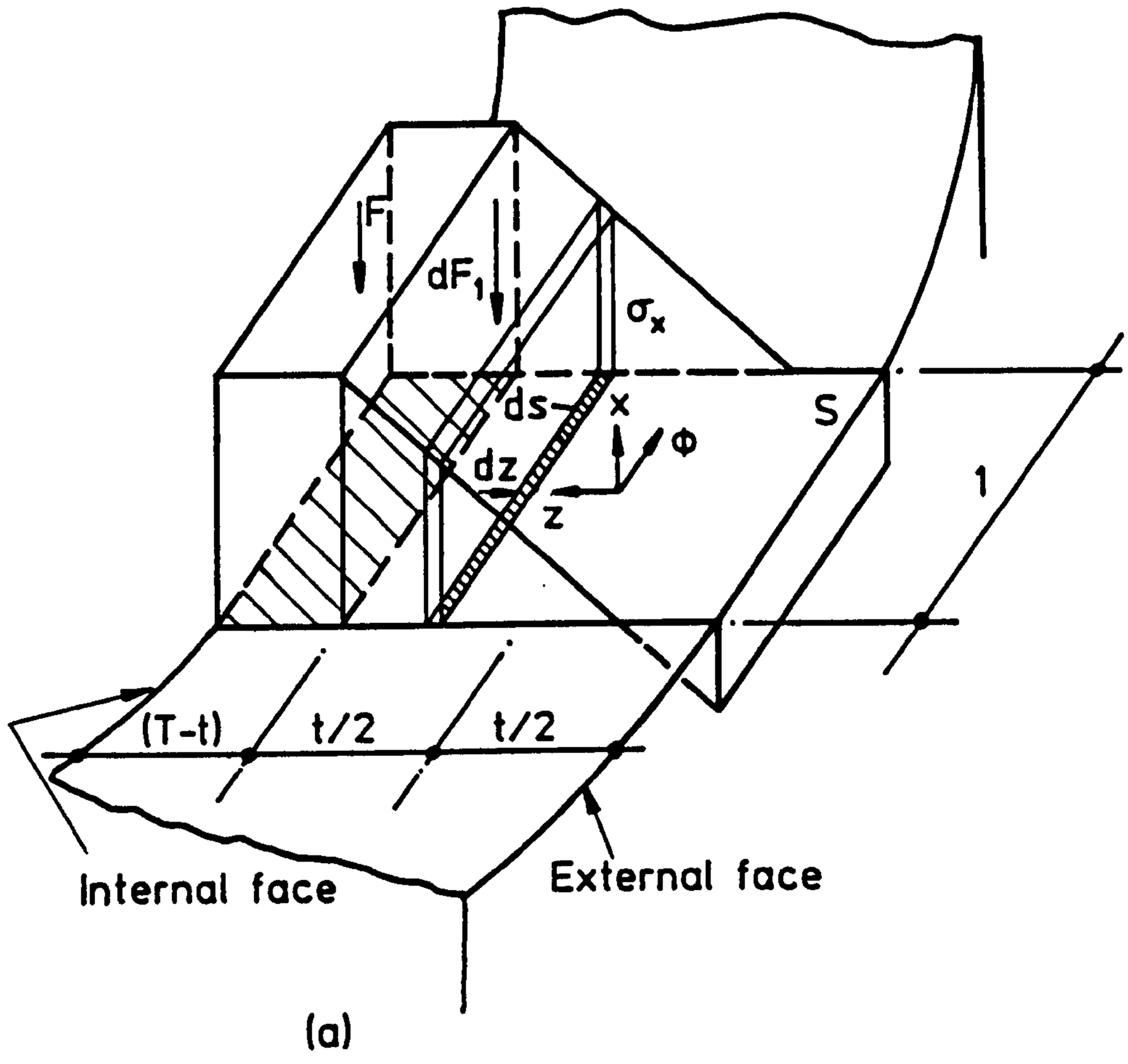

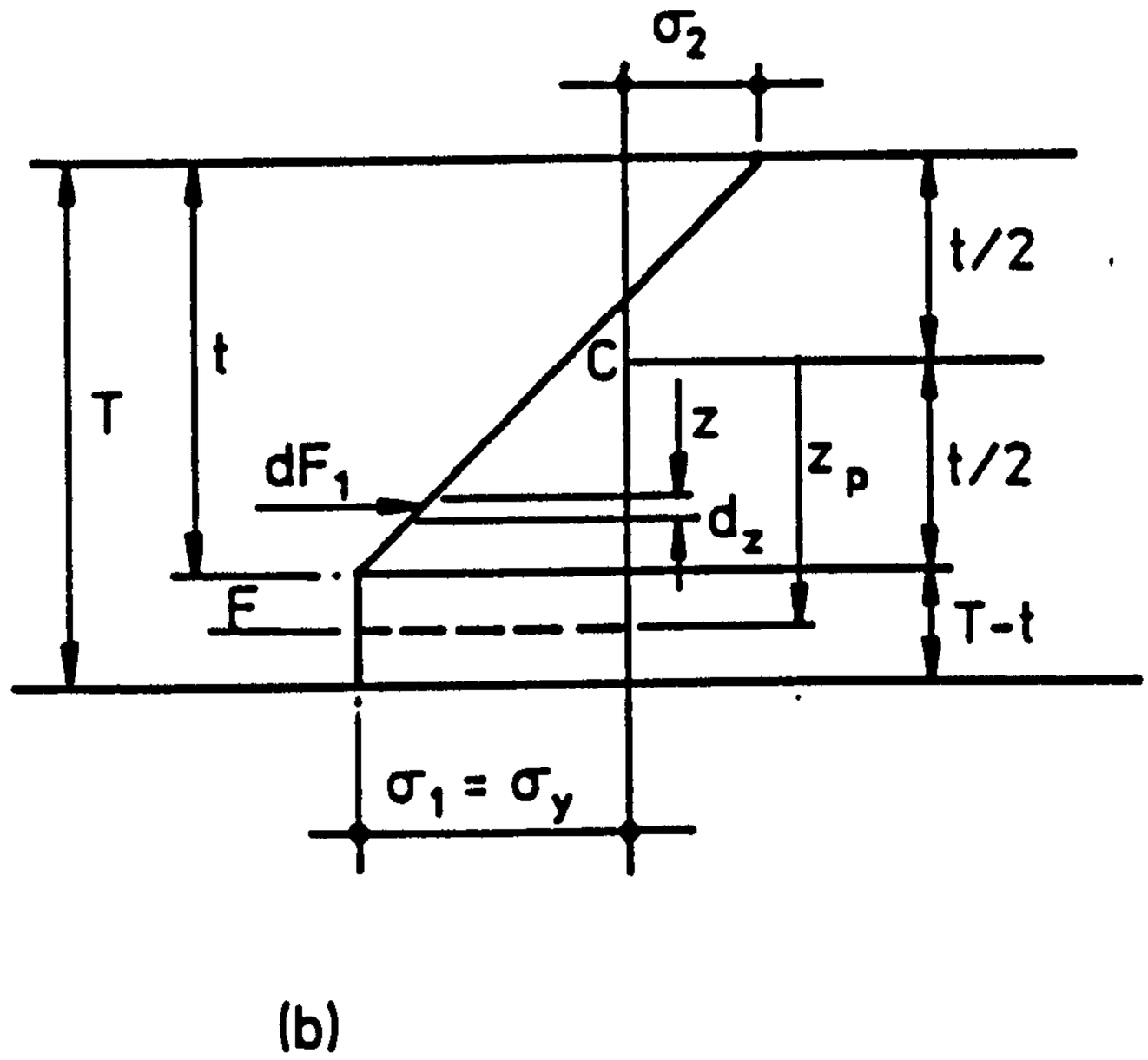

FIG A6 STRESS DISTRIBUTION FOR ELASTIC/PERFECTLY PLASTIC MATERIAL

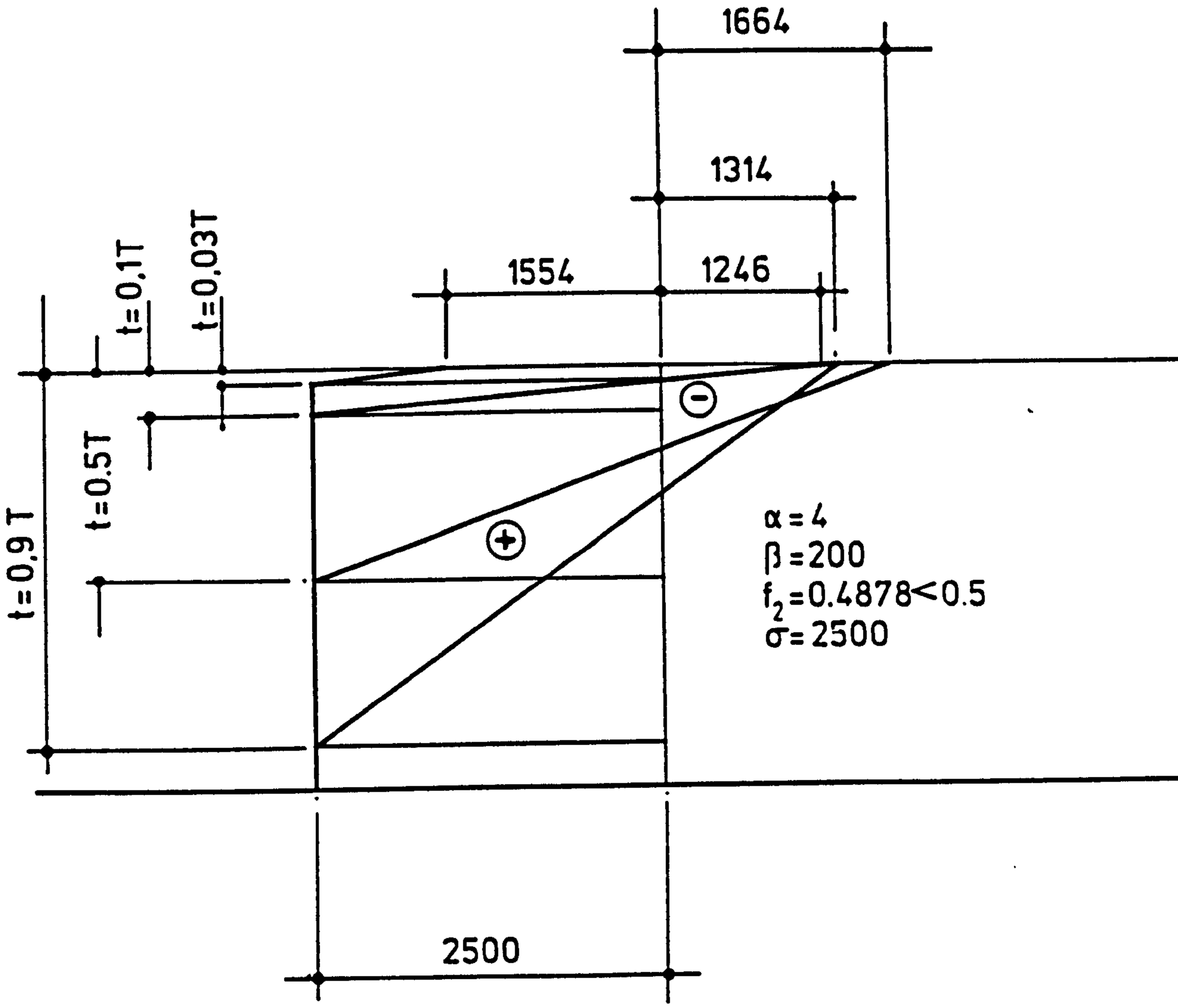

FIG. A7 STRESS DISTRIBUTION FOR $f_2 < 0.5$

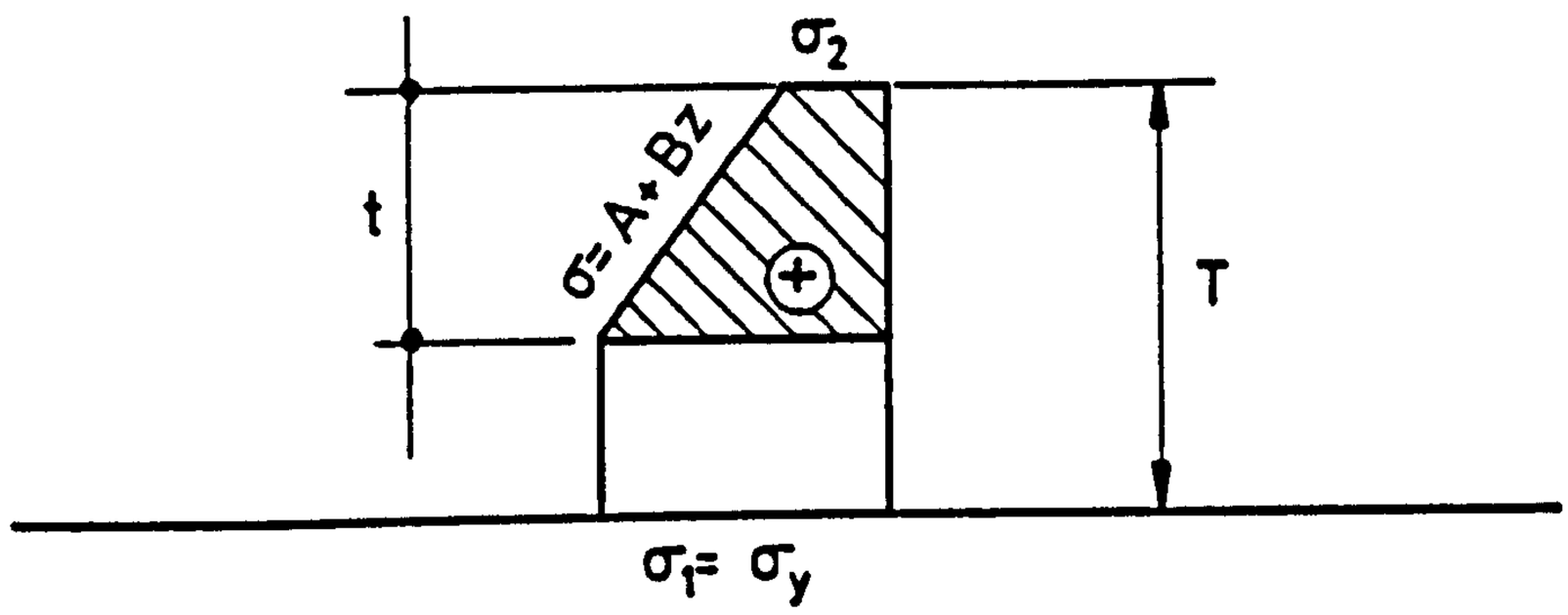

FIG. A8 STRESS DISTRIBUTION FOR $A > Bt/2$

APPENDIX B

DISPLACEMENT AND STRAIN FIELDS FOR AXI-SYMMETRIC SHELLS DISCRETIZED INTO FINITE ELEMENTS

The displacement field for an element i of such a type of structure will be described in terms of global displacements in the outward horizontal direction W(s) and in the downward vertical direction U(s) as shown in Fig. 6.3. Such global displacements are assumed to be interpolated by linear functions in terms of nodal values as

$$U(s) = U_i + \frac{s}{\ell_i}(U_{i+1} - U_i) \qquad \text{B1}$$

$$W(s) = \left(1 - \frac{s}{\ell_i}\right) W_i + \frac{s}{\ell} W_{i+1} \qquad \text{B2}$$

In a matrix form, the vectors representing the total displacement field and the rigid body translation may be respectively written as

$$\{u_e(s)\} = \begin{Bmatrix} U(s) \\ W(s) \end{Bmatrix}; \ \{U_o\} = \begin{Bmatrix} U_i \\ 0 \end{Bmatrix}. \qquad \text{B3}$$

The global displacement field can be written in a matrix form, in terms of a nodal values vector

$$\{U_o\} = \begin{Bmatrix} U_i \\ \\ 0 \end{Bmatrix}; \ \{U_n\} = \begin{Bmatrix} U_{i+1}-U_i \\ W_i \\ W_{i+1} \end{Bmatrix} \qquad \text{B4}$$

and a matrix of shape functions

$$[\Omega(s)] = \begin{bmatrix} \frac{s}{\ell_i} & 0 & 0 \\ 0 & \left(1 - \frac{s}{\ell_i}\right) & \frac{s}{\ell_i} \end{bmatrix} \qquad \text{B5}$$

as follows

$$\{U_e(s)\} = \begin{Bmatrix} U(s) \\ \\ W(s) \end{Bmatrix} = \begin{Bmatrix} U_i \\ \\ 0 \end{Bmatrix} + \begin{bmatrix} s/\ell_i & 0 & 0 \\ \\ 0 & (1-s/\ell_i) & s/\ell_i \end{bmatrix} \begin{Bmatrix} U_{i+1}-U_i \\ W_i \\ W_{i+1} \end{Bmatrix} \qquad \text{B6}$$

The local displacement field is obtained by simple transformation as

$$\{u_e^i(s,\phi)\} = [T]^i \ \{U_e^i(s)\} \qquad \text{B7}$$

where

$$\{u_e(s,\phi)\} = \begin{Bmatrix} u(s,\phi) \\ w(s,\phi) \end{Bmatrix} \qquad \text{B8}$$

which gives

$$\begin{Bmatrix} u(s,\phi) \\ \\ w(s,\phi) \end{Bmatrix} = \begin{Bmatrix} U_i \sin\phi \\ \\ -U_i \cos\phi \end{Bmatrix} + \begin{bmatrix} \frac{s}{\ell_i}\sin\phi & \left(1 - \frac{s}{\ell_i}\right)\cos\phi & \frac{s}{\ell_i}\cos\phi \\ \\ \frac{s}{\ell_i}\cos\phi & \left(1 - \frac{s}{\ell_i}\right)\sin\phi & \frac{s}{\ell_i}\sin\phi \end{bmatrix} \begin{Bmatrix} U_{i+1}-U_i \\ W_i \\ W_{i+1} \end{Bmatrix} . \qquad \text{B9}$$

In a matrix form it becomes

$$\{u_e(s)\} = \{u_o\} + [H(s)]\ \{U_n\} \qquad \text{B10}$$

The strain field is obtained from such a local displacement field, without the rigid body motion vector $\{u_o\}$, by means of (2.5) and as stated in Chapter 2, it will be defined only by the meridional and circumferential strains, with no curvature involved. In the case of thin shells of revolution, Equation (2.5) is given by, for example, Timoshenko and Krieger [77] which in terms of nodal values is

$$\{\varepsilon(s,\phi)\} = \begin{Bmatrix} \varepsilon_\phi(s,\phi) \\ \\ \varepsilon_\theta(s,\phi) \end{Bmatrix} = \begin{bmatrix} \frac{d}{ds} & \frac{1}{R_1} \\ \\ \frac{\cot\phi}{R_2} & \frac{1}{R_2} \end{bmatrix} [H]\ \{U_n\} \qquad \text{B11}$$

Matrix [B] in Equation (6.10) is defined as

$$[B] = \begin{bmatrix} \frac{d}{ds} & \frac{1}{R_1} \\ \\ \frac{\cot\phi}{R_2} & \frac{1}{R_2} \end{bmatrix} [H] \qquad \text{B12}$$

which gives rise to

$$[B] = \begin{bmatrix} \frac{\sin\phi}{\ell_i} & 0 & 0 \\ \\ 0 & \frac{1}{R_2}\left(1 - \frac{s}{\ell_i}\right)\frac{1}{\sin\phi} & \frac{1}{R_2}\frac{s}{\ell_i}\ \frac{1}{\sin\phi} \end{bmatrix} \qquad \text{B13}$$

when [H] is given by (B10).

APPENDIX C

AVERAGING THE NODAL CONSISTENT RELATIONSHIP BETWEEN THE GLOBAL DISPLACEMENTS W'S AND THE PLASTIC MULTIPLIERS λ'S

The consistent displacement formulation proposed in Chapter 6 gives rise to a relationship between nodal values of W's and λ's for each element. Consequently, two of such relationship for each node is produced since adjacent elements share one node as illustrated in Fig. C1. In order to obtain a single nodal relation and therefore a continuous displacement field, the average of the two equations corresponding to the adjacent elements was adopted.

From Equation (6.41) and Fig. C1 the consistent relationships for such adjacent elements can be written as

Element i-1

$$\begin{Bmatrix} U_i - U_{i-1} \\ W_{i-1} \\ W_i \end{Bmatrix} = \begin{bmatrix} L_{11}^{i-1} & L_{12}^{i-1} \cdots & L_{16}^{i-1} & L_{17}^{i-1} & L_{18}^{i-1} \cdots & L_{112}^{i-1} \\ L_{21}^{i-1} & L_{22}^{i-1} \cdots & L_{26}^{i-1} & L_{27}^{i-1} & L_{28}^{i-1} \cdots & L_{212}^{i-1} \\ L_{31}^{i-1} & L_{32}^{i-1} \cdots & L_{36}^{i-1} & L_{37}^{i-1} & L_{38}^{i-1} \cdots & L_{312}^{i-1} \end{bmatrix} \begin{Bmatrix} \lambda_1^{i-1} \\ \vdots \\ \lambda_6^{i-1} \\ \lambda_1^{i} \\ \vdots \\ \lambda_6^{i} \end{Bmatrix} \quad \text{C1}$$

Element i

$$\begin{Bmatrix} U_{i+1} - U_i \\ W_i \\ W_{i+1} \end{Bmatrix} = \begin{bmatrix} L^i_{11} & L^i_{12} \ldots L^i_{16} & L^i_{17} & L^i_{18} \ldots L^i_{112} \\ L^i_{21} & L^i_{22} \ldots L^i_{26} & L^i_{27} & L^i_{28} \ldots L^i_{212} \\ L^i_{31} & L^i_{32} \ldots L^i_{36} & L^i_{37} & L^i_{38} \ldots L^i_{312} \end{bmatrix} \begin{Bmatrix} \lambda^i_1 \\ \vdots \\ \lambda^i_6 \\ \lambda^{i+1}_1 \\ \vdots \\ \lambda^{i+1}_6 \end{Bmatrix} \qquad \text{C2}$$

A single general equation representing a single relationship between W's and λ's for a node i can thus be written from (C1) and (C2) as

$$W_i = \frac{1}{2} \left\{ \sum_{k=1}^{6} \left[L^{i-1}_{3k} \lambda^{i-1}_k + (L^{i-1}_{3k+6} + L^i_{2k}) \lambda^i_k + L^i_{2k+6} \lambda^{i+1}_k \right] \right\} \qquad \text{C3}$$

which involves plastic multipliers from three nodes i-1, i and i+1. In a matrix form such single relationships for all the nodes can be written as

$$\begin{Bmatrix} W_1 \\ \vdots \\ W_i \\ \vdots \\ W_N \end{Bmatrix} = \frac{1}{2} \begin{bmatrix} 0 \ \ldots & 0 & 2xL^1_{21} \ldots & 2xL^1_{26} & 2xL^1_{27} \ldots & 2xL^1_{212} \\ L^{i-1}_{31} \ldots & L^{i-1}_{36} (L^{i-1}_{37} + L^i_{21}) \ldots & & (L^{i-1}_{312} + L^i_{26}) & L^i_{27} \ldots & L^i_{212} \\ 2xL^{N-1}_{31} \ldots & 2xL^{N-1}_{36} & 2xL^{N-1}_{37} \ldots & 2xL^{N-1}_{312} & 0 \ \ldots & 0 \end{bmatrix} \begin{Bmatrix} \lambda^{i-1}_1 \\ \vdots \\ \lambda^{i-1}_6 \\ \lambda^i_1 \\ \vdots \\ \lambda^i_6 \\ \lambda^{i+1}_1 \\ \vdots \\ \lambda^{i+1}_6 \end{Bmatrix} \qquad \text{C4}$$

or

$$\begin{Bmatrix} W_1 \\ \vdots \\ W_i \\ \vdots \\ W_N \end{Bmatrix} = \begin{bmatrix} L_W^{1\,1} & \cdots & L_W^{1\,18} \\ \vdots & & \\ L_W^{i\,1} & \cdots & L_W^{i\,18} \\ \vdots & & \vdots \\ L_W^{N\,1} & & L_W^{N\,18} \end{bmatrix} \begin{Bmatrix} \lambda_1^{i-1} \\ \vdots \\ \lambda_6^{i-1} \\ \lambda_1^{i} \\ \vdots \\ \lambda_6^{i} \\ \lambda_1^{i+1} \\ \vdots \\ \lambda_6^{i+1} \end{Bmatrix} \qquad \text{C5}$$

Thus

$$\{W_i\} = [L_W^i] \begin{Bmatrix} \lambda_k^{i-1} \\ \lambda_k^{i} \\ \lambda_k^{i+1} \end{Bmatrix} \quad \text{for } k = 1,6 \qquad \text{C6}$$

FIG. C1 GENERIC ADJACENT ELEMENTS SHARING NODE i

APPENDIX D

THE GENERAL CONSTRAINT EQUATION AND THE COST FUNCTION IN TERMS OF PLASTIC MULTIPLIERS

The General Constraint Equation

Equation (6.64), representing the external work due to the internal pressure, can be rearranged in terms of nodal contributions as shown below

$$W_E = 2\pi p \left\{ \sum_{i=1}^{NE} [IFWUI(i)U_i + IFWU(i)](U_{i+1}-U_i) + \sum_{i=1}^{NN} [IFWIP1(i-1) + IFWI(i)]W_i \right\} \qquad D1$$

Such an equation needs to be introduced to the Linear Programming, as a general constraint equation, in terms of plastic multipliers, according to condition (6.41) assumed in Chapter (6). The nodal displacement components (U_{i+1} - U_i) and W_i appearing in (D1) may be directly substituted in terms of plastic multipliers by means of (C2) in Appendix C. The nodal axial displacement U_i, however, is given by the end conditions and the first line of matrix (C2) in Appendix C for any node i as follows:

Node		Node	
1	$U_2-U_1 = f_1(\lambda)$	i	$U_{i+1}-U_i = f_i(\lambda)$
2	$U_3-U_2 = f_2(\lambda)$	i+1	$U_{i+2}-U_{i+1} = f_{i+1}(\lambda)$
.	. . .	.	. . .
.	. . .	.	. . .
.	. . .	.	. . .
i-1	$U_i-U_{i-1} = f_{i-1}(\lambda)$	N-1	$U_N-U_{N-1} = f_{N-1}(\lambda)$

$$\sum_{i=1}^{i-1}(U_{i+1}-U_i) = U_i-U_1 = \sum_{k=1}^{i-1} f_k(\lambda) \qquad \sum_{i=i}^{N-1}(U_{i+1}-U_i) = U_N-U_i = \sum_{k=i}^{N-1} f_k$$

for U_1 prescribed for U_N prescribed

D2 D3

If Equation (D3) is adopted, the axial displacements U_i's can then be written in terms of λ's by means of matrix (6.41) as

$$U_i = -\sum_{i=i}^{N} [L^{i-1}_{1k+6}+L^{i}_{1k}]\{\lambda^i_k\} \quad \text{for } k = 1,6 \qquad \text{D4}$$

The general constraint Equation (D1) is then given by the contribution of the three displacement components U_i, U_{i+1} - U_i and W_i, which are all functions of nodal λ's.

The Cost Function

In Chapter 6, the cost function for a particular element i and a yield stress independent of the temperature was given by Equation (6.60) to be integrated over the hinge and element volumes.

where I2 is given by

$$I_2 = \sum_{k=1}^{6} \int_{V_{Hinge}} \left[\sigma_{ij}^{c} - \hat{\sigma}_{ij}^{\theta}(t_k) \right] d\varepsilon_{ij}(t_k) dV \qquad \text{D5}$$

and will be discussed later in this Appendix. Assuming the Tresca yield condition (Fig. 6.4) and that $\lambda_k(s)$ may be interpolated in terms of nodal values

$$\lambda^{i}(s) = \left(1 - \frac{s}{\ell_i}\right) \lambda_k^{i} + \frac{s}{\ell_i} \lambda_k^{i+1} \quad \text{for } k = 1,6 \qquad \text{D6}$$

the integral over the element volume for a particular $\lambda_k(s)$ may be written

$$\int_V \left[\sigma_{ij}^{c} - \hat{\sigma}_{ij}^{\theta}(t_k) \right] \{N_{ij}\}_k \{\lambda_k^{i}(s)\} dV =$$

$$2\pi \left\{ \int_{-h/2}^{h/2} \left[\sigma_{ij}^{c} - \hat{\sigma}_{ij}^{\theta}(t_k) \right] dy \{N_{ij}\}_k \left[\int_{o}^{\ell_i} r(s) \left(1 - \frac{s}{\ell_i}\right) \lambda_k^{i} ds + \int_{o}^{\ell_i} r(s) \frac{s}{\ell_i} \lambda_k^{i+1} ds \right] \right\} \qquad \text{D7}$$

where $dV = 2\pi r(s) dy ds$.

The integral I1 of the cost function for an element i becomes thus,

$$I_1 = 2\pi \sum_{k=1}^{6} \left\{ \int_{-h/2}^{h/2} \left[\sigma_{ij}^{c} - \hat{\sigma}_{ij}^{\theta}(t_k) \right] dy \{N_{ij}\}_k \left[F_1 \lambda_k^{i} + F_2 \lambda_k^{i+1} \right] \right\} \qquad \text{D8}$$

where

$$F_1 = \int_{o}^{\ell_i} r(s) \left(1 - \frac{s}{\ell_i}\right) ds \qquad \text{D9}$$

$$F_2 = \int_0^{\ell_i} r(s) \frac{s}{\ell_i} ds \qquad \text{D10}$$

When the assemblage of the elements is performed the total integral becomes the sum of the contribution of each individual element to give

$$TI_1 = 2\pi \sum_{i=1}^{NE} \sum_{k=1}^{6} \left\{ \int_{-h/2}^{h/2} \left[\sigma_{ij}^c - \hat{\sigma}_{ij}^\theta(t_k)\right] dy \{N_{ij}\}_k \left[F_1^i \lambda_k^i + F_2^i \lambda_k^{i+1}\right] \right\} \qquad \text{D11}$$

which in terms of nodal contributions becomes

$$TI_1 = 2\pi \sum_{i=1}^{NN} \sum_{k=1}^{6} \left\{ \int_{-h/2}^{h/2} \left[\sigma_{ij}^c - \hat{\sigma}_{ij}^\theta(t_k)\right] dy \{N_{ij}\}_k \left[F_1^{i-1} + F_2^i\right]_k \lambda_k^i \right\} \qquad \text{D12}$$

The second integral I2 in (6.60) is performed over the volume of a hinge and perhaps can be described as the difference between the energy dissipation during the formation of such a hinge and the external work produced by the thermal stresses due to the hinge rotation. For an axi-symmetric shell I2 can be split in two parts to give

$$I_2 = \int_V \left[\sigma_\phi^c - \hat{\sigma}^\theta(t_k)\right] d\varepsilon dV + \int_V \left[\sigma_\partial^c - \hat{\sigma}^\theta(t_k)\right] d\varepsilon_\theta dV \qquad \text{D13}$$

where $dV = 2\pi r_i ds dy$.

Let Fig. 6.8 represent a nodal hinge circle for an axi-symmetric shell, at the intersection of two generic elements. Details of such a hinge is shown in Fig. D1. For small values of the angle Θ_i, $ds = r_c\ \Theta i$. It may be seen from Fig. D1 that the length of the fibres at nodal points, initially the same as the neutral line, has varied linearly

with the formation of the hinge. It can also be seen that the layers above the neutral line are in compression whilst those below it are in tension. Considering a general fibre at a distance y from the neutral line (Fig. D1), the meridional strain may be determined by

$$d\varepsilon_\phi = \frac{(ds+\Delta ds) - ds}{ds} \qquad \text{D14}$$

where $ds + \Delta ds = (r_c + y)\theta_i$. Thus,

$$d\varepsilon_\phi = \frac{(r_c+y)\theta_i - r_c\theta_i}{r_c\ \theta_i} \qquad \text{D15}$$

or

$$d\varepsilon_\phi = \frac{y}{r_c} = \frac{y\theta_i}{ds} \qquad \text{D16}$$

The uniform circumferential strain is given by

$$d\varepsilon_\theta = W_i/r_i \qquad \text{D17}$$

Equation (D13) may now be written as

$$I_2 = 2\pi r_i \left\{ \int_{-h/2}^{h/2} \left[\sigma_\phi^c - \hat{\sigma}_\phi^\theta(t_k)\right] \frac{y\theta_i}{ds}\, ds dy + ds \int_{-h/2}^{h/2} \left[\sigma_\theta^c - \hat{\sigma}_\theta^\theta(t_k)\right] d\varepsilon_\theta dy \right\} \qquad \text{D18}$$

Assuming ds as very small the second term on the right hand side can be neglected. Thus

$$I_2 = 2\pi r_i \left\{ \int_{-h/2}^{h/2} \left[\sigma_\phi^c - \hat{\sigma}_\phi^\theta(t_k)\right] y\theta_i dy \right\} \qquad \text{D19}$$

Note that when the thermal stress is zero, (D19) becomes identical to the term representing the energy dissipation during the formation of a hinge for $\sigma_\phi^c = \sigma_y$, ie,

$$I_2 = 2\pi r_i \sigma_y \frac{h^2}{4} \theta_i \qquad \text{D20}$$

(6.60)

The cost function, Equation ( ), may now be written as

$$I = 2\pi \sum_{i=1}^{NN} \sum_{k=1}^{6} \left\{ \int_{-h/2}^{h/2} \left[\sigma_{ij}^c - \hat{\sigma}_{ij}^\theta(t_k)\right] dy \{N_{ij}\}_k \, A_k \lambda_k^i + r_i \int_{-h/2}^{h/2} \left[\sigma_\phi^c - \hat{\sigma}_\phi^\theta(t_k)\right] y dy \theta_i \right\} \qquad \text{D21}$$

where

$$A_k = [F_1^{i-1} + F_2^i]_k \qquad \text{D22}$$

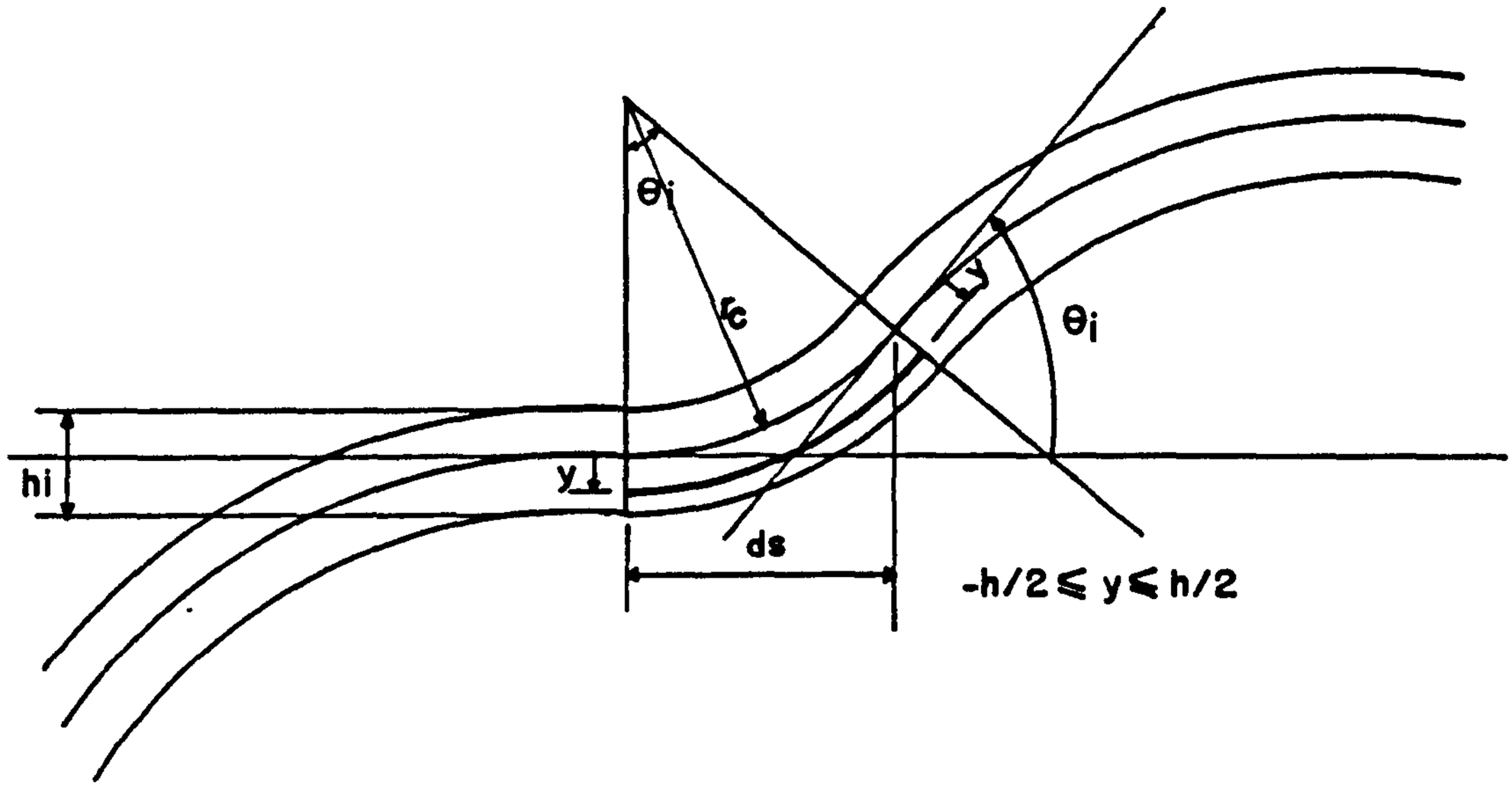

Fig. D1 - HINGE CIRCLE

APPENDIX E

GOVERNING EQUATIONS FOR THE DIFFERENT MODES OF BEHAVIOUR OF PORTAL FRAMES AT 400°C SUBJECTED TO SIMULATED THERMAL CYCLIC LOADING AND CONSTANT MECHANICAL LOAD

Before determining the required equations some definitions must be made which will be used through the whole set of calculations. These definitions are the following:

a) Moment Required to Form a Plastic Hinge(M_L)

The definition of a plastic hinge is easily available in the literature [13,14,15,16] within the classical theory of plasticity and associated with it there is the definition of plastic moment which will be widely used in this section. Stress distributions for both perfectly plastic and isotropic material models on a retangular cross section are illustrated by Figs. E1a,b,c and Figs. E2a,b,c. The definition of the plastic moment for the isotropic hardening model is the moment which yields a stress distribution diagram of equal area as that corresponding to the plastic moment of a perfectly plastic material model.

The value of the plastic moment is then

$$M_L = \frac{\sigma_y b t^2}{4} \qquad \text{E1}$$

b) The Collapse Mechanical Load

The collapse mechanical load will be assumed as the load necessary to produce plastic hinges at the nodes B,C and D of the portal frame. The collapse mechanism is shown in Fig. E3.

The collapse load is then given by $P_L = 3*M_L/L$

c) The Magnitude of δ to Form a Plastic Hinge

The expressions for the elastic moments due to the cyclic load in Table (5.1) show that the maximum moment occurs at node B where the first plastic hinge will form. When that happens the moment at node B will be equal to the plastic moment previously defined which as function of P_L is given by $M_L = P_L L/3$. Equating the value of M_L in terms of P_L to the expression obtained from Table (5.1) for the elastic moment at node B, gives:

$$\frac{LP_L}{3} = \frac{12}{11}\frac{EI}{\ell^2}\delta_L \qquad \text{E2}$$

Hence,

$$\delta_L = \frac{11}{36} \frac{\ell^3}{EI} P_L \qquad \text{E3}$$

With these values defined one can now start the determination of the governing equations for the different modes of response of the structure corresponding to the different regions shown in Fig. 5.17.

Fully Elastic Behaviour(Region E in Fig. 5.17)

The elastic boundary is defined by two bounds which depend on the combination of the loads. The bending moment receives contributions from both the mechanical and cyclic thermal loads. For the structure to behave elastically the stress due to the total bending moment needs to be, at the most, equal to the yield stress of the material at any time of the cycle. The equality will provide bounds beyond which some sort of plasticity will occur in the structure. The bounds which will confine the elastic region are defined by two modes of behaviour at the limit of elasticity.

- limit of elasticity is reached at node B where the moment due to the cyclic thermal load prevails upon the moment due to the mechanical load

- limit of elasticity is reached at node D where a high mechanical load imposes a reverse situation

The general condition for the elastic behaviour of a structure with rectangular cross section subjected to

bending moments is

$$\sigma = \frac{6M_i}{bt^2} \lesssim \sigma_y \qquad \text{E4}$$

where σ_y is the yield stress, M_i is the bending moment at a generic cross section i. Then,

$$\frac{3M_i}{2} \lesssim \frac{\sigma_y bt^2}{4} = M_L \qquad \text{E5}$$

If the elastic limit is reached at node B the first elastic bound can be determined by substituting into Equation (E5) the expressions for the moment at node B due to the mechanical and cyclic loads obtained from Table (5.1). This bound in terms of non-dimensional quantities is given by

$$\frac{15}{22}\frac{P}{P_L} + \frac{\delta}{\delta_L} = \frac{2}{3} \qquad \text{E6}$$

The second bound is obtained likewise by assuming similar conditions at node D to give

$$\frac{15}{11}\frac{P}{P_L} + \frac{3}{4}\frac{\delta}{\delta_L} = \frac{2}{3} \qquad \text{E7}$$

These two bounds constitute the boundary for a fully elastic response of the portal frame.

<u>Elastic Shakedown Region(Region S in Fig. 5.17)</u>

Any operating point outside this boundary and inside the shakedown region S will still lead the structure to a fully

elastic behaviour after the accumulation of some transient plastic deformation during the first few cycles. Different operating points in the shakedown region will only produce yielding in different parts of the portal frame. The boundary for this region is the one used in present design codes which is obtained by the strict use of the shakedown concept. The boundary, in fact, is composed of two bounds; one separating the shakedown region S from the reversed plasticity region F and the other separating it from the ratchetting region R. The shakedown/reversed plasticity bound is defined by value of the cyclic thermal load necessary to form a hinge at node B, ie $\delta_A/\delta_L = 1$. The S/R bound will be obtained by applying the upper bound shakedown theorem (Equation 2.50) to an incremental mechanism consisting of plastic hinges at nodes B,C and D, likewise the collapse mechanism shown in Fig. E3. The upper bound theorem will then give :

$$3 M_L \theta = P.L.\theta + |M_B||\theta| + |M_C||\theta| + |M_D||\theta| \qquad \text{E8}$$

From Table (5.1) the expressions for the moments can be substituted into (E8) to give

$$3M_L = P.L + \frac{24}{11}\frac{EI}{\ell^2}\delta_A \qquad \text{E9}$$

which in terms of non-dimensional parameters becomes:

$$1 = \frac{P}{P_L} = \frac{2}{3}\frac{\delta}{\delta_L} \qquad \text{E10}$$

These two bounds can now be plotted on a Bree type diagram

in terms of the non-dimensional parameter to define the classical shakedown boundary currently used for designing structures under such conditions of mechanical and cyclic thermal loading.

Reversed Plasticity(Region F in Fig. 5.17)

The region of reversed plasticity F will be defined by a safe estimate of bounds which separate a state of zero strain growth of the structure under complete reversed loading and that state of incremental growth when the structure operates in ratchetting region R. For a safe prediction of the boundary between the F and R cyclic hardening must be taken into account and the extended upper bound theorem proposed by Ponter and Karadeniz [36,37] will be used for its determination. In the case of the portal frame under analysis here, the moment at any section of the structure when the operating point is outside the elastic region, is given by:

$$M^* = M_p + M_\delta + M_R \qquad \text{E11}$$

where M_p and M_δ are the elastic solutions in Table (5.1). For any operating point in the region of reversed plasticity F, the moment due to δ_A will be greater than M_L at some part of the structure. Assuming that wherever it occurs that region will behave as a plastic hinge and that

$$M_p + M_R = 0 \qquad \text{E12}$$

give^{s} rise to $M_\delta = M_L$ in V_F (hinge) and the application of the extended upper bound theorem becomes restricted to the remainder of the structure (V_s). Hence, Equation (E10) is valid until the plastic moment M_L is exceeded somewhere in the frame. This first occurs at node B for $\delta_A/\delta_L = 1$ which taken into Equation (E10) gives

$$\frac{P}{P_L} = \frac{1}{3} \qquad \text{E13}$$

Applying the extended upper bound theorem to the remainder of the structure (Fig. 5.9) and assuming an incremental collapse mechanism as shown in Fig. E4 with no contribution from node B to the energy dissipation gives:

$$2M_L\theta = P.L.\theta + |M_C||\theta| + M_D|\theta| \qquad \text{E14}$$

and hence

$$1 = \frac{3}{2}\frac{P}{P_L} + \frac{1}{2}\frac{\delta}{\delta_L} \qquad \text{E15}$$

Similarly, Equation (E16) will be valid until the plastic moment M_L is reached again somewhere else in the structure. The way the frame actually behaves with the increase of load is by having the plastic hinge spreading along the bars AB or BC from node B and M_L will therefore be exceeded first in the cross sections adjacent to it. It is still a reasonable approximation to assume that this will occur next, at node D instead. The moment at node D due to the cyclic load will be equal to the plastic moment for

$$\frac{\delta}{\delta_L} = \frac{4}{3} \qquad \text{E16}$$

which subtituting into (E16) gives $P/P_L = 2/9$. The extended upper bound theorem can again be applied to the remainder of the structure (Fig. 5.10) with its corresponding incremental mechanism shown in Fig. E5 where no contribution to the work is given by nodes B and D. The new bound is given by:

$$M_L\theta = P.L.\theta + |M_C||\theta| \qquad \text{E17}$$

and hence

$$1 = 3\frac{P}{P_L} + \frac{1}{4}\frac{\delta}{\delta_L} \qquad \text{E18}$$

completing though the boundaries in the Bree type diagram which separate the several regions of different modes of behaviour of the portal frame.

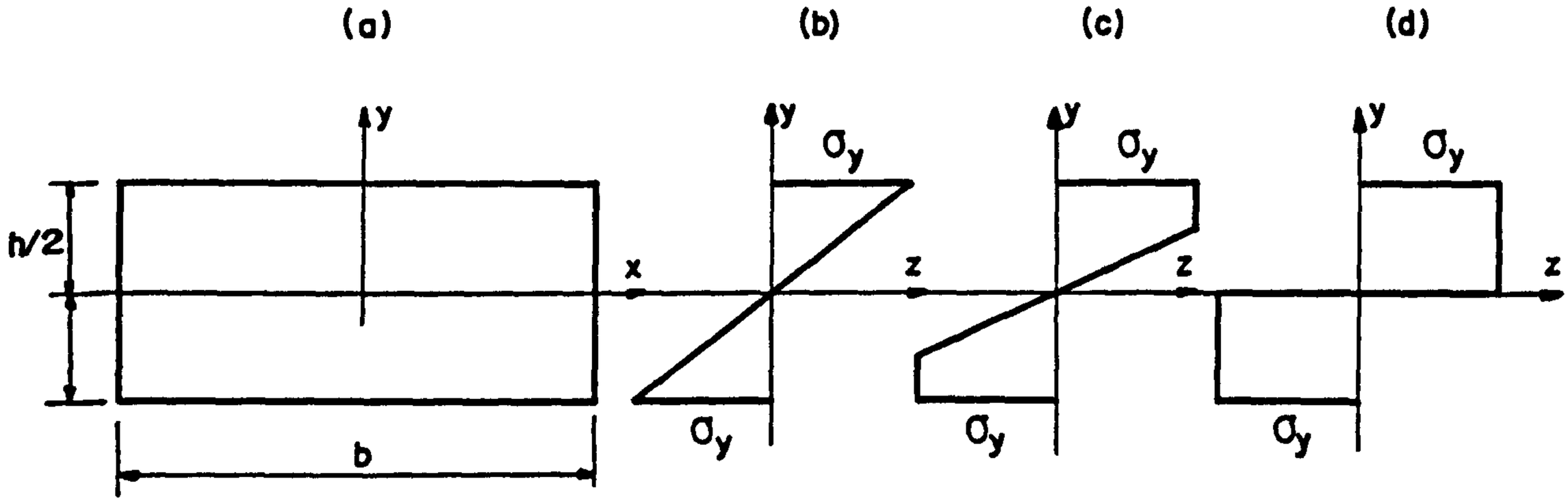

FIG: E1 - STRESS DISTRIBUTION (Perfectly Plastic Material Model)
(a) CROSS SECTION (b) AT LIMIT OF ELASTICITY
(c) HINGE IN FORMATION (d) AT PLASTIC MOMENT (Hinge Formed)

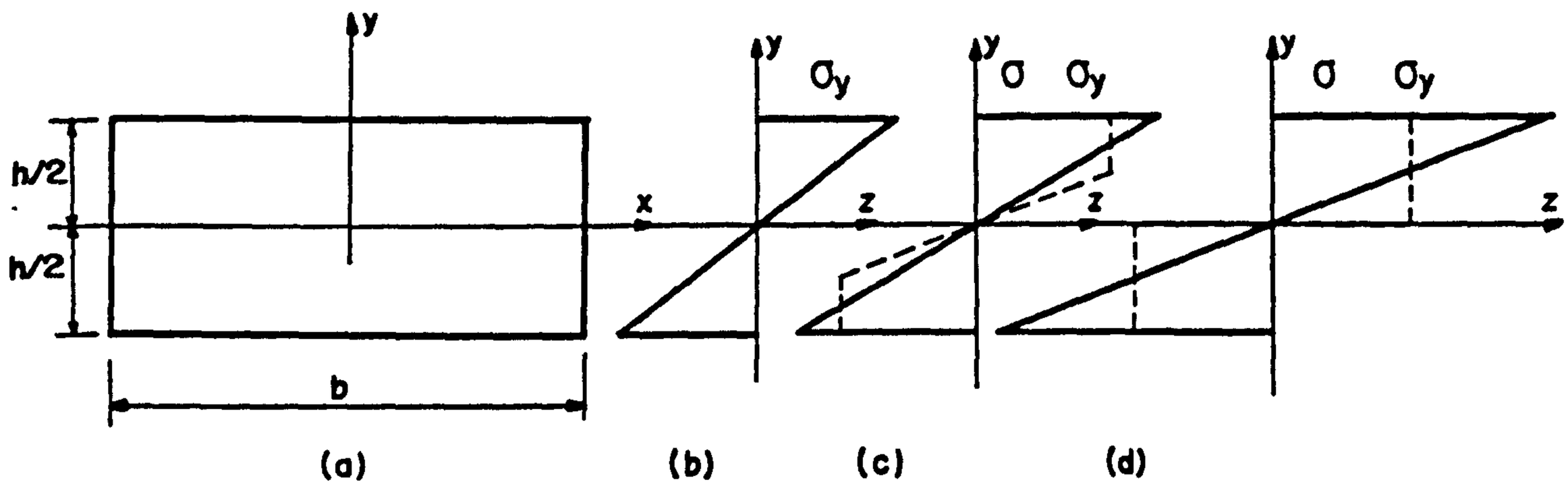

FIG. E2 - STRESS DISTRIBUTION (Isotropic Hardening Model)
(a) CROSS SECTION (b) AT LIMIT OF ELASTICITY)
(c) HINGE IN FORMATION (d) AT PLASTIC MOMENT (Hinge Formed)

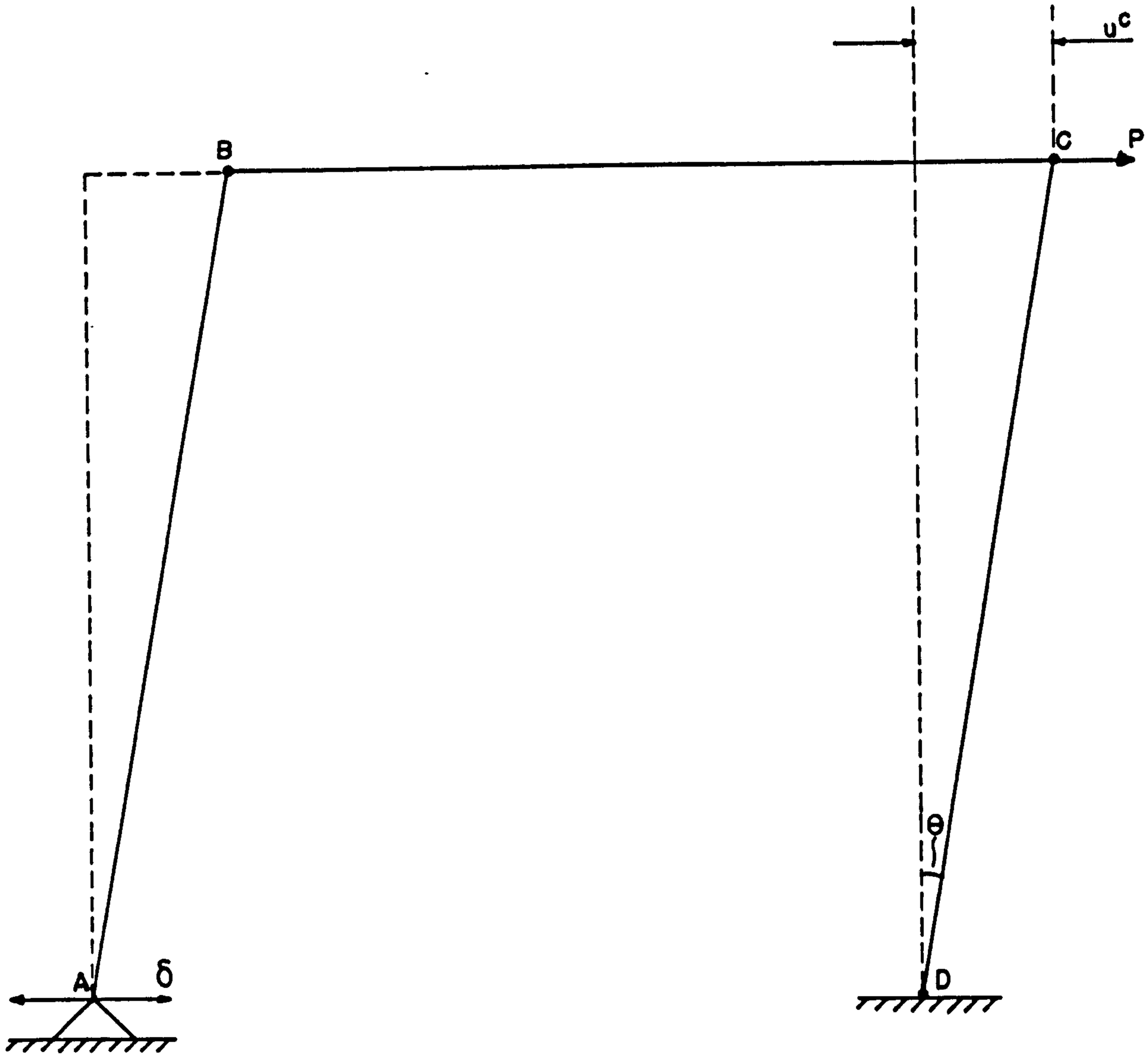

FIG.E3 COLLAPSE MECHANISM

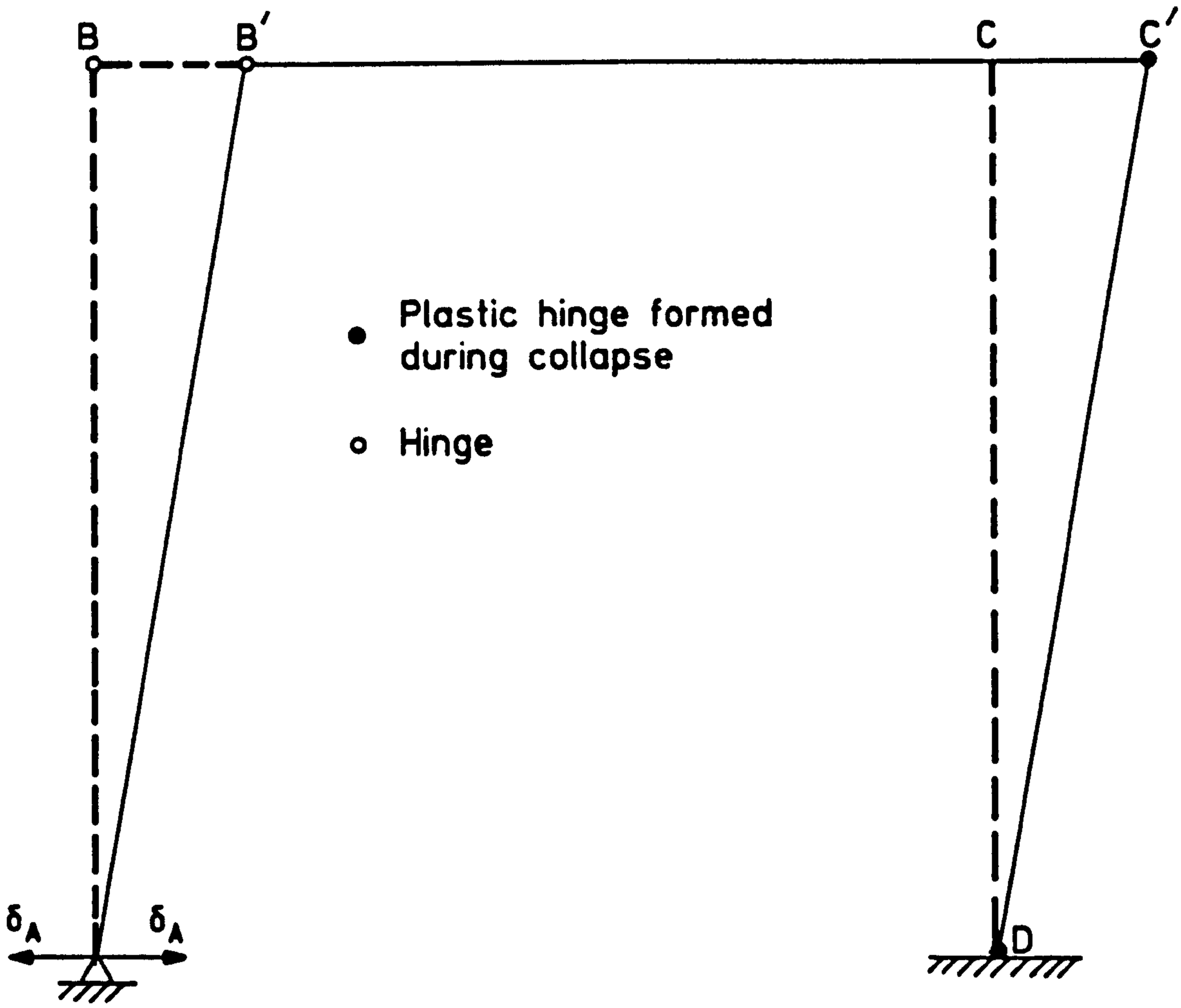

FIG. E4 INCREMENTAL COLLAPSE MECHANISM FOR THE REMAINDER OF THE PORTAL FRAME AFTER THE FORMATION OF A HINGE AT NODE B

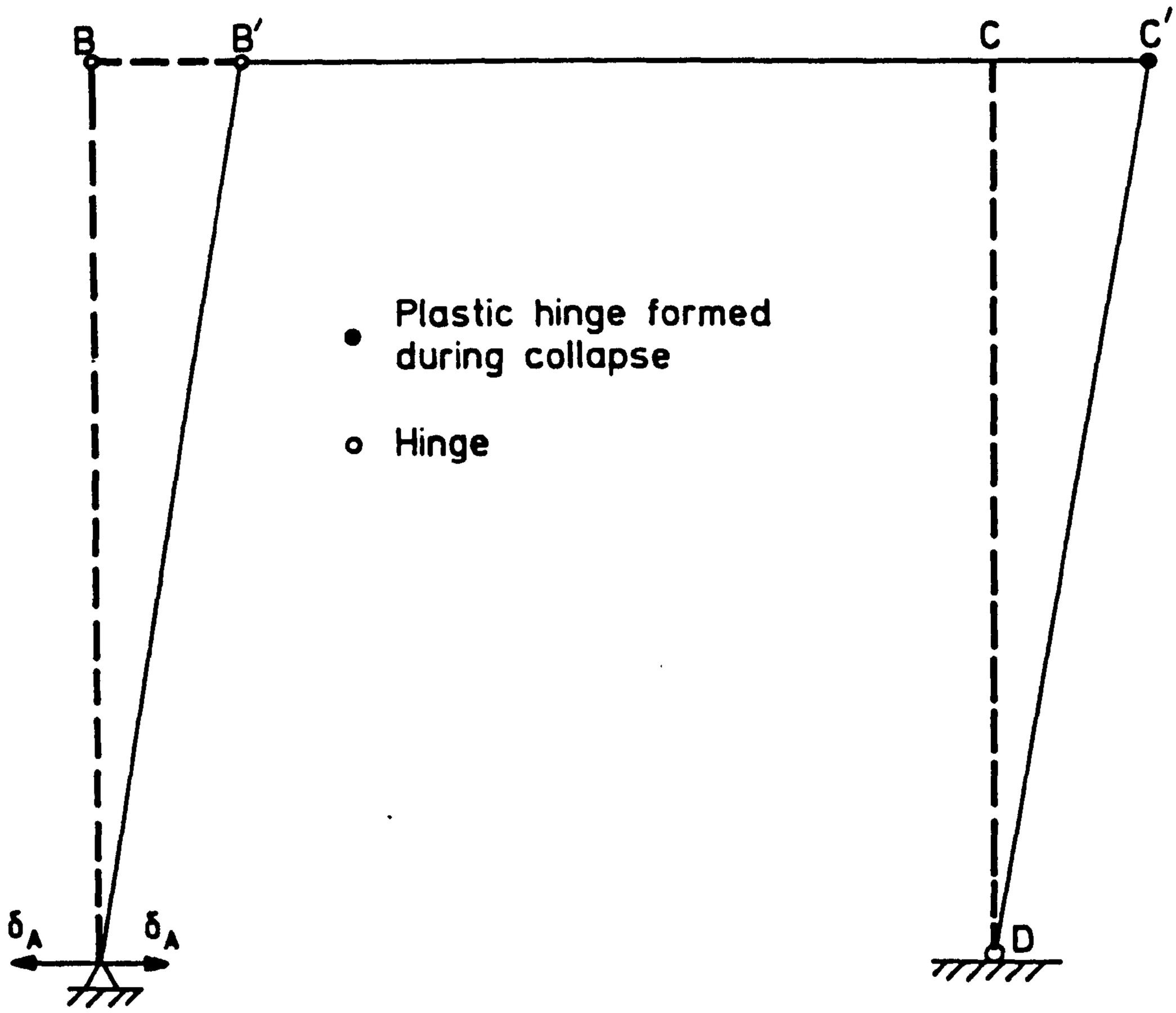

FIG. E5 INCREMENTAL COLLAPSE MECHANISM FOR THE REMAINDER OF THE PORTAL FRAME AFTER THE FORMATION OF HINGES AT NODES B AND D

R E F E R E N C E S

1. Gruning, M. "Die Tragfahigkeit statisch unbestimmter Tragwerke aus Stahl bei beliebig haufig wiederholter Belastung", Julius Springer,Berlin, 1926.

2. Rose, R.T. "New Design Method for Pressure Vessel Nozzle", The Engineer, July 1962 no. 20

3. Leckie, F.A. and Penny, R.K. "Stress Concentration Factors for the Stresses at Nozzle Intersections in Pressure Vessels", Welding Research Council Bulletin No. 90, September 1963.

4. Leckie, F.A. "Shakedown Pressures for Flush Cylinder-Sphere Shell Intersections", J. Mech. Engr. Sci. Vol. 7 no. 4, 1965.

5. Leckie, F.A. "Shakedown Loads for Radial Nozzles in Spherical Pressure Vessels", Int. J. Solids Structures Vol. 3, 1967.

6. Leckie, F.A. and Payne, D.J. " Some Observations on the design of Spherical Pressure Vessels with Flush Cylindrical Nozzles", Proc. Instr. Mech. Engrs., 1965-66.

7. Findlay, G.E. and Spence, J. "Applying the Shakedown Concept to Pressure Vessel Design", The Engineer, 1968, 12 July.

8. Leckie, F.A. and Penny, R.K. "Shakedown as a Guide to the Design of Pressure Vessels", Journal of Engineering Industry, Paper No. 68, Transation of the ASME, 1969.

9. Robinson, M. "Some Comments on the Stress Concentration and Shakedown Factors for Spherical Pressure Vessels with Flush Radial Cylindrical Nozzles", J. Mech. Eng. Science, Vol. 21, No. 3, 1979.

10. Armstrong, P.J. and Townley, C.H.A. "Shaded/own Experiments on a T-Section Beam", CEGB Report RD/B/N907, 1987.

11. Procter, E. and Flinders, R.F. "Experimental Investigation into Elastic/Plastic Behaviour of Isolated Nozzles in Spherical Shells", Part II, "Shakedown and Plastic Analysis", CEGB Report RD/B/N.861, 1967.

12. Findlay, G.E., Moffat, D.G. and Stanley, P. "Torispherical Drumheads: A Limit Pressure and Shakedown Investigation", J. Strain Analysis, Vol. 6, No. 3, 1971.

13. Leckie, F.A. "A Review of Bounding Techniques in Shakedown and Ratcheting at Elevated Temperature", WRC Bulletin, No. 195, June 1974.

14. Ponter, A.R.S. "Shakedown and Ratcheting Below the Creep Range", Part I,II Department of Engineering, University of Leicester, May 1981.

15. Saint-Venant, B. "Memoire sur l'Etablissement des Equations Differentielles des Mouvements Interieurs Operes dans les Corps Solides ductiles au dela des Limites ou l'Elasticite Pourrait les Ramener a leur Premier Etat", Compt. Rend, 70, 1870, pp. 473-480.

16. Levy, M. "Memoire sur les Equations Generales des Mouvements Interieurs des Corps Solides Ductile au dela Limites ou l'Elasticite Pourrait les Ramener a leur Premier Etat", Compt. Rend., 70, 1870, pp. 1323-1325.

17. von Mises, R. "Mechanik der Festen Koerper in Plastisch Deformablem Zustand", Goettinger Nachr. Math. Phys., Kl. 1913,pp.582,592.

18. Prantl. L. "Spannungsverteilung in plastischen Koerpern", Proceedings of the 1st International Congress on Applied Mechanics, Delft, TYechnische Boekhandel en Druckerij, J,Waltman, Jr., 1925,pp.43-54.

19. Reuss, E. "Beruecksichtigung der elastischen Formaenderungen in der Plastizitaetstheorie",Z. Angew. Math.Mech., 10, 1930, pp. 266-274.

20. Drucker, D.C. "Some Implications of Work Hardening and Ideal Plasticity", Quart. Appl. Math., 7, 1950, pp. 411-418.

21. Drucker, D.C. "A More Fundamental Approch to Plastic Stress-Strain Relations", 1st U.S. Congress of Applied Mechanics, ASME, New York, 1952, pp - 487-491.

22. Drucker, D.C. "Extension of the Stability Postulate with Emphasis on Temperature Changes", Proc. of the Second Symposium on Naval Structural Mechanics: Pergamon Press, 1960, pp. 170-184.

23. Mendelson, A. "Theory of Plasticity", The MacMillan Company, New York, 1968.

24. Melan, E. "Theorie Statich Unbestimmter Systeme aus Idealplastischen Baustoff", Sitzungsberiche der Akademie der Wissenshaften, Wien, Abt IIa, Vol. 145, 1936,pp. 195-218.

25. Melan, E. "Der Spannungszustand Eines Mises-Henckey'schen Kontinuums bei veranderlicher Belastung", Sitzingsberd. Akad. d. Wiss., abt. IIa, Vol. 147, 1938, pp. 73-87.

26. Melan, E. "Zur Plastizitat des Raumlichen Kontinuums", Ingeniuer-Archiv, Vol. 9, 1938, pp. 116-126.

27. Symmonds, P.S. "Shakedown in Continuous Media", J. Appl. Mech., Vol. 18, 1951, pp. 85-89.

28. Koiter, W.T. "General Theorems for Elastic-Plastic Solids", Progress in Solid Mechanics, Ed. by Hill, R. and Sneddon, I., 2nd Edition, North Holland Publishing Com., Amsterdam, Vol. 2, 1964, pp.167-219.,

29. Koiter, W.T. "A New General Theorem on Shakedown of Elastic Plastic Structures", Proc. Konk. Ned. Akad. Wett., B. 59, 1956, pp.24-34.

30. Martin J. "Plasticity", M.I.T. Press, Boston, 1975.

31. Prager, W. "Shakedown in Elastic, Plastic Media Subjected to Cycles of Load and Temperature", Symposium Su la Plasticita Nella Scienza Delle Construzioni, Bologna, 1957, pp. 239-244.

32. Roseblum, V.I. "On Shakedown of Nonuniformily Heated Elastic Plastic Bodies", (in Russian), Izv ANSSSR OTN Mekh. Mashinostr 7, 1957,pp. 136-138.

33. Maier, G. "Shakedown Theory in Perfect Elastoplasticity with Associated and Nonassociated Flow-Laws: A Finite Element, Linear Programming Approach", Meccanica, Vol. 4, no. 3, 1969, pp. 250-260.

34. De Donato, O. "Second Shakedown Theorem Allowing for Cycles of Both Loads and Temperature", Istituto Lombardo(Rend. Sc.)A 104, 1970, pp. 265-277.

35. Roseblum, V.I. "On Shakedown Analysis of Non-Uniformily Heated Elastic-Plastic Solids",(in Russian) Zhurn. Prikl. Mekh. Tekh. Fiz. (PMTF), No. 5, 1965, pp. 98-101.

36. Ponter, A.R.S. and Karadeniz, S. "An Extended Shakedown Theory for Structures That Suffer Cyclic Thermal Loading", Part 1: Theory, J. Appl. Mech., Vol. 52, DEC/1985, pp. 877-882.

37. Ponter, A.R.S. and Karadeniz, S. "An Extended Shakedown Theory for Structures That Suffer Cyclic Thermal Loading", Part 2: Applications, J. Appl. Mech., Vol. 52, DEC/1985, pp. 883-889.

38. Pellisier-Tanon, A., Rabbe, P. & Amzallag, C. "Defining a Proper Material Characteristic for the Shakedown Analysis", 3rd Int. Conf. on Pressure Vessel Technology, Tokyo, ASME, 1977, pp. 223-232.

39. Miller, D.R. "Thermal-Stress Ratchet Mechanism in Pressure Vessels", J. Basic Engineering, Trans. ASME, Vol. 96,1974, pp. 190-196.

40. Bree, J. "Elastic-Plastic Behaviour of Thin Tubes Subjected to Internal Pressure and Intermittent

High-Heat Fluxes with Applications to Fast-Nuclear-Reactor Fuel Elements", J. Strain Analysis, Vol. 2, No. 3, pp. 226-238.

41. Bree, J. "Incremental Growth Due to Creep and Plastic Yielding of Thin Tubes Subjected to Internal Pressure and Cyclic Thermal Stresses", J. Strain Analysis, Vol. 3, No. 2, 1968, pp. 122-127.

42. Burgreen, D. "The Thermal Ratchet Mechanism", J. Basic Enginnering, Trans. ASME, Series D, Vol. 90, No. 3, 1968, pp. 319-324.

43. Burgreen, D. "Structural Growth Induced by Thermal Cycling", J. Basic Enginnering, Trans. ASME, Series D, Vol. 90, No.3, 1968, pp. 469-475.

44. Edmonds, H.G. and Beer, F.J., "Notes on Incremental Collapse in Pressure Vessels". Jnl. Mech. Enginnering Sci., Vol. 3, 1961.

45. Anderson, W.F. "Ratchetting Deformation as Affected by Relative Variations of the Loading Sequence", 2nd Int. Conf. Pressure Vessel Technol., Part I - Design And Analysis, San Antonio, Texas, USA, ASME 1973, pp. 277-289.

46. Uga, T. "An Experimantal Study on Thermal-Stress Ratchetting of Austenic Stainless Steel by a Three Bars Specimen", Trans. ASME, Jnl. of Engn. Materials and Techn., Vol 100, 1978, pp. 150-156.

47. Mulcahy, T.M. "An Assement of Kinematic Hardening Thermal Ratchetting", J. Enginnering Mat. and Techn., Trans. ASME, Vol. 96, 1974, pp. 214-221.

48. Mulcahy, T.M. "Thermal Ratchetting of a Beam Element Having an Idealized Buaschinger Effect", J. Enginnering Materials and Techn., Trans. ASME, Vol. 98, 1976, pp. 264-271.

49. Arnaudeau, F., Zarka, J. & Gerij, J. "Thin Circular Cylinder under Axisymmetrical Thermal and Mechanical Loading", Paper 16/5, Proceedings 4th Int. Conf. on Struc. Mech. in Reactor Techn. Vol. L, San Francisco, USA, 1977.

50. Megahed, M.M. "on the Inelastic Deformation of Structures Subjected to Variable Loading", Ph.D. Thesis, University of Leicester, November 1977.

51. Karadeniz, S. and Ponter, A.R.S. "A Linear Programming Upper Bound Approach to the Shakedown Limit of Thin Shells Subjected to Variable Thermal Loading", J. of Strain Analysis, Vol. 19, No. 4, 1984, pp. 221-229.

52. Kraus, H. "International Benchmark Project on Simplified Methods for Elevated Temperature Design and Analysis; Problem II - The Saclay Fluctuating Sodium

Level Experiment", WRC Bulletin, No. 258, May 1980.

53. ASME Boiler and Pressure Code Case 1592, Asme, New York, 1974.

54. Goodman A.M. "Incremental Plastic Deformation of a Cylinder Subjected to Cyclic Thermal Loading", "Non-Linear Problems in Stress Analysis", Ed. Staley, P., Applied Science Publishers Ltd., London, 1978, pp. 317-344, and CEGB, Berkeley Nuclear Laboratories, report RD/B/N3851, Nov. 1977.

55. Goodman, A.M. "The Infuence of Rapid Thermal Transients on Elastic-Plastic Ratchetting", CEGB, Berkeley Nuclear Laboratories, Report No. RD/B/N4492, Feb. 1979.

56. Bell, R.T. "Ratchetting Experiments on Thin Cylinders Subjected to Axially Moving Temperature Fronts", UKAEA, Risley Nuclear Power Development Establishment, Memorandum ND-m-1325(R), Risley, Oct. 1980.

57. Timoshenko, S.P. and Woinowsky-Kreiger, S. "Theory of Plates and Shells", 2nd Ed. McGraw-Hill, 1959.

58. Flugge, W.F. "Stresses in Shells", Springer-Verlag, Berlin,1960.

59. Euromech 185 "Colloquium on Matematical Programming Methods for the Plastic Analysis of Structures" Imperial College, London, Sept. 1984.

60. Karadeniz, S. "The Development of Upper Bound and Associated Finite Element Techniques for the Plastic Shakedown of Thermally Loaded Structures", PhD Thesis, Leicester University, Feb. 1983.

61. Morelle, P. and Hung, N.D. "Etude Numerique de L'adaptation Plastique des Plaques et des Coques de Revolution par les Elements Finis D'equilibre", J. de Mecanique Theorique et Appliquee, Vol. 2, No. 4, 1983, pp. 567-599.

62. Morelle, P. "Numerical Shakedown Analysis of Axisymmetric Sandwich Shells", To be Published.

63. Karadeniz, S. Ponter, A.R.S., Carter, K. "The Plastic Ratchetting of Thin Cylindrical Shells Subjected to Axisymmetric Thermal and Mechanical Loading. Report CEC RAP 054 UK (H) to the Commission of the European Coomunities Directorate-General for Science, Research and Development, Brussels, Jan. 1985

64. Ponter, A.R.S., Carter, K.F. & Karadeniz, S. "The Effects of Thermal Loading on The Deformation of Shells Structures", Inelastic Behaviour of Plates and Shells, IUTAM Symposium Rio de Janeiro 1985, Springer,Berlin Heidelberg 1986.

65. Zarka, J. et Inglebert, G. "Sur une Nouvelle Analuse

Simple des Structures Inelastiques", CISM Seminar on Simplified Analysis of Inelastic Structures Subjected to Statical or Dynamical Loadings, Laboratorie de Mecanique des Solides, Ecole Polytechnique, Oct. 1985.

66. Corradi, L. "A Displacement Formulation for the Finite Element Elastic-Plastic Problem", Meccanica, 18, 1983, pp.77-91.

67. Corradi, L. and Zavelani, A. "A Linear Programming Approach to Shakedown Analysis of Structures", Computer Methods in Applied Mechanics and Enginnering, 3, 1974, pp. 37-53, North-Holland Publishing Company.

68. Maier, G. and Munro, J. "Mathematical Programming Methods in Engineering Plasticity", Proc.5th Int. Conf. on Struct. Mech. in Reactor Tech., Berlin, Vol. 1 1979.

69. Drucker, D.C. "Limit Analysis of Cylindrical Shells Under Axially-symmetric Loading", Proc. 1st. Midwest. Conf. Solids Mech., Urbana,Ill, 1953, pp. 158-163.

70. Onat, E.T. "Tha Plastic Collapse of Cylindrical Shells Under Axially Symmetrical Loading", Quart. of Appl. Math., Vol. 13, 1955, pp. 63-72.

71. Hodge Jr., P.G. and Brooklyn, N.Y. "Rigid-Plastic Analysis of Symmetrically Loaded Cylindrical Shells", J. Appl. Mech. Dec. Vol. 76, 1954, pp. 336-342.

72. Hodge Jr., P.G. "Plastic Analysis of Structures, McGraw-Hill, New York, 1959.

73. Agrawal, P.K. and Hodge Jr, P.G. "Yield-point Ring Load Filled Circular Cylindrical Shells", In J. Mech. Sci. Vol. 12, 1970, pp. 935-947.

74. Onat, E.T. and Prager, W. "Limit Analysis of Shells of Revolution" Proc. of Koninklijke Nederlandshe Akad. van Wet., B, Vol. 57, 1954, pp. 534-548.

75. Drucker, D.C. and Shield, R.T. "Limit Anlysis of Symmetrically Loaded Thin Shells of Revolution", J. Appl. Mech., Vol 25, TRans. ASME 1958.

76. Shield, R.T. and Drucker, D.C. "Limit Strength of Thin Walled Pressure Vessels with an ASME Standard Torispherical Head", #rd Congr. of Appl. Mech., June 1958, pp. 665-672.

77. Robinson, M. "A comparison of Yield Surfaces for Thin Shells", Int. J. Mech. Sci. Vol. 13, 1971, pp. 345-354.

78. Hodge Jr., P.G. "Limit Analysis of Rotationally Symmetric Plates and Shells", Prentice-Hall Inter. serire in Theory of Appl. Mech., 1963.

79. Gill S.S. "The Limit pressure for a Flush Cylindrical

Nozzle in a Spherical Pressure Vessel", Int. J. Mech. Sci., Vol. 6, 1964, pp. 105-115.

80. Dinno, K.S. and Gill, S.S. "The Effect of the Circumferential Bending Moment and Change of Circumferential Curvature on the Calculation of the Limit Pressure of Symmetrically Loaded Shells of Revolution", Int. J. Mech. Sci. Vol. 7, 1965, pp. 15-19.

81. Drucker, D.C., Prager, W. & Greenberg, H.J. "Extended Limit Design Theorems for Continuous Media", Quart. J. appl. Math., Vol. 9, 1952, pp. 381-389.

82. Allman D.J. and Gill, S.S. "The Effect of Change of Geometry on the Limit Pressure of a Flush Nozzle in a Spherical Pressure Vessel", Engiineering Plasticity, Cambridge University Press, 1968.

83. Robinson, M. and Gill, S.S. "The Effect of Finite Changes of Geometry on the Rigid-Plastic Limit Pressure of Flush Nozzles in Spherical Pressure Vessels", In J. Mech. Sci., Vol. 11, 1969 pp. 253-267.

84. Biron A. and Charleux, G. "Limit analysis of Axisymmetric Pressure Vessel Intersections of Arbitrary Shape", Int. J. Mech. Sci. Vol. 14, 1972, pp. 25-41.

85. Oden, J.T. and Brauchli H.J. "On the Calculation of Consistent Stress Distribution in Finite Element Approximations", Int. J. for Num. Meth. in Eng., Vol. 3, 1971, pp. 317-325.

86. Oden, J.T. and Reddy, J.N. "Note on the Approximate Method for Computing Consistent Conjugate Stresses in Elastic Finite Elements", Int. J. for Num. Meth. in Eng., Vol. 6, 1973, pp. 55-61.

87. Prager, W. "In Introduction to Plasticity", Addison-Wesley Publishing Company Inc., 1959.

88. Zienkiewicz, O.C. "The Finite Element Method", McGraw-Hill, 1977.

89. Hodge Jnr., P.G. and Sun, C.K. "Yield-Point Load of a Circular Plate Sealing an Incompressible Fluid", Int. J. Mech. Sci., Vol. 9, 1967, p. 405.

90. Eason, G. and Shield, R.T., "The Influence of Free Ends on the Load Carrying Capacities of Cylindrical Shells", J. Mech. Phys. Solids, Vol. 4, 1955, p. 17.

91. Eason, G, "The Load Carrying Capacities of Cylindrical Shells Subjected to a Ring of Force", J. Mech. Phys. Solids, Vol. 4, 1958-59, pp. 169-180.

92. Biron, A. and Chawla, U.S. "Numerical Method for Limit Analysis of Rotationally Symmetric Shells", Bulletin de l'Academie Ponolaise des Sciences, Vol. 18, No. 3,

1970, pp. 109-117.

93. Nguyen Dang Hung, Trapeletti, M. and Ransart, D. "Bornes Quasi-Inferieures et Bornes Superieures de la Pression de Ruine des Coques de Revolution par la Methode des Elements Finis et par la Programmation Non Lineaire", Int. J. Non-Linear Mechanics, Vol. 13, 1978, pp. 79-102.

94. Ponter, A.R.S. and Carter, K.F., to be published.

95. Hodge Jnr., P.G. "The Collapse Load of a Spherical Cap", Proc. Fourth Midwest Conf. Solid Mech., Austin, 1959, pp. 108-126.

96. Hodge Jnr., P.G. "Yield Conditions for Rotationally Symmetric Shells under Axisymmetric Loading", J. Appl. Mech. 2, Vol. 27, 1960, pp. 323-331.

97. Mroz, Z. and Xu, B.Y. "The Load Carrying Capacities of Symmetrically Loaded Spherical Shells", Arch. Mech. Stos. 2, Vol. 15, 1963, pp. 245-266.

98. Lee, L.C. and Onat, E.T. "Analysis of Plastic Spherical Shells", Brown University, 1965.

99. Heyman, J. "Beams and Framed Structures", 2nd edition, Pergamon Press, 1974.

100. Neal, B.G., "The Plastic Methods of Structural Analysis", 3rd edition, Chapman and Hall, 1974.

101. Horne, M.R. "Plastic Theory of Structures", 2nd edition, Pergamon Press, 1979.

102. Megahed, M.M. Ponter, A.R.S., Morrison, C.J. "Experimental Investigations into the Influence of Cyclic Phenomena of Metals on Structural Ratchetting Behaviour" University of Leicester ,Department of Engineering, Internal Report, 1983.

103. Morrow, J. "Cyclic plastic Strain Energy and Fatigue of Metals", ASTM STP 378, 1965, pp. 45-87.

104. Landgraf, R.W., "Resistance of Metals to Cyclic Deformation", ASTM pp. 1970, pp. 3-36.

105. Landgraf, R.W., Morrow, J., Endo, T. "Determination of the Cyclic Stress-Strain Curves", Journal of Materials, JMLSA, Vol. 4, 1969, pp. 176-188.

106. Manson, S.S. "Thermal Stress and Low Cyclic Fatigue", McGraw-Hill, New York, 1966.

107. Oldroyd, P.W.J., "Modifications to an Intron-Testing Machine for Cyclic Loading in the Plastic Range", Proc. Instn. Mech. Engrs., Vol. 180, Pt. 3A, 1965-1966, pp. 229-236.

108. Oldroyd, P.W.J., Burns, D.J., Benham, P.P., "Strain

Hardening and Softening of Metals Induced by Cycles of Plastic Deformations", Proc. Instn. Mech. Engrs., Vol. 180, Pt. 3I, 1965-1966, pp. 392-402.

109. Fenn. O., "Behaviour of Structures Subjected to Cyclic Plastic Deformation", M.Phil, Thesis, University of Leicester, October 1980.

110. Megahed, M.M., "Influence of Hardening Rules on the Elasto-Plastic Behaviour of a Simple Structure Under Cyclic Loading", Int. J. Mech. Sci., Vol. 23, 1981, pp. 169-182.

111. Karadeniz, S. and Ponter, A.R.S., "The Influence of Transient Thermal Loading on the Bree Plate; A Simplified Analysis", Journal of Nuclear Enginnering and Design, Vol. 180, 1984, pp. 359-374.

112. Shield, R.T. and Ziegler, H. "On Prager's Hardening Rule", Contract No. 562(10) to the Office of Naval Research, Brown University, Division of Applied Mathematics, 1958.

113. Prager, W., "The Theory of Plasticity; A Survey of Recent Achievements", James Clayton Lecture, Proc. Inst. Mech. Engrs., Vol. 169, 1955, pp. 41-57.